



SUMMARY OF ACTIVITIES 2016





GEOSCIENCE BC SUMMARY OF ACTIVITIES 2016



© 2017 by Geoscience BC.

All rights reserved. Electronic edition published 2017.

This publication is also available, free of charge, as colour digital files in Adobe Acrobat® PDF format from the Geoscience BC website: <http://www.geosciencebc.com/s/DataReleases.asp>.

Every reasonable effort is made to ensure the accuracy of the information contained in this report, but Geoscience BC does not assume any liability for errors that may occur. Source references are included in the report and the user should verify critical information.

When using information from this publication in other publications or presentations, due acknowledgment should be given to Geoscience BC. The recommended reference is included on the title page of each paper. The complete volume should be referenced as follows:

Geoscience BC (2017): Geoscience BC Summary of Activities 2016; Geoscience BC, Report 2017-1, 264 p.

ISSN 1916-2960 Summary of Activities (Geoscience BC)

Cover photo: Installing piezometers near Coles Lake, northeastern British Columbia

Photo credit: S. Abadzadesahraei, 2016

Acknowledgments

I would like to express appreciation for the leaders in British Columbia's mineral exploration, mining and energy sectors who support our organization through their guidance, use and recognition of the information that we collect and distribute. I would also like to thank the Province of British Columbia for its ongoing support of Geoscience BC and recognize the \$5 million investment made in 2016, enabling our continued delivery of projects that generate new earth science information for everyone.

Robin Archdekin
President & CEO
Geoscience BC
www.geosciencebc.com

Foreword

Geoscience BC is pleased to present results from several of our ongoing geoscience projects in our tenth edition of the *Geoscience BC Summary of Activities*. The volume is divided into two sections, 'Energy' and 'Minerals', and contains a total of 33 papers from Geoscience BC-funded projects and 2016 scholarship winners.

The 'Energy' section contains 14 papers from oil and gas and geothermal projects in northeastern British Columbia (BC). Three papers, by Bustin and Bustin, Babaie Mahani et al. and Wang et al., examine the monitoring and impact of induced seismicity due to hydraulic fracturing. Hayes et al. provide an update on a new project examining resource oil plays, and petroleum systems analyses are presented for the Doig Formation by Silva and Bustin, and Upper Devonian shales of the Horn River and Liard basins by Wilson and Bustin. Vaisblat et al. present a diagenetic model for the Montney Formation.

Water is once again a key focus of Geoscience BC Energy projects. Two papers, by Morgan et al. and Abadzadesahraei et al., highlight research aimed at increasing the regional understanding of groundwater in northeastern BC. Owen and Bustin discuss the geochemistry of flowback waters from hydraulic fracturing, Gupta et al. examine the uptake of water by Horn River basin shales during hydraulic fracturing and the resulting hydration-induced stress and strain, and Quinton et al. provide an update on permafrost and hydrological monitoring and modelling in northeastern BC.

Evans and Whiticar introduce a new project aimed at geochemically 'fingerprinting' natural gas in northeastern BC and compiling the results into a publicly available database. Finally, Palmer-Wilson et al. introduce a new project aimed at the development of a methodology for assessing geothermal potential of sedimentary basins by using data from oil and gas exploration.

The 'Minerals' section contains 19 papers from minerals geoscience projects throughout BC. Madu provides an update of the Search project, which has now completed a second phase of airborne magnetic data collection.

Geochemistry is once again a main focus of Geoscience BC projects. Sacco et al., Geffen and Bluemel, and Bluemel and Geffen highlight advances in analyzing and interpreting TREK project till geochemical data, and Jackaman summarizes Geoscience BC's ongoing updates to the provincial RGS databases. Three papers, one by Yehia et al. and two by Heberlein and Dunn, highlight the ongoing development of new geochemical techniques in BC (using a field-portable photometer and voltammeter, and through the analysis of halogen and other volatile compounds, respectively). Hart and Jenkins present a summary of a recently completed Mineral Deposit Research Unit project focused on compiling and interpreting surficial geochemistry around BC porphyry deposits.

Four student papers are focused on important mineral deposits or mining districts in BC: Highland Valley (Chouinard et al. and Byrne et al.), Brucejack (McLeish et al.) and Kerr-Sulphurets-Mitchell (Campbell and Dilles). South-central BC is the focus of Mortensen et al. and Bouzari et al., who characterize the basement of the Quesnel terrane and porphyry-fertile plutons in the region, respectively. Chapman et al. provide an update on using detrital gold as an indicator mineral in central BC.

Two papers, by Hoy et al. and Cook, describe new mapping and geophysical interpretation being produced in southeastern BC. Finally, Flynn and Madu highlight an innovative partnership between Geoscience BC and the Canada Mining Innovation Council aimed at compiling and disseminating key water quality data related to the mining sector.

Geoscience BC Publications 2016

In addition to this *Summary of Activities* volume, Geoscience BC releases interim and final products from our projects as Geoscience BC reports. Highlights from 2016 include the Search Phase I airborne survey data in west-central BC, a new airborne EM survey in northeastern BC, a tree-top biogeochemical survey in central BC and a report highlighting direct-use geothermal resources in BC.

The most up-to-date listing of all Geoscience BC data and reports can be accessed through our website at www.geosciencebc.com/s/DataReleases.asp. Most final reports and data can be viewed through our Earth Science Viewer at <http://www.geosciencebc.com/s/WebMaps.asp>.

All releases of Geoscience BC reports and data are announced through our website and e-mail list. If you are interested in receiving e-mail regarding these reports and other Geoscience BC news, please contact info@geosciencebc.com.



Acknowledgments

Geoscience BC would like to thank all authors and reviewers of the *Summary of Activities* papers for their contributions to this volume. RnD Technical is also thanked for their work in editing and assembling the volume.

Christa Pellett
Project Co-ordinator
Geoscience BC
www.geosciencebc.com

Contents

Energy Projects

- A.M.M. Bustin and R.M. Bustin:** Monitoring and risk assessment of anomalous induced seismicity due to hydraulic fracturing in the Montney Formation, northeastern British Columbia 1
- A. Babaie Mahani, H. Kao, J. Johnson and C.J. Salas:** Ground motion from the August 17, 2015, moment magnitude 4.6 earthquake induced by hydraulic fracturing in northeastern British Columbia 9
- B.J.R. Hayes, B. Nassichuk, R. Bachman, J.S. Clarke, R. Wust and K. Michaud:** Identification and evaluation of new resource oil plays in northeastern British Columbia 15
- B. Wang, R. Harrington, Y. Liu and H. Kao:** Remote dynamic triggering of earthquakes in three Canadian shale gas basins, northeastern British Columbia and Alberta, Northwest Territories and New Brunswick: progress report. 21
- P.L. Silva and R.M. Bustin:** Status report on petroleum system analysis study of the Triassic Doig Formation, Western Canada Sedimentary Basin, northeastern British Columbia 25
- T.K. Wilson and R.M. Bustin:** Unconventional petroleum systems analysis of Upper Devonian organic-rich shale units in the Horn River and Liard basins, northeastern British Columbia and adjacent western Alberta: preliminary report 29
- N. Vaisblat, N.B. Harris, C. DeBhur, T. Euzen, M. Gasparrini, V. Crombez, S. Rohais, F. Krause and K. Ayranci:** Diagenetic model for the deep Montney Formation, northeastern British Columbia . . . 37
- J.N. Owen and R.M. Bustin:** Implications of the inorganic geochemistry of flowback water from the Montney Formation, northeastern British Columbia and northwestern Alberta: progress report. 49
- A. Gupta, M. Xu, H. Dehghanpour and D. Bearinger:** Preliminary report on hydration-induced swelling of shale in the Horn River Basin, northeastern British Columbia 55
- S.E. Morgan, D.M. Allen, D. Kirste and C.J. Salas:** Investigating the role of buried valley aquifer systems in the regional hydrogeology of the Peace River region, northeastern British Columbia. 63
- S. Abadzadesahraei, S.J. Déry and J. Rex:** Quantifying the water balance of Coles Lake in northeastern British Columbia using in situ measurements and comparisons with other regional sources of water information 69
- C. Evans and M.J. Whiticar:** British Columbia Natural Gas Atlas project: 2016 project update 75
- W.L. Quinton, J.R. Adams, J.L. Baltzer, A.A. Berg, J.R. Craig and E. Johnson:** Consortium for Permafrost Ecosystems in Transition: traversing the southern margin of discontinuous permafrost with hydrological, ecological and remote sensing research, northeastern British Columbia and southwestern Northwest Territories 79
- K. Palmer-Wilson, W. Walsh, J. Banks and P. Wild:** Techno-economic assessment of geothermal energy resources in the Western Canada Sedimentary Basin, northeastern British Columbia. 87

Minerals Projects

- B.E. Madu:** Search project: Phase II activities in west-central British-Columbia 91
- W. Jackaman:** Ongoing development of British Columbia's regional geochemical database using material saved from previous field surveys. 95
- D.A. Sacco, W. Jackaman, R.E. Lett and B. Elder:** Identifying mineral exploration targets in the TREK project area, central British Columbia, using a multimedia and multivariate analysis of geochemical data and a preliminary method of sediment transport modelling 101
- P.W.G. van Geffen and E.B. Bluemel:** Clay-fraction till geochemistry of the TREK project area, central British Columbia: progress report 113
- E.B. Bluemel and P.W.G. van Geffen:** Adding value to regional till geochemical data through exploratory data analysis, TREK project area, central British Columbia. 115
- R.L. Chouinard, P.A. Winterburn, M. Ross and R.G. Lee:** Surficial geochemical footprint of buried porphyry Cu-Mo mineralization at the Highland Valley Copper operations, south-central British Columbia: project update 125
- R. Yehia, D.R. Heberlein and R.E. Lett:** Rapid, field-based hydrogeochemical-survey analysis and assessment of seasonal variation using a field-portable photometer and voltammeter, Marmot Lake NTS area, south-central British Columbia 133
- D.R. Heberlein and C.E. Dunn:** Preliminary results of a geochemical investigation of halogen and other volatile compounds related to mineralization, part 1: Lara volcanogenic massive-sulphide deposit, Vancouver Island. 141
- D.R. Heberlein and C.E. Dunn:** Preliminary results of a geochemical investigation of halogen and other volatile compounds related to mineralization, part 2: Mount Washington epithermal gold prospect, Vancouver Island. 151

C.J.R. Hart and S. Jenkins: Surficial geochemical map packages for British Columbia porphyry systems	159	district, Guichon batholith, south-central British Columbia	213
J.K. Mortensen, K. Lucas, J.W.H. Monger and F. Cordey: Synthesis of U-Pb and fossil age, lithogeochemical and Pb-isotopic studies of the Paleozoic basement of the Quesnel terrane in south-central British Columbia and northern Washington state	165	D.F. McLeish, A.E. Williams-Jones and W.S. Board: Nature and origin of the Brucejack high-grade epithermal gold deposit, northwestern British Columbia	223
F. Bouzari, C.J.R. Hart, T. Bissig and G. Lesage: Mineralogical and geochemical characteristics of porphyry-fertile plutons: Guichon Creek, Takomkane and Granite Mountain batholiths, south-central British Columbia	189	M.E. Campbell and J.H. Dilles: Magmatic history of the Kerr-Sulphurets-Mitchell copper-gold porphyry district, northwestern British Columbia	233
R.J. Chapman, D.A. Banks and C. Spence-Jones: Detrital gold as a deposit-specific indicator mineral, British Columbia: analysis by laser-ablation inductively coupled plasma-mass spectrometry	201	T. Höy and G.M. DeFields: Geology of the northern extension of the Rock Creek graben, Christian Valley map area, south-central British Columbia	245
K. Byrne, G. Lesage, S.A. Gleeson and R.G. Lee: Large-scale sodic-calcic alteration around porphyry copper systems: examples from the Highland Valley Copper		F.A. Cook: Merging geological, seismic-reflection and magnetotelluric data in the Purcell Anticlinorium, southeastern British Columbia	257
		M.J. Flynn and B.E. Madu: Unlocking the value of open data in British Columbia: a Mining Industry Knowledge Hub	259

Monitoring and Risk Assessment of Anomalous Induced Seismicity Due to Hydraulic Fracturing in the Montney Formation, Northeastern British Columbia

A.M.M. Bustin, The University of British Columbia, Vancouver, BC, abustin@eos.ubc.ca

R.M. Bustin, The University of British Columbia, Vancouver, BC

Bustin, A.M.M. and Bustin, R.M. (2017): Monitoring and risk assessment of anomalous induced seismicity due to hydraulic fracturing in the Montney Formation, northeastern British Columbia; *in* Geoscience BC Summary of Activities 2016, Geoscience BC, Report 2017-1, p. 1–8.

Introduction

Shale gas operations in northeastern British Columbia (NEBC) have induced the largest occurrence and magnitude of anomalous induced seismicity (AIS) due to hydraulic fracturing. Occurrences of AIS with magnitudes of up to M_L 4.6 have been recorded in seven clusters within the Montney play due to hydraulic fracturing (Figure 1). Two of these clusters have been linked to waste-water disposal and another five to hydraulic fracturing. Environmental and safety concerns associated with wellbore damage resulting from AIS are important, as are public concerns, especially as shale-gas extraction is expected to ramp up over the next several years.

The goal of this Geoscience BC research project is to better understand AIS due to hydraulic fracturing in NEBC. The project is designed to investigate the variables and processes controlling AIS and its associated ground motions, as well as to investigate and develop methods or protocols for the reduction and mitigation of the seismicity. The program has two objectives in order to accomplish these goals:

- build and deploy additional accelerograph and three-component (3C) seismometer sensors (up to 15 additional sensors during the tenure of the grant) to monitor hydraulic fracturing in the Montney Formation for the purpose of mitigating AIS through the development of a traffic-light/early-warning protocol based on ground motions, and to develop attenuation models (i.e., the relationship between magnitude and ground motions)
- develop probabilistic hydrogeomechanical models for the occurrence and magnitude of AIS due to hydraulic fracturing in the Montney Formation by integrating data from field studies and laboratory analysis into numerical simulations

Keywords: British Columbia, hydraulic fracturing, induced seismicity, Montney Formation, attenuation model, traffic-light protocol, hydrogeomechanical modelling

This publication is also available, free of charge, as colour digital files in Adobe Acrobat® PDF format from the Geoscience BC website: <http://www.geosciencebc.com/s/DataReleases.asp>.

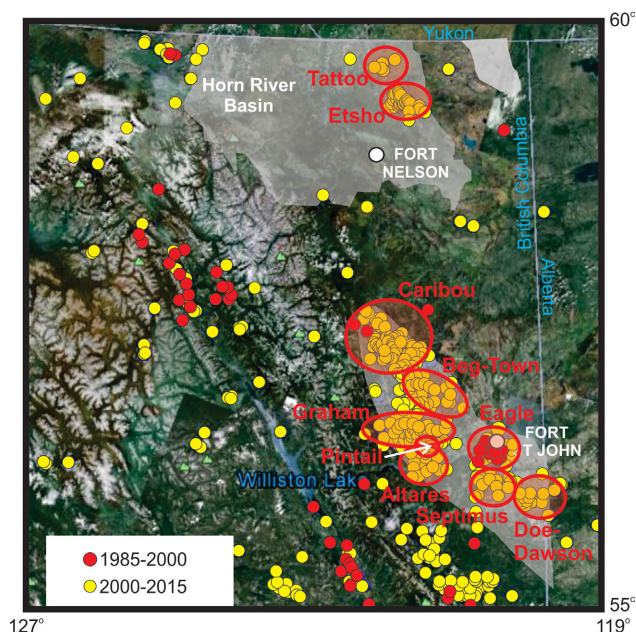


Figure 1. Anomalous induced seismicity in northeastern British Columbia from 1985 to 2000 (red circles) and from 2000 to 2015 (yellow circles). The Eagle cluster is related to conventional production and secondary recovery; the Graham and Pintail clusters are associated with waste-water injection; the Etsho and Tattoo clusters are linked to hydraulic fracturing in the Horn River Basin; whereas the remaining five clusters are linked to hydraulic fracturing in the Montney play.

The data necessary to develop an effective AIS traffic-light protocol (TLP) based on ground motions will be provided by expanding the currently operational five-sensor array. These sensors are low cost, mobile and easy to deploy (sensors need only be buried beneath any loose material using a shovel), consisting of both an accelerograph and 3C seismometer to cover the full frequency bandwidth necessary for monitoring both microseismicity and AIS, as well as accurately measure ground motions. The design for the sensors was modified from that developed at the University of British Columbia (UBC) and currently deployed for British Columbia's earthquake early-warning system and, hence, is extensively tested and proven technology. The sensors will be instrumental in providing industry with an efficient, accurate and inexpensive monitoring option for the BC Oil

and Gas Commission's collaborative monitoring model. The array will be used to densely monitor the hydraulic fracturing of 3–5 multilateral well pads in the Montney play and to obtain a dataset of reliably located events and associated ground motions. The spatiotemporal and magnitude-frequency distributions of microseismicity, AIS and associated ground motions will be analyzed to develop TLP. The increased positional accuracy of source locations and magnitudes will be calibrated with, and integrated into, the Canadian National Seismograph Network (CNSN), as well as any commercial arrays put in place by industry partners. Monitoring of the array will provide a better understanding of the relationship between ground motions and magnitudes for induced events and assist in the development of an attenuation relationship for the Montney Formation.

Earth models for the monitored regions will be developed to better understand the processes resulting in AIS, quantify the sensitivity of the occurrence and magnitude of the AIS to the hydrogeomechanical parameters, identify regions with higher probability of encountering critically stressed faults and provide estimates of maximum-event magnitudes, as well as test mitigation techniques. The modelling parameters will be obtained from the seismic monitoring as well as the analysis of well logs, injection fall-off tests and 'mini fracs', and combined with the hydraulic-fracture stimulation parameters provided by industry partners. The results from geomechanical tests being undertaken in sister studies at UBC will provide further metrics for the modelling. The field and laboratory data will be linked to numerical simulations incorporating advanced 3-D hydrogeomechanical bonded-block distinct-element modelling (3DEC™), which uses algorithms to estimate event magnitudes from simulated induced seismicity.

Background

British Columbia (BC) has tremendous resources of natural gas (estimated at $\sim 8.5 \times 10^{13} \text{ m}^3$) in mainly low-permeability rocks, which require hydraulic fracturing to achieve economic production rates (BC Ministry of Energy and Mines, 2011). It is estimated that natural gas will contribute some 100 billion dollars over the next 30 years to the BC economy and at the same time reduce greenhouse-gas emissions (BC Ministry of Energy and Mines, 2012). To supply five liquefied natural gas (LNG) export facilities would require an estimated 40 000 additional wells in NEBC by the year 2040 (Paulson, 2015). Reducing and mitigating AIS associated with hydraulic fracturing as well as other geohazards, minimizing water use, and developing more effective and efficient fracturing techniques are important challenges that must be met for this development to be economically and environmentally viable.

Anomalous induced seismicity is a known risk in any earth-engineering project that changes the effective stress in a

rock mass. Such a change in effective stress can result from injecting or extracting fluids from the Earth during activities associated with energy technologies. The most notable example of fluid-disposal-induced seismicity occurred in Denver, Colorado, in the 1960s, when liquid-waste disposal at the Rocky Mountain Arsenal resulted in a series of magnitude 4 events. The largest was a magnitude 4.8 event in 1967, which caused half a million dollars in minor structural damages. Subsequent research (e.g., Healy et al., 1968; Van Poolen and Hoover, 1970; Hsieh and Bredehoeft, 1981) indicated a strong relationship between injection volumes and earthquake frequency; it was generally agreed that the seismicity could be described by the Hubbert-Rubey mechanism (Hubbert and Rubey, 1959), which is in accordance with the Mohr-Coulomb failure criterion ($\tau = \mu[\rho_n - p]$). In this mechanism, shear failure occurs on pre-existing failure surfaces as a result of fluid injection, which increases the pore pressure and, hence, reduces the effective normal stress. The reduction in effective normal stress lowers the critical shear stress on the failure surface, bringing the stress regime into a state of failure. This is the mechanism generally used to describe all fluid-injection-induced seismicity. In general, the fluid injection increases the pore pressure in the vicinity of the injection source, which then diffuses along natural and induced planes of weakness (e.g., fractures, faults, joints and bedding planes) into pre-existing faults that slip once the pore pressure exceeds the critical threshold.

The hydraulic fracturing of reservoirs typically only induces microseismicity ($M < 0$). However, stronger events, up to magnitude 1, are known to occur when increased pore pressures penetrate pre-existing faults (e.g., Warpinski et al., 2012). There are four known exceptional regions where hydraulic fracturing has induced seismicity with greater magnitudes: Oklahoma (Holland 2011, 2013) and Ohio, United States (Skoumal et al., 2015); Blackpool, England (de Pater and Baisch, 2011; Clarke et al., 2014); and the Western Canada Sedimentary Basin (BC Oil and Gas Commission 2012, 2014; Schultz et al. 2015a, b).

Shale-gas operations in NEBC, within the Western Canada Sedimentary Basin, have induced the largest occurrence and magnitude of AIS due to hydraulic fracturing (BC Oil and Gas Commission, 2014). Occurrences of AIS have been recorded in seven clusters within the Montney play, with magnitudes of up to M_L 4.6. Two of these clusters have been linked to waste-water disposal and another five to regions where hydraulic fracturing of the Montney shale-gas play occurs (BC Oil and Gas Commission, 2014). Although some events have been felt, the remote location and magnitude of the seismicity did not cause any damage or pose any risk of harm to the public or the environment in NEBC. However, given the current public and media perception of hydraulic fracturing of shale-gas reservoirs, simply alerting the public to the issue can cause problems for the indus-

try's development plans. The lower population in NEBC has helped industry avoid significant media attention, but safety and social concerns due to ground motions, in addition to environmental concerns associated with potential aquifer and wellbore damage (BC Oil and Gas Commission, 2012) resulting from AIS, are important issues, which are likely to worsen as more wells are drilled to meet proposed LNG commitments.

Regions where the risk is higher of inducing large events can be identified through hydrogeomechanical modelling and probabilistic risk assessment (e.g., Gischig and Wiemer, 2013; Hakimhashemi et al., 2014; Bommer et al., 2015; Hajati et al., 2015; Rutqvist et al., 2015; Tutuncu and Bui, 2016). Such assessments require a large quantity of data, which has yet to be integrated for the Montney Formation in NEBC. Even though research has provided a better understanding of the processes and parameters controlling the magnitude and occurrence of large induced events and identifying higher risk regions, it is currently impossible to measure or model the heterogeneity and scale necessary to prevent all induced events. Therefore, it is also necessary to develop and implement protocols for mitigating events. The events induced by fluid injection typically increase in magnitude and distance from the injector with time due to the diffusion of pore pressures (Figures 2, 3; e.g., Baisch and Harjes, 2003; Baisch et al., 2006; Baisch et al., 2010; Shapiro et al. 2011). The occurrence of events with increasing magnitude and distance from the injector can thus be considered precursor events and TLP are typically used to determine the nature and timing of the actions that should be taken in an attempt to mitigate larger future events (Figure 4; e.g., Bommer et al. 2006; Bachmann et al., 2011; Maxwell, 2013; Mignan et al., 2015). A TLP has yet to be developed for the Montney, where the current regulation

simply requires all injected activities to stop after a magnitude 4 event. However, it is not the magnitude of an event, but the intensity of the ground shaking that controls whether an event is felt and causes damage. Therefore, the development of a traffic-light protocol requires an understanding of the ground motions and attenuation of seismic waves, in addition to understanding the spatiotemporal and magnitude-frequency distribution of events, and the nature of the actions that may help mitigate the increase in magnitude and occurrence of events.

Objectives

In order to investigate the hydrogeomechanical parameters and processes controlling AIS and its associated ground motions in NEBC, as well as to develop methods or protocols for reducing and mitigating AIS, this research program has two objectives, which are described in detail below.

Develop Protocols to Manage and Mitigate AIS

The main objective of this study is to develop effective TLP for mitigating AIS based on ground motions for the Montney Formation in NEBC. An array of five accelerograph and 3C-seismometer sensors with telemetry for real-time monitoring of fluid injection activities has been designed and built for this purpose. The design for the sensors was modified from those built for BC's earthquake early-warning system. The array will be expanded to densely monitor 3–5 hydraulic-fracturing stimulations in the Montney play to obtain a dataset of reliably located events and associated ground motions due to AIS. The spatiotemporal and magnitude-frequency distributions of microseismicity, AIS and the associated ground motions will be analyzed to develop TLP based on ground motions. The goal to developing TLP, and combining them with current research on

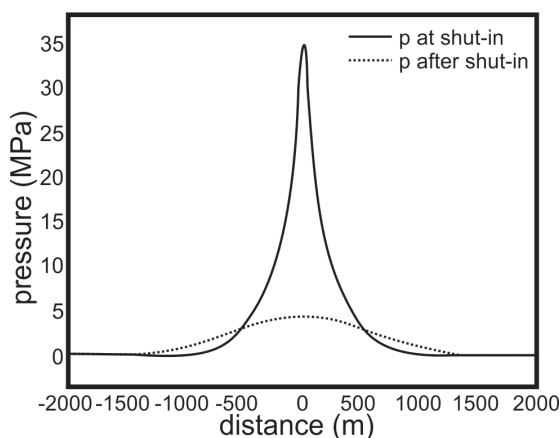


Figure 2. Graphical representation of pore pressure versus distance from an injector during injection (solid curve) and following shut-in (dotted curve), illustrating the process of pore-pressure diffusion. After shut-in, a larger area of a fault experiences elevated pore pressures resulting in larger magnitude events (modified from Baisch et al., 2006).

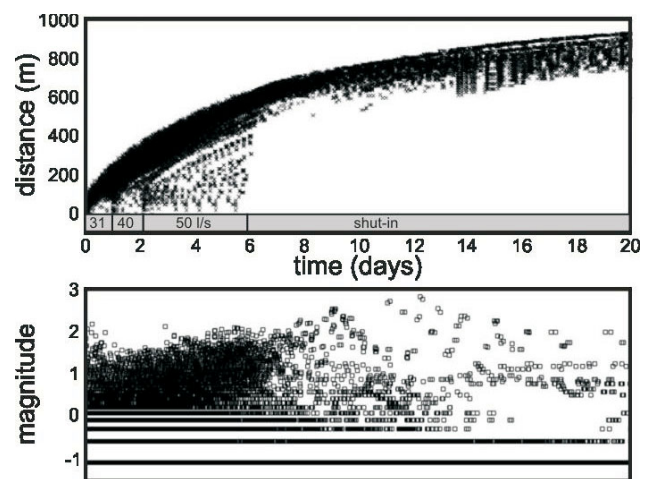


Figure 3. Example of the increase in distance from the injector (top) and the magnitude of earthquakes (bottom) during injection and following shut-in. Example is drawn from the enhanced geothermal project at Soultz-sous-Forêts in France (modified from Baisch et al., 2010).

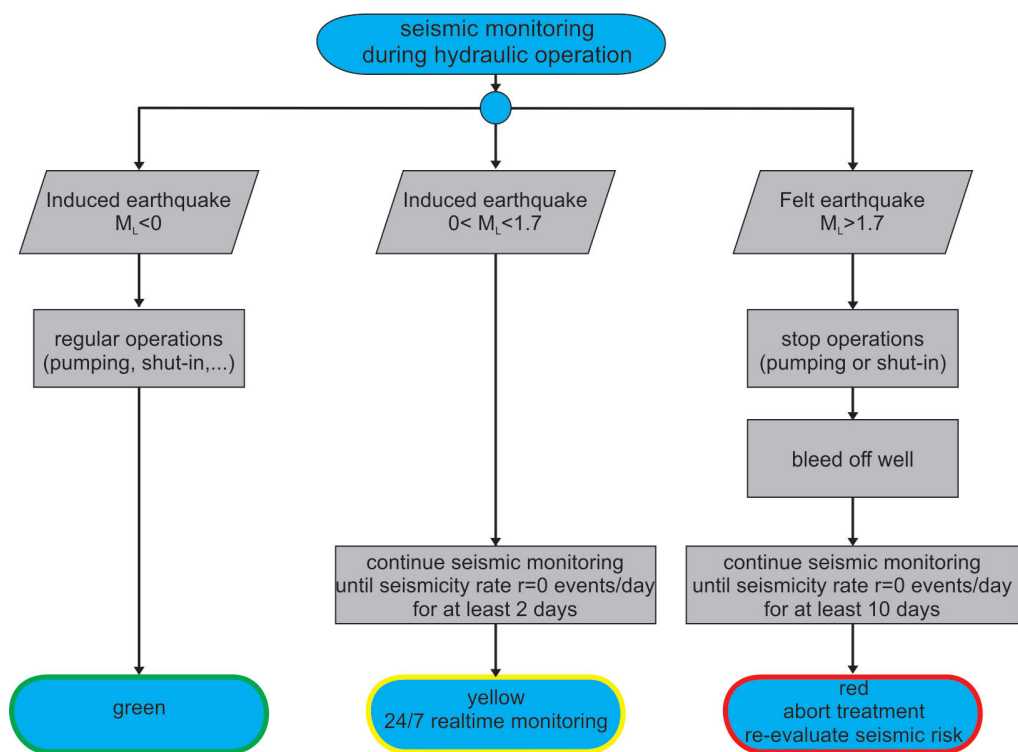


Figure 4. Example of a traffic-light protocol developed for mitigating anomalous induced seismicity due to hydraulic fracturing in the Bowland Shale in England (modified from de Pater and Baisch, 2011).

reservoir geomechanics, is to develop real-time adjustments to completion programs for mitigating AIS and, at the same time, optimize the stimulation. The data from the monitoring arrays will also be used to develop an attenuation relationship for predicting ground motions from the magnitude of AIS in the Montney Formation.

Reducing AIS through Hydrogeomechanical Modelling

Hydrogeomechanical modelling will help prevent AIS due to hydraulic fracturing in NEBC by providing a better understanding of the relative importance of hydrogeomechanical parameters, by identifying regions with a higher probability of hosting critically stressed faults, and by providing insights into the maximum magnitude of events. Mitigation techniques will also be investigated through modelling. The modelling parameters will be obtained from the results of the seismic monitoring and the analysis of well logs, injection fall-off and mini-frac tests, combined with the hydraulic-fracture stimulation parameters provided by industry partners and geomechanical tests being undertaken in sister studies at UBC. The field and laboratory data will be integrated into numerical simulations using 3DEC™, a discontinuum-modelling code based on distinct-element method (DEM) software developed by Itasca™ Consulting Group, Inc.

Methods and Approaches

There are two components to the research: a field component, whereby the array will allow hydraulic-fracture completions to be densely monitored, and a hydrogeomechanical modelling component. These approaches will be investigated in parallel, with results from the field studies being combined with ancillary data provided by laboratory analyses and industry collaborators providing the metrics for the modelling portion of the study.

Densely Monitoring Hydraulic Completions

Working with the Earthquake Engineering Research Facility (EERF) at UBC, the authors designed and built a five-station array of sensors, which include an accelerograph (Tetra 2) and a 3C seismometer. The design for the sensors was modified from the EERF's early earthquake detectors installed in BC schools for BC's earthquake early-warning system (<http://globalnews.ca/news/2429129/early-warning-system-successfully-detects-b-c-earthquake/>). The Tetra 2 accelerometers, which consist of 78 microelectromechanical systems (MEMS), are custom built based on the Tetra 1 sensors designed, built and installed for BC's earthquake early-warning system. The units are powered by a solar panel with an absorbed glass mat (AGM) deep-cycle battery and an uninterruptible power supply (UPS)

gel battery inside the pelican box for backup. The pelican box also encloses a GPS as well as a next unit of computing (NUC) to store the data and run the system. The configuration and a photo of the field setup of one of the units are shown in Figure 5. The accelerograph and seismometer have individual enclosures, which are approximately 10 by 5 by 20 cm and need only be buried under any loose material using a shovel.

The first test-monitoring project for the array is complete and the data is currently being processed. Following the first test, the stations were upgraded to include the 3C seismometers and telemetry by cell-phone modem to enable real-time monitoring. Additional modifications to reduce power consumption, due to the remoteness of the deployment areas, are currently underway. Following the next deployment, the array of inexpensive and easily deployable stations will be expanded in such a way as to allow 3–5 completions to be densely monitored (ideally 10 stations over a 10 by 10 km area) in real-time over a short period of time to obtain a dataset of reliably located events and the associated ground motions. The goal is to monitor hydraulic-fracturing stimulations of pads in the Montney play operated by industry collaborators, as well as by operators of nearby pads, through a collaborative model. The arrays will

be integrated with downhole or surface (depending on the operators' preference) microseismic monitoring arrays. A major hydraulic-fracturing service company operating in NEBC has also offered to work with them on operations with certain clients. The design criteria of the arrays will depend on the surface geology, microseismic monitoring array, the location of nearby monitoring arrays, as well as the number of sensors that are available.

The spatiotemporal and magnitude-frequency distributions of microseismicity, AIS and the associated ground motions will be analyzed to develop TLP. Similar waveforms from the same fault system will first be grouped together through cross-correlations (events rupturing the same fault system will have similar waveforms), then the post-injection time-lag and magnitude increase will be quantified to better understand pore-pressure diffusion and the resulting spatiotemporal distribution. In addition to developing TLP for regions of NEBC, the data will be used to develop an attenuation relationship for NEBC, to better understand the relationship between ground motions and recorded magnitudes.

The increased positional accuracy of source locations and magnitudes will be integrated and calibrated with the

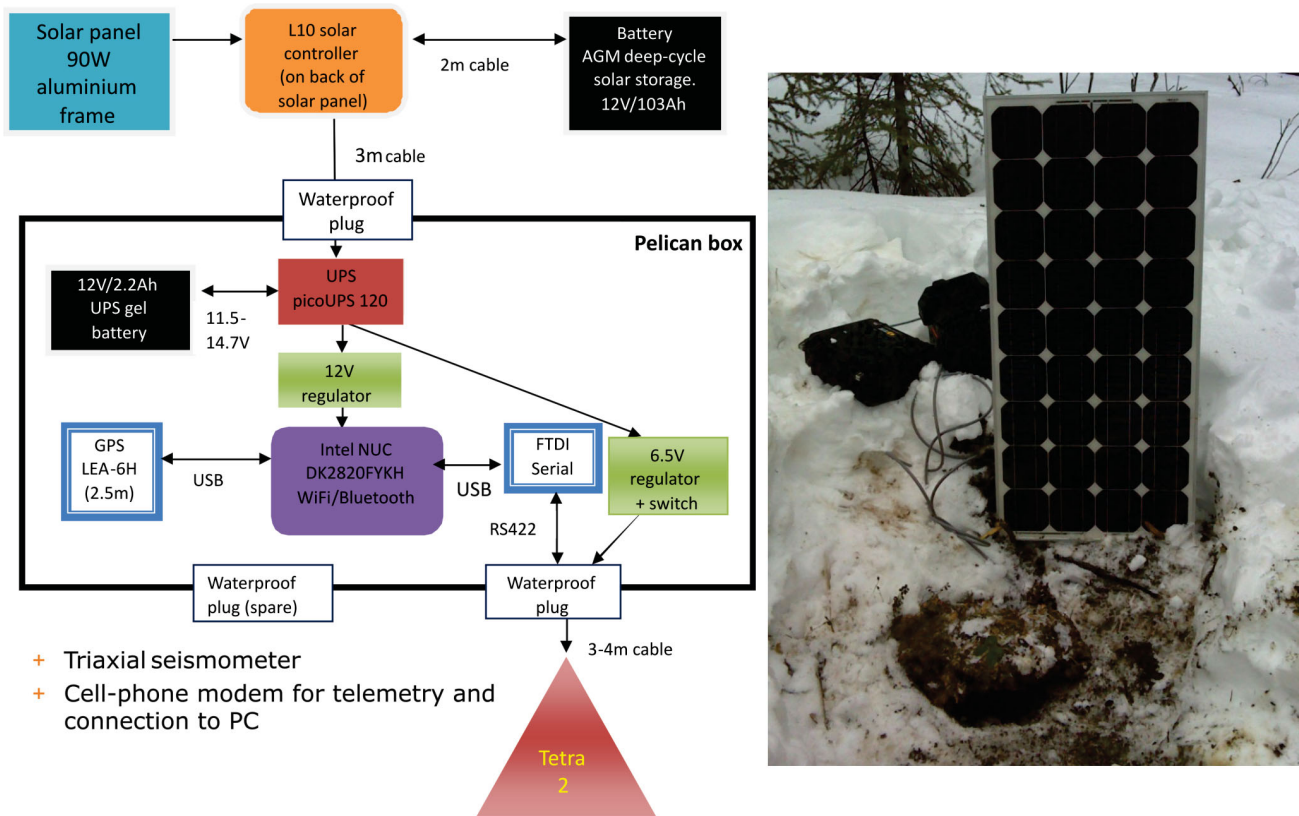


Figure 5. Configuration (left) and photo of the field setup (right) of one of the accelerograph and 3C-seismometer sensors used to monitor hydraulic fracturing in the Montney Formation. Abbreviations: AGM, absorbed glass mat; Ah, amp hour; FTDI, Future Technology Devices International; GPS, global positioning system; NUC, next unit of computing; UPS, uninterruptible power supply; USB, universal serial bus; V, volt.

CNSN, as well as any commercial arrays deployed by industry partners. The calibration of the data from the study's monitoring arrays with that provided by other sensor types will aid in understanding hypocentre accuracy and magnitude distributions and thresholds, as well as serve as a comparison to illustrate the advantages provided by these sensors. Additionally, the monitoring projects will help optimize the design criteria for monitoring arrays in NEBC.

Hydrogeomechanical Modelling

Hydrogeomechanical modelling provides the opportunity to evaluate the potential response of naturally stressed rock to fluid injection under various conditions. The first step of the modelling is to create a database of the parameters needed to create a hydrogeomechanical model. The necessary parameters include: 3-D stress profiles; pore pressure; rock mechanical properties (including those for fault characterization); spacing, geometry, and orientation of natural and induced fractures and faults; and bedding thickness and orientation. In order to determine the above parameters, agreements are in place with many operators in NEBC to provide data and/or interpretations from well-pressure tests, well logs, and seismic and microseismic monitoring. Information on completions, including wellbore pressures, injected volumes and rates, type and amount of proppant, and flow-back volumes and rates, in addition to well designs, are also being obtained.

To establish metrics for the hydrogeomechanical and reservoir models, laboratory tests will be combined with interpretation and analysis of well logs and well tests, in addition to the results of the seismic monitoring. Part of the research will involve characterizing the relationship between the lithostratigraphy, rock moduli (mechanical stratigraphy) and the established or estimated in situ stress field to better predict the fracture fabric that will be induced with various drilling and hydraulic-fracturing strategies. Therefore, a necessary component of the research involves the detailed analysis and integration of petrophysical properties, including stress-dependent permeability and porosity, measurement of rock moduli from triaxial tests on core, and stress-dependent acoustic P- and S-wave velocities at various degrees of saturation and pore pressure. These data, when combined with analysis of calibrated wireline dipole sonic and dipole shear logs and well tests, will contribute to upgrading the regional stress map of NEBC at a scale that can be integrated into a geohazard map. Using EXbase¹ and UBC data allows access to a broad sampling of rock mechanical data that provide a starting point for the study.

Once the hydrogeomechanical parameters are collected, they will provide inputs for simulating seismicity induced

by the monitored hydraulic completions using a 3-D modelling program. Each recorded event with a magnitude >1 will first be associated with a stage of hydraulic fracturing, by allowing for large time windows to account for post-injection seismicity and by considering the event's location with respect to the perforations and previous events. The hydrogeomechanical and completion parameters from those stages, laterals, regions and fields that induced seismicity will be compared with the parameters from those that did not. Relating each induced event with a period of fluid injection will also allow the spatial and temporal distribution of the events to be examined. Understanding the migration in time and space of the occurrence and magnitude of the seismicity will provide insight into the pore-pressure diffusion taking place.

The first stage of the hydrogeomechanical modelling will involve history matching specific hydraulic-fracturing stages to match the spatial and temporal pattern of the seismicity and microseismicity as well as the wellbore-pressure variations that were monitored. The history matching will provide insight into the source parameters of the induced seismicity as well as into the mechanisms taking place. A complete parametric analysis will then be conducted on the best-fit models by comparing the occurrence and maximum magnitude of induced seismicity for variations in the hydrogeomechanical parameters, including the stress field, rock mechanical properties and structural setting. Parametric analysis will be used to determine which variables are controlling the induced seismicity, to identify regions with a higher probability of hosting critically stressed faults and to provide insights into the maximum possible magnitude of events. For comparison, stages which only induced microseismicity will also be history matched and the sensitivity of the parameters will be analyzed.

Different mitigation techniques will also be tested using hydrogeomechanical modelling, such as the impact of reducing or stopping injection at different thresholds and flow-back volumes, and controlling leak-off rates by modifying the completion-fluid chemistry. Another technique involves varying the hydraulic-fracturing parameters (i.e., wellbore pressures, injected volumes and rates, type and amount of proppant, and flow-back volumes and rates) and well designs, which can help optimize disposal and completions. For example, the effect of zipper fracturing, simultaneous fracturing, number of stages, injection rates and pressures, fluid viscosity, as well as orientation, spacing and pattern of laterals can also be examined.

The current model of choice is 3DECTM, a discontinuum-modelling code based on DEM software. The utility of this program was evaluated by first using UDECTM (Universal Distinct Element Code), the two dimensional version of the numerical software developed by ItascaTM Consulting Group, Inc., to model both pore-pressure buildup and its

¹EXbase is a proprietary historical database of mainly geochemical data.

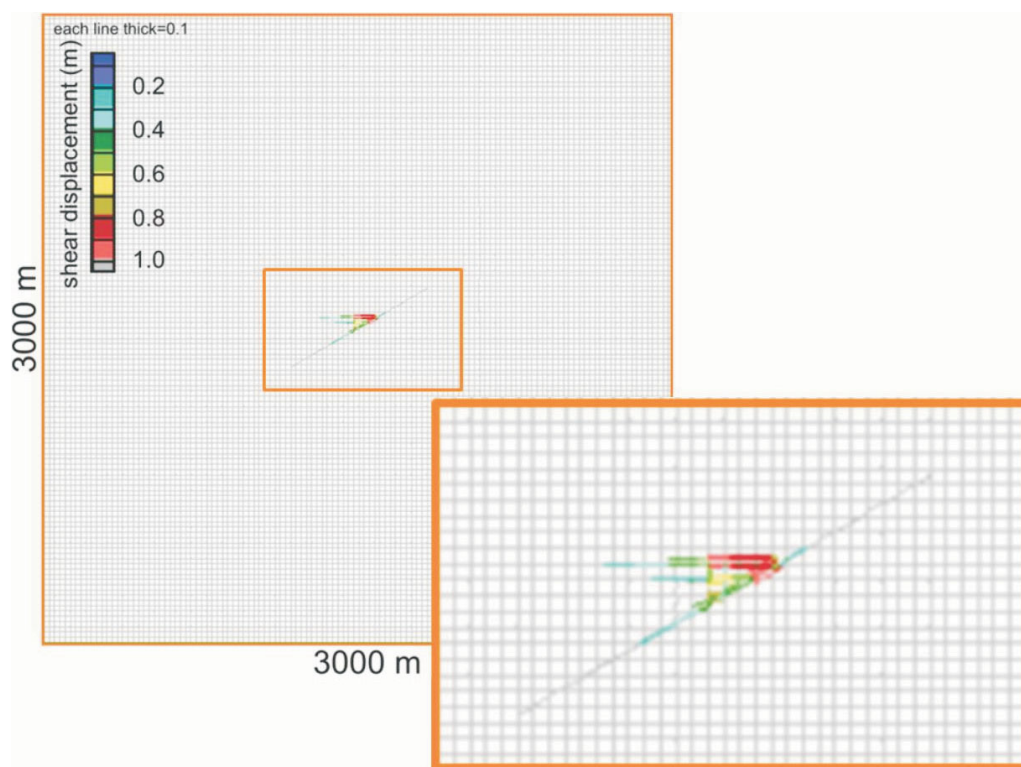


Figure 6. Example of the results from modelling using UDEC™ (Universal Distinct Element Code), the two dimensional version of the distinct-element method (DEM) numerical software chosen for the hydraulic fracturing monitoring project in the Montney Formation. The plot shows the shear displacement along a 1500 m fault and fractures surrounding the hydraulic fracture caused by injection 100 m from the fault.

diffusion along rock discontinuities into a critically stressed fault in response to fluid injection and the subsequent changes to the effective stress field (Figure 6). The problem domain is discretized into blocks, where the boundaries represent fractures/joints/faults or planes subject to possible failure. Failure occurs by both shear slip and dilation along the pre-specified surfaces; therefore, both shear and normal displacements can be quantified. The Mohr-Coulomb slip model with residual strength is used to quantify the displacements. The blocks are subdivided into a mesh of finite difference elements and their deformation is modelled based on the basic Mohr-Coulomb slip criterion. A coupled hydrogeomechanical analysis models the fluid flow through the discontinuities, whereas the blocks are impermeable.

Legacy

In addition to the development of methods and protocols for the reduction and mitigation of AIS in the Montney Formation in NEBC, the legacy of this research will be the commissioning of up to 15 mobile sensors that can be optimally positioned throughout field development as needed. In addition, a world-class research nexus is being created at UBC–Geoscience BC dealing with AIS and hydraulic frac-

turing that will serve the province during the exploration and exploitation of its vast shale-gas and shale-oil resources during the next 40 years.

Acknowledgments

The authors thank Geoscience BC for their support and funding of this study. They also thank K. Johansen and C. Ventura of the Earthquake Engineering Research Facility for the construction of the sensors and M. Longobardi for her review of this manuscript.

References

- Bachmann, C.E., Wiemer, S., Woessner, J. and Hainzl, S. (2011): Statistical analysis of the induced Basel 2006 earthquake sequence: introducing a probability-based monitoring approach for Enhanced Geothermal Systems; *Geophysical Journal International*, v. 186, p. 793–807.
- Baisch, S. and Harjes, H.-P. (2003): A model for fluid injection induced seismicity at the KTB; *Geophysical Journal International*, v. 152, p. 160–170.
- Baisch, S., Weidler, R., Voros, R. and Jung, R. (2006): A conceptual model of post-injection seismicity at Soultz-sous-Forêts; *GRC Transactions*, v. 30, p. 601–605.
- Baisch, S., Voros, R., Rothert, E., Stang, H., Jung, R. and Schellschmidt, R. (2010): A numerical model for fluid injection

- tion induced seismicity at Soultz-sous-Forêts; *International Journal of Rock Mechanics and Mining Sciences*, v. 47, p. 405–413.
- BC Oil and Gas Commission (2012): Investigation of observed seismicity in the Horn River Basin, URL <<https://www.bcogc.ca/node/8046/download>> [March 2015].
- BC Oil and Gas Commission (2014): Investigation of observed seismicity in the Montney Trend, URL <<https://www.bcogc.ca/node/12291/download>> [March 2015].
- BC Ministry of Energy and Mines (2011): British Columbia Natural Gas and Petroleum. Yours to Explore 2010, URL <<http://www.empr.gov.bc.ca/OG/oilandgas/royalties/infdevcredit/Documents/YourstoExplore18Mar2010web.pdf>> [March 2015].
- BC Ministry of Energy and Mines (2012): British Columbia's natural gas strategy: Fuelling BC's economy for the next decade and beyond, URL <http://www.gov.bc.ca/ener/popt/down/natural_gas_strategy.pdf> [March 2015].
- Bommer, J.J., Oates, S., Cepeda, J.M., Lindholm, C., Bird, J., Torres, R., Marroquin, G. and Rivas, J. (2006): Control of hazard due to seismicity induced by a hot fractured rock geothermal project; *Engineering Geology*, v. 83, p. 287–306.
- Bommer, J.J., Crowley, H. and Pinho, R. (2015): A risk-mitigation approach to the management of induced seismicity; *Journal of Seismology*, v. 19, p. 633–646.
- Clarke, H., Eisner, L., Styles, P. and Turner, P. (2014): Felt seismicity associated with shale gas hydraulic fracturing: the first documented example in Europe; *Geophysical Research Letters*, v. 41, p. 8308–8314.
- de Pater, C.J. and Baisch, S. (2011): Geomechanical study of Bowland Shale Seismicity, URL <<https://www.rijksoverheid.nl/binaries/rijksoverheid/documenten/rapporten/2011/11/04/rapport-geomechanical-study-of-bowland-shale-seismicity/rapport-geomechanical-study-of-bowland-shale-seismicity.pdf>> [March 2015].
- Gischig, V.S. and Wiemer, S. (2013): A stochastic model for induced seismicity based on non-linear pressure diffusion and irreversible permeability enhancement; *Geophysical Journal International*, v. 194, p. 1229–1249.
- Hajati, T., Langenbruch, C. and Shapiro, S.A. (2015): A statistical model for seismic hazard assessment of hydraulic-fracturing-induced seismicity; *Geophysical Research Letters*, v. 42, doi: 10.1002/2015GL066652
- Hakimhashemi, A.H., Yoon, J.S., Heidbach, O., Zang, A. and Grunthal, G. (2014): Forward induced seismic hazard assessment: application to a synthetic seismicity catalogue from hydraulic stimulation modeling; *Journal of Seismology*, v. 18, p. 671–680.
- Healy, J.H., Rubey, W.W., Griggs, D.T. and Raleigh, C.B. (1968): The Denver earthquakes; *Science*, v. 27, p. 1301–1310.
- Holland, A.A. (2011): Examination of possibly induced seismicity from hydraulic fracturing in the Eola field, Garvin County Oklahoma; Oklahoma Geological Survey, Open-File Report OFI-2011.
- Holland, A.A. (2013): Earthquakes triggered by hydraulic fracturing in south-central Oklahoma; *Bulletin of the Seismological Survey of America*, v. 103, doi: 10.1785/0120120109
- Hubbert, M.K. and Rubey, W.W. (1959): Role of fluid pressure in mechanics of overthrust faulting; *Bulletin of the Geological Society of America*, v. 70, p. 115–166.
- Hsieh, P.A. and Bredehoeft, J.D. (1981): A reservoir analysis of the Denver earthquakes: a case of induced seismicity; *Journal of Geophysical Research*, v. 86, p. 903–920.
- Maxwell S. 2013: Unintentional seismicity induced by hydraulic fracturing; *Canadian Society of Exploration Geophysicists, Recorder*, v. 38, p. 8.
- Mignan, A., Landtwing, D., Kastli, P., Mena, B. and Wiemer, S. (2015): Induced seismicity risk analysis of the 2006 Basel, Switzerland, Enhanced Geothermal System project: influence of uncertainties on risk mitigation; *Geothermics*, v. 53, p. 133–146.
- Paulson, K. (2015): Natural gas development in BC Today and Tomorrow, BCEIA Luncheon on LNG Initiatives, URL <http://www.bceia.com/media/78728/bceia_ken_paulson_oct_2_2015.pdf> [September 2016].
- Rutqvist, J., Rinaldi, A.P., Cappa, F. and Morigidis, G.J. (2015): Modeling of fault activation and seismicity by injection directly into a fault zone associated with hydraulic fracturing of shale-gas reservoirs; *Journal of Petroleum Science and Engineering*, v. 127, p. 377–386.
- Schultz, R., Stern, V., Novakovic, M., Atkinson, G. and Gu, Y.J. (2015a): Hydraulic fracturing and the Crooked Lake sequence: insights gleaned from regional seismic networks; *Geophysical Research Letters*, v. 41, doi: 10.1002/2015GL063455
- Schultz, R., Mei, S.L., Pana, D., Stern, V., Gu, Y.J., Kim, A. and Eaton, D. (2015b): The Cadston earthquake swarm and hydraulic fracturing of the Exshaw Formation (Alberta Bakken Play); *Bulletin of the Seismological Society of America*, v. 105, p. 2871–2884.
- Shapiro, S., Kruger, O.S., Dinske, C. and Langenbruch, C. (2011): Magnitudes of induced earthquakes and geometric scales of fluid-stimulated rock volumes; *Geophysics*, v. 76, doi: 10.1190/gEO2010-0349.1
- Skoumal, R.J., Brudzinski, M.R. and Currie, B.S., (2015): Earthquakes induced by hydraulic fracturing in Poland Township, Ohio; *Bulletin of the Seismological Society of America*, v. 105, p. 189–197.
- Tutuncu, A.N. and Bui, B.T. (2016): A coupled geomechanics and fluid flow model for induced seismicity in oil and gas operations and geothermal applications; *Journal of Natural Gas Science and Engineering*, v. 29, p. 110–124.
- Van Poolen, H.K. and Hoover, S.B. (1970): Waste disposal and earthquakes at the Rocky Mountain Arsenal, Derby, Colorado; *Journal of Petroleum Technology*, v. 22, no. 8, p. 983–993.
- Warpinski, N.R., Du, J. and Zimmer, U. (2012): Measurements of hydraulic-fracture-induced seismicity in gas shales; *Society of Petroleum Engineers, Paper SPE-151597*, doi: 10.2118/151597-PA

Ground Motion from the August 17, 2015, Moment Magnitude 4.6 Earthquake Induced by Hydraulic Fracturing in Northeastern British Columbia

A. Babaie Mahani, Geoscience BC, Vancouver, BC, ali.mahani@mahangeo.com

H. Kao, Natural Resources Canada, Geological Survey of Canada-Pacific, Sidney, BC

J. Johnson, BC Oil and Gas Commission, Victoria, BC

C.J. Salas, Geoscience BC, Vancouver, BC

Babaie Mahani, A., Kao, H., Johnson, J. and Salas, C.J. (2017): Ground motion from the August 17, 2015, moment magnitude 4.6 earthquake induced by hydraulic fracturing in northeastern British Columbia; *in* Geoscience BC Summary of Activities 2016, Geoscience BC, Report 2017-1, p. 9–14.

Introduction

Analysis of earthquake ground motion from data recorded by regional and local seismograph networks is essential in understanding the potential seismic hazard in a region. Ground motion prediction equations (GMPE) are routinely developed and modified as more data become available, then they are used to update the available seismic hazard maps and building codes. However, the majority of the available GMPE lack data resolution at distances close to the source of the earthquakes. This lack of resolution is especially important with regard to the ground motion from larger, shallow, fluid-injection-induced events, which has the potential to damage the structures around the injection point (Novakovic and Atkinson, 2015).

Earthquakes caused by fluid injection are now common in central and eastern US (Keranen et al., 2014; Skoumal et al., 2015) and western Canada in the provinces of Alberta and British Columbia (Atkinson et al., 2016; Babaie Mahani et al., 2016). Although damage from these induced earthquakes has been observed after the larger magnitude events, such as the moment magnitude (M_w) 5.7 earthquake in November 2011 in Prague, Oklahoma (Keranen et al., 2013), smaller events in western Canada with magnitudes of 4 and higher (Atkinson et al., 2015; Eaton and Babaie Mahani, 2015; Babaie Mahani et al., in press) also require special attention due to the shallow depth of these events.

On August 17, 2015, an M_w 4.6 event occurred in the northern Montney play of British Columbia (BC), in an area where intensive hydraulic fracturing and long-term injection of gas and wastewater have taken place for decades (Babaie Mahani et al., in press). The regional seismographic stations operated by Natural Resources Canada

(NRCan) in the area are too sparse to provide ground motion data at close distances. However, a local seismograph network owned by Progress Energy Canada Ltd. (Progress Energy) provided a unique dataset ranging in distance from 5 to 100 km (Figure 1a). Waveforms from this event, however, were clipped at epicentral distances as far as ~40 km, therefore, direct observation of maximum ground motion amplitudes is not possible. In this paper, ground motion amplitudes from the M_w 4.6 event at the clipped stations are estimated using the unclipped waveforms from an aftershock (M_w 3.0), which happened approximately three hours after the main shock.

Database

In this study, the availability of data from the Progress Energy three-component broadband sensors (Figure 1a), situated close to the hydraulic fracturing operations, provided an excellent opportunity to investigate the level of ground motion at close distances caused by induced events. Figure 1b shows seismicity and injection activity during the months of August and September 2015. Earthquakes are well clustered around the hydraulic fracturing wells. Babaie Mahani et al. (in press) studied seismic activity and fluid injection in this region from October 2014 to the end of 2015. It was found that events are better correlated in space and time with hydraulic fracturing than other types of fluid injection in the area. Events occurred at shallow depths (<2.5 km) on northwest-trending thrust faults, based on results from double difference relocation and moment tensor inversion (Babaie Mahani et al., in press).

Figure 2 shows sample raw waveforms (horizontal east-west component) from the three largest events in August and September 2015. For the August 17, M_w 4.6 event, waveform amplitudes were clipped at distances as far as ~40 km from the epicentre whereas waveform clipping was observed only at the closest station for the September 2, M_w 3.2 event (epicentral distance 7.5 km). None of the waveforms from the M_w 3.0 event on August 17 were

Keywords: British Columbia, induced seismicity, ground motion
This publication is also available, free of charge, as colour digital files in Adobe Acrobat® PDF format from the Geoscience BC website: <http://www.geosciencebc.com/s/DataReleases.asp>.

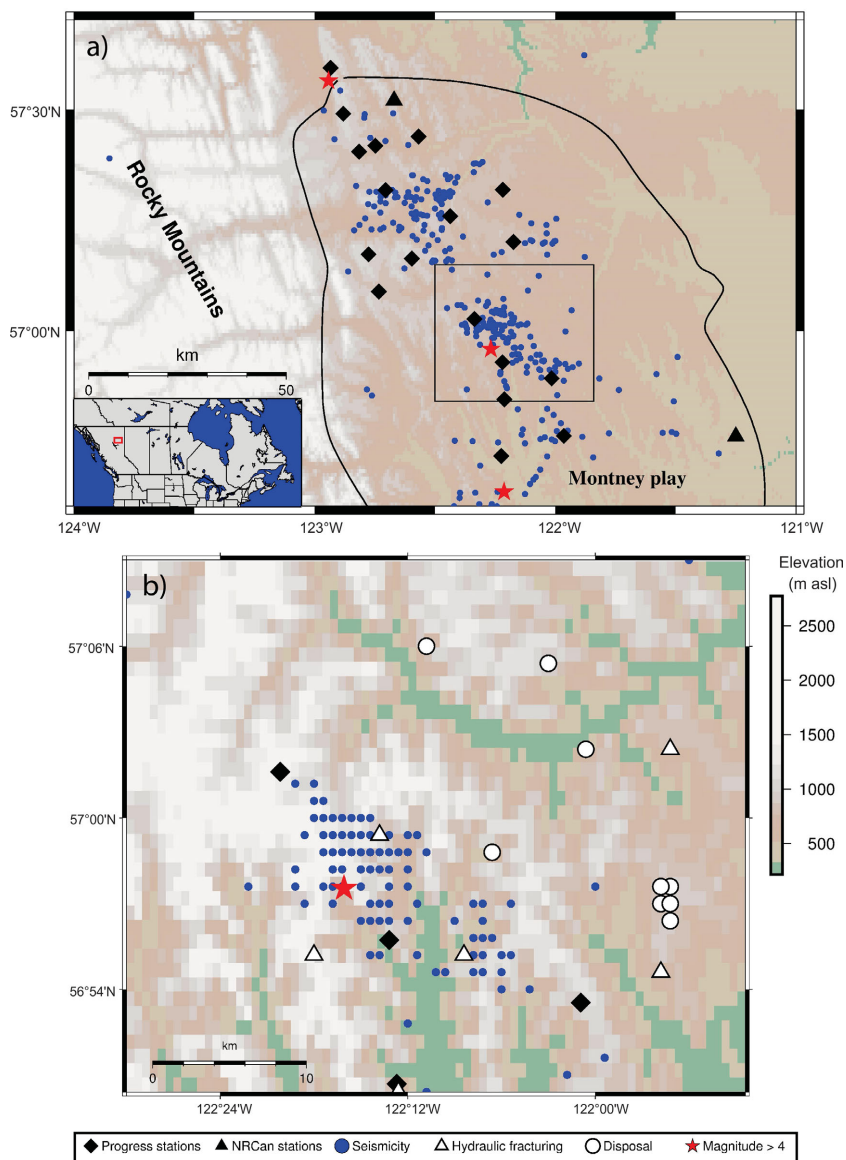


Figure 1. a) Seismic activity from 1985 to 2016 in the northern Montney play of British Columbia from Natural Resources Canada (NRCAN) earthquake catalogue (Natural Resources Canada, 2016). The inset shows the region in North America. Boundary of the Montney shale gas play is shown with a black outline. The black box is the area shown in 1b. **b)** Seismic activity during the months of August and September 2015 from the Progress Energy Canada Ltd. (Progress) earthquake catalogue. The location of all wastewater disposal and gas injection wells that have been active in this area in the past five years are shown (circles). Hydraulic fracturing is shown for the months of August and September only (triangles). The star is the location of the moment magnitude (M_w) 4.6 event on August 17, 2015. Background image from Linquist et al. (2004).

clipped. Acceleration time series were obtained from the unclipped waveforms by removing the instrument response and filtering the waveforms using a second-order Butterworth bandpass filter with corner frequencies of 0.5 and 12 hertz (Hz). Figure 3 shows the three-component peak ground acceleration (PGA) versus epicentral distance for the events shown in Figure 2. In Figure 3, only values from the unclipped waveforms are shown.

Ground Motion Amplitude from the M_w 4.6 Event

Ground motion at close distances provides insights into the hazard potential of moderate-sized induced earthquakes (magnitudes of 4 and higher) to nearby structures. Analysis of ground motion from possibly induced earthquakes in the magnitude range of 3.8–4.4 in the Western Canada Sedi-

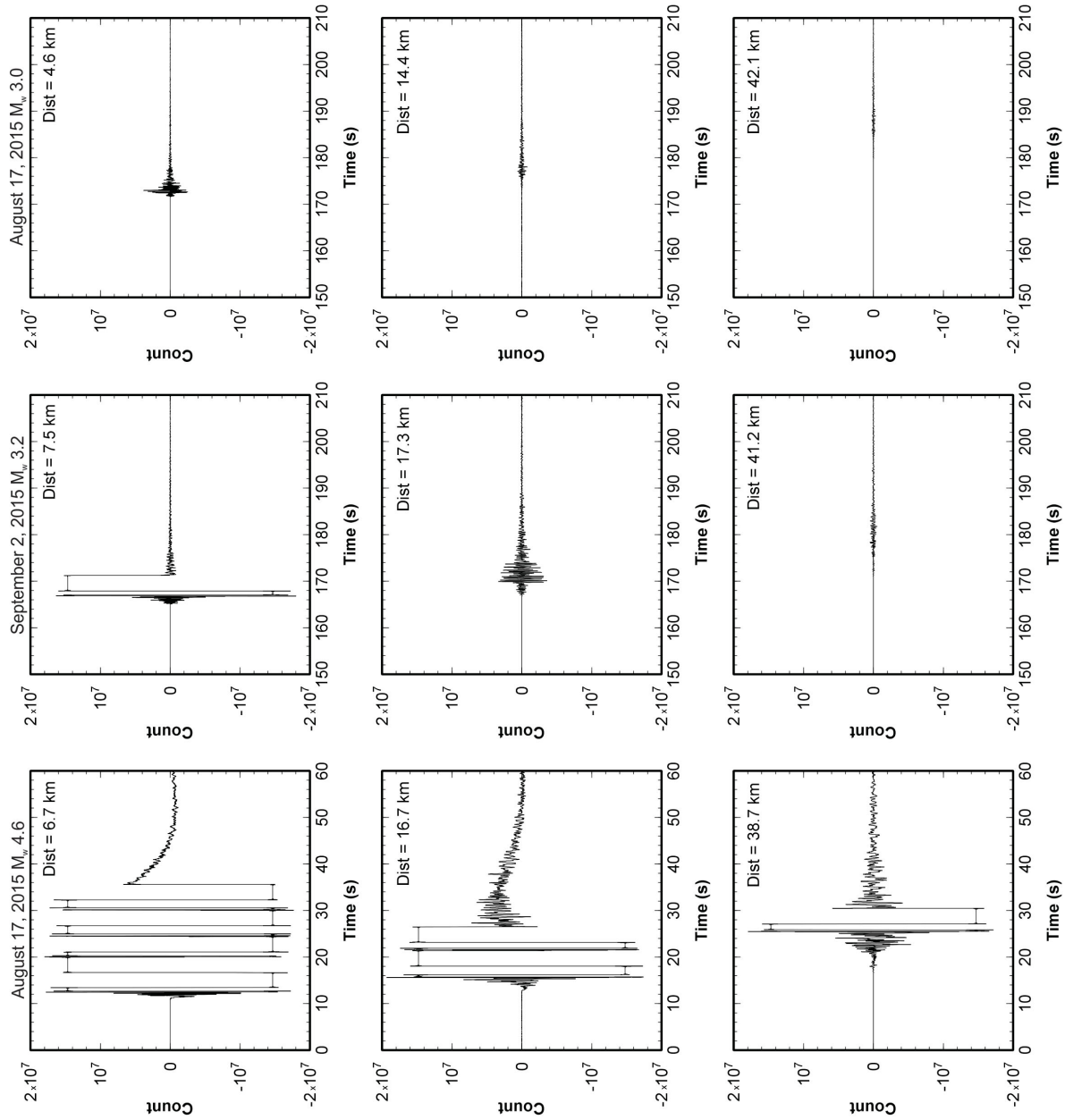


Figure 2. Sample raw seismograms (east-west component) from the three largest induced earthquakes in the months of August and September 2015. Waveforms were recorded by the broadband seismographic stations operated by Progress Energy Canada Ltd. For the August 17, moment magnitude (M_w) 4.6 event, waveform amplitudes were clipped at distances up to ~40 km. In contrast, only one station located near the September 2, M_w 3.2 event epicentre had clipped waveforms. Abbreviation: Dist, distance.

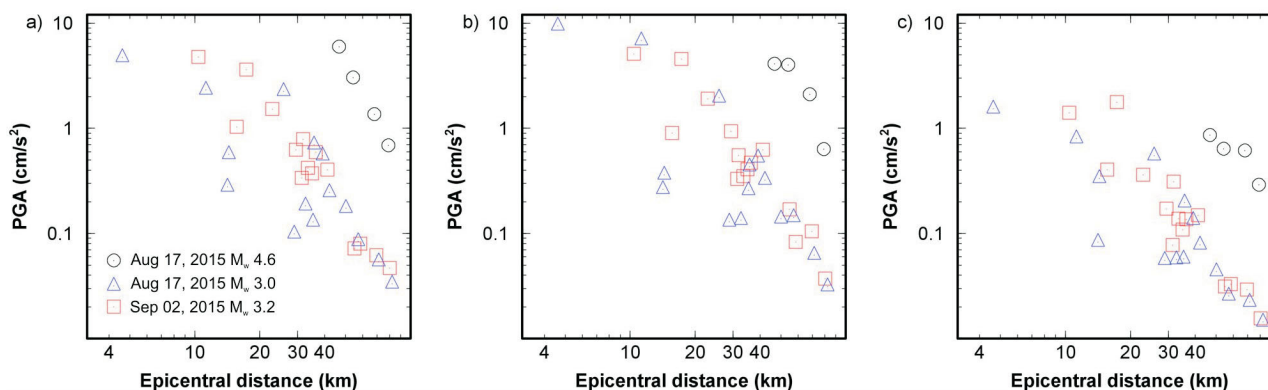


Figure 3. Three-component peak ground acceleration (PGA) versus epicentral distance for the three largest events in August and September 2015: **a)** east-west component, **b)** north-south component, and **c)** vertical component. Waveforms were recorded by the seismographic stations operated by Progress Energy Canada Ltd. Waveforms were filtered between 0.5 and 12 hertz (Hz) using a second-order Butterworth bandpass filter. Only values from unclipped waveforms are shown. Abbreviation: M_w , moment magnitude.

mentary Basin has revealed that this level of motion can be potentially damaging to nearby infrastructure due to the shallow depths of these events, although the lower stress drop as a result of shallow focal depths might limit the high frequency content of the ground motion (Atkinson, 2015; Atkinson et al., 2015). Although broadband waveform clipping as a result of instrument limitation can be common, especially at close distances (Yang and Ben-Zion, 2010), it can lead to a critical knowledge gap in characterizing the distribution of near-field ground motion when co-located strong-motion data are not available. In this case, innovative efforts should be made to derive as much ground motion information as possible from the available imperfect dataset. Here, unclipped waveforms from a smaller aftershock (August 17, 2015, M_w 3.0) that occurred approximately three hours after the M_w 4.6 event were used as a reference dataset to estimate the ground motion amplitudes for the clipped waveforms from the larger event. Both events occurred in proximity of each other with similar source and depth characteristics and were recorded by the same stations.

The total energy of a unit mass at a recording station can be related to the seismic moment, M_0 , as

$$\frac{\Delta\sigma}{2\mu} M_0 = 2\rho\pi^2 \frac{A^2}{T^2} \quad (1)$$

(Lay and Wallace, 1995), where $\Delta\sigma$ is the stress drop, μ is the shear modulus, ρ is density and A is the amplitude of a wave with period T . By rearranging equation (1), a relationship can be found between the seismic moment and amplitude:

$$M_0 = 4\mu\rho\pi^2 \frac{A^2}{\Delta\sigma T^2} \quad (2)$$

Here, it is assumed that μ , ρ and $\Delta\sigma$ are similar for the two events, although, stress drop can vary from one event to another depending on depth and magnitude. With these as-

sumptions, the ratio of seismic moments for the two events becomes

$$\frac{M_{0,4.6}}{M_{0,3.0}} = \frac{A_{4.6}^2}{A_{3.0}^2} \quad (3)$$

In equation (3), subscripts 4.6 and 3.0 refer to the M_w 4.6 and 3.0 earthquakes, respectively. The M_w 3.0 event generated a PGA value of ~ 10 cm/s^2 ($A_{3.0}$) at the closest distance of ~ 5 km on the north-south component (Figure 3b). Considering the seismic moment ratio of ~ 300 between the two events (i.e., $M_{0,4.6}/M_{0,3.0} = 300$), the peak amplitude of ground acceleration generated by the M_w 4.6 event at this distance (~ 5 km) can be estimated to be ~ 173 cm/s^2 ($\sim 17\%$ gravity [g]). Ground motion from the M_w 3.0 event at a distance of ~ 40 km is ~ 0.5 cm/s^2 on the north-south component, therefore, the equivalent ground motion at this distance for the M_w 4.6 event could be ~ 9 cm/s^2 .

Figure 4 shows the estimated, three-component PGA values as a function of epicentral distance for the M_w 4.6 event. For distances >40 km, the estimated values can be verified by the observed ones from unclipped waveforms (triangles, Figure 4). The good match between the estimated and observed data points confirms the validity of equation (3). The felt threshold (0.3% g), damage threshold (6.2% g) and moderate damage threshold (22% g) levels shown in Figure 4 are based on Worden et al. (2012). From the observed values in Figure 4, the M_w 4.6 event could have been felt at distances as far as 60 km from the epicentre. This is consistent with the felt reports received by NRCAN with some coming from far away communities, such as Charlie Lake, BC (located ~ 100 km to the southeast of the M_w 4.6 epicentre). Also, based on the results shown in Figure 4, the zone of potential damage could be as far as ~ 10 km.

The uncertainty of the estimated PGA values for the M_w 4.6 event is an important factor that deserves further investigation. For the purpose of verification, the possible level of

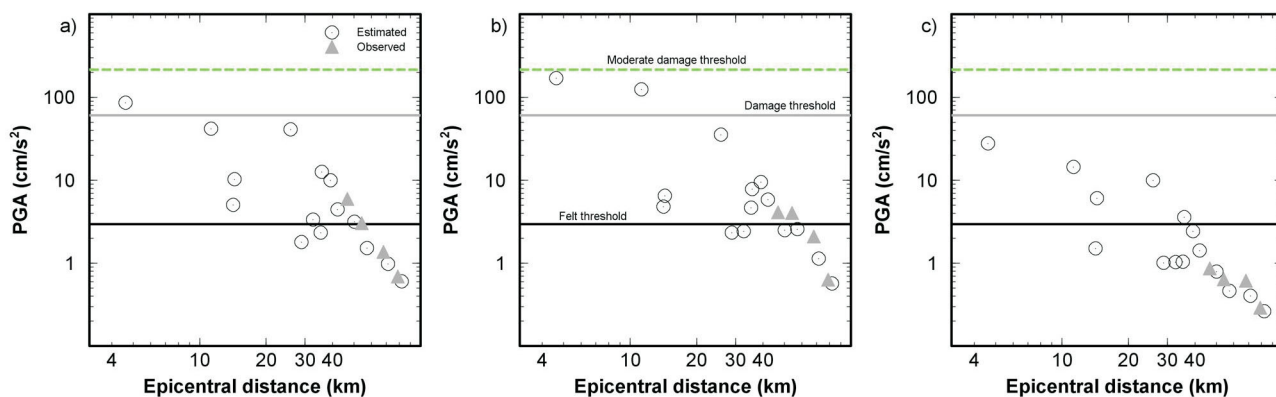


Figure 4. Estimated peak ground acceleration (PGA) for the **a)** east-west, **b)** north-south and **c)** vertical components of the August 17, 2015, moment magnitude (M_w) 4.6 event determined from the unclipped ground motion data of the smaller M_w 3.0 event using equation (3). Values as high as $\sim 173 \text{ cm/s}^2$ ($\sim 17\%$ gravity) are estimated for places close to the epicentre ($\sim 5 \text{ km}$ or less). The three thresholds (felt, damage, moderate damage) are taken from Worden et al. (2012). The estimated PGA values are remarkably consistent with the observed ones from unclipped waveforms at distances of $>40 \text{ km}$ (shown as grey triangles).

errors when equation (3) is used for ground motion prediction is quantitatively assessed. Specifically, the M_w 3.0 event is first used to estimate the PGA values of the M_w 3.2 event on September 2, which had only one clipped waveform at the closest epicentral distance of 7.5 km (Figure 2). The estimated values for distances $>7.5 \text{ km}$ were then compared to the observed ones measured directly from the unclipped waveforms and the results are shown in Figure 5. For each data point in Figure 5, the epicentral distance for the M_w 3.0 event (which is used to obtain the estimated PGA) differs from that of the M_w 3.2 event by $<5 \text{ km}$, thus the propagation and attenuation effects are negligible. Overall, the majority of the difference between observed

and estimated PGA values is a factor of ~ 3 . It seems that equation (3) tends to overestimate the PGA by a factor of ~ 2 for most data points at distances $\geq 40 \text{ km}$. In contrast, both underestimation and overestimation can happen at closer distances. Although it is difficult to determine the exact cause of this discrepancy with this limited dataset, it could be speculated that perhaps variations in local geological setting and site condition could be important factors.

Finally, Figure 6 shows the estimated and observed PGA of the geometric mean of the horizontal components from the M_w 4.6 event versus hypocentral distance (the source depth is set at 2 km). The solid line corresponds to the prediction

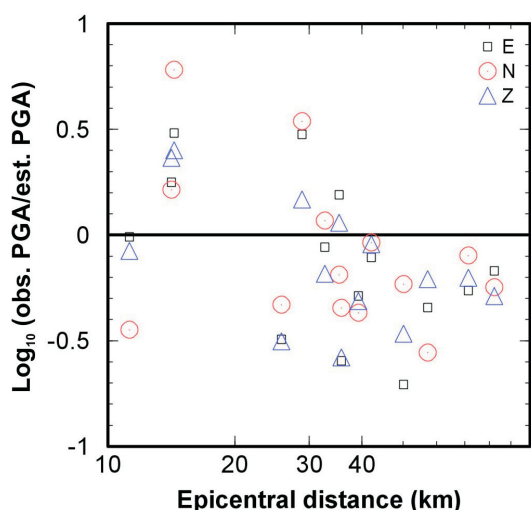


Figure 5. Plot of the ratio between the observed and estimated peak ground acceleration (PGA) of the three components for the September 2, 2015, moment magnitude (M_w) 3.2 event. Waveforms from the smaller August 17, 2015, M_w 3.0 event were used in the calculation using equation (3). Abbreviations: E, east-west component; est., estimated; N, north-south component; obs., observed; Z, vertical component.

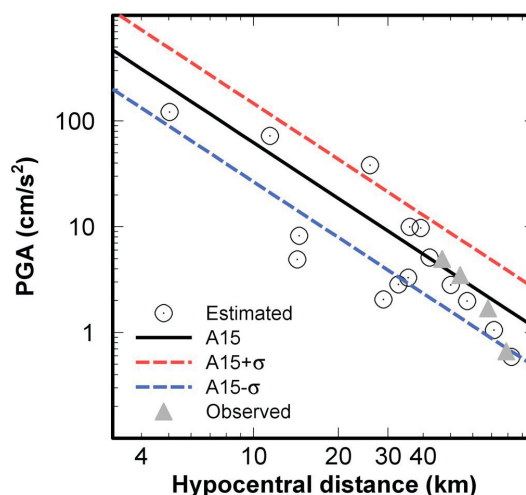


Figure 6. Estimated and observed peak ground acceleration (PGA) values of the geometric mean of the horizontal components from the M_w 4.6 event, August 17, 2015. Solid line (A15) corresponds to the prediction by the Atkinson (2015) model. Dashed lines mark the ± 0.37 deviation (in logarithmic unit) from the solid line, corresponding to one standard deviation (σ) of the ground motion prediction model.

by the Atkinson (2015) model for small to moderate events at short hypocentral distances. This model is based on the Next Generation Attenuation (NGA)-West2 database (Ancheta et al., 2014) at hypocentral distances <40 km, which is suitable for applications to seismic hazard from induced earthquakes. Both the estimated and observed values appear to be in good agreement with the prediction model within its standard deviation (dashed lines, Figure 6).

Conclusion

Waveforms from the August 17, 2015, moment magnitude (M_w) 4.6 event were clipped at distances up to ~40 km from the epicentre; an indicator of large ground motion at close distances. Using the unclipped ground motion from a smaller M_w 3.0 aftershock, the authors estimate that the peak ground acceleration (PGA) from the M_w 4.6 event could have been as high as ~173 cm/s^2 (~17% gravity) at an epicentral distance of ~5 km. Although there was no reported damage from this shallow induced event, ground motion from this event could have exceeded the damage threshold of structures if it had happened in a populated area.

Acknowledgments

The authors would like to thank M. Norton with Progress Energy Canada Ltd. for providing waveform data and constructive comments on the manuscript. Financial support for this project was partially provided by the Canadian Association of Petroleum Producers and the BC Oil and Gas Research and Innovation Society.

References

- Ancheta, T.D., Darragh, R.B., Stewart, J.P., Seyhan, E., Silva, W.J., Chiou, B.S.J., Wooddell, K.E., Graves, R.W., Kottke, A.R., Boore, D.M., Kishida, T. and Donahue, J.L. (2014): NGAWest2 database; *Earthquake Spectra*, v. 30, no. 3, p. 989–1005.
- Atkinson, G.M. (2015): Ground-motion prediction equation for small-to-moderate events at short hypocentral distances, with application to induced-seismicity hazards; *Bulletin of Seismological Society of America*, v. 105, p. 981–992.
- Atkinson, G., Assatourians, K., Cheadle, B. and Greig, W. (2015): Ground motions from three recent earthquakes in western Alberta and northeastern British Columbia and their implications for induced-seismicity hazard in eastern regions; *Seismological Research Letters*, v. 86, p. 1022–1031.
- Atkinson, G.M., Eaton, D., Ghofrani, H., Walker, D., Cheadle, B., Schultz, R., Scherbakov, R., Tiampo, K., Gu, Y.J., Harrington, R., Liu, Y., van der Baan, M. and Kao, H. (2016): Hydraulic fracturing and seismicity in the Western Canada Sedimentary Basin; *Seismological Research Letters*, v. 87, p. 631–647.
- Babaie Mahani, A., Kao, H., Walker, D., Johnson, J. and Salas, C. (2016): Performance evaluation of the regional seismograph network in northeast British Columbia, Canada, for monitoring of induced seismicity; *Seismological Research Letters*, v. 87, p. 648–660.
- Babaie Mahani, A., Schultz, R., Kao, H., Walker, D., Johnson, J. and Salas, C. (in press): Fluid injection and seismic activity in the northern Montney play, British Columbia, Canada, with special reference to the 17 August 2015 M_w 4.6 induced earthquake; *Bulletin of Seismological Society of America*.
- Eaton, D.W. and Babaie Mahani, A. (2015): Focal mechanisms of some inferred induced earthquakes in Alberta, Canada; *Seismological Research Letters*, v. 86, p. 1078–1085.
- Keranen, K.M., Savage, H.M., Abers, G.A. and Cochran, E.S. (2013): Potentially induced earthquakes in Oklahoma, USA: links between wastewater injection and the 2011 M_w 5.7 earthquake sequence; *Geology*, v. 41, p. 699–702.
- Keranen, K.M., Weingarten, M., Abers, G.A., Bekins, B.A. and Ge, S. (2014): Sharp increase in central Oklahoma seismicity since 2008 induced by massive wastewater injection; *Science*, v. 345, p. 448–451.
- Lay, T. and Wallace, T.C. (1995): *Modern Global Seismology*; Academic Press, San Diego, California, 522 p.
- Lindquist, K.G., Engle, K., Stahlke, D. and Price, E. (2004): Global topography and bathymetry grid improves research efforts; *Eos, Transactions, American Geophysical Union*, v. 85, no. 19, p. 186, URL <<http://onlinelibrary.wiley.com/doi/10.1029/2004EO190003/full>> [November 2016].
- Natural Resources Canada (2016): *Earthquakes Canada*; Natural Resources Canada, URL <<http://earthquakescanada.nrcan.gc.ca>> [November 2016].
- Novakovic, M. and Atkinson, G.M. (2015): Preliminary evaluation of ground motions from earthquakes in Alberta; *Seismological Research Letters*, v. 86, p. 1086–1095.
- Skoumal, R.J., Brudzinski, M.R. and Currie, B.S. (2015): Earthquakes induced by hydraulic fracturing in Poland Township, Ohio; *Bulletin of Seismological Society of America*, v. 105, p. 189–197.
- Worden, C.B., Gerstenberger, M.C., Rhoades, D.A. and Wald, D.J. (2012): Probabilistic relationships between ground-motion parameters and modified Mercalli intensity in California; *Bulletin of Seismological Society of America*, v. 102, p. 204–221.
- Yang, W. and Ben-Zion, Y. (2010): An algorithm for detecting clipped waveforms and suggested correction procedures; *Seismological Research Letters*, v. 81, p. 53–62.

Identification and Evaluation of New Resource Oil Plays in Northeastern British Columbia

B.J.R. Hayes, Petrel Robertson Consulting Ltd., Calgary, AB, bhayes@petrelrob.com

B. Nassichuk, Trican Geological Solutions Ltd., Calgary, AB

R. Bachman, CGG Geoconsulting Calgary, Calgary, AB

J.S. Clarke, Petrel Robertson Consulting Ltd., Calgary, AB

R. Wust, Trican Geological Solutions Ltd., Calgary, AB

K. Michaud, Petrel Robertson Consulting Ltd., Calgary, AB

Hayes, B.J.R., Nassichuk, B., Bachman, R., Clarke, J.S., Wust, R. and Michaud, K. (2017): Identification and evaluation of new resource oil plays in northeastern British Columbia; *in* Geoscience BC Summary of Activities 2016, Geoscience BC, Report 2017-1, p. 15–20.

Introduction

Horizontal drilling and multiple-stage hydraulic fracturing (multi-frac) stimulation technologies have greatly augmented gas and liquids resources and reserves in the unconventional reservoirs of British Columbia (BC) over the past several years. However, little new unconventional oil potential has been identified, even though substantial conventional oil pools have been producing for decades. To address this issue, Geoscience BC commissioned a study to determine the potential for new tight oil exploration and exploitation fairways, accessible through modern drilling and completions technologies.

Clarkson and Pedersen (2011) analyzed the spectrum of known unconventional oil plays, and assigned them to three categories:

- Tight oil plays—clastic or carbonate rock reservoirs with low permeability, requiring horizontal drilling and multi-frac stimulation to produce oil at economic rates. The middle Bakken Formation sandstone of the Williston Basin and portions of the Montney Formation in Alberta and BC are good examples.
- Halo oil plays—lower permeability fringes flanking conventional clastic and carbonate rock reservoirs, which can be developed with horizontal multi-frac wellbores to enlarge the original play area. Halo oil plays may extend vertically from a conventional pool, as well as laterally. The Cardium Formation in west-central Alberta is the best Canadian example.
- Shale oil plays—oil accumulations hosted by true shales and/or mudrocks. These are relatively rare, and there is a

body of work suggesting that pore networks in true shales can produce liquids-rich gas, but not actual oil (Dembicki, 2014). The Second White Specks Formation of west-central and southern Alberta has been suggested as an example of a shale oil play, but detailed work suggests that associated tight sandstone beds with extensive natural fracturing are responsible for much of the production. Appraisal of other potential shale oil reservoirs, such as the Duvernay Formation and Gordondale Member (“Nordegg” Member), has failed to produce oil at economic rates to date.

Petrel Robertson Consulting Ltd., Trican Geological Solutions Ltd. and CGG Consulting Calgary have undertaken an assessment of new resource oil potential in northeastern BC, guided by the Clarkson and Pedersen (2011) classification. The Montney Formation was excluded from the project, as its tight oil potential has been the subject of considerable work to date (e.g., Ferri et al., 2013).

Progress Summary

Twenty-one potential resource oil plays were identified in northeastern BC and they were classified according to their overall productive potential, based upon the team’s extensive knowledge of BC conventional and unconventional petroleum geology (Table 1). Existing analytical data were compiled to support play analysis, grouping the information into the following categories:

- source rock analysis, including thermal maturity, organic richness and hydrocarbon composition parameters;
- adsorption/desorption tests;
- X-ray diffraction (XRD) and X-ray fluorescence (XRF);
- scanning electron microscopy (SEM);
- standard petrographic (thin section) analysis; and
- geomechanical testing.

Keywords: *British Columbia, resource oil, tight oil, halo oil, reservoir engineering, Maxhamish field, geochemistry, geomechanics, hydrogeology, resource assessment*

This publication is also available, free of charge, as colour digital files in Adobe Acrobat® PDF format from the Geoscience BC website: <http://www.geosciencebc.com/s/DataReleases.asp>.

Table 1. Listing of resource oil plays being addressed in this study, northeastern British Columbia (BC).

Group, formation, member	Play type	Producing	Potential	New data	Comments
Muskwa	Shale	Oil (Alberta); gas (Horn River)	Local	?	Worked extensively in Alberta. Primarily in gas window in BC, but may be oil-bearing in specific areas.
Jean Marie	Tight carbonate	Gas, minor oil	Local	No	Extensively developed as tight gas play. Seeking areas of oil potential—likely related to maturity of Muskwa Fm.
Kakisa	Tight carbonate	Minor gas	Local	Yes	Seeking areas of oil potential—likely related to maturity of Muskwa Fm.
Kotcho	Tight carbonate	No	Local	Yes	Seeking areas of oil potential—likely related to maturity of Muskwa Fm.
Tetcho	Tight carbonate	Minor gas and oil	Local	Yes	Seeking areas of oil potential—likely related to maturity of Muskwa Fm.
Besa River/Exshaw	Shale/tight carbonate	Gas, oil tested	Moderate	Yes	Seeking areas with potential productivity in oil window.
Banff	Tight sandstone	Minor gas	Low	?	Secondary target, limited data.
Rundle	Halo(?)/tight sandstone	Oil and gas	High(?)	?	Need to understand Desan area and subcrop edge potential in general.
Golata	Shale	No	Low	Yes	Peace River Embayment area—organic richness appears low.
Stoddart (Kiskatinaw)	Tight sandstone	Yes	Low	?	Limited and structurally/stratigraphically isolated reservoirs—limited potential.
Belloy	Tight sandstone	Yes	Low	?	Limited and structurally/stratigraphically isolated reservoirs—limited potential.
Doig	Halo(?)/tight sandstone, shale	Yes	Moderate	No	Extensive existing data in both Doig phosphate and sandstone.
Toad/Grayling	Tight sandstone	No	High	Yes	Horn River and Liard basins; potential possibly in conjunction with overlying Chinkeh Fm.
Halfway	Halo sandstone	Yes	Low	No	Oil pools generally very mature, with discrete structural/stratigraphic boundaries—limited potential.
Charlie Lake	Halo/tight sandstone	Yes	Low	No	Little potential around existing conventional pools; assess potential for Worsley-type play.
Baldonnel	Halo/tight carbonate	Yes	Low	No	Existing production appears conventional with downdip water and limited halo potential.
"Nordegg"/Gordondale	Shale	Minor oil (Alberta)	Moderate	Yes	Good source rock, abundant existing data; little success in horizontal/multiple-stage hydraulic fracturing development to date.
Rock Creek	Tight sandstone	No	Low	No	Conceptual play, appears to have low potential, but just above Nordegg source rock.
Chinkeh	Tight sandstone	Oil and gas	High	Yes	Extensive oil resource downdip of Chinkeh oil pool.
Bluesky	Tight sandstone	Oil and gas	Low	No	Existing pools are conventional; stratigraphic work to identify tight oil potential.
Buckinghorse	Shale/tight sandstone	Gas	Moderate	Yes	Seeking areas with potential productivity in oil window.

Table 2. Source rock analysis data generated for samples from the Chinkeh and Toad/Grayling formations in core from the GSENR (ECA) Maxhamish D-48-B/94-O-11 well (universal well identifier 200D048B094O1100, BC Oil and Gas Commission, 2016), northeastern British Columbia. Abbreviations: HI, hydrogen index; OI, oxygen index; PC, pyrolyzed carbon; PI, production index; S1, free hydrocarbons present in sample; S2, hydrocarbons formed during pyrolysis; S3, CO₂ yield during breakdown of kerogen; T_{max}, temperature at maximum release of hydrocarbons; TOC, total organic carbon.

Sample ID	Formation	Sample type	Depth (m)	T _{max} (°C)	S1 (mg/g)	S2 (mg/g)	S3 (mg/g)	PC (%)	PI	S2/S3	S1/TOC	TOC (%)	HI	OI	T _{max} data quality
1466.06	Upper Chinkeh	Core	1466.06	450	0.64	1.74	0.47	0.20	0.27	3.70	0.43	1.50	116	31	Good
1467.11	Upper Chinkeh	Core	1467.11	451	0.55	2.05	0.49	0.22	0.21	4.18	0.39	1.41	145	35	Good
1468.05	Upper Chinkeh	Core	1468.05	453	0.49	1.80	0.69	0.19	0.21	2.61	0.33	1.48	122	46	Good
1468.97	Upper Chinkeh	Core	1468.97	455	0.45	1.50	0.52	0.16	0.23	2.88	0.35	1.29	116	40	Good
1470.08	Upper Chinkeh	Core	1470.08	453	0.41	1.40	0.52	0.15	0.23	2.69	0.34	1.21	115	43	Good
1470.96	Upper Chinkeh	Core	1470.96	451	0.75	0.74	0.69	0.12	0.50	1.07	0.91	0.82	90	84	Okay
1472.08	Top porosity Chinkeh	Core	1472.08	434	1.24	0.84	0.56	0.17	0.60	1.50	1.57	0.79	106	70	Poor
1472.96	Top porosity Chinkeh	Core	1472.96	449	1.26	1.15	0.68	0.20	0.52	1.69	1.12	1.13	101	60	Good
1474.18	Top porosity Chinkeh	Core	1474.18	458	1.22	0.71	0.42	0.16	0.63	1.69	1.44	0.85	82	49	Okay
1475.01	Top porosity Chinkeh	Core	1475.01	459	1.29	0.72	0.47	0.17	0.64	1.53	1.93	0.67	107	71	Okay
1475.51	Toad/Grayling	Core	1475.51	455	2.41	0.76	0.45	0.26	0.76	1.69	2.65	0.91	83	49	Okay
1475.92	Toad/Grayling	Core	1475.92		2.06	0.61	0.81	0.22	0.77	0.75	3.68	0.56	108	145	No good
1476.08	Toad/Grayling	Core	1476.08	455	0.62	0.45	0.61	0.09	0.58	0.74	1.29	0.48	94	127	Okay
1476.47	Toad/Grayling	Core	1476.47	446	0.89	1.51	0.36	0.20	0.37	4.19	0.73	1.22	123	29	Good
1476.74	Toad/Grayling	Core	1476.74	457	0.47	0.61	0.60	0.09	0.44	1.02	0.87	0.54	112	110	Okay
1477.05	Toad/Grayling	Core	1477.05	454	0.12	0.39	0.58	0.04	0.24	0.67	0.18	0.65	60	89	Okay
1478.03	Toad/Grayling	Core	1478.03	460	0.07	0.26	0.46	0.03	0.21	0.57	0.19	0.36	72	127	Poor
1478.95	Toad/Grayling	Core	1478.95	463	0.08	0.28	0.51	0.03	0.22	0.55	0.22	0.36	78	144	Poor
1480.05	Toad/Grayling	Core	1480.05	471	0.09	0.31	0.52	0.03	0.23	0.60	0.20	0.44	69	116	Poor
1481.03	Toad/Grayling	Core	1481.03	464	0.08	0.30	0.65	0.03	0.21	0.46	0.19	0.42	71	154	Poor
1482.03	Toad/Grayling	Core	1482.03	483	0.09	0.29	0.60	0.03	0.24	0.48	0.21	0.42	68	141	Poor
1483.04	Toad/Grayling	Core	1483.04	479	0.10	0.30	0.60	0.03	0.25	0.50	0.24	0.41	73	145	Poor
1483.50	Toad/Grayling	Core	1483.50	476	0.11	0.34	0.93	0.04	0.24	0.37	0.14	0.76	44	121	Poor

Table 3. Mineralogical data generated by X-ray diffraction analysis for samples from the Chinkeh and Toad/Grayling formations in core from the GSENR (ECA) Maxhamish D-48-B/94-O-11 well (universal well identifier 200D048B094O1100, BC Oil and Gas Commission, 2016), northeastern British Columbia. Abbreviations: T_{max} , temperature at maximum release of hydrocarbons; TOC, total organic carbon; tr, trace.

Sample ID	Formation	Sample type	Depth (m)	T_{max} (°C)	TOC (%)	Quartz (%)	Feldspar			Carbonate rocks			Clays			Sulphides	
							Albite (%)	Microcline (%)	Calcite (%)	Dolomite, Fe-dolomite (%)	Siderite (%)	Illite/mica (%)	Chlorite (%)	Pyrite (%)	Apatite (%)		
1466.06	Upper Chinkeh	Core	1466.06	450	1.50	46.2	7.3	2.4	0.7	9.0	26.3	4.6	3.4	0.1			
1467.11	Upper Chinkeh	Core	1467.11	451	1.41	52.3	5.2	1.9	15.7	19.9	4.3	0.6	0.1				
1468.05	Upper Chinkeh	Core	1468.05	453	1.48	44.1	6.4	2.5	0.8	8.3	30.1	6.3	1.6	0.1			
1468.97	Upper Chinkeh	Core	1468.97	455	1.29	56.1	6.2	2.2	0.5	5.8	23.8	4.0	1.4				
1470.08	Upper Chinkeh	Core	1470.08	453	1.21	55.2	7.2	2.1	8.3	21.0	5.1	1.1					
1470.96	Upper Chinkeh	Core	1470.96	451	0.82	68.9	6.6	1.8	6.9	10.9	4.0	0.8					
1472.08	Top porosity Chinkeh	Core	1472.08	434	0.79	69.9	5.5	1.9	3.4	14.2	3.9	0.8	0.3				
1472.96	Top porosity Chinkeh	Core	1472.96	449	1.13	66.5	7.3	1.8	7.5	10.4	5.3	0.8	0.5				
1474.18	Top porosity Chinkeh	Core	1474.18	458	0.85	88.4	3.8	1.5	1.2	1.0	0.8	2.3	0.2	0.8			
1475.01	Top porosity Chinkeh	Core	1475.01	459	0.67	88.1	5.6	1.1	0.2	0.5	1.2	1.9	0.5	0.8			
1475.51	Toad/Grayling	Core	1475.51	455	0.91	89.7	2.3	1.6	2.8	0.1	1.3	1.6	0.1	0.5			
1475.92	Toad/Grayling	Core	1475.92		0.56	74.7	4.8	1.8	4.9	0.5	10.2	1.9	1.3	tr			
1476.08	Toad/Grayling	Core	1476.08	455	0.48	85.6	5.8	2.0	1.7	0.7	1.5	2.6					
1476.47	Toad/Grayling	Core	1476.47	446	1.22	73.3	8.1	3.2	0.1	5.4	3.8	5.1	1.0				
1476.74	Toad/Grayling	Core	1476.74	457	0.54	76.0	7.6	2.7	0.2	6.1	3.1	3.9	0.4				
1477.05	Toad/Grayling	Core	1477.05	454	0.65	37.2	7.7	3.8		2.8	35.2	11.7	1.7				
1478.03	Toad/Grayling	Core	1478.03	460	0.36	34.0	4.0	4.0	0.6	1.0	41.2	13.7	1.5				
1478.95	Toad/Grayling	Core	1478.95	463	0.36	57.4	5.5	2.4	1.9	2.8	18.9	10.5	0.6				
1480.05	Toad/Grayling	Core	1480.05	471	0.44	45.7	4.5	3.5	1.1	1.1	31.4	11.8	1.0				
1481.03	Toad/Grayling	Core	1481.03	464	0.42	31.0	4.1	4.0	1.0	0.8	43.8	13.3	1.2				
1482.03	Toad/Grayling	Core	1482.03	483	0.42	59.5	5.6	2.1	2.1	3.1	16.8	10.2	0.5				
1483.04	Toad/Grayling	Core	1483.04	479	0.41	51.1	5.3	2.6	1.5	1.3	26.8	10.7	0.7				
1483.50	Toad/Grayling	Core	1483.50	476	0.76	46.8	5.2	3.3	1.3	1.3	30.5	11.0	0.6				

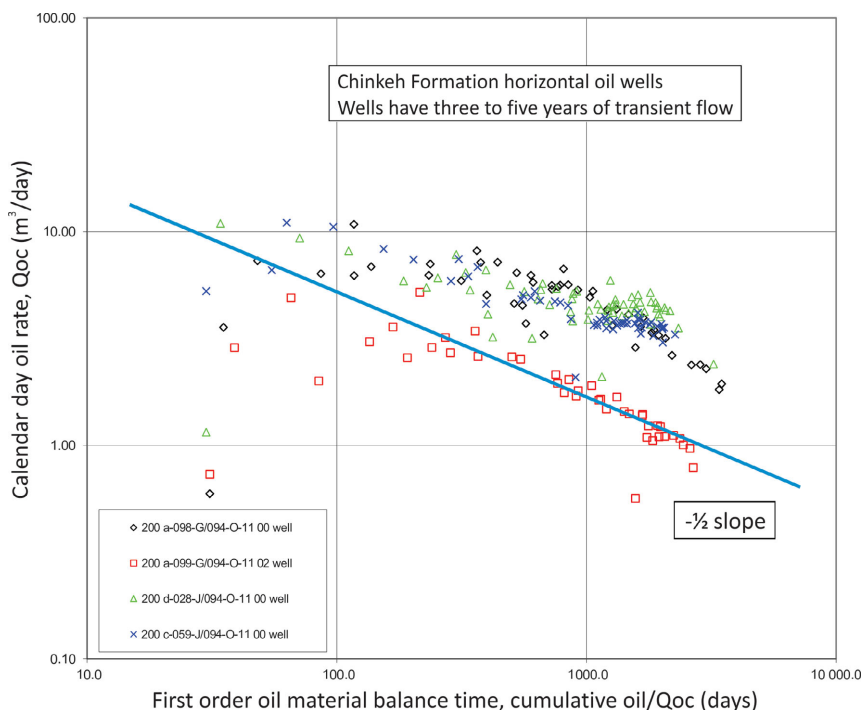


Figure 1. Oil production rate versus first order material balance time for four horizontal wells completed in the Chinkeh Formation on the western flank of the gas pool in the Maxhamish field, northeastern British Columbia. Three of the four wells have a slope less than the reference $\frac{1}{2}$ slope which indicates transient flow, meaning that the wells are not seeing production interference from offset wells or from geological barriers, for at least 3–5 years. In other words, the oil in place contacted by each well is continually increasing throughout transient flow, indicating potentially large untapped oil resources.

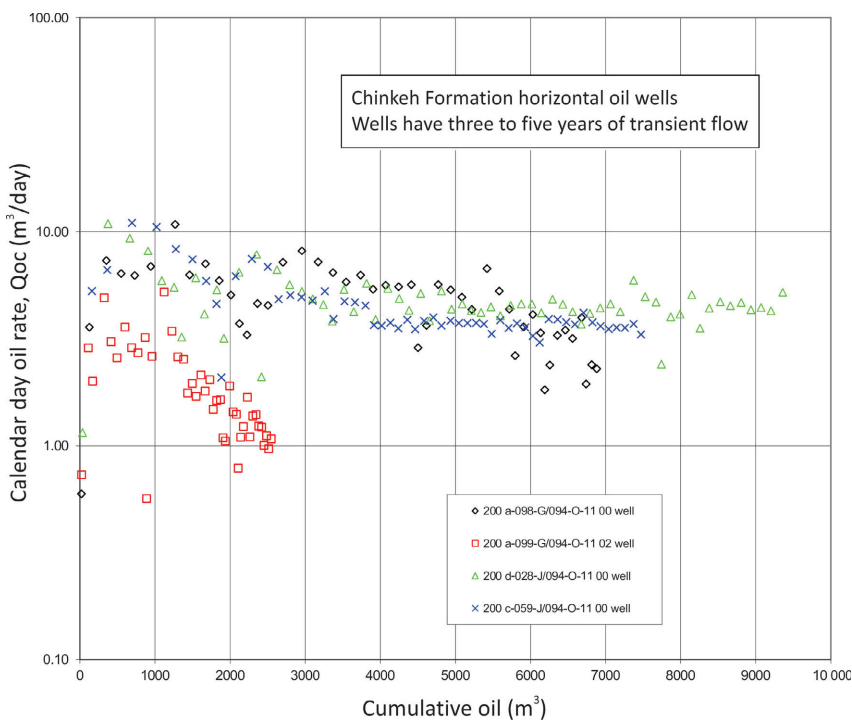


Figure 2. Oil production rate versus cumulative oil production for the same four horizontal wells in Figure 1, completed in the Chinkeh Formation on the western flank of the Maxhamish gas pool, northeastern British Columbia. On this graph, the so-called harmonic plot, three of the four wells show no sharp decrease in oil rate with increasing cumulative production. This provides additional corroboration that the wells are in long-term transient flow.

Data were gathered from the technical literature, government survey reports and analytical files submitted to the BC Oil and Gas Commission (BCOGC) by operators, yielding results from 752 wells. Between one and five stratigraphic units were analyzed in each well. Creating a comprehensive compilation was a much larger task than originally contemplated, but was essential to play characterization and to guide acquisition of new datasets. The BCOGC facilitated this work by providing partial compilations and access to data files. Some analytical work completed in the past, when BCOGC did not require submission of reports, is not available and therefore not included in the compilation.

Comparing existing analytical data against the spectrum of resource oil plays, new laboratory sampling of cores and analytical testing was identified to fill gaps in existing datasets. Trican Geological Solutions Ltd. (Trican) undertook the sampling work, and by the end of September 2016 had sampled, described and photographed cores from 12 wells, and had completed much of the analytical work for those wells. Table 2 illustrates results of source rock analysis on samples from the Chinkeh and Toad/Grayling formations in the core from the GSENR (ECA) Maxhamish D-48-B/94-O-11 well (universal well identifier 200D048B094O1100, BC Oil and Gas Commission, 2016), and Table 3 displays mineralogical compositions derived from XRD work on the same samples. After completing the compilation of existing data and consultation on results of Trican's work to date, the team will select additional core for sampling and analytical testing. Drill cuttings may also be sampled to fill critical dataset vacancies.

CGG Consulting Calgary is undertaking reservoir engineering analysis of potential resource oil plays with two primary goals: characterizing the fracability of potential reservoirs, and identifying fairways where existing oil production data suggest the presence of substantial oil resources occurring in low-permeability halo accumulations. Analysis of oil production from horizontal and vertical wells in the Chinkeh Formation on the western (down-dip) flank of the gas pool in the Maxhamish field shows long-term transient flow from many wells, indicating potential for regionally extensive low-permeability oil accumulations (Figures 1, 2). Future productive behaviour of tight oil

prospects, like the Chinkeh Formation, will be modelled once all data are compiled.

Deliverables

For each resource oil play, final project reporting will include

- reservoir mapping and facies characterization, related to existing conventional pools, where applicable;
- reservoir quality assessment, incorporating mineralogical data and porosity/permeability characteristics;
- assessment of geochemistry (source rock analysis), hydrogeology and fluid distributions
 - identification of abnormally pressured fairways, where present and supported by pressure and production data;
- assessment of geomechanical properties and resulting productive potential; and
- summary of resource potential characterization, including volumetric resource estimates and estimates of producible potential, guided by existing production and reservoir engineering analysis.

The study will wrap up with discussion and recommendations regarding exploration for and appraisal of the highest potential resource oil plays.

Acknowledgments

The authors wish to thank K. Dorey for her thoughtful review of this manuscript.

References

- BC Oil and Gas Commission (2016): Well lookup and reports; BC Oil and Gas Commission, web application, URL <<http://www.bco.gc.ca/online-services>> [December 2016].
- Clarkson, C.R. and Pedersen, P.K. (2011): Production analysis of Western Canadian unconventional light oil plays; Society of Petroleum Engineers, Canadian Unconventional Resources Conference, November 15–17, 2011, Calgary, Alberta, SPE-149005-MS, 23 p.
- Dembicki, H. (2014): Challenges to black oil production from shales; American Association of Petroleum Geologists/Datapages, Inc., Search and Discovery Article #80355, 22 p.
- Ferri, F., Hayes, M. and Nelson, A. (2013): Liquids potential of the Lower to Middle Triassic Montney and Doig formations, British Columbia; in Geoscience Reports 2013, BC Ministry of Natural Gas Development, p. 1–11.

Remote Dynamic Triggering of Earthquakes in Three Canadian Shale Gas Basins, Northeastern British Columbia and Alberta, Northwest Territories and New Brunswick: Progress Report

B. Wang, McGill University, Montréal, QC, bei.wang@mail.mcgill.ca

R. Harrington, McGill University, Montréal, QC

Y. Liu, McGill University, Montréal, QC

H. Kao, Natural Resources Canada, Geological Survey of Canada-Pacific, Sidney, BC

Wang, B., Harrington, R., Liu, Y. and Kao, H. (2017): Remote dynamic triggering of earthquakes in three Canadian shale gas basins, northeastern British Columbia and Alberta, Northwest Territories and New Brunswick: progress report; *in* Geoscience BC Summary of Activities 2016, Geoscience BC, Report 2017-1, p. 21–24.

Introduction

The Earth's crust is full of faults, and several studies indicate that the brittle crust is in a critically stressed state with failures on the verge of happening (Zoback and Zoback, 2002; Hill, 2008). Local faults can be activated by the transient stress from the seismic waves of distant mainshocks with hypocentre distances ranging from hundreds to thousands of kilometres, this is called dynamic triggering (Hill et al., 1993; Gomberg et al., 2001; Prejean et al., 2004; Hill and Prejean, 2007). The organized study of dynamic triggering could help to interpret the mechanism of earthquake nucleation and fault activation. Meanwhile, testing the minimum transient stress necessary to trigger an earthquake could help to investigate the stress state of local faults (Brodsky and Prejean, 2005; van der Elst et al., 2013; Aiken and Peng, 2014; Wang et al., 2015).

In this project, a search for dynamic triggering in three shale basins in Canada will be undertaken to see if these three regions, which represent different types of tectonic regimes, are susceptible to triggering. At the same time, the current stress state of local faults will also be investigated. If triggering happens, the specific triggering response properties for each of the different basins will be examined, as well as the factors that could be causing dynamic triggering. For the three shale basins (Figure 1), one basin is situated in northeastern British Columbia and western Alberta (BCAB), one basin is situated in the Northwest Territories (NWT) and one basin is situated in New Brunswick (NB). These three areas have all seen an increase in the number of seismic stations installed; studies show that they have experienced relatively high seismicity rates recently, which may

be related to the fluid injection from unconventional oil/gas production (Rivard et al., 2014; Schultz et al., 2014, 2015; Eaton and Mahani, 2015; Farahbod et al., 2015; Lamontagne et al., 2015; Atkinson et al., 2016). For example, the number of earthquakes catalogued by Natural Resources Canada (NRCAN) in BCAB was 24 in 2002 compared with a total of 168 in 2014 (Natural Resources Canada, 2016). Figure 2 shows the newly installed seismic stations and catalogued earthquakes (2013–2015) in the three areas of this study.

Method

The multi-station matched method (MMF) detects similar signals by cross-correlating the waveforms of known events, referred to as templates, with continuous waveform data at multiple stations to detect the small and uncatalogued earthquakes. Templates will be built using earthquake data from the NRCAN catalogue (Natural Resources Canada, 2016).

Statistical Measure of the Level of Triggering

After detecting and counting earthquakes from the continuous waveforms, the β statistical value will be used as the quantitative measure of the level of dynamic triggering. The β statistical value represents differences between the number of events in a specific time window and the expected number of events in that time window (Matthews and Reasenberg, 1988). The following equation will be used to calculate the β statistical value (Aron and Hardebeck, 2009):

$$\beta(N_a, N, T_a, T) = \frac{N_a - N(T_a/T)}{\sqrt{N(T_a/T)(1 - T_a/T)}}$$

where T_a is the length of time window after the mainshock and T is the total length of time window, variable N_a is the number of events after the mainshock and N is the total number of events. Here the total time window has been set

Keywords: *British Columbia, dynamic triggering, shale basins, induced seismicity*

This publication is also available, free of charge, as colour digital files in Adobe Acrobat® PDF format from the Geoscience BC website: <http://www.geosciencebc.com/s/DataReleases.asp>.

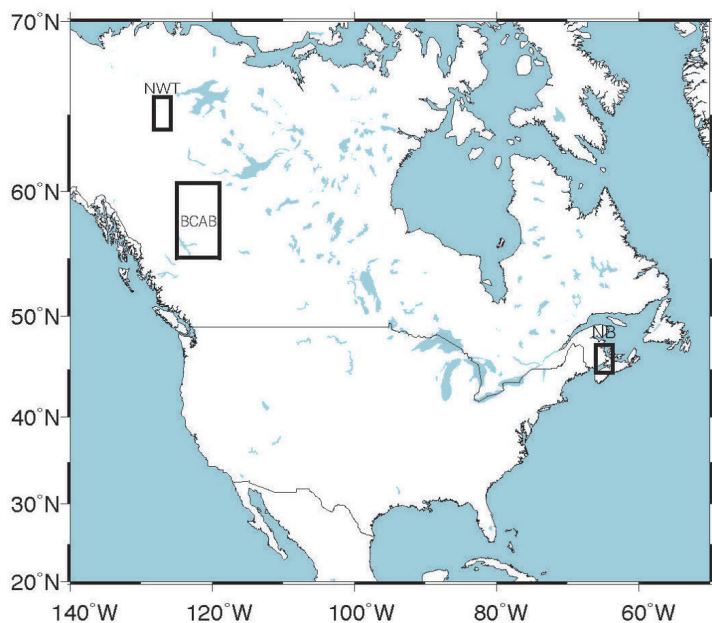


Figure 1. Black boxes show the locations of the three shale basins in Canada. Abbreviations: BCAB, British Columbia and Alberta; NB, New Brunswick; NWT, Northwest Territories.

to be even, meaning $T_a = 1/2 \times T$. The maximum time windows used in the MMF detection for each of the three basins are 10, 5 and 5 days. The β statistical value varies slightly as a function of time window length.

Next Steps

Since project initiation at the beginning of 2016, coding, waveform processing and the building of candidate templates from waveform selections have been completed, and the code is running for the detections. After determining seismicity rates in the windows surrounding each mainshock, the β statistic value will be calculated to quantify if statistically significant triggering has occurred or not. Where triggering occurs, calculations of triggered earthquake focal mechanisms may help explain how pre-existing receiver faults become critically stressed, and what physical factors are directly correlated with dynamic triggering. Cases of observed triggering may imply that the seismic response to

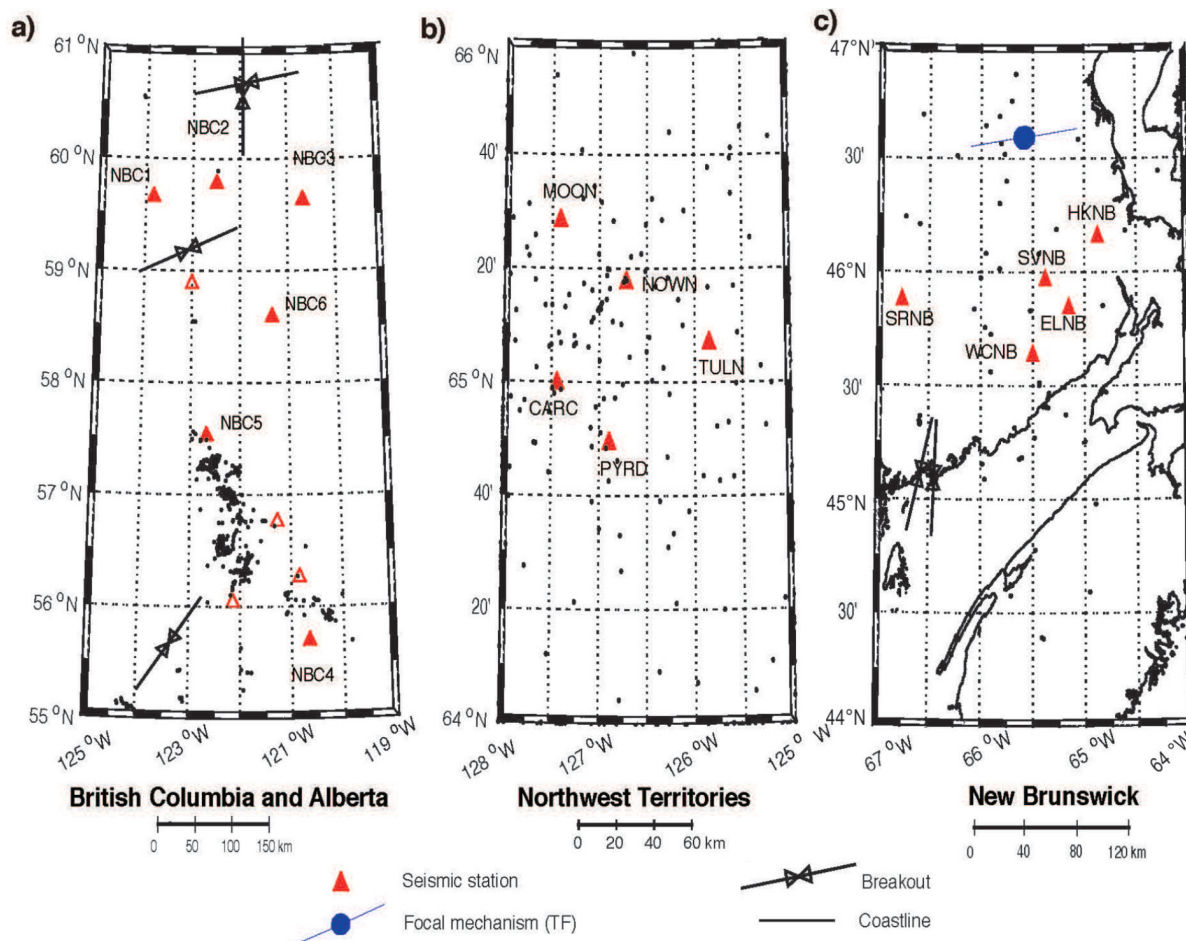


Figure 2. Locations of the newly installed Natural Resources Canada seismic stations in each of the study areas: **a)** British Columbia and Alberta, **b)** Northwest Territories and **c)** New Brunswick. Seismic stations used in the analysis shown as filled red triangles, remaining stations shown as unfilled red triangles and catalogued earthquakes (2013–2015) shown as black dots (Natural Resources Canada, 2016). Abbreviation: TF, thrust fault.

injection activity could be intense. Alternatively, if triggering occurs but the seismic response to injection activity is limited, it could imply that hydraulic communication with basement faults is key to inducing earthquakes. This project will be finished at the beginning of 2017.

Acknowledgments

This project is funded by two Natural Sciences and Engineering Research Council of Canada Discovery grants to R. Harrington and Y. Liu at McGill University, as well as partial funding from the McGill University FRQNT – New University Researchers Start Up Program. Support was given to B. Wang through the Geoscience BC scholarship fund.

The authors would also like to thank H. Yu for providing guidance on this project.

References

- Aiken, C. and Peng, Z.G. (2014): Dynamic triggering of microearthquakes in three geothermal/volcanic regions of California; *Journal of Geophysical Research Solid Earth*, v. 119, no. 9, p. 6992–7009, doi:10.1002/2014jb011218
- Aron, A. and Hardebeck, J.L. (2009): Seismicity rate changes along the central California coast due to stress changes from the 2003 M 6.5 San Simeon and 2004 M 6.0 Parkfield earthquakes; *Bulletin of the Seismological Society of America*, v. 99, no. 4, p. 2280–2292.
- Atkinson, G.M., Eaton, D.W., Ghofrani, H., Walker, D., Cheadle, B., Schultz, R., Shcherbakov, R., Tiampo, K., Gu, J., Harrington, R.M., Liu, Y.J., van der Baan, M. and Kao, H. (2016): Hydraulic fracturing and seismicity in the Western Canada Sedimentary Basin; *Seismological Research Letters*, v. 87, no. 3, p. 631–647, doi:10.1785/0220150263
- Brodsky, E.E. and Prejean, S.G. (2005): New constraints on mechanisms of remotely triggered seismicity at Long Valley caldera; *Journal of Geophysical Research Solid Earth*, v. 110, no. B4, doi:Artn B04302
- Eaton, D.W. and Mahani, A.B. (2015): Focal mechanisms of some inferred induced earthquakes in Alberta, Canada; *Seismological Research Letters*, v. 86, no. 4, p. 1078–1085.
- Farahbod, A.M., Kao, H., Walker, D.M., Cassidy, J.F. and Calvert, A. (2015): Investigation of regional seismicity before and after hydraulic fracturing in the Horn River Basin, northeast British Columbia; *Canadian Journal of Earth Sciences*, v. 52, no. 2, p. 112–122.
- Gomberg, J., Reasenberg, P.A., Bodin, P. and Harris, R.A. (2001): Earthquake triggering by seismic waves following the Landers and Hector mine earthquakes; *Nature*, v. 411, no. 6836, p. 462–466, doi:10.1038/35078053
- Hill, D.P. (2008): Dynamic stresses, Coulomb failure, and remote triggering; *Bulletin of the Seismological Society of America*, v. 98, no. 1, p. 66–92, doi:10.1785/0120070049
- Hill, D.P. and Prejean, S.G. (2007): 4.09 - dynamic triggering; *in* *Treatise on Geophysics*, G. Schubert (ed.), Elsevier, Amsterdam, The Netherlands, p. 257–291.
- Hill, D.P., Reasenberg, P.A., Michael, A., Arabaz, W.J., Beroza, G., Brumbaugh, D., Brune, J.N., Castro, R., Davis, S., Depolo, D., Ellsworth, W.L., Gomberg, J., Harmsen, S., House, L., Jackson, S.M., Johnston, M.J., Jones, L., Keller, R., Malone, S., Munguia, L., Nava, S., Pechmann, J.C., Sanford, A., Simpson, R.W., Smith, R.B., Stark, M., Stickney, M., Vidal, A., Walter, S., Wong, V. and Zollweg, J. (1993): Seismicity remotely triggered by the magnitude 7.3 Landers, California, earthquake; *Science*, v. 260, no. 5114, p. 1617–1623, doi:10.1126/science.260.5114.1617
- Lamontagne, M., Lavoie, D., Ma, S., Burke, K.B. and Bastow, I. (2015): Monitoring the earthquake activity in an area with shale gas potential in southeastern New Brunswick, Canada; *Seismological Research Letters*, v. 86, no. 4, p. 1068–1077.
- Matthews, M.V. and Reasenberg, P.A. (1988): Statistical methods for investigating quiescence and other temporal seismicity patterns; *Pure and Applied Geophysics*, v. 126, no. 2–4, p. 357–372, doi:10.1007/Bf00879003
- Natural Resources Canada (2016): Earthquakes Canada; Natural Resources Canada, URL <<http://earthquakescanada.nrcan.gc.ca/>> [November 2016].
- Prejean, S., Hill, D., Brodsky, E.E., Hough, S., Johnston, M., Malone, S., Oppenheimer, D., Pitt, A. and Richards-Dinger, K. (2004): Remotely triggered seismicity on the United States west coast following the Mw 7.9 Denali fault earthquake; *Bulletin of the Seismological Society of America*, v. 94, no. 6B, p. S348–S359.
- Rivard, C., Lavoie, D., Lefebvre, R., Séjourné, S., Lamontagne, C. and Duchesne, M. (2014): An overview of Canadian shale gas production and environmental concerns; *International Journal of Coal Geology*, v. 126, p. 64–76.
- Schultz, R., Stern, V. and Gu, Y.J. (2014): An investigation of seismicity clustered near the Cordell Field, west central Alberta, and its relation to a nearby disposal well; *Journal of Geophysical Research Solid Earth*, v. 119, no. 4, p. 3410–3423.
- Schultz, R., Stern, V., Novakovic, M., Atkinson, G. and Gu, Y.J. (2015): Hydraulic fracturing and the Crooked Lake sequences: insights gleaned from regional seismic networks; *Geophysical Research Letters*, v. 42, no. 8, p. 2750–2758, doi:10.1002/2015gl063455
- van der Elst, N.J., Savage, H.M., Keranen, K.M. and Abers, G.A. (2013): Enhanced remote earthquake triggering at fluid-injection sites in the midwestern United States; *Science*, v. 341, no. 6142, p. 164–167, doi:10.1126/science.1238948
- Wang, B., Harrington, R.M., Liu, Y., Yu, H., Carey, A. and Elst, N.J. (2015): Isolated cases of remote dynamic triggering in Canada detected using catalogued earthquakes combined with a matched-filter approach; *Geophysical Research Letters*, v. 42, no. 13, p. 5187–5196.
- Zoback, M.D. and Zoback, M.L. (2002): 34 – state of stress in the Earth’s lithosphere; *in* *International Handbook of Earthquake and Engineering Seismology, Part A*, W.H.K. Lee, H. Kanamori, P.C. Jennings and C. Kisslinger (ed.), *International Geophysics*, v. 81, p. 559–568.

Status Report on Petroleum System Analysis Study of the Triassic Doig Formation, Western Canada Sedimentary Basin, Northeastern British Columbia

P.L. Silva, The University of British Columbia, Vancouver, BC, pablols@alumni.ubc.ca

R.M. Bustin, The University of British Columbia, Vancouver, BC

Silva, P.L. and Bustin, R.M. (2017): Status report on petroleum system analysis study of the Triassic Doig Formation, Western Canada Sedimentary Basin, northeastern British Columbia; *in* Geoscience BC Summary of Activities 2016, Geoscience BC, Report 2017-1, p. 25–28.

Introduction

The Triassic section of the Western Canada Sedimentary Basin (WCSB) is the richest interval in terms of volume of oil per volume of rock in the basin (Marshall et al., 1987). An important part of the succession is the Lower and Middle Triassic Doig Formation, which historically has been known for limited production from its conventional reservoirs in British Columbia (BC) and Alberta. More recently, the Doig has been recognized as an important unconventional reservoir for gas and natural-gas liquids (NGL), with estimates of total gas-in-place ranging from 1.1 to 5.6 trillion m³ (Walsh et al., 2006). Little is currently known, however, about the unconventional portion of the Doig succession: the spatial and stratigraphic distribution of litho- and reservoir facies is poorly constrained and measurements of petrophysical properties are sparse and limited in scope. The distribution of unconventional reservoir properties within the Doig succession and the geological controls on these properties and their distribution are therefore unknown. Furthermore, there is an uncertainty in the distribution of hydrocarbon phase and composition, due to variations in thermal maturity, depth of burial and organic-matter type. The purpose of the ongoing research project reported herein is to determine the unconventional hydrocarbon potential of the Doig Formation through a petroleum system analysis (PSA). The principal goal of the study is to delineate the distribution of producible liquids from tight reservoirs in northeastern BC.

The PSA approach used in this study consists of three inter-related elements (Figure 1):

- Source rock evaluation: thorough quantification and mapping of the source-rock properties across the basin, such as thermal-maturity levels and organic-matter abundance and type

Keywords: British Columbia, shale gas, shale oil, unconventional reservoir, petroleum system analysis

This publication is also available, free of charge, as colour digital files in Adobe Acrobat® PDF format from the Geoscience BC website: <http://www.geosciencebc.com/s/DataReleases.asp>.

- Basin modelling: modelling of the Doig petroleum system on a basin scale, incorporating structural, lithological, geochemical and burial-history data, in order to determine the timing of thermogenic hydrocarbon generation and retention
- Reservoir properties: characterizing the reservoir potential of the Doig Formation in terms of storage capacity, producibility and response to hydraulic stimulation

Geological Background

The Doig Formation consists of mudstone, siltstone and subordinate sandstone, bioclastic packstone and grainstone, deposited under marine conditions in environments ranging from shoreface through offshore (Evoy and Moslow, 1995). It has long been recognized that the Doig can be broadly subdivided into a lower, more organic-rich and phosphatic zone, known as the Doig Phosphate Zone (DPZ); and an upper, relatively organic-lean siltstone interval. A more detailed subdivision has been proposed by Chalmers and Bustin (2012), who recognized three units: a basal Doig A, composed mainly of interbedded dark argillaceous and calcareous siltstones, corresponding to the DPZ and distinguishable in well logs by a gamma-ray signature; an intermediate section, named Doig B, corresponding to medium to dark grey argillaceous siltstone containing localized sand beds; and an upper Doig C, composed of siltstone and argillaceous fine sandstone.

Ongoing Work

To date, 470 m of core from fifteen wells in BC and 190 m from seven wells in Alberta (Table 1) have been logged for lithology, sedimentary structures, bioturbation, diagenetic features and structural features. These wells comprise three strike and six dip cross-sections (Figure 2), covering the entire lateral extent of the Doig Formation in BC and Alberta. The primary selection criterion was availability and length of core in the Doig, in an attempt to adequately represent its stratigraphic and spatial variability. Another factor taken into consideration when selecting wells was the availability of a complete well-log suite over the Doig interval. The minimum requirement for this study is a quad-combo

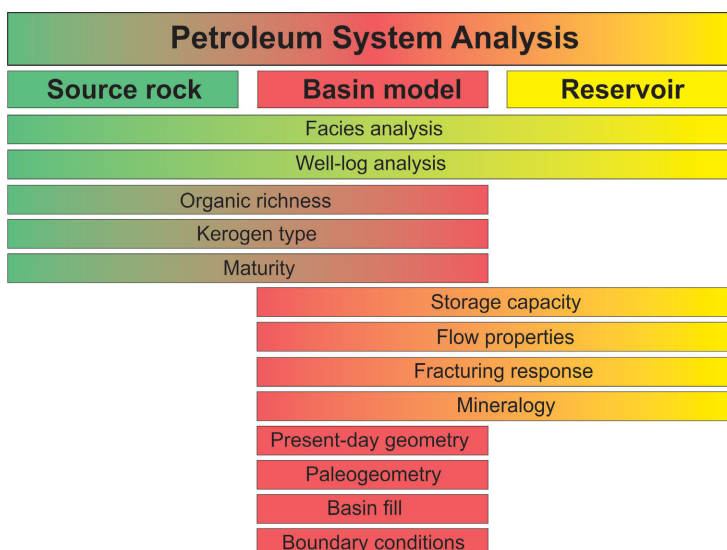


Figure 1. Elements of the petroleum system analysis approach to reservoir evaluation and their respective inputs as implemented in this study.

(gamma ray, density/neutron, resistivity and compressional slowness), and preference was given to wells with shear slowness, nuclear magnetic resonance, elemental capture spectroscopy and spectral gamma ray. These logs, although not available for all wells in the study, will aid in the development of neural-network models and in the extrapolation of petrophysical and organic geochemical properties measured on core and on cuttings to non-cored sections and wells.

Analytical work in progress includes X-ray diffraction for quantitative mineralogy, Rock-Eval pyrolysis for organic geochemical properties, helium pycnometry and mercury intrusion for porosity and pore size distribution, pressure pulse-decay permeameter measurements of permeability, and triaxial cell tests for geomechanical properties. These properties will be extrapolated to non-cored intervals and wells using quad-combo well logs through multiresolution graph-based clustering and neural-network techniques.

Table 1. Wells from which core of the Doig Formation was logged. See Figure 2 for location.

UWI	Well Name	Length (m)	Interval
100/01-10-082-23W6/00	ADU MONIAS 01-10-082-23	37	Upper Doig, DPZ
100/01-32-083-25W6/00	PROGRESS ET AL HZ ALTARES A01-32-083-25	81	DPZ
100/08-36-081-14W6/00	HUSKY MICA 08-36-081-14	10	Upper Doig
100/04-09-084-22W6/00	ARCRES ATTACHIE 04-09-084-22	29	DPZ
100/05-04-088-14W6/00	CHINOOK N BOUNDARY 05-04-088-14	22	Upper Doig
100/09-33-079-21W6/00	TALISMAN GROUND BIRCH 09-33-079-21	83	Upper Doig
100/12-04-086-20W6/00	CNRL ET AL W STODDART 12-04-086-20	18	Upper Doig
100/15-34-080-18W6/00	SHELL SUNSET 15-34-080-18	26	DPZ
200/a-063-A 093-P-09/00	MURPHY HERITAGE A 063-A/093-P-09	25	Upper Doig
200/a-070-A 093-P-10/00	ARCRES SUNDOWN A-B 070-A/093-P-10	37	Upper Doig
200/b-008-L 094-H-07/00	CNRL ET AL ZAREMBA B 008-L/094-H-07	18	Upper Doig
200/b-046-E 094-A-15/00	TALISMAN ET AL BEAVERTAIL B 046-E/094-A-15	18	Upper Doig
200/c-073-J 094-A-12/00	ARCRES INGA C 073-J/094-A-12	19	Upper Doig
200/c-075-A 094-G-16/00	CNRL TOMMY C 075-A/094-G-16	17	Upper Doig
200/c-082-F 094-H-01/00	CNRL DRAKE C 082-F/094-H-01	30	Upper Doig
100/03-22-078-10W6/00	CNRL PROGRESS 3-22-78-10	33	Upper Doig
100/04-10-079-05W6/00	CNRL ET AL HOWARD 4-10-79-5	18	Upper Doig
100/06-22-074-10W6/00	NORTHROCK KNOPCIK 6-22-74-10	48	Upper Doig
100/15-01-074-04W6/00	CNRL TEEPEE 15-1-74-4	19	Upper Doig
100/06-03-070-04W6/00	GULF GOLD CREEK 6-3-70-4	18	Upper Doig
100/08-28-071-07W6/00	RANCHWEST DIMSD 8-28-71-7	23	Upper Doig
102/15-05-071-12W6/00	HUSKY 102 ELM 15-5-71-12	36	Upper Doig

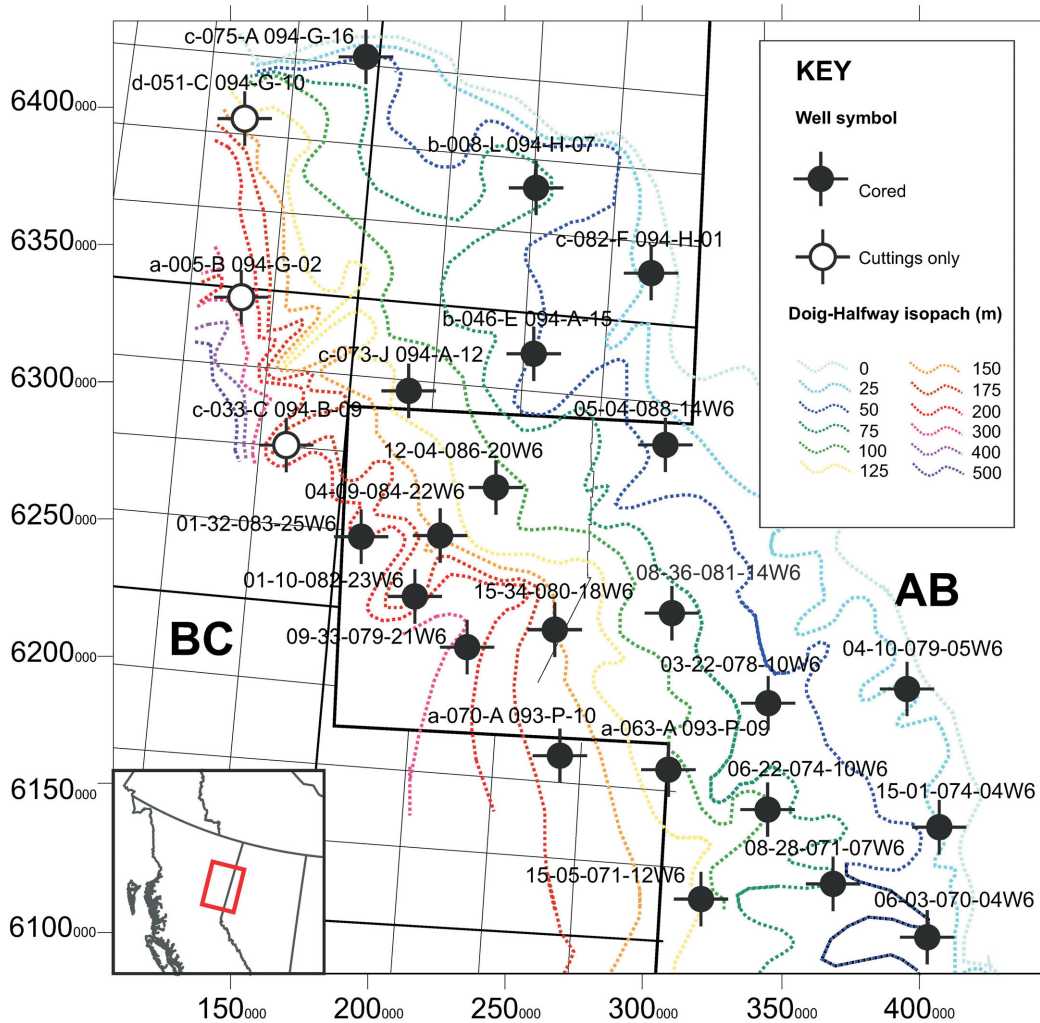


Figure 2. Location of the wells used in this study overlain on the isopach map of the Doig Formation–Halfway Formation interval.

Thermal maturity from pyrolysis will be used in a basin-modelling platform to constrain the maturity of the Doig Formation across the basin. The maps of kerogen type and total organic carbon, also derived from pyrolysis, will constrain the spatial distribution and timing of thermal hydrocarbon generation.

Preliminary core logging reveals a wide variety of lithofacies and complex stacking patterns that confer a high degree of heterogeneity on the succession. Preliminary work has identified ten lithofacies, defined based on colour, lithology and fabric. Diagenetic and structural features add another layer of heterogeneity within individual lithofacies. These facies have distinctly different reservoir properties, such as porosity, distribution of pore-throat size, permeability, elastic moduli and organic content. It has been shown that petrophysical properties vary significantly between the different Doig lithofacies, with median pore-throat size spanning one order of magnitude and permeabil-

ity spanning four orders of magnitude, despite a narrow range in grain size (Chalmers and Bustin, 2012; Chalmers et al., 2012). It is further anticipated that the degree of bioturbation, which changes the fabric of the sediments, may also control porosity and permeability (Pemberton and Gin-gras, 2005; Baniak et al., 2015).

There are currently no publicly available regional studies with a systematic petrophysical characterization of the lithofacies found in the Doig Formation. This study aims to fill this gap and will serve as the foundation for a full petrophysical and organic-geochemical characterization of these facies and their spatial and stratigraphic distribution across the WCSB. Ultimately, the lithofacies will be grouped into facies associations to enable work at the log scale, and the facies associations with their petrophysical properties keyed to cored wells will be extrapolated through logs to adjacent wells.

Acknowledgments

The authors acknowledge financial support from Geoscience BC, Trican Geological Solutions Ltd., EnCana Corporation, Husky Energy Inc., Chevron Canada Limited and Canadian Natural Resources Limited. Additionally, the thorough review by E. Letham, Ph.D. candidate at The University of British Columbia, is greatly appreciated.

References

- Baniak, G.M., Gingras, M.K., Burns, B.A. and Pemberton, S.G. (2015): Petrophysical characterization of bioturbated sandstone reservoir facies in the Upper Jurassic Ula Formation, Norwegian North Sea, Europe; *Journal of Sedimentary Research*, v. 85, no. 1, p. 62–81.
- Chalmers, G.R.L. and Bustin, R.M. (2012): Geological evaluation of Halfway-Doig-Montney hybrid gas shale–tight gas reservoir, northeastern British Columbia; *Marine and Petroleum Geology*, v. 38, no. 1, p. 53–72.
- Chalmers, G.R.L., Bustin, R.M. and Bustin, A.A.M. (2012): Geological controls on matrix permeability of the Doig-Montney hybrid shale-gas–tight-gas reservoir, northeastern British Columbia (NTS 093P); *in* Geoscience BC Summary of Activities 2011, Geoscience BC, Report 2012-1, p. 87–96 URL <http://www.geosciencebc.com/i/pdf/SummaryofActivities2011/SoA2011_Chalmers.pdf> [November 2016].
- Evoy, R.W. and Moslow, T.F. (1995): Lithofacies associations and depositional environments in the Middle Triassic Doig Formation, Buick Creek Field, northeastern British Columbia; *Bulletin of Canadian Petroleum Geology*, v. 43, no. 4, p. 461–475.
- Marshall, G.M., Noble, I.A. and Tang, R.C.W. (1987): Triassic/Jurassic fields; *in* Geophysical Atlas of Western Canadian Hydrocarbon Pools, N.L. Anderson, L.V. Hills and D.A. Cederwall (ed.), Canadian Society of Exploration Geophysicists–Canadian Society of Petroleum Geologists, p. 187–215, URL <http://www.cspg.org/cspg/documents/Publications/Atlas/geophysical/L_Chapter_7.pdf> [November 2016].
- Pemberton, S.G. and Gingras, M.K. (2005): Classification and characterizations of biogenically enhanced permeability; *AAPG Bulletin*, v. 89, no. 11, p. 1493–1517, URL <<http://archives.datapages.com/data/bulletns/2005/11nov/1493/1493.HTM>> [November 2016].
- Walsh, W., Adams, C., Kerr, B. and Korol, J. (2006): Regional “shale gas” potential of the Triassic Doig and Montney formations, northeastern British Columbia; BC Ministry of Energy and Mines, Oil and Gas Division, Resource Development and Geoscience Branch, Petroleum Geology Open File 2006-02, 19 p., URL <<http://www2.gov.bc.ca/assets/gov/farming-natural-resources-and-industry/natural-gas-oil/petroleum-geoscience/petroleum-open-files/pgof20062.pdf>> [November 2016].

Unconventional Petroleum Systems Analysis of Upper Devonian Organic-Rich Shale Units in the Horn River and Liard Basins, Northeastern British Columbia and Adjacent Western Alberta: Preliminary Report

T.K. Wilson, The University of British Columbia, Vancouver BC, twilson@eos.ubc.ca

R.M. Bustin, The University of British Columbia, Vancouver BC

Wilson, T.K. and Bustin, R.M. (2017): Unconventional petroleum systems analysis of Upper Devonian organic-rich shale units in the Horn River and Liard basins, northeastern British Columbia and adjacent western Alberta: preliminary report; *in* Geoscience BC Summary of Activities 2016, Geoscience BC, Report 2017-1, p. 29–36.

Introduction

The Horn River and Liard basins located in northeastern British Columbia (BC), southern Yukon and Northwest Territories, and adjacent western Alberta contain immense volumes of hydrocarbons that are held within multiple stratigraphic intervals. The estimates of marketable gas reserves are significant, with volumes in the Liard Basin surpassing 200 trillion cubic feet (tcf), and another 78 and 8.8 tcf in the Horn River Basin and Cordova Embayment, respectively, as well as potential for significant liquid reserves (BC Ministry of Energy and Mines and National Energy Board, 2011; Ferri and Griffiths, 2014; BC Ministry of Natural Gas Development, 2015; National Energy Board, 2016). The majority of these gas reserves are hosted within Devonian strata. The Devonian stratigraphy of these basins comprises thick accumulations of organic-rich, highly prospective fine-grained formations including the Muskwa, Besa River and Horn River (Evie and Otter Park members) formations that occur over a large areal extent.

The objective of this study is to contribute to the prediction of hydrocarbon distribution, reservoir quality and producibility of Devonian shales in the Horn River and Liard Basins, Cordova Embayment, and adjacent western Alberta. Specifically, the goal is to determine the geological factors controlling the distribution of potentially producible wet gas, condensate and oil. The multifaceted study uses petroleum systems analysis, ground-truthed with fluid analysis, and petrophysical and geochemical analyses of cuttings and core samples, to predict the types and volumes of generated and retained hydrocarbons throughout the basins' evolution (Figure 1).

Detailed core-based analysis of samples from across the study area will help refine the reservoir characterization of

important intervals and elucidate regional trends. The emphasis of such laboratory work will be put on characterizing the porosity, pore structure and pore-size distribution of the core samples, and generating additional thermal-maturity data to add to the public database. In addition, basin modelling with a focus on thermal history will be used to resolve the timing of hydrocarbon generation and migration and to quantify hydrocarbon charge and retention within the formations. Since the study region encompasses a large area with spatially variable tectonic history but comprises strata of the same general lithology and kerogen type, this study further provides an opportunity to test the impact of tectonic history and variable heat flow on the timing of hydrocarbon generation.

This preliminary report outlines the main research goals of this study, and presents initial results of petrophysical and organic-content measurements of the Muskwa Formation.

Study Area

The Liard and Horn River basins are located in northernmost BC, and southern Yukon and Northwest Territories (Figure 2). Although the focus of the study is within the BC portion of the basins, the study area extends north of the 60° parallel into the territories and includes wells west of the 6th meridian in Alberta to encompass the geographic extent of the formations. The majority of wells in the study area are located within the Horn River Basin, Cordova Embayment and west into Alberta, where initial unconventional petroleum exploration has occurred. The Liard Basin has only recently become an area of active exploration (Ferri et al., 2015) due to the expense and difficulty associated with drilling to reach Paleozoic strata that are deeply buried as a result of displacement in the Bovie fault zone.

Geological Framework

During the Devonian and Mississippian periods northeastern BC was situated along the edge of the North American protocontinent. As in other parts of the Western Canada Sedimentary Basin, the stratigraphy during that time was dominated by shale and carbonate packages, which were

Keywords: *British Columbia, shale gas, unconventional reservoirs, petrophysics, porosity, basin modelling, thermal maturity*

This publication is also available, free of charge, as colour digital files in Adobe Acrobat® PDF format from the Geoscience BC website: <http://www.geosciencebc.com/s/DataReleases.asp>.

related to major transgressive and regressive cycles. The basal setting of the study area resulted in deposition of thick packages of fine-grained sedimentary rocks, whereas stratigraphically equivalent carbonate units further to the east were deposited in shallower water (Figure 3). Exten-

sional block faulting synchronous with the Antler orogeny further influenced Paleozoic deposition by creating salient features such as the Liard Basin and Fort St. John graben (Wright et al., 1994).

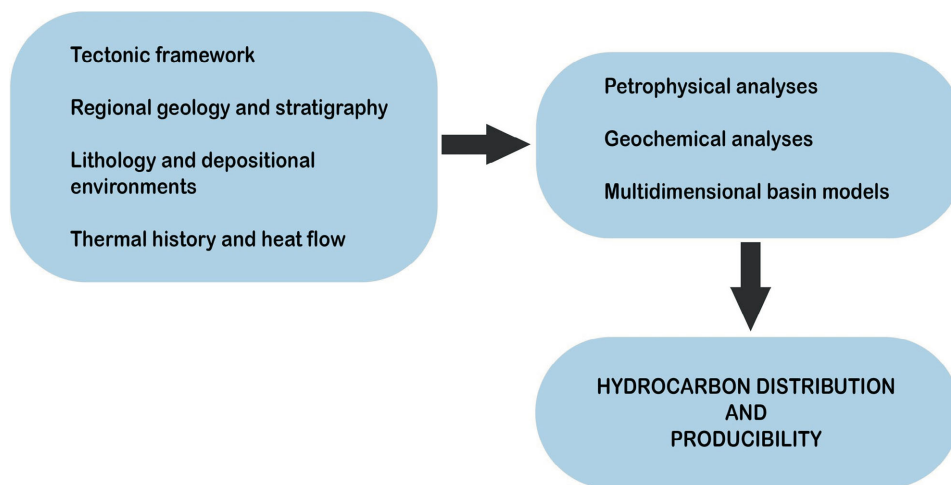


Figure 1. Flowchart illustrating the protocol for this study.

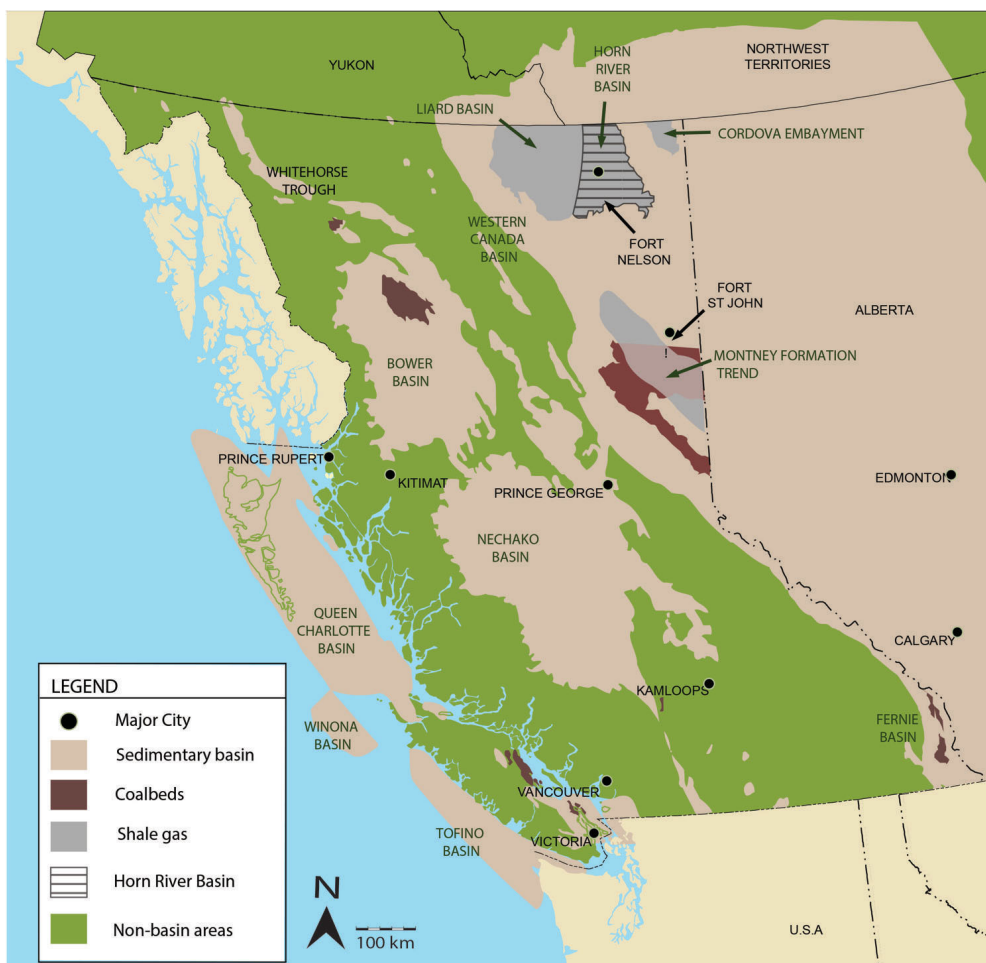


Figure 2. Location of the Liard and Horn River basins, and Cordova Embayment within northeastern British Columbia (modified from BC Ministry of Energy and Mines and National Energy Board et al., 2011).

The Besa River Formation dominates the stratigraphy of the Liard Basin, representing an extended period of deposition in a sediment-starved anaerobic environment (Ross and Bustin, 2009). The formation contains organic-rich markers representative of the Muskwa and Exshaw formations (Ferri et al., 2011, 2015). In contrast to the more basinal Liard Basin, the Horn River Basin contains a number of carbonate packages interlayered with regionally extensive organic-rich transgressive shale intervals, including the Muskwa and Exshaw formations (Switzer et al., 1994; Ferri et al., 2011). The most common lithofacies within the Muskwa and Horn River formations is massive mudstone with abundant pyrite laminations (Dong et al., 2015). These formations thin and become shallow overall toward the east, where the Horn River Formation pinches out against the

edge of the Presqu'île barrier reef. The Muskwa Formation extends into Alberta (BC Ministry of Natural Gas Development, 2015). Maturity of the source rocks, which is a function of the interplay between burial depth, thermal history and kerogen type, is within the dry-gas window for most of the study area.

Preliminary Results and Work in Progress

To date, core samples have been collected from nine wells in BC along a southwest-trending transect. The location of the wells was selected to capture the variation in depth of burial and thermal history across the basins, and therefore the associated variability in reservoir quality. Additionally, drill cuttings samples were collected from six wells along an adjacent southwest-trending transect. A total of ~300

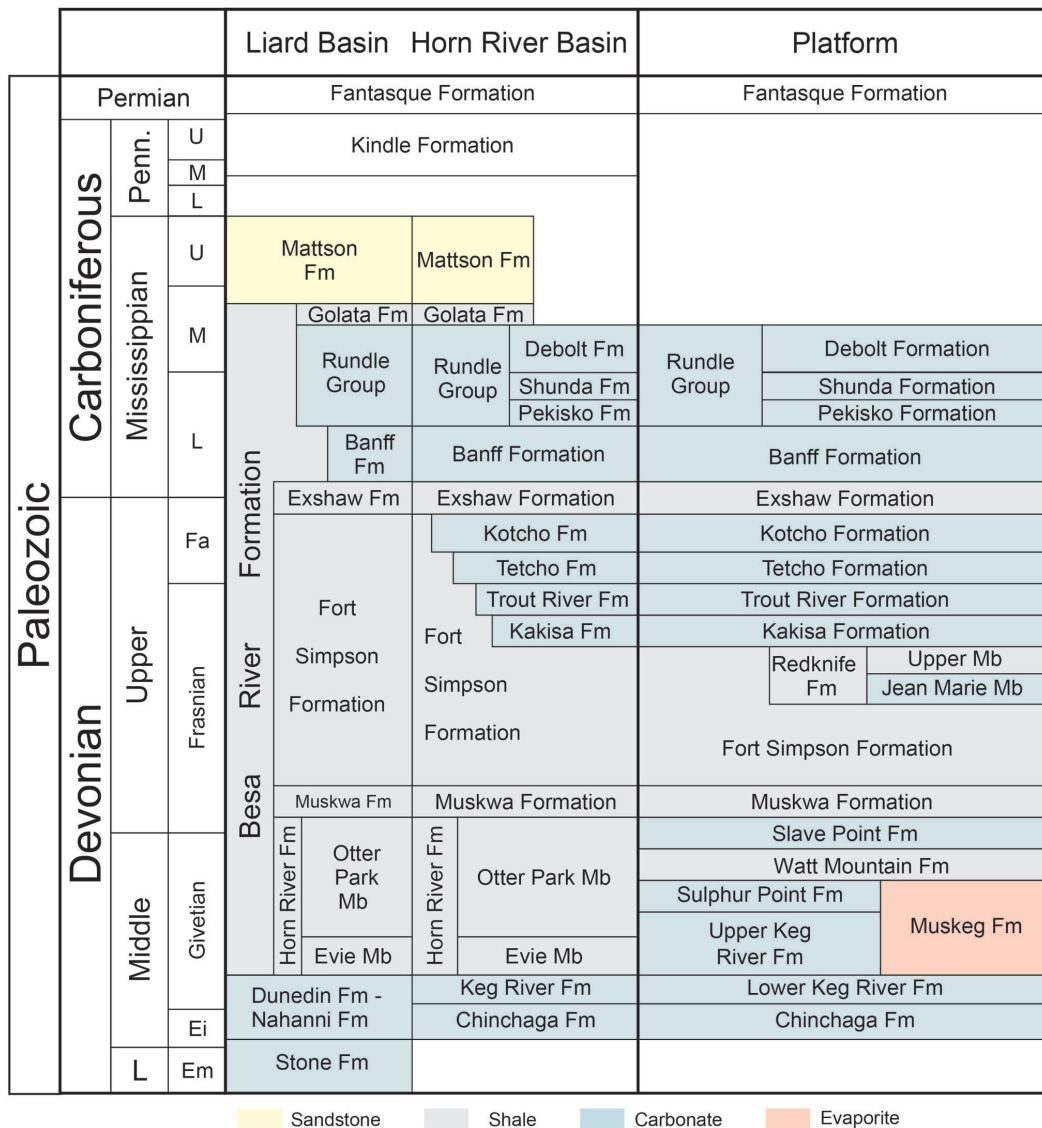


Figure 3. Upper Paleozoic stratigraphy for northeastern British Columbia (modified from Ferri et al., 2011). Abbreviations: Ei, Eifelian; Em, Emsian; Fa, Famennian; Fm, formation; L, lower; M, middle; Mb, member; Penn., Pennsylvanian; U, upper.

samples were collected by sampling at 30 to 50 m intervals along the entire length of each well. Initial data have been collected for a suite of samples from the Muskwa Formation in the Horn River Basin and Cordova Embayment, and include results from total organic carbon (TOC)/pyrolysis, helium pycnometry and mercury intrusion porosimetry (MIP). In addition, TOC/pyrolysis data have been collected for the entire suite of ~300 cuttings samples.

TOC/Pyrolysis

The average TOC of the Muskwa Formation was mapped across the study area using a dataset that includes both publicly available data and new analyses from cuttings and core samples collected for this study. The TOC is generally <2%, with the highest organic potential being located in the northwestern corner of the Horn River Basin (Figure 4). Due to sampling bias, the densest region shown by the dataset is located in the Horn River Basin and Cordova Embayment areas, where the database for the Muskwa Formation is more extensive. There is a positive correlation between porosity and TOC (Figure 5), although the correlation itself does not necessarily suggest a direct genetic relationship. For instance, it has been demonstrated in this area that there is a correlation between quartz content and TOC (Chalmers et al., 2012; Dong et al., 2015). Future mineralogical analysis as a part of this study will address such relationships.

Mercury Intrusion Porosimetry and Helium Pycnometry

The pore structure of shale-oil and shale-gas-reservoir rocks in part determines their storage capacity and fluid-transport properties, which in turn govern the economic producibility of the hydrocarbons. Due to their importance, pore structures will be characterized in this study using a

combination of mercury intrusion porosimetry (MIP), helium pycnometry, CO₂ and N₂ gas adsorption, and field emission scanning electron microscopy. Each technique has limitations, but collectively they will provide a quantitative and qualitative understanding of pore structure within the study area.

Results of MIP and helium pycnometry/bulk density obtained to date are summarized in Figure 6. The MIP data were corrected using the workflow outlined by Munson (2015; Figure 7). When comparing porosity values from MIP and helium pycnometry, helium porosity is always higher (Figure 6), as anticipated, due to helium molecules being smaller than mercury molecules and therefore able to access smaller pores. Initial pore-size-distribution results from MIP indicate that most samples contain pores in the mesopore range (Figure 8). Additionally, CO₂ and N₂ gas adsorption will provide insight as to the quantity and size distribution of micropores in the samples.

Basin History

One-dimensional basin modelling is underway, beginning with wells that contain extensive thermal maturity data. Numerous one-dimensional models will provide control points for a three-dimensional model that will assess basin history throughout the area of interest. A preliminary model for a well in the northwestern corner of the Horn River Basin has been constructed to show the general basin history and present-day temperature for this portion of the study area (Figure 9).

Future Work

The petrophysical and geochemical analyses in progress will be used to map lateral trends in reservoir properties and thermal maturity. Construction of basin models using these

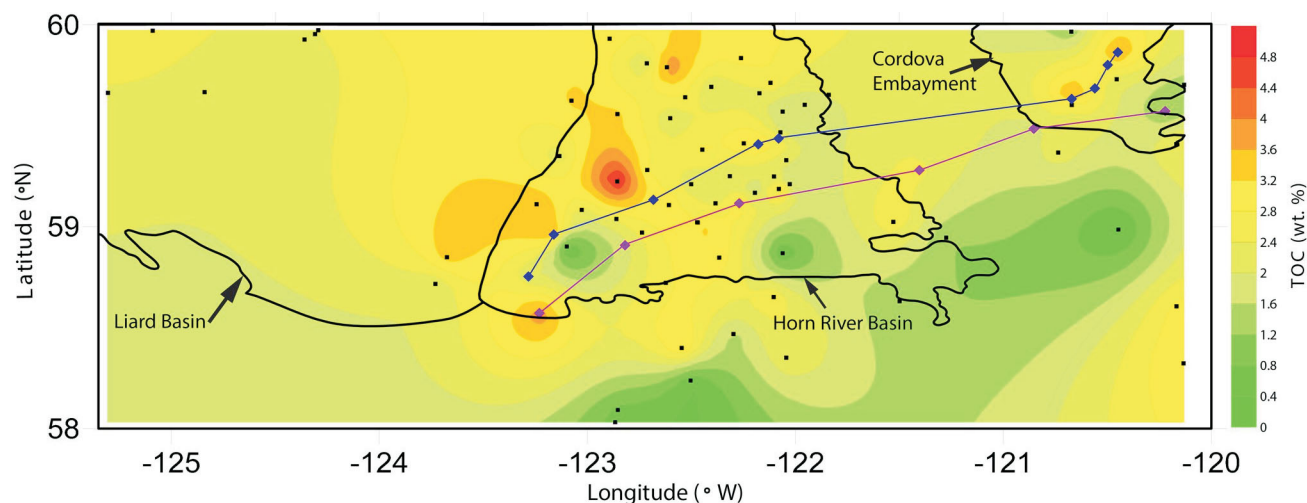
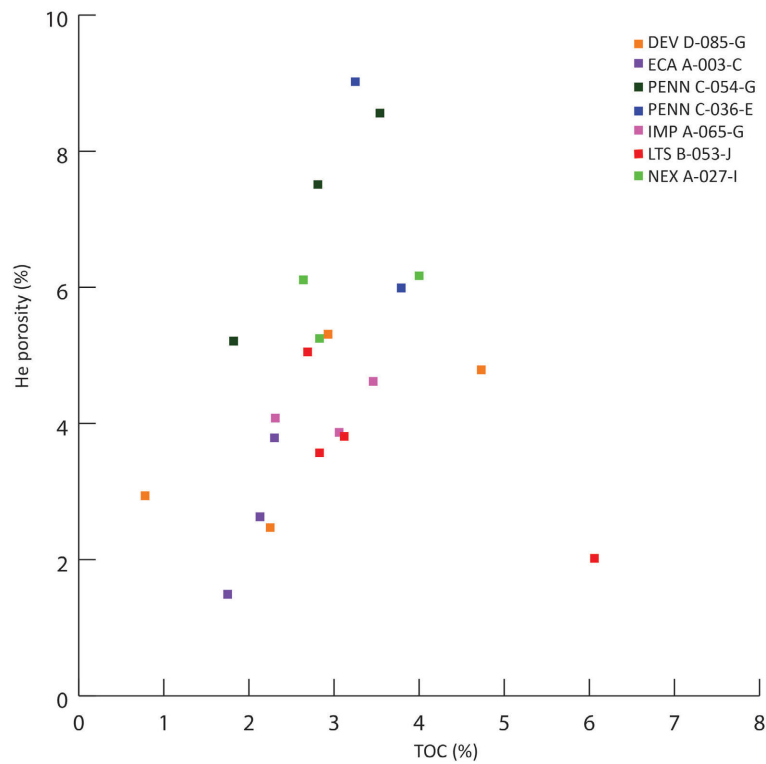


Figure 4. Average total organic carbon (TOC; wt. %) map of the study area. The Liard and Horn River basins and Cordova Embayment are outlined from west to east. The purple and blue cross-sections correspond to the well location of collected cuttings and core samples, respectively. The remaining well locations (black) contain publicly available TOC data.



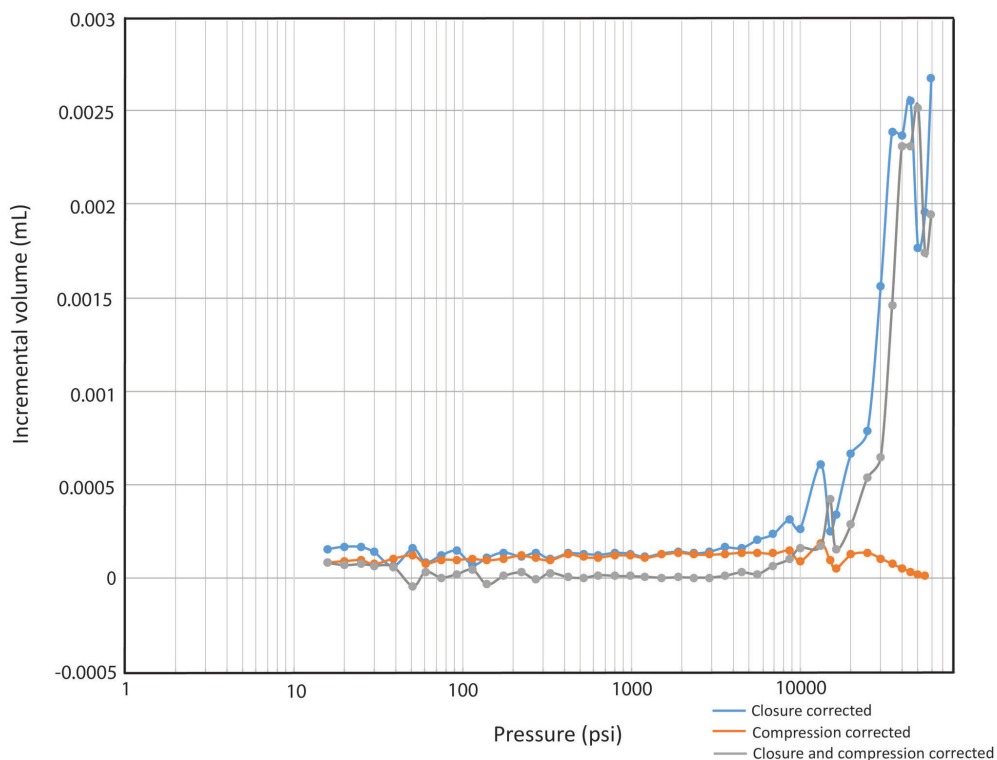


Figure 7. Incremental intrusion (mL) versus injection pressure (psi)—an example of applying closure and compression corrections to uncorrected raw mercury intrusion porosimetry data using the workflow developed by Munson (2015).

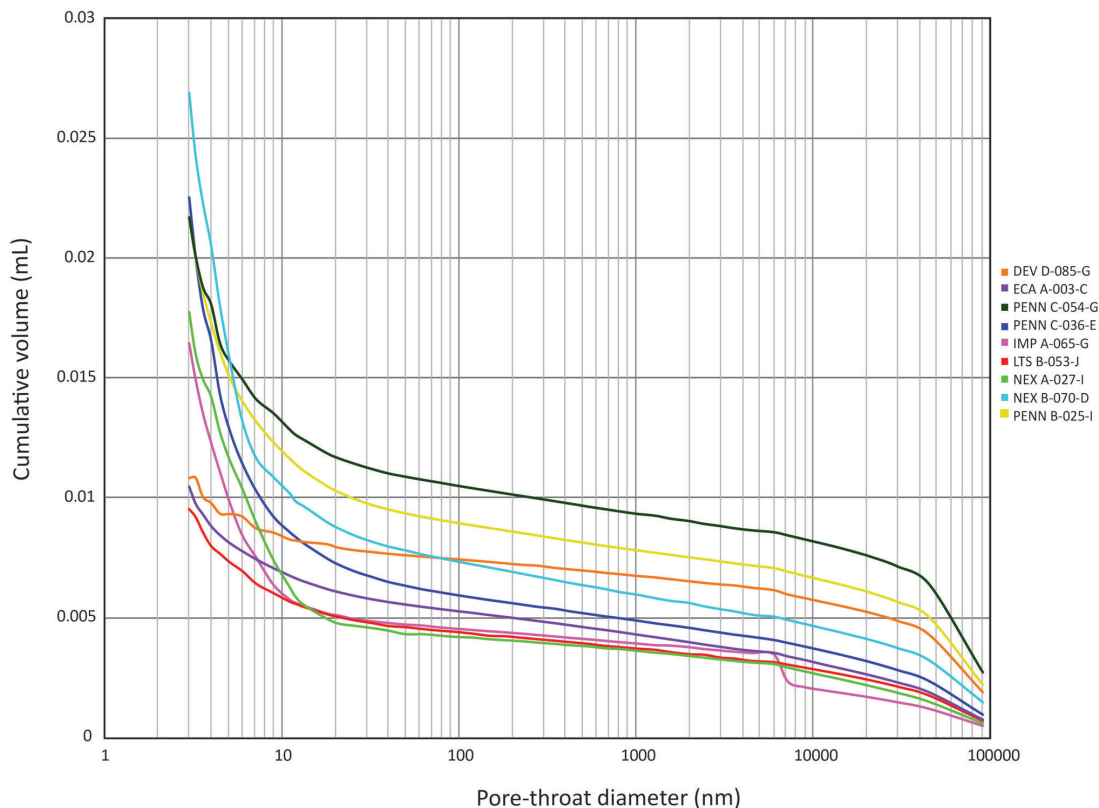


Figure 8. Cumulative intrusion (mL) versus pore-throat diameter (nm)—initial pore-size distributions for Muskwa Formation samples all exhibit similar results with the majority of pores measuring from 3 to 20 nm, which is in the mesopore range. The coloured symbols correspond to data points from different well locations that have been analyzed thus far.

ECOG Maxhamish

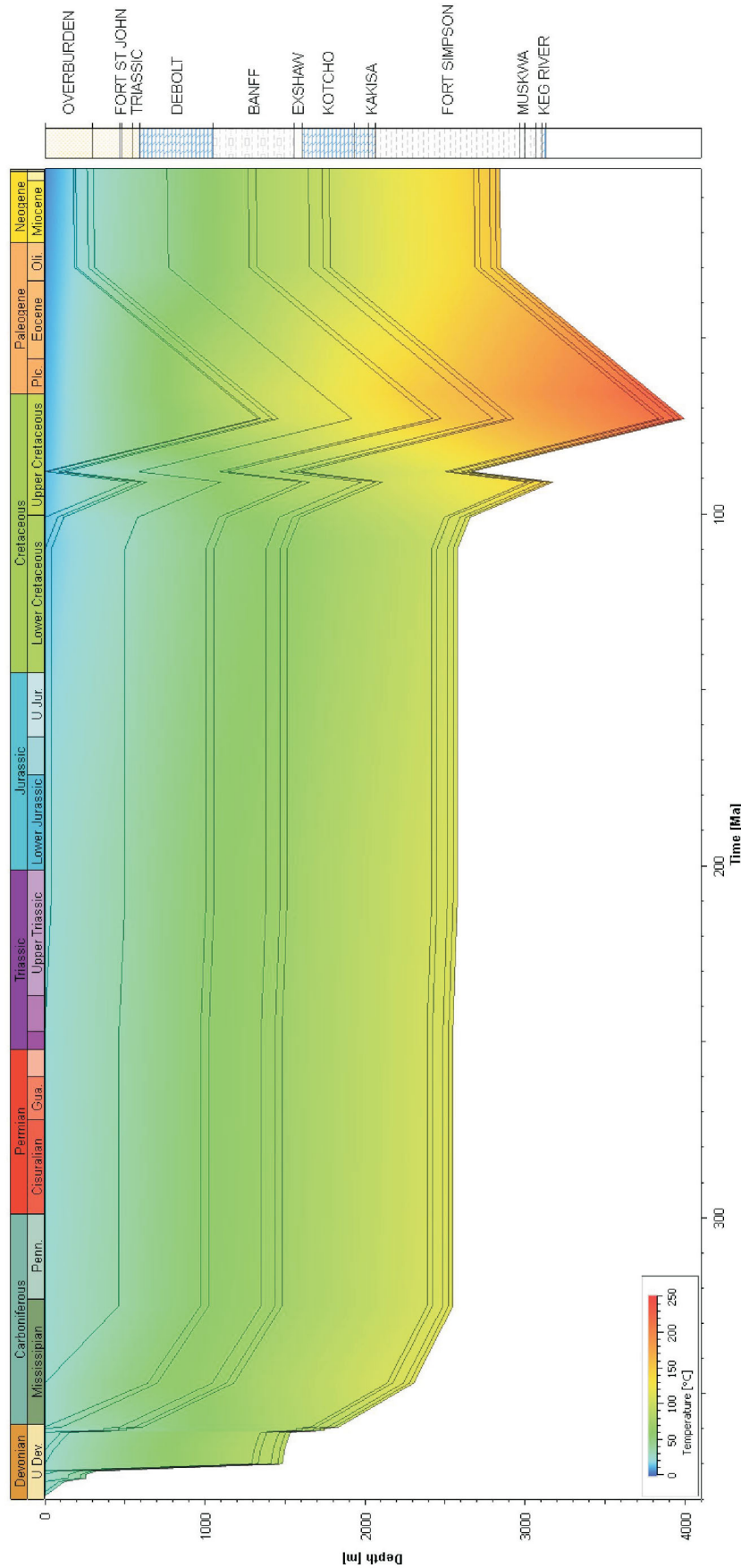


Figure 9. An example of a one-dimensional basin model showing burial depth (m) versus time (Ma) for a well in the Horn River Basin. The colour overlay on the burial history is a present-day temperature profile for this location. The stratigraphic column on the right is based on formation tops from well logs. Abbreviations: Gua, Guadalupian; L Jur., Lower Jurassic; Mio., Miocene; Oli., Oligocene; Plc., Paleocene; U Crt., Upper Cretaceous; U Dev., Upper Devonian; U Jur., Upper Jurassic.

data combined with lithostratigraphy and interpretation of tectonic history will provide a framework for determining the thermal history and the timing of hydrocarbon generation and migration. Together, these research aspects will assess the impact of basin history on the type and quantity of migrated and retained hydrocarbons, and ultimately their producibility.

Acknowledgments

The authors thank Trican Geological Solutions for their logistic support and generosity in providing laboratory analyses. Financial support from Geoscience BC, Encana Corporation, Devon Energy Corporation, Husky Energy Inc., Chevron Canada Limited, Canadian Natural Resources Limited and geoLOGIC systems ltd. are greatly appreciated. The senior author thanks Geoscience BC for the awarding of their research scholarship for 2016. This paper benefited from a careful review by E. Letham.

References

- BC Ministry of Energy and Mines and National Energy Board (2011): Ultimate potential for unconventional natural gas in northeastern British Columbia's Horn River Basin; BC Ministry of Energy and Mines and National Energy Board Report, Oil and Gas Reports 2011-1, 50 p.
- BC Ministry of Natural Gas Development (2015): Unconventional natural gas assessment for the Cordova embayment in northeastern British Columbia; BC Ministry of Natural Gas Development, Oil and Gas Report 2015-1, 12 p.
- Chalmers, G.R., Ross, D.J.K. and Bustin, R.M. (2012): Geological controls on matrix permeability of Devonian gas shales in the Horn River and Liard basins, northeastern British Columbia, Canada; *International Journal of Coal Geology*, v. 103, p. 120–131.
- Dong, T., Harris, N.B., Ayranci, K., Twemlow, C.E. and Nassichuk, B.R. (2015): Porosity characteristics of the Devonian Horn River shale, Canada: insights from lithofacies classification and shale composition; *International Journal of Coal Geology*, v. 141–142, p. 74–90.
- Ferri, F. and Griffiths, M. (2014): Thermal maturity and regional distribution of the Muskwa Formation, northeastern British Columbia, *in* Oil and Gas Geoscience Reports 2014, BC Ministry of Natural Gas Development, p. 37–45.
- Ferri, F., Hickin, A.S. and Huntley, D.H. (2011): Besa River Formation, western Liard Basin, British Columbia (NTS 094N): geochemistry and regional correlations; *in* Geoscience Reports 2011, BC Ministry of Energy and Mines, p. 1–18.
- Ferri, F., McMechan, M. and Creaser, R. (2015): The Besa River Formation in Liard Basin, British Columbia; *in* Oil and Gas Geoscience Reports 2015, BC Ministry of Natural Gas Development, p. 1–27.
- Munson, E.O. (2015): Reservoir characterization of the Duvernay Formation, Alberta: a pore to basin-scale investigation; Ph.D. thesis, University of British Columbia, Vancouver, 289 p.
- National Energy Board (2016): The unconventional gas resources of Mississippian–Devonian shales in the Liard Basin of British Columbia, the Northwest Territories, and Yukon—Energy Briefing Note; National Energy Board, 16 p., URL <<https://www.neb-one.gc.ca/nrg/sttstc/ntrlg/rprt/lmtptntlbcnwtkn2016/index-eng.html>> [October 2016]
- Ross, D.J.K. and Bustin, R.M. (2009): Investigating the use of sedimentary geochemical proxies for paleoenvironment interpretation of thermal mature organic rich strata: examples from the Devonian–Mississippian shales, Western Canadian Sedimentary Basin; *Chemical Geology*, v. 260, p. 1–19.
- Switzer, S.B., Holland, W.G., Christie, D.S., Graf, G.C., Hedinger, A.S., McAuley, R.J., Wierzbicki, R.A. and Packard, J.J. (1994): Devonian Woodbend–Winterburn strata of the Western Canada Sedimentary Basin; *in* Geological Atlas of the Western Canadian Sedimentary Basin, G.D. Mossop and I. Shetsen (comp.), Canadian Society of Petroleum Geologists, Calgary, Alberta and Alberta Research Council, Edmonton, Alberta, p. 165–202.
- Wright, G. N., McMechan, M.E. and Potter, D.E.G. (1994): Structure and architecture of the Western Canadian Sedimentary Basin; *in* Geological Atlas of the Western Canadian Sedimentary Basin, G.D. Mossop and I. Shetsen (comp.), Canadian Society of Petroleum Geologists, Calgary, Alberta and Alberta Research Council, Edmonton, Alberta, p. 25–39.

Diagenetic Model for the Deep Montney Formation, Northeastern British Columbia

N. Vaisblat, University of Alberta, Edmonton, AB, vaisblat@ualberta.ca

N.B. Harris, University of Alberta, Edmonton, AB

C. DeBhur, University of Calgary, Calgary, AB

T. Euzen, IFP Technologies Inc., Calgary, AB

M. Gasparrini, IFP Energies nouvelles, Rueil-Malmaison, France

V. Crombez, IFP Energies nouvelles, Rueil-Malmaison, France

S. Rohais, IFP Energies nouvelles, Rueil-Malmaison, France

F. Krause, University of Calgary, Calgary, AB

K. Ayranci, University of Alberta, Edmonton, AB

Vaisblat, N., Harris, N.B., DeBhur, C., Euzen, T., Gasparrini, M., Crombez, V., Rohais, S., Krause, F. and Ayranci, K. (2017): Diagenetic model for the deep Montney Formation, northeastern British Columbia; *in* Geoscience BC Summary of Activities 2016, Geoscience BC, Report 2017-1, p. 37–48.

Introduction

The Lower Triassic Montney Formation of the Western Canada Sedimentary Basin (WCSB) is a world-class unconventional resource with 450 Tcf gas reserves, 14 520 mmbbl natural gas liquids reserves and 1125 mmbbl oil reserves (National Energy Board, 2013). Although commonly described as a shale, the Montney Formation is a siltstone in most of its subcrop. Unlike sandstone and shale reservoirs, little is known about the diagenetic evolution and pore development of siltstone reservoirs, and a better understanding of diagenetic controls on reservoir quality in this type of reservoir is essential to improve resource and reserve estimates and to maximize hydrocarbon recovery. This work focuses on the deepest section of the Montney Formation in British Columbia (BC). An isopach map of the formation thickness and the location of the study area are presented in Figure 1. In this area, the Montney Formation is within the gas window and highly mature (temperature at maximum release of hydrocarbons [T_{\max}] is $>470^{\circ}\text{C}$, vitrinite reflectance [R_o] is 1.3%).

Diagenetic studies are crucial for understanding pore system evolution and predicting reservoir quality. The objective of this paper is to describe the major authigenic phases that are present in the Montney Formation siltstone and in-

terpret the temporal sequence of events leading to the consolidation of the formation.

Geological Background

The Montney Formation is a west-dipping clastic wedge, deposited on the western continental shelf of Pangea. The Montney Formation consists of three third-order sequences prograding from east to west. In the western part of the basin, the Montney Formation is topped by a major intra-Triassic erosive surface and overlain by the transgressive Doig Formation (Crombez, 2016). The formation reaches a maximum thickness of 350 m adjacent to the Rocky Mountains deformation front, and thins eastward to an erosional zero edge in the east (Figure 1). The centre of the Montney Formation depositional basin was positioned at a paleolatitude of approximately 30°N (Golonka et al., 1994; Davies et al., 1997; Deep Times Maps Inc.TM, 2013), experiencing a semi-arid to desert climate (Gibson and Barclay, 1989; Davis et al., 1997), and dominated by west winds (Edwards et al., 1994; Golonka et al., 1994).

Grain sizes in the Montney Formation range from silt to very fine sand, with grains typically moderately to well sorted, and subrounded to rounded (Davies et al., 1997; Barber, 2003). Sorting and roundness indicate a predominantly aeolian transport mechanism with periodic fluvial influence (Davies et al., 1997; Barber, 2003; Moslow and Zonneveld, 2012). The mineralogy of the Montney Formation (high in feldspar and detrital dolomite) supports the interpretations of an arid climate and suggests a depositional model of wind-blown, recycled immature material originating from the quartz-rich shield in the east (Edwards et al., 1994; Davies et al., 1997; Barber, 2003; Moslow and

Keywords: British Columbia, Montney Formation, diagenesis, paragenesis, quartz cement, dolomite cement, dissolution, reservoir quality, clay minerals

This publication is also available, free of charge, as colour digital files in Adobe Acrobat[®] PDF format from the Geoscience BC website: <http://www.geosciencebc.com/s/DataReleases.asp>.

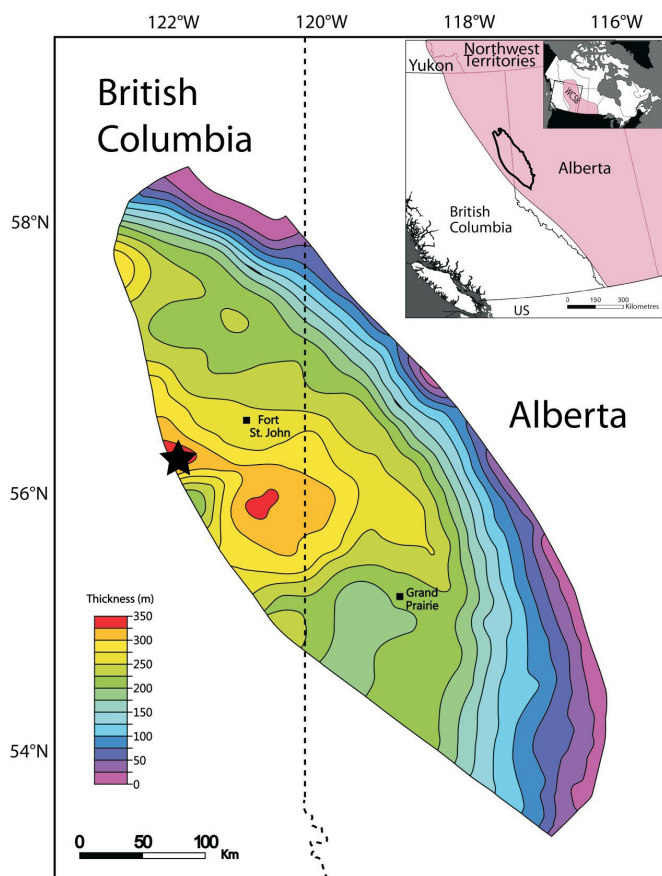


Figure 1. Isopach map of the thickness of the Montney Formation (modified from Edwards et al., 1994) and its location within the Western Canada Sedimentary Basin (WCSB). Study area is marked by the black star.

Zonneveld, 2012). Deposition of the Montney Formation took place in an anoxic to dysoxic environment, with several periods of higher oxygen levels evidenced by bioturbated intervals (Robbins, 1999; Nassichuk, 2000; LaMothe, 2008; Zonneveld et al., 2010a, b, 2011; Moslow and Zonneveld, 2012; Playter, 2013; Crombez, 2016; Crombez et al., 2016).

Previous Work

Few diagenetic studies have been conducted on the Montney Formation. Davies et al. (1997) and Barber (2003) studied diagenesis in the Montney Formation of west-central Alberta (Sturgeon Lake South ‘F’ pool), and Nassichuk (2000), Chalmers and Bustin (2012) and Playter (2013) investigated the diagenetic sequences of the Montney Formation in northeastern BC. Investigation methods vary between studies, and paragenetic interpretations are inconsistent. The major diagenetic phases described are calcite, dolomite, feldspar and quartz cements. Pyrite is reported to be widely present throughout the Montney Formation. Authigenic clays identified are fibrous illite, chlorite and glauconite, and diagenetic illitization of smectite.

Secondary porosity resulted from grain dissolution (aragonite, calcite, feldspar and quartz) or dedolomitization (Playter, 2013). Carbonate cementation is usually described as the earliest pore-occluding event, followed by quartz cement. Pyrite precipitation is thought to have occurred more or less continuously (Davies et al., 1997; Playter, 2013). Authigenic clay precipitation occurred in an intermediate stage, followed by quartz and feldspar dissolution and a second phase of carbonate (calcite and/or dolomite) precipitation. Ducros et al. (2014) estimated 2200 m of erosion above the Montney Formation in the research area during the Laramide orogeny, bringing the Montney Formation to a maximum burial depth of approximately 4700 m. The modelled maximum temperature for the Montney Formation at maximum burial depth is 180°C (Vaisblat and Harris, 2016).

Dataset

The majority of the samples for this study were selected from the Progress et al. Altares 16-17-083-25 wellcore (universal well identifier 100161708325W600, BC Oil and Gas Commission, 2016), which represents the entire section of the Montney Formation at its thickest location in the basin (sequences 1, 2 and 3 of Crombez et al. [2016], equivalent to the lower and upper Montney Formation). Sixty-eight samples were taken from this core between 2258 and 2530 m. Fifteen additional samples were made available for this study from the Suncor PC HZ Kobes D-048-B/094-B-09 wellcore (universal well identifier 200D048A094B0900, 200B079A094B0902), representing Spathian age strata (Golding et al., 2015).

Those samples were the focus of the work done by Playter (2013). Both wells are situated in the study area (Figure 1).

Methods

Since grain size in the Montney Formation, particularly in the deep section, is very fine, standard thin section analysis has proven ineffective for detailed diagenetic study. For this reason, all analyses were carried out using a scanning electron microscope (SEM).

Rock Composition

Samples were cut perpendicular to bedding, mounted in epoxy and polished to expose a surface of approximately 1.5 cm². Inorganic rock composition of these samples was determined by QEMSCAN[®] (Quantitative Evaluation of Minerals by SCANNing electron microscopy) at SGS Canada Inc. (Vancouver, BC). The QEMSCAN method is based on an FEI Company Quanta 650 with multiple energy dispersive spectrometry (EDS) detectors. Mineral identification was made by matching the spectral response with a proprietary species identification protocol (SIP), a comprehensive mineral library, which includes reference composi-

tions and solid solution series. The composition of three randomly selected samples was also determined by quantitative X-ray diffraction (XRD) analysis on a homogenized sample, representing approximately 10 cm of core. Clay minerals expandability potential was determined using oriented, glycolated mounts of the <2 µm fraction. Analysis was done at the James Hutton Institute (Aberdeen, Scotland). Whole rock X-ray powder diffraction patterns were recorded from 3–70° 2θ, and clay mounts were recorded from 3–45° 2θ, using copper Kα radiation. Organic rock composition, also performed on ~10 cm homogenized sample, was obtained by LECO TOC (total organic carbon) analysis at GeoMark Research, Ltd. laboratories (Houston, Texas).

Diagenetic Phases

Both freshly broken surfaces and polished surfaces were examined in order to identify the diagenetic phases present in the rock. Some of the samples were coated with gold and examined on a JEOL Ltd. 6301F field emission SEM (FE-SEM) with an accelerating voltage of 20 kilovolts (kV) at the University of Alberta (Edmonton, Alberta). Other samples were coated with carbon and examined on a Zeiss EVO LS15 extended pressure SEM (EP-SEM) with an accelerating voltage of 20 kV, also at the University of Alberta. Elemental content was determined using an energy dispersive X-ray analyzer attached to the SEM.

Selected samples were polished with an E.A. Fischione Instruments, Inc. 1060 SEM mill at 5 kV, 3° and continuous rotation for three hours. Samples were examined on an FEI Company Quanta 250 FEG with a Gatan, Inc. MonoCL4™ detector (SEM-CL) at the University of Calgary (Calgary, Alberta). For each sample, three or four areas were randomly selected and analyzed for mineralogical composition and luminescence patterns. Image analysis was con-

ducted to differentiate mineralogical and diagenetic phases for each mineral.

Results and Morphological Observations

Since the two well locations examined in this study are <40 km apart, results will be presented for both cores together.

Minerals present in the rock include quartz, feldspar, plagioclase, carbonate minerals, pyrite, apatite, muscovite, chlorite, mixed-layered illite-smectite (MLIS) and kaolinite, and minor amounts of other sulphides and heavy minerals (Table 1). Total organic carbon values in the samples range between 0.5 and 4 wt. % with an average of 1.5 wt. %. Organic matter in the formation displays a wide spectrum of morphologies from nonporous to extremely porous. This phenomenon was previously recognized in shales, and attributed by Curtis et al. (2011) to differences in organic matter composition.

Diagenetic Processes

Diagenetic processes were interpreted through a combination of compositional analysis, SEM-imaging observations and cathodoluminescence image interpretation.

Porosity Occluding Processes

Compaction

Physical compaction followed by chemical compaction is evidenced in all samples by pressure solutions of framework grains, mainly quartz, feldspars and dolomite (Figure 2).

Dolomite

Dolomite in the deep Montney Formation varies in origin and composition. Detrital dolomite, evidenced by weathered rounded cores, is surrounded by rhombs of authigenic dolomite cement. Small rhombohedral dolomite crystals do not always contain a detrital core. At least seven genera-

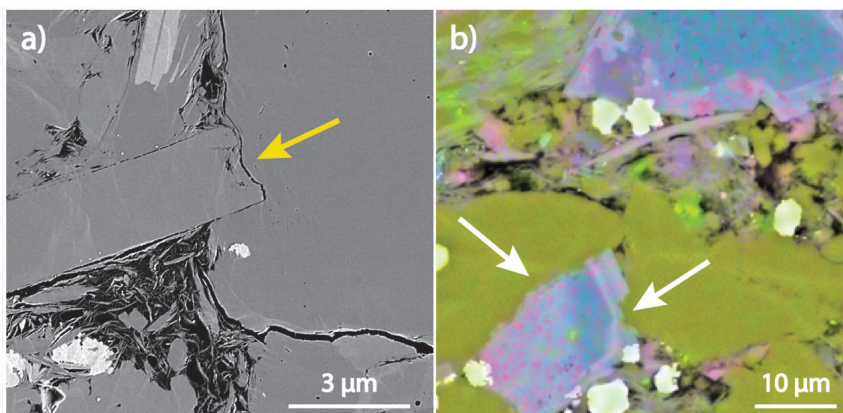


Figure 2. Evidence for chemical compaction in Montney Formation, northeastern British Columbia: **a)** backscattered electron (BSE) image of mica penetrating a quartz grain and **b)** energy dispersive spectrometry (EDS) image of quartz grain (greenish-yellow) dissolving dolomite (light blue) with authigenic rims.

Table 1. Mineralogical composition (%) and total organic carbon (wt. %) for samples from the Progress et al. Altares 16-17-083-25 wellcore (universal well identifier 100161708325W600, BC Oil and Gas Commission, 2016) were obtained by QEMSCAN® analysis.

Depth ¹	TOC	Quartz	K-feldspar	Plagioclase	Muscovite	Biotite	Kaolinite	Chlorite	Illite/ MLIS	Calcite	Dolomite	Fe- dolomite	Fe oxide and siderite	Pyrite	Sulphides ²	Fluorite	Ti silicates	Apatite	Heavy minerals
2260	0.98	36.66	9.59	7.44	2.40	0.08	0.40	0.20	6.48	6.95	22.09	0.01	0.00	4.17	0.32	0.01	0.40	1.74	0.08
2265	--	38.40	11.03	10.10	4.19	0.08	0.40	0.16	10.10	8.80	11.51	0.01	0.00	3.91	0.21	0.02	0.45	0.50	0.12
2268	2.21	37.04	9.86	9.11	2.97	0.09	0.41	0.17	8.27	9.72	14.13	0.03	0.00	4.66	0.32	0.02	0.42	0.49	0.08
2273	--	35.91	10.18	8.85	3.80	0.11	0.44	0.16	10.90	9.82	14.70	0.07	0.00	3.94	0.23	0.01	0.40	0.43	0.06
2275	1.30	30.94	9.06	6.81	4.26	0.17	0.67	0.16	13.68	5.97	22.32	0.40	0.00	3.14	0.22	0.01	0.36	0.47	0.07
2278	--	31.88	9.06	7.66	3.44	0.13	0.50	0.18	11.18	10.86	17.13	3.30	0.00	3.56	0.24	0.01	0.40	0.42	0.06
2282	3.25	35.25	10.16	8.27	3.48	0.08	0.41	0.12	10.67	12.36	10.65	1.47	0.00	2.50	0.40	0.02	0.41	0.40	0.09
2286	--	34.39	10.76	8.33	4.71	0.13	0.53	0.16	14.43	9.14	11.52	1.97	0.00	2.60	0.28	0.02	0.44	0.54	0.07
2290	3.14	34.30	9.91	8.43	3.85	0.09	0.46	0.14	12.85	11.97	10.03	1.43	0.00	2.30	0.24	0.03	0.39	0.37	0.07
2293	--	36.63	8.87	8.49	3.08	0.17	0.58	0.26	8.93	6.97	18.90	4.20	0.01	1.76	0.15	0.01	0.40	0.51	0.09
2299	1.03	34.38	8.87	8.84	3.59	0.11	0.45	0.28	8.00	6.85	14.50	10.47	0.04	1.37	0.11	0.02	0.38	0.36	0.06
2301	--	35.30	8.88	9.58	4.53	0.16	0.60	0.31	10.27	3.83	16.86	6.77	0.03	1.74	0.18	0.01	0.43	0.43	0.08
2306	1.30	38.26	11.21	11.38	4.94	0.09	0.39	0.18	12.17	5.52	7.76	3.72	0.02	2.03	0.15	0.01	0.44	0.36	0.08
2308	--	37.70	10.99	11.44	5.69	0.12	0.50	0.26	11.36	3.31	11.19	4.25	0.02	1.97	0.22	0.01	0.43	0.44	0.08
2310	2.21	33.40	10.92	9.83	6.40	0.14	0.51	0.20	16.70	2.30	10.93	2.89	0.01	2.56	0.19	0.00	0.41	0.37	0.05
2324	--	18.11	3.10	3.91	2.09	0.17	0.69	0.37	4.69	3.32	35.08	26.67	0.20	1.08	0.07	0.01	0.21	0.20	0.03
2328	1.81	37.88	8.25	9.38	4.05	0.12	0.58	0.24	11.94	5.35	13.10	3.75	0.17	2.05	0.21	0.01	0.39	0.64	0.08
2332	--	25.21	5.46	5.82	2.43	0.22	0.64	0.39	8.45	2.62	28.26	17.31	0.07	2.34	0.12	0.01	0.28	0.31	0.04
2334	1.00	37.66	10.59	11.01	5.71	0.12	0.47	0.23	13.74	3.37	9.34	3.53	0.08	2.10	0.21	0.01	0.39	0.36	0.08
2338	--	36.26	11.21	10.56	5.57	0.13	0.52	0.23	13.69	4.82	10.86	3.23	0.19	1.75	0.16	0.01	0.39	0.34	0.09
2343	0.82	38.60	8.53	10.43	4.68	0.09	0.50	0.25	10.24	6.71	10.27	5.12	0.42	2.05	0.32	0.02	0.45	0.41	0.09
2346	0.90	37.55	8.90	11.31	5.82	0.09	0.56	0.23	11.65	6.54	9.05	4.25	0.25	1.84	0.24	0.01	0.40	0.32	0.09
2350	--	39.74	8.66	10.91	4.53	0.08	0.51	0.26	9.11	7.42	9.62	5.51	0.49	1.95	0.21	0.02	0.41	0.44	0.13
2354	1.02	34.27	8.15	10.07	7.42	0.11	0.66	0.28	14.21	5.12	9.10	5.68	0.43	2.30	0.21	0.01	0.40	0.49	0.07
2356	1.90	34.95	8.26	9.43	6.87	0.11	0.62	0.20	15.78	6.88	8.60	2.26	0.62	2.50	0.24	0.02	0.36	0.33	0.07
2360	--	27.93	7.11	7.12	4.05	0.15	0.67	0.33	11.07	4.88	22.68	10.18	0.13	2.90	0.16	0.01	0.30	0.26	0.06
2364	2.68	35.85	8.58	9.69	6.12	0.13	0.62	0.22	16.02	5.36	9.33	2.22	0.16	1.98	0.19	0.01	0.37	0.38	0.09
2368	--	28.48	9.47	6.00	3.82	0.13	0.50	0.15	16.45	7.33	10.60	2.03	0.13	1.76	0.19	0.01	0.24	12.67	0.04
2372	1.95	37.46	11.50	11.21	5.32	0.11	0.47	0.22	13.08	4.15	8.37	1.87	0.02	3.17	0.22	0.00	0.47	0.35	0.07
2376	--	38.25	11.06	11.40	3.76	0.21	0.32	0.30	15.61	5.22	4.54	2.58	0.01	5.61	0.27	0.00	0.51	0.29	0.08
2381	3.86	35.95	10.53	10.65	4.52	0.08	0.49	0.20	12.41	7.43	7.65	0.65	0.01	4.34	0.28	0.01	0.37	0.50	0.07
2386	--	33.77	8.82	9.23	4.89	0.19	0.69	0.26	13.60	4.74	18.22	0.70	0.00	3.85	0.28	0.01	0.35	0.35	0.06
2387	0.68	36.57	9.79	10.81	4.66	0.12	0.52	0.23	12.44	4.89	13.16	2.29	0.02	2.85	0.24	0.01	0.36	0.28	0.08
2395	--	32.46	4.20	9.15	4.73	0.14	1.04	0.27	10.66	13.35	19.15	1.58	0.17	2.14	0.16	0.04	0.29	0.42	0.07
2396	1.18	37.33	4.46	10.22	5.08	0.57	0.87	1.33	10.99	4.35	17.48	2.39	0.06	2.66	0.18	0.01	0.33	0.40	0.09

Table 1 (continued)

Depth ¹	TOC	Quartz	K-feldspar	Plagioclase	Muscovite	Biotite	Kaolinite	Chlorite	Illite/ MLIS	Calcite	Dolomite	Fe- dolomite	Fe oxide and siderite	Pyrite	Sulphides ²	Fluorite	Ti silicates	Apatite	Heavy minerals
2401	0.48	37.15	4.46	10.98	6.54	0.95	0.98	1.62	16.05	3.76	10.93	0.96	0.02	3.83	0.51	0.01	0.36	0.36	0.05
2404	0.69	38.22	5.80	12.32	5.91	0.70	0.73	1.73	12.81	5.12	9.66	1.58	0.02	3.51	0.32	0.01	0.42	0.39	0.07
2408	--	39.14	5.76	12.08	3.99	0.50	0.66	1.62	9.22	7.81	11.30	4.40	0.07	2.49	0.14	0.02	0.42	0.33	0.06
2410	0.57	38.41	5.72	11.61	6.06	0.86	0.74	1.95	14.77	4.89	8.98	1.35	0.02	3.10	0.16	0.01	0.35	0.35	0.09
2414	--	41.86	6.35	10.75	4.91	0.73	0.65	1.65	14.57	5.56	7.20	1.58	0.02	3.20	0.16	0.01	0.37	0.35	0.07
2416	0.53	35.98	3.47	6.79	5.49	1.09	1.36	1.43	16.16	5.41	17.33	1.30	0.01	2.70	0.16	0.01	0.26	0.48	0.04
2425	1.06	44.59	6.12	12.13	3.69	0.46	0.60	1.71	13.41	5.91	5.34	0.80	0.02	3.23	0.19	0.01	0.36	0.32	0.06
2427	--	39.85	7.20	12.87	4.88	0.58	0.60	1.54	16.56	5.75	5.63	0.65	0.01	2.95	0.14	0.01	0.35	0.33	0.10
2431	0.83	41.20	6.35	11.41	4.89	0.73	0.69	1.54	14.41	4.25	9.63	0.88	0.00	2.32	0.10	0.01	0.39	0.27	0.09
2436	--	37.07	5.52	10.77	3.71	0.67	0.85	1.52	14.10	5.29	14.92	1.55	0.04	2.98	0.21	0.01	0.33	0.40	0.05
2440	0.87	32.32	3.10	5.36	3.40	0.86	1.29	1.07	19.84	2.98	21.37	1.21	0.00	5.58	0.24	0.01	0.23	0.24	0.03
2444	--	41.53	6.25	9.16	4.76	0.69	0.61	1.46	19.32	3.24	6.99	1.10	0.03	3.81	0.34	0.01	0.33	0.30	0.07
2448	1.60	41.20	6.05	9.23	4.62	0.75	0.72	1.44	20.13	2.90	6.05	0.70	0.02	3.67	0.22	0.01	0.36	0.26	0.08
2452	2.12	39.03	5.48	6.41	4.40	0.72	0.71	1.10	24.73	2.56	6.82	0.76	0.01	4.24	0.33	0.01	0.32	0.22	0.05
2457	--	33.14	3.57	7.49	3.24	0.65	0.99	1.50	15.15	3.50	22.46	4.67	0.09	2.80	0.19	0.01	0.30	0.20	0.05
2472	--	39.49	4.36	9.39	4.17	0.65	0.81	1.73	14.80	3.98	13.27	3.35	0.06	3.06	0.20	0.01	0.38	0.24	0.05
2474	1.35	38.97	4.30	7.11	2.63	0.87	0.49	1.05	25.75	4.80	6.67	1.40	0.03	3.67	0.23	0.00	0.40	0.24	0.04
2476	--	40.20	4.79	10.09	4.57	0.68	0.80	1.59	17.94	4.18	9.37	1.36	0.04	3.52	0.22	0.01	0.37	0.23	0.05
2479	1.38	35.10	3.58	7.18	2.50	0.88	0.68	1.19	23.11	5.32	11.11	3.59	0.03	3.47	0.20	0.00	0.40	0.23	0.05
2481	--	41.86	4.65	9.69	4.39	0.70	0.77	1.76	19.73	3.99	6.75	1.11	0.03	3.78	0.17	0.01	0.33	0.20	0.07
2483	0.97	41.39	4.44	8.30	4.05	0.65	0.74	1.39	20.29	3.94	7.61	1.11	0.05	4.17	0.28	0.01	0.32	0.23	0.06
2487	--	37.18	3.67	8.90	4.51	0.72	1.07	1.64	18.02	3.35	12.48	2.97	0.10	4.55	0.26	0.01	0.32	0.20	0.05
2492	0.97	40.76	4.14	9.04	4.70	0.76	0.89	1.56	19.68	4.00	7.63	0.98	0.04	4.07	0.20	0.01	0.35	0.20	0.04
2495	0.74	40.61	3.39	7.79	6.30	0.86	0.84	1.47	22.75	2.74	6.43	0.65	0.03	4.62	0.21	0.00	0.31	0.20	0.04
2498	--	26.33	1.67	4.08	2.90	0.78	1.83	1.36	12.79	2.27	34.74	7.47	0.27	3.03	0.10	0.01	0.19	0.15	0.03
2499	0.56	18.57	0.96	2.96	1.09	0.40	1.22	1.25	5.85	0.88	41.67	22.14	0.86	1.28	0.06	0.01	0.15	0.08	0.03
2501	0.96	43.60	3.85	7.81	5.11	0.80	0.74	1.45	22.95	3.49	4.70	0.61	0.03	3.23	0.13	0.01	0.32	0.15	0.07
2505	--	46.79	4.78	8.95	3.40	0.48	0.61	1.16	20.30	3.31	5.67	0.60	0.03	3.13	0.15	0.00	0.38	0.18	0.07
2509	1.40	45.39	4.21	6.95	3.23	0.41	0.66	0.98	19.73	3.27	7.79	1.24	0.07	3.83	0.20	0.01	0.38	0.18	0.05
2514	--	44.89	4.52	5.18	3.18	0.36	0.60	0.76	25.63	3.87	4.83	0.85	0.03	4.52	0.25	0.01	0.32	0.17	0.04
2518	2.10	38.93	3.79	3.97	1.89	0.28	0.74	0.55	27.24	5.75	8.44	1.45	0.01	4.23	0.20	0.01	0.24	0.14	0.04
2524	1.42	41.51	4.89	4.31	2.38	0.34	0.69	0.56	25.52	3.39	9.03	1.12	0.02	4.02	0.31	0.01	0.30	0.13	0.04
2528	--	44.95	5.30	4.42	3.41	0.25	0.44	0.47	29.23	1.31	4.39	0.23	0.01	4.45	0.66	0.00	0.29	0.14	0.05

¹Depths (in metres) in this table are shifted to match core gamma log with downhole gamma log.

²includes barite, sphalerite and gypsum.

Abbreviations: MLIS, mixed-layer illite-smectite; TOC, total organic carbon.

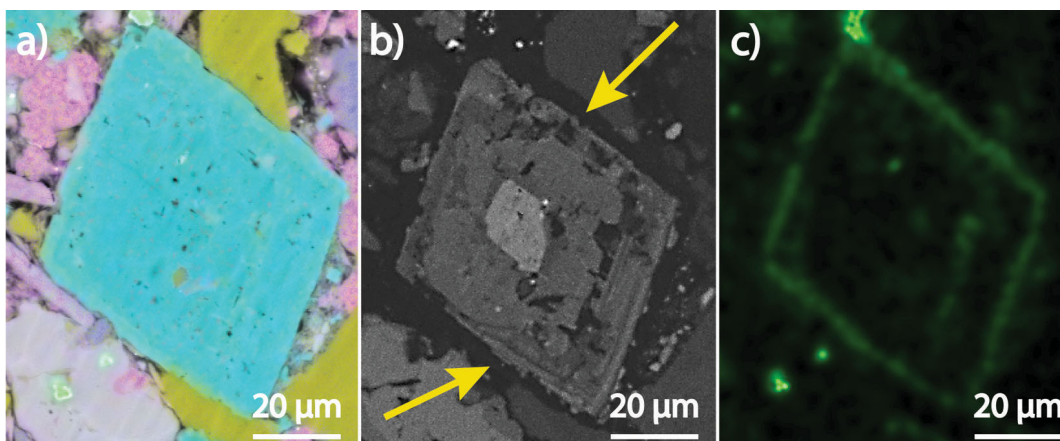


Figure 3. Dolomite cement in the Montney Formation, northeastern British Columbia. **a)** Energy dispersive spectrometry (EDS) image of dolomite (light blue). **b)** Scanning electron microscope (SEM) cathodoluminescence (CL) images of the crystals revealing complex internal structure with detrital rounded core and multiple rims. Some of the internal rims are corroded. Note the nonluminescent Fe-rich rim (yellow arrows). **c)** An EDS image showing Fe-rich external rim.

tions of dolomite cement were identified. Rims differ in Ca and Mg content (evidenced by HCl etching), with the outermost rim characterized by high Fe concentration (Figure 3). Several of the internal rims show corroded edges (Figure 3c). In some intervals, Ca-phosphate was incorporated into the dolomite structure. Dolomite dissolution is attributed to pressure solution (partially missing grain) or contact with organic acids (ragged edges; Figure 4a). Secondary porosity is developed in detrital dolomite, particularly along cleavage planes (Figure 4b).

Calcite

Calcite appears as isolated grains, sometimes enclosing large pyrite crystals (Figure 5a). The SEM-CL images show that calcite is composed of two generations (Figure 5b). Calcite was found to replace K-feldspar (Figure 5c) and dolomite (Figure 5d).

Ca-Phosphate (Apatite)

Ca-phosphate is present in the samples as grain-coating cement or nodules, and is locally incorporated into dolomite cement.

Pyrite

Pyrite is present in all samples, forming framboids or large crystals, and is commonly associated with organic matter. Framboids and crystals range from <1 to 10 µm in diameter (Figure 6).

K-Feldspar

Potassium-feldspar cement surrounds detrital K-feldspar grains as a one-phase cement (Figure 7a), or appears as discrete crystals with several generations of cement separated by dissolved ragged edges (Figure 7b). In addition, non-luminescent K-feldspar is detected in the centre of Na-feldspar and quartz grains (Figure 8). Most of the authigenic K-feldspar, though much darker than detrital K-feldspar in SEM-CL images, is moderately luminescent.

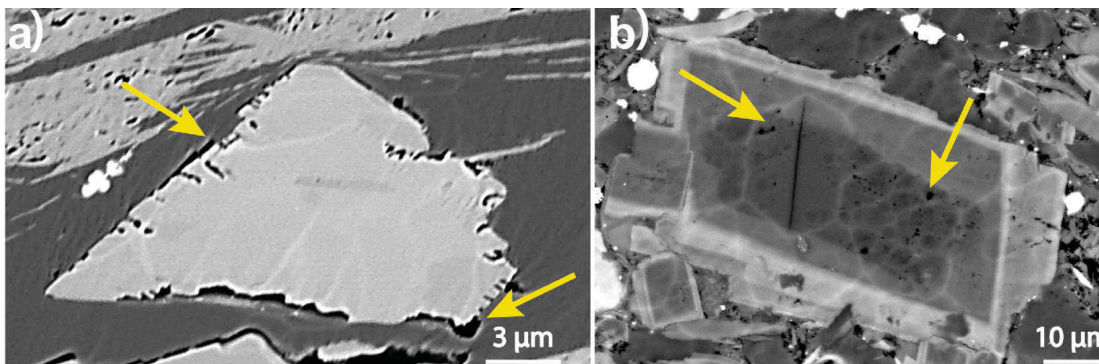


Figure 4. Backscattered electron–scanning electron microscope (BSE-SEM) images showing dolomite dissolution in the Montney Formation, northeastern British Columbia: **a)** dissolution of dolomite grain edges where dolomite is in direct contact with organic matter detrital grain and **b)** dissolution of detrital dolomite grain. Note preferred dissolution along cleavage planes.

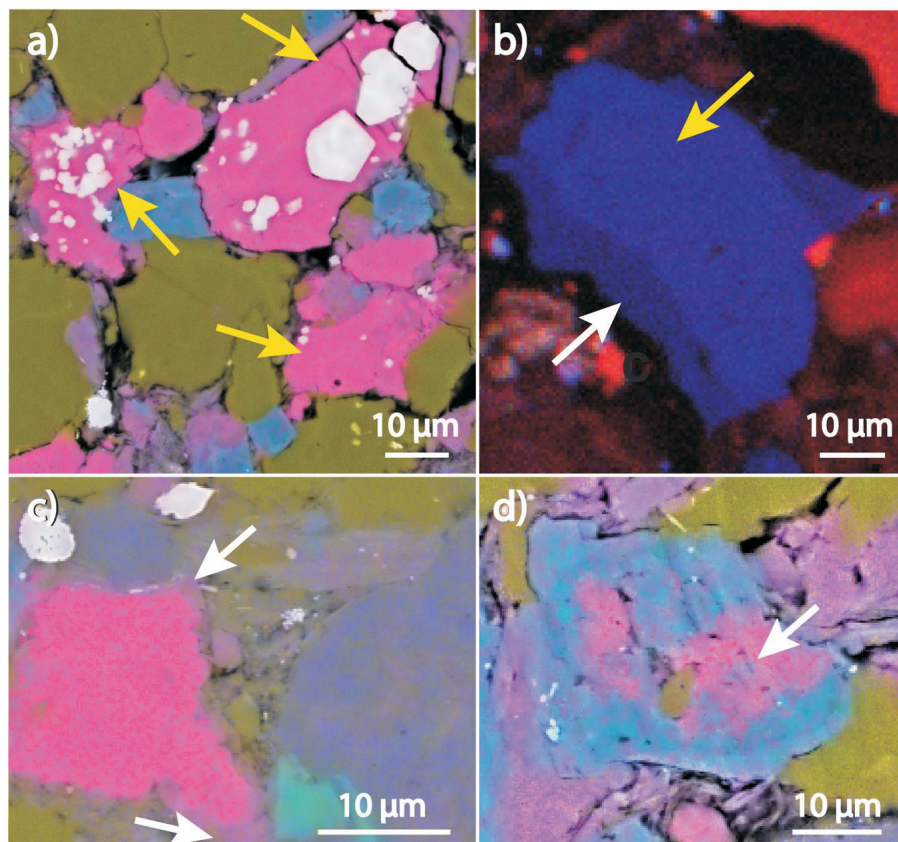


Figure 5. Scanning electron microscope images of calcite cement in the Montney Formation, northeastern British Columbia. **a)** Scanning electron microscope–energy dispersive spectrometry (SEM-EDS) image showing calcite (bright pink) enclosing pyrite crystals (white). **b)** Scanning electron microscope–cathodoluminescence (SEM-CL) image showing two different generations of calcite cement (different shades of blue) marked by arrows. **c)** An SEM-EDS image showing calcite (bright pink) replacing K-feldspar (light pink). In this image calcite has replaced most of the K-feldspar grain. Remaining K-feldspar is marked with arrows. **d)** An SEM-EDS image showing calcite replacing dolomite grain.

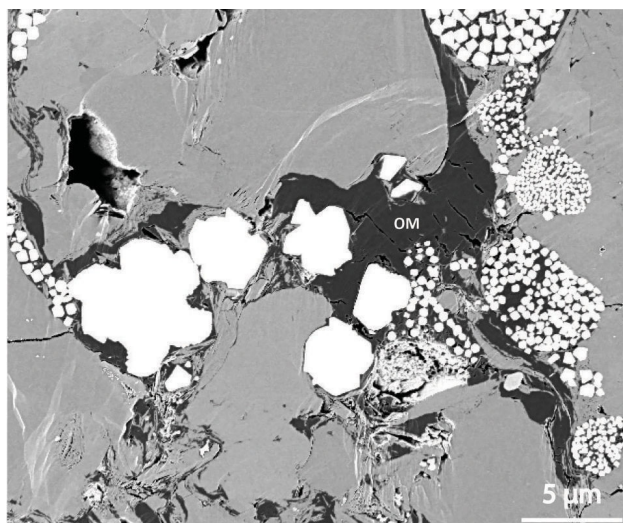


Figure 6. Backscattered electron–scanning electron microscope (BSE-SEM) image of a milled surface showing pyrite framboids and crystals (white) of varying sizes (Montney Formation, northeastern British Columbia). Note association with organic matter (OM, dark).

Na-Feldspar

In the deep Montney Formation, Na-feldspar largely occurs as detrital grains. Some samples contain nonluminescent Na-feldspar overgrowths with sharp, straight edges—both indicative of authigenic cement growth (Figure 9a). Nonluminescent Na-feldspar also replaces detrital and authigenic dolomite and detrital K-feldspar (Figure 9b, c). Sodium-feldspar alteration is usually incomplete and easily identifiable through EDS maps and backscattered electron (BSE)–SEM images.

Quartz

In the deep part of the Montney Formation, authigenic quartz occurs in three different morphologies: a) overgrowths, b) microcrystalline cements and c) amorphous opaline silica (Figure 10).

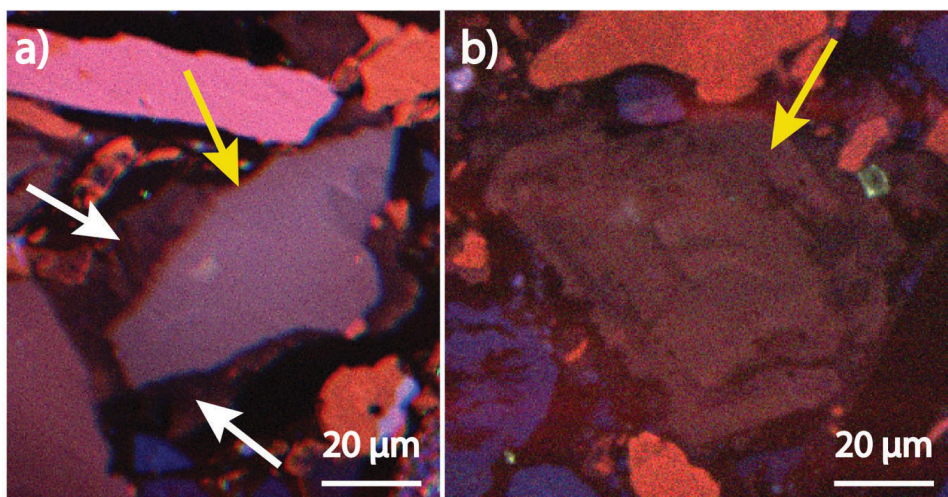


Figure 7. Scanning electron microscope–cathodoluminescence (SEM-CL) images of K-feldspar in the Montney Formation, northeastern British Columbia: **a)** detrital K-feldspar (yellow arrow) surrounded by K-feldspar cement (white arrows) and **b)** detrital rhombic K-feldspar showing cement rims (yellow arrow).

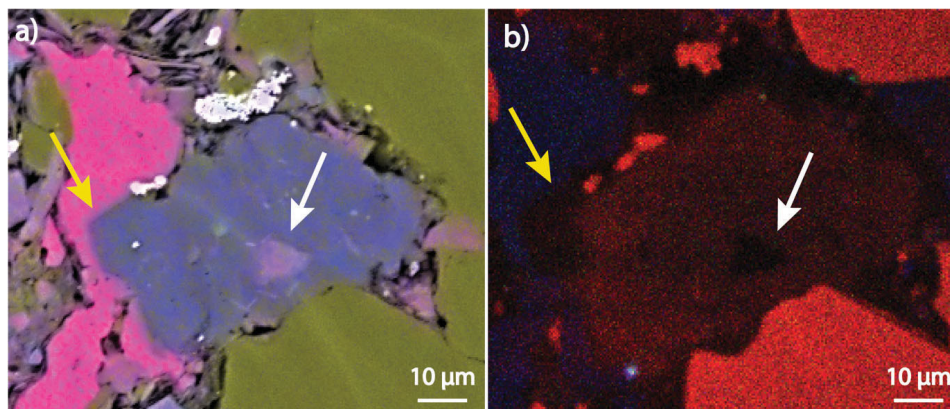


Figure 8. Sample from Montney Formation, northeastern British Columbia showing K-feldspar replacing Na-feldspar. **a)** Scanning electron microscope–energy dispersive spectrometry (SEM-EDS) image. Na-feldspar is represented by the blue colour and K-feldspar by the pink light colour and the white arrow. Yellow arrow points to straight edges of Na-feldspar cement. **b)** Scanning electron microscope–cathodoluminescence (SEM-CL) image. White arrow points to authigenic, nonluminescent K-feldspar. Note the straight edges of the Na-feldspar nonluminescent overgrowth (yellow arrow).

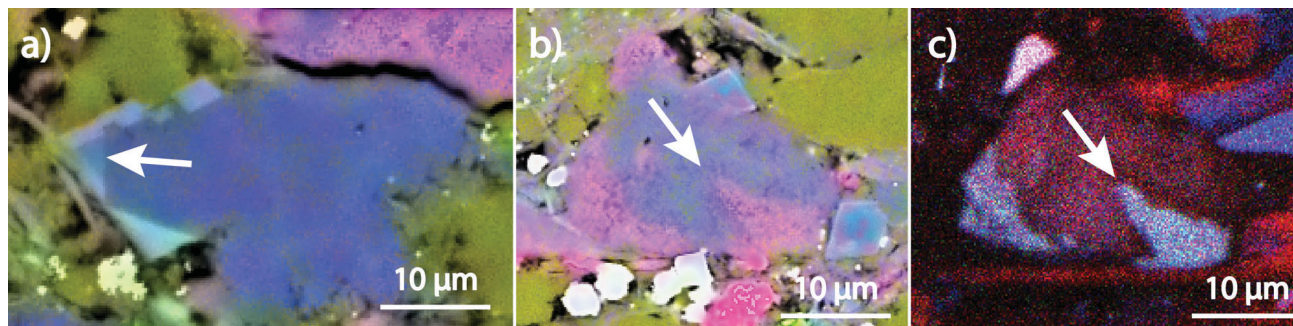


Figure 9. Examples of Na-feldspar replacement in the Montney Formation, northeastern British Columbia. **a)** Scanning electron microscope–energy dispersive spectrometry (SEM-EDS) image showing Na-feldspar (blue) replacing dolomite (light blue). Note two shades in the dolomite; the darker colour (white arrow) represents a detrital core and the lighter colour represents cement. **b)** An SEM-EDS image of Na-feldspar (blue) replacing detrital K-feldspar grain (pink). **c)** Scanning electron microscope–cathodoluminescence (SEM-CL) image of 9b. Note the bright colour of the K-feldspar (blue), indicating detrital origin.

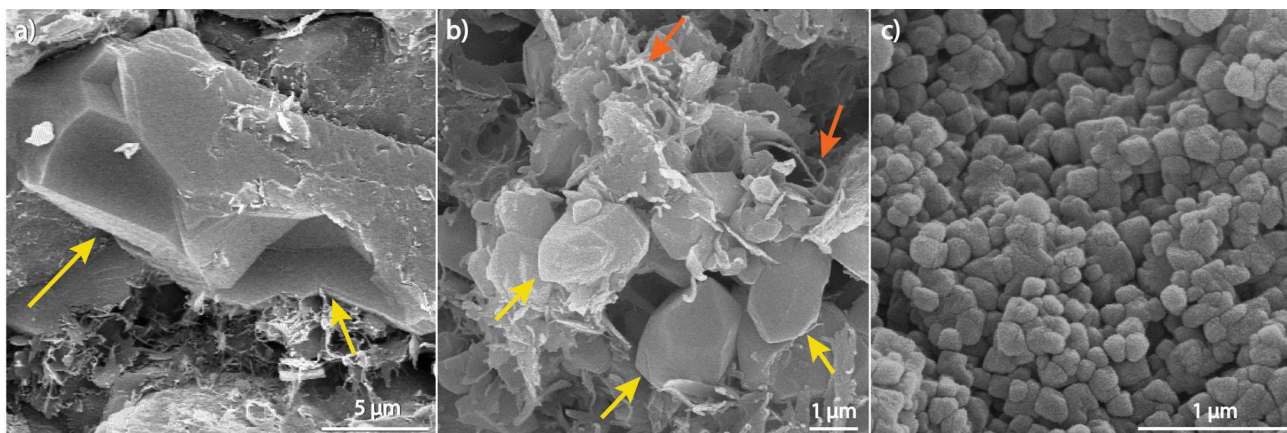


Figure 10. Secondary electron–scanning electron microscopy (SE-SEM) images of authigenic quartz morphologies in the deep Montney Formation, northeastern British Columbia: **a)** crystal overgrowth (arrows), note authigenic fibrous illite in the bottom section of the image; **b)** microcrystalline quartz cements (yellow arrows) and authigenic fibrous illite growing off the edges of detrital clay (orange arrow); and **c)** amorphous opaline silica.

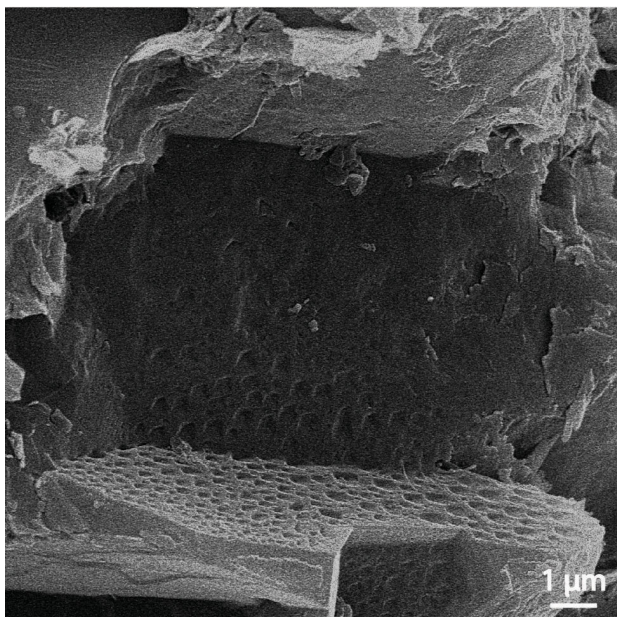


Figure 11. Secondary electron–scanning electron microscope (SE-SEM) image of a sample treated with HCl to remove carbonate. Angular small pits are visible on exposed quartz surfaces that were in contact with now dissolved carbonate cements. Pits are interpreted to be local quartz dissolution patterns. Sample from the Montney Formation, northeastern British Columbia.

Clay

Fibrous illite is present in the rock in varying abundance. Fibrous illite nucleates on the edges of detrital clay and locally on weathered mica grains (Figure 10b).

Porosity Enhancing Processes

Dolomite

Dolomite dissolution is evident by partially missing grains (Figure 2b) and ragged edges (Figure 4a). Secondary po-

rosity is developed in detrital dolomite, particularly along cleavage planes (Figure 4b).

Quartz

Small angular pits are present on the surface of some quartz grains (Figure 11). These pits are similar to previously reported quartz dissolution patterns (Freidman et al., 1976; Georgiev and Stoffers, 1980; Brantley et al., 1986; Burley and Kantorowicz, 1986; Hurst and Bjørkum, 1986; Bennett and Siegel, 1987; Knauss and Wolery, 1988; Wahab, 1998) and suggest local quartz dissolution in the Montney Formation caused by compaction.

Discussion

The Montney Formation in the study area is composed of compacted, well-cemented siltstone, containing detrital and authigenic phases, and organic matter. The QEM-SCAN results show that clay content in the deep Montney Formation ranges from 5 to 30 wt. %, with an average of 15 wt. %. These findings contrast with lower estimates of clay content previously published for the Montney Formation (<8 wt. %; Davies et al., 1997; Derder, 2012; Playter, 2013). Based on qualitative SEM observations most of the clay is of detrital origin.

The paragenesis of the Montney Formation in the deep basin was interpreted from a detailed study of crosscutting relationships between different phases. The paragenetic sequence is presented in Figure 12. In accord with other authors (Davies et al., 1997; Nassichuk, 2000; Barber, 2003; Chalmers and Bustin, 2012; Playter, 2013), the authors interpret dolomite as the earliest authigenic phase in the deep Montney Formation. Davies et al. (1997) analyzed fluid inclusions in the dolomite and concluded that dolomite was formed below 60°C. Dolomite precipitated in a series of rims, differing in composition (Ca/Mg), width and degree of corrosion on edges (Figure 3c). The outermost

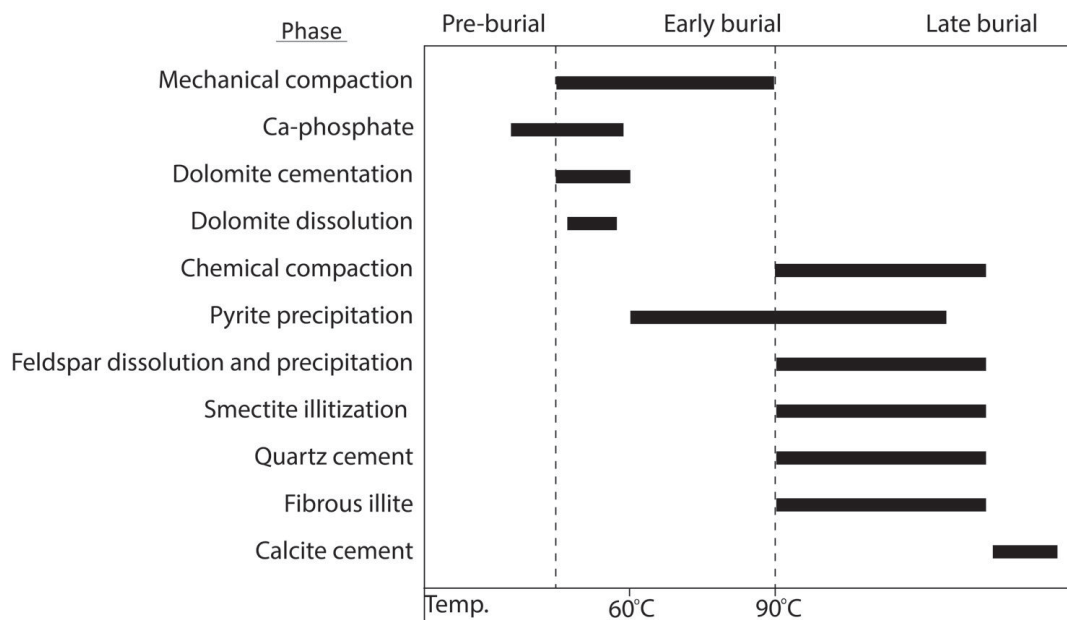


Figure 12. The paragenetic sequence for the Montney Formation in the deep basin, northeastern British Columbia.

Fe-rich rim of the dolomite is similar to that recognized by Davies et al. (1997) and Nassichuk (2000). Like Davies et al. (1997), the authors believe that Ca-phosphate precipitation is a syndepositional phase. Calcium phosphate, incorporated into dolomite cement, was probably remobilized during early burial (Tribovillard et al., 2006). Following dolomite precipitation, increasing burial led to chemical compaction and grain dissolution. The major phases that were dissolved are quartz, dolomite and feldspars. Since pyrite framboids and crystals are present in all cement phases in the Montney Formation (other than quartz, below), pyrite formation was interpreted to be a continuous diagenetic process.

The evolution of the feldspars in the deep Montney Formation is complicated and the temporal relationships between feldspar cementation and Na-feldspar to K-feldspar replacement remains unclear. The XRD analyses on glycolated samples resulted in 5% expandability of the MLIS, indicating extensive conversion of smectite to illite. In addition to smectite illitization, fibrous illite nucleated on detrital clay clumps or micas. Davies et al. (1997), Barber (2003) and Nassichuk (2000) described similar illitization processes as a result of K-feldspar dissolution.

The SEM imaging of freshly broken surfaces indicate relatively small authigenic quartz crystals (commonly <3 µm, occasionally up to 10 µm). Localized quartz dissolution is interpreted to occur during chemical compaction on contact surfaces between quartz and dolomite. Nassichuk (2000) reported that quartz partly or completely replaces dolomite, but this was not confirmed in this study. Playter (2013) proposed that dedolomitization occurred in the deep

Montney Formation, which was confirmed in this study (Figure 12), though not as a widespread phenomenon.

Future Work

This paper is part of a project that investigates the diagenesis of the Montney Formation. Future work will provide details on rock composition, diagenetic phases and the paragenetic sequence for the Montney Formation along a cross-section from the deep to shallow basin.

Conclusions

The Lower Triassic Montney Formation in the deep basin is composed of silt-size detrital and authigenic grains. Mixed-layer illite-smectite clay composes up to 30 wt. % of the rock. Diagenetic processes in the deep Montney Formation started with early burial and rock composition altered significantly over time. Dolomitization and feldspar alteration are the most volumetrically significant modifications. Both pore occluding and pore enhancing processes were observed, but porosity reduction processes are by far more substantial and significantly affect reservoir quality.

Acknowledgments

This work was supported by CMG Reservoir Simulation Foundation (Foundation CMG). The authors would like to thank M. Powers from SGS Canada Inc. for providing QEMSCAN® results and M. French for reviewing the manuscript. The authors would also like to warmly thank B. Jones for his comments and suggestions.

References

- Barber, L.M. (2003): Sedimentology, diagenesis and reservoir characterization of the Montney Formation at Sturgeon Lake South 'F' pool, west-central Alberta; M.Sc. thesis, University of Calgary, 557 p.
- BC Oil and Gas Commission (2016): Well lookup and reports; BC Oil and Gas Commission, web application, URL <<http://www.bcogc.ca/online-services>> [December 2016].
- Bennett, P. and Siegel, D.I. (1987): Increased solubility of quartz in water due to complexing by organic compounds; *Nature*, v. 326, p. 684–686.
- Brantley, S.L., Crane, S.R., Crerar, D.A., Hellmann, R. and Stallard, R. (1986): Dissolution at dislocation etch pits in quartz; *Geochimica et Cosmochimica Acta*, v. 50, p. 2349–2361.
- Burley, S.D. and Kantorowicz, J.D. (1986): Thin section and SEM textural criteria for the recognition of cement-dissolution porosity in sandstones; *Sedimentology*, v. 3, p. 587–604.
- Chalmers, G.R.L. and Bustin, R.M. (2012): Geological evaluation of Halfway-Doig-Montney hybrid gas shale-tight gas reservoir, northeastern British Columbia; *Marine and Petroleum Geology*, v. 38, p. 53–72.
- Crombez, V. (2016): Petrofacies, sedimentology and stratigraphic architecture of organic rich rocks. Insights from a multi-disciplinary study of the Montney and Doig formations (Lower and Middle Triassic, Alberta - British Columbia, Canada); Ph.D. thesis, Paris VI University, 238 p.
- Crombez, V., Baudin, F., Rohais, S., Riquier, L., Euzen, T., Pauthier, S., Mathieu, D., Caron, B. and Vaisblat, N. (2016): Basin scale distribution of organic matter in marine fine-grained sedimentary rocks: insight from sequence stratigraphy and multi-proxies analysis in the Montney and Doig formations; *Marine and Petroleum Geology*, in press, corrected proof, URL <<http://www.sciencedirect.com/science/article/pii/S0264817216303518>> [December 2016].
- Curtis, M.E., Ambrose, R.J., Sondergeld, C.H. and Rai, C.S. (2011): Transmission and scanning electron microscopy investigation of pore connectivity of gas shales on the nanoscale; Society of Petroleum Engineers, North American Unconventional Gas Conference and Exhibition, Woodlands, Texas, June 14–16, 2011, SPE-144391-MS, 10 p., URL <<https://www.onepetro.org/conference-paper/SPE-144391-MS>> [December 2016].
- Davies, G.R., Moslow, T.F. and Sherwin, M.D. (1997): The Lower Triassic Montney Formation, west-central Alberta; *Bulletin of Canadian Petroleum Geology*, v. 45, p. 474–505.
- Deep Times Maps Inc.TM (2013): North America 245 Ma Triassic (Early to Middle); Deep Times Maps Inc.TM, paleogeography map, URL <https://deeptimemaps.com/wp-content/uploads/2016/05/NAM_key-245Ma_ETri.png> [November 2016].
- Derder, O.M. (2012): Characterizing reservoir properties for the Lower Triassic Montney Formation based on petrophysical methods; M.Sc. thesis, University of Calgary, 231 p.
- Ducros, M., Euzen, T., Vially, R. and Sassi, W. (2014): 2-D basin modeling of the WCSB across the Montney-Doig system: implications for hydrocarbon migration pathways and unconventional resources potential; *in* Geoconvention 2014: Focus, Canadian Society of Petroleum Geologists, Canadian Society of Exploration Geophysicists, Canadian Well Logging Society, Joint Annual Meeting, Calgary, Alberta, May 12–14, 2014, abstract, 5 p. URL <http://www.geoconvention.com/archives/2014/185_GC2014_2D_basin_modeling_of_the_WCSB_across_the_Montney-Doig_system.pdf> [December 2016].
- Edwards, D.E., Barclay, J.E., Gibson, D.W., Kvill, G.E. and Halton, E. (1994): Triassic Strata of the Western Canada Sedimentary Basin; *in* Geological Atlas of the Western Canada Sedimentary Basin, G.D. Mossop and I. Shetsen (comp.), Canadian Society of Petroleum Geologists, Calgary, Alberta and Alberta Research Council, Edmonton, Alberta, p. 259–275.
- Freidman, G.M., Ali, S.A. and Krinsley, D.H. (1976): Dissolution of quartz accompanying carbonate precipitation and cementation in reefs: example from the Red Sea; *Journal of Sedimentary Research*, v. 46, p. 970–973.
- Georgiev, V.M. and Stoffers, P. (1980): Surface textures of quartz grains from late Pleistocene to Holocene sediments of the Persian Gulf/ Gulf of Oman - an application of the scanning electron microscope; *Marine Geology*, v. 36, p. 85–96.
- Gibson, D.W. and Barclay, J.E. (1989): Middle Absaroka Sequence - the Triassic Stable Craton; *in* Western Canada Sedimentary Basin - A Case History, B.D. Ricketts (ed.), Canadian Society of Petroleum Geologists, Special Publication No. 30, p. 219–232.
- Golding, M.L., Orchard, M.J., Zonneveld, J.P. and Wilson, N.S.F. (2015): Determining the age and depositional model of the Doig Phosphate Zone in northeastern British Columbia using conodont biostratigraphy; *Bulletin of Canadian Petroleum Geology*, v. 63, p. 143–170.
- Golonka, J., Ross, M.I. and Scotese, C.R. (1994): Phanerozoic paleogeographic and paleoclimatic modeling maps; *in* Pangea: Global Environments and Resources, A.F. Embry, B. Beauchamp and D.J. Glass (ed.), Canadian Society of Petroleum Geologists, Memoir no. 17, p. 1–48.
- Hurst, A. and Bjørkum, P.A. (1986): Thin section and SEM textural criteria for the recognition of cement-dissolution porosity in sandstones; *Sedimentology*, v. 33, p. 605–614.
- Knauss, K.G. and Wolery, T.J. (1988): The dissolution kinetics of quartz as a function of pH and time at 70°C; *Geochimica et Cosmochimica Acta*, v. 52, p. 43–53.
- LaMothe, J.T. (2008): Sedimentology, ichnology, stratigraphy and depositional history of the contact between the Triassic Doig and Montney formations in west-central Alberta, Canada: presence of an unconformity bound sand wedge; M.Sc. thesis, University of Alberta, 184 p.
- Moslow, T.F. and Zonneveld, J.-P. (2012): The Montney Formation; unpublished industry course notes, Calgary, Alberta, May 29–31, 2012.
- Nassichuk, B.R. (2000): Sedimentology, diagenesis and reservoir development of the Lower Triassic Montney Formation, northeastern BC; M.Sc. thesis, University of British Columbia, 151 p.
- National Energy Board (2013): Canada's energy future 2013, energy supply and demand projections to 2035; National Energy Board, report, 87 p., URL <<https://www.neb-one.gc.ca/nrg/ntgrtd/fttr/2013/2013nrgftr-eng.pdf>> [November 2016].
- Playter, T.L. (2013): Petrographic and X-ray microtomographic analysis of the upper Montney Formation, northeastern British Columbia, Canada; M.Sc. thesis, University of Alberta, 111 p.

- Robbins, D.J.C. (1999): Ichnology and palaeoenvironment of the Lower Triassic Montney Formation, Kaybob and Kaybob South Fields area, west-central Alberta; M.Sc. thesis, University of Alberta, 165 p.
- Tribovillard, N., Algeo, T.J., Lyons, T. and Riboulleau, A. (2006): Trace metals as paleoredox and paleoproductivity proxies: an update; *Chemical Geology*, v. 232, p. 12–32.
- Vaisblat, N. and Harris, N.B. (2016): A burial history model for the Montney Formation - an insight to porosity distribution and hydrocarbon migration; *in* Geoconvention 2016: Optimizing Resources, Canadian Society of Petroleum Geologists, Canadian Society of Exploration Geophysicists, Canadian Well Logging Society, Joint Annual Meeting, Calgary, Alberta, March 7–11, 2016, abstract, 1 p., URL <http://www.geoconvention.com/uploads/2016abstracts/278_GC2016_A_Burial_History_Model_for_the_Montney_Fm.pdf> [December 2016].
- Wahab, A.A. (1998): Diagenetic history of Cambrian quartzarenites, Ras Dib-Zeit Bay area, Gulf of Suez, eastern desert, Egypt; *Sedimentary Geology*, v. 121, p. 121–140.
- Zonneveld, J.-P., Gingrass, K.M. and Beatty, T.W. (2010a): Diverse ichnofossil assemblages following the P-T mass extinction, Lower Triassic, Alberta and British Columbia, Canada: evidence for shallow marine refugia on the north-eastern coast of Pangea; *PALAIOS*, v. 25, p. 368–392.
- Zonneveld, J.-P., MacNaughton, R.B., Utting, J., Beatty, T.W., Pemberton, S.G. and Henderson, C.M. (2010b): Sedimentology and ichnology of the Lower Triassic Montney Formation in the Pedigree-Ring/Border-Kahntah River area, northwestern Alberta, and northeastern British Columbia; *Bulletin of Canadian Petroleum Geology*, v. 58, p. 115–140.
- Zonneveld, J.-P., Golding, M., Moslow, T.F., Orchard, M.J., Playter, T. and Wilson, N. (2011): Depositional framework of the Lower Triassic Montney Formation, west-central Alberta and northeastern British Columbia; *in* recovery 2011, Canadian Society of Petroleum Geologists, Canadian Society of Exploration Geophysicists, Canadian Well Logging Society, Joint Annual Meeting, Calgary, Alberta, May 9–13, 2011, abstract, 4 p.

Implications of the Inorganic Geochemistry of Flowback Water from the Montney Formation, Northeastern British Columbia and Northwestern Alberta: Progress Report

J.N. Owen, The University of British Columbia, Vancouver, BC, jowen@eoas.ubc.ca

R.M. Bustin, The University of British Columbia, Vancouver, BC

Owen, J.N. and Bustin, R.M. (2017): Implications of the inorganic geochemistry of flowback water from the Montney Formation, northeastern British Columbia and northwestern Alberta: progress report; *in* Geoscience BC Summary of Activities 2016, Geoscience BC, Report 2017-1, p. 49–54.

Introduction

The development of unconventional oil and gas resources requires injections of large volumes of fluid at high pressures and rates, in order to hydraulically fracture the reservoir and hence create a system permeability high enough that hydrocarbons can be produced economically. Fracturing fluid, used in completions of the Montney Formation in the Western Canada Sedimentary Basin as well as almost all shale completions elsewhere, previously consisted mainly of freshwater as the base fluid. There is currently a trend to blend freshwater with flowback water from previously fractured wells and/or produced water from other wells to reduce freshwater usage. Much of the motivation for reducing freshwater usage during hydraulic fracturing is based on economics and real, or perceived, environmental issues related to depletion of freshwater resources.

The flowback water volume from hydraulic fracturing is generally significantly less than the injected volumes due to imbibition of the completion fluid into the reservoir matrix (i.e., Engelder et al., 2014). The actual amount of flowback fluid varies greatly between wells with most flowback volumes measuring significantly less than 25% (i.e., Haluszczak et al., 2013) of the injected fluid volume, although the actual values vary significantly and some wells flow back more fluid than the volumes injected.

The chemistry of the flowback water is a complex product of the volumes and chemistry of the injected completion fluid, reservoir connate water, plus reactions that occur between the fluids and the reservoir rock and tubulars. The flowback fluids thus provide important data and insights relevant to optimizing reservoir completions, and recognizing, preventing and/or remediating damage to the reservoir, fluid system, proppant pack and tubulars. Addition-

ally, knowledge of the chemistry and volumes of flowback water are critical to designing optimal blends for recycling, treatment and/or disposal of the fluids.

In support of the Geoscience BC–supported study on the controls on producible hydrocarbons in northeastern British Columbia (NEBC), a study of the flowback water chemistry from wells completed in the Montney Formation in NEBC and northwestern Alberta has been undertaken. To date, this study includes the collection of flowback samples, produced water samples (from selected wells) and ancillary information from 31 wells in six geographic areas (Figure 1). These studies have been made possible by close co-operation with industry. The sampled wells include

- 18 wells completed in the upper Montney Formation,
- 11 wells completed in the middle Montney Formation, and
- 2 wells completed in the lower Montney Formation.

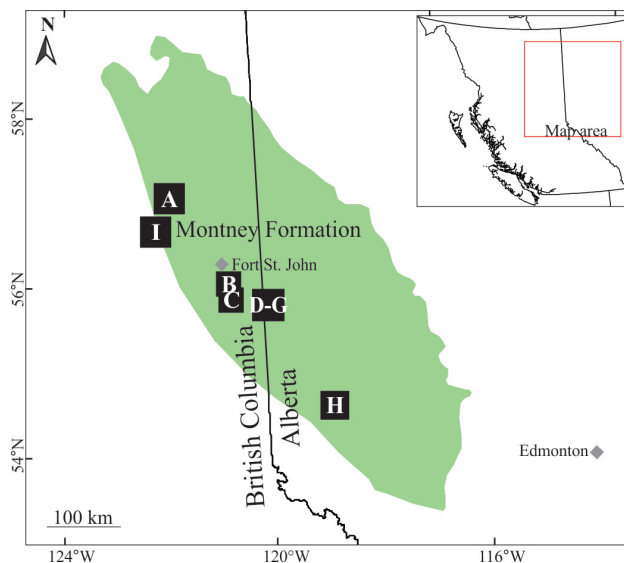


Figure 1. The location of the study sites in northeastern British Columbia and northwestern Alberta. The locations of the sites (A–I) are shown as black squares. The extent of the Montney Formation is shown in green (modified from Edwards et al., 1994).

Keywords: British Columbia, inorganic geochemistry, stable isotopes, hydraulic fracturing, flowback water, Montney Formation

This publication is also available, free of charge, as colour digital files in Adobe Acrobat® PDF format from the Geoscience BC website: <http://www.geosciencebc.com/s/DataReleases.asp>.

In this paper, some preliminary results will be provided and the nature of the ongoing work will be described.

Experimental Methods

Flowback water samples were collected on site throughout the flowback period, with more frequent sampling (2–3 samples per day) earlier in the flowback period and decreasing to one sample per day after the first week of sampling. The higher frequency of sampling earlier in the program allows for the capture of the higher variability in the initial flowback water. In addition to the flowback water samples, produced water samples were collected at two of the sites following the flowback period (sites A and B). The samples were stored at 4°C prior to analysis. As samples were not preserved on site, the samples were heated in a hot water bath back to reservoir temperature (~75–80°C) for 24 hours prior to subsampling. After heating, the samples were subsampled for 1) pH, conductivity and alkalinity analysis; 2) anion analysis; and 3) dissolved metals analysis. Prior to heating, a subsample was collected for stable water isotope analysis. The pH, conductivity and alkalinity tests were conducted at The University of British Columbia (UBC; Vancouver, BC) on filtered, unpreserved samples. The anion analysis is currently in progress at a commercial laboratory. The dissolved metal samples were filtered and preserved with nitric acid to pH <1. These samples were processed further by acid digestion in order to remove any organics in the fluid. The acid digestion process involved an initial step of adding trace metal grade nitric acid and hydrochloric acid in a 2:1 ratio to the sample and heating it on a hot plate until evaporated. This heating and evaporating step was then repeated with only nitric acid added to the sample. The dried sample was then rediluted in a 1% HNO₃ solution. The dissolved metals were measured using inductively coupled plasma–optical emission spectrometry (ICP-OES) and inductively coupled plasma–mass spectrometry (ICP-MS). The isotope samples were mixed with activated charcoal to remove organics and then filtered. These samples were run on a liquid-water isotope analyzer and analyzed for $\delta^{18}\text{O}$ and $\delta^2\text{H}$. The ICP-MS, ICP-OES and isotope analyses were conducted at laboratory facilities in the Department of Earth, Ocean and Atmospheric Sciences at UBC (Vancouver, BC).

In support of this study, an analysis of the hydraulic fracturing fluids was also completed. This generally involved creating a composite sample by combining the fluids used in different fracturing stages based on similar conductivity readings. The composite samples were then submitted for the same suite of analyses as the flowback and produced waters.

In addition to the geochemical analyses, a mineralogical analysis is also being undertaken. Core samples from adjacent wells (as the studied wells were not cored) are being

analyzed using X-ray diffraction. These results will be used to support the geochemical modelling.

Preliminary Results

General Parameters – pH, Alkalinity, Conductivity and Total Dissolved Solids

The pH of sampled flowback waters are typically near neutral (pH 6–8) and in general decrease over the flowback period. There is some variability in the flowback water from the site D wells completed in the upper Montney Formation, with values ranging from acidic (pH <4.5) to slightly basic (pH >9). In addition, produced waters from the two site B wells are slightly acidic (pH 4.6–5.7).

The alkalinity of the flowback fluids generally decreases over the flowback period. Overall, the flowback waters from the upper Montney Formation wells have low alkalinity with values remaining between 100 and 200 mg/L as CaCO₃. The early flowback water from the middle and lower Montney Formation can have alkalinity values up to 400 mg/L as CaCO₃.

Conductivity is high in the Montney Formation flowback water (Figure 2a–d). In flowback samples from the upper Montney Formation and the upper portion of the middle Montney Formation, the conductivity generally ranges from 50 to 200 millisiemens (mS) per cm (Figure 2a–c). The flowback water from the lower portion of the middle Montney Formation has lower conductivity with values below 100 mS/cm (Figure 2c). The conductivity in the flowback water from the lower Montney Formation ranges from approximately 15 mS/cm to approximately 130 mS/cm (Figure 2d).

The total dissolved solids (TDS) range, estimated from conductivity, for the upper Montney Formation flowback and the upper portion of the middle Montney Formation flowback is approximately 30 000–130 000 mg/L. Relative to these flowback waters, the TDS for flowback from the lower portion of the middle Montney Formation is lower with a range of 4500–65 000 mg/L. The flowback from one of the lower Montney Formation wells falls within this range with TDS values from 7000 to 55 000 mg/L, whereas the other lower Montney Formation well is higher (12 000–83 000 mg/L). These TDS values are approximate and once all of the anion results are available the TDS will be recalculated using all ion concentrations.

Major Cations

The major cations increase in abundance over the flowback period resulting in an increase in TDS. The dominant cation in all Montney Formation flowback water is Na. All Na concentrations in the flowback water samples are above 1000 mg/L and the maximum values in the different wells range from approximately 5000 to 50 000 mg/L (Figure 3a–d).

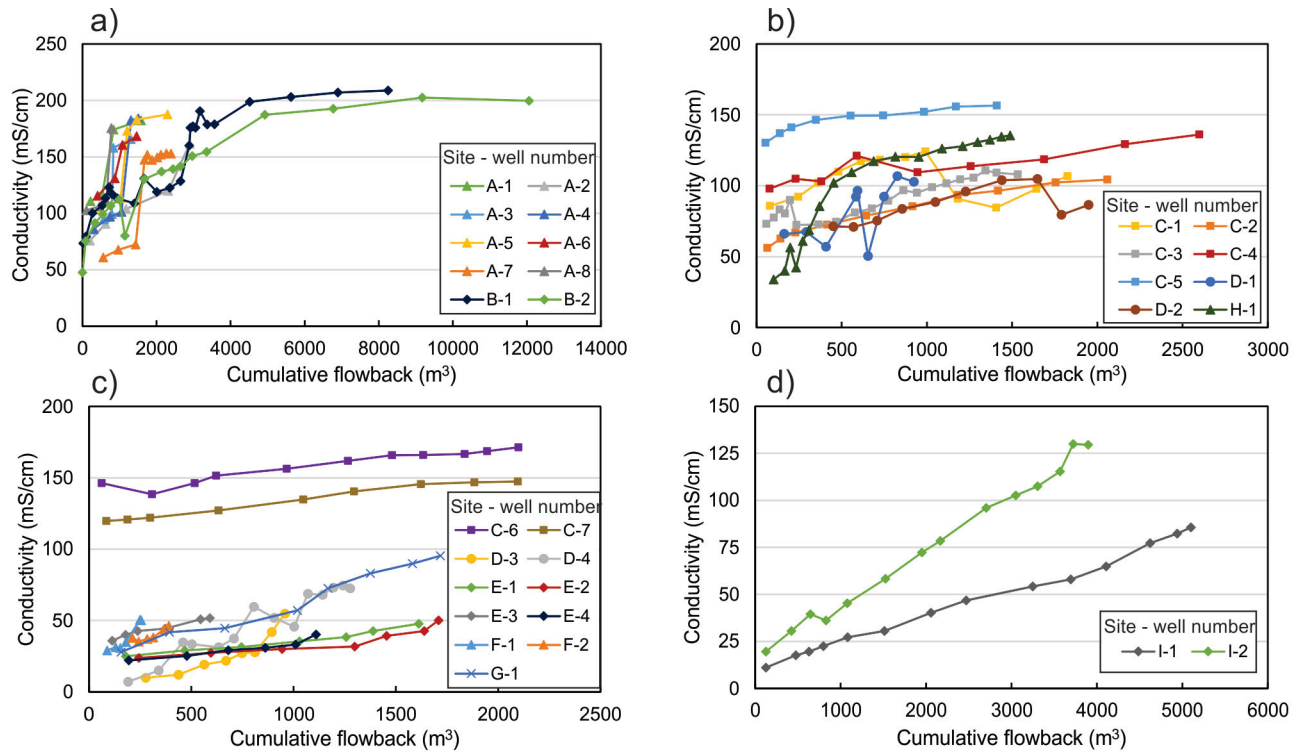


Figure 2. Conductivity in flowback water throughout the flowback period, from wells in northeastern British Columbia and northwestern Alberta: **a)** upper Montney Formation wells from sites A and B, includes both flowback and produced waters; **b)** upper Montney Formation wells from sites C, D, H; **c)** middle Montney Formation wells from sites C–G; and **d)** lower Montney Formation wells from site I. Note the variability in the scales. Abbreviation: mS, millisiemens.

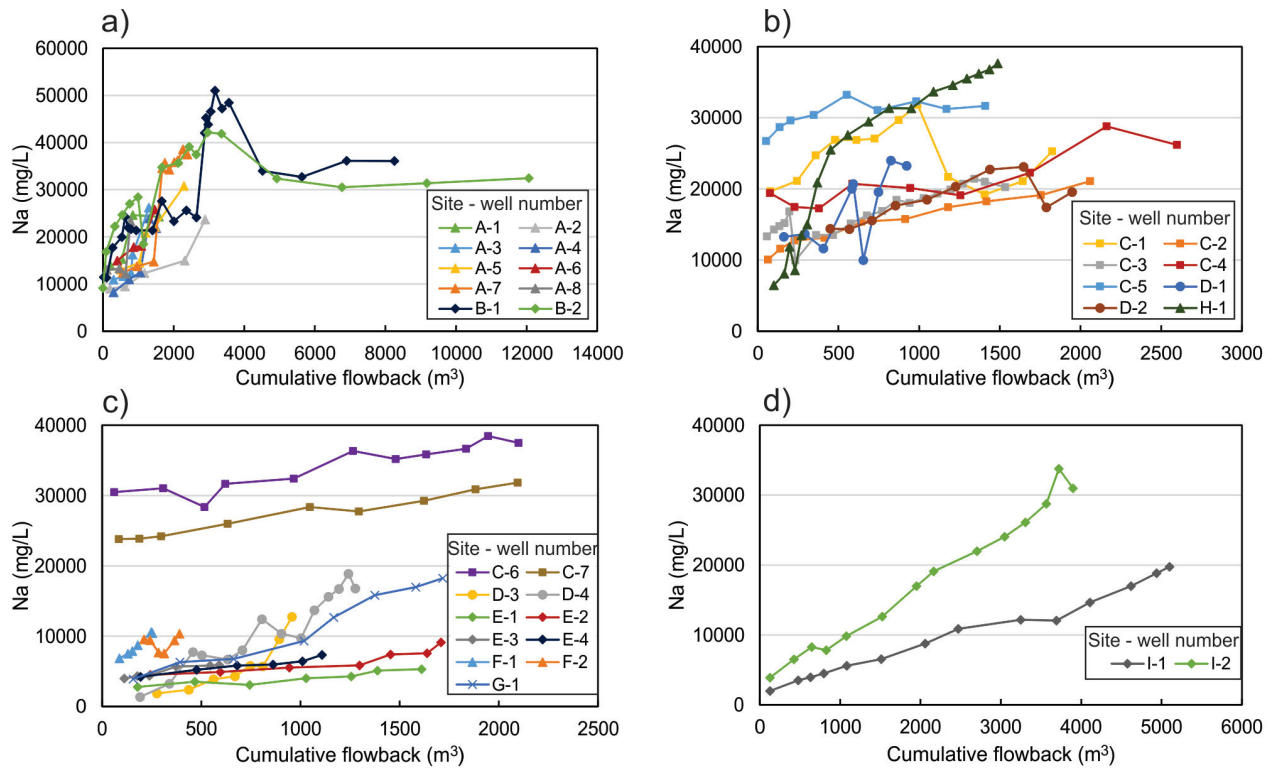


Figure 3. Concentrations of Na in flowback water throughout the flowback period, from wells in northeastern British Columbia and northwestern Alberta: **a)** upper Montney Formation wells from sites A and B, includes both flowback and produced waters; **b)** upper Montney Formation wells from sites C, D, H; **c)** middle Montney Formation wells from sites C–G; and **d)** lower Montney Formation wells from site I. Note the different scale for the y-axis in 3a.

Following Na, the order of elements from highest to lowest concentration is Ca, K, Mg and Sr. Concentrations of Sr are higher than Mg concentrations in flowback water from some wells. Concentrations of Ca range between 10 and 17 000 mg/L, with the majority of values below 10 000 mg/L. Concentrations of K, Mg and Sr remain below 2500 mg/L in all samples and are often much lower than this.

Variability in Major Cation Flowback Water Chemistry

In general, the major cation concentrations are higher in flowback water from wells in the upper Montney Formation and the upper portion of the middle Montney Formation. These wells have higher concentrations from the beginning of the flowback period onward relative to other wells completed in different stratigraphic intervals of the formation. The one area with wells completed in the lower portion of the middle Montney Formation has consistently lower major cation concentrations whereas the two lower Montney Formation wells, situated in the northwestern part of the study area, have intermediate concentrations. The flowback waters from the two lower Montney Formation wells initially have low TDS and low cation concentrations that are comparable to the early flowback water chemistry for the wells completed in the lower portion of the middle Montney Formation. However, the cation concentrations in

the lower Montney Formation flowback show a greater increase over the flowback period, most notably for Na, K and Sr (e.g., Na concentrations in Figure 3d).

Barium

Barium (Ba) concentrations display the greatest amount of variability in Montney Formation flowback water (Figure 4a–d). The Ba concentrations are low (<25 mg/L) at sites A, B and D–H, which include wells from both the upper and middle Montney Formation (Figure 4a, c). At site C, which is located in the same area as sites B and D–G, the Ba concentrations are higher (Figure 4b). The maximum Ba concentrations for both middle and upper Montney Formation flowback waters at this site are in the range of 200–300 mg/L. Similar Ba values are measured in the flowback water from the two wells completed in the lower Montney Formation at site I (Figure 4d). The concentrations at these two wells increase from <5 mg/L in early flowback up to maximum values of approximately 200 and 450 mg/L at the end of the flowback period. Initial results indicate that there is a negative correlation between Ba and sulphate. The site I wells initially have higher sulphate concentrations and the Ba concentrations only begin to increase once the sulphate values begin to decrease. Other wells that have consistently high sulphate concentrations (e.g., one well at site G and the site H well) have low Ba concentrations (<1.5 mg/L).

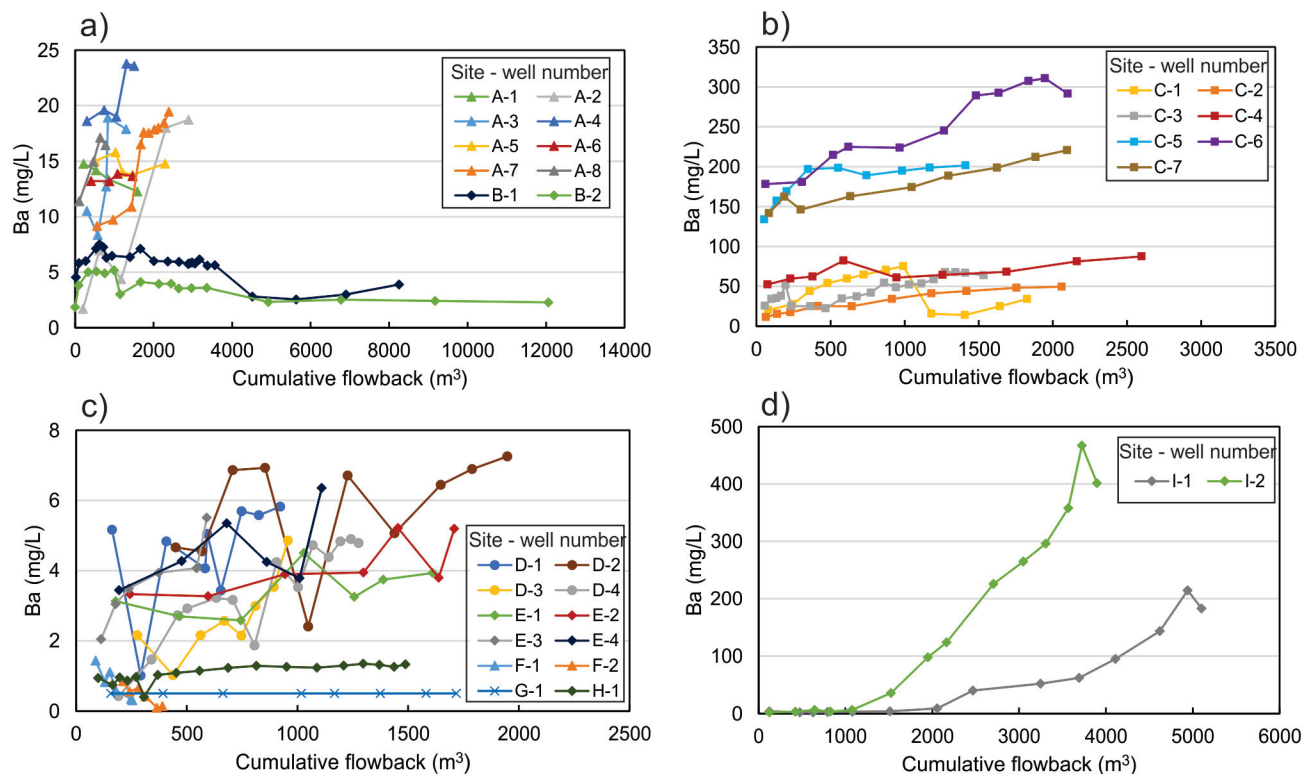


Figure 4. Concentrations of Ba in flowback water throughout the flowback period, from wells in northeastern British Columbia and northwestern Alberta: **a)** upper Montney Formation wells from sites A and B, includes both flowback and produced waters; **b)** upper and middle Montney Formation wells with high Ba concentrations from site C; **c)** upper and middle Montney Formation wells with low Ba concentrations from sites D–H; and **d)** lower Montney Formation wells from site I. Note the variability in the scales of the axes.

Currently, the sulphate results are only available for a limited number of wells as the anion analysis is still in progress. The relationship between Ba and sulphate will be investigated in more detail once the remaining sulphate data becomes available.

Isotopes of $\delta^{18}\text{O}$ and $\delta^2\text{H}$

The isotope analysis included an analysis of both the flowback water and the hydraulic fracturing fluids. The isotope values will supplement the inorganic geochemical data by providing additional information that can be used to estimate the connate water contribution to flowback water. Overall, the hydraulic fracturing fluids have $\delta^{18}\text{O}$ and $\delta^2\text{H}$ isotope values that plot on or close to the global meteoric water line (GMWL, defined as $\delta^2\text{H} = 8 \cdot \delta^{18}\text{O} + 10\text{‰}$; Figure 5). However, there are some samples that plot away from this line, which indicate the hydraulic fracturing fluids have a base of a blend of freshwater and recycled flowback water. Water produced from deep formations, including waters produced during hydraulic fracturing, typically have elevated $\delta^{18}\text{O}$ and $\delta^2\text{H}$ isotope values relative to meteoric water and results that plot to the right of the GMWL (i.e., Sharma et al., 2014; Rowan et al., 2015). The flowback waters analyzed as part of this study generally have values that plot away from the GMWL indicating mixing of the hydraulic fracturing fluid with another more saline end member (i.e., the connate water; Figure 5). The change in the isotope values of the flowback waters over time is interpreted to be due to mixing with connate water rather than water-rock interactions as the time for water-rock interactions (between the injected hydraulic fracturing fluid and the rock) is not sufficient to significantly change the isotopic signature of the water (Rowan et al., 2015).

Further Work

The work for this study is currently ongoing. Full anion results to complete the geochemical analysis are being run and compiled, after which detailed analysis of the chemistry of both the flowback waters and the hydraulic fracturing fluids will be completed. The full dataset will allow for further interpretation of the results, which will provide insight into the variability across the formation as well as assist with determining the sources of the ions in flowback water. The combined geochemical results of the flowback water and the hydraulic fracturing fluid from this study, along with the mineralogy from the X-ray diffraction analysis and existing produced water geochemical results, will be used for geochemical modelling to determine the dominant geochemical processes that are impacting the flowback water chemistry.

The results of this study will determine the variability in flowback water chemistry within the Montney Formation and contribute to the understanding of the geochemical

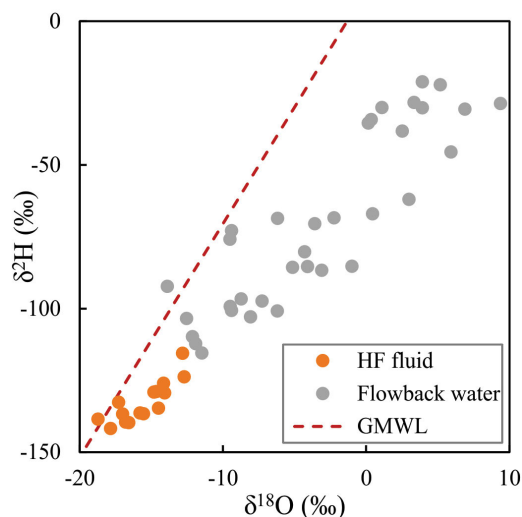


Figure 5. The $\delta^{18}\text{O}$ and $\delta^2\text{H}$ isotope values for hydraulic fracturing fluids and flowback waters from the eight wells at site A. Results for this site are provided as an example of the isotope results obtained as part of this study. The hydraulic fracturing (HF) fluid samples plot close to or slightly away from the global meteoric water line (GMWL). In general, the later flowback samples have higher values and plot farther to the right. The GMWL is plotted for reference.

processes that cause flowback water to change over time and to vary between different sites. Characterizing the flowback water chemistry in different areas of the Montney Formation will in turn assist in flowback water management for future oil and gas development in the region. Potential beneficial outcomes related to the geochemical analysis undertaken in this study include optimizing the selection of hydraulic fracturing fluid chemical additives when recycling flowback water and determining the ideal mixing ratios to use in the make-up water for future hydraulic fracturing jobs.

Acknowledgments

The authors would like to thank ARC Resources Ltd., Black Swan Energy Ltd., Unconventional Gas Resources, and other companies, which wish to remain anonymous, for collecting the samples and providing other data in support of this study. Geoscience BC is also thanked for the funding provided in support of this study. This manuscript benefited from review by S. Hazell.

References

- Edwards, D.E., Barclay, J.E., Gibson, D.W., Kvill, G.E. and Halton, E. (1994): Triassic strata of the Western Canada Sedimentary Basin; *in* Geological Atlas of the Western Canada Sedimentary Basin, G.D. Mossop and I. Shetsen (comp.), Canadian Society of Petroleum Geologists and Alberta Research Council, Edmonton, Alberta, p. 257–275, URL <<http://ags.aer.ca/publications/chapter-16-triassic-strata.htm>> [October 2016].

- Engelder, T., Cathles, L.M. and Bryndzia, L.T. (2014): The fate of residual treatment water in gas shale; *Journal of Unconventional Oil and Gas Resources*, v. 7, p. 33–48.
- Haluszczak, L.O., Rose, A.W. and Kump, L.R. (2013): Geochemical evaluation of flowback brine from Marcellus gas wells in Pennsylvania, USA; *Applied Geochemistry*, v. 28, p. 55–61.
- Rowan, E.L., Engle, M.A., Kraemer, T.F., Schroeder, K.T., Hammack, R.W. and Doughten, M.W. (2015): Geochemical and isotopic evolution of water produced from Middle Devonian Marcellus shale gas wells, Appalachian basin, Pennsylvania; *American Association of Petroleum Geologists, AAPG Bulletin*, v. 99, no. 2, p. 181–206.
- Sharma, S., Mulder, M.L., Sack, A., Schroeder, K. and Hammack, R. (2014): Isotope approach to assess hydrologic connections during Marcellus shale drilling; *Groundwater*, v. 52, no. 3, p. 424–433.

Preliminary Report on Hydration-Induced Swelling of Shale in the Horn River Basin, Northeastern British Columbia

A. Gupta, University of Alberta, Edmonton, AB, aadish@ualberta.ca

M. Xu, University of Alberta, Edmonton, AB

H. Dehghanpour, University of Alberta, Edmonton, AB

D. Bearinger, Nexen Energy ULC, Calgary, AB

Gupta, A., Xu, M., Dehghanpour, H. and Bearinger, D. (2017): Preliminary report on hydration-induced swelling of shale in the Horn River Basin, northeastern British Columbia; *in* Geoscience BC Summary of Activities 2016, Geoscience BC, Report 2017-1, p. 55–62.

Introduction

In the past decade, multistage hydraulic fracturing has become an essential completion technique, resulting in prolific development of low-permeability sandstone and shale reservoirs. Although such reservoirs are found to be abundant in many parts of the world, most of the developed ones are found in major North American basins (Energy Information Administration, 2013; Charlez, 2015). The practice of multistage hydraulic fracturing involves pumping water or oil-based fluids at high pressure to create fracture networks in low-permeability rocks. As a result, a significant amount of water is used in such an operation (King, 2012, 2014). The range in volumes of water used for fracturing treatments varies significantly among formations. However, it is widely reported that up to 80% of the water pumped during a fracturing treatment is typically not recovered when the well is put back on production (Fan et al., 2010; King, 2012; Tipton, 2014).

Poor water recovery is attributed partly to spontaneous or forced imbibition of water into the rock matrix and clay system, particularly in clay-rich rocks (Makhanov et al., 2012; Roychaudhuri et al., 2013; Lan et al., 2014). Major mechanisms responsible for the spontaneous water uptake by shale rocks are high capillary suction (due to nanometre-size pores) due to sub-irreducible water saturation, diffusion, advection and surface-osmotic hydration (Al-Bazali, 2005; Zhang, 2005; Ghanbari, 2015; Roshan et al., 2016). Clay-rich shale can act as a membrane when immersed in water with lower ion concentration. This produces an osmotic potential (Zhang et al., 2004; Al-Bazali, 2005; Ghanbari and Dehghanpour, 2014). In addition to osmosis, diffusion results in ion transport in and out of the shale rock

(Al-Bazali, 2005; Zhang, 2005; Ghanbari, 2015). This causes a change in electrical conductivity of the fluid.

Earlier studies examined the physicochemical changes that occur as a result of clay hydration in shales, but mostly in the context of drilling engineering. Chenevert (1970) conducted a comprehensive study on hydration of shales from various formations in the United States. He found that hydration of shales resulted in tensile stress and expansion in all rock samples. Adsorption of water by clay minerals also reduced the overall strength in his shale rock samples, which can be detrimental for wellbore-stability applications (Chenevert, 1970; Bol et al., 1994). In subsequent studies on shale hydration, researchers developed swelling or hydration indices to compare the swelling potential of various shales (Bol, 1986; Hayatdavoudi, 1999).

Recent studies have also connected the concept of clay hydration to wettability. Significantly higher uptake of water than of oil by oil-wet gas shales of the Horn River (HR) Basin has been attributed to water adsorption by clay minerals (Dehghanpour et al., 2012; Dehghanpour et al., 2013). Anisotropy in water imbibition, swelling stress and expansion, have also been shown as characteristics of laminated mudstones (Ghanbari and Dehghanpour, 2014; Makhanov et al., 2014). Furthermore, fabric changes, such as induced tensile microfractures and sample expansion have also been observed during imbibition (Dehghanpour et al., 2013; Ghanbari and Dehghanpour, 2014; Yang et al., 2015). Ghanbari and Dehghanpour (2014) reported a reduced spontaneous imbibition of water into samples confined with epoxy, raising questions on how much tensile stress and resultant expansion can be generated from hydration.

Furthermore, in the context of geomechanics, rock elastic properties (Young's modulus and Poisson's ratio) from laboratory compression tests are widely used as key inputs in creating hydraulic-fracture design models (Lacy, 1997; Dunphy and Campagna, 2011; Dong, 2016). However, most compression tests for unconventional rock samples in

Keywords: British Columbia, hydraulic fracturing optimization, soaking of gas shale, hydration-induced tensile stress, expansion of clay-rich shale, clay swelling, Horn River shales

This publication is also available, free of charge, as colour digital files in Adobe Acrobat® PDF format from the Geoscience BC website: <http://www.geosciencebc.com/s/DataReleases.asp>.

the laboratory still follow the workflow for conventional rocks. This workflow does not account for hydration-induced tensile stresses due to clay swelling. Incorporating hydration-induced stress and strain into geomechanical models can result in more realistic models for hydraulic fracturing.

Research Objectives

The goals of this study are to 1) extend previous work on water uptake of HR Basin shales and quantify its hydration-induced stress and expansion characteristics, 2) investigate the effects of fluid chemistry on water uptake and swelling, and 3) investigate the effects of hydration-induced stress and strain on enhancement of hydrocarbon production. In this paper are presented the preliminary results of the most direct measurements of hydration-induced tensile stress and strain in HR Basin shales.

Methodology

A three-step approach is taken to investigate the effects of hydration in the rock samples. Total water uptake by gas shales is due to a combination of high capillarity of nanopores and adsorption by clay minerals (Dehghanpour et al., 2012). Hence, all measurements will be linked to spontaneous imbibition and rock-mineralogy data.

In the first phase, spontaneous water- and oil-imbibition experiments are conducted on the shale samples. The purpose of the water-imbibition experiments is to obtain a relationship between the amount of ions that leach out of the sample and the mass of fluid that imbibe into the sample. By recording the imbibed mass and change in electrical conductivity, an imbibed mass–electrical conductivity crossplot (IM-EC crossplot) can be created to be used in phase 3. Imbibition and electrical conductivity are normalized to the mass of rock sample used. Comparisons are made between the imbibition of water and oil.

In the second phase, the expansion of the shale samples is measured during imbibition. During water imbibition, expansion is measured parallel and perpendicular to the plane of lamination, whereas expansion is measured only perpendicular to the plane of lamination for oil imbibition. This test does not restrain the sample, meaning the sample is free to expand during imbibition in customized imbibition cell 1 (described in the ‘Materials and Equipment’ section). Strain is computed from the displacement (as measured) and original length of the rock sample. The imbibition data from phase 1 are used to correlate the strain with the imbibed mass of fluid.

During the third phase, the hydration-induced tensile stress is measured in the samples when they are immersed in deionized water. Customized imbibition cell 2 (described in the ‘Materials and Equipment’ section) allows for the re-

striction of axial expansion and concurrent measurement of the expansive force generated by rock samples during imbibition of water. This test gives the hydration-induced tensile force with respect to the soaking time. Axial stress is computed from the force (as measured by the load cell) and the cross-sectional area of the rock sample. This phase will be extended by measuring the hydration-induced tensile stress (and change in water-uptake profile) of rock samples subjected to a constant axial compressive load during imbibition.

Since the sample is under an axial restraint, further fluid imbibition may be hindered as tensile force accumulates (Chenevert, 1970; Ghanbari and Dehghanpour, 2014). As a result, the imbibition profile in this test may not resemble that of a sample under zero accumulated-stress conditions (phase 1). Therefore, it is also of interest to determine the imbibed fluid mass that results in the recorded tensile force. However, the rock samples cannot be removed from the cell during the tests in this phase because that would create perturbation in the state of stress. To mitigate this problem, the electrical conductivity of the aqueous phase surrounding the rock sample in the imbibition cell is measured periodically. Subsequently, the electrical conductivity (normalized to the mass of the rock sample) is correlated with the imbibed mass of water using the IM-EC crossplot from phase 1.

Materials and Equipment

Core Samples

The core samples used in this study come from a well drilled in the Horn River Basin of northeastern British Columbia (BC). Figure 1a shows a geographic overview of Western Canada, indicating the Horn River Basin. Figure 1b shows the major formations of the Middle Devonian Elk Point Group in the Horn River Basin, with the three zones of interest outlined in red.

Tests are planned on rock samples from two formations of the Horn River Basin: the Muskwa (MU) and Horn River (HR) formations (Figure 1b). The Muskwa Formation is a siliceous pyritic shale with moderate to high total organic carbon (TOC). The Horn River Formation is further divided into the Otter Park (OP) and Evie (EV) members, both of them mid-Devonian shale units (Mossop and Shetsen, 1994; Hulsey, 2011; BC Oil and Gas Commission, 2014; Dong, 2016). The OP is a medium- to dark-grey, slightly calcareous mudstone with a lower TOC than the EV (McPhail et al., 2008). The EV is a dark grey to black shale with a higher average TOC than the MU and OP (Mossop and Shetsen, 1994; McPhail et al., 2008; Hulsey, 2011; BC Oil and Gas Commission, 2014; Dong, 2016). All MU and HR shales are brittle and exhibit strong fissility, mostly along the plane of lamination (Figure 2).



Figure 2: Shale sample from the Evie (EV) Member of the Horn River Formation, showing fissility along the plane of lamination, and natural and induced fractures.

Twenty-one samples are to be used in this study (seven each from the MU, OP and EV). Table 1 gives the depth, porosity and permeability for each sample. Representative mineralogy of powdered rock measured by X-ray diffraction (XRD) is shown in Table 2.

Rock samples used in all phases of this study were oven dried at 250°F to evaporate both capillary and clay-bound water (Luffel and Guidry, 1992). This ensures that all samples start at a similar water saturation (as capillary water evaporates first, followed by the water molecules electrostatically bound to the clay). Early water uptake by dried samples results from a combination of capillarity and adsorption by clay minerals. Hence, the oven-dried state of the samples provides the opportunity to capture the trends of imbibition and hydration swelling early in the soaking process.

Equipment

During the first phase, imbibition cells (Figure 3) are used to fully immerse the rock sample in water. A portable electrical-conductivity meter and mass balance are used to record the electrical conductivity and mass, respectively, of the rock sample during imbibition.

In the second phase, the rock sample is placed inside the glass chamber of a customized imbibition cell 1 (CIC-1; Figure 4), which is then filled with fluid until the rock is completely submerged. This cell is equipped with a linear variable differential transformer (LVDT) mounted on the side wall of the imbibition chamber. Stabilizer mounts prevent lateral movement of the rock sample. Any axial expansion

Table 1: Approximate depth, porosity and permeability of samples used in this study.

Sample ID	Approximate depth (m)	Formation/ member	Average porosity (%)	Average permeability (nD)
MU-1	2610	Muskwa	2.92	180
MU-2				
MU-3				
MU-4				
MU-5				
MU-6				
MU-7				
OP-1	2617	Horn River / Otter Park	3.25	271
OP-2				
OP-3				
OP-4				
OP-5				
OP-6				
OP-7				
EV-1	2681	Horn River / Evie	4.17	384
EV-2				
EV-3				
EV-4				
EV-5				
EV-6				
EV-7				

Table 2: Representative mineralogy of powdered shale samples from the Muskwa Formation (MU) and the Evie (EV) and Otter Park (OP) members of the Horn River Formation, as measured by X-ray diffraction.

Sample	Mineral (wt. %)								Total clay
	Quartz	K-feldspar	Plagioclase	Carbonate	Pyrite	Illite/smectite	Illite/mica	Kaolinite	
MU	65	3	3	10	3	5	11	0	16
EV	52	5	6	16	3	7	12	0	19
OP	76	0	3	6	3	4	9	0	13

sion exhibited by the rock causes a displacement of the LVDT core. The LVDT and its data acquisition system are set to acquire the displacement data every 10 seconds.

For the third phase, a specialized setup (customized imbibition cell 2) was designed to measure the hydration-induced tensile stress during spontaneous imbibition of fluid (Figure 5). Customized imbibition cell 2 (CIC-2) consists of an imbibition cell housed inside a load frame. The rock sample is placed in the imbibition cell filled with water. The sample is overlain by a circular spacer disk and a circular through-hole load cell. The spacer disk prevents rusting and damage to the load cell by eliminating direct physical contact between the fluid and the load cell. The shaft of the load frame firmly attaches into the through-hole load cell. At this point, from bottom to top, the rock sample, spacer disk, load cell and shaft are in rigid vertical alignment. This system prevents any axial expansion of the rock sample during the tests. Axial restraint at the top and bottom ends of the rock sample allows the swelling force generated within the rock sample to be directed toward the load cell. In addition to the axial restraint, the load frame allows for a constant compressive load to be applied to the rock sample through controlled downward motion of the shaft. Once the desired compressive load is reached, the shaft remains locked in position until manually unscrewed. The data acquisition

system and associated computer program are set up to acquire the force on the load cell every 10 seconds. The portable electrical-conductivity meter from phase 1 is used to periodically measure the electrical conductivity of the fluid.

Experiments

This section describes the experiments for each phase. Table 3 summarizes the experiments to be performed on each rock sample.

Phase 1

Spontaneous imbibition experiments are conducted with water and kerosene on nine shales samples (three each from MU, OP and EV) for 7 days, to obtain three sets of imbibition data. The first and second sets of data (with water and kerosene, respectively) are used in conjunction with the free-expansion results (phase 2). The third set of imbibition data (with water), which includes electrical conductivity of the fluid, is used in phase 3.

Phase 2

Three sets of free-expansion experiments are conducted on MU, OP and EV rock samples. The first and second sets of experiments are carried out with water and kerosene, re-



Figure 3: Imbibition cells used in phase 1. Rock samples were immersed in aqueous or oleic phases. Change in mass of the rock samples and electrical conductivity of the fluid (for aqueous-phase experiments) were recorded periodically.

spectively. Rock samples are placed in the customized imbibition cell 1 such that planes of lamination are horizontal. Hence, the LVDT measures axial expansion along the direction perpendicular to the plane of laminations. The third set of experiments, carried out with water, are rotated 90° to align the axis of LVDT parallel to the plane of laminations. This arrangement measures axial expansion parallel to the plane of laminations.

Phase 3

One sample each from MU, OP and EV is tested for hydration-induced tensile stress. Force is measured in the direction perpendicular to the plane of laminations.

Preliminary Results and Future Work

From the rock samples tested thus far, it is apparent that imbibition-induced microfractures observed in previous stud-

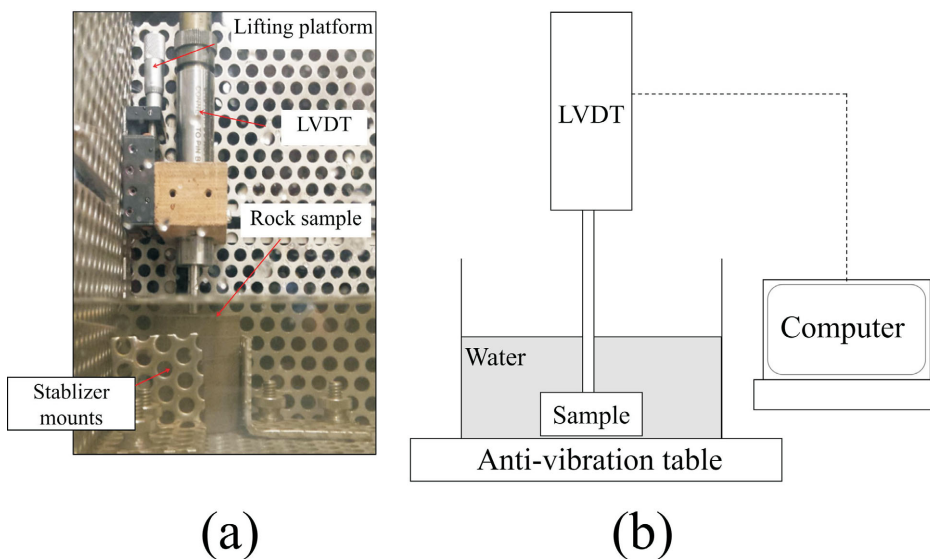


Figure 4: Photo (a) and schematic diagram (b) of customized imbibition cell 1, used in phase 2 of this study. The linear variable differential transformer (LVDT) records the axial displacement of the rock sample during imbibition.

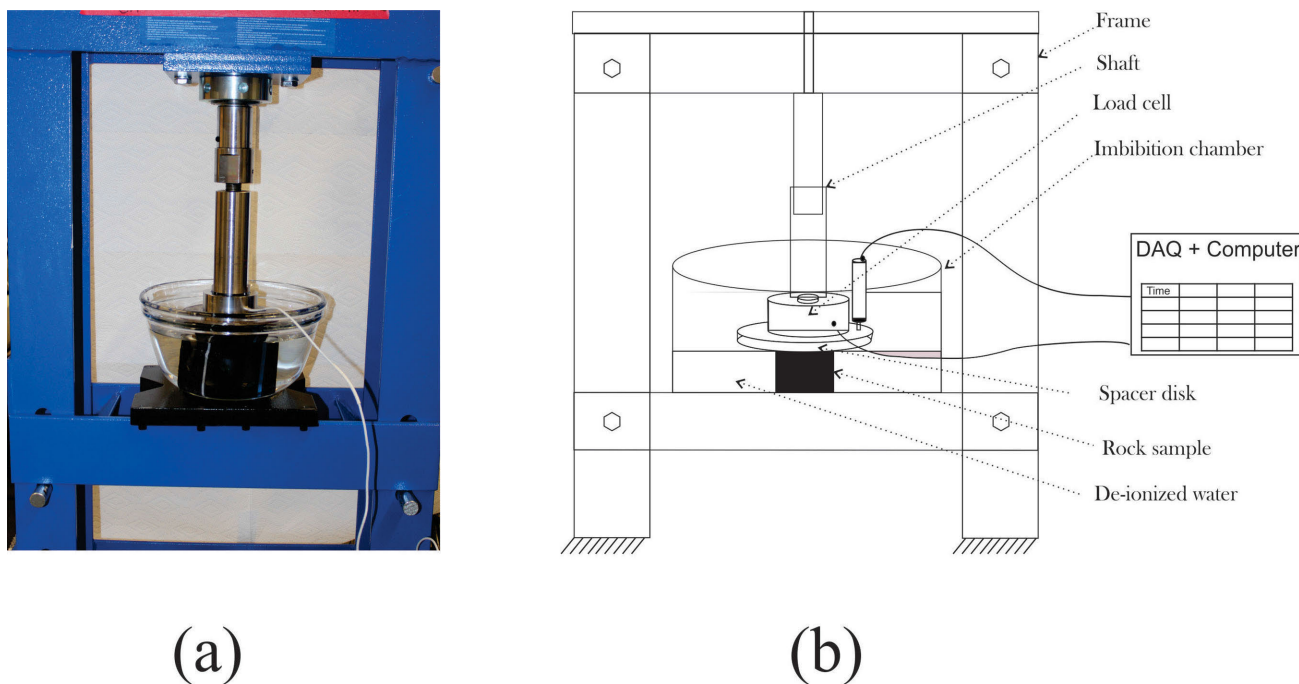


Figure 5: Photo (a) and schematic diagram (b) of customized imbibition cell 2, used in phase 3 of this study. The load cell measures the expansive (tensile) force generated by the rock sample during imbibition.

Table 3: Experiments to be performed on each rock sample.

Sample ID	Experiment	Test direction	Fluid
MU-1	Imbibition	-	Water
MU-2	Imbibition	-	Oil
MU-3	Imbibition + conductivity	-	Water
MU-4	Hydration stress	Perpendicular to lamination	Water
MU-5	Free expansion	Perpendicular to lamination	Water
MU-6	Free expansion	Perpendicular to lamination	Oil
MU-7	Free expansion	Parallel to lamination	Water
OP-1	Imbibition	-	Water
OP-2	Imbibition	-	Oil
OP-3	Imbibition + conductivity	-	Water
OP-4	Hydration stress	Perpendicular to lamination	Water
OP-5	Free expansion	Perpendicular to lamination	Water
OP-6	Free expansion	Perpendicular to lamination	Oil
OP-7	Free expansion	Parallel to lamination	Water
EV-1	Imbibition	-	Water
EV-2	Imbibition	-	Oil
EV-3	Imbibition + conductivity	-	Water
EV-4	Hydration stress	Perpendicular to lamination	Water
EV-5	Free expansion	Perpendicular to lamination	Water
EV-6	Free expansion	Perpendicular to lamination	Oil
EV-7	Free expansion	Parallel to lamination	Water

ies can, in fact, result in measurable expansion of rock samples. Strain of up to 0.75% is observed in the free-expansion imbibition cell (CIC-1). Expansion anisotropy is observed in directions parallel to and perpendicular to the plane of lamination. When the expansion is restricted, tensile stress of up to 18 psi accumulates in the samples, due to hydration (CIC-2). Rock samples will be tested under various added axial-compressive loads to investigate any changes in water-imbibition behaviour and accumulation of tensile stress. More samples will be incorporated into this study to assess the effect of fluid salinity on imbibition, expansion and tensile stress. It is projected that the work will be concluded by August 2017.

Acknowledgments

This research is supported by Nexen Energy ULC, the Natural Sciences and Engineering Research Council of Canada (NSERC) and Natural Resources Canada. The first author is grateful to Geoscience BC for a graduate study award. The authors also thank O. Ezulike, Y. Fu and Y. Xu for their reviews of this paper.

References

Al-Bazali, T.M., 2005. Experimental study of the membrane behavior of shale during interaction with water-based and oil-based muds; Ph.D. thesis, The University of Texas at Austin.

BC Ministry of Energy and Mines and National Energy Board (2011): Ultimate potential for unconventional natural gas in northeastern British Columbia's Horn River Basin; BC Ministry of Energy and Mines and National Energy Board, Oil and Gas Report 2011-1, <<https://www.neb-one.gc.ca/nrg/sttstc/ntrlgs/rprt/archive/ncnvtntnltrlgshrnrvrbsnhrrvr2011/ncnvtntnltrlgshrnrvrbsnhrrvr2011-eng.pdf>> [November 2016].

BC Oil and Gas Commission (2014): Horn River Basin unconventional shale gas play atlas; BC Oil and Gas Commission, <<https://www.bcogc.ca/node/11238/download>> [November 2016].

Bol, G.M. (1986): The effect of various polymers and salts on borehole and cutting stability in water-base shale drilling fluids; SPE/IADC Drilling Conference, Dallas, Texas, February 9–12, 1986, Paper SPE-14802-MS, URL <<https://www.onepetro.org/conference-paper/SPE-14802-MS>> [November 2016].

Bol, G.M., Wong, S.W., Davidson, C.J. and Woodland, D.C. (1994): Borehole stability in shales; SPE Drilling & Completion, v. 09, no. 2, URL <<https://www.onepetro.org/journal-paper/SPE-24975-PA>> [November 2016].

Charlez, P.A. (2015): How to export the unconventional revolution out of North America?; 12th Offshore Mediterranean Conference and Exhibition 2015, Ravenna, Italy, March 25–27, 2015, Paper OMC-2015-226, URL <<https://www.onepetro.org/conference-paper/OMC-2015-226>> [November 2016].

Chenevert, M.E. (1970): Shale alteration by water adsorption; Journal of Petroleum Technology, v. 22, no. 9, Paper SPE-2401-PA, URL <<https://www.onepetro.org/journal-paper/SPE-2401-PA>> [November 2016].

Dehghanpour, H., Lan, Q., Saeed, Y., Fei, H. and Qi, Z. (2013): Spontaneous imbibition of brine and oil in gas shales: effect of water adsorption and resulting microfractures; Energy & Fuels, v. 27, no. 6, p. 3039–3049, <<http://pubs.acs.org/doi/abs/10.1021/ef4002814>> [November 2016].

Dehghanpour, H., Zubair, H.A., Chhabra, A. and Ullah, A. (2012): Liquid intake of organic shales; Energy & Fuels, v. 26, no. 9, p. 5750–5758, <<http://pubs.acs.org/doi/abs/10.1021/ef3009794>> [November 2016].

Dong, T. (2016): Geochemical, petrophysical and geomechanical properties of stratigraphic sequences in Horn River Shale, Middle and Upper Devonian, northeastern British Columbia, Canada; Ph.D. thesis, Department of Earth and Atmospheric Sciences, University of Alberta.

- Dunphy, R. and Campagna, D. (2011): Fractures, elastic moduli & stress: geological controls on hydraulic fracture geometry in the Horn River Basin; CSPG/CSEG/CWLS GeoConvention 2011, Calgary, Alberta, <http://www.cspg.org/documents/Conventions/Archives/Annual/2011/154-Fractures_Elastic_Moduli_and_Stress.pdf> [November 2016].
- Energy Information Administration (2013): Technically recoverable shale oil and shale gas resources: an assessment of 137 shale formations in 41 countries outside the United States; United States Department of Energy, Energy Information Administration, <<http://www.eia.gov/analysis/studies/worldshalegas/pdf/overview.pdf>> [November 2016].
- Fan, L., Thompson, J.W. and Robinson, J.R. (2010): Understanding gas production mechanism and effectiveness of well stimulation in the Haynesville Shale through reservoir simulation; Canadian Unconventional Resources and International Petroleum Conference 2010, Calgary, Alberta, October 19–21, 2010, Paper SPE-136696-MS, URL <<https://www.onepetro.org/conference-paper/SPE-136696-MS>> [November 2016].
- Ferri, F., Hickin, A.S. and Huntley, D.H. (2011): Besa River Formation, western Liard Basin, British Columbia (NTS 094N): geochemistry and regional correlations; in Geoscience Reports 2011, BC Ministry of Energy and Mines, p. 1–18, <http://www2.gov.bc.ca/assets/gov/farming-natural-resources-and-industry/natural-gas-oil/petroleum-geoscience/geoscience-reports/2011/2011_ferri1_besa.pdf> [November 2016].
- Ghanbari, E. (2015): Water imbibition and salt diffusion in gas shales: a field and laboratory study; M.Sc. thesis, Department of Civil and Environmental Engineering, University of Alberta.
- Ghanbari, E. and Dehghanpour, H. (2014): Impact of rock fabric on water imbibition and salt diffusion in gas shales; International Journal of Coal Geology, v. 138, p. 55–67, URL <<http://www.sciencedirect.com/science/article/pii/S0166516214002286>> [November 2016].
- Hayatdavoudi, A. (1999): Changing chemophysical properties of formation and drilling fluid enhances penetration rate and bit life; SPE International Symposium on Oilfield Chemistry, Houston, Texas, February 16–16, 1999, Paper SPE-50729-MS, <<https://www.onepetro.org/conference-paper/SPE-50729-MS>> [November 2016].
- Hulseay, K. (2011): Lithofacies characterization and sequence stratigraphic framework for some gas-bearing shales within the Horn River Basin, northeastern British Columbia; M.Sc. thesis, Department of Geology and Geophysics, University of Oklahoma.
- King, G.E. (2012): Hydraulic fracturing 101: what every representative, environmentalist, regulator, reporter, investor, university researcher, neighbor, and engineer should know about hydraulic fracturing risk; Journal of Petroleum Technology, v. 64, no. 4, <<https://www.onepetro.org/conference-paper/SPE-152596-MS>> [November 2016].
- King, G.E. (2014) 60 years of multi-fractured vertical, deviated and horizontal wells: what have we learned?; SPE Annual Technical Conference and Exhibition, Amsterdam, The Netherlands, October 27–29, 2014, Paper SPE-170952-MS, URL <<https://www.onepetro.org/conference-paper/SPE-170952-MS>> [November 2016].
- Lacy, L.L. (1997): Dynamic rock mechanics testing for optimized fracture designs; SPE Annual Technical Conference and Exhibition, San Antonio, Texas, October 5–8, 1997, Paper SPE-38716-MS, URL <<https://www.onepetro.org/conference-paper/SPE-38716-MS>> [November 2016].
- Lan, Q., Ghanbari, E., Dehghanpour, H. and Hawkes, R. (2014): Water loss versus soaking time: spontaneous imbibition in tight rocks; Energy Technology, v. 2, p. 1033–1039. doi:10.1002/ente.201402039
- Luffel, D.L., and Guidry, F.K. (1992): New core analysis methods for measuring reservoir rock properties of Devonian shale; Journal of Petroleum Technology, v. 44, no. 11, URL <<https://www.onepetro.org/journal-paper/SPE-20571-PA>> [November 2016].
- Makhanov, K., Dehghanpour, H. and Kuru, E. (2012): An experimental study of spontaneous imbibition in Horn River shales; SPE Canadian Unconventional Resources Conference, Calgary, Alberta, October 30–November 1, 2012, Paper SPE-162650-MS, URL <<https://www.onepetro.org/conference-paper/SPE-162650-MS>> [November 2016].
- Makhanov, K., Habibi, A., Dehghanpour, H. and Kuru, E. (2014): Liquid uptake of gas shales: a workflow to estimate water loss during shut-in periods after fracturing operations; Journal of Unconventional Oil and Gas Resources, v. 7, p. 22–32, URL <<http://www.sciencedirect.com/science/article/pii/S221339761400024X>> [November 2016].
- McPhail, S., Walsh, W., Lee, C. and Monahan, P. (2008): Shale units of the Horn River Formation, Horn River Basin and Cordova Embayment, northeastern British Columbia; BC Ministry of Energy and Mines, <<http://www2.gov.bc.ca/assets/gov/farming-natural-resources-and-industry/natural-gas-oil/petroleum-geoscience/petroleum-open-files/pgof20081.pdf>> [November 2016].
- Mossop, G.D. and Shetsen, I., compilers (1994): Geological atlas of the Western Canada Sedimentary Basin; Canadian Society of Petroleum Geologists, Calgary, Alberta and Alberta Research Council, Edmonton, Alberta, 510 p.
- Roshan, H., Andersen, M.S., Rutledge, H., Marjo, C.E. and Acworth, R.I. (2016): Investigation of the kinetics of water uptake into partially saturated shales; Water Resources Research, v. 52, p. 2420–2438.
- Roychaudhuri, B., Tsotsis, T.T. and Jessen, K. (2013): An experimental investigation of spontaneous imbibition in gas shales; Journal of Petroleum Science and Engineering, v. 111, p. 87–97.
- Tipton, D.S. (2014): Mid-continent water management for stimulation operations; SPE Hydraulic Fracturing Technology Conference, The Woodlands, Texas, February 4–6, 2014, Paper SPE-168593-MS, URL <<https://www.onepetro.org/conference-paper/SPE-168593-MS>> [November 2016].
- Yang, L., Ge, H., Shen, Y., Zhang, J., Yan, W., Wu, S. and Tang, X. (2015): Imbibition inducing tensile fractures and its influence on in-situ stress analyses: a case study of shale gas drilling; Journal of Natural Gas Science and Engineering, v. 26, p. 927–939.
- Zhang, J. (2005): The impact of shale properties on wellbore stability; Ph.D. thesis, The University of Texas at Austin.
- Zhang, J., Chenevert, M.E., Al-Bazali, T. and Sharma, M.M. (2004): A new gravimetric-swelling test for evaluating water and ion uptake in shales; SPE Annual Technical Conference and Exhibition 2004, Houston, Texas, September 26–29, 2004, Paper SPE-89831-MS, URL <<https://www.onepetro.org/conference-paper/SPE-89831-MS>> [November 2016].

Investigating the Role of Buried Valley Aquifer Systems in the Regional Hydrogeology of the Peace River Region, Northeastern British Columbia (Parts of NTS 094A, B)

S.E. Morgan, Department of Earth Sciences, Simon Fraser University, Burnaby, BC, sem16@sfu.ca

D.M. Allen, Department of Earth Sciences, Simon Fraser University, Burnaby, BC

D. Kirste, Department of Earth Sciences, Simon Fraser University, Burnaby, BC

C.J. Salas, Geoscience BC, Vancouver, BC

Morgan, S.E., Allen, D.M., Kirste, D. and Salas, C.J. (2017): Investigating the role of buried valley aquifer systems in the regional hydrogeology of the Peace River region, northeastern British Columbia (parts of NTS 094A, B); in Geoscience BC Summary of Activities 2016, Geoscience BC, Report 2017-1, p. 63–68.

Introduction

Buried valleys are channel-form depressions, or paleo-valleys, that have been infilled by sediment and buried following their formation (Cummings et al., 2012). Within these buried valleys, permeable material can form thick units that have the potential to store and transmit significant amounts of water, hence the term ‘buried valley aquifers’. Buried valleys have been identified below glaciated terrains in North America and northern Europe, and when filled with permeable sediments, they can represent attractive targets for groundwater exploitation (Shaver and Pusc, 1992; Andriashek, 2000; Cummings et al., 2012; Oldenborger et al., 2013). Studying buried valleys and gaining an understanding of their architecture, lateral extent and the continuity of the permeable units is crucial to managing groundwater resources (Hickin et al., 2016).

Several studies have explored the hydraulic role of buried valley aquifers through both field techniques (e.g., Troost and Curry, 1991; Shaver and Pusc, 1992; van der Kamp and Maathuis, 2012) and numerical modeling (e.g., Shaver and Pusc, 1992; Seifert et al., 2008; Seyoum and Eckstein, 2014). Investigations into buried valley aquifers using numerical modeling have incorporated their geological structure and have explored the continuity of the permeable units within their fill, which are among the key factors that control the effect that buried valleys have on groundwater flow (Russell et al., 2004). These studies, however, tend to be localized (e.g., one buried valley). “At the regional scale, there has been limited investigation of aquifer extent and continuity along buried valleys, the groundwater re-

source potential of buried valley aquifer systems, and the hydraulic role of buried valleys on regional flow” (Russell, 2004). To examine the resource potential of buried valley aquifers, the impact that buried valleys have on the regional groundwater flow regime must be investigated.

The purpose of this research is to contribute to the knowledge of buried valley aquifer hydrogeology and explore the influence that buried valley aquifers have on groundwater flow at a regional scale. The study area is the Peace River region of northeastern British Columbia (BC). The aim of this work is also to extend the research conducted for Geoscience BC’s Peace Project, a project aimed at contributing new information about the available water resources in northeastern BC.

The specific objectives of the research are to

- determine the nature of the continuity of the permeable units within the buried valley network in the Peace River region,
- characterize the regional groundwater flow system for the buried valley aquifer network, and
- analyze the regional water budget under the influence of the buried valley aquifers and assess the validity of the buried valley aquifers as a water resource.

Study Area

Northeastern BC has seen a large increase in shale gas development during the last 15 years. To access the gas in the tight shale units, industry hydraulically fractures the rock (fracking) to increase its permeability. This fracking requires large volumes of water, with a single well requiring potentially more than 20 000 m³ of water. Currently, most of the water used for hydraulic fracturing in northeastern BC is surface water; however, increased development may increase the demand for other water sources, specifically groundwater found in northeastern BC’s aquifers.

Keywords: British Columbia, buried valley aquifers, regional groundwater flow, hydrogeology, Petrel, MODFLOW, SkyTEM, northeastern BC, Peace River region

This publication is also available, free of charge, as colour digital files in Adobe Acrobat® PDF format from the Geoscience BC website: <http://www.geosciencebc.com/s/DataReleases.asp>.

Unconsolidated aquifers that are particularly important to this region are in Neogene (preglacial; existed prior to glaciation) and Quaternary (glacial; cut during glaciation) buried valleys eroded into overlying sediments and/or bedrock. Both types of buried valleys occur in the Peace River region, and the valley-fill material can sometimes contain sand and gravel aquifers (Lowen, 2011), making them appealing targets for groundwater exploration. Most, however, have little to no surface expression because following the deposition of the valley-fill material, processes such as aggradation subsequently buried these valleys (Hickin, 2011; Hickin et al., 2016). This makes the process of identifying and mapping these buried valley aquifers challenging.

In the Peace River region, the approximate extent of a large network of buried valleys has been delineated (Figure 1; Petrel Robertson Consulting Ltd., 2015); however, the hydrogeological characteristics of these buried valleys, in particular the potential continuity of high permeability materials, is largely unknown. Moreover, the broader role that these buried valleys play in the regional groundwater flow regime of the Peace River region has yet to be explored.

Methods

Buried valley geometry is quite complex (Oldenborger et al., 2014); therefore, the incorporation of high-resolution geophysical data is necessary to interpret their architecture. This study will incorporate the geological data and interpretations from two geophysical techniques: electromagnetic surveys and gamma-ray logging.

Airborne Electromagnetic Survey Data

During the last several years, airborne time-domain electromagnetic (TEM) systems have been developed and proven successful for hydrogeophysical studies of buried valleys (e.g., Steuer et al., 2009; Høyer et al., 2011; Oldenborger et al., 2013). As part of Geoscience BC's Peace Project, approximately 21 000 line-kilometres were flown with the SkyTEM system (Sørensen and Auken, 2004) to collect airborne TEM data for the Peace River region. SkyTEM is an airborne TEM system specifically designed for environmental investigations (Sørensen and Auken, 2004). The TEM data were subject to one-dimensional and three-dimensional inversion and are presented as interpreted horizontal subsurface resistivity slices (Figure 2) and vertical resistivity cross sections. Generally, low resistivity is interpreted to represent fine-grained material such as clay or material containing saline water, whereas high resistivity is interpreted to represent coarse-grained material such as sand and gravel or bedrock.

Gamma-Ray Logs

Gamma-ray logs are used to measure the natural radioactivity emitted by sediments. High gamma-ray values generally relate to clays and result from higher concentrations of radioactive elements found in clay minerals, such as uranium, potassium and thorium (Quartero et al., 2014). Low gamma-ray values generally relate to sand and coarse-grained material. Gamma-ray logs are commonly used to determine subsurface lithology and stratigraphy; however, the steel surface casing in the well mutes the gamma-ray response from the formation, reducing the amplitude and variance of the data (Quartero et al., 2014). While surface casing enhances wellbore stability and protects shallow groundwater from surface contamination, the attenuation caused by the casing lowers the overall gamma-ray response and is problematic for geological interpretation (Quartero et al., 2014).

The gamma-ray logs from approximately 1400 wells in the Peace River region have been corrected for the attenuation of the gamma-ray response caused by the surface casing using the statistical correction technique developed by Quartero et al. (2014). This technique allows the cased and noncased log intervals to be merged into one continuous gamma-ray curve for stratigraphic correlation (Figure 3).

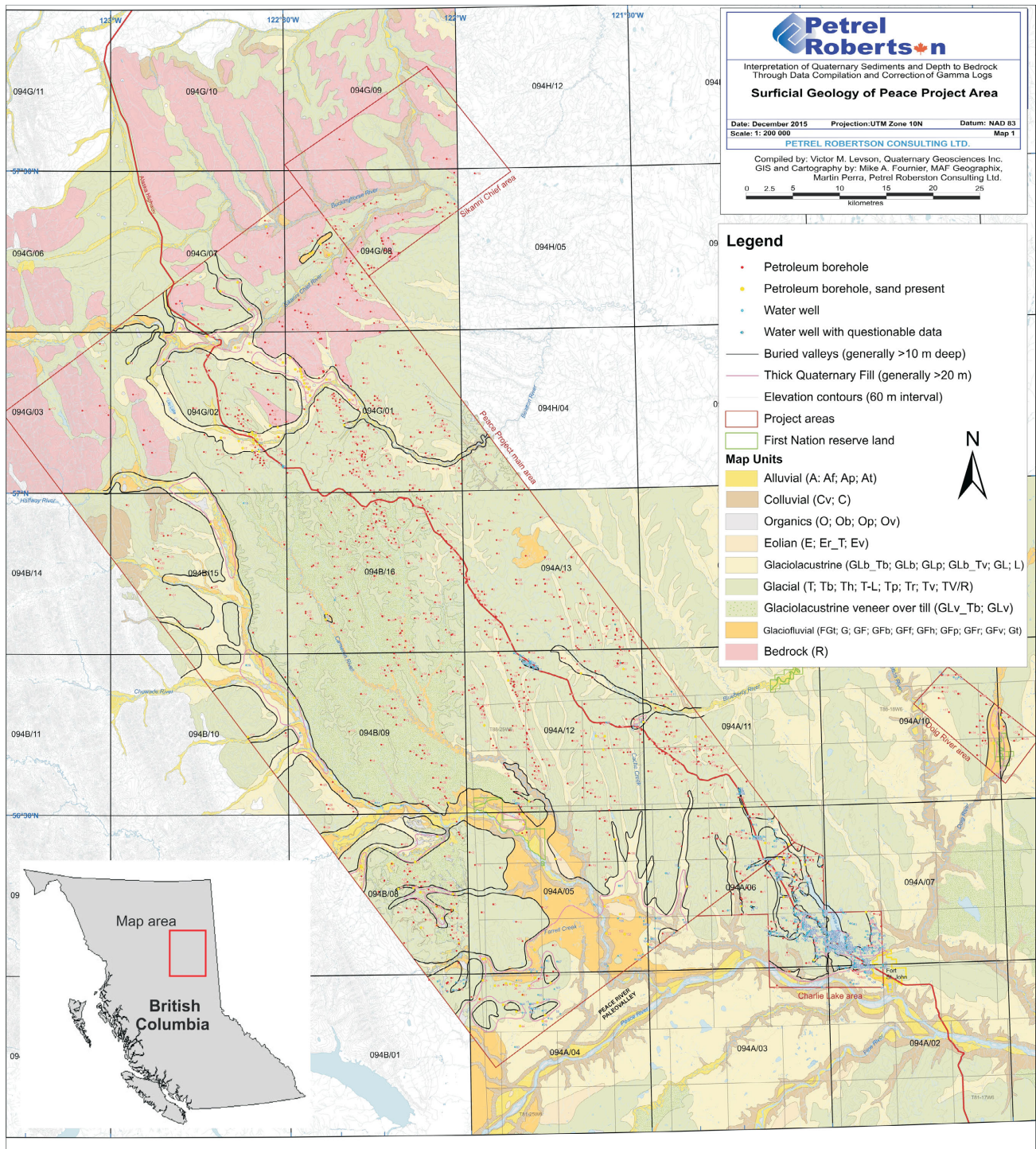
Objective 1: Geological Model

The surficial geology map of the Peace Project area in Figure 1 shows the outline of a large buried valley network. This large network will be the focus for this research, thus, the developed geological model will likely be in this area. The exact area of the model will be defined at a later stage in the research, once all available data have been examined.

The geological and geophysical datasets will be imported into the reservoir software, Petrel (Schlumberger Limited, 2011), and used to design a 3-D geological model of the buried valley network. Two options will be explored for the model domain:

- The vertical extent of the geological model will be from ground surface to the top of bedrock. Bedrock topography (from Petrel Robertson Consulting Ltd., 2015) and a digital elevation model (DEM) will be used as the top and bottom surfaces of the geological model, respectively. This geological model and the following hydrogeological model will only consider the unconsolidated sediments. The bedrock will be considered impermeable.
- A full geological model will be generated that includes the bedrock, down to approximately 200 m, below which there is likely limited groundwater flow.

The interpreted geology from the TEM resistivity slices and cross sections will be used to differentiate fine- and coarse-grained material within the valley fill (and possibly



lithological differences in bedrock) and, in combination with bedrock topography, to visualize the structure of the buried valleys themselves. The surficial geology map, available gamma-ray logs for oil and gas wells, and lithology logs reported by well drillers (from the WELLS database; BC Ministry of Environment, 2016) will supplement

the TEM data to help confirm the depth to bedrock and verify the geological interpretation from the TEM data. There is also a possibility that a few targeted boreholes will be drilled in the study area to confirm the geological interpretation of the geophysical data. The information collected from these boreholes would be included in the study.

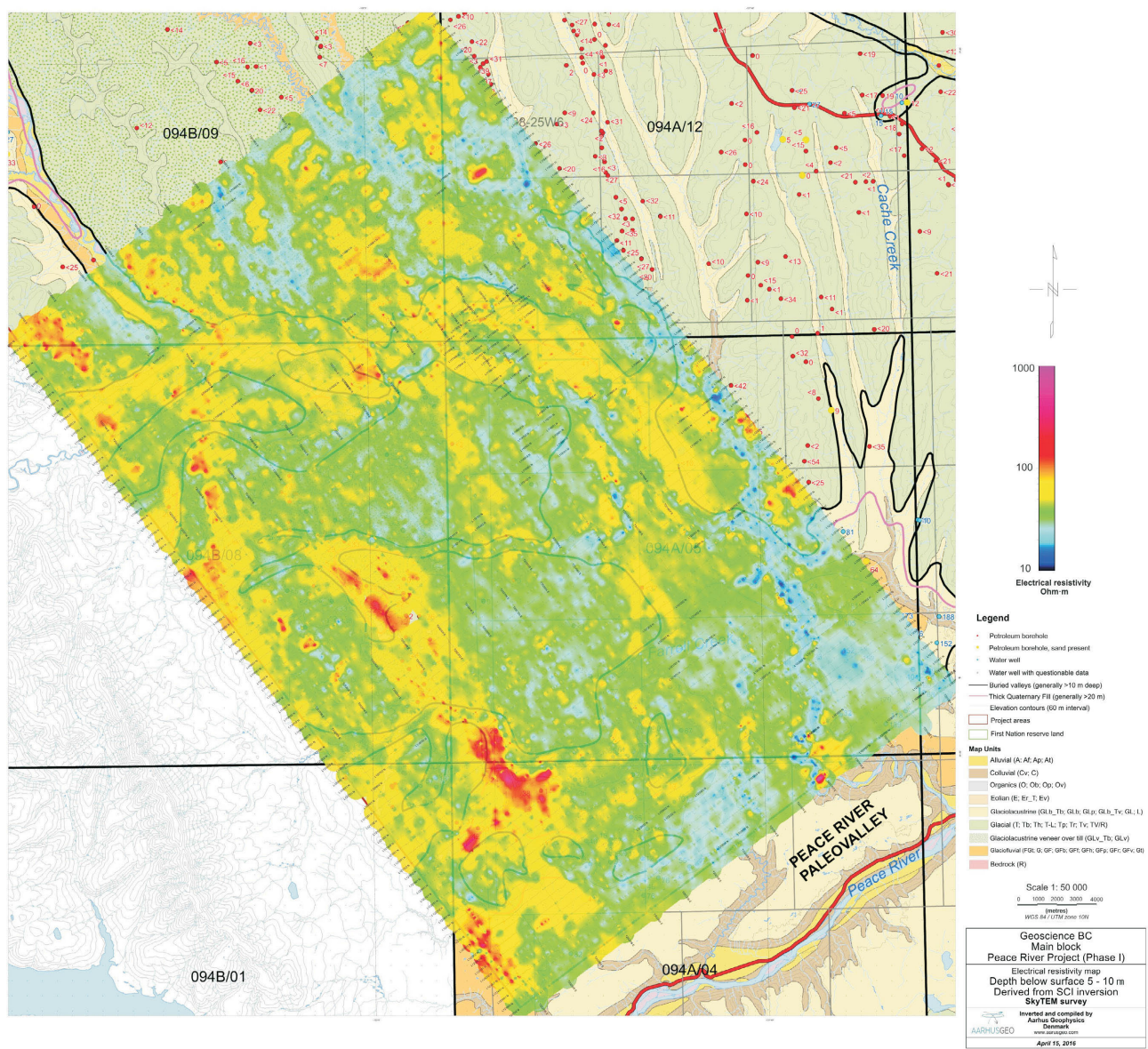


Figure 2. Example of a horizontal subsurface resistivity slice showing interpreted resistivity distribution from 5 to 10 m below ground surface in the Peace Project Main area of the Peace Project. Resistivity distribution was derived from spatially constrained inversion (SCI). Depth to bedrock in metres is shown next to the petroleum and water wells in the figure. Modified from Aarhus Geophysics ApS (2016).

The hydraulic properties of the geological units will be estimated primarily from the literature based on the texture of the Quaternary deposits in the Peace River region. These will be supplemented by estimates obtained from pumping tests and possibly grain size data. Based on distinct hydraulic conductivity contrasts between the dominant material types (e.g., till versus glaciofluvial), unique hydrostratigraphic units will be defined.

Objective 2: Numerical Groundwater Flow Model

Characterizing a groundwater flow system requires a geological model, defined recharge areas and amounts of recharge, delineation of flow paths and the volume of flow, and defined discharge areas. Numerical groundwater flow

models are valuable tools for characterizing groundwater flow systems. The most commonly used groundwater flow model is MODFLOW, and since its release in 1988, it has become the industry standard for numerical groundwater modeling (Zhou and Li, 2011). MODFLOW is a block-centred, finite-difference code that can handle complex boundaries and spatial and temporal variations of the system (Pisinaras et al., 2007). MODFLOW can also import geological models generated in other programs, such as Petrel (Schlumberger Limited, 2011).

Using the 3-D geological model developed in Objective 1, an interpretive, steady-state, 3-D numerical groundwater flow model will be created for the Peace River study area to characterize the regional groundwater flow system of the

buried valley network. The model boundary conditions are uncertain, but will be approximated based on existing information. Spatial recharge has been estimated for the Peace River region by Holding and Allen (2015), who provide a range of average mean annual recharge between 88 and 1006 mm/year. Based on the model location and the spatial distribution of recharge from Holding and Allen (2015), recharge rates within the range of 0 and 300 mm/year will be tested and applied to the top surface of the numerical model. Other boundary conditions thought to control the flow within the buried valley aquifer system will be investigated prior to model construction. These may include major rivers, such as the Peace River, and other water bodies. Available hydrometric data will be used where rating curves are available (to obtain the river stage from discharge measurements).

The Particle Tracking tool in MODFLOW will be used to identify and delineate likely recharge and discharge areas of the buried valley aquifer network. The groundwater travel paths will also be observed to explore the regional groundwater flow system and investigate the hydraulic gradient.

Objective 3: Regional Water Budget

In MODFLOW, the Zone Budget analysis tool will be used to quantify the amount of recharge to and discharge from the buried valleys, respectively, and to estimate how much water is moving through the buried valley aquifer network. If the model domain includes bedrock, the Zone Budget tool will also be used to estimate how much water is moving outside the buried valleys in the bedrock. This amount will be compared with the amount of flow within the buried valley network to address the question of the impact of buried valley aquifers on regional groundwater flow.

Additionally within the numerical model, simulations will be carried out to assess the potential of these buried valley aquifers as a long-term, sustainable groundwater resource. This will be achieved through adding to the steady-state model pumping wells that are completed in the buried valley aquifers. Abstraction will be simulated, and the Particle Tracking tool will be used identify capture zones in the steady-state flow field.

Future Work

Objective 1 is currently underway for this project. The geological and geophysical data will be brought into Petrel (Schlumberger Limited, 2011), and these datasets will be used to design the geological model of the buried valley network in the Peace River study area. Based on the developed geological model, a numerical groundwater flow model will be constructed for the study area. This flow model will be used to assess the impact of buried valley aquifers on regional groundwater flow. It is hoped that the

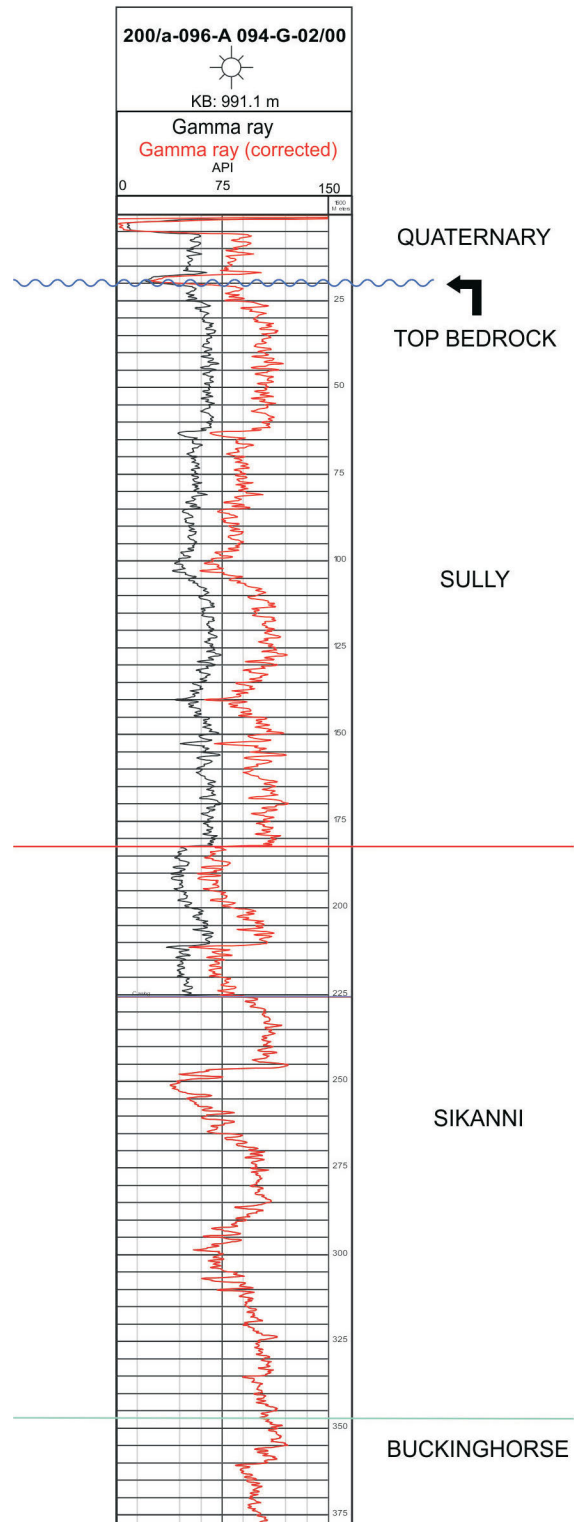


Figure 3. Example of a gamma-ray log from the Peace Project area corrected using the Quartero et al. (2014) method. The gamma-ray curve from the cased-hole interval is shown in black and the corrected gamma-ray curve is shown in red. Stratigraphic picks are also shown on the gamma-ray log, beginning with the youngest: Quaternary sediments, Upper Cretaceous Sully Formation, Lower Cretaceous Sikanni Formation and Lower Cretaceous Buckinghamhorse Formation. Modified from Petrel Robertson Consulting Ltd. (2015).

results of this study can provide insight to future investigations of regional groundwater systems containing buried valleys. This research will be completed and documented as an M.Sc. thesis.

References

- Aarhus Geophysics ApS (2016): Processing and inversion of SkyTEM data, Peace River main area – phase 1; Geoscience BC, Report 2016-09a, 28 p., URL <<http://www.geosciencebc.com/s/Report2016-09.asp>> [December 2016].
- Andriashek, L.D. (2000): Quaternary stratigraphy of the buried Birch and Willow bedrock channels, NE Alberta; Alberta Energy and Utilities Board, EUB/AGS Earth Sciences, Report 2000-15, 61 p.
- BC Ministry of Environment (2016): WELLS database; BC Ministry of Environment, URL <<https://a100.gov.bc.ca/pub/wells/public/indexreports.jsp>> [November 2016].
- Cummings, D.I., Russell, H.A.J. and Sharpe, D.R. (2012): Buried-valley aquifers in the Canadian prairies: geology, hydrogeology, and origin; Canadian Journal of Earth Sciences, v. 49, no. 9, p. 987–1004.
- Hickin, A.S. (2011): Preliminary bedrock topography and drift thickness of the Montney Play area; BC Ministry of Energy and Mines, BC Geological Survey, Open File 2011-1 and Geoscience BC, Report 2011-07, 2 maps, 1:500 000 scale, URL <<http://www.geosciencebc.com/s/Report2011-07.asp>> [November 2016].
- Hickin, A.S., Best, M.E. and Pugin, A. (2016): Geometry and valley-fill stratigraphic framework for aquifers in the Groundbirch paleovalley assessed through shallow seismic and ground-based electromagnetic surveys; BC Ministry of Energy and Mines, BC Geological Survey, Open File 2016-05, 46 p., URL <<http://www.empr.gov.bc.ca/Mining/Geoscience/PublicationsCatalogue/OpenFiles/2016/Pages/2016-5.aspx>> [November 2016].
- Holding, S. and Allen, D.M. (2015): Shallow groundwater intrinsic vulnerability mapping in northeast British Columbia; Simon Fraser University, Final report prepared for Pacific Institute for Climate Solutions and BC Ministry of Energy and Mines, 41 p., URL <http://pics.uvic.ca/sites/default/files/uploads/publications/NEBC%20DRASTIC%20Report_Final.pdf> [November 2016].
- Høyer, A., Lykke-Andersen, H., Jørgensen, F. and Auken, E. (2011): Combined interpretation of SkyTEM and high-resolution seismic data; Physics and Chemistry of the Earth, Parts A/B/C, v. 36, no. 16, p. 1386–1397.
- Lowen, D. (2011): Aquifer classification mapping in the Peace River region for the Montney water project; *in* EcoCat: the ecological reports catalogue, BC Ministry of Environment, Report 23 247, 51 p.
- Oldenborger, G.A., Logan, C.E., Hinton, M.J., Sapia, V., Pugin, A.J.M., Sharpe, D.R., Calderhead, A.I. and Russell, H.A.J. (2014): 3D hydrogeological model building using airborne electromagnetic data; Near Surface Geoscience 2014, 20th European Meeting of Environmental and Engineering Geophysics, Athens, Greece, September 14–18, 2014, 5 p.
- Oldenborger, G.A., Pugin, A.J.M. and Pullan, S.E. (2013): Airborne time-domain electromagnetics, electrical resistivity and seismic reflection for regional three-dimensional mapping and characterization of the Spiritwood Valley aquifer, Manitoba, Canada; Near Surface Geophysics, v. 11, no. 1, p. 63–74.
- Petrel Robertson Consulting Ltd. (2015): Interpretation of Quaternary sediments and depth to bedrock through data compilation and correction of gamma logs; Geoscience BC, Report 2016-04, 24 p., URL <<http://www.geosciencebc.com/s/Report2016-04.asp>> [November 2016].
- Pisinaras, V., Petalas, C., Tsihrintzis, V. and Zagana, E. (2007): A groundwater flow model for water resources management in the Ismarida plain, North Greece; Environmental Modeling and Assessment, v. 12, no. 2, p. 75–89.
- Quartero, E., Bechtel, D., Leier, A. and Bentley, L. (2014): Gamma-ray normalization of shallow well-log data with applications to the Paleocene Paskapoo formation, Alberta; Canadian Journal of Earth Sciences, v. 51, no. 5, p. 452–465.
- Russell, H.A.J., Hinton, M.J., van der Kamp, G. and Sharpe, D.R. (2004): An overview of the architecture, sedimentology and hydrogeology of buried-valley aquifers in Canada; *in* Proceedings of the 57th Geotechnical Conference and the 5th Joint CGS-IAH Conference, Québec, Quebec, October 24–27, 2004, p. 2B (26–33), doi:10.4095/215602
- Schlumberger Limited (2011): Petrel 2011 for Windows; Schlumberger Limited, online help (not available in libraries).
- Seifert, D., Sonnenborg, T.O., Scharling, P. and Hinsby, K. (2008): Use of alternative conceptual models to assess the impact of a buried valley on groundwater vulnerability; Hydrogeology Journal, v. 16, no. 4, p. 659–674.
- Seyoum, W.M. and Eckstein, Y. (2014): Hydraulic relationships between buried valley sediments of the glacial drift and adjacent bedrock formations in northeastern Ohio, USA; Hydrogeology Journal, v. 22, no. 5, p. 1193–1206.
- Shaver, R.B. and Pusc, S.W. (1992): Hydraulic barriers in Pleistocene buried-valley aquifers; Ground Water, v. 30, no. 1, p. 21–28.
- Sørensen, K.I. and Auken, E. (2004): SkyTEM—a new high-resolution helicopter transient electromagnetic system; Exploration Geophysics, v. 35, no. 3, p. 194–202.
- Steuer, A., Siemon, B. and Auken, E. (2009): A comparison of helicopter-borne electromagnetics in frequency- and time-domain at the Cuxhaven valley in Northern Germany; Journal of Applied Geophysics, v. 67, no. 3, p. 194–205.
- Troost, K.G. and Curry, B.B. (1991): Genesis and continuity of Quaternary sand and gravel in glaciogenic sediment at a proposed low-level radioactive waste disposal site in East-Central Illinois; Environmental Geology and Water Sciences, v. 18, no. 3, p. 159–170.
- van der Kamp, G. and Maathuis, H. (2012): The unusual and large drawdown response of buried-valley aquifers to pumping; Ground Water, v. 50, no. 2, p. 207–215.
- Zhou, Y. and Li, W. (2011): A review of regional groundwater flow modeling; Geoscience Frontiers, v. 2, no. 2, p. 205–214.

Quantifying the Water Balance of Coles Lake in Northeastern British Columbia Using In Situ Measurements and Comparisons with Other Regional Sources of Water Information

S. Abadzadesahraei, University of Northern British Columbia, Prince George, BC, sina@unbc.ca

S.J. Déry, University of Northern British Columbia, Prince George, BC

J. Rex, British Columbia Ministry of Forests, Lands and Natural Resource Operations, Prince George, BC

Abadzadesahraei, S., Déry, S.J. and Rex, J. (2017): Quantifying the water balance of Coles Lake in northeastern British Columbia using in situ measurements and comparisons with other regional sources of water information; *in* Geoscience BC Summary of Activities 2016, Geoscience BC, Report 2017-1, p. 69–74.

Introduction

Northeastern British Columbia (BC) is undergoing rapid development for oil and gas extraction, largely depending on subsurface hydraulic fracturing (fracking), which relies on freshwater. Even though this industrial activity has made substantial contributions to regional and provincial economies, it is important to ensure that sufficient and sustainable water supplies are available for socioeconomic sectors dependent on the resource, including ecological systems. This, in turn, demands a comprehensive understanding of how water in all its forms interacts within the watershed and an identification of the potential impacts of changing climatic conditions on these processes. The aim of this study is to characterize and quantify all components of the water balance in the Coles Lake watershed, northeastern BC, through a combination of fieldwork and observational data analysis. Baseline information generated from this study will support the assessment of the sustainability of current and future plans for freshwater extraction in the region by the oil and gas industry. The initial results of fieldwork and a partial observational analysis were already published by Abadzadesahraei et al. (2016). This paper provides a complete observational analysis for the hydrological year 2013–2014, providing a better understanding of boreal wetland dynamics by identifying the water balance of Coles Lake. In addition, the outcomes of this study are compared with other available regional sources of water in northeastern BC.

Overview of Past Research

Shale gas exploration and development near Fort Nelson has increased demand for surface water in these wetland-

dominated landscapes, prompting several studies to assess the sustainable function of such natural ecosystems. For instance, Johnson (2010) developed a conceptual water balance model for the Horn River Basin near Fort Nelson and identified knowledge gaps including the identification of wetlands, delineation of fens and bogs, location and distribution of permafrost, identification of the spatial distribution of evapotranspiration, and increased monitoring of discharge. Further contributions to water allocation planning efforts have also been made by Chapman et al. (2012) with the development of the NorthEast Water Tool (NEWT)—a web-based hydrological model and planning tool for prediction of water availability based on modelled annual, seasonal and monthly runoff (BC Oil and Gas Commission and BC Ministry of Forests, Lands and Natural Resource Operations, 2016). Additionally, the BC Water Portal (WP), which is an online map-based water information tool, was designed in 2014 to provide a wide range of water-related data and information for northeastern BC (BC Ministry of Forests, Lands and Natural Resource Operations and BC Oil and Gas Commission, 2016). The WP contains water quantity and quality data wherever the data are available for both surface water and groundwater. Furthermore, it links climate information and historical hydrographs of mean monthly water depth of provincial observation wells (Holding et al., 2015).

Recent studies indicate that the combination of climate change, shale gas development activities and the physical characteristics of northeastern BC watersheds make hydrological studies in this region particularly challenging (Johnson, 2010). These challenges are exacerbated by the combination of gentle topography, relatively fine-textured surficial materials, extensive wetlands, discontinuous permafrost and seasonally frozen ground (Golder Associates, 2010; Johnson, 2010). Although several studies have explored these concerns, there are still many knowledge gaps (e.g., role of vegetation canopies in the water balance) that need to be addressed.

Keywords: northeastern British Columbia, water resources, Coles Lake watershed, oil and gas extraction

This publication is also available, free of charge, as colour digital files in Adobe Acrobat® PDF format from the Geoscience BC website: <http://www.geosciencebc.com/s/DataReleases.asp>.

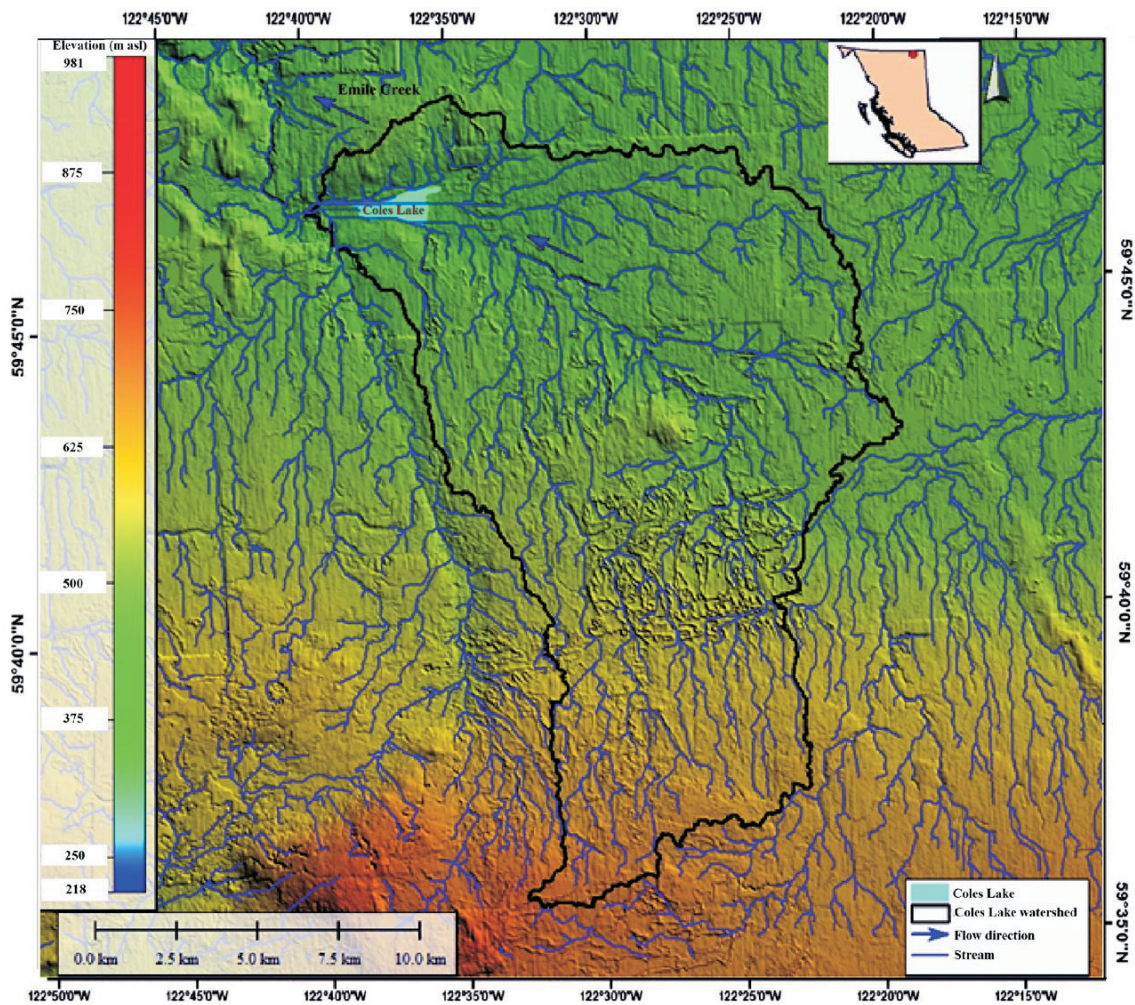


Figure 1. Location of Coles Lake and its topography, northeastern British Columbia. Data from HydroSHEDS (World Wildlife Fund, 2009).

Study Area Characteristics

The Coles Lake watershed is in northeastern BC, between Fort Nelson and the Northwest Territories border. The watershed is about 140 km northeast of Fort Nelson and has a drainage area of approximately 227 km² (Figure 1). Its elevation ranges from 311 to 550 m above sea level (asl) with an average elevation of 524 m asl and contains an elevated central highland, which acts as a drainage divide. According to the BC biogeoclimatic ecosystem classification (BEC) system, the Coles Lake watershed is located in the moist cool boreal white and black spruce zone (DeLong et al., 2011). This zone contains 10% of BC’s total land area, which makes it the province’s largest biogeoclimatic zone (DeLong et al., 1991). This zone is characterized by black and white spruce forests and wetland complexes of discontinuous permafrost, fens, bogs, swamps and marshes on a glaciolacustrine plain, with extensive organic deposits and a lesser component of streamlined tills (Golder Associates, 2010; Johnson, 2010; Huntley et al., 2011; Kabzems et al.,

2012). Based on a vegetation resource inventory (VRI) and the BC Land Cover Classification Scheme, approximately 43.3% of this watershed is open, 51.4% has a mixed vegetation canopy and 5.3% has a closed vegetation canopy. Only crown closure is used to identify open, mixed and closed vegetation canopies ($\leq 25\%$ open, $>25\text{--}61\%$ mixed, $>61\%$ closed).

Coles Lake is a small and shallow water body, with a maximum depth of 2.2 m, situated in the northwestern corner of the Coles Lake watershed. Coles Lake is part of the Peace River Land District and it is situated at 59°46'57"N latitude and 122°36'27"W longitude with an area of 1.72 km² (Figure 1). The southern and western side of the study area drains to the west and north through Emile Creek and flows into the Petitot River, whereas the northern and eastern side of the study area drains to the east and north through Fortune Creek and also flows into the Petitot River. Based on data from an automated weather station installed near Coles Lake (latitude 59°47'22.2"N, longitude 122°36'42.8"W, el-

elevation 480 m asl), the mean annual air temperature was 1.7°C with a total annual precipitation of 429.5 mm for the 2013–2014 hydrological year. Permanent snow cover typically lasts from early November until early to mid-May.

Methodology

Estimating the Water Balance

Determination of Coles Lake’s water balance requires an estimation of stored water and fluxes. Precipitation (rain and snow), stream inflow and groundwater to the lake are considered the main inputs; evaporation, stream outflow and water extraction from the lake are considered outputs as follows:

$$\Delta S = P + I + G - E - Q - W \quad (1)$$

where ΔS is the change in stored water; P is precipitation ($P = R + S$, where R denotes rainfall and S represents snowfall); I is the mean annual stream inflow to Coles Lake; G is the groundwater exchange; E is evaporation; Q is discharge (outflow) and W is the licensed withdrawal of water. Although the water balance has been computed for the entire Coles Lake watershed, results presented here are only for the lake itself. All terms are expressed in units of millimetres. A water-year from October 1, 2013 to September 30, 2014 was used as the temporal framework within which to estimate the balance, as this period begins and ends when both discharge and storage are at their minimum levels (Winkler et al., 2010).

Data Collection

Fieldwork was conducted from May 2012 to September 2014 to examine the hydrological components of this watershed in detail. Challenges to the field efforts included the remoteness of the basin and difficult access to the area, as well as frequent adverse weather conditions. The results of this work will support the quantification and understanding of the Coles Lake water balance. A general description of each field procedure used and its purpose is available in Abadzadesahraei et al. (2016).

Water Balance Components

Wetlands are an essential part of the hydrological cycle within this region, with water balance components including precipitation, evaporation, surface water and groundwater flows (Ingram, 1983). Each of these components and results from the 2013–2014 hydrological year are discussed below.

Rainfall (R)

Local rainfall data were collected every 15 min at the automated weather station and then summed for a daily total to calculate the total contribution of rainfall on Coles Lake. Rainfall from November 1, 2013 to May 15, 2014 is taken

as zero because temperatures are continuously subfreezing during this period and reported data during this period is from snowfall rather than rainfall. In total, 262.1 mm of rainfall is reported, with maximum rainfall occurring in June (73.9 mm) and July (61.9 mm).

Snowfall (S)

Based on Environment and Climate Change Canada standard equivalences, 1 cm of snow is assumed to correspond to 1 mm of water. Therefore, snowfall for the Coles Lake weather station totals 167.4 mm (water equivalent) based on the ultrasonic ranging sensor.

Evaporation (E)

Multiple steps were required to compute the total evaporation over the Coles Lake area. The first step was to identify the ice-free (open-water) period. Landsat images were downloaded and reviewed to determine the start and end time of freezing and melting of the ice cover at Coles Lake. Based on the Landsat images, Coles Lake began freezing around November 1, 2013, and the melting period began near to May 15, 2014. Once the ice-free period was identified, the Food and Agriculture Organization (FAO) of the United Nations’ Penman-Monteith method was selected to estimate evaporation from the lake surface (Hendriks, 2010). To use the FAO Penman-Monteith method, the net radiation at the earth’s surface, air temperature, wind speed, relative humidity and air pressure were collected for the duration of the open-water period. The results suggested that maximum evaporation occurred in July (97.7 mm) and minimum evaporation occurred in December (2.6 mm). This demonstrates a correlation with temperature, with a total loss of 368.5 mm during the ice-free months. In addition, the potential contribution of blowing snow sublimation to the water balance of Coles Lake was assessed using the Pietruk blowing snow model (Déry et al., 1998). This model indicates that blowing snow sublimation does not contribute significantly to the water balance of Coles Lake and can be safely neglected in this study.

Inflow and Outflow (I, Q)

Discharge measurements were made at both the inflow and the outflow stations. Unfortunately, it was not possible to use the stage–discharge relationship to measure the streamflow because beaver dams altered flow during the field campaign. Since these structures blocked water, the water level recorded by transducers in July, August and September stayed mostly the same. As a result of this natural phenomenon, water levels were raised in the upstream stage and therefore rendered the rating curve invalid. In light of this challenge, an alternative method of obtaining representative streamflow data was employed. To compute the amount of discharge, the streamflow data from Emile Creek and two Coles Lake stations were compared. The

Emile Creek hydrometric station is located about 4 km downstream from Coles Lake. Four days of onsite discharge measurements of inflow and outflow using the mid-point method were correlated with data for the same days from the Emile Creek station. A high degree of correspondence is demonstrated between the Emile Creek station and each of the inflow and outflow stations. The high correlation coefficients show that discharge measurements are consistent (Table 1). The obtained regression allowed extrapolation of the daily discharges at each site for each day of the study period with total inflow of 106.6 mm and total outflow of 198.5 mm for the hydrological year.

Groundwater (G)

To estimate the contribution of groundwater fluxes to the lake, nine piezometers in three transects were installed on February 5, 2014 (Abadzadesahraei et al., 2016). Groundwater fluxes were only estimated from February 5, 2014 to September 30, 2014, and only during the ice-free period. In fact, there are no data available prior to this study. In addition, it is assumed that the water fluxes are zero during the freezing period. Although this logical inference is based on sound assumptions, there may be an underestimation of the flux. To compute the net average annual flow of water at Coles Lake, Darcy's equation was employed (Lohman, 1972):

$$Q = q \times A \quad (2)$$

where Q is water flow ($\text{m}^3 \cdot \text{s}^{-1}$), q is the net flux (has a dimension of velocity in $\text{m} \cdot \text{s}^{-1}$) and A (m^2) is the cross-sectional area of the shoreline segment, representing a vertical plane at the shoreline through which water passes to either enter or leave the surface-water body. This method assumes that the aquifer is homogeneous and isotropic within the segment; however, its assumption of a constant aquifer thickness is violated where the water table slopes in the vicinity of a surface water body.

According to the analysis, a total of 4.1 mm of groundwater contributed to the water balance of the lake each month from the three transects (flow = $Q \times$ number of seconds for the specific months / the area that each transect covers in m^2). Flows to and from the surface-water body were summed to calculate the net groundwater contribution to the entire

Table 1. The t- and p-values between Coles Lake and Emile Creek stations with the computed Pearson's product-moment correlation coefficients. The t-value reflects the value of the 't' test statistic for the test, and the p-value reflects whether the significance of the correlation (<0.05) is significant.

	t-value	p-value	Correlation
Between inflow station and Emile Creek station	9.39	0.011	0.99
Between outflow station and Emile Creek station	9.78	0.010	0.99

lake. Based on these assumptions, 22.6 mm ($4.1 \text{ mm} \times 5.5$ months) of groundwater had flowed into the lake during the ice-free period.

Water Withdrawal (W)

The BC Oil and Gas Commission (BCOGC) gave Quicksilver Resources Canada Inc. (Quicksilver) a maximum water withdrawal allocation of 38.5 mm for the 2013–2104 hydrological year from Coles Lake. However, actual water withdrawal was zero because the plant was closed in response to low natural gas prices (Quicksilver Resources Canada Inc., pers. comm., 2013).

Water Balance Results

After computing the hydrological components, it was possible to determine the final water balance components, listed in Table 2.

Evaluation of the Coles Lake Hydrological Components

This section evaluates the hydrological components of Coles Lake using comparisons with other available sources of water information in northeastern BC. The sources employed were the NEWT and WP, as well as hydrometeorological data from the Fort Nelson climate normals (FNCN) station (Environment and Climate Change Canada, 2016a) and Fisheries and Environment Canada (FEC) lake evaporation data (Fisheries and Environment Canada, 1978). The precipitation data reported by the NEWT are from Climate-WNA (Centre for Forest Conservation Genetics, 2015) and hydrometric data originate from Water Survey of Canada (Environment and Climate Change Canada, 2016b) gauging stations with various periods of record. The WP is based on observational data for the 2013–2014 water year. The FNCN are the average climatic data from 1981 to 2010 recorded at Fort Nelson, whereas the FEC data represents the mean value of the annual evaporation of open water bodies, based on the 10-year period 1957–1966.

Table 2. Summary of water balance components, the hydrological year 2013–2014, Coles Lake, northeastern British Columbia.

Component	Total (mm)
Rainfall (R)	262.1
Snowfall (S)	167.4
Inflow (I)	106.6
Outflow (Q)	198.5
Evaporation (E)	368.5
Groundwater (G)	22.6
Water withdrawal (W)	0*
Change in stored water (ΔS)	-8.3

*Although, the potential maximum water allocation is 38.5 mm, the total amount of water withdrawal is zero since there was no water extracted during this study period.

For the 2013–2014 water year, observed precipitation totals 429.5 mm over Coles Lake. The estimated observed precipitation for Coles Lake is within an appropriate range compared to results from the NEWT (435.3 mm; BC Oil and Gas Commission and BC Ministry of Forests, Lands and Natural Resource Operations, 2013), WP (430.3 mm) and FNCN (451.7 mm). In addition, the estimated rainfall during the ice-free period at Coles Lake (262.1 mm) varied only by 27.5 mm compared to FNCN (289.6 mm). Additionally, the total amount of computed snowfall at Coles Lake (167.4 mm) matches well the reported data by FNCN (169.8 mm).

A total amount of 106.6 mm as inflow and 198.5 mm as outflow was estimated for Coles Lake. To evaluate these estimated results, an attempt was made to compare these findings with the NEWT and WP. It was concluded that the results of Coles Lake are not consistent with the results of NEWT for two main reasons. Firstly, NEWT does not separate the total amount of runoff into and out of Coles Lake. Secondly, NEWT does not consider the effect of beaver dams in the area. Thus, only WP values are used for the evaluation, however, the WP values are only representative of the flow in Emile Creek (located downstream of Coles Lake) and not for Coles Lake itself. It was still possible to employ values from WP because Coles Lake streamflow was constructed based on recorded data from Emile Creek. After comparison, the recorded data from Emile Creek highly correlated with the WP data. Furthermore, the WP reported that the streamflow in 2014 approached zero in October, confirming this study's assumption regarding the ice-free period.

The total amount of evaporation estimated for Coles Lake during the ice-free period was 368.5 mm. According to FEC data, the mean annual lake evaporation at Coles Lake varies from 300 to 500 mm. It can be concluded that the estimated results are located within this range reported by FEC.

Although the groundwater data are currently unavailable for comparison, previous studies by Quicksilver indicated a low hydraulic conductivity and consequently low permeability at the Coles Lake watershed. This fact may explain a low computed value of groundwater contribution to Coles Lake.

Summary and Future Approach

In this paper, the water balance of Coles Lake, including its inputs, outputs and storage terms, is quantified, and the obtained results were compared with other available sources of water information in northeastern BC. In the next phase of this work, historical water balance of Coles Lake and its associated hydrological processes will be quantified using a hydrological model—MIKE SHE (DHI Water & Environment, 2007). The MIKE SHE hydrological model is se-

lected to identify the interactions among the atmosphere, surface and subsurface in this region. In addition, the water balance tool within MIKE SHE is used to estimate the historical water balance of northeastern BC watersheds over 35 years. Simulated results will be compared to other watersheds to investigate the differences/similarities of the Coles Lake watershed with others in the region. Therefore, the main goal of this research is to advance and improve the knowledge of hydrological processes and water resources in northeastern BC. Outcomes of this study may assist regulators in balancing multiple priorities in a way that will not compromise the long-term sustainability of water resources. More specifically, this study can help determine how much freshwater can be extracted by oil and gas operations by forecasting balance thresholds to avoid the over-allocation of local water resources.

Acknowledgments

The authors thank Geoscience BC for their support of this project. Comments from S. Islam improved the quality of this manuscript. In particular, the authors thank D. Allen, D. Ryan and E. Petticrew for their insights into this research. In addition, the BC Ministry of Forests, Lands and Natural Resource Operations is thanked for providing funding for this project. Also, gratitude is extended to Quicksilver Resources Canada Inc. for their collaboration.

References

- Abadzadesahraei, S., Déry, S.J. and Rex, J. (2016): Quantifying the water budget for a northern boreal watershed: the Coles Lake study, northeastern British Columbia; *in* Geoscience BC Summary of Activities 2015, Geoscience BC, Report 2016-1, p. 95–100.
- BC Ministry of Forests, Lands and Natural Resource Operations and BC Oil and Gas Commission (2016): BC water portal; BC Ministry of Forests, Lands and Natural Resource Operations and BC Oil and Gas Commission, URL <<http://www.bcwatertool.ca/waterportal/>> [August 2016].
- BC Oil and Gas Commission and BC Ministry of Forests, Lands and Natural Resource Operations (2013): NorthEast Water Tool query, Lower Petitot River, British Columbia, Tuesday November 12, 2013; BC Oil and Gas Commission, query results, 4 p.
- BC Oil and Gas Commission and BC Ministry of Forests, Lands and Natural Resource Operations (2016): NorthEast Water Tool; BC Oil and Gas Commission, GIS-based hydrology decision-support tool, URL <<https://water.bcogc.ca/newt/>> [December 2016].
- Centre for Forest Conservation Genetics (2015): ClimateBC/WNA/NA; The University of British Columbia, Faculty of Forestry, URL <<http://cfcg.forestry.ubc.ca/projects/climate-data/climatebcwna/>> [September 2015].
- Chapman, A., Kerr, B. and Wilford, D. (2012): Hydrological modelling and decision-support tool development for water allocation, northeastern British Columbia; *in* Geoscience BC Summary of Activities 2011, Geoscience BC, Report 2012-1, p. 81–86.

- DeLong, C., Annas, R.M. and Stewart, A.C. (1991): Boreal white and black spruce zone; *in* Ecosystems of British Columbia, D. Meidinger and J. Pojar (ed.), BC Ministry of Forests, Special Report Series 6, p. 237–250.
- DeLong, C., Banner, A., MacKenzie, W.H., Rogers, B.J. and Kaytor, B. (2011): A field guide to ecosystem identification for the boreal white and black spruce zone of British Columbia; BC Ministry of Forests, Lands and Natural Resource Operations, BC Land Management Handbook No. 65, 250 p., URL <<https://www.for.gov.bc.ca/hfd/pubs/Docs/Lmh/Lmh65.htm>> [August 2013].
- Déry, S.J., Taylor, P.A. and Xiao, J. (1998): The thermodynamic effects of sublimating, blowing snow in the atmospheric boundary layer; *Boundary-Layer Meteorology*, v. 89, no. 2, p. 251–283.
- DHI Water & Environment (2007): MIKE SHE user manual, volume 2: reference guide; DHI Water & Environment, Horsholm, Denmark, 386 p.
- Environment and Climate Change Canada (2016a): Canadian climate normals 1981–2010 station data; Environment and Climate Change Canada, URL <http://climate.weather.gc.ca/climate_normals/results_1981_2010_e.html?searchType=stnName&txtStationName=fort+nelson&searchMethod=contains&txtCentralLatMin=0&txtCentralLatSec=0&txtCentralLongMin=0&txtCentralLongSec=0&stnID=1455&dispBack=1> [August 2016].
- Environment and Climate Change Canada (2016b): Wateroffice; Environment and Climate Change Canada, database, URL <<https://wateroffice.ec.gc.ca/>> [January 2016].
- Fisheries and Environment Canada (1978): Mean annual lake evaporation; *in* Hydrological Atlas of Canada, Fisheries and Environment Canada, plate 17, URL <<http://geogratis.gc.ca/api/en/nrcan-rncan/ess-sst/67de4f04-855d-5d23-bb4a-2a270d1488d0.html>> [August 2016].
- Golder Associates (2010): Surface water study – Horn River Basin; draft report prepared for BC Ministry of Natural Gas Development, Oil and Gas Division, 61 p., URL <http://www.geosciencebc.com/i/pdf/RFP/App2_Water_Supply_in_HRB_Mar31_2010_1.pdf> [November 2015].
- Hendriks, M. (2010): *Introduction to Physical Hydrology*; Oxford University Press, Oxford, United Kingdom, 352 p.
- Holding, S., Allen, D.M., Notte, C. and Olewiler, N. (2015): Enhancing water security in a rapidly developing shale gas region; *Journal of Hydrology: Regional Studies*, in press, corrected proof, 12 p., URL <<http://dx.doi.org/10.1016/j.ejrh.2015.09.005>> [December 2016].
- Huntley, D., Hickin, A. and Chow, W. (2011): Surficial geology, geomorphology, granular resource evaluation and geohazard assessment for the Maxhamish Lake map area (NTS 94-O), northeastern British Columbia; Geological Survey of Canada, Open File 6883, 20 p., doi:10.4095/289306
- Ingram, H.A.P. (1983): *Hydrology*; *in* Mires: Swamp, Bog, Fen and Moor, Ecosystems of the World, 4A, A.J.P. Gore (ed.), Elsevier, New York, New York, p. 67–158.
- Johnson, E. (2010): Conceptual water model for the Horn River Basin, northeast British Columbia (NTS 094O, parts of 094P, J); BC Ministry of Natural Gas Development, Geoscience Report 2010, p. 99–121.
- Kabzems, R., D’Aloia, M., Rex, J., Geertsema, M., Maloney, D. and MacKenzie, W. (2012): Monitoring indicators of wetland dynamics and hydrologic function in Fort Nelson watersheds; unpublished report prepared for BC Ministry of Forest, Lands and Natural Resource Operations, 26 p.
- Lohman, S.W. (1972): *Ground-Water Hydraulics*; United States Department of the Interior, Geological Survey Professional Paper 708, 70 p.
- Winkler, R.D., Moore, R.D., Redding, T.E., Spittlehouse, D.L., Carlyle-Moses, D.E. and Smerdon, B.D. (2010): Hydrologic processes and watershed; *in* Compendium of Forest Hydrology and Geomorphology in British Columbia, R.G. Pike, T.E. Redding, R.D. Moore, R.D. Winkler and K.D. Bladon (ed.), BC Ministry of Forests, Lands and Natural Resource Operations and FORREX Forum for Research and Extension in Natural Resources, BC Land Management Handbook 66, v. 1, p. 133–177.
- World Wildlife Fund (2009): HydroSHEDS; World Wildlife Fund, dataset, URL <<http://www.hydrosheds.org>> [October 2016].

British Columbia Natural Gas Atlas Project: 2016 Project Update

C. Evans, School of Earth and Ocean Sciences, University of Victoria, Victoria, BC, c2evans@uvic.ca

M.J. Whiticar, School of Earth and Ocean Sciences, University of Victoria, Victoria, BC

Evans, C. and Whiticar, M.J. (2017): British Columbia Natural Gas Atlas project: 2016 project update; *in* Geoscience BC Summary of Activities 2016, Geoscience BC, Report 2017-1, p. 75–78.

Introduction

Natural gas is associated with many sedimentary basins and marine depositional areas in British Columbia (BC). The BC Natural Gas Atlas (BC NGA) project (http://bc-NGA.ca/BC-NGA_Home.html) has just launched and proposes to map the major known gas occurrences throughout BC during the next few years, in a series of mapping phases. The initial phase of mapping has been focused on the areas of commercial natural gas production in northeastern BC (NEBC). The BC NGA project was initiated in response to regulatory changes, industry need and increased public recognition for geochemical data and basic interpretation. The industry uses gas geochemistry to understand hydrocarbon occurrences to aid in the identification and prioritization of areas of interest. Public interest stems from increased awareness of potential contamination issues, fugitive emissions, and supply and demand issues, such as the need for gas pipelines and LNG terminals.

The BC NGA project is using the concept of a ‘gas fingerprint’ based on molecular composition and analysis of stable isotopes of carbon and hydrogen to categorize and map gas sources, flow paths and destinations, both in geological/stratigraphic time and on a human timescale.

Background

Natural gas is a combination of naturally occurring hydrocarbons—primarily methane (CH₄), plus other non-hydrocarbon gases (in small amounts)—that can exist in a free or adsorbed phase in various types of reservoirs, frequently associated with possible hydrocarbon fluids. Economic production of natural gas as a fuel has a long history in BC, with most of the development in and production from NEBC. Environmental sensitivity of the public with regard to natural gas is increasing, with not only health effects from natural seeps and fugitive emissions being a significant concern (e.g., sour-gas effects on rural populations), but also the net effects of the same events on larger

systems such as the economy (e.g., increased national gross domestic product from exporting to international markets), climate change (e.g., methane as a greenhouse gas more important than CO₂) and public safety (e.g., pipeline explosion and/or fire occurrences).

In 2006, the BC Ministry of Energy and Mines (MEM) published the first edition of the Conventional Natural Gas Play Atlas of Northeast British Columbia in three parts (BC Ministry of Energy and Mines, 2006a–c). This document was a series of synopses of each of the stratigraphic targets for natural gas development and commercial production. The focus of the Natural Gas Play Atlas was the overall description of each conventional gas play by its geological (depositional, sedimentological, diagenetic, structural) and reservoir characteristics. The BC NGA project is adding a geochemical section to many, but not all, of the intervals presented and is also adding strata that was previously considered unconventional.

The regulatory requirement for the isotopic portion of the geochemistry was initiated by the BC Oil and Gas Commission (BCOGC) in October 2015 with further clarification early in 2016 (BC Oil and Gas Commission, 2015, 2016). The requirements for operators to test and submit results of molecular composition of natural gas, including public release of data, have resulted in more data being available over a longer timeframe (BC Oil and Gas Commission, 2010, 2015b). In support of the requirements for the isotopic portion, Geoscience BC initiated this project, but with the intent to also include mapping of the natural gas molecular composition.

Area of Study

Location and Access

As noted above there are many regions within BC that have natural gas occurrences, but the BC NGA project is currently focusing on the NEBC portion of the Western Canadian Sedimentary Basin (WCSB) as phase 1 (Figure 1). Current natural gas exploration and development within the NEBC portion of the WCSB (highlighted in green) is more focused in the four areas marked within the WCSB on Figure 1: the Montney, Liard Basin, Horn River Basin and Cordova Embayment. There are other portions of the

Keywords: British Columbia, natural gas, methane, isotopes, geochemistry, mapping, update

This publication is also available, free of charge, as colour digital files in Adobe Acrobat® PDF format from the Geoscience BC website: <http://www.geosciencebc.com/s/DataReleases.asp>.

WCSB in BC, but the strata elsewhere are in the mountainous physiographic region with very little gas production and even less data available. Further review of other areas with gas occurrences are discussed as future phases of the project. The project area covers almost 120 000 km² of the province, with the eastern edge being more than 630 km long and the northern edge being more than 280 km long. Much of the area is boreal forest of the Interior Plains physiographic region.

Geology

Many of the natural gas occurrences in BC are in intermontane basins or in basins associated with accreted terranes. The NEBC region is unique in that it is a portion of the WCSB, which is a preserved foreland basin. Future publications on this project will present the geology in more detail once the strata for analysis have been determined.

Sampling

Field sampling of mud gas from chip samples and production gas from shut-in commercial wells was proposed for both industry and project staff, but field access has only been permitted for industry staff. The large volumes of archival chip samples required to generate the equivalent of mud gas analysis are generally not available in long term storage after drilling is completed. This difficulty has required adjustments to the project, as described below.

The number of mud gas samples was expected to be more than 500, but only 116 mud gas samples have been received to date from industry. Due to the otherwise low activity by industry in drilling the categories described in the legislation, the project allowed an additional 29 samples of production gas (16 originals plus duplicates) and completed the same analysis. More samples of production gas are being received by the project and samples of mud gas from all categories of drilling are expected in the future.

Further sampling is anticipated from industry sources once issues of safe collection, transport and analysis of samples containing sour gas (H₂S) are resolved.

Methods

The samples were received by the lab at the Biogeochemistry Facility at the University of Victoria School of Earth and Ocean Sciences (Victoria, BC).

The samples were stored in a secure location and isotope analysis was completed in summer 2016. First, the molecular composition of the gas was determined by gas chromatography (GC) with flame ionization detection for C₁–C₄ hydrocarbon gases and thermal conductivity detection for the nonionizable gas, CO₂. Molecular composition was not completed for all possible chemical components (for example, noble gases are not analyzed). Stable isotope ratios

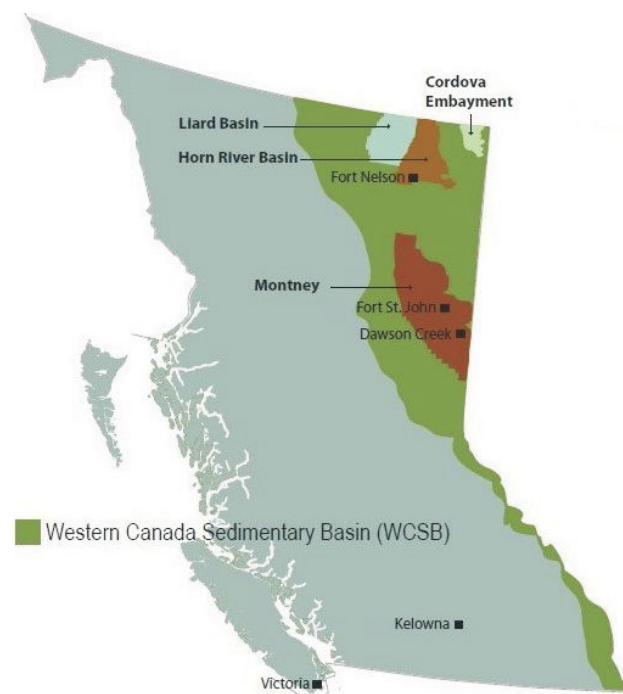


Figure 1. Location of the northeastern British Columbia portion of the Western Canadian Sedimentary Basin (in green), which is the project area for phase 1. The four sub-basins shown are current targets of natural gas exploration and development by industry (used with permission of the BC Oil and Gas Commission).

were measured by continuous flow–isotope ratio mass spectrometry (CF-IRMS), which is also referred to as GC-combustion-IRMS.

The carbon isotope ratio ($\delta^{13}\text{C}$) of the C₁–C₄ hydrocarbon gases are measured by online GC separation of the gas mixture (with He as carrier gas) followed by sequential oxidation of the individual species (CH₄, C₂H₆, C₃H₈, C₄H₁₀) to combustion CO₂ over a Cu-Pt wire microcombustion oven at approximately 1050°C. This combustion CO₂ is ported to an isotope ratio mass spectrometer (Finnigan™ MAT 252 or Delta+) to measure the isotopically different CO₂ molecules with atomic masses of 44, 45 and 46. These masses and their ratios are used to calculate the ¹³C/¹²C of the C₁–C₄ hydrocarbon gases, which is converted to conventional delta notation ($\delta^{13}\text{C}$) in ‰ (per mil) relative to the Vienna Pee Dee Belemnite (VPDB) standard. The accuracy and linearity of the measurements is determined by external calibration standards (Isometric Instruments standard gases). The external $\delta^{13}\text{C}$ accuracy and precision is $\pm 0.2\%$ for samples with >100 nmol hydrocarbon available.

Hydrogen isotope ratio ($\delta^2\text{H}$) or (δD) of the C₁–C₄ hydrocarbon gases are similarly measured by online GC separation of the gas mixture (with He as carrier gas), but is instead followed by sequential reduction of the individual species (CH₄, C₂H₆, C₃H₈, C₄H₁₀) to reduction H₂ over a Ni microreduction oven at approximately 1400°C. This reduc-

tion H_2 is ported to an isotope ratio mass spectrometer (Finnigan MAT 252 or Delta+) to measure the isotopically different H_2 molecules with the atomic masses of 2, 3 and 4. These masses and their ratios are used to calculate the $^2H/^1H$ (also known as D/H) of the C1–C4 hydrocarbon gases, which is converted to conventional delta notation (δ^2H) or (δD) in per mil relative to the Vienna standard mean ocean water (VSMOW) standard. The same statement applies for the accuracy and linearity but the precision is ± 0.3 – 0.4% , depending on compound and amount.

Data

Molecular composition data were downloaded from the server at the BCOGC and subjected to rigorous data quality assurance–quality control (QA-QC). A substantial portion of the more recent data is from horizontal wells with numerous multilateral (HZML) legs tested in each well. This detailed analysis is especially valuable for local mapping and gas fingerprinting; however, the concentration of data points from a single area that HZML emulates can lead to data ‘clusters’. This can lead to distortions when mapping at a regional scale and create geostatistical trends that ‘plateau’ the values. A consequence is that part of the data handling procedure is to manually decluster the data. The project method, which is undergoing constant refinement, will also elucidate any multimodal occurrences.

The addition of the new carbon and hydrogen stable isotope data into the integrated mapping results is expected to start in late 2016. The data will be eventually published as tables and associated maps on the Geoscience BC website (<http://www.geosciencebc.com/s/BCNaturalGasAtlas.asp>).

Analysis

Some of the early analyses were presented as a series of maps at the Unconventional Gas Technical Forum (UGTF) hosted by the BCOGC in April 2016 (Evans and Whiticar, 2016a, b). Those maps are not duplicated here because they are preliminary and subject to further QA-QC corrections as described above. The primary type of mapping algorithm is kriging using an unconstrained spherical variogram with octant search. Data will be presented on cross-sections through the strata in 2017. It is expected that the deliverables from the BC NGA project will include a full set of regional maps including contour plots and isopleths of gas compositions, and carbon plus hydrogen stable isotope ratios of methane and other light hydrocarbons. Where sufficient detailed depth data coverages allow, local cross-sections will be produced.

Future Work

The current discussion is somewhat restricted because the project is still in the start-up phase. As the project proceeds, web-based, analytical, database and visual products will be

generated. It is anticipated that the results may initiate a review of the points mentioned in the conclusion of this paper.

The ongoing activities include the collection, submission and analyses of industry gas samples from NEBC. Future sampling is expected to include increasing numbers of sour gas samples. As a consequence, sampling, transport, handling and analytical SOPs must be adjusted. Map generation will continue to integrate both existing and additional incoming data.

Conclusions

This project is creating new regional geochemistry maps to

- assemble a catalogue of unique natural gas compositional IDs for active gas operations in NEBC,
- characterize and map the geochemical conditions of BC’s major ongoing and future regions of petroleum exploration and production,
- contribute to understanding the geological framework of natural gas deposits at scales of fields to basins,
- assist petroleum system models to de-risk plays by understanding and predicting generation occurrences, histories and potential productivity of natural gas in BC,
- provide a robust baseline of gas signatures to identify and track fugitive emissions of natural gas (groundwater and atmosphere),
- offer a ‘geochemical DNA’ catalogue for different gas sources for provenance work in production, well completions, processing and transport and
- establish a database for fugitive emissions in surface waters and the atmosphere.

Most of the geochemistry is yet to be described and conclusions will be determined once the data review is completed.

Acknowledgments

The authors thank Geoscience BC and the Province of British Columbia for the opportunity to undertake this project. Support for the BC NGA project has been sustained from the BCOGC and the MEM and the staff at both organizations have been very helpful in supplying data, explaining data analysis and providing updates to the source database. Discussions with staff at Geoscience BC have influenced the direction of studies and will be supporting future releases of map products. Further support has been provided by the members of the Project Advisory Committee, who established this project as being very proactive in a challenging time for the energy industry. Also, the active operators have been very open with discussions and have provided support for the interim results.

References

- BC Ministry of Energy and Mines (2006a): Conventional natural gas play atlas, part 1; Petroleum Geology Publication 2006-01, BC Ministry of Energy and Mines, Oil & Gas Division, Resource Development & Geoscience Branch, URL <http://www2.gov.bc.ca/assets/gov/farming-natural-resources-and-industry/natural-gas-oil/petroleum-geoscience/oil-gas-reports/og_report_2006-1_nebc_atlas_part1.pdf> [October 2016].
- BC Ministry of Energy and Mines (2006b): Conventional natural gas play atlas; Petroleum Geology Publication 2006-01, BC Ministry of Energy and Mines, Oil & Gas Division, Resource Development & Geoscience Branch, URL <http://www2.gov.bc.ca/assets/gov/farming-natural-resources-and-industry/natural-gas-oil/petroleum-geoscience/oil-gas-reports/og_report_2006-1_nebc_atlas-2_part2.pdf> [October 2016].
- BC Ministry of Energy and Mines (2006c): Conventional natural gas play atlas; Petroleum Geology Publication 2006-01, BC Ministry of Energy and Mines, Oil & Gas Division, Resource Development & Geoscience Branch, URL <http://www2.gov.bc.ca/assets/gov/farming-natural-resources-and-industry/natural-gas-oil/petroleum-geoscience/oil-gas-reports/og_report_2006-1_nebc_atlas_part3.pdf> [October 2016].
- BC Oil and Gas Commission (2010): Section 17: well reports and well data; *in* Oil and Gas Activities Act: general regulation; B.C. Reg. 274/2010, URL <http://www.bclaws.ca/civix/document/id/loo83/loo83/274_2010#section17> [November 2016].
- BC Oil and Gas Commission (2015a): Isotopic analysis and submission guideline, URL <<https://www.bcogc.ca/isotopic-analysis-and-submission-guideline>> [October 2016].
- BC Oil and Gas Commission (2015b): Section 34: tests, analyses, surveys and logs; *in* Oil and Gas Activities Act: Drilling and Production Regulation, B.C. Reg. 165/2015, URL <http://www.bclaws.ca/civix/document/id/loo97/loo97/282_2010#section34> [November 2016].
- BC Oil and Gas Commission (2016): Industry bulletin 2016-07 submission of isotopic gas analyses; BC Oil and Gas Commission, March 8, 2016, URL <<https://www.bcogc.ca/indb-2016-07-submission-isotopic-gas-analyses>> [October 2016].
- Evans, C. and Whiticar, M.J. (2016a): BC Natural Gas Atlas: geochemical characterization of our energy resources; poster at Unconventional Gas Technical Forum, April 4, 2016, Victoria, British Columbia, URL <<https://www.bcogc.ca/10th-bc-unconventional-gas-technical-forum>> [October 2016].
- Evans, C. and Whiticar, M.J. (2016b): BC Natural Gas Atlas: initial results of gas geochemical mapping; poster at Unconventional Gas Technical Forum, April 4, 2016, Victoria, British Columbia, URL <<https://www.bcogc.ca/10th-bc-unconventional-gas-technical-forum>> [October 2016].

Consortium for Permafrost Ecosystems in Transition: Traversing the Southern Margin of Discontinuous Permafrost with Hydrological, Ecological and Remote Sensing Research, Northeastern British Columbia and Southwestern Northwest Territories

W.L. Quinton, Cold Regions Research Centre, Wilfrid Laurier University, Waterloo, ON, wquinton@wlu.ca

J.R. Adams, Cold Regions Research Centre, Wilfrid Laurier University, Waterloo, ON

J.L. Baltzer, Cold Regions Research Centre, Wilfrid Laurier University, Waterloo, ON

A.A. Berg, Department of Geography, University of Guelph, ON

J.R. Craig, Department of Civil and Environmental Engineering, University of Waterloo, Waterloo, ON

E. Johnson, Northeast Water Strategy, Government of British Columbia, Victoria, BC

Quinton, W.L., Adams, J.R., Baltzer, J.L., Berg, A.A., Craig, J.R. and Johnson, E. (2017): Consortium for Permafrost Ecosystems in Transition: traversing the southern margin of discontinuous permafrost with hydrological, ecological and remote sensing research, northeastern British Columbia and southwestern Northwest Territories; *in* Geoscience BC Summary of Activities 2016, Geoscience BC, Report 2017-1, p. 79–86.

Introduction and Project Scope

The southern margin of discontinuous permafrost, over a region comprising northeastern British Columbia (NEBC) and southwestern Northwest Territories (NWT), has experienced rising air temperatures in recent decades (Quinton et al., 2009). Analysis of streamflow records from gauged basins in the lower Liard River valley of this region shows that discharge is also increasing over a similar period despite no apparent changes to total annual precipitation (St. Jacques and Sauchyn, 2009; Connon et al., 2014). The land cover of this region mainly consists of upland and lowland forests and wetlands (e.g., bogs and fens), with a portion of the forested land cover underlain by permafrost. Bogs and fens have unique hydrological functions. Bogs are storage features whereas fens are channels that transport water laterally through the landscape. Degradation of permafrost ultimately leads to the conversion of forested plateaus to wetlands (Baltzer et al., 2014). Reported estimates of permafrost degradation for this region indicate that the change in aerial extent of permafrost coverage (i.e., decrease in forest/wetland expansion) is 28% from 1970 to 2012 (Coleman et al., 2015), 27% from 1947 to 2008 (Chasmer et al., 2010) and up to 50% from ~1950 to 2000 (Beilman and Robinson, 2003). Accordingly, various studies have attributed rising streamflow in gauged basins over the region to both shrinking aerial extent and thickness of

permafrost (e.g., St. Jacques and Sauchyn, 2009; Quinton and Baltzer, 2013a; Connon et al., 2014).

In addition to correlated trends among rising air temperature and streamflow records concomitant with estimates of permafrost loss, industrial activities are occurring or have historically occurred over parts of the region in the form of exploration and extraction for oil and natural gas. These influences add extra complexity to understanding and predicting future hydrological consequences of climate warming over the region. Industrial activities have two major implications for land cover change and water resources availability: 1) permanent impacts of linear disturbances (i.e., deforested corridors created for seismic exploration, winter roads and pipelines; Lee and Boutin, 2006) and 2) industrial uses of large volumes of surface water for hydraulic fracturing of shale gas in NEBC (Hayes, 2010; Johnson, 2010). Linear disturbances have been made throughout the landscape of the NEBC–NWT border region since at least the 1970s. There is evidence that the removal of vegetation for linear disturbances significantly alters the thermal properties of the ground so much that, over time, this leads to permafrost-free corridors (Williams and Quinton, 2013; Braverman and Quinton, 2016). It has been suggested that the permafrost degradation along these corridors imposes surface water flow paths over the landscape, which connect forest and wetland land cover types (i.e., permafrost and permafrost-free areas), accelerate permafrost thaw, and potentially promote wetland drainage along topographic gradients (Williams et al., 2013). In terms of hydraulic fracturing present in NEBC, high volumes of water and other materials are injected into the ground to gain access to trapped geological deposits of shale gas. Johnson

Keywords: *British Columbia, permafrost, environmental change, linear disturbances*

This publication is also available, free of charge, as colour digital files in Adobe Acrobat® PDF format from the Geoscience BC website: <http://www.geosciencebc.com/s/DataReleases.asp>.

(2010) and Hayes (2010) report that an estimated 1200 to >4000 m³ of water are needed per fracture, which among other environmental concerns, represents a major demand on surface water and groundwater availability. This significant industrial demand must be managed effectively relative to the regional water balance, local community needs and considerations for future availability (Johnson, 2010).

Accurate estimation of future water resources in the NEBC–NWT border region is of interest for industry, community groups and governments across the region, as it will enable them to promote sustainable water use among users, assist in environmental change adaptation strategies and mitigate environmental impacts from climate warming and industrial development (e.g., Government of the Northwest Territories, 2008; Johnson, 2010). However, scientific knowledge of the changing hydrology of this region under coupled climate warming and industrial impact scenarios is relatively limited. It is commonly recognized among industry, community and government stakeholders that this issue is complicated by a lack of baseline and continuous hydrological monitoring data. Additionally, relatively few scientific studies have been completed to understand climate-driven and industrial impacts to land cover change and water availability across the region. Consequently, present efforts to apply hydrological models to the estimation of future water availability under varied scenarios of industrial disturbance and climate warming are subject to considerable uncertainty. Modelling efforts are further complicated by a lack of publicly available land cover datasets, such as detailed wetland and topography maps, as many current products are either outdated, inaccurate or developed at insufficient spatial resolutions.

The Consortium for Permafrost Ecosystems in Transition (CPET) was formed in 2015 among academic researchers, industry partners, and community and government groups

to address the aforementioned issues being faced by the NEBC–NWT border region. The long-term goal of CPET is to produce robust scientific knowledge of, and datasets on, climate-driven and industrial-imposed environmental changes to reduce uncertainty of water resources modelling. The CPET has five science objectives, which are listed in Table 1. The purpose of this paper is to summarize and report on CPET progress to date from 2015. For an extended project description and a literature synthesis on the science background of CPET, the reader is referred to Quinton et al. (2016).

Development of Study Sites

The CPET research activities are completed over an approximately 175 km transect oriented north-south, which traverses the zone of discontinuous permafrost in southwestern NWT and northeastern BC (Figure 1). Field studies are concentrated at two research basins, which form latitudinal end members of the study region. Scotty Creek research basin (north) was established prior to the formation of CPET. Suhm Creek research basin (south) was established by CPET as a research site in 2015–2016 to act as a paired basin to Scotty Creek. The ongoing development of instrumentation capacity and datasets for Suhm Creek research basin is anticipated as a key legacy of CPET. From a hydrological modelling perspective, the development of a paired research basin to the south of Scotty Creek is a major advantage for developing and evaluating models at sites representing different latitudinal positions along the southern margin of discontinuous permafrost. It is noted that a significant difference between Scotty Creek and Suhm Creek basins is that Scotty Creek has no industrial presence, other than linear disturbances from prior to 1985, whereas Suhm Creek is representative of current industrial activity in NEBC (e.g., shale gas exploration in the Horn River geological basin). This allows for insights into as-

Table 1. Five science objectives of the Consortium for Permafrost Ecosystems in Transition (CPET).

Objective 1	Map the changing spatial distribution of permafrost, wetland and forest coverage over the study area using aerial photography, satellite images and light detection and ranging (LiDAR) images.
Objective 2	For different ground thaw and moisture conditions, conduct field studies to improve the understanding of the volume and timing of runoff from a) peat plateau–bog complexes and b) the adjacent channel fens, which convey the runoff that they receive from plateau-bog complexes to streams and rivers. For each setting, the water flux and storage processes that control runoff will be examined.
Objective 3	Simulate the major water flux and storage processes controlling runoff from the plateau-bog complexes using the cold regions hydrological model (CRHM) and the Raven hydrological modelling framework, and, where needed, make improvements to both models based on the improved process understanding arising from objective 2.
Objective 4	Improve the ability to characterize permafrost impacts at larger scales through field investigation and subsequent adaptation of the northern ecosystem soil temperature (NEST) regional-scale permafrost model to handle the unique thaw response of bogs, fens and plateaus.
Objective 5	Use information generated from the improved hydrological models (in objective 3) and the permafrost model (in objective 4) to estimate future quantities of runoff and surface water storage within boreal and subarctic landscapes with discontinuous permafrost under possible scenarios of climate warming and human disturbance.

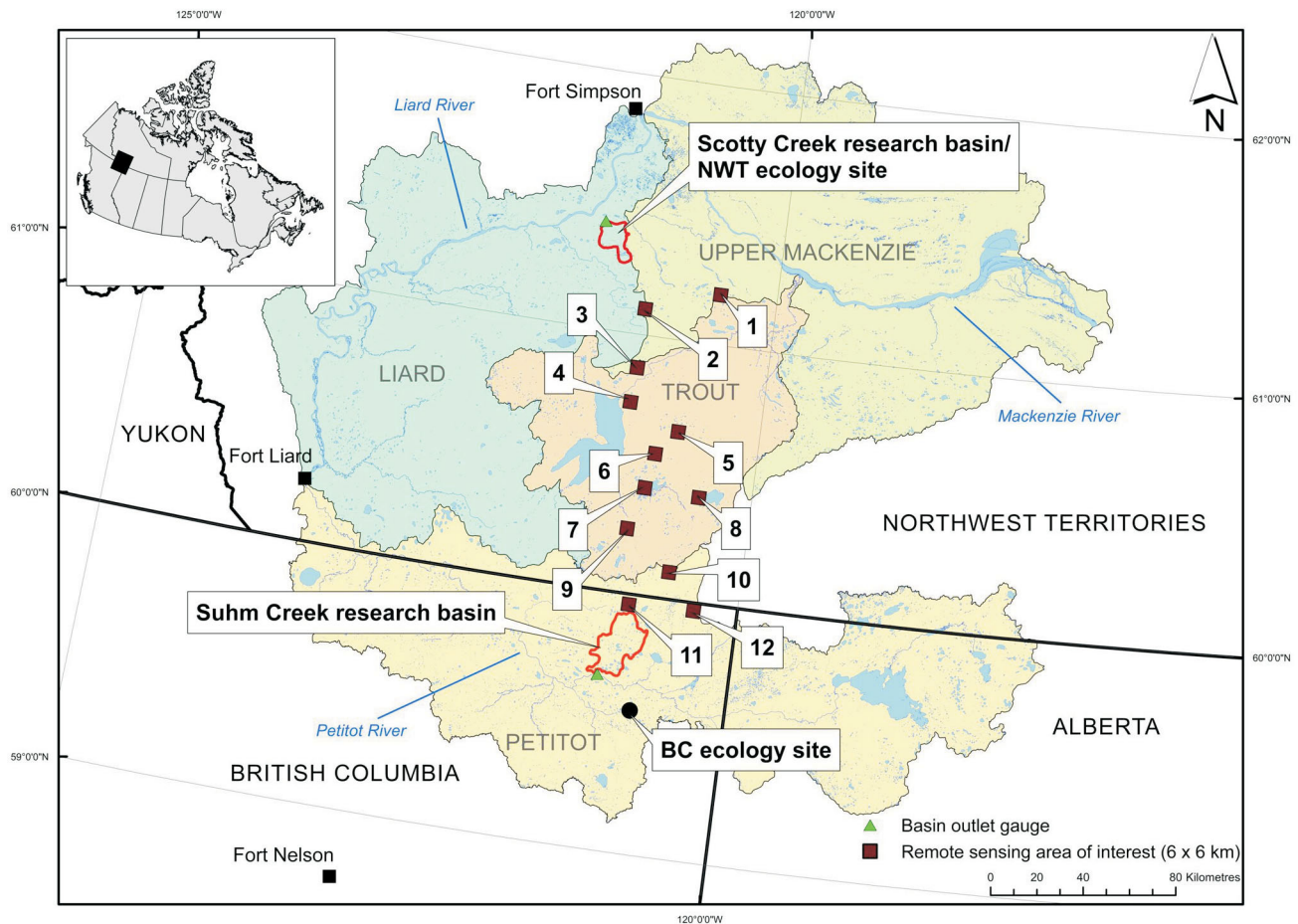


Figure 1. The Consortium for Permafrost Ecosystems in Transition (CPET) focuses on a north-south oriented study region traversing the southern margin of discontinuous permafrost (refer to Heginbottom and Radburn, 1992), northeastern British Columbia (BC) and south-western Northwest Territories (NWT). Field studies are concentrated at Scotty Creek and Suhm Creek research basins and additional observations are done at remote sensing areas of interest over the region. Note: streamflow gauge indicated for Suhm Creek is planned for installation during the CPET project but had not been installed at the time of publication. Base maps of watershed boundaries (red line) and water features are from the national hydro network (GeoBase®, 2014).

sessing impacts of industrial activities on basins in the zone of discontinuous permafrost. For example, this is demonstrated by the contrast in linear disturbance densities over Scotty Creek and Suhm Creek research basins shown in Figure 2.

Scotty Creek

Scotty Creek basin is estimated to be approximately 140 km² and drains into the Liard River. Discharge from the basin has been measured continuously since 1996 by the Water Survey of Canada (Connon et al., 2014). The basin is located approximately 50 km south of Fort Simpson, NWT. The topography is relatively flat (~250 m relief) and land cover is dominated by upland forest, treed plateaus, flat bogs and channel fens (for further description, refer to Quinton et al., 2011; Chasmer et al., 2014). Approximately half the basin consists of peat plateaus, bogs and fens. Research involving data from field studies, automated instruments and remote sensing has been conducted at Scotty

Creek continuously since 1999. A growing body of scientific literature regarding hydrology of the discontinuous permafrost zone has been produced from this site, giving important insights for hydrological modelling. For example, understanding the functions of major land cover types (e.g., peat plateaus, channel fens and flat bogs) and their roles in runoff generation (e.g., Quinton et al., 2003; Wright et al., 2009), linkages between land cover change and streamflow (e.g., Connon et al., 2014), hydraulic properties of peatlands (e.g., Quinton and Baltzer, 2013b) and ecological responses to permafrost thaw (e.g., Patankar et al., 2015). A significant amount of infrastructure is currently in place at Scotty Creek, including a simple field camp for researchers (e.g., tents) and an array of automated instrumentation measuring climate and hydrological variables across different land cover types (e.g., bogs, fens and peat plateaus). These instruments measure variables such as precipitation, air temperature, relative humidity, wind speed, incoming and outgoing radiation, snow height, soil

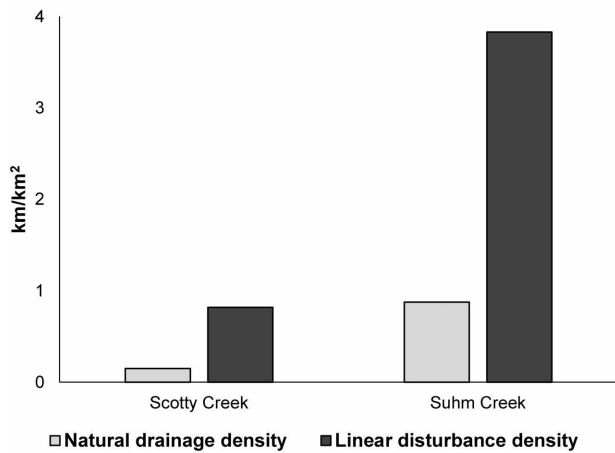


Figure 2. Linear disturbance densities for Scotty Creek and Suhm Creek research basins (Northwest Territories and British Columbia, respectively) compared to natural drainage densities. Data for Scotty Creek is from Quinton et al. (2009). Linear disturbance densities for Suhm Creek are estimated from digitizing disturbances visible within a 143 km² sample of the basin using high resolution airphotos (<1 m). The drainage density of Suhm Creek is calculated using stream network length (obtained from Natural Resources Canada as a GIS vector layer) relative to the corresponding estimated basin area.

moisture and soil temperature at sites across the basin. A large volume of field sampling has been conducted at Scotty Creek, including measurements of active layer depth and talik formation (e.g., using ground penetrating radar), snow water equivalent, soil moisture and vegetation properties (e.g., leaf area index [LAI]).

Suhm Creek

Suhm Creek basin is approximately 150 km northeast of Fort Nelson, BC, and drains into the Petitot River, which flows into the Liard River at Fort Liard (Figure 1). Suhm Creek basin is estimated to be 365 km² and there is ~200 m of topographic relief over the basin. Johnson (2010) conducted a review of basic hydrological modelling needs in the NEBC region (e.g., Suhm Creek) and identified key information gaps necessary for modelling. Johnson (2010) included 1) delineation of wetlands to identify proportions of fens and bogs; 2) knowledge of permafrost spatial distribution; 3) climate monitoring for major land cover types; 4) stream gauging; 5) water table measurement; and 6) topography data. For example, identifying the proportions of land cover types is important for modelling basin runoff because different land cover types have been shown to control unique runoff responses (Quinton et al., 2003). Specifically, it has been demonstrated that an increased proportion of bogs is inversely related to runoff, whereas a greater proportion of fens is positively correlated with runoff (Connon et al., 2014). Although the types of land covers are relatively similar between Suhm Creek and Scotty Creek basins (mixed forested peatlands and wetlands), work to

characterize the differences in distributions of these land covers is in progress.

Much of the data requirements for hydrological modelling identified by Johnson (2010) have been addressed for Scotty Creek basin (Quinton et al., 2016), however, significant work is necessary to address these needs at Suhm Creek basin. As such, ongoing work is being conducted at Suhm Creek to address these gaps by installing automated instruments, completing field sampling and obtaining remote sensing datasets. Various instrumentation has been installed in the basin in 2015–2016 to provide continuous monitoring data of hydrological variables. Specifically, two climate monitoring stations were installed in late 2015 with analogous measurement capabilities to those at Scotty Creek basin. One climate station is located in a forested peat-plateau and the other is in an open wetland site. Data from these stations are used to characterize energy budgets of each land cover type. Pressure transducers have also been deployed at six nodes of Suhm Creek basin to measure water level and to assist in understanding the flow routing of streams over the basin and parameterize routing in distributed hydrological models. Installation of an automated stream discharge gauge near the outlet of Suhm Creek at Petitot River is also planned for the future to monitor total basin discharge (Figure 1). In terms of field sampling, distributed measurements are being done along transects of peat plateaus during site visits to Suhm Creek basin to determine permafrost presence relative to forested land cover and characterize depth to permafrost relative to distances from forested edges. The CPET researchers have obtained remote sensing datasets over Suhm Creek basin and work is being completed to map both forest and wetland land covers at high resolutions, similar to that of Scotty Creek basin (Chasmer et al., 2014). A light detection and ranging (LiDAR)-derived digital elevation model has also been obtained and can be used to estimate surface water pathways along topographic gradients.

Remote Sensing Areas of Interest

In addition to field studies and data development of Suhm Creek and Scotty Creek basins, remote sensing areas of interest (AOI) have been established along a north-south configuration in the NEBC–NWT border region (Figure 1). These AOI connect the two research basins and enable sampling of land cover distributions along a latitudinal distribution over the southern margin of discontinuous permafrost (Figure 1). Each of the 12 AOI has a footprint of 36 km² (432 km² total area). Imagery stacking over these sites includes recent Landsat 8 (30 m resolution) and WorldView-1 and -2 (50 cm resolution) datasets and historical aerial photographs acquired in 1970–1971 (1.2 m resolution). Detailed statistical characterization of the land covers within these AOI is being developed at high resolutions, providing information on proportions of major land cover

types, and changes to these land cover types over a 40-year period. For example, one aspect of this work is examining changes to the total areas of forested plateaus and bogs. This can be useful as an indicator of decreased permafrost areal extent over time because the total area of bogs increases as plateaus underlain by permafrost decrease (Beilman and Robinson, 2003). Also within the remote sensing AOI, linear disturbance densities (Figure 3) and proportions of land cover intersected by these disturbances are being mapped. For example, Figure 3 illustrates the distribution of linear disturbance densities across selected remote sensing AOI of the study region.

Progress Toward Science Objectives

Assessing the Rate and Pattern of Permafrost Loss and Related Vegetation Change Using Remote Sensing

Analysis of satellite remote sensing datasets acquired over Scotty Creek and Suhm Creek research basins and remote sensing AOI commenced in 2015–2016 to determine rates and spatial extent of forest and bog changes over a 40-year period. From these, information on permafrost degradation is inferred from the changing vegetation composition. A very large coverage of spatial information is being generated from analysis of these remote sensing datasets providing robust estimates of land cover change across the NEBC–NWT region. Unlike previous small-scale estimates of change using remote sensing change detection (e.g., Chasmer et al., 2010), this work involves distributed sampling across the discontinuous permafrost region. To support this work, field verification was conducted in 2016 to validate permafrost presence according to vegetation distribution and ensure correct identification of land cover types during visual and automated interpretation of remote sensing images.

Field Studies on Water Flux and Storage Processes

The CPET is using modelling as a tool for hypothesis testing at local scales to evaluate the efficacy of conceptual models developed from field observations, which describe specific hydrological processes. These local predictions of hydrological processes can then be upscaled to estimate hydrological fluxes over an entire basin. A significant amount of field studies was completed at Scotty Creek research basin in 2015–2016 and prior to the formation of CPET (Quinton et al., 2016), from which conceptual models of local-scale hydrological processes are being developed. For example, in the past year sampling was done at points throughout Scotty Creek basin to survey talik formation (unfrozen layer within permafrost ground) and frost table measurements. These data are applicable to parameterizing subsurface water flow and con-

nectivity within computational models. Very high resolution imagery (3 cm) was gathered from fixed-wing and rotary unmanned aerial vehicle (UAV) platforms for specific areas of interest within Scotty Creek research basin, including multispectral, thermal and infrared sensors. These data are used to develop very high resolution elevation products and identify surface temperatures of land cover features. This information contributes toward development of hydraulic roughness algorithms for modelling runoff between land cover types (e.g., isolated bogs and interconnected bogs). Data are now being analyzed from pressure transducers installed along stream nodes in Scotty Creek and Suhm Creek research basins in 2015–2016 to characterize hydrological routing. Finally, data are being analyzed from sap flow sensors installed on trees at Scotty Creek and a site near Suhm Creek (NWT and BC ecology sites on Figure 1) in 2015–2016 to characterize evapotranspirative fluxes over forested areas underlain by permafrost for inclusion in hydrological modelling calculations.

Development and Testing of Hydrological Models to Simulate Water Flow and Storage

The CPET uses both the cold regions hydrology model (CRHM; Pomeroy et al., 2007) and Raven model (The Raven Development Team, 2014). Knowledge developed from field studies at Scotty Creek is being incorporated to parameterize these models to predict hydrological processes over local and basin scales. Both CHRM and Raven are object-oriented frameworks developed for simulating the energy and water balance of hydrological response units (HRU). The HRU corresponds to a spatial footprint of similar biophysical features and processes, in which mass and energy balances can be generalized (Pomeroy et al., 2007). Therefore, in a given HRU, a model can be parameterized with a single set of parameters and state variables. Important achievements were made in 2015–2016 to parameterize HRU in hydrological models, building off existing work. The CRHM computations of snowmelt, active

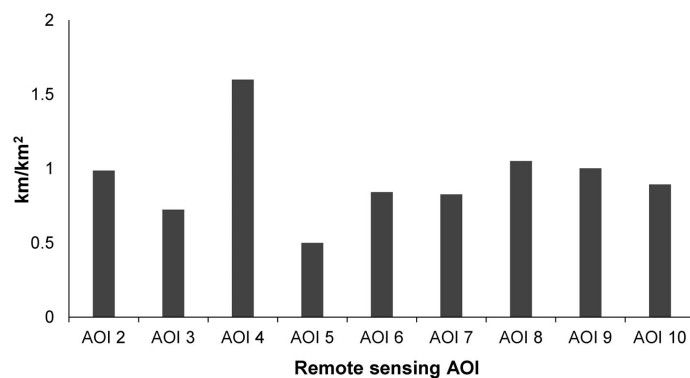


Figure 3. Linear disturbance densities for selected remote sensing areas of interest (AOI; 36 km² each) shown in Figure 1, numbered from north to south (Northwest Territories to British Columbia). Data are determined from digitizing visible seismic lines, winter roads and pipelines within 50 cm resolution WorldView-1 and -2 images.

layer thaw and subsurface flux have been conducted for Scotty Creek at bogs, fens and plateaus (Quinton et al., 2016). The current focus for Scotty Creek basin is on model development of these computations within the Raven platform.

Conclusion

Industry, government and community groups in the NEBC–NWT border region acknowledge that there is a lack of monitoring data related to water resources. As a result, there are currently high levels of uncertainty in existing hydrological modelling tools for predicting water resources availability in the future under climate warming and industrial development scenarios. The CPET is filling this gap by developing new science-based conceptual and computational models to predict future permafrost thaw and determine the implications for water resources availability. This information is integral to plan for, and adapt to, impacts of permafrost thaw under varied scenarios. For example, the knowledge generated by CPET can be applied to limit damage to infrastructure caused by permafrost thaw (Government of the Northwest Territories, 2008) or be applied so that industry can confidently plan future operations, such as hydraulic fracturing, based on available water supplies (Johnson, 2010).

Next Steps

The CPET work in 2016–2017 will build on existing knowledge and continue development of study sites to focus on 1) permafrost modelling and 2) basin-scale hydrological prediction under future scenarios. In addition, further field studies and modelling work will be done at Suhm Creek basin to test the similarity and reproducibility of conceptual models developed for Scotty Creek basin. Activities for permafrost modelling will concentrate on field studies to better understand the energy dynamics of receding permafrost at the edges of treed plateaus. One example of this is sampling the subsurface permafrost composition using electrical resistivity imaging. As well, work will be completed to predict permafrost thaw using the northern ecosystem soil temperature (NEST) model (Zhang et al., 2006). Permafrost models are typically run at relatively coarse resolutions (e.g., 1000 km²), however, information generated from ongoing work (e.g., land cover distributions generated from remote sensing) will be leveraged to scale this model for application at finer spatial scales (e.g., 1 km²). Activities toward basin-scale hydrological prediction will include preparing CHRM and Raven hydrological models to simulate streamflow in Scotty Creek and Suhm Creek research basins. The accuracy of these models will be evaluated using instruments deployed throughout the basins, and adjustments to model parameters can be incorporated as necessary. Once it has been established that reasonable modelling accuracy has been achieved, these

models will be coupled with NEST to simulate future water resources scenarios according to hypothetical land cover changes.

Acknowledgments

Consortium for Permafrost Ecosystems in Transition is funded by a Natural Sciences and Engineering Research Council of Canada Collaborative Research and Development grant with partner contributions from Nexen Energy ULC, Petroleum Technology Alliance of Canada, Geoscience BC and BC Oil and Gas Research and Innovation Society. The authors gratefully acknowledge the support of Fort Nelson First Nation, Liidlii Kue First Nation, Jean Marie River First Nation, Government of the Northwest Territories and Government of British Columbia. This article benefited from a review by M. English at Wilfrid Laurier University.

References

- Baltzer, J.L., Veness, T., Chasmer, L.E., Sniderhan, A. and Quinton W.L. (2014): Forests on thawing permafrost: fragmentation, edge effects, and net forest loss; *Global Change Biology*, v. 20, no. 3, p. 824–834, doi:10.1111/gcb.12349
- Beilman, D.W. and Robinson, S.D. (2003): Peatland permafrost thaw and landform type along a climate gradient; *in* Proceedings of the Eighth International Conference on Permafrost, M. Phillips, S.M. Springman and L.U. Arenson (ed.), Zurich, Switzerland, July 21–25, 2003, A.A. Balkema, v. 1, p. 61–65.
- Braverman, M. and Quinton, W.L. (2016): Hydrological impacts of seismic lines in the wetland-dominated zone of thawing, discontinuous permafrost, Northwest Territories, Canada; *Hydrological Processes*, v. 30, p. 2617–2627, doi:10.102/hyp.10695
- Chasmer, L., Hopkinson, C. and Quinton, W. (2010): Quantifying errors in plateau changes from optical data, Northwest Territories, Canada: 1947–2008; *Canadian Journal of Remote Sensing*, v. 36, no. S2, p. S211–S223, doi:10.5589/m10-058
- Chasmer, L., Hopkinson, C., Veness, T., Quinton, W. and Baltzer, J. (2014): A decision-tree classification for low-lying complex land cover types within the zone of discontinuous permafrost; *Remote Sensing of Environment*, v. 143, p. 73–84, doi:10.1016/j.rse.2013.12.016
- Coleman, K.A., Palmer, M.J., Korosi, J.B., Kokelj, S.V., Jackson, K., Hargan, K.E., Courtney Mustaphi, C.J., Thienpont, J.R., Kimpe, L.E., Blais, J.M., Pisaric, M.F.J. and Smol, J.P. (2015): Tracking the impacts of recent warming and thaw of permafrost peatlands on aquatic ecosystems: a multi-proxy approach using remote sensing and lake sediments; *Boreal Environment Research*, v. 20, no. 3, p. 363–377.
- Connon, R.F., Quinton, W.L., Craig, J.R. and Hayashi, M. (2014): Changing hydrologic connectivity due to permafrost thaw in the lower Liard River valley, NWT, Canada; *Hydrological Processes*, v. 28, no. 14, p. 4163–4178, doi:10.1002/hyp.10206
- GeoBase® (2014): National hydro network; Natural Resources Canada, URL <[http://geogratis.gc.ca/api/en/nrcan-rncan/ess-sst/-\(urn:iso:series\)geobase-national-hydro-network-nhn?sort-field=relevance](http://geogratis.gc.ca/api/en/nrcan-rncan/ess-sst/-(urn:iso:series)geobase-national-hydro-network-nhn?sort-field=relevance)> [October 2016].

- Government of the Northwest Territories (2008): NWT Climate Change Impacts and Adaptation Report, 2008; Northwest Territories, Environment and Natural Resources, 31 p., URL <http://www.enr.gov.nt.ca/sites/default/files/reports/nwt_climate_change_impacts_and_adaptation_report.pdf> [December 2016].
- Hayes, B.J.R. (2010): Horn River Basin aquifer characterization project, northeastern British Columbia (NTS 094I, J, O, P); progress report; *in* Geoscience BC Summary of Activities 2009, Geoscience BC, Report 2010-1, p. 245–248, URL <http://www.geosciencebc.com/i/pdf/SummaryofActivities2009/SoA2009_Hayes.pdf> [November 2016].
- Heginbottom, J.A. and Radburn, L.K., compilers (1992): Permafrost and ground ice conditions of northwestern Canada; Geological Survey of Canada, Map 1691A, scale 1:1 000 000.
- Johnson, E. (2010): Conceptual water model for the Horn River Basin, northeast British Columbia (parts of NTS 094I, J, O, P); *in* Geoscience Reports 2010, BC Ministry of Energy, Mines and Petroleum Resources, p. 99–121.
- Lee, P. and Boutin, S. (2006): Persistent and developmental transition in wide seismic lines in the western boreal plains of Canada; *Journal of Environmental Management*, v. 78, no. 3, p. 240–250, doi:10.1016/j.jenvman.2005.03.016
- Patankar, R., Quinton, W.L., Hayashi, M. and Baltzer, J.L. (2015): Sap flow responses to seasonal thaw and permafrost degradation in a subarctic boreal peatland; *Trees – Structure and Function*, v. 29, no. 1, p. 129–142, doi:10.1007/s00468-014-1097-8
- Pomeroy, J.W., Gray, D.M., Brown, T., Hedstrom, N.R., Quinton, W.L., Granger, R.J. and Carey, S.K. (2007): The cold regions hydrological model: a platform for basing process representation and model structure on physical evidence; *Hydrological Processes*, v. 21, no. 19, p. 2650–2667, doi:10.1002/hyp.6787
- Quinton, W.L. and Baltzer, J.L. (2013a): Changing surface water systems in the discontinuous permafrost zone: implications for streamflow; *in* Cold and Mountain Region Hydrological Systems Under Climate Change: Towards Improved Projections, Proceedings of H02, IAHS-IAPSO-IASPEI Assembly, Gothenburg, Sweden, July 2013, International Association of Hydrological Sciences, Publication 360, p. 85–92.
- Quinton, W.L. and Baltzer, J.L. (2013b): The active-layer hydrology of a peat plateau with thawing permafrost (Scotty Creek, Canada); *Hydrogeology Journal*, v. 21, no. 1, p. 201–220, doi:10.1007/s10040-012-0935-2
- Quinton, W.L., Adams, J.R., Baltzer, J.L., Berg, A.A., Craig, J.R. and Johnson, E. (2016): Permafrost ecosystems in transition: understanding and predicting hydrological and ecological change in the southern Taiga Plains, northeastern British Columbia and southwestern Northwest Territories; *in* Geoscience BC Summary of Activities 2015, Geoscience BC, Report 2016-1, p. 89–94, URL <http://www.geosciencebc.com/i/pdf/SummaryofActivities2015/SoA2015_Quinton.pdf> [November 2016].
- Quinton, W.L., Hayashi, M. and Chasmer, L.E. (2009): Peatland hydrology of discontinuous permafrost in the Northwest Territories: overview and synthesis; *Canadian Water Resources Journal*. v. 34, no. 4, p. 311–328.
- Quinton, W.L., Hayashi, M. and Chasmer, L.E. (2011): Permafrost-thaw-induced land-cover change in the Canadian subarctic: implications for water resources; *Hydrological Processes (Scientific Briefing)*, v. 25, no. 1, p. 152–158, doi:10.1002/hyp.7894
- Quinton, W.L., Hayashi, M. and Pietroniro, A. (2003): Connectivity and storage functions of channel fens and flat bogs in northern basins; *Hydrological Processes*, v. 17, no. 18, p. 3665–3684, doi:10.1002/hyp.1369
- St. Jacques, J.M. and Sauchyn, D.J. (2009): Increasing winter base flow and mean annual streamflow from possible permafrost thawing in the Northwest Territories, Canada; *Geophysical Research Letters*, v. 36, no. L01401, doi:10.1029/2008GL035822
- The Raven Development Team (2016): Raven, version 2.6; modelling framework, University of Waterloo, <<http://www.civil.uwaterloo.ca/jrcraig/Raven/Main.html>> [May 2016].
- Williams, T.W. and Quinton, W.L. (2013): Modelling incoming radiation on a linear disturbance and its impact on the ground thermal regime in discontinuous permafrost; *Hydrological Processes*, v. 27, no. 13, p. 1854–1865, doi:10.1002/hyp.9792
- Williams, T.W., Quinton, W.L. and Baltzer, J.L. (2013): Linear disturbances on discontinuous permafrost: implications for thaw-induced changes to land cover and drainage patterns; *Environmental Research Letters*, v. 8, no. 025006, p. 1–12, doi:10.1088/1748-9326/8/2/025006
- Wright, N., Hayashi, M. and Quinton, W.L. (2009): Spatial and temporal variations in active-layer thawing and their implication on runoff generation; *Water Resources Research*, v. 45, no. W05414, doi:10.1029/2008WR006880
- Zhang, Y., Chen, W. and Riseborough, D.W. (2006): Temporal and spatial changes of permafrost in Canada since the end of the Little Ice Age; *Journal of Geophysical Research-Atmospheres*, v. 111, no. D22103, doi:10.1029/2006JD007284

Techno-Economic Assessment of Geothermal Energy Resources in the Western Canada Sedimentary Basin, Northeastern British Columbia

K. Palmer-Wilson, University of Victoria, Victoria, BC, kevinpw@uvic.ca

W. Walsh, BC Ministry of Energy and Mines, Victoria, BC

J. Banks, University of Alberta, Edmonton, AB

P. Wild, University of Victoria, Victoria, BC

Palmer-Wilson, K., Walsh, W., Banks, J. and Wild, P. (2017): Techno-economic assessment of geothermal energy resources in the Western Canada Sedimentary Basin, northeastern British Columbia; *in* Geoscience BC Summary of Activities 2016, Geoscience BC, Report 2017-1, p. 87–90.

Introduction

To date, no commercial geothermal electric power plant has been successfully developed in Canada. Much of the research and development activities in British Columbia (BC) have concentrated around the high-temperature volcanic geology of the Mount Meager complex, but these have yet to yield a commercial power plant. The Western Canada Sedimentary Basin (WCSB) in northeastern BC has received less attention, in part due to its lower temperature resource. However, this region has been subject to substantial oil and gas development, and a significant amount of data from drilling activities is available (Grasby et al., 2012). This data has been successfully applied to estimate the electric power potential for a project in the Clarke Lake gas field (Walsh, 2013). In this study, this data is applied to a broader region to assess the potential and the cost for geothermal power plants in the WCSB within BC (Figure 1).

The latest, most comprehensive techno-economic study of geothermal resources in BC was recently released by Geoscience BC (Kerr Wood Leidal Associates Ltd., 2016). Here, 19 sites were pre-evaluated for their feasibility, taking into account factors like distance to transmission and road access, as well as a number of other parameters. The 11 favourable sites were evaluated in detail for technical and economic potential. The volume method (Williams et al., 2008) was applied to assess the potential electric power. Further, the Geothermal Electricity Technology Evaluation Model (GETEM) was applied to assess the levelized cost of electricity (LCOE) for each project. Two of the projects assessed in this study are located in the WCSB, namely Clarke Lake and Jedney (Figure 1). Their projected LCOE

was \$297 per megawatt-hour (MWh) and \$398/MWh, respectively, higher than any other project in the study.

Since the release of this study, a number of questions have been raised regarding the assumptions that led to the assessed LCOE values. For example, drilling costs were based on the situation in 2012, a boom year for the oil and gas industry. Since then, the significant decline of oil and gas prices has caused drilling costs to drop considerably. A decrease in this cost item is expected to have a significant impact on LCOE.

Further, the required exploration plan for the sedimentary basin projects may be less elaborate than assumed in the Geoscience BC study. Considering the number of oil and gas wells already existing in the area, it has been assumed that the number of required exploration wells is lower and the success rate of confirmation wells is higher than previously anticipated. This research project will therefore use data from oil and gas exploration (files provided by the BC Oil and Gas Commission) to refine costs for projects in the sedimentary basin.

Methodology

In order to assess the economic feasibility of geothermal power plants in northeastern BC, the first step is to locate those areas where economic feasibility is most likely. A favourability map that takes geological and economic factors into account is created. This map is used to select particular locations that are representative for their geological and economic environment. In the second step, the economic feasibility of a geothermal power plant at those select locations is assessed.

Site Selection

Identifying the most favourable site for a geothermal power plant is a spatial decision-making problem. In this study, an adaptation of the weighted linear combination (Malczewski, 2000; Nyerges and Jankowski, 2009) is employed,

Keywords: *British Columbia, geothermal energy, favourability map, spatial decision making, GETEM, economic assessment*

This publication is also available, free of charge, as colour digital files in Adobe Acrobat® PDF format from the Geoscience BC website: <http://www.geosciencebc.com/s/DataReleases.asp>.



Figure 1. Project area and two of the potential sites for geothermal development, northeastern British Columbia. Background map created using ArcGIS® software by Esri. ArcGIS® and ArcMap™ are the intellectual property of Esri and are used herein under license. Copyright® Esri. All rights reserved. For more information about Esri® software, please visit www.esri.com.

due to its relative simplicity for dealing with a small number of input criteria. The process (Figure 2) will be implemented in a geographic information system (GIS), such as ArcGIS or QGIS.

The favourability map depicts the favourability score for each grid point within the project area. The score is a mea-

sure of the potential economic feasibility of developing a geothermal power plant. A higher favourability score indicates a higher likelihood of a geothermal plant being economically feasible at a particular location. Therefore, several criteria that contribute to geothermal favourability are taken into account.

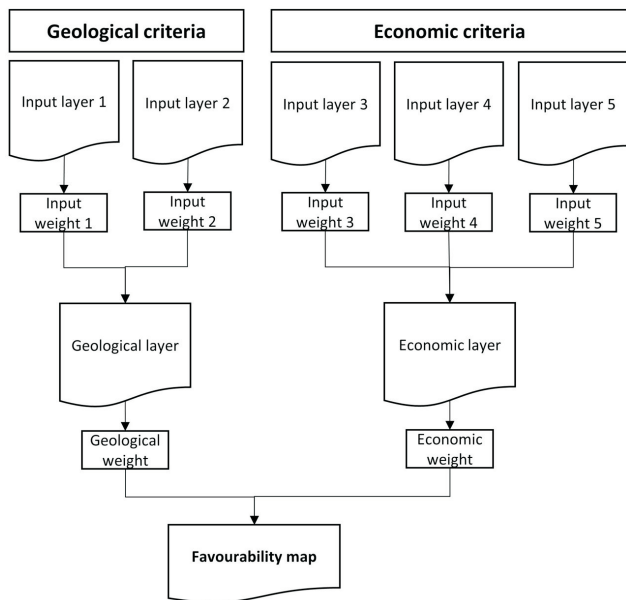


Figure 2. Flow diagram illustrating the favourability mapping process for potential geothermal development site selection.

Geological criteria include temperature and permeable aquifer data. This data will be extracted from drill-stem test logs and records pertaining to natural gas producing fields. It is then filtered for data from strata of the Middle Devonian Elk Point Group, as those strata a) potentially contain aquifers and b) are located at depths that potentially possess a temperature sufficient for binary geothermal power plants (above 80°C). Economic criteria include proximity to electrical infrastructure as well as towns and small communities. Areas where future natural gas extraction is expected to occur will be taken into account as potential sites of geothermal electricity consumption.

Sites at Clarke Lake and Jedney have already been identified as suitable sites for geothermal development (Kerr Wood Leidal Associates Ltd., 2016) and will be investigated within this research. Further potentially suitable sites will be identified, with candidates including Fort Nelson, Dawson, the Horn River Basin and Fort St. John.

Economic Assessment

The objective of the economic assessment is to quantify the amount of energy available, and the cost of that energy, at each of the representative locations selected in the previous section. Focus lies on harnessing electrical energy. The possibility to supply heat energy will be a secondary goal wherever proximity to potential consumers justifies this investigation.

The economic assessment consists of three parts. First, the size of the geothermal reservoirs and their associated power outputs will be assessed using the volume method (Williams et al., 2008). Secondly, literature regarding the economic modelling of geothermal power projects will be reviewed, in order to identify the most suitable model. Thirdly, the most suitable model will be applied to assess the LCOE. Here, appropriate values for the cost of drilling, depreciation of assets, currency conversion and capital costs will be input into the model. Appropriate values will be retrieved from literature as well as recent cost estimates provided by industry. These include

- a class C cost estimate for an organic Rankine cycle geothermal power plant (5 megawatt [MW] output, 110°C fluid inlet temperature), and
- cost estimates for drilling and well completion.

Results from the selected economic model will be compared to at least one other model. Further, the sensitivity of results to varying technical parameters (temperature, flow rate) and economic parameters (drilling costs, drilling success rate, capital costs) will be assessed in a Monte Carlo simulation.

Conclusions

It is expected that several locations, beyond Clarke Lake and Jedney, will be found that are potentially suitable for geothermal development. It is further expected that the LCOE at Clarke Lake and Jedney will be lower in this assessment than previously estimated for Geoscience BC (Kerr Wood Leidal Associates Ltd., 2016). This study will devise a methodology for assessing sedimentary basin geothermal energy by using data from oil and gas exploration. In future work, this methodology can be applied to Alberta, where an additional body of data is available.

Current Status and Project Timeline

The first part of this study, namely site selection via favourability mapping, has been completed to date. Results from this section are still under review and therefore not yet presented here. The second part of the study, the economic assessment, is ongoing. Results of this study will be submitted to a peer reviewed journal by May 2017. After publication, a full report will be released by Geoscience BC.

Acknowledgments

The authors would like to thank Geoscience BC and the Pacific Institute for Climate Solutions for making this project possible. The BC Ministry of Energy and Mines and the University of Victoria (British Columbia) are also thanked for their in-kind contributions. The authors want to acknowledge A. Rowe, C. Salas and C. Pellett for reviewing this work. This study is part of the 2060 Project, researching the path to a low-carbon Canadian energy system.

References

- Grasby, S.E., Allen, D.M., Bell, S., Chen, Z., Ferguson, G., Jessop, A., Kelman, M., Ko, M., Majorowicz, J., Moore, M., Raymond, J. and Therrien, R. (2012): Geothermal energy resource potential of Canada; Geological Survey of Canada, Open File 6914, 322 p., doi:10.4095/291488
- Kerr Wood Leidal Associates Ltd. (2016): An assessment of the economic viability of selected geothermal resources in British Columbia; report prepared for Geoscience BC, Report 2015-11, 53 p. plus appendices, URL <http://www.geosciencebc.com/i/project_data/GBCReport2015-11/GBC2015-11_KWL_Geothermal_Economics_Project_Report_27Sep16.pdf> [November 2016].
- Malczewski, J. (2000): On the use of weighted linear combination method in GIS: common and best practice approaches; Transactions in GIS, v. 4, no. 1, p. 5–22, doi:10.1111/1467-9671.00035
- Nyerges, T.L. and Jankowski, P. (2009): Regional and Urban GIS: A Decision Support Approach; The Guilford Press, New York, New York, 299 p.
- Walsh, W. (2013): Geothermal resource assessment of the Clarke Lake gas field, Fort Nelson, British Columbia; Bulletin of Canadian Petroleum Geology, v. 61, no. 3, p. 241–251, doi:10.2113/gscpgbull.61.3.241
- Williams, C., Reed, M. and Mariner, R. (2008): A review of methods applied by the U.S. Geological Survey in the assessment of identified geothermal resources; United States Geological Survey, Open-File Report 2008–1296, 27 p.

Search Project: Phase II Activities in West-Central British Columbia (Phases I and II, covering NTS 093E, F, G, K, L, M, N, 103I)

B.E. Madu, Geoscience BC, Vancouver, BC, madu@geosciencebc.com

Madu, B.E. (2017): Search project: Phase II activities in west-central British Columbia (phases I and II, covering NTS 093E, F, G, K, L, M, N, 103I); in Geoscience BC Summary of Activities 2016, Geoscience BC, Report 2017-1, p. 91–94.

Introduction

The Search project was conceived by Geoscience BC's Minerals Technical Advisory Committee to generate regional magnetic data and complementary geoscience information for prospective mineral areas of British Columbia (BC). The exploration sector will use this new information to focus or renew its efforts in discovering and developing opportunities within the province. Communities, First Nations and governments will also benefit from new geoscience data that will assist in making informed resource-management decisions and highlighting economic opportunities.

The project name 'Search' was selected as it contains the word 'arch', which refers to the program's initial focus on the Skeena arch: a paleotopographic high that was eroded into the Bowser and Nechako Basins (Tipper and Richards, 1976) and today bridges the span between the Stikine and Quesnel geological terranes. Proximity to infrastructure, modest topography and skilled labour are some of the advantages that make developing projects in this region attractive.

The Search project started with an initial budget of \$2.415 million to fund Phase I and II activities and is planned to be completed in four phases (Figure 1). A primary objective of the project is to complete airborne magnetic surveys with a line spacing of 250 m—creating an opportunity to formulate new geological interpretations at a property-size scale as an aid to explorers. Other Geoscience BC-funded projects making use of similar high-resolution magnetic surveys are the TREK, Northern Vancouver Island, QUEST-Northwest and Jennings River projects. The regional scale of the surveys also supports the development of a refined tectonic framework, especially in areas with poor access or limited rock outcrop such as those identified in the adjoining TREK project area.

Keywords: *British Columbia, Search Project, airborne survey, geophysics, magnetic data, radiometric data, Skeena Arch, Stikine terrane, Quesnel terrane*

This publication is also available, free of charge, as colour digital files in Adobe Acrobat® PDF format from the Geoscience BC website: <http://www.geosciencebc.com/s/DataReleases.asp>.

Phases I and II boundaries roughly coincide with the QUEST-West project. This project completed airborne time-domain electromagnetic (TEM) and gravity surveys at a line spacing of 4 and 2 km, respectively, in this region (Kowalczyk, 2009).

Geophysical Program

Phase I field activities were completed in November 2015 and included the helicopter-borne magnetic survey of an area that encompassed the communities of Kitimat, Terrace and Smithers (Madu, 2016). Owing to fall weather in steep mountainous terrain, it was a challenge to complete the project. Results of the 6756 km² survey were released at the Mineral Exploration Roundup 2016 conference in map and digital format through Geoscience BC's website. They were also made available as an interactive map layer on the organization's Earth Science Viewer, a web mapping application that allows a broad client base to immediately access Geoscience BC's data alongside other public information such as current mineral tenures and the BC Geological Survey's geological, MINFILE and ARIS data.

Phase II field activities began in late June 2016, and a contract was awarded to Ottawa-based Sander Geophysics Ltd., who flew an estimated 105 000 line kilometres using fixed-wing aircraft (Figure 2) at a predetermined height and drape over the project area. The survey followed east-west-trending flight lines at 250 m intervals, with north-south tie lines specified at 2500 m intervals. Although not identified as one of its major priorities, radiometric data was also collected in the course of the survey; this task did not interfere with the acquisition of the magnetic data as flights were not altered to optimize conditions for radiometric data collection. Quality assurance and quality control services for the program were provided by in3D Geoscience Inc. and S.E. Geoscience and Exploration. In addition, Hemmera created an ungulate management plan to minimize the program's impact on wildlife in the area. Survey pilots had operating procedures for wildlife observations and were empowered to deviate from planned flight patterns to mitigate negative impacts on animals.

The total flight-line distance flown, including tie lines, was estimated at 116 900 km. This represents an 11% expansion of the originally planned survey coverage owing to the

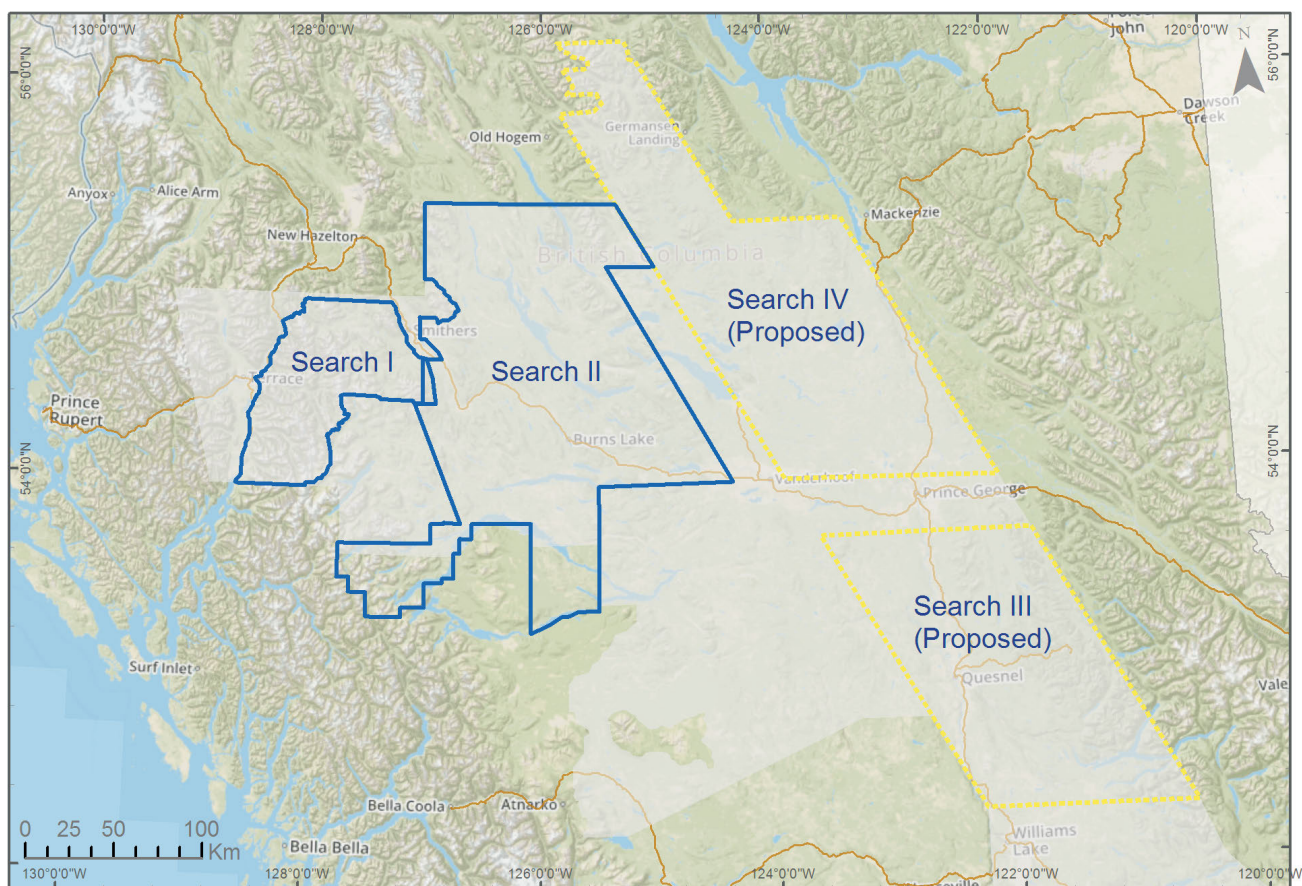


Figure 1. Conceptual location of the four proposed blocks of the Search Project in west-central British Columbia and their phased completion. Planning and consultation processes for upcoming phases are expected to alter ultimate activity areas. Blue outline, Search Phase I and II actual survey area; dashed yellow outlines, coverage of proposed phases of the Search Project; transparent mask, coverage of previous airborne geophysical surveys conducted by Geoscience BC. Background data from Natural Resources Canada (2016).

availability of three aircraft and timely progress during the program; total area covered was 21 122 km² (Figure 3). The 2016 survey connects the area covered in the 2015 Phase I survey to that covered in the 2014 TREK project survey for a combined coverage of 58 737 km².

The TREK project area surrounds the proposed Blackwater gold-silver mine and the results of the Phase II magnetic survey (to be published in January 2017) will provide new regional geophysical data of an area lying just north of this significant deposit. The survey also overflow, or covered areas adjacent to, six active, proposed or closed mines: Morrison, Bell, Granisle, Equity Silver, Endako and Huckleberry (MINFILE 093M 007, 093M 001, 093L 146, 093L 001, 093K 006 and 093E 037, respectively; BC Geological Survey, 2015; Figure 3).

Planning for Phase III activities is expected to commence in late fall 2016, with the goal of continued geophysical surveying in 2017.



Figure 2. The total flight-line distance flown to complete the Phase II airborne geophysical survey in west-central British Columbia was approximately 116 900 km, making it the most extensive of all surveys ever undertaken by Geoscience BC. Phase II was completed using up to three Cessna Grand Caravan aircraft operated by Sander Geophysics Ltd.

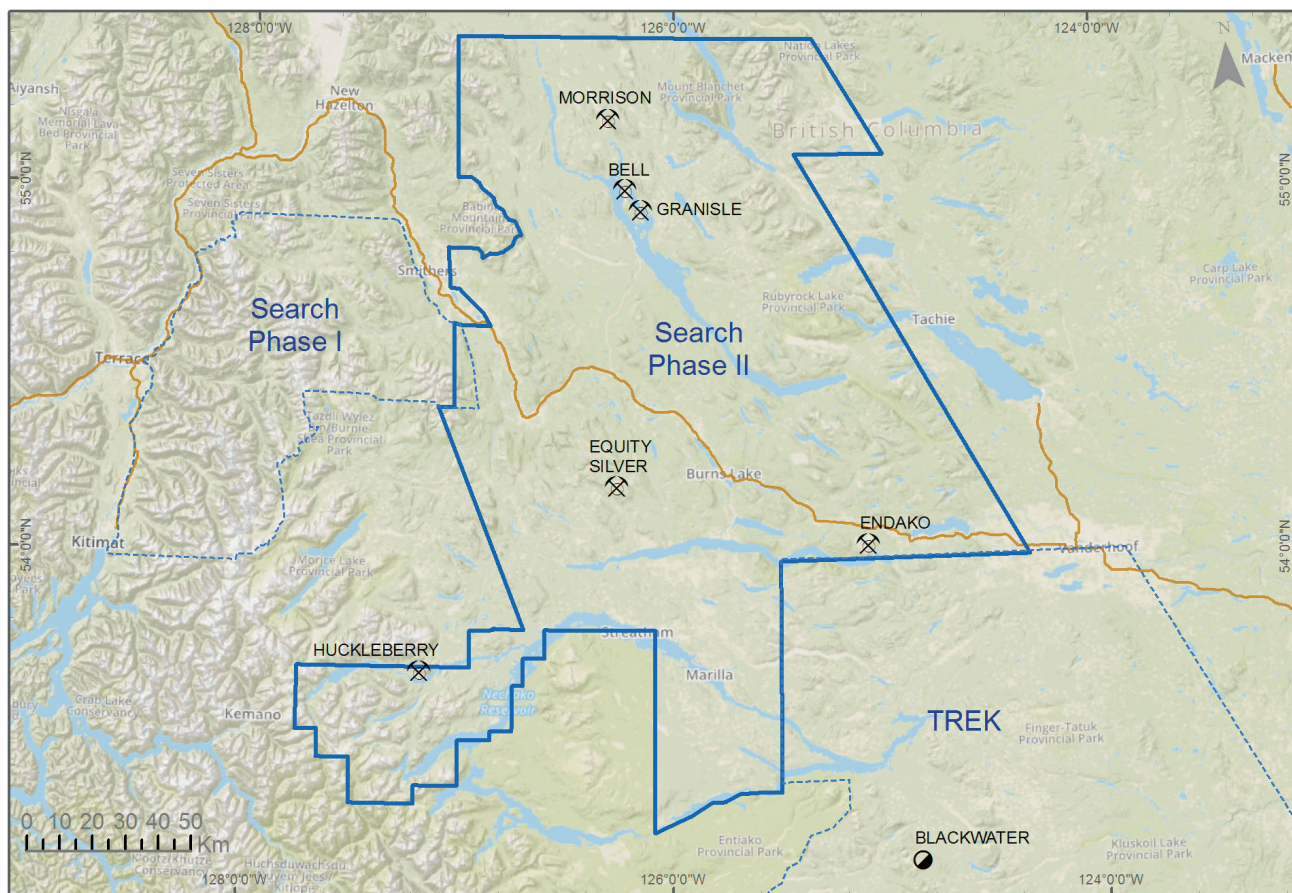


Figure 3. The Phase II airborne geophysical program ultimately surveyed a 21 122 km² area (outlined in blue) in west-central British Columbia in 2016, producing new, high-resolution magnetic and radiometric data. The survey overflow or covered areas adjacent to several active, proposed or closed mines. Background data from Natural Resources Canada (2016) and DataBC (2016).

Geochemical Program

The Search project area has excellent geochemical coverage owing to re-analyses and infill sampling under previous Geoscience BC projects, such as QUEST-West (Jackman et al., 2009). Phases I and II of this program did not include funding for new geochemical-sample collection; however, future proposals may be sought that add value to existing datasets, sponsor innovative techniques or present other original concepts.

Integration Program

A desired outcome when generating new datasets is to integrate them into added-value products that promote new understanding about the geological potential of an area. The Search Project is expected to stimulate renewed interest in an already data-rich region. Recent geological mapping by the BC Geological Survey in the Terrace-Kitimat area (Nelson, 2009) may benefit from new, high-resolution geophysical information and conversely provide better constraints and interpretation of the survey data itself. East of the Terrace area, the Nechako Project of the Geological Survey of Canada's National Geoscience Mapping Program

(NATMAP) produced a comprehensive data library of digital geoscience information (Struik et al., 2007). Geoscience BC strives to ensure explorers benefit from data it collects by releasing it in both raw and interpreted forms, by integrating all relevant data into its Earth Science Viewer web mapping application and by funding projects that add value to the data.

Collaboration between Geoscience BC, the BC Geological Survey and the Mineral Deposit Research Unit of the University of British Columbia led to the development of a field mapping initiative in map areas NTS 093L, 103H and 103I in 2016. The project will enhance the geological dimension of the Search Project by allowing geological components extracted from both the new geophysical survey data and satellite imagery to be validated through ground-truthing methods and targeted field mapping. This region hosts numerous porphyry prospects, a belt of which was the focus of recent exploration activity in map area NTS 093L/13.

Geoscience BC will pursue data integration proposals as the Search Project continues into its third and fourth phases.

Summary

The Search Project is a multiyear project for Geoscience BC that is focused on generating high-resolution regional magnetic-survey data and complementary geoscience data for key prospective mineral areas of the province. In 2016, the program included an airborne survey covering 21 122 km² and targeted geological mapping. Data from the survey will be made available through both Geoscience BC's website and its web mapping application—the Earth Science Viewer.

Acknowledgments

This paper benefited from an insightful review by B. Brusche. Numerous prospectors and geoscientists provided input that guided the selection of the survey's ultimate location and ensured it will provide the best-quality new geoscience information needed for their exploration efforts. The communities of Burns Lake and Smithers warmly welcomed the survey crews for the duration of their stay in the region. Several First Nation communities reached out to Geoscience BC to learn more about the program and outreach to all communities in the region is planned during the next phases of the project. Sander Geophysics Ltd. provided excellent service in completing this extensive survey in a professional and efficient manner.

References

- BC Geological Survey (2015): MINFILE BC mineral deposits database; BC Ministry of Energy and Mines, BC Geological Survey, URL <<http://www.minfile.ca>> [October 2015].
- DataBC (2016): MINFILE Mineral occurrence database; BC Ministry of Energy and Mines, BC Geological Survey, URL <<https://catalogue.data.gov.bc.ca/dataset/minfile-mineral-occurrence-database>> [September 2016].
- Jackaman, W., Balfour, J.S. and Reichheld, S.A. (2009): QUEST-West project geochemistry: field survey and data reanalysis (parts of NTS 093E, F, J, K, L, M, N), central British Columbia; *in* Geoscience BC Summary of Activities 2008, Geoscience BC, Report 2009-1, p. 7–14, URL <http://www.geosciencebc.com/i/pdf/SummaryofActivities2008/SoA2008-JackamanQW_original.pdf> [October 2016].
- Kowalczyk, P.K. (2009): QUEST-West geophysics in central British Columbia (NTS 093E, F, G, K, L, M, N, 103I): new regional gravity and helicopter time-domain electromagnetic data; *in* Geoscience BC Summary of Activities 2008, Geoscience BC, Report 2009-1, p. 1–6, URL <http://www.geosciencebc.com/i/pdf/SummaryofActivities2008/SoA2008-Kowalczyk_original.pdf> [October 2016].
- Madu, B.E. (2016): Search: Geoscience BC's new minerals project in west-central British Columbia (phases I and II covering NTS 093E, F, G, K, L, M, N, 103I); *in* Geoscience BC Summary of Activities 2015, Geoscience BC, Report 2016-1, p. 39–42.
- Natural Resources Canada (2016): Transport networks in Canada – CanVec – transport features; Natural Resources Canada, Esri file geodatabase, scale 1:1 000 000, URL <http://ftp.geogratis.gc.ca/pub/nrcan_rncan/vector/canvec/fgdb/Transport/> [July 2016].
- Nelson, J.L. (2009): Terrace regional mapping project, year 4: extension of Paleozoic volcanic belt and indicators of volcanogenic massive sulphide-style mineralization near Kitimat, British Columbia (NTS 103I/02, 07) *in* Geological Fieldwork 2008, BC Ministry of Energy and Mines, BC Geological Survey, Paper 2009-01, p. 7–20, URL <http://www.empr.gov.bc.ca/Mining/Geoscience/Publications/Catalogue/Fieldwork/Documents/2008/02_Nelson.pdf> [October 2016].
- Struik, L.C., MacIntyre, D.G. and Williams, S.P. (2007): Nechako NATMAP project: a digital suite of geoscience information for central British Columbia (NTS map sheets 093N, 093K, 093F, 093G/W, 093L/9, 16 and 093M/1, 2, 7, 8), BC Ministry of Energy and Mines, BC Geological Survey, Open File 2007-10, URL <<http://www.empr.gov.bc.ca/Mining/Geoscience/PublicationsCatalogue/OpenFiles/2007/2007-10/Pages/default.aspx>> [October 2016].
- Tipper, H.W. and Richards, T.A. (1976): Jurassic stratigraphy and history of north-central British Columbia; Geological Survey of Canada, Bulletin 270, 73 pages.

Ongoing Development of British Columbia's Regional Geochemical Database Using Material Saved from Previous Field Surveys

W. Jackaman, Noble Exploration Services Ltd., Jordan River, BC, wjackaman@shaw.ca

Jackaman, W. (2017): Ongoing development of British Columbia's regional geochemical database using material saved from previous field surveys; in Geoscience BC Summary of Activities 2016, Geoscience BC, Report 2017-1, p. 95–100.

Introduction

Reconnaissance-scale regional geochemical surveys (RGS) are designed to produce high-quality information that can be used to guide mineral exploration activities. These government-funded programs have been conducted throughout British Columbia (BC) since the early 1970s. At the outset, stringent methodologies were developed and have been maintained to ensure survey results remain useful and comparable (Ballantyne, 1991; Friske, 1991; Cook, 1997; Levson, 2001; Dunn, 2007). Opportunely, the original survey design included archiving representative splits of all samples collected. Having access to these materials saved from previous RGS field programs has contributed to the long-term viability and utility of the database.

To date, thousands of archived samples have been successfully reanalyzed using modern analytical techniques such as instrumental neutron activation analysis (INAA) and by inductively coupled plasma–mass spectrometry (ICP-MS). The methods are cost effective and provide significant upgrades to original analytical data reports (McCurdy et al., 2014). They provide lower detection levels for base and precious metals as well as pathfinder and rare-earth elements. They also generate improved data continuity between surveys completed at different times and samples analyzed by different commercial laboratories.

In 2017, results of a Geoscience BC–funded reanalysis project will be released for six regions in BC. Previously unavailable trace-metal data determined by ICP-MS will be available for 5579 stream sediment samples. The work represents the ongoing effort of Geoscience BC and government agencies to maintain and upgrade this important geochemical data resource.

BC RGS Projects and Database

More than 100 reconnaissance-scale regional geochemical surveys funded by Geoscience BC and both provincial and

Keywords: *British Columbia, geochemistry, regional geochemical survey, RGS, sample archive, multimedia, multi-element, analytical data, mineral exploration*

This publication is also available, free of charge, as colour digital files in Adobe Acrobat® PDF format from the Geoscience BC website: <http://www.geosciencebc.com/s/DataReleases.asp>.

federal governments have been conducted in BC since 1976. These projects included the collection of a variety of samples, including

- stream and lake sediments,
- stream and lake water,
- till samples and
- biogeochemical material.

Results of the RGS projects have been compiled into publicly available digital databases that provide site descriptions, details on sample constituents plus analytical determinations for a range of trace metals. Figure 1 shows the provincial distribution of the more than 76 000 samples that have been collected to date. The surveys cover close to 75% of the province at sample-site densities that average from one site per 5 km² to one site per 14 km².

Since inception, modifications and upgrades have been implemented to improve the utility of the geochemical database. These have included the completion of surveys in areas not previously sampled; infill sampling to increase existing survey density; targeted field surveys using innovative methods; and reanalysis, using up-to-date analytical techniques, of sample pulps saved from older surveys. The availability of these samples has proved to be a valuable resource in generating enhanced analytical information for samples collected during older surveys. In the 1990s, more than 24 000 of these samples were reanalyzed by INAA (Jackaman et al., 1991), and starting in 2005, more than 45 000 samples have been reanalyzed by ICP-MS as part of Geoscience BC–funded initiatives and BC Geological Survey projects (Jackaman, 2011; Jackaman et al., 2015).

BC RGS Sample Storage

Material from more than 76 000 BC RGS samples have been saved, catalogued and stored in secure government facilities located in Ottawa, Ontario and Victoria, BC. This collection includes sediments acquired from stream, lake and till field sites, plus bark, needles and twigs collected from trees. Table 1 lists the type and number of field surveys completed in BC and the total number of samples that have been collected. Figure 1 shows the distribution of these sample sites.

Archived samples are stored in plastic containers that are labelled with each sample's unique identification number and placed sequentially in boxes organized by survey location and year (Figure 2). For each sample type, vials contain a representative split of the processed pulp used during initial laboratory analysis. Depending on the type of sample and year collected, the character of the archived pulp material may vary in fraction size and available weight.

For more recent stream sediment surveys, samples were air-dried and sieved through an -80 mesh screen (<0.177 mm). In surveys completed prior to 1986, the stream sediment samples were air-dried, ball milled and sieved to a -80 mesh (<0.177 mm) fraction. Lake sediment samples were air-dried and then crushed using a ceramic puck mill and sieved through an -80 mesh screen (<0.177 mm). Till-sample pulps were air-dried, crushed and sieved to produce splits of the silt plus clay-sized (<0.063 mm) fraction and in some cases a clay-sized fraction (<0.002 mm) was generated. Tree bark and twigs were macerated and needles were reduced to ash at 475°C. In general, sample weights for archived stream, lake and till pulps average 10–20 g. Based on previous sample recovery projects, approximately 95% of the samples will have more than 2 g of available material.

In addition to the pulps, the archive includes raw unprocessed stream sediment material consisting of coarse

Table 1. Type and number of Geoscience BC- and government-funded, reconnaissance-scale regional geochemical survey (RGS) programs conducted in British Columbia since 1976.

Survey type	Number of surveys	Number of samples
Stream	66	56 256
Lake	15	9 180
Till	18	9 898
Tree	5	1 412
Total	104	76 746

gravel, fine sediment and organic constituents. For more recent surveys (i.e., after 1986), a representative sample split of material sieved to -18 mesh (<2 mm) fraction was saved. There are more than 50 000 of these samples that are stored in containers that hold less than 100–400 g of material (Figure 3). For some till surveys, splits of the original till samples were also preserved in the archives (Figure 4).

The archived unprocessed samples have not been included in any systematic reanalysis initiatives and remain an underutilized resource. The availability of this material provide opportunities to apply analytical instruments such as a Mineral Liberation Analyzer (MLA) or automated scanning electron microscopy systems (QEMSCAN®) for mineral identification. These units can conduct automated mineralogy investigations significantly more quickly and

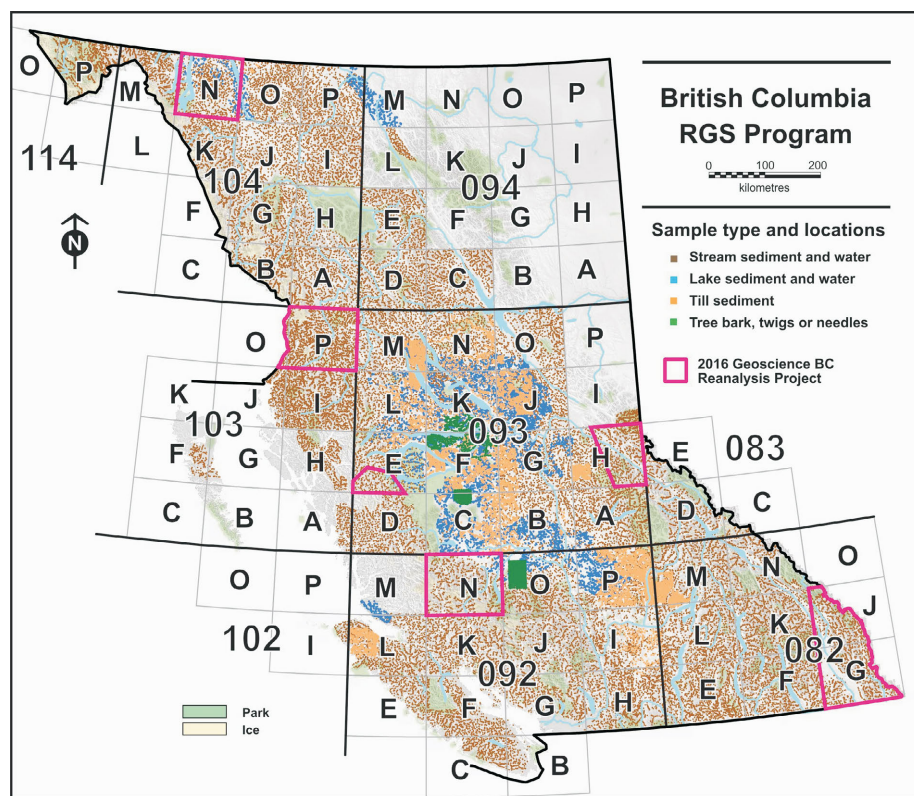


Figure 1. Distribution of all British Columbia regional geochemical survey (RGS) samples and location of survey areas targeted by the 2016 reanalysis project.

effectively than traditional non-automated methods (Page, 1991; Sylvester, 2012; Mackay et al., 2015). These applications are relatively new but have the potential to generate mineralogical information that could complement the existing trace-metal database.



Figure 2. Geological Survey of Canada's sample archive facility in Ottawa, Ontario, showing an example of warehoused regional geochemical survey (RGS) stream sediment pulps. The samples are stored in plastic vials, which are contained in boxes that hold 79 samples. Each box is placed in a metal cabinet.



Figure 3. Geological Survey of Canada's sample archive facility in Ottawa, Ontario, showing an example of a raw unprocessed regional geochemical survey (RGS) stream sediment sample collected in 1977.

Current RGS Database Upgrades

In 2016, as part of Geoscience BC's ongoing commitment to maintaining the BC RGS database, a total of 5579 RGS stream sediment pulps were recovered from archive storage in Ottawa. Permission to access these samples was provided by Natural Resources Canada (NRCan). The sample splits plus inserted quality-control reference materials were delivered to the Bureau Veritas Minerals laboratory (Vancouver, BC), where they will be analyzed for 56 minor and trace elements by ICP-MS following aqua-regia digestion. Results from this project are scheduled to be released in early 2017.

Recovered sample pulps originated from surveys conducted prior to 1986 in NTS map areas 093E, 093H, 103O, 103P and 104N (Figure 1). At that time, initial analytical results using an aqua-regia digestion and atomic absorption spectrometry (AAS) reported less than 20 elements in stream sediments. Also included in this reanalysis project are stream sediment pulps from NTS map areas 082G, 082J and 092N. Completed in the early 1990s, analytical results from these surveys also included a relatively limited number of elements determined by AAS. Table 2 provides the location and count of samples included in the 2016 ICP-MS reanalysis work, along with a list of remaining RGS stream sediment samples located outside of designated park land and other restricted areas that have not been analyzed by ICP-MS.

Summary

During the last decade, Geoscience BC-funded projects have established the agency as a leader in the development and maintenance of the BC RGS database. Building on the significant contributions by the Geological Survey of Canada (GSC) and the BC Geological Survey (BCGS), Geoscience BC has furthered the utility of this geochemical re-



Figure 4. Geological Survey of Canada's sample archive facility in Ottawa, Ontario, showing an example of a raw unprocessed split of a till sample originally collected in 1997.

source through new field surveys and sample reanalysis initiatives. To date, Geoscience BC–funded projects have included the collection of 14 253 new RGS samples, the reanalysis by INAA of 1152 RGS samples and the reanalysis by ICP-MS of more than 44 500 RGS samples. This information further augments the highly regarded BC RGS geochemical database that is routinely used as a standalone

mineral exploration tool and as a complementary resource to other exploration activities. Providing an expanded suite of metals that outlines geochemical anomalies and regional geochemical trends (e.g., the Mo distribution shown in Figure 5) helps focus exploration. Reanalysis initiatives have produced a multi-element geochemical database that offers contiguous provincial coverage. This coverage further pro-

Table 2. List of previous stream sediment regional geochemical survey (RGS) programs targeted in the 2016 Geoscience BC Reanalysis Project, and list of remaining RGS datasets that do not include stream sediment results determined by inductively coupled plasma–mass spectrometry (ICP-MS).

NTS map area	Survey name	Survey year	Sample count	ICP-MS release year
082G, J	Southern Rockies	1990	1526	2017
092N	Waddington	1991	714	2017
093E	Whitesail Lake	1986	63	2017
093H	McBride	1984–1985	646	2017
104N	Atlin	1977	862	2017
103O, P	Nass River	1978	1768	2017
Total			5579	
104M, 114P	Skagway	1992	973	Future
092K, L	Bute Inlet	1988	1312	Future
092F, G	Vancouver	1989	951	Future
Total			3236	

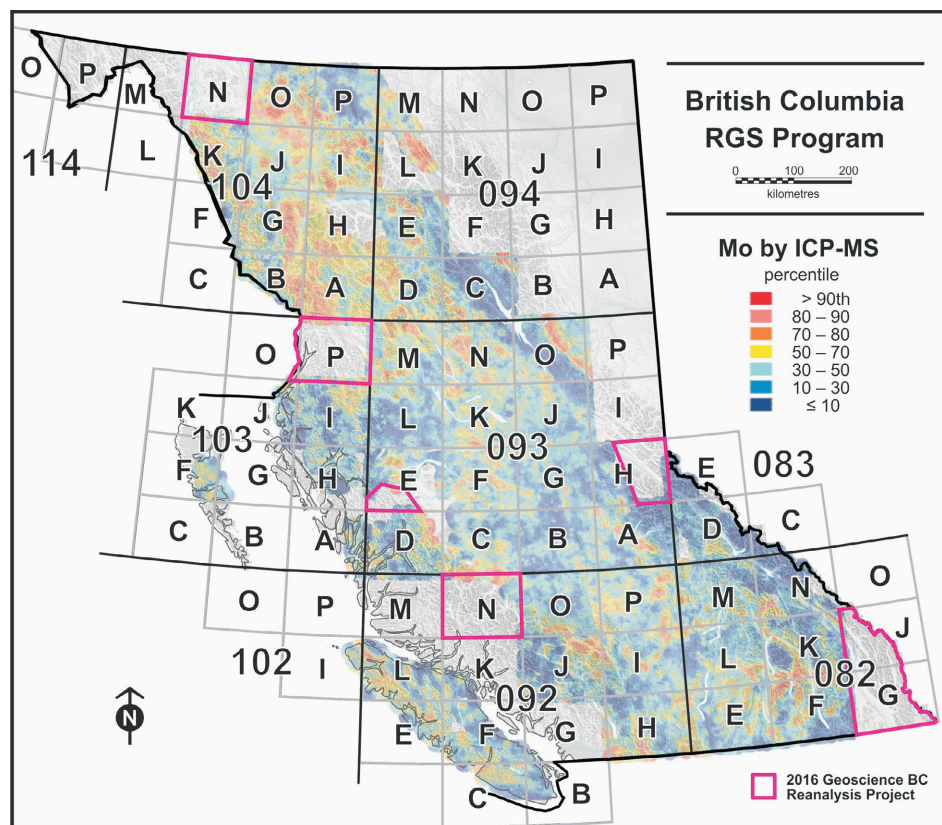


Figure 5. Geochemical distribution of Mo determined by aqua-regia digestion followed by inductively coupled plasma–mass spectrometry (ICP-MS) for stream, lake, till and tree samples from regional geochemical surveys. Threshold values are based on percentiles that were determined separately for each sample type.

motes the utility of the information to assist in the identification new areas of mineral potential, reassess known mining camps and support other complementary exploration work such as geophysical surveys, geological mapping and environmental evaluations.

Acknowledgments

The ongoing maintenance and development of RGS databases and RGS sample storage facilities remains a challenge due to staff limitations and budget constraints. Agencies such as Geoscience BC, the BCGS and the GSC are commended for their ongoing efforts to protect the long-term security of this valuable geochemical resource. Thanks to M. McCurdy, S. Day, R. McNeil, A. Plouffe and A. Grenier of the GSC; A. Rukhlov, T. Ferbey and A. Hickin of the BCGS; and R. Lett (consultant, formerly BCGS) for their efforts to promote and maintain the sample materials collections. This paper was much improved by the editing of R. Lett. Geoscience BC provided the funding for the 2016 reanalysis project.

References

- Ballantyne, S.B. (1991): Stream geochemistry in the Canadian Cordillera: conventional and future applications for exploration; *in* Exploration Geochemistry Workshop, Geological Survey of Canada, Open File 2390, p. 6.1–6.7, URL <<http://geoscan.ess.nrcan.gc.ca/cgi-bin/starfinder/0?path=geoscan.fl&id=fastlink&pass=&format=FLFULL&search=R=132388>> [November 2016].
- Cook, S.J. (1997): Regional and property-scale application of lake sediment geochemistry in the search for buried mineral deposits in the southern Nechako Plateau area, British Columbia (093C, E, F, K, L); *in* Interior Plateau Geoscience Project: Summary of Geological, Geochemical and Geophysical Studies, L.J. Diakow, P. Metcalfe and J.M. Newell (ed.), BC Ministry of Energy and Mines, Paper 1997-2, p. 175–203, URL <<http://www.empr.gov.bc.ca/mining/geoscience/publicationscatalogue/papers/pages/1997-2.aspx>> [November 2016].
- Dunn, C.E. (2007): Biogeochemistry in mineral exploration; Volume 9 *in* Handbook of Exploration and Environmental Geochemistry, M. Hale (ser. ed.), Elsevier, Amsterdam, 462 p.
- Friske, P.W.B. (1991): The application of lake sediment geochemistry in mineral exploration; *in* Exploration geochemistry workshop, Geological Survey of Canada, Open File 2390, p. 4.1–4.2, URL <<http://geoscan.ess.nrcan.gc.ca/cgi-bin/starfinder/0?path=geoscan.fl&id=fastlink&pass=&format=FLFULL&search=R=132388>> [November 2016].
- Jackaman, W. (2011): British Columbia Regional Geochemical Survey Program: new analytical data and sample archive upgrades; *in* Geoscience BC Summary of Activities 2010, Geoscience BC, Report 2011-1, p. 181–188, URL <http://www.geosciencebc.com/i/pdf/SummaryofActivities2010/SoA2010_Jackaman.pdf> [November 2016].
- Jackaman, W., Matysek, P.F. and Cook, S.J. (1991): The Regional Geochemical Survey Program: summary of activities; *in* Geological Fieldwork 1991, BC Ministry of Energy and Mines, Paper 1992-1, p. 307–318, URL <<http://www.empr.gov.bc.ca/Mining/Geoscience/PublicationsCatalogue/Fieldwork/Documents/1991/307-318-jackaman.pdf>> [November 2016].
- Jackaman, W., Sacco, D. and Lett, R.E. (2015): Geochemical reanalysis of archived till samples, TREK project, Interior Plateau, central BC (parts of NTS 093C, 093B, 093F & 093K); Geoscience BC, Report 2015-09, 5 p., URL <<http://www.geosciencebc.com/s/Report2015-09.asp>> [November 2016].
- Levson, V.M. (2001): Regional till geochemical surveys in the Canadian Cordillera: sample media, methods, and anomaly evaluation; *in* Drift Exploration in Glaciated Terrain, M.B. McClenaghan, P.T. Bobrowsky, G.E.M. Hall and S.J. Cook (ed.), Geological Society, London, Special Publication, no. 185, p. 45–68.
- Mackay, D.A.R., Simandl, G.J., Ma, W., Gravel, J. and Redfearn, M. (2015): Indicator minerals in exploration for specialty metal deposits: a QEMSCAN[®] approach; *in* Symposium on Strategic and Critical Materials Proceedings, G.J. Simandl and M. Neetz (ed.), November 13–14, 2015, Victoria, British Columbia, BC Ministry of Energy and Mines, Paper 2015-3, p. 211–217, URL <<http://www.empr.gov.bc.ca/Mining/Geoscience/PublicationsCatalogue/Papers/Pages/2015-3.aspx>> [November 2016].
- McCurdy, M.W., Spirito, W.A., Grunsky, E.C., Day, S.J.A., McNeil, R.J. and Coker, W.B. (2014): The evolution of the Geological Survey of Canada's regional reconnaissance geochemical drainage sediment and water surveys; *Explore*, no. 163, p. 1, 3–4, 6–10, URL <<http://www.appliedgeochemists.org/images/Explore/Explore%20Number%20163%20June%202014.pdf>> [November 2016].
- Page, J.W. (1991): Stream-sediment petrography using the coarse fraction of stream sediments; *in* Geological Fieldwork 1991, BC Ministry of Energy and Mines, Paper 1992-1, p. 301–306, URL <<http://www.empr.gov.bc.ca/Mining/Geoscience/PublicationsCatalogue/Fieldwork/Documents/1991/301-306-page.pdf>> [November 2016].
- Sylvester, P. (2012): Use of the Mineral Liberation Analyzer (MLA) for mineralogical studies of sediments and sedimentary rocks; Chapter 1 *in* Quantitative mineralogy and microanalysis of sediments and sedimentary rocks, Mineralogical Association of Canada, Short Course Series 42, p. 1–16.

Identifying Mineral Exploration Targets in the TREK Project Area, Central British Columbia (Parts of NTS 093B, C, F, G), Using a Multimedia and Multivariate Analysis of Geochemical Data and a Preliminary Method of Sediment Transport Modelling

D.A. Sacco, Palmer Environmental Consulting Group Inc., Vancouver, BC, david@pecg.ca

W. Jackaman, Noble Exploration Services Ltd., Jordan River, BC

R.E. Lett, Consultant, Victoria, BC

B. Elder, Consultant, Vancouver, BC

Sacco, D.A., Jackaman, W., Lett, R.E. and Elder, B. (2017): Identifying mineral exploration targets in the TREK project area, central British Columbia (parts of NTS 093B, C, F, G), using a multimedia and multivariate analysis of geochemical data and a preliminary method of sediment transport modelling; *in* Geoscience BC Summary of Activities 2016, Geoscience BC, Report 2017-1, p. 101–112.

Introduction

Geoscience BC's Targeting Resources through Exploration and Knowledge (TREK) project has produced a comprehensive collection of geoscience information for a highly prospective area in central British Columbia (BC). Up to this point, the surficial geochemistry component of the project has focused on new till and lake sediment sampling combined with a reanalysis and genetic interpretation of similar archived data, resulting in one of the largest, high-quality, and directly comparable raw exploration datasets in North America. This value-added project provides advanced processing of the TREK geochemical data that incorporates a bedrock and surficial context into the evaluation to better understand the complex nature of this information and promote its potential as a mineral exploration tool.

This project has two primary objectives: identify low-risk exploration targets within the TREK project area, and develop and test a method to delineate potential source regions for till and lake sediment samples. Exploration targets will be identified through a multimedia and multivariate analysis that highlights samples with geochemical signatures similar to specific common deposit types. Till and lake sediment samples are good candidates for the multimedia comparison as they have been shown to correlate (Cook et al., 1995). This correlation is likely a result of erosion and transport of the region's ubiquitous till cover by watercourses. Priority will be placed on targets that show spatially correlative dispersal in both till and lake sediment geochemistry.

Keywords: British Columbia, TREK, regional geochemical survey, target generation, multivariate analysis, anomaly

This publication is also available, free of charge, as colour digital files in Adobe Acrobat® PDF format from the Geoscience BC website: <http://www.geosciencebc.com/s/DataReleases.asp>.

Potential source areas, or areas of influence (AOI), for the two media are delineated using their unique transport mechanisms. Lake sediment samples are transported by watercourses, so a catchment basin analysis will be used that is similar to those used for stream sediment samples (e.g., Bonham-Carter and Goodfellow, 1986; Arne and Bluemel, 2011; Heberlein, 2013). Till samples are transported by glaciers, so their AOI will be delineated using ice-flow data, and will build on concepts related to provenance envelopes (Stea and Finck, 2001; Plouffe et al., 2011). Till AOI are designed to spatially link till samples to a dominant bedrock source unit. Contrasting rock types forming the bedrock geology within the TREK project area will be reflected in the till geochemistry. The till data will be levelled using the dominant bedrock source unit to mitigate the influence of these contrasting rock types on the regional dataset, which should improve anomaly identification.

Project Area

A summation and references for the known bedrock and surficial geology for the project area are provided in Sacco et al. (2014k). The project area is in the Interior Plateau (Mathews, 1986), south of Vanderhoof and approximately 60 km west of Quesnel. It occupies parts of NTS map areas 093B, C, F and G and covers more than 28 1:50 000 scale NTS map areas, and approximately 25 000 km² (Figure 1). Access is through a network of forest service roads in the Vanderhoof, Quesnel, Chilcotin and Central Cariboo forest districts.

The project area includes parts of the Nechako Plateau, Fraser Plateau and Fraser Basin physiographic regions (Holland, 1976). Thick surficial deposits composed dominantly of till and glacial lake sediments obscure most bedrock exposures. Higher relief features include the Nechako and Fawnie mountain ranges of the Nechako Plateau and the Ilgachuz and Itcha mountain ranges of the Fraser Plateau.

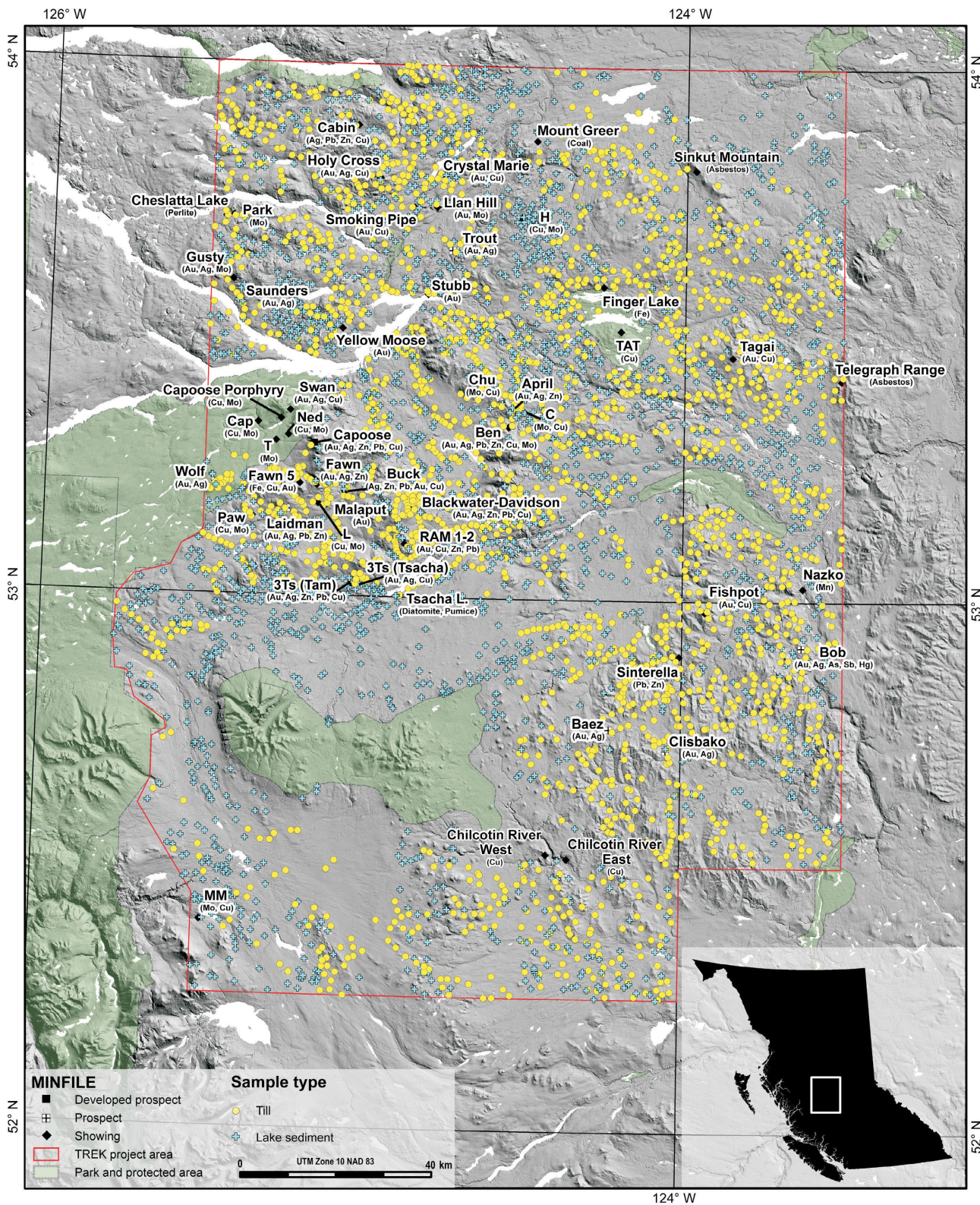


Figure 1. Location map showing the study area, till (yellow symbols) and lake sediment (blue symbols) sample locations, and MINFILE mineral occurrences (BC Geological Survey, 2016a). Digital elevation model from Canadian digital elevation data (GeoBase®, 2007).

Methods

This section outlines the proposed workflow and methods for the study (Figure 2). All procedures are carried out using a combination of ArcGIS™, Reflex® ioGAS and Microsoft® Excel® computer software.

Data

This project integrates data from multiple sources listed in Table 1. Due to the complex nature of this collection of information, inherent data discrepancies exist that may affect the results. Significant effort has gone into the assessment, compilation and processing of these data to ensure the best

possible results. The specific procedures used are outlined in the appropriate method subsections below.

Bedrock Compilation and Simplification

The bedrock geology is an integral part of this study, so it is essential to have the most accurate and consistent mapping possible. The most continuous bedrock geology in the project area is compiled by Cui et al. (2015); however, more recent, higher resolution bedrock mapping conducted for parts of the project area by Mihalynuk et al. (2008), Angen et al. (2015) and Bordet (2016) is not in Cui et al. (2015). A new, uniform and continuous geology layer is being pro-

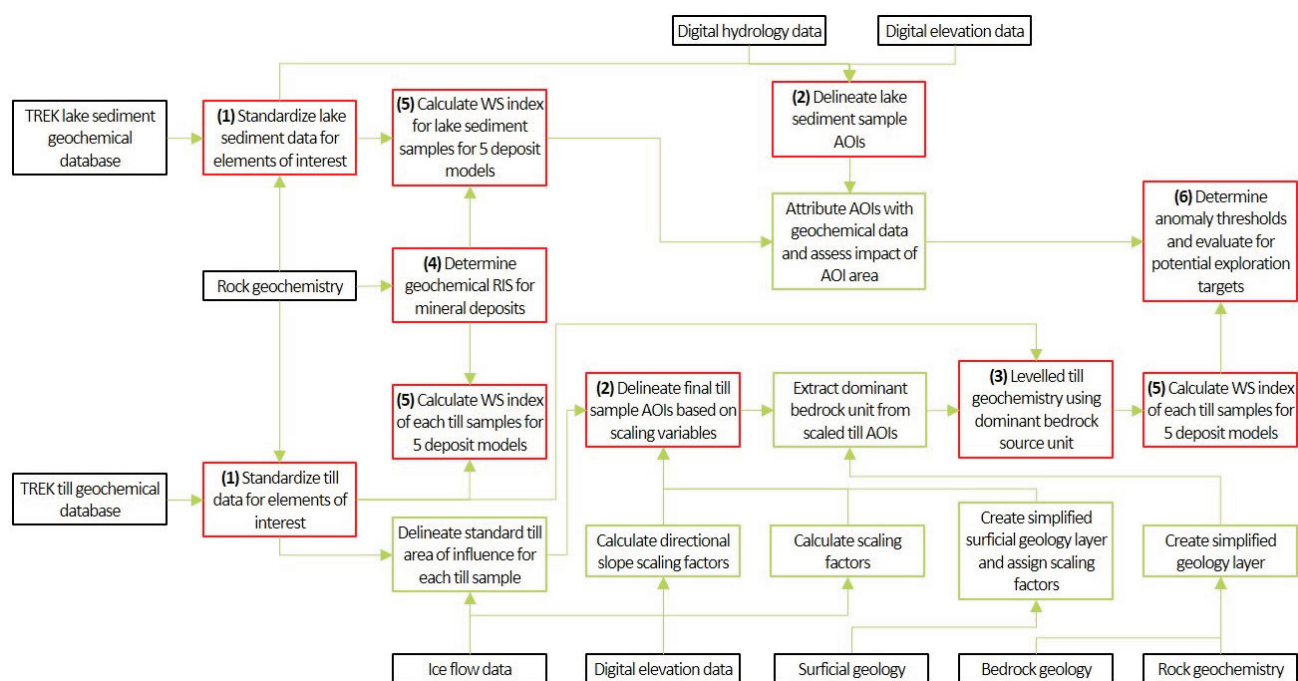


Figure 2. Flowchart illustrating the workflow for this study. Black boxes identify data sources, green boxes identify processing steps and red boxes identify final products. Bold bracketed numbers refer to the final product list in the conclusions section of this paper. Abbreviations: AOI, areas of interest; RIS, relative importance signature; TREK, Targeting Resources through Exploration and Knowledge; WS, weighted sums.

Table 1. Datasets and their references used in this study.

Data sets	Reference
TREK till geochemistry	Jackaman and Sacco (2014); Jackaman et al. (2015a)
Reanalyzed archive till geochemistry	Jackaman et al. (2015b)
TREK lake sediment geochemistry	Jackaman and Sacco (2014)
Archive lake sediment geochemistry	Jackaman (2006, 2008a, 2009a)
Reanalyzed archive lake geochemistry	Jackaman (2009a, 2009b)
Rock geochemistry	Mihalynuk et al. (2008a, b); Angen et al. (2016); additional data to be collected from MINFILE (BC Geological Survey, 2016) and ARIS (BC Ministry of Energy and Mines, 2016)
Geology	Cui et al. (2015); Bordet (2016); Mihalynuk (unpublished data)
Surficial geology	Kerr and Giles (1993); Plouffe et al. (2004); Sacco et al. (2014a–j)
Elevation data (SRTM, CDED)	Canadian Digital Elevation Data (CDED), GeoBase® (2007), Shuttle Radar Topography Mission (SRTM), NASA LP DAAC (2015)
Ice flow data	Ferby and Arnold (2013); Plouffe and Sacco (unpublished data)
Hydrology	GeoBC (2016)

duced for this study that will combine these data sources. The data sources are first overlaid to assess the spatial comparability, unit designation and descriptions. From this assessment, the most suitable sources will be determined. The selected layers will then be converted to a comparable legend based on the most extensive data source (i.e., Cui et al., 2015), and spliced into the compilation. No attempts at edge matching will be made between the units as it is a complicated process that requires resources beyond the scope of this project. The new layer will then be simplified so that the geology is represented by major bedrock units that are most likely to influence the till geochemistry. Simplifications will be based largely on unit descriptions and supplemented with available rock geochemistry where possible.

TREK Geochemical Data Standardization

Data standardization refers to a series of processing steps required to create a genetically comparable, normally distributed and statistically equivalent dataset. Only sediments with similar genesis should be compared to eliminate variation associated with different transport and deposition mechanisms. Non-normal and censored data distributions can cause issues when applying mathematical or statistical analytical procedures (cf. Grunsky, 2010). Similarly, variation in analytical results from external factors can limit anomaly recognition within the dataset. A combination of filtering, data transformations and substitutions, and levelling techniques are applied to the raw data to improve its utility.

The geochemical data used for this study is a compilation of new till and lake sediment samples, and reanalyzed archive samples. Details for the datasets can be found in the references in Table 1 and sample locations in Figure 1. To ensure genetic continuity within the datasets, all till and lake sediment data were assessed separately. In addition, till samples that are not basal till are removed from the analysis based on genetic interpretations conducted earlier in the TREK surface sediment geochemistry program (Jackaman et al., 2015b). Basal till is well suited to assessing mineral potential of an area because it is a first derivative of bedrock (Shilts, 1993); therefore, it has a similar geochemical signature. It was eroded, transported and deposited under ice, thus its transport history is relatively simple and can be determined by reconstructing ice-flow histories. Furthermore, it produces a geochemical signature that is areally more extensive than the bedrock source and potentially easier to locate (Levson, 2001).

The data distribution of each element is assessed numerically and graphically to determine which data require the \log_{10} transformation to produce more normal data distributions. Most data are positively skewed and require the transformation. Censored data distributions occur when enough data points fall below detection limits. A sufficient

proportion of censored data artificially skews the data distribution. For elements with <1% of data points below the detection limit, the data below the detection limit are substituted with half of the lower detection limit. For elements with >1% of the data points below the detection limit, the data below the detection limit are substituted with predicted values based on linear regression coefficients of the data. This is accomplished by fitting a line by linear regression on a normal probability plot, and then replacing the censored data with their expected values.

The inductively induced neutron activation analysis (INAA) was conducted at Activation Laboratories Ltd. (Ancaster, Ontario) or Becquerel Laboratories Inc. (Mississauga, Ontario) laboratories, depending on the survey. An assessment of analytical results indicates there is minor variation in the analytical results from each lab. There is significant spatial overlap of the sampling regions for the two labs, thus it is unlikely the difference is related to geology. Instead, the variation is attributed to differences between the labs. To mitigate this variation, the data are levelled using a robust z-score method. The z-score levelling method was chosen because it does not change the shape of the data distribution and it preserves genuine outliers. This method converts each data point into a group-based z-score, expressing the data in units of standard deviation from the central tendency. The median is used as a robust estimate of the mean and the interquartile range (IQR) multiplied by 0.7413 as a robust estimate of standard deviation. It is defined by the equation

$$z = \frac{\text{input value} - \text{median}}{\text{IQR} \times 0.7413}$$

Sample Areas of Influence

An AOI is designed to identify the potential source region for a sediment sample. Because till and lake sediments have different geneses, the AOI of each media is determined based on different transport mechanisms and represents a different source material. Basal till is eroded and transported by glacial ice and is dominantly derived from bedrock. The shape of each till sample AOI is dependent on variables related to ice-flow dynamics, and the AOI delineates a region of bedrock that has influenced the composition of the till sample. Lake sediment samples are transported through drainage networks; therefore, the AOI for lake sediment samples is defined by the catchment basin of the sampled lake.

Till Sample AOI

Till sample AOI represent the potential source region for a specific sample point, defined by a sector of a circle that is centred on the sample location. The angle of the sector is a function of the range of ice-flow directions that affected the location, and the length of the radii (arms) is a function of estimated sediment-transport distance (Figure 3). Delinea-

tion of a till sample AOI is an iterative process that begins with a standard till sample AOI that has a standard length and an arc length that is specific to the ice-flow history at each sample location. The standard AOI is used to extract scaling factors that reflect increased or decreased sediment transport distances. These scaling factors are then applied to the standard AOI to create the final till sample AOI that will be used to determine dominant bedrock influence (Figure 3).

Delineation of a Standard Till Sample AOI

The length of a standard AOI is determined based on average anomaly dispersion distances in till from known mineral deposits within the region. The dispersal distance is measured from the deposit to the location where associated element concentrations are below the 75th percentile. Based on the references listed in Table 2, the average dispersal length is approximately 2.5 km.

The angle of a standard AOI is based on the range of ice-flow directions that affected a sample location (Figure 2). Ice-flow directions were determined from the azimuth of small- and large-scale ice-flow indicators (see Table 1 for references). Ice-flow histories were determined where relative chronologies could be assigned to the indicators, and from regional ice-flow patterns. A 2 km buffer was created for each till sample location, and the maximum and minimum azimuth values from all ice-flow indicators were attributed to the sample point. The range for each sample location was assessed for the influence of spurious values and adjusted accordingly. During this assessment, modifications were made based on known ice-flow histories and topographic influences.

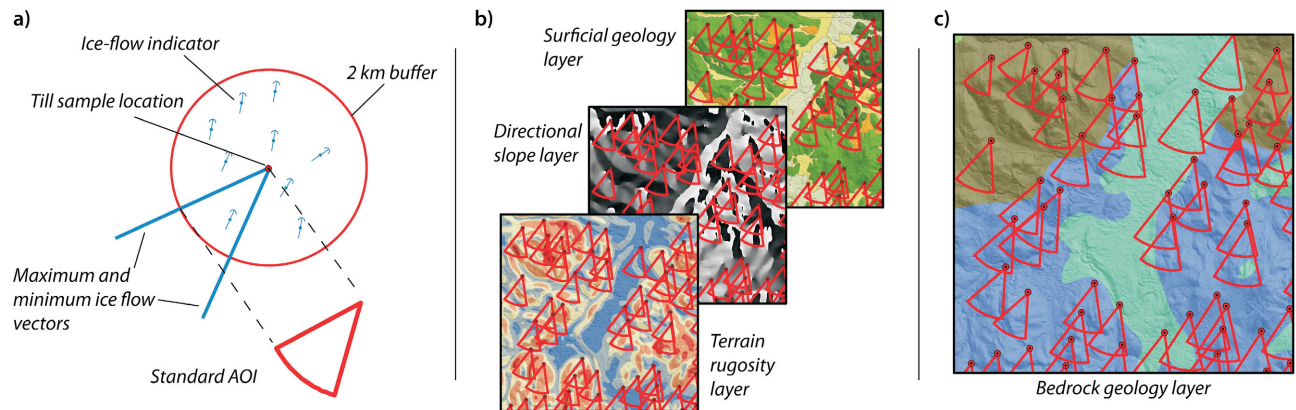


Figure 3. Conceptual diagram of till sample area of influence (AOI) delineation and utilization to extract the dominant bedrock source: **a)** standard till sample AOI are delineated based on sample locations and ice-flow vectors; **b)** length-scaling factors are extracted from layers that affect sediment transport distances using standard till AOI; **c)** the length of standard till sample AOI are multiplied by the scaling factors, and the dominant bedrock units affecting the samples are calculated.

Table 2. Geochemical dispersal distances in till to the 75th percentile from known mineral occurrences in central British Columbia.

Dispersal distance (km)	NTS 1:250 000 map area	Reference
2	093M, L	Ferbey et al. (2009)
5	093M, L	Ferbey et al. (2009)
1–3	93L	Stumpf (2012)
2.5–5	093F	Levson et al. (1994)
1–2	093F	Levson et al. (1994)
2	093F	Levson et al. (1994)
3–7	093F	O'Brien et al. (1997)
2–4	093F	O'Brien et al. (1997)
2	093F	O'Brien et al. (1997)
>1	093O	Plouffe (1997)
>1	082E	Lett et al. (2001)
2–4	093F	Sibbick et al. (1996)
1.6	093E	Ferbey et al. (2012)
1–2	O92P	Paulen et al. (2000a)
3	082M	Paulen et al. (2000b)
2–5	various	Weary et al. (1997)

Length-Scaling Variables and Factors

Length-scaling factors are used to modify the length of a till sample AOI based on the specific surface conditions to improve the accuracy of the estimated transport distance of each sample. It has been shown that transport distances increase with velocity of ice flow (Clark, 1987; Bouchard and Solonen, 1990; Aario and Peuraniemi, 1992). The ice velocity cannot be directly determined; thus, the scaling factors are based on three surface characteristics (i.e., scaling variables) that can affect ice velocity: slope, surface rugosity and surficial material. Transport distances can also be affected by the physical properties of the source (e.g., areal extent, erodibility, topographic position) and re-entrainment potential (Parent et al., 1996). The physical properties of the exploration targets are yet to be identified, and determining re-entrainment potential is not feasible across the study area so these factors will not be addressed here.

Glaciers generally accelerate downslope and decelerate upslope. Directional slope is measured using SRTM elevation data and the generalized ice-flow directions from the ice-flow indicator compilation. Thiessen polygons are created for the generalized ice-flow indicators. Spurious results are assessed and adjusted where necessary ensuring coordination with surrounding values. The polygon file is converted to an ice-flow direction raster with an equivalent cell size to the SRTM data. The ice-flow direction raster is smoothed using a roaming average of 10 cells to reduce sudden directional changes along polygon borders. The SRTM dataset is smoothed using a 25-cell roaming average to remove the influence of minor topographic features that are either too small to affect ice flow, or did not exist during glaciation (e.g., meltwater channels and postglacial landforms). Slope and aspect raster layers are calculated from the SRTM data, and the directional slope was calculated using the formula

$$S_D = \left(S \cos \left((D - A) \frac{\pi}{180} \right) \right),$$

where S_D = directional slope, S = slope raster, D = direction of ice-flow raster and A = aspect raster.

Increased surface rugosity increases basal drag and decreases ice velocity. Surface rugosity is calculated using a modified version of the terrain ruggedness index (TRI) by Riley et al. (1999). Several other methods of measuring

rugosity were tested and were deemed unsuitable due to issues with scale and the resolution of the elevation data. For example, the true rugosity of a surface is probably best indicated by the 2-D area to 3-D area ratio. This method, however, could not produce accurate results at a scale that would affect a glacier and is better suited to higher resolution data.

The Riley et al. (1999) TRI is the difference between the value of a cell and the mean of a neighbourhood of surrounding cells. This calculation is performed on the SRTM dataset that is smoothed using a 10-cell roaming average to remove minor topographic irregularities from the calculation. Minimum and maximum 25 by 25-cell neighbourhood raster layers are derived from the smoothed DEM, then the TRI is calculated using the formula

$$TRI = \sqrt{\left(\text{abs}(\text{max}^2 - \text{min}^2) \right)},$$

where max = maximum 25 by 25-cell neighbourhood raster and min = minimum 25 by 25-cell neighbourhood raster.

The surface expression and thickness of the surficial materials are used as qualitative proxies for ice-flow velocity and transport distance, respectively. Thicker till units are generally transported farther (e.g., Levson and Giles, 1995; Paulen, 2001) and streamlined landforms (notably with a length-to-width ratios of 10:1) suggest higher ice-flow velocities (Stokes and Clark, 2002; Briner, 2007; King et al., 2009). Sediment thickness and surface expressions were extracted from surficial mapping compiled from several sources (see Table 1). The mapping was combined using a common legend, with higher resolution mapping favoured where overlap occurred.

Quantifying the effects of the scaling variables on ice-flow velocity, and ultimately on sediment transport distance, is beyond the scope of this preliminary study. The scaling factors for this preliminary study are, therefore, relative rather than absolute. Each scaling variable is divided into five factor categories, with each representing a scaling factor of 0.1 (Table 3). The relative scaling factors are based on the average condition. For example, the average condition is scaled by a factor of 1; one below the average condition is scaled by a factor of 0.9; one above the average condition is scaled

Table 3. Length-scaling variables and factors used to adjust till sample areas of interest (AOI) based on surface characteristics that affect till transport distances.

Scaling factor	Category breaks	Slope value (°)	TRI index value	Surficial geology map unit description
0.8	> -1.5 standard deviation from mean	>5	<71	No surficial material (e.g., dominantly rock with lesser amounts of thin material; R.Tv)
0.9	-1.5 to -0.5 standard deviation from mean	5 to 2.1	72-263	Thin surficial material (e.g., veneers; Tv)
1	-0.5 to 0.5 standard deviation from mean	-2 to 2	264-454	Thick surficial material (e.g., blankets; Tb)
1.1	0.5 to 1.5 standard deviation from mean	-2.1 to -5	455-646	Thick material with some streamlining (e.g., till blanket with some streamlining; Tb.Ts)
1.2	>1.5 standard deviation from mean	<-5	>646	All material is streamlined (Ts)

Note: Thin and thick material categories are based on material thickness and not genesis, thus can include all material types.

by a factor of 1.1. Directional slope and rugosity variables are numerical indices. The average condition for these indices will be determined by the mean, and the scaling-factor divisions measured in units of standard deviation (Table 3). Surficial material characteristics are more qualitative and require a different approach. Based on areal distribution, thick material is the average condition and is assigned a scaling factor of 1. The scaling factors increase as the amount of streamlining increases, and decrease as the material becomes thinner.

The percent coverage of the scaling factors for each scaling variable are measured from within the standard AOI. A final scaling factor for each variable is determined by weighting each category based on the percent coverage. The standard AOI length is then multiplied by each variable's weighted scaling factor and the final till sample AOI are delineated using those lengths.

Levelling Geochemical Data Based on Bedrock

The final till sample AOI spatially link each till sample to a probable source region. The dominant bedrock source unit can be determined by extracting the dominant bedrock unit within the AOI. The efficacy of the bedrock attribution will be measured by examining the pebble lithologies of till samples, and by comparing the geochemistry of till samples with that of the bedrock source. Till samples collected in 2013 and 2014, in association with the TREK project, included the collection of 50 clasts (Jackaman and Sacco, 2014; Jackaman et al., 2015a). The proportion of clasts collected will be compared to the source area bedrock attribution and assessed for consistency. Similarly, the geochemical concentrations of till samples will be compared with those of the bedrock source regions to determine if they match. These quality-control measures are limited by the fact that not all samples have pebble data and not all rock units have available geochemical data that are comparable to the till geochemical data.

If the bedrock attributions are found suitable, the till geochemical data will be levelled to mitigate the variance in geochemical concentrations related to bedrock source. The levelling procedure will use the same methods outlined in the data standardization section because it does not change the shape of the data distribution and it preserves genuine outliers.

Lake Sediment Sample AOI

Lake sediment sample AOI represent the potential area from which lake sediment was derived, and are delineated in the same manner as a catchment basin. For the purposes of this study, a lake catchment is defined as the drainage area from the outlet of the sampled lake to the outlet of the next upstream sampled lake. Lake sediment sample AOI are delineated by computing the catchments of sampled lakes using Canadian digital elevation data (CDED;

GeoBase[®], 2007). The CDED was chosen because it was created using hydrographic elements, and more accurately represents the hydrological system compared with the SRTM elevation data.

The CDED is processed to remove linear artifacts that affect the drainage system modelling. The data are resampled to a resolution of 10 m and smoothed using the minimum value of the surrounding eight cells. The minimum value is used to ensure lower elevation areas representing drainage networks are not artificially raised, resulting in disconnected upstream areas.

Preliminary catchments are delineated for all sampled lakes by using the Arc Hydro tool set, and generally following the method for modelling deranged drainage systems (Djokic, 2008). The elevation values under the sampled lakes are reduced to below the minimum value of the elevation dataset to ensure the modelling does not allow for water flow through the lake. A flow direction raster is created specifying the sampled lakes as sinks. During this process, each cell that would eventually drain into an identified sink was defined, which delineated the possible sediment source area for each sampled lake.

Errors can occur in the catchment delineation for lakes with upstream, adjacent wetlands. If the upstream wetland is flat in the elevation model, no flow direction can be computed and the upstream area is cut off from the lake catchment. All wetlands that are adjacent to lakes are identified and screened for potential impact on catchment delineation. Upstream wetlands that impact the preliminary catchment delineation are merged into the lake, and the process is rerun using the modified lakes.

Lake sediment sample AOI represent the potential source region for a sample; therefore, they represent the source for geochemical anomalies within that sample. The geochemistry of the lake sediment samples is attributed to the AOI to indicate the ground coverage of the sampling, and an area to focus exploration efforts.

In several large lakes, sediment samples were collected from what was interpreted as different basins (Jackaman, 2006, 2008a; Jackaman and Sacco, 2014). The geochemical concentrations of lake sediment samples collected from the same lake are compared for variation prior to attribution to the AOI. If the variation between key mineralization pathfinder elements (e.g., Cu, Zn) are within 25%, estimated as percent relative standard deviation, the values are averaged and applied to the AOI. If significant variation is observed, the catchment is manually modified based on topographic and hydrological considerations to best represent input into the sampled basins within the lake (Figure 4).

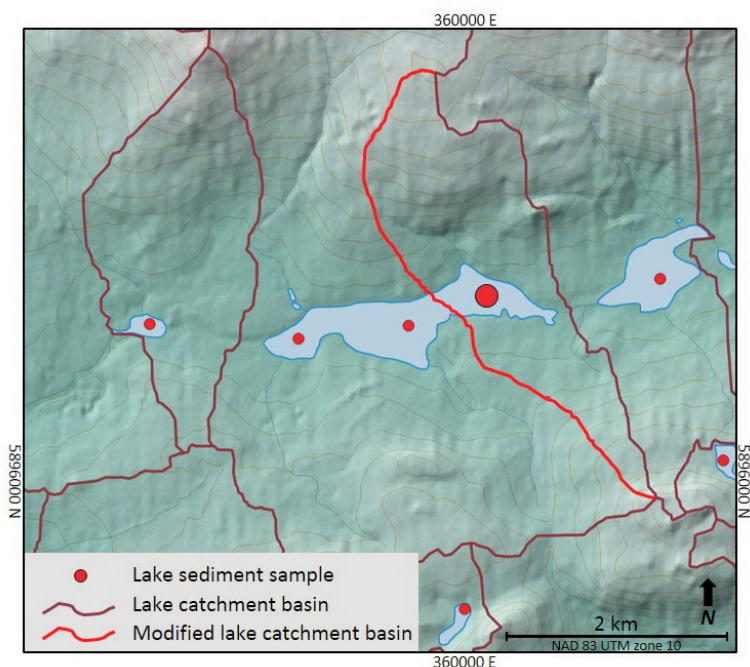


Figure 4. Example of catchment basin delineations for lake sediment samples (burgundy lines). Catchments are manually modified based on topographic and hydrological considerations where samples within the same lake have percent relative standard deviations that are greater than 25% (red lines).

Evaluation of the lake sediment geochemistry will include consideration for AOI size. It is expected that samples with larger AOI will have geochemical values that are closer to background levels due to dilution. The effect of dilution will be assessed empirically using concentration versus AOI area scatterplots to identify samples from large catchments that are above the mean concentrations. If AOI are prohibitively large, the sample may be removed from the dataset or evaluated separately.

A weighted sums (WS) analysis creates a single index that considers multiple elements and is specific to the geochemical signature of the exploration targets. The WS analysis uses a priori knowledge of mineralization to reduce its multi-element signature to a single linear function (see Garrett and Grunsky [2001] for a description of the calculation). The specific RIS will be used to calculate the WS index for each deposit type. The relative importance values are converted to weights by dividing each importance by

Data Evaluation

Deposit Types and Relative Importance Signatures

The deposit types used in this study will be based on nomenclature from the BC mineral deposit profiles (BC Geological Survey, 2016b). The weighted sums (WS) analysis uses elements that are diagnostic of mineral deposit types common to the region (Table 4). Preliminary elements of interest were determined through a review of available rock geochemistry from those mineral deposit types and information in MINFILE (BC Geological Survey, 2016a). A specific relative importance signature (RIS) will be determined for each deposit type through factor analysis and correlation matrices of surface sediment and rock geochemistry. Positive values in the RIS indicate that elevated concentrations of pathfinder elements are significant and negative values indicate that depleted concentrations are significant. Preliminary experiments will be carried out to determine which deposit types will be used in the final analysis.

Weighted Sums Analysis

Table 4. British Columbia Geological Survey mineral deposit profiles (BC Geological Survey, 2016b) with examples from MINFILE (BC Geological Survey, 2016a) in the Targeting Resources through Exploration and Knowledge (TREK) project area, and preliminary mineralization pathfinder elements that will be used for the relative importance signatures. Preliminary experiments will be carried out to determine deposit types used in final analysis.

Deposit profile	Au	Ag	As	Ba	Cu	Bi	Co	F	Fe	Hg	Mn	Mo	Ni	Pb	S	Sb	Te	V	W	Zn	
L04: Porphyry Cu±Mo±Au, e.g., Capoose (MINFILE 093F 022)	x	x	x	x	x		x		x			x		x		x	x	x		x	
L05: Porphyry Mo, e.g., Nithi (MINFILE 093F 014)					x			x	x			x								x	x
H04: Epithermal Au-Ag-Cu: high sulphidation, e.g., CH (MINFILE 093F 085)	x	x	x		x					x				x	x	x	x			x	x
H05: Epithermal Au-Ag: low sulphidation, e.g., Blackwater Davidson (MINFILE 093F 037)	x	x	x	x	x			x		x	x			x	x		x				x
H02: Hot spring: Hg (no known examples in TREK area)	x		x							x							x				
D03: Redbed volcanic copper, e.g., Pickle (Angen et al., 2016)	x	x			x																x
E03: Carbonate-hosted disseminated Au-Ag, e.g., Bob (MINFILE 093B 054)	x	x	x								x		x				x	x			
K04: Au skarn, e.g., Fawn 5 (MINFILE 093F 053)	x		x		x	x	x		x					x							x
I01: Au-quartz veins, e.g., Laidman (MINFILE 093F 067)	x	x	x														x	x			x
I05: Polymetallic veins Ag-Pb-Zn±Au, e.g., 3Ts (MINFILE 093F 068)	x	x	x	x	x					x	x			x							x

Note: Fluorine (F) only determined for lake sediment samples.

the square root of the sum of the squares of all the importance values, resulting in the sum of squares of the weights equating to 1. The WS analysis will be carried out on the standardized geochemical datasets for the till and lake sediment, and again on the till dataset that has been levelled using dominant bedrock source.

Anomaly Evaluation

Specific anomaly thresholds will be determined for each element of interest and WS indices by assessing data distributions on probability graphs (cf. Sinclair, 1981; Grunsky, 2010). Once the anomaly thresholds are determined, the data will be symbolized in a GIS and assessed to identify the locations of anomalies and spatially correlate anomalies between the different media. Clustered anomalous samples and spatially correlative anomalies between the two media will be identified as high-priority exploration targets.

Discussion

The aim of this project is to identify exploration targets through the multivariate analysis of both till and lake sediment samples. Efficacy of the study relies heavily on the quality of the data, the accurate delineation of sample AOI and the RIS. Geochemical data quality has been improved through recent reanalysis and genetic interpretations. Further improvements are made in this study through data standardization to create a genetically comparable, normally distributed and statistically equivalent dataset.

Areas of influence are delineated for till and lake sediment samples to assist in the evaluation of the TREK geochemical dataset. This method is based on catchment analysis that is typically applied to stream sediment samples (e.g., Arne and Bluemel, 2011; Heberlein, 2013). Provided here are preliminary methods to delineate the AOI for till and lake sediment samples, which can be built upon and improved in future studies. Till sample AOI are meant to spatially link each sample to a dominant bedrock source so that the influence of varying bedrock geology can be removed from the regional geochemical dataset. In this study, the determination of till transport distances (i.e., length of till sample AOI) is relative and based on factors that influence glacier velocity. Future efforts to delineate till sample AOI could also use the length of streamlined bedforms as a proxy for ice-flow velocity. Attempts to apply more absolute scaling values based on sediment transport studies (e.g., Clark, 1987; Parent et al., 1996) may also improve the accuracy of the delineation. The accuracy of the bedrock mapping and simplifications are also very important. Inaccurate mapping will result in the incorrect attribution of bedrock source units and cause spurious data levelling results. Efforts are made to incorporate the highest resolution, comparable bedrock mapping into one layer and to create accurate simplifications. Future work should concentrate on improving the assimilation of bedrock data from different

sources and the acquisition of extensive geochemical data, which will improve the simplification process.

Lake sediment sample AOI are delineated from the outlet of the sampled lake to the outlet of the next upstream sampled lake. This definition assumes that there is minimal sediment transfer through the sampled lakes; however, the catchments of upstream lakes that were not sampled are included in the delineation in order to not exclude potential source areas. A comparative analysis of geochemical data using nested and non-nested catchments may provide empirical evidence to inform whether upstream catchments should be included in the AOI delineation.

Using catchment basins as lake sediment sample AOI presumes that any sediment within the catchment is available for erosion and transport to the lake. In reality, soil erosion in most areas is limited by vegetation, and likely only occurs in significant amounts near the stream networks. Incorporating a buffer around active watercourses may provide a more precise delineation of the major contributing sediment sources to the lakes. This delineation would reduce the size of the exploration target, and may provide a better estimate of catchment area, which can be used to determine dilution during data evaluation.

Conclusions

This paper presents the methods that will be used to identify mineral exploration targets in the TREK project area using multivariate and multimedia geochemical data analysis, and a preliminary method of sediment transport modelling. These methods are suitable for the evaluation of surficial exploration data in most regions, particularly in other areas of BC where there is a large collection of geochemical data. The completed study will produce (numbers in parentheses are referenced in Figure 2)

- a database of standardized till and lake sediment geochemical data for elements of interest (1);
- polygon shapefiles of AOI for all till and lake sediment samples (2);
- levelled till geochemistry using dominant bedrock source (3);
- RIS of geochemistry for six common mineral deposits in central BC (4);
- WS indices for deposit models calculated with standardized till and lake sediment geochemistry, and levelled till geochemistry (5);
- potential exploration targets (6); and
- georeferenced maps (e.g., eight 1:100 000 scale maps in PDF) to display WS indices using proportional dot symbols, and gridded data if the sample spacing allows.

Acknowledgments

Funding for this project was provided by Geoscience BC. The authors thank D. Turner for his review of this manuscript and E. Grunsky for his thoughtful advice.

References

- Aario, R. and Peuraniemi, V. (1992). Glacial dispersal of till constituents in moraine landforms of different types; *Geomorphology*, v. 6, p. 9–25.
- Angen, J.J., Logan, J.M., Hart, C.J.R. and Kim, R. (2016): TREK geological mapping project, year 2: update on bedrock geology and mineralization in the TREK project area, central British Columbia (parts of NTS 093B, C, F, G); *in* Geoscience BC Summary of Activities 2015, Geoscience BC, Report 2016-1, p. 1–16, URL <http://www.geosciencebc.com/i/pdf/SummaryofActivities2015/SoA2015_Angen.pdf> [November 2016].
- Angen, J.J., Westberg, E., Hart, C.J.R., Kim, R. and Rahami, M. (2015): Preliminary geological map of the TREK project area, central British Columbia; Geoscience BC, Report 2015-10, URL <<http://www.geosciencebc.com/s/Report2015-10.asp>> [November 2016].
- Arne, D.C. and Bluemel, E.B. (2011): Catchment analysis and interpretation of stream sediment data from QUEST South, British Columbia; Geoscience BC, Report 2011-5, 24 p., URL <<http://www.geosciencebc.com/s/2011-05.asp>> [November 2016].
- BC Geological Survey (2016a): MINFILE BC mineral deposits database; BC Ministry of Energy and Mines, URL <<http://minfile.ca/>> [August 2016].
- BC Geological Survey (2016b): British Columbia mineral deposit profiles; BC Geological Survey, URL <<http://www.empr.gov.bc.ca/MINING/GEOSCIENCE/MINERALDEPOSITPROFILES/Pages/default.aspx>> [November 2016].
- BC Ministry of Energy and Mines (2016): Assessment Report Indexing System (ARIS); BC Ministry of Energy and Mines, BC Geological Survey, URL <<http://www.empr.gov.bc.ca/Mining/Geoscience/ARIS/Pages/default.aspx>> [November 2016].
- Bonham-Carter, G.F. and Goodfellow, W.D. (1986): Background corrections to stream geochemical data using digitized drainage and geological maps: application to Selwyn Basin, Yukon and Northwest Territories; *Journal of Geochemical Exploration*, v. 25, p. 139–155.
- Bordet, E. (2016): Geology of the Eocene Ootsa Lake Group in the Nazko area, Chilcotin Plateau, central British Columbia; Geoscience BC Map 2016-12 and MDRU Map M-10, scale 1:100 000, URL <<http://www.geosciencebc.com/s/Report2016-12.asp>> [November 2016].
- Bouchard, M.A. and Salonen, V.-P. (1990): Boulder transport in shield areas; *in* Glacial Indicator Tracing, R. Kujansuu and M. Saarnisto (ed.), A.A. Balkema, Rotterdam, p. 87–107.
- Briner, J.P. (2007): Supporting evidence from the New York drumlin field that elongate subglacial bedforms indicate fast ice flow; *Boreas*, v. 36, no. 2, p. 143–147.
- Clark, P.U. (1987): Subglacial sediment dispersal and till composition; *The Journal of Geology*, v. 95, no. 4, p. 527–541.
- Cook, S.J., Levson, V.M., Giles, T.R. and Jackaman, W. (1995): A comparison of regional lake sediment and till geochemistry surveys: a case study from the Fawnie Creek area, central British Columbia; *Exploration Mining Geology*, v. 4, p. 93–101.
- Cui, Y., Miller, D., Nixon, G. and Nelson, J. (2015): British Columbia digital geology; BC Geological Survey, Open File 2015-2, URL <<http://www.empr.gov.bc.ca/mining/geoscience/bedrockmapping/pages/bcgeomap.aspx>> [May 2016].
- Djokic, D. (2008): Comprehensive terrain preprocessing using Arc Hydro tools; Esri Support, 61 p., URL <http://downloads2.esri.com/resources/datamodels/Comprehensive terrain preprocessing using Arc Hydro tools_2008.zip> [February 2016].
- Ferbey, T. and Arnold, H. (2013): Micro- to macro-scale ice-flow indicators for the Interior Plateau, central British Columbia; BC Ministry of Energy and Mines, BC Geological Survey, Open File 2013-03, scale 1:900 000, URL <<http://www.empr.gov.bc.ca/Mining/Geoscience/PublicationsCatalogue/OpenFiles/2013/Pages/2013-036.aspx>> [November 2016].
- Ferbey, T., Levson, V.M. and Lett, R.E. (2009): Till geochemical exploration targets, Babine porphyry copper belt, central British Columbia; BC Ministry of Energy and Mines, Open File 2009-4 and Geoscience BC, Report 2009-10, 38 p., URL <<http://www.geosciencebc.com/s/2009-10.asp>> [November 2016].
- Ferbey, T., Levson, V.M. and Lett, R.E. (2012): Till geochemistry of the Huckleberry mine area, west-central British Columbia (NTS 93E/11); BC Geological Survey, Open File 2012-02, 56 p., URL <<http://www.empr.gov.bc.ca/Mining/Geoscience/PublicationsCatalogue/OpenFiles/2012/Documents/2012-2/OF2012-02.pdf>> [November 2016].
- Garrett, R.G. and Grunsky, E.C. (2001): Weighted sums – knowledge based empirical indices for use in exploration geochemistry; *Geochemistry: Exploration, Environment, Analysis*, v. 1 2001, p. 135–141.
- GeoBase® (2007): Canadian digital elevation data, edition 3.0; Natural Resources Canada, URL <<http://geogratis.gc.ca/api/en/nrcan-rncan/ess-sst/3A537B2D-7058-FCED-8D0B-76452EC9D01F.html>> [November 2016].
- GeoBC (2016): Freshwater atlas, British Columbia; Integrated Land Management Bureau, BC Ministry of Natural Resource Operations, URL <<http://geobc.gov.bc.ca/base-mapping/atlas/fwa/index.html>> [November 2016].
- Grunsky, E.C. (2010): The interpretation of geochemical survey data; *Geochemistry: Exploration, Environment, Analysis*, v. 10, p. 27–74.
- Heberlein, D. (2013): Enhanced interpretation of RGS data using catchment basin analysis and weighted sums modeling: examples from map sheets NTS 105M, 105O and part of 105P; Yukon Geological Survey, Open File 2013-16, 18 p.
- Holland, S.S. (1976): Landforms of British Columbia: a physiographic outline; BC Ministry of Energy and Mines, BC Geological Survey, Bulletin 48, 138 p.
- Jackaman, W. (2006): Regional drainage sediment and water geochemical data Anahim Lake & Nechako River, central British Columbia (NTS 93C & 93F); Geoscience BC, Report 2005-4 and BC Ministry of Energy and Mines, BC Geological Survey, GeoFile 2006-11, 463 p., URL <<http://www.empr.gov.bc.ca/Mining/Geoscience/PublicationsCatalogue/GeoFiles/Pages/2006-11.aspx>> [October 2013].

- Jackaman, W. (2008a): Regional lake sediment and water geochemical data, northern Fraser Basin, central British Columbia (parts of NTS 093G, H, J, K, N & O); Geoscience BC, Report 2008-5, 446 p., URL <<http://www.geosciencebc.com/s/2008-05.asp>> [October 2013].
- Jackaman, W. (2008b): QUEST project sample reanalysis; Geoscience BC, Report 2008-3, 4 p., URL <<http://www.geosciencebc.com/s/2008-03.asp>> [October 2013].
- Jackaman, W. (2009a): QUEST-West project sample reanalysis; Geoscience BC, Report 2009-5, 4 p., URL <<http://www.geosciencebc.com/s/2009-05.asp>> [October 2013].
- Jackaman, W. (2009b): Regional drainage sediment and water geochemical data, central British Columbia (parts of NTS 93E, F, G, J, K, L, M, N & O); Geoscience BC, Report 2009-11, 347 p., URL <<http://www.geosciencebc.com/s/2009-11.asp>> [October 2013].
- Jackaman, W. and Sacco, D. (2014): Geochemical and mineralogical data, TREK project, Interior Plateau, British Columbia; Geoscience BC, Report 2014-10, 13 p., URL <<http://www.geosciencebc.com/s/Report2014-10.asp>> [November 2016].
- Jackaman, W., Sacco, D.A. and Lett, R.E. (2015a): Regional geochemical and mineralogical data, TREK project – year 2, Interior Plateau, British Columbia; Geoscience BC, Report 2015-12, URL <<http://www.geosciencebc.com/s/Report2015-12.asp>> [November 2016].
- Jackaman, W., Sacco, D. and Lett, R.E. (2015b): Geochemical reanalysis of archived till samples, TREK project, Interior Plateau, central BC (parts of NTS 093C, 093B, 093F & 093K); Geoscience BC, Report 2015-09, 5 p., URL <<http://www.geosciencebc.com/s/Report2015-09.asp>> [November 2016].
- Kerr, D.E. and Giles, T.R. (1993): Surficial geology of the Chezacut area (NTS 093C/08); BC Ministry of Energy and Mines, BC Geological Survey, Open File 1993-17, scale 1:50 000.
- King, E.C., Hindmarsh, R.C. and Stokes, C.R. (2009): Formation of mega-scale glacial lineations observed beneath a West Antarctic ice stream; *Nature Geoscience*, v. 2, p. 585–588.
- Lett, R., Levson, V. and Dunn, C. (2001): A provisional geochemical exploration model (GEM) for the Sappho property, BC (82E/2E); *in* Geological Fieldwork 2001, BC Ministry of Energy and Mines, BC Geological Survey, p. 389–396, URL <<http://www.empr.gov.bc.ca/Mining/Geoscience/PublicationsCatalogue/Fieldwork/Documents/2001/29-RL-p389-396.pdf>> [November 2016].
- Levson, V.M. (2001): Regional till geochemical surveys in the Canadian Cordillera: sample media, methods, and anomaly evaluation; *in* Drift Exploration in Glaciated Terrain, M.B. McClenaghan, P.T. Bobrowsky, G.E.M. Hall and S.J. Cook (ed.), Geological Society, Special Publication, no. 185, p. 45–68.
- Levson, V.M. and Giles, T.R. (1995). Glacial dispersal patterns of mineralized bedrock: with examples from the Nechako Plateau, central British Columbia; *in* Drift Exploration in the Canadian Cordillera, BC Ministry of Energy and Mines, BC Geological Survey, Paper 1995-2, p. 67–76.
- Levson, V.M., Giles, T.R., Cook, S.J. and Jackaman, W. (1994): Till geochemistry of the Fawnie Creek map area (93F/03); BC Ministry of Energy and Mines, BC Geological Survey, Open File 1994-18, 40 p., URL <<http://www.empr.gov.bc.ca/Mining/Geoscience/PublicationsCatalogue/OpenFiles/1994/Pages/1994-18.aspx>> [October 2013].
- Mathews, W.H. (1986): Physiographic map of the Canadian Cordillera; Geological Survey of Canada, “A” Series Map 1701A, scale 1:5 000 000.
- Mihalynuk, M.G., Orovan, E.A., Larocque, J.P., Friedman, R.M. and Bachiu, T. (2008a): Geology, geochronology and mineralization of the Chilanko Forks to Southern Klusko River area, west-central British Columbia (NTS 093C/01, 08, 09S); *in* Geological Fieldwork 2008, BC Ministry of Energy and Mines, BC Geological Survey, Paper 2009-1, p. 81–100, URL <http://www.empr.gov.bc.ca/Mining/Geoscience/PublicationsCatalogue/Fieldwork/Documents/2008/08_Mihalynuk.pdf> [November 2016].
- Mihalynuk, M.G., Peat, C.R., Orovan, E.A., Terhune, K., Ferbey, T. and McKeown, M.A. (2008b): Chezacut area geology (NTS 093C/08); BC Ministry of Energy and Mines, BC Geological Survey, Open File 2008-2, 1:50 000 scale, URL <<http://www.empr.gov.bc.ca/Mining/Geoscience/PublicationsCatalogue/OpenFiles/2008/Pages/2008-2.aspx>> [November 2016].
- NASA LP DAAC (2015): ASTER level 1 precision terrain corrected registered at-sensor radiance, version 3; National Aeronautic Space Administration (NASA) Earth Observing System Data and Information System (EOSDIS) Land Processes Distributed Active Archive Centre (LP DAAC), USGS Earth Resources Observation and Science (EROS) Center, Sioux Falls, South Dakota, URL <http://dx.doi.org/10.5067/ASTER/AST_L1T.003> [February 2016].
- O’Brian, E.K., Levson, V.M. and Broster, B.E. (1997): Till geochemistry dispersal in central British Columbia; BC Ministry of Energy and Mines, BC Geological Survey, Open File 1997-12, 114 p., URL <<http://www.empr.gov.bc.ca/Mining/Geoscience/PublicationsCatalogue/OpenFiles/1997/Pages/1997-12.aspx>> [November 2016].
- Parent, M., Paradis, S.J. and Doiron, A. (1996): Palimpsest glacial dispersal trains and their significance for drift prospecting; *Journal of Geochemical Exploration*, v. 56, p. 123–140.
- Paulen, R.C. (2001): Glacial transport and secondary hydro-morphic metal mobilization: examples from the southern interior of British Columbia, Canada; Geological Society, London, Special Publications, v. 185, p. 323–337.
- Paulen, R.C., Bobrowsky, P.T., Lett, R.E., Jackaman, W., Bichler, A.J. and Wingerter, C. (2000a): Till geochemistry of the Chu Chua–Clearwater area, BC (parts of NTS 92P/8 and 92P/9); BC Ministry of Energy and Mines, BC Geological Survey, Open File 2000-17, 25 p., URL <<http://www.empr.gov.bc.ca/Mining/Geoscience/PublicationsCatalogue/OpenFiles/2000/Documents/OF2000-17.pdf>> [November 2016].
- Paulen, R.C., Bobrowsky, P.T., Lett, R.E., Jackaman, W., Bichler, A.J. and Wingerter, C. (2000b): Till geochemistry of the Shuswap Highlands area, BC (parts of NTS 82M/3, 82L/13 and 92P/9); BC Ministry of Energy and Mines, BC Geological Survey, Open File 2000-18, 26 p., URL <<http://www.empr.gov.bc.ca/Mining/Geoscience/PublicationsCatalogue/OpenFiles/2000/Documents/OF2000-18.pdf>> [November 2016].

- Plouffe, A. (1997): Reconnaissance till geochemistry on the Chilcotin Plateau (92O/5 and 12); *in* Interior Plateau Geoscience Project: Summary of Geological, Geochemical and Geophysical Studies, L.J. Diakow and J.M. Newell (ed.), Geological Survey of Canada, Open File 3448 and BC Geological Survey, Paper 1997-2, p. 147–157, URL <http://geochem.nrcan.gc.ca/cdogs/content/pub/pub00541_e.htm> [November 2016].
- Plouffe, A., Anderson, R.G., Gruenwald, W., Davis, W.J., Bednarski, J.M. and Paulen, R.C. (2011): Integrating ice-flow history, geochronology, geology, and geophysics to trace mineralized glacial erratics to their bedrock source: an example from south-central British Columbia; *Canadian Journal of Earth Sciences*, v. 48, no. 6, p. 1113–1129.
- Plouffe, A., Levson, V.M. and Mate, D.J. (2004): Surficial geology of the Nechako River map area (NTS 093F); Geological Survey of Canada, “A” series map, scale 1:100 000, URL <<http://geogratings.gc.ca/api/en/nrcan-rncan/ess-sst/c12f712d-fa92-5119-81a3-adffb7db2076.html>> [November 2016].
- Riley, S.J., DeGloria, S.D. and Elliot, R. (1999): A terrain ruggedness index that quantifies topographic heterogeneity; *Intermountain Journal of Sciences*, v. 5, p. 23–27.
- Sacco, D., Ferbey, T. and Jackaman, W. (2014a): Basal till potential of the Clusko River map area (NTS093C/09), British Columbia; BC Ministry of Energy and Mines, BC Geological Survey, Open File 2014-06 and Geoscience BC, Map 2014-06-01, scale 1:50 000, URL <<http://www.geosciencebc.com/s/Report2014-06.asp>> [November 2016].
- Sacco, D., Ferbey, T. and Jackaman, W. (2014b): Basal till potential of the Clisbako River map area (NTS093B/12), British Columbia; BC Ministry of Energy and Mines, BC Geological Survey, Open File 2014-07 and Geoscience BC, Map 2014-06-02, scale 1:50 000, URL <<http://www.geosciencebc.com/s/Report2014-06.asp>> [November 2016].
- Sacco, D., Ferbey, T. and Jackaman, W. (2014c): Basal till potential of the Marmot Lake map area (NTS093B/13), British Columbia; BC Ministry of Energy and Mines, BC Geological Survey, Open File 2014-08 and Geoscience BC, Map 2014-06-03, scale 1:50 000, URL <<http://www.geosciencebc.com/s/Report2014-06.asp>> [November 2016].
- Sacco, D., Ferbey, T. and Jackaman, W. (2014d): Basal till potential of the Toil Mountain map area (NTS093B/16), British Columbia; BC Ministry of Energy and Mines, BC Geological Survey, Open File 2014-09 and Geoscience BC, Map 2014-06-04, scale 1:50 000, URL <<http://www.geosciencebc.com/s/Report2014-06.asp>> [November 2016].
- Sacco, D., Ferbey, T. and Jackaman, W. (2014e): Basal till potential of the Suscha Creek map area (NTS093F/01), British Columbia; BC Ministry of Energy and Mines, BC Geological Survey, Open File 2014-10 and Geoscience BC, Map 2014-06-05, scale 1:50 000, URL <<http://www.geosciencebc.com/s/Report2014-06.asp>> [November 2016].
- Sacco, D., Ferbey, T. and Jackaman, W. (2014f): Basal till potential of the Coglistiko River map area (NTS093G/04), British Columbia; BC Ministry of Energy and Mines, BC Geological Survey, Open File 2014-11 and Geoscience BC, Map 2014-06-06, scale 1:50 000, URL <<http://www.geosciencebc.com/s/Report2014-06.asp>> [November 2016].
- Sacco, D., Ferbey, T. and Jackaman, W. (2014g): Basal till potential of the Pelican Lake map area (NTS093G/05), British Columbia; BC Ministry of Energy and Mines, BC Geological Survey, Open File 2014-12 and Geoscience BC, Map 2014-06-07, scale 1:50 000, URL <<http://www.geosciencebc.com/s/Report2014-06.asp>> [November 2016].
- Sacco, D., Ferbey, T. and Jackaman, W. (2014h): Basal till potential of the Eucheniko River map area (NTS093F/08), British Columbia; BC Ministry of Energy and Mines, BC Geological Survey, Open File 2014-13 and Geoscience BC, Map 2014-06-08, scale 1:50 000, URL <<http://www.geosciencebc.com/s/Report2014-06.asp>> [November 2016].
- Sacco, D., Ferbey, T. and Jackaman, W. (2014i): Basal till potential of the Chilako River map area (NTS093G/12), British Columbia; BC Ministry of Energy and Mines, BC Geological Survey, Open File 2014-14 and Geoscience BC, Map 2014-06-09, scale 1:50 000, URL <<http://www.geosciencebc.com/s/Report2014-06.asp>> [November 2016].
- Sacco, D., Ferbey, T. and Jackaman, W. (2014j): Basal till potential of the Hulatt map area (NTS 93G/13), British Columbia; BC Ministry of Energy and Mines, BC Geological Survey, Open File 2014-15 and Geoscience BC, Map 2014-06-10, scale 1:50 000, URL <<http://www.geosciencebc.com/s/Report2014-06.asp>> [November 2016].
- Sacco, D.A., Jackaman, W. and Ferbey, T. (2014k): Targeted geochemical and mineralogical surveys in the TREK project area, central British Columbia (parts of NTS 093B, C, F, G); *in* Geoscience BC Summary of Activities 2013, Geoscience BC, Report 2014-1, p. 19–34, URL <<http://www.geosciencebc.com/s/SummaryofActivities.asp?ReportID=619756>> [November 2016].
- Shilts, W. (1993): Geological Survey of Canada’s contributions to understanding the composition of glacial sediments; *Canadian Journal of Earth Sciences*, v. 30, p. 333–353.
- Sibbick, S.J., Balma, R.G. and Dunn C.E. (1996): Till geochemistry of the Mount Milligan area (parts of 93N/1 and 93O/4); BC Ministry of Energy and Mines, BC Geological Survey, Open File 1996-22, 18 p. <<http://www.empr.gov.bc.ca/Mining/Geoscience/PublicationsCatalogue/OpenFiles/1996/Documents/OF1996-22.pdf>> [November 2016].
- Sinclair, A.J. (1981): Application of probability graphs; *The Association of Exploration Geochemists, Special Publication 4*, 95 p.
- Stea, R.R. and Finck, P.W. (2001): An evolutionary model of glacial dispersal and till genesis in Maritime Canada; *Geological Society, London, Special Publications*, v. 185, p. 237–265.
- Stokes, C.R. and Clark, C.D. (2002). Are long subglacial bedforms indicative of fast ice flow?; *Boreas*, v. 31, p. 239–249.
- Stumpf, A.J. (2012): Till geochemistry and clast lithology studies of the Bulkley River Valley, West-Central British Columbia (parts of NTS 093L); Geoscience BC, Report 2012-11, 59 p., URL <<http://www.geosciencebc.com/s/Report2012-11.asp>> [November 2016].
- Weary, G.F., Levson, V.M. and Broster, B.E. (1997): Till geochemistry of the Chedakuz Creek map area (NTS 93F/7); BC Ministry of Energy and Mines, BC Geological Survey, Open File 1997-11, 97 p., URL <<http://www.empr.gov.bc.ca/Mining/Geoscience/PublicationsCatalogue/OpenFiles/1997/Documents/OF1997-11.pdf>> [November 2016].

Clay-Fraction Till Geochemistry of the TREK Project Area, Central British Columbia (Parts of NTS 093B, C, F, G): Progress Report

P.W.G. van Geffen, REFLEX Geosciences, Vancouver, BC, pim.vangeffen@imdexlimited.com

E.B. Bluemel, REFLEX Geosciences, Vancouver, BC

van Geffen, P.W.G. and Bluemel, E.B. (2017): Clay-fraction till geochemistry of the TREK project area, central British Columbia (parts of NTS 093B, C, F, G): progress report; in Geoscience BC Summary of Activities 2016, Geoscience BC, Report 2017-1, p. 113–114.

Introduction

Large parts of central British Columbia (BC) are underexplored because of extensive Quaternary cover that obscures much of the underlying geology from direct observation. Consequently, resource companies are faced with increased exploration risk and must rely on indirect detection of mineralization by geophysical or geochemical methods. As these methods evolve and improve over time, the cumulative geoscience that is generated over covered areas enables the integration of various data types, which in turn increases confidence in the understanding of the bedrock lithology.

Geoscience BC has actively engaged in the generation of high-quality public geoscience in the province for more than a decade, including geoscience in large areas of covered terrain such as the Targeting Resources through Exploration and Knowledge (TREK) project area, which covers parts of the NTS map areas 093B, C, F and G (Figure 1). The size fraction that was selected for the till geochemistry in the TREK project was $<63\ \mu\text{m}$ (silt + clay). Although this is standard practice in till analysis because dry sieving to a finer fraction would be impractical, the geo-

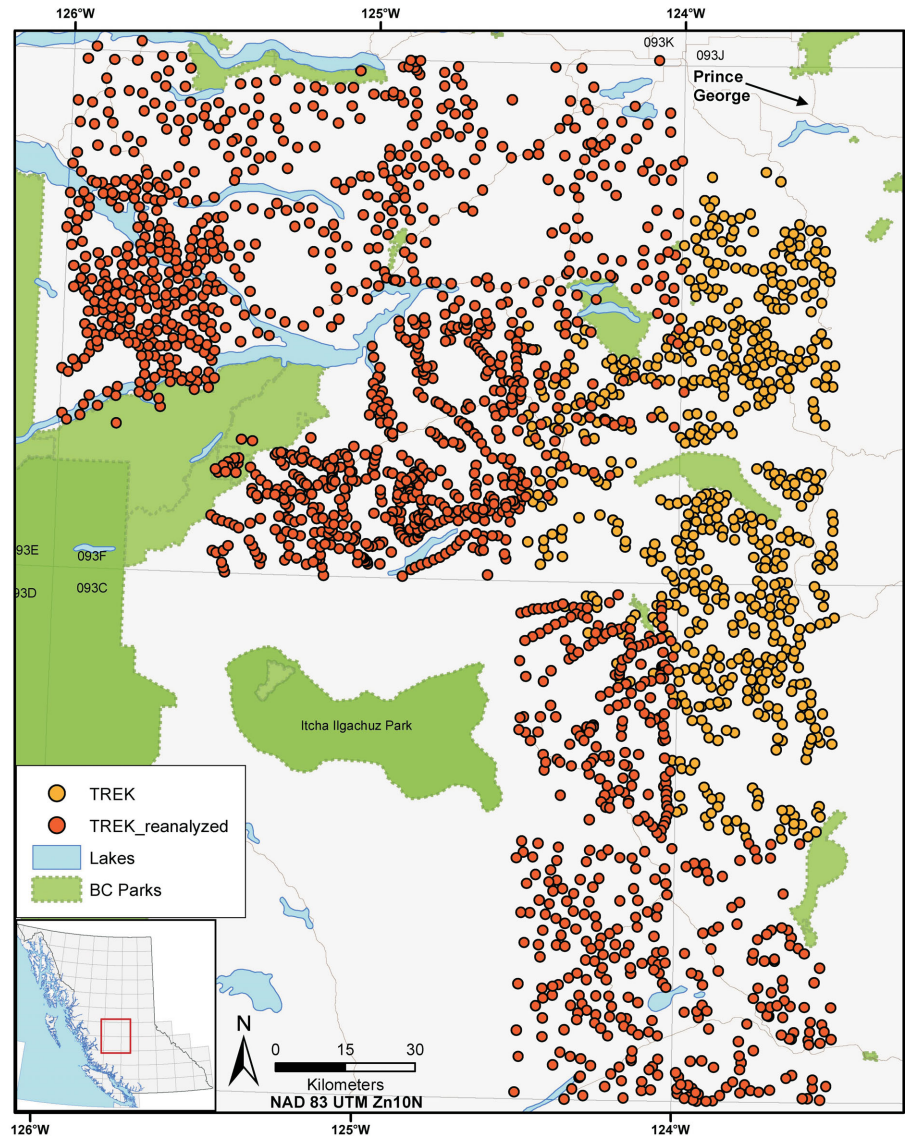


Figure 1. TREK project till sample locations, central British Columbia.

Keywords: British Columbia, till geochemistry, hydromorphic dispersion, exploration

This publication is also available, free of charge, as colour digital files in Adobe Acrobat® PDF format from the Geoscience BC website: <http://www.geosciencebc.com/s/DataReleases.asp>.

chemical response may still be overwhelmed by matrix components such as carbonate minerals and organic matter. To remedy the effect of matrix materials on the analysis of till and reduce its heterogeneity, the clay fraction ($<2\ \mu\text{m}$) can be extracted and analyzed, which has been known to provide superior results for trace elements transported by

hydromorphic dispersion through the till cover (Slavek and Pickering, 1981; DiLabio, 1995; van Geffen et al., 2012).

Geoscience BC Report 2009-10 (Ferbey et al., 2009) reported the analysis of the clay fraction of archived till samples from the Babine porphyry belt, which were sampled in the earlier NATMAP sampling program (Levson, 2002). The paper described the relative abundances of a range of elements with limited data processing and interpretation. This study will include data validation and basic exploratory data analysis to add value to the generated data and comment on the comparison with the original data from the silt + clay fraction.

Status and Future Work

Till samples that were collected in the TREK project area in 2013 and 2014 were archived by the BC Geological Survey (BCGS) in Victoria, BC (Jackaman and Sacco, 2014; Sacco et al., 2014; Sacco and Jackaman, 2015). To date, 613 ‘character splits’ of the archived samples have been retrieved for clay extraction and analysis, with help from R. Lett, consultant, formerly BCGS. These samples have been submitted to the Bureau Veritas Mineral laboratory in Vancouver, BC, for preparation and analysis. The analytical method is a clay-fraction separation followed by aqua-regia digestion and inductively coupled plasma–mass spectrometry (ICP-MS) finish for 53 elements on 0.5 g aliquots.

Previous campaigns in the TREK area produced till samples that were recovered and submitted for reanalysis as part of the TREK project in 2015 (Jackaman et al., 2015), but the sample volumes remaining at the BCGS archive are considered insufficient for clay extraction. The Geological Survey of Canada published till geochemical data from the area in 2001 (Plouffe et al., 2001), including inductively coupled plasma–atomic emission spectroscopy (ICP-AES) data of both the <63 and <2 µm fractions. These data will be used for reference and, where appropriate, included in the final data analysis of this study.

It is anticipated that this study will be completed by January 2017 and the results presented at the Association of Mineral Exploration Roundup. The final report will be published as a separate Geoscience BC report in early 2017.

References

- DiLabio, R.N.W. (1995): Residence sites of trace elements in oxidized till; *in* Drift Exploration in the Canadian Cordillera, P.T. Bobrowsky, S.J. Sibbick, J.M. Newell and P. Matyssek (ed.), BC Ministry of Energy and Mines, BC Geological Survey, Paper 1995-2, p. 139–148.
- Ferbey, T., Levson, V.M. and Lett, R.E. (2009): Till geochemical exploration targets, Babine porphyry copper belt, central British Columbia; BC Geological Survey, Open File 2009-4 and Geoscience BC, Report 2009-10, URL <<http://www.geosciencebc.com/s/2009-10.asp>> [October 2016].
- Jackaman, W. and Sacco, D.A. (2014): Regional geochemical and mineralogical data TREK project Interior Plateau, British Columbia; Geoscience BC, Report 2014-10, URL <<http://www.geosciencebc.com/s/Report2014-10.asp>> [October 2016].
- Jackaman, W., Sacco, D.A. and Lett, R.E. (2015): Geochemical reanalysis of archived till samples TREK project, Interior Plateau, central BC; Geoscience BC, Report 2015-09, URL <<http://www.geosciencebc.com/s/Report2015-09.asp>> [October 2016].
- Levson, V.M. (2002): Quaternary geology and till geochemistry of the Babine porphyry copper belt, British Columbia (NTS 93 L/9,16, M/1, 2, 7, 8); BC Ministry of Energy and Mines, Bulletin 110, 278 p.
- Plouffe, A., Levson, V.M. and Mate, D.J. (2001): Till geochemistry of the Nechako River map area (NTS 93F), central British Columbia; Geological Survey of Canada, Open File 4166.
- Sacco, D.A. and Jackaman, W. (2015): Targeted geochemical and mineralogical surveys in the TREK project area, central British Columbia (parts of NTS 093B, C, F, G): year two; *in* Geoscience BC Summary of Activities 2014, Geoscience BC, Report 2015-1, p. 1–12, URL <http://www.geosciencebc.com/i/pdf/SummaryofActivities2014/SoA2014_Sacco.pdf> [October 2016].
- Sacco, D.A., Jackaman, W. and Ferbey, T. (2014): Targeted geochemical and mineralogical surveys in the TREK project area, central British Columbia (parts of NTS 093B, C, F, G); *in* Geoscience BC Summary of Activities 2013, Geoscience BC, Report 2014-1, p. 19–34, URL <http://www.geosciencebc.com/i/pdf/SummaryofActivities2013/SoA2013_Sacco.pdf> [October 2016].
- Slavek, J. and Pickering, W. (1981): The effect of pH on the retention of Cu, Pb, Cd, and Zn by clay-fulvic acid mixtures; *Water, Air, & Soil Pollution*, v. 16, no. 2, p. 209–221.
- van Geffen, P.W.G., Kyser, T.K., Oates, C.J. and Ihlenfeld, C. (2012): Till and vegetation geochemistry at the Talbot VMS Cu–Zn prospect, Manitoba, Canada: implications for mineral exploration; *Geochemistry, Exploration, Environment & Analysis*, v. 12, p. 67–86.

Adding Value to Regional Till Geochemical Data through Exploratory Data Analysis, TREK Project Area, Central British Columbia (parts of NTS 093B, C, F, G)

E.B. Bluemel, REFLEX Geosciences, Vancouver, BC, britt.bluemel@imdexlimited.com

P.W.G. van Geffen, REFLEX Geosciences, Vancouver, BC

Bluemel, E.B. and van Geffen, P.W.G. (2017): Adding value to regional till geochemical data through exploratory data analysis, TREK project area, central British Columbia (parts of NTS 093B, C, F, G); in Geoscience BC Summary of Activities 2016, Geoscience BC, Report 2017-1, p. 115–124.

Introduction

The most efficient use of resources in mineral exploration is to add value to existing data products. The utility of existing geochemical data can be greatly improved by first order interpretation, because derivative data products (which are common in geophysics) account for surficial processes. These derivative data products can spur interest in areas that may have been otherwise overlooked.

Over the past 11 years, Geoscience BC has supported the continued collection and chemical analysis of till geochemical samples in efforts to promote mineral exploration throughout British Columbia (BC). The TREK (Targeting Resources through Exploration and Knowledge) project was initiated in 2013 to generate new information on BC's northern Interior Plateau region, an area which is highly prospective for mineral resources and may also have some geothermal potential. However, the area is underexplored for these resources due to overburden of variable thickness covering complicated and poorly understood bedrock geology. Across the TREK project area almost 3000 samples were collected by the British Columbia Geological Survey (BCGS), Geological Survey of Canada (GSC) and Geoscience BC (Figure 1). Samples from the BCGS and GSC campaigns were reanalyzed as part of the TREK project (Jackaman et al., 2015) to ensure state-of-the-art data quality.

The geochemical interpretation presented in this study has three main steps, the deliverables of which will contribute to Geoscience BC's mandate to stimulate mineral exploration:

- 1) All available till geochemical analyses in the TREK area were evaluated and assessed for comparability and utility on an element by element basis. Data artefacts

were visible between original survey areas, but their effects were suitably circumvented during the remainder of the interpretation.

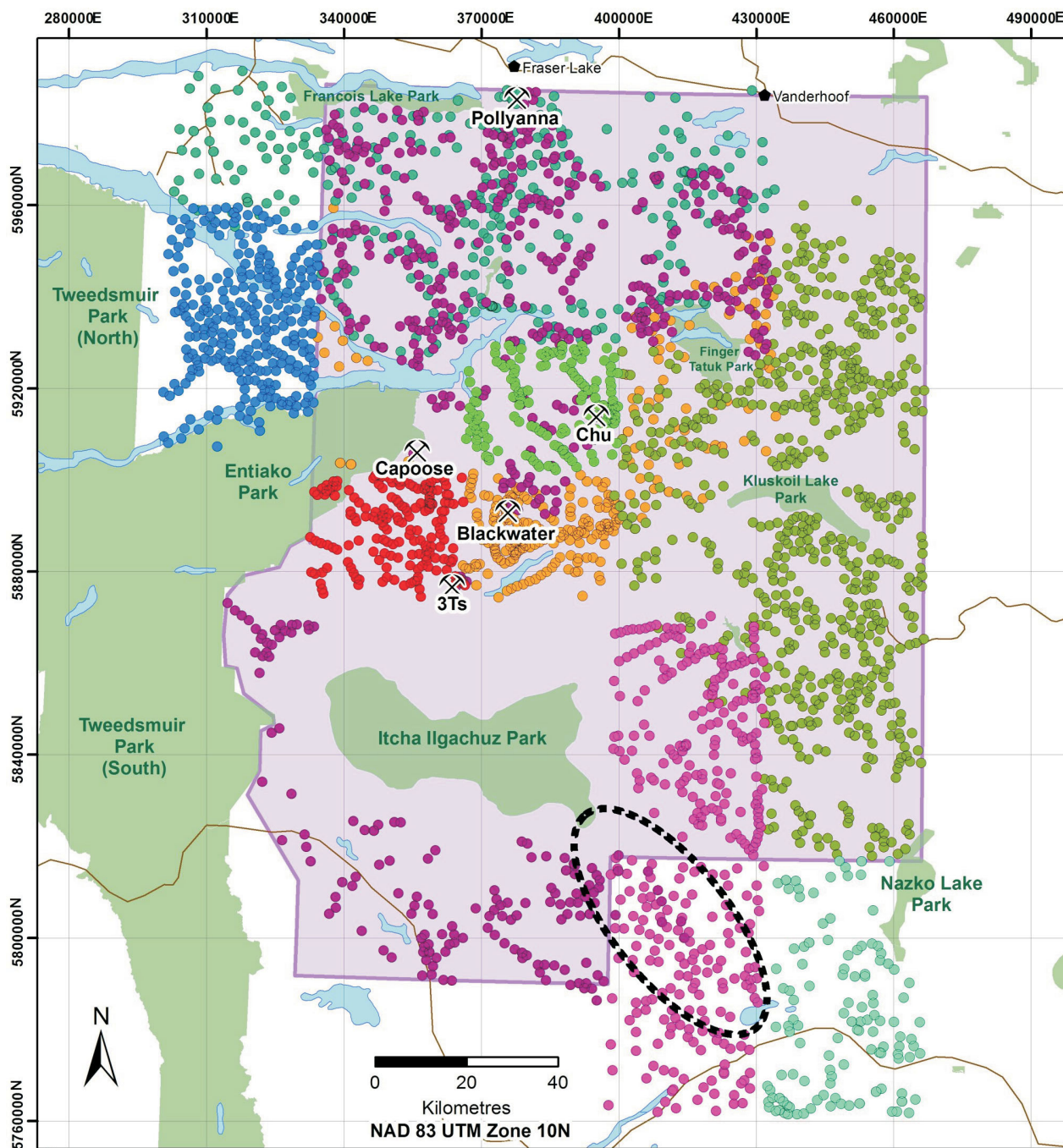
- 2) A thorough interpretation of the till geochemical data selected in the first step was accomplished using exploratory data analysis (EDA) techniques, including cluster analysis to determine till signature. Further geochemical techniques, such as regression analyses to account for secondary surficial processes, were also employed.
- 3) Robust, second order, geochemical derivative products (compared to known mineral occurrences where possible) that delineate areas of increased mineral potential based on ranked multi-element anomalies were provided.

Data Validation and Assessment

Before data analysis can be properly undertaken, it is necessary to assess the quality and distribution of the available geochemical data. The data quality was assessed using ioGAS software and common data format issues were addressed, such as replacement of below-detection values, 'no-data' values (in this dataset no-data was listed as "-9999") and zeroes with null values to allow further statistical analysis. The full dataset (number of samples [n] = 2970) comprises 1259 new till survey samples and 1711 reanalyzed till samples from previous campaigns in the area (Jackaman et al., 2015), data from which will be included as an appendix in the final report. The newly collected and reanalyzed samples were all subjected to the same analytical method at the same lab (aqua-regia digestion with inductively coupled plasma–mass spectrometry [ICP-MS] finish at Bureau Veritas Minerals [Vancouver, BC]) eliminating the need for data processing to remove lab method effects. Normal probability plots were used to evaluate the distributions of each element and to flag those elements with limited quality and precision. The TREK till geochemistry dataset was generally of very good quality, with the exception of a few elements (W, S, Se, Te, Ge, Ta, In, Re, Pd, Pt, B, Na), and a group of 255 samples that contained null values for all elements. Also, a handful of samples (n = 6) were omitted from

Keywords: British Columbia, geochemistry, exploratory data analysis, till, anomaly, mineral exploration, provenance

This publication is also available, free of charge, as colour digital files in Adobe Acrobat® PDF format from the Geoscience BC website: <http://www.geosciencebc.com/s/DataReleases.asp>.



- Till sample site**
- Levson et al. (1994)
 - Weary et al. (1997)
 - Levson et al. (2002)
 - Lett et al. (2006)
 - Ferbey (2009)
 - Jackaman and Sacco (2014)
 - Jackaman et al. (2015)
 - Plouffe and Williams (1998)
 - Plouffe et al. (2001)

- ⚡ Developed prospect
- Road
- Lake
- Provincial park
- TREK area



Figure 1. The Targeting Resources through Exploration and Knowledge (TREK) project location map with till samples coloured based on the associated geoscience report ('original report'). Note that the black-dashed circle represents the area of survey overlap used to determine spatial versus survey influence in the exploratory data analysis.

the interpretation because of extreme values in elements of secondary interest (Fe, Mn, Na).

In total, the interpreted dataset ($n = 2709$) spans nine survey areas, including five zones where spatial sample collection overlap. To investigate whether changes in elemental concentrations were influenced by the survey area ('original report'), these five zones were isolated and then all element ranges were evaluated. If the ranges of element concentrations vary significantly when only looking at data from within one zone, it can be confidently surmised that the data variation is due to some other factor than original report (i.e., changes in slope or underlying geology rather than survey effect). Four of the five zones showed acceptable variation when comparing the immobile elements, but one zone (Figure 1) showed considerable differences (up to three times greater median values in immobile elements between areas), between Jackaman et al. (2015) and Lett et al. (2006), and this variation will be addressed in further interpretations.

The main concern with the variation of data between survey areas is actually the quality of the till sample collected. Jackaman et al. (2015) re-evaluated the basal till potential (BTP) for the historic till samples and found large degrees of variation between survey years. Jackaman et al. assigned a BTP score to all samples, and 2581 till samples were classified "basal till or very likely basal till", whereas 389 samples were classified "unlikely to be basal till". The latter samples require more careful interpretation because they were likely transported farther from their protolith.

Exploratory Data Analysis - Methodology

Exploratory data analysis is well documented in geochemical literature, and has been used in mineral exploration for the past 50 years. Grunsky (2007) describes it as the process of detecting trends or structures within the data, which can "provide insight into the geochemical/geological processes". By having a greater understanding of the processes that create, channel and ultimately control geochemical anomalies that are expressed at surface, the likelihood of correctly interpreting these anomalies is drastically increased and therefore the likelihood of discovering buried mineralization. Exploratory data analysis (EDA) was performed on the 2709 till samples selected from the full dataset of 2970 samples based on data quality.

Part I: Cluster Analysis to Define Till Provenance

Till geochemical samples, even if they are basal till and a first derivative of the underlying bedrock, are still the product of a surficial process and thus their data must be treated accordingly. Assigning a protolith unit to a till sample based on its actual sample

collection location is inappropriate because the till may have been derived from bedrock as much as tens of kilometres away (Ferbey et al., 2014). The provenance of these till samples was determined by a multivariate analysis of both immobile and trace elements, and initially five different till types were identified using a hard-partitioning k-means cluster analysis. This method aims to partition a number of observations into k-clusters in which each observation is assigned to the most similar group based on a subset of variables. The optimum number of clusters will have the smallest sum of squares between observations and the cluster's central node. The purpose of this analysis is to minimize the within-cluster variation and maximize the between-cluster variation based on the selected elements of interest.

The elements used in the first pass clustering analysis were (Na+K)/Al, Ca, Ti, Zr, Y, Th and Nb. The (Na+K)/Al term can be used as a proxy for till evolution; more evolved, or distal, till samples will have a lower (Na+K)/Al value because they are more weathered and therefore more of the Na or K has been mobilized and removed from the till sample (Figure 2). The dark green group has been identified as evolved due to its lower relative (Na+K)/Al values, and also its higher Zr and Ti values (Zr can be correlative to the sand fraction of the till sample, also indicating a higher degree of transport). The till samples were analyzed using an aqua-regia digestion, which is an incomplete digestion method that does not dissolve certain silicates, oxides, and some of the minerals that contain high-field strength elements (HFSE), meaning that the results for many elements are only partial, and elements such as Zr will have poorer data quality. The blue group is likely derived from carbonate materials, inferred from their high Ca content.

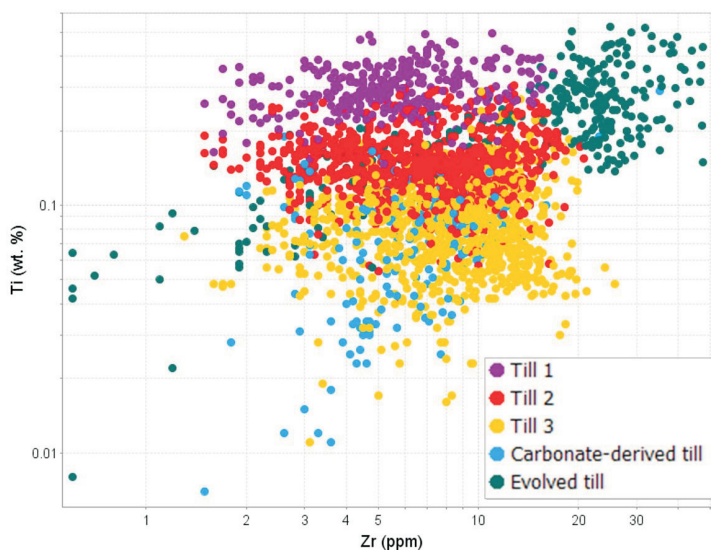


Figure 2. Biplot of Ti as a function of Zr, coloured by first pass clustering analysis using immobile and trace elements to separate till types, Targeting Resources through Exploration and Knowledge [TREK] project area, central British Columbia.

The carbonate-derived and evolved tills were then temporarily removed from the dataset and the remaining three till groups were further separated into five groups based on the distributions of major elements and a selection of trace elements (Ti, Al, Fe, Mg, Mn, Ca, Na, K, Cr, U, Ni; Figure 3) resulting in a total of seven chemically distinct till compositions or types in the TREK area (Figure 4). These till types were spatially coherent but do not correspond with the original report areas, which indicates the influence of survey area has been overcome. Till signature was assigned based on differences in till geochemistry and the lithological affinity of major and trace elements.

Part II: Regression Analysis (by Provenance) to Identify Outliers

Regression analysis predicts the behaviour of a response variable relative to an explanatory variable, and also allows the calculation of a residual value, which is the difference between the predicted value and the observed value of the dependent variable. The linear equation resulting from a regression analysis models the relationship between the predictor and response variables. A robust regression analysis down-weights the influence of outliers, thus the robust regression equation most closely approximates the majority of the data, and allows outliers to be identified more clearly. The algorithm used is the least median of squares (LMS) method described in Rousseeuw and Leroy (1987).

In this regression analysis, the predictor variables used were Fe and Al. Iron oxides in the surficial environment are very efficient at binding mobile chalcophile elements (e.g., Cu, Zn, Pb, Ag, As) and Al can be used as a proxy for clay

content in till samples because mobile elements can be adsorbed onto clay particles. In this interpretation, the regression analysis was carried out by till type, meaning that outliers were identified for each different till type as defined and separated by signature. This is significant because some till types naturally contain more chalcophile elements based on their protolith. The example in Figure 5 shows that the mafic-signature (high Fe) till type has the highest proportion of Cu, so by calculating a regression analysis by till type the effect of varying signatures can be levelled out at the same time a robust residual is calculated. Of note is the elevated Fe content coinciding with the elevated Cu content in the mafic-signature (high Fe) till type; this alludes to either Fe control on hydromorphic dispersion of Cu, or that Fe and Cu have a common source in this till type.

Residuals are the measure of the difference between the observed value and the expected value (of the response variable, i.e., Cu) compared to the predictor or explanatory variable, in this case Fe (Figure 6). Robust standardized residual values (residual divided by the standard deviation of the residuals) were then calculated for the pathfinder elements (Cu, Mo, Zn, Pb, As, Ag) as a function of both Fe and Al (independently), as well as per till type and plotted on the map along with known developed prospects to validate the results (Figure 7, Cu as a function of Fe). Calculated robust standardized residuals for all pathfinder elements are presented with the data compilation as an appendix to the final report.

The results of the interpretation show excellent spatial relation of residual values with known developed prospects (Blackwater [MINFILE 093H 037, BC Geological Survey, 2016], 3Ts [MINFILE 093F 055], Pollyanna [MINFILE 093F 15W], Chu [MINFILE 093F 07E]) in the TREK area. One exception is the Capoose prospect (MINFILE 093F 06E), which is just outside the till sampling coverage area. Even though these observations are helpful in validating the method, the more important results of the interpretation are the several new areas that have been highlighted by this approach of second-order geochemical data interpretation. These prospective areas, which have not yet been identified as areas of mineralization, may warrant follow-up by more detailed fieldwork in the future (Figure 7).

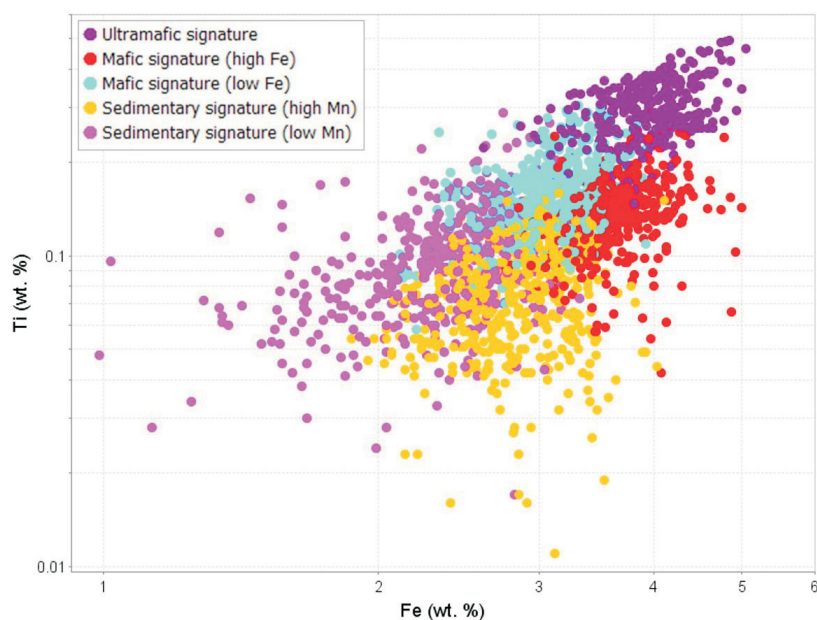


Figure 3. Biplot of Ti as a function of Fe, coloured by the second iteration of clustering analysis to differentiate the five till types, Targeting Resources through Exploration and Knowledge (TREK) project area, central British Columbia (note that carbonate-derived and evolved tills are omitted from this diagram for clarity).

Discussion

In the initial stages of EDA, two main observations about the structure of the data

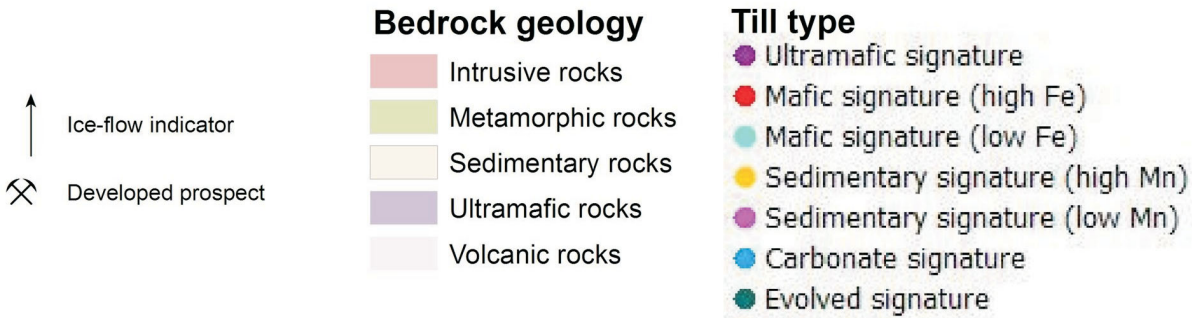
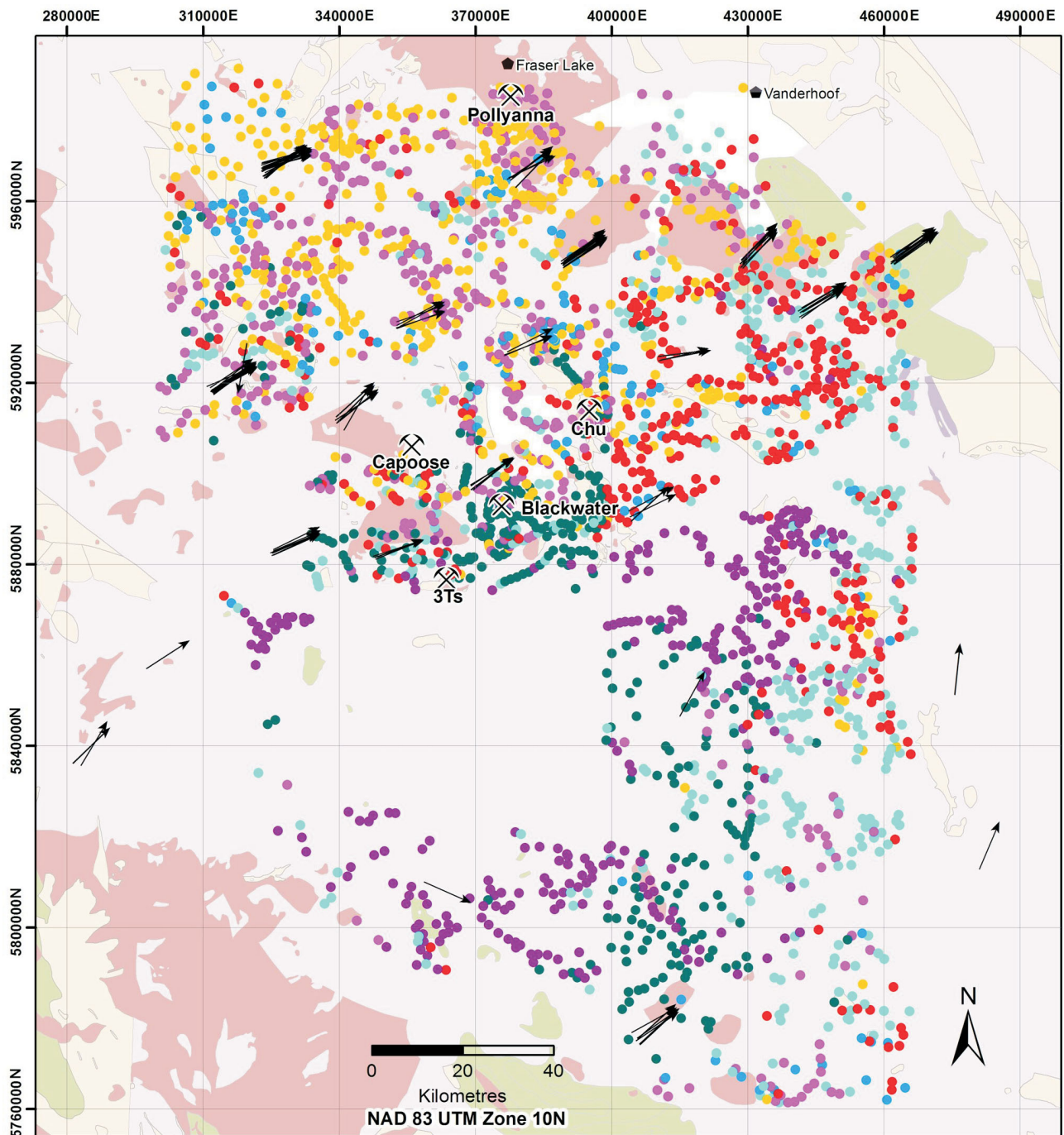


Figure 4. Map of till geochemical samples, colour is based on till type (signature), Targeting Resources through Exploration and Knowledge (TREK) project area, central British Columbia. Bedrock geology modified from Massey et al. (2005).

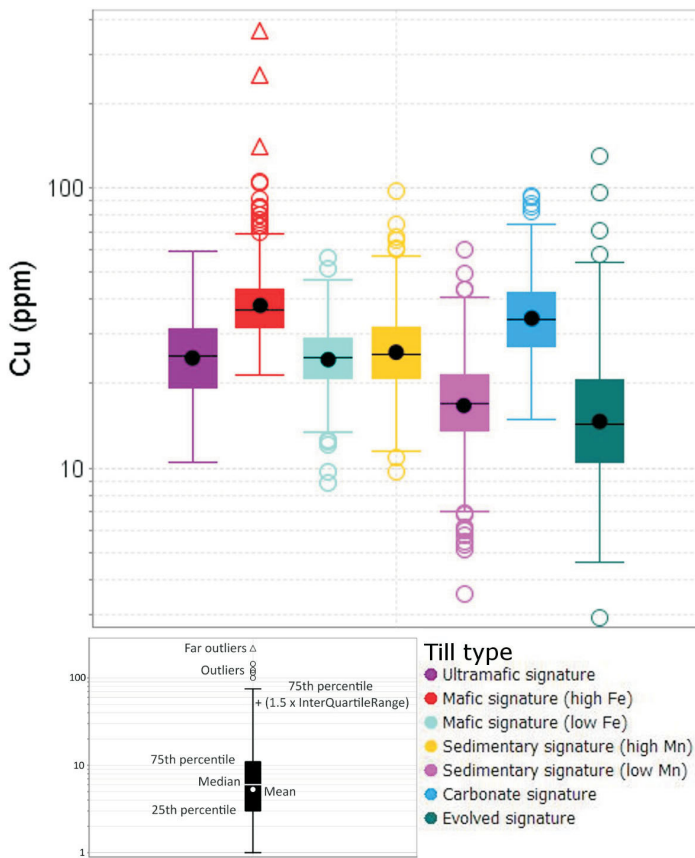


Figure 5. Boxplot of Cu content of till samples grouped by till type (signature), Targeting Resources through Exploration and Knowledge (TREK) project area, central British Columbia.

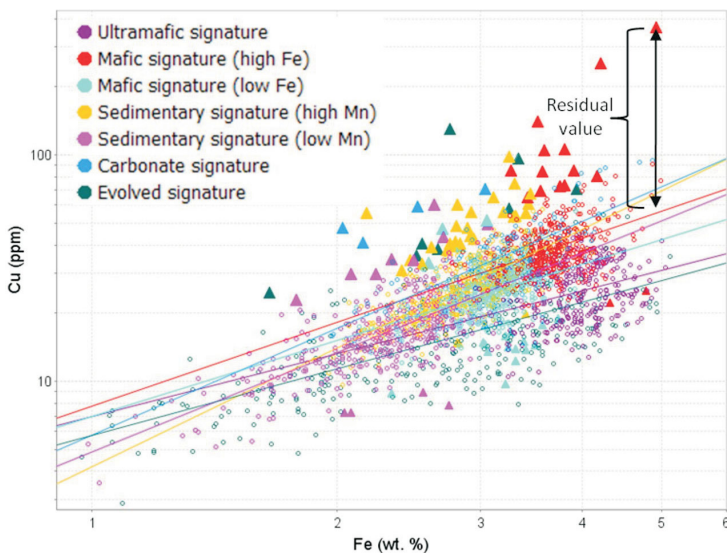


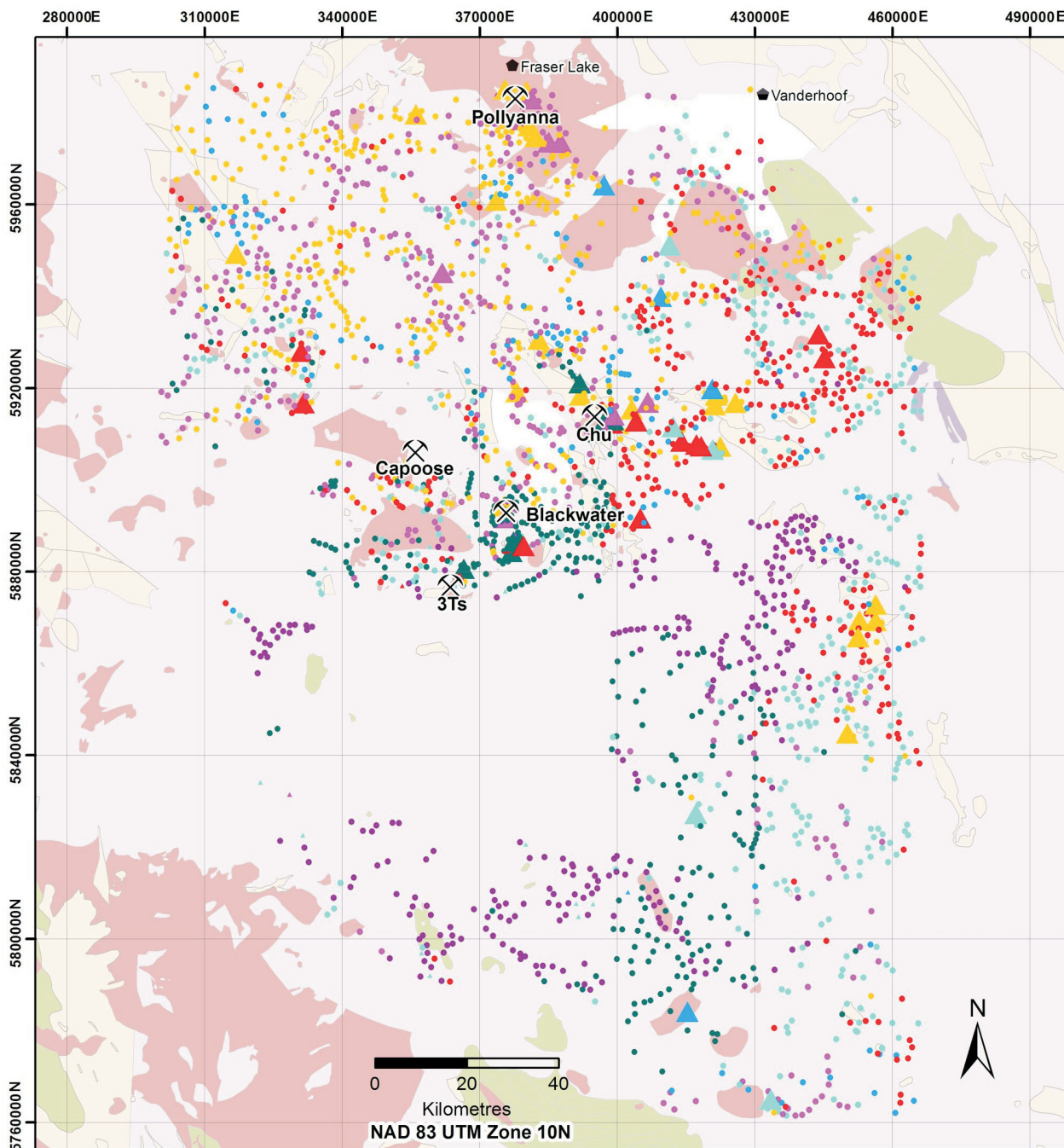
Figure 6. Regression analysis of Cu as a function of Fe (till samples from Targeting Resources through Exploration and Knowledge [TREK] project area, central British Columbia). Samples with standardized residual values >3 are presented as large filled triangles. Residuals are the value of the difference between the observed and the expected result. Standardized residuals = residual / standard deviation of the residuals by till type.

were obvious. Firstly, several elements of interest, including the porphyry pathfinder and immobile elements, were incomparable between the original reports, and this effect had to be investigated more closely. Secondly, the main changes in the BTP score (Jackaman et al., 2015) were coincident with survey boundaries. This is not surprising because earlier surveys were not as rigorous about the type of till collected, which became important in later surveys, so in many cases ablation or supraglacial flow tills were collected rather than basal tills. Since the collected material differed in origin, differences in trace and immobile element chemistry were also incomparable by their BTP. This is a boon for the interpretation because it is possible to account for either of those factors and the influence of the other will also be accounted for.

To investigate the original report effect more closely, five small areas containing samples from two spatially overlapping reports were selected and that data was subset and examined. In this interpretation, several of the immobile elements evaluated still showed large variation within each spatial subset, so original report was accounted for in the regression step of the interpretation.

Cluster analysis using (Na+K)/Al, Ca, Ti, Zr, Y, Th and Nb was performed on the 2709 till samples, and was done in two parts resulting in seven chemically distinct till types, which were then named based on their signature. Once the till samples were separated into signature groups, a robust regression analysis was performed on appropriate porphyry pathfinder elements and a robust residual was calculated for each pathfinder element within each till type. This removes the effect of varying chemistry based on till source, and also removes the effect of survey area – recall in the first steps of the EDA the comparability issue that was spotted between survey areas and these boundaries roughly matched the boundaries defined by changing BTP. These boundaries are also coincident with the chemically distinct till types (Figure 8).

Finally, the robust residual values for the pathfinder elements (Ag, As, Cu, Mo) were evaluated using an anomaly assessment test, which is the combination of univariate Tukey box-and-whisker plot statistics (Tukey, 1977) and multivariate Mahalanobis distance calculation (Mahalanobis, 1936), which takes correlated sample behaviour into account. The most interesting resultant anomalies are larger symbols on Figure 9 because the size of the symbol is directly proportional to the number of anomalous elements in that sample. Of



Bedrock geology

- Intrusive rocks
- Metamorphic rocks
- Sedimentary rocks
- Ultramafic rocks
- Volcanic rocks

Till type

- Ultramafic signature
- Mafic signature (high Fe)
- Mafic signature (low Fe)
- Sedimentary signature (high Mn)
- Sedimentary signature (low Mn)
- Carbonate signature
- Evolved signature

Standard residuals for Cu

- 3.0 to 3.0
- > 3.0
- Developed prospect

Figure 7. Map of Cu residuals (regression analysis of Cu as a function of Fe), Targeting Resources through Exploration and Knowledge (TREK) project area, central British Columbia. New target areas are indicated by the large filled triangles that are not coincident with known prospects. Bedrock geology modified from Massey et al. (2005).



Figure 8. Comparison maps of **a)** original report, **b)** basal till potential (BTP) and **c)** till type, Targeting Resources through Exploration and Knowledge (TREK) project area, central British Columbia (NAD 83, UTM Zone 10N). Boundaries from original report are also visible in the BTP and till type maps, which means accounting for till provenance in the interpretation will automatically explain the variation in BTP and original report.

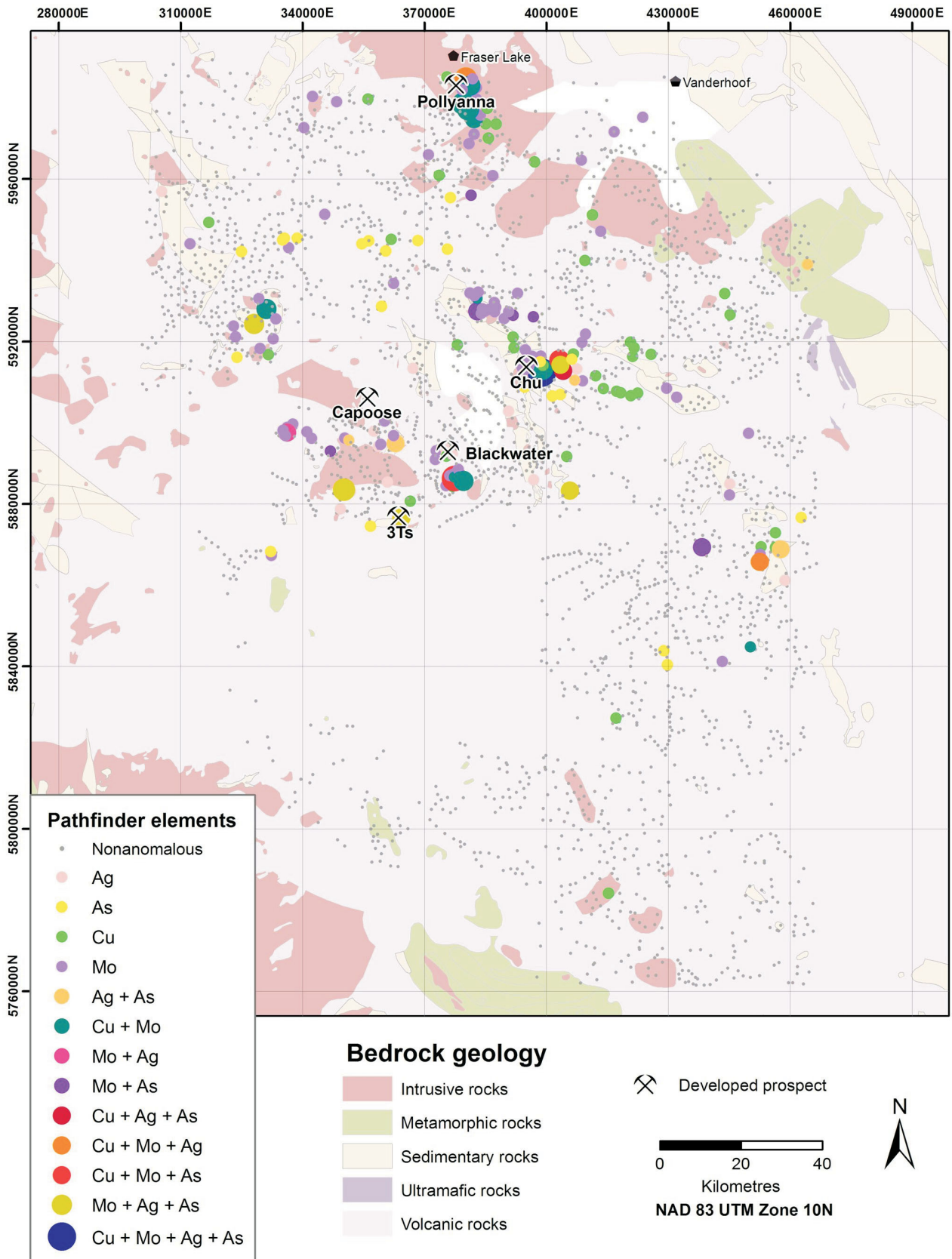


Figure 9. Map of multivariate anomaly assessment results from till samples, Targeting Resources through Exploration and Knowledge (TREK) project area, central British Columbia. The colour and sizing scheme is based on the input variables (Cu, Mo, Ag, As). Larger symbols are samples with anomalous values (>3 standard deviations [sd]) in one or more pathfinder elements. Bedrock geology modified after Massey et al. (2005).

note is the Cu+Mo+Ag target 77 km east-southeast of Blackwater, the Cu+Mo+As, Cu+Mo and Mo+As target 7 km southeast of Blackwater and also the Cu+Mo and Mo+Ag+As target 32 km northwest of Capoose.

Conclusions

Basic geochemical interpretation methods, such as clustering and regression analyses, allowed greater insight into the architecture of the till geochemical data in the TREK project area. Data effects, such as changes in survey area, were overcome and the till samples were classified into till types based on immobile and trace element chemistry (signature). Anomalous samples were then identified in each till type based on a selection of chalcophile elements, and these anomalies were quantified using a robust regression analysis and combined using an anomaly assessment test. The residual results show spatial coincidence with known developed prospects, and several targets were generated in areas without known mineralization.

Future Work

Multivariate anomaly assessment analysis highlights several areas of interest, which have been ranked based on multivariate element combinations as well as their coincidence with developed prospects (anomalies not associated with known mineralization have a higher ranking). These ranked areas can be followed up with more detailed fieldwork to validate potential targets and advance prospectivity.

Acknowledgments

This interpretation was funded by Geoscience BC and supported by REFLEX Instrument North America Ltd. The report greatly benefited from the thoughtful edits of S. Sugden of REFLEX Asia-Pacific in Perth, Australia.

References

BC Geological Survey (2016): MINFILE BC mineral deposits database; BC Ministry of Energy and Mines, URL <<http://minfile.ca/>> [October 2016].

Ferbey, T. (2009): Till geochemical exploration targets, Redstone and Loomis Lake map areas, central British Columbia (NTS 093B/04, 05); BC Ministry of Energy and Mines, BC Geological Survey, Open File 2009-09, 52 p.

Ferbey, T., Plouffe, A. and Anderson, R.G. (2014): An integrated approach to search for buried porphyry-style mineralization in central British Columbia using geochemistry and mineralogy: a TGI-4 project; Geological Survey of Canada, Current Research 2014-2, 12 p., URL <http://publications.gc.ca/collections/collection_2015/rncan-nrcan/M44-2014-2-eng.pdf> [November 2016].

Grunsky, E.C. (2007): The interpretation of regional geochemical survey data; *in* Proceedings of Exploration 07: Fifth Decen-

ennial International Conference on Mineral Exploration, B. Milkereit (ed.), Decennial Mineral Exploration Conferences, Toronto, Canada, September 9–12, 2007, p. 139–182, URL <http://www.esd.mun.ca/~spiercey/Piercey_Research_Site/ES4502_6510_files/Grunsky_2007.pdf> [November 2016].

Jackaman, W. and Sacco, D. (2014): Geochemical and mineralogical data, TREK Project, Interior Plateau, British Columbia; Geoscience BC, Report 2014-10, 13 p., URL <<http://www.geosciencebc.com/s/Report2014-10.asp>> [November 2016].

Jackaman, W., Sacco, D. and Lett, R.E. (2015): Geochemical reanalysis of archived till samples, TREK project, Interior Plateau, central BC (parts of NTS 093C, 093B, 093F & 093K); Geoscience BC, Report 2015-09, 5 p.

Jackaman, W., Sacco, D.A. and Lett, R.E. (2015): Regional geochemical and mineralogical data, TREK project - year 2, Interior Plateau, British Columbia; Geoscience BC, Report 2015-12, 13 p. plus 3 appendices, URL <<http://www.geosciencebc.com/s/Report2015-12.asp>> [November 2016].

Lett, R., Cook, S. and Levson, V. (2006): Till geochemistry of the Chilanko Forks, Chezacut, Clusko River and Toil Mountain area, British Columbia (NTS 93C/1, C/8, C/9, C/16); BC Ministry of Energy and Mines, BC Geological Survey, GeoFile 2006-1, 12 p. plus appendices.

Levson, V.M., Giles, T.R., Cook, S.J. and Jackaman, W. (1994): Till geochemistry of the Fawnie Creek area (NTS 93F/03); BC Ministry of Energy and Mines, BC Geological Survey, Open File 1994-18, 34 p. plus appendices.

Levson, V.M., Mate, D. with contributions from Dubois, J.E., O'Brian, E.K., Stewart, A. and Stumpf, A.J. (2002): Till geochemistry of the Tetachuck Lake and Marilla map areas (NTS 93F/5 and F/12); BC Ministry of Energy and Mines, BC Geological Survey, Open File 2002-11, 32 p.

Mahalanobis, P.C. (1936): On the generalized distance in statistics; Proceedings of the Indian National Science Academy, v. 2, no. 1, p. 49–55.

Massey, N.W.D., MacIntyre, D.G., Desjardins, P.J. and Cooney, R.T. (2005): Digital geology map of British Columbia: whole province; BC Ministry of Energy and Mines, GeoFile 2005-1, scale 1:250 000.

Plouffe, A. and Williams, S.P., compilers (1998): Regional till geochemistry, gold and pathfinder elements, northern Nechako River, British Columbia; Geological Survey of Canada, Open File 3687, 1 diskette.

Plouffe, A., Levson, V.M. and Mate, D.J. (2001): Till geochemistry of the Nechako River map area (NTS 93F), central British Columbia; Geological Survey of Canada, Open File 4166, 66 p. (includes CD-ROM).

Rousseeuw, P.J. and Leroy, A.M. (1987): Robust Regression and Outlier Detection; Wiley Series in Applied Probability and Statistics, John Wiley and Sons, Hoboken, New Jersey, 329 p.

Tukey, J.W. (1977): Exploratory Data Analysis; Addison-Wesley, Reading, Pennsylvania, 688 p.

Weary, G.F., Levson, V.M. and Broster, B.E. (1997): Till geochemistry of the Chedakuz Creek map area (NTS 93F/7); BC Ministry of Energy and Mines, BC Geological Survey, Open File 1997-11, 97 p.

Surficial Geochemical Footprint of Buried Porphyry Cu-Mo Mineralization at the Highland Valley Copper Operations, South-Central British Columbia: Project Update

R.L. Chouinard, Mineral Deposit Research Unit, The University of British Columbia, Vancouver, BC, rchouina@eoas.ubc.ca

P.A. Winterburn, Mineral Deposit Research Unit, The University of British Columbia, Vancouver, BC

M. Ross, University of Waterloo, Waterloo, ON

R.G. Lee, Mineral Deposit Research Unit, The University of British Columbia, Vancouver, BC

Chouinard, R.L., Winterburn, P.A., Ross, M. and Lee, R.G. (2017): Surficial geochemical footprint of buried porphyry Cu-Mo mineralization at the Highland Valley Copper operations, south-central British Columbia: project update; *in* Geoscience BC Summary of Activities 2016, Geoscience BC, Report 2017-1, p. 125–132.

Introduction

South-central British Columbia (BC) is well known for its endowment in porphyry copper deposits (McMillan and Panteleyev, 1995). These deposits include calcalkaline porphyry Cu-Mo (\pm Au) and alkaline porphyry Cu-Au systems (Logan and Schroeter, 2013). The economy of BC has benefited greatly from the development of many of these deposits, mostly discovered from mineralized outcrop or geochemical anomalies from suboutcropping mineralization under till of reasonably local origin. As the number of outcropping and suboutcropping discoveries declines, exploration geologists must develop ways to explore through to those covered with glacial material of remote origin, such as glaciofluvial cover that conceals mineralized bedrock.

This research is part of the Porphyry Cu Subproject of the National Sciences and Engineering Research Council (NSERC) and Canada Mining Innovation Council (CMIC)'s mineral exploration Footprints Project. This subproject aims to quantify and identify the footprint of porphyry Cu-(Mo) mineralization at the Highland Valley Copper (HVC) operations in south-central BC, through a multidisciplinary, integrated approach. The research is also part of the Mineral Deposit Research Unit (MDRU) Exploration Geochemistry Initiative, a collaborative research program established at the University of British Columbia (UBC) to understand mobility and transport of elements from buried mineralized bedrock to surface environment.

The identified deposits at HVC comprise five main clusters of porphyry-style mineralization, whose current state of production varies from developed to undeveloped. The J.A. and Highmont South targets comprise two mineralized areas that are both undeveloped and buried under variable thicknesses of glacial and preglacial sedimentary cover. Surficial geochemical studies at these two buried targets aim to fully characterize mineralogical and chemical changes that manifest themselves in the surficial environment after glacial dispersal and soil development over mineralized bedrock. The research will help develop surficial geochemical exploration models that can be applied to the search for other buried Cu-(Mo) porphyry mineralization. This paper provides an update on the progress of the project, which is expected to be completed by August 2017.

Background

Teck Resources Limited ('Teck') has a 100% interest in Highland Valley Copper (HVC), which is located in south-central BC, 15 km west of the Municipality of Logan Lake, and consists of five known porphyry-style Cu-Mo mineralized bodies (Figure 1). These clusters include: 1) the active producing Valley, Lornex and Highmont pits; 2) the past producing Bethlehem deposit; and 3) the buried J.A. deposit, all of which are centrally located within the Guichon Creek batholith (GCB; Byrne et al., 2013). The sulphide-bearing mineralized bedrock buried under glacially transported cover at HVC makes it an interesting site to test surficial geochemical exploration techniques.

Bedrock Geology

The GCB is part of the Quesnel terrane, which represents an island-arc setting (Northcote, 1969; Logan and Schroeter, 2016). The batholith was emplaced in the Late Triassic into the sedimentary and volcanic strata of the Permian Cache Creek and Late Triassic Nicola groups. The GCB has a sur-

Keywords: British Columbia, exploration, geochemistry, surficial geology, footprints, porphyry, surficial mapping, buried deposit

This publication is also available, free of charge, as colour digital files in Adobe Acrobat® PDF format from the Geoscience BC website: <http://www.geosciencebc.com/s/DataReleases.asp>.

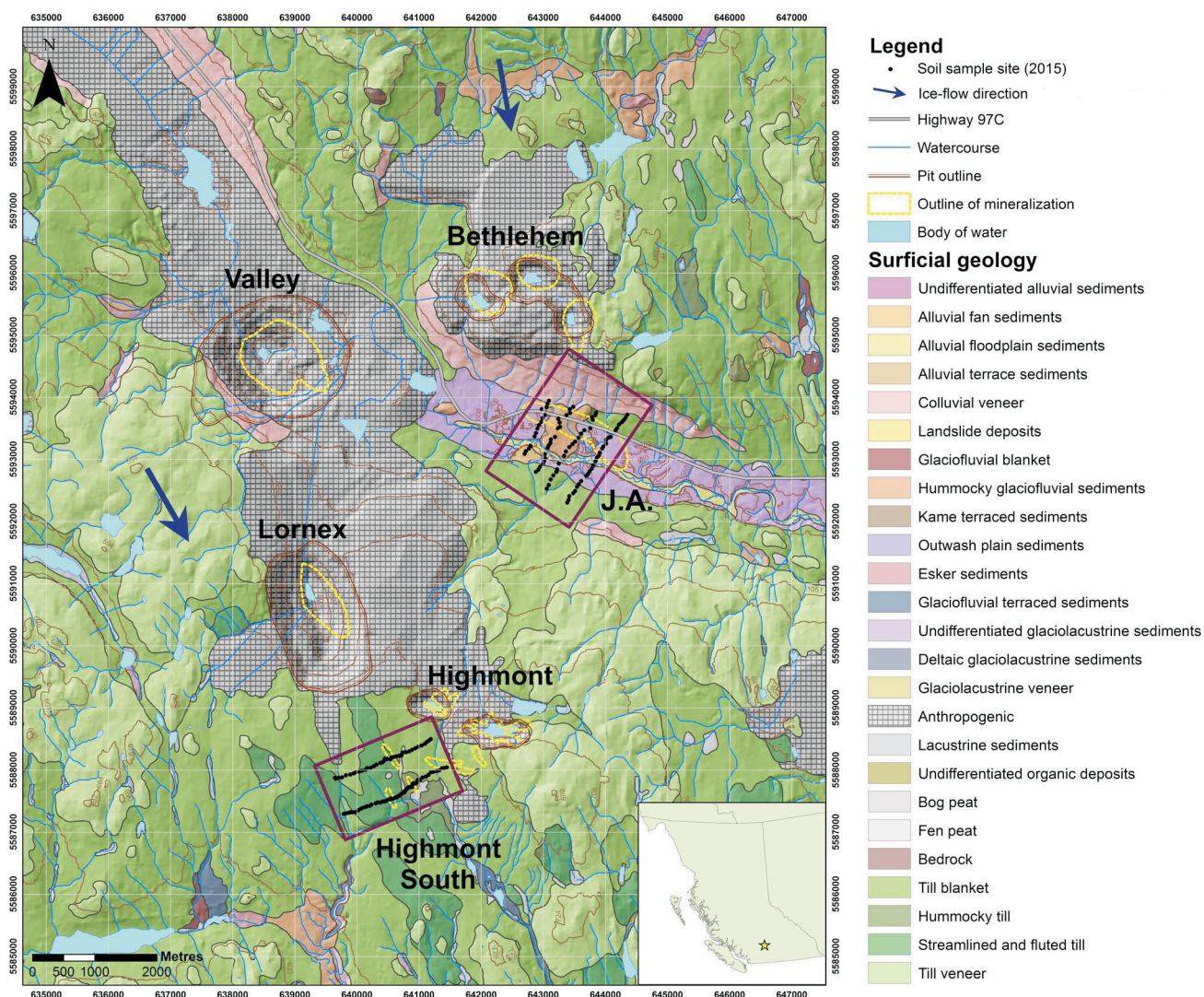


Figure 1. Surficial geology of the Highland Valley Copper mine operations area, south-central British Columbia (surficial geology and ice-flow direction from Plouffe and Ferbey, 2015).

face area of approximately 1100 km² and is calcalkalic in composition. The batholith was unroofed by the Jurassic period, with Early Jurassic to Eocene sedimentary and volcanic strata unconformably overlying the batholith (Northcote, 1969).

Zones of buried, undeveloped mineralized bedrock at HVC include: J.A. and Highmont South, which is interpreted as a small area of auxiliary mineralization to the main Highmont deposits. The buried Highmont South targets occur near the lithological boundary between the Skeena variety of quartz diorite and the Bethsaida quartz monzonite (Reed and Jambor, 1976). A large composite quartz-feldspar porphyry dike, the Gnawed Mountain porphyry dike, is emplaced to the north of Highmont South and is interpreted to have had a significant influence on the development of the Highmont deposits as a whole, specifically by controlling sulphide zoning (Byrne et al., 2013). The J.A. target is lo-

cated in a down-dropped fault block, straddling the contact between the Bethlehem granodiorite and the quartz diorite to granodiorite of the Guichon variety. The Guichon–Bethlehem contact is cut by a zone of quartz-plagioclase porphyry (possible Bethsaida-phase offshoot) in the southern portion of the deposit (McMillan, 1976).

Surficial Geology

Present-day physiography of the study area is strongly influenced by the style of deglaciation experienced. Rolling uplands and steep-walled, flat-floored valleys characteristic to the field sites are a function of ice retreating northward and the development of ice-contact and proglacial land systems, including various glaciolacustrine and glaciofluvial deposits (Figure 1; Bobrowsky et al, 2002). The resultant geography supports open grasslands with sagebrush, and slopes dominated by species of pine and spruce.

The study area (Figure 1) is covered by varying thicknesses of glacial sediments, with ice flow trending predominantly south-southeast (Plouffe and Ferbey, 2015). The Highmont South target (Figure 2) subcrops beneath 2–10 m of till (averaging 5–6 m). The J.A. target (Figure 3) sits beneath significantly thicker overburden, averaging 170 m and up to 300 m in thickness. Between the glacial overburden and the bedrock at the J.A. deposit sit sequences of preglacial sediments, which shielded the mineralized bedrock from glacial erosion (Plouffe and Ferbey, 2015). This may pose a problem for till-based exploration, such as the search for porphyry indicator minerals, as the till will not include fragments of the mineralized bedrock from the targeted mineralization.

Objectives of the Research Project

Geochemical investigations were undertaken in the field and laboratory to support the following research objectives:

- define the surficial response, in different materials, to the presence of buried mineralization;
- identify processes contributing to the generation of false anomalies and noise in data; and
- evaluate various exploration methods to develop a future framework for surficial geochemical exploration of buried porphyry-Cu deposits in glacially-covered terrain.

The following fieldwork was conducted to address these research questions through characterization of the surficial materials and processes at both field areas.

Surficial Mapping

Detailed surficial mapping is required for an exploration geochemical survey in order to select the most suitable sample sites, and to integrate and fully understand geochemical data in terms of different regolith units and surface processes. Fieldwork in 2015 started with surficial mapping to identify soil-sampling sites in the least disturbed areas, which showed the least variability in material type and amount of water saturation. The field area was traversed and mapping was completed at 1:2500 scale, recording all anthropogenic features that would influence sample-site selection such as exploration trenches, drill pads, old agricultural infrastructure, roads, zones of mechanical reforestation and forestry burn piles. Natural disturbances such as intense animal activity and past forest fires were noted. Additional information recorded included observations on geomorphology, water saturation and vegetation type.

Additional reconnaissance carried out during the 2016 field season aided in the development of regolith maps for both the J.A. and Highmont South field areas (Figures 2, 3). Both regolith maps make use of surficial geology presented in BC Geological Survey Geoscience Map 2015-3 (Plouffe and Ferbey, 2015), incorporating surficial interpretations

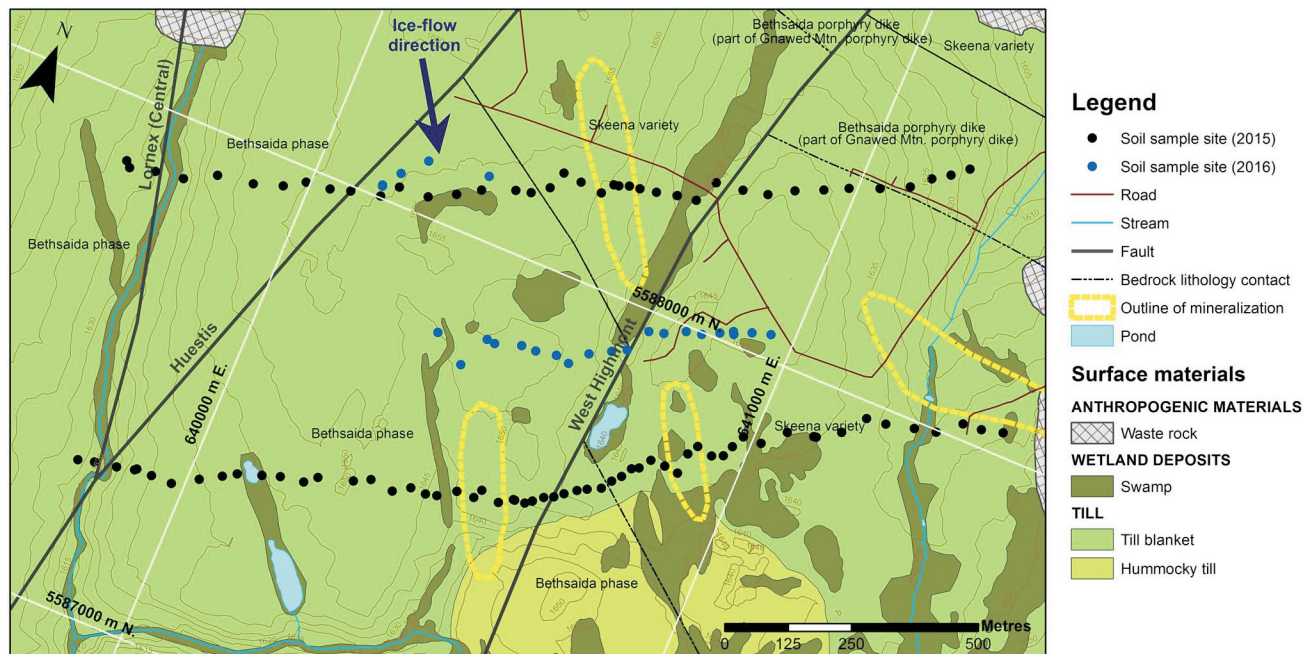


Figure 2. Surficial geology of the Highmont South study area at the Highland Valley Copper mine operations; surficial geology is modified from Plouffe and Ferbey (2015), using the Geological Survey of Canada’s data model for surficial geology, version 1.2 (Deblonde et al., 2012); bedrock geology and structure adapted from McMillan et al. (2009) based on work done in August 2016 by Teck Resources Limited and the Canadian Mining Innovation Council. Abbreviation: Mtn., mountain.

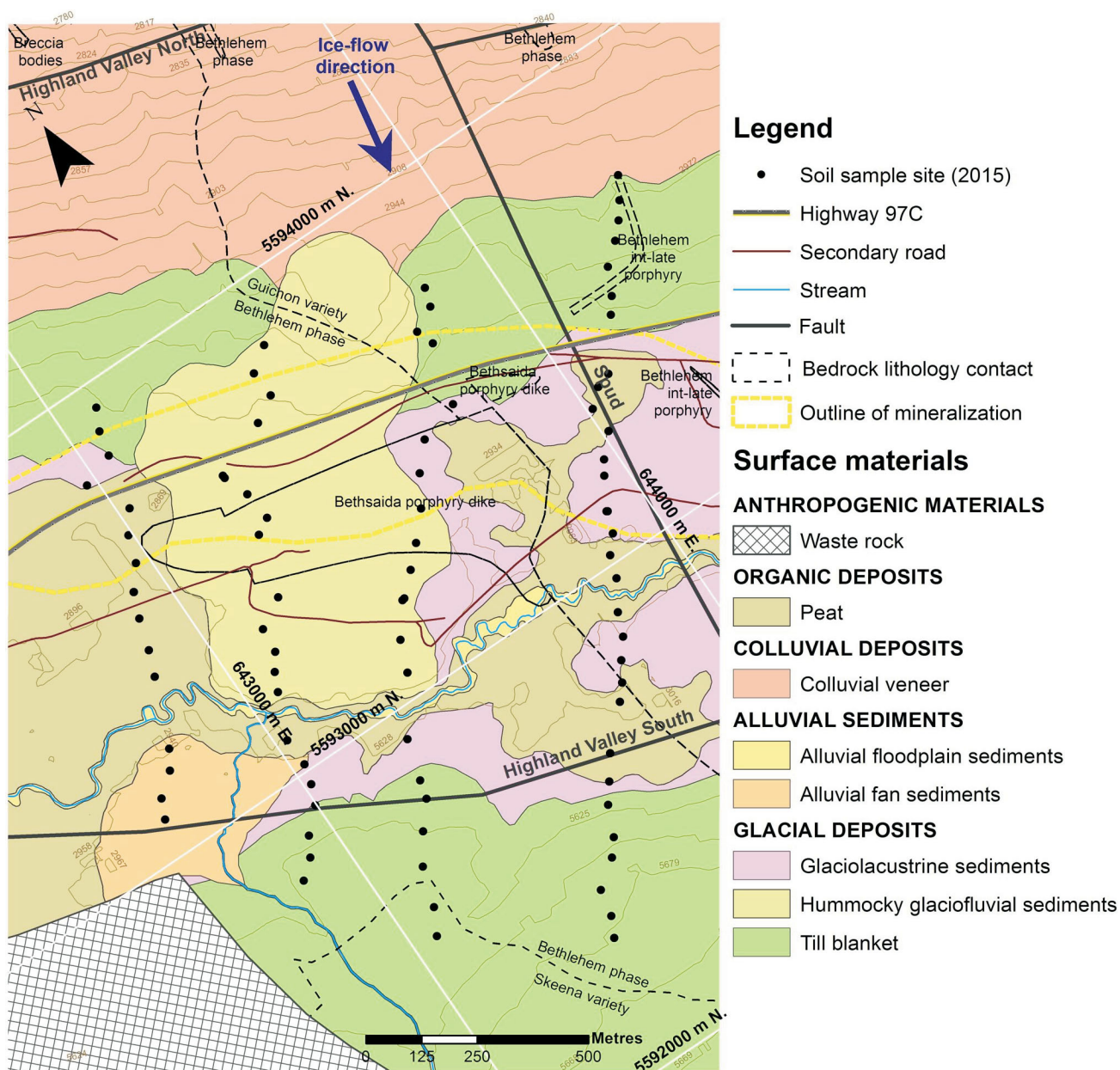


Figure 3. Surficial geology of the J.A. study area at the Highland Valley Copper mine operations; surficial geology is modified from Plouffe and Ferbey (2015), using the Geological Survey of Canada’s data model for surficial geology, version 1.20 (Deblonde et al., 2012); bedrock geology and structure adapted from McMillan et al. (2009) based on work done in August 2016 by Teck Resources Limited and the Canadian Mining Innovation Council.

and field observations to bring the details from a 1:50 000 scale to an approximately 1:10 000 scale representation.

Soil Sampling and Field Measurements

Two soil transects were sampled crossing buried targets perpendicular to mineralization at Highmont South, with 25 m site spacing close to and over the top of the targets, and 50 m site spacing out into background areas. A total of 93 soil samples were collected at the Highmont South targets in 2015. Four soil transects cross the buried J.A. target, again perpendicular to mineralization, all with 50 m spac-

ing between sample sites and with approximately 200–300 m spacing between transects. A total of 85 soil samples were collected at the J.A. target. A full quality assurance–quality control program was implemented with the samples, including insertion of certified reference materials and duplicate samples.

At each sample site, a detailed description was recorded and in situ physicochemical measurements were conducted for each soil horizon identified. Typical soil profiles encountered during sampling at both Highmont South and J.A. can be seen in Figure 4a–f. The upper 10 cm of the

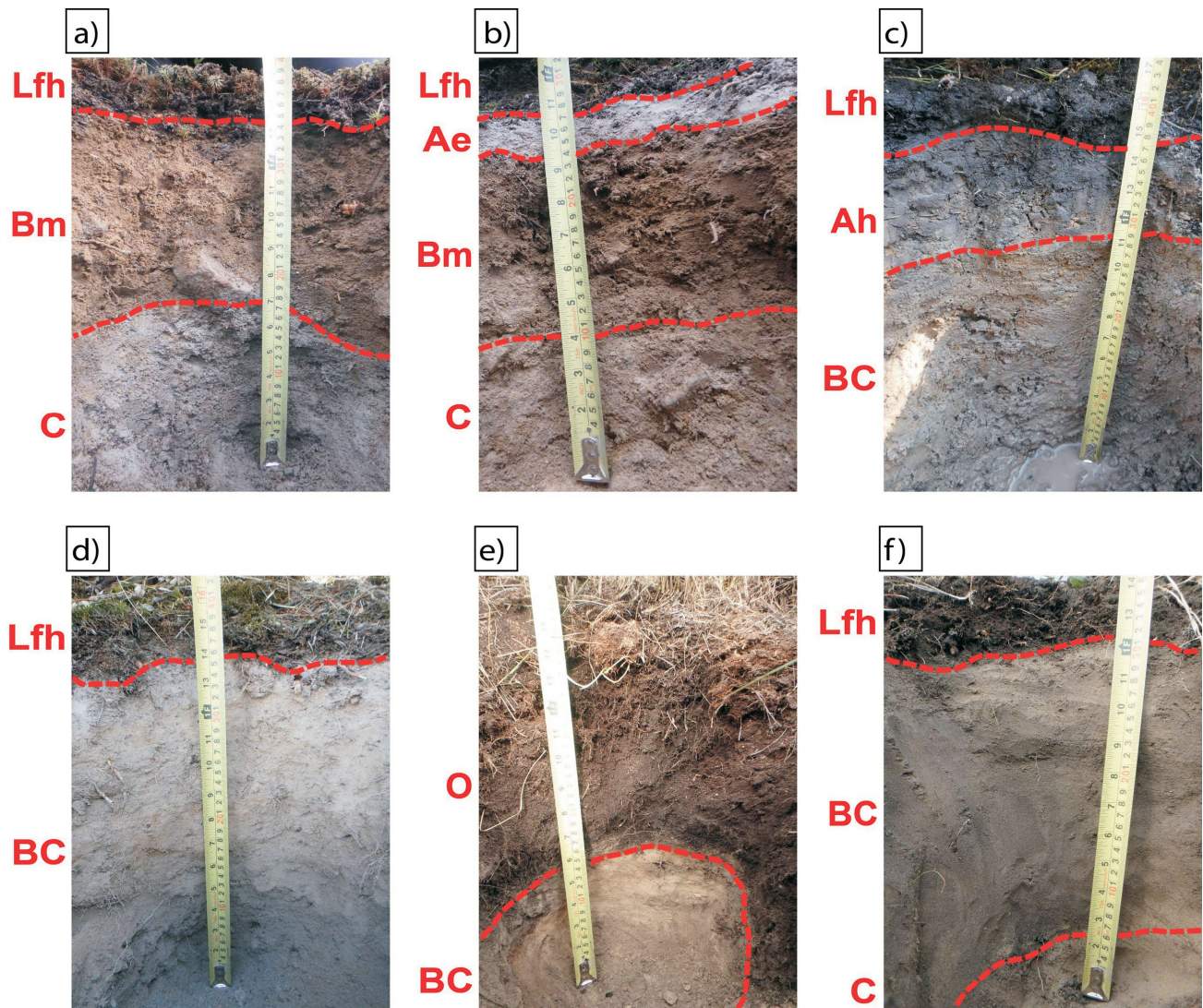


Figure 4. Typical soil profiles encountered during sampling at Highmont South (a–c) and J.A. (d–f), showing **a)** a Brunisol developed over till blanket material; **b)** a more well-developed Brunisol with an Ae horizon, developed over till blanket material; **c)** a clay-rich, water-saturated soil (Gleysol); **d)** a Brunisol developed over sandy glaciofluvial sediments; **e)** a sand-rich soil profile with no real B horizon (Regosol); **f)** an organic soil (peat) developed over glaciolacustrine sediments. Soil horizons are named based on the Canadian system of soil classification (Soil Classification Working Group, 1998).

B horizon was targeted for the soil sample itself and subsequent soil-slurry tests. The in situ measurements included electrical conductivity (EC), soil moisture and pH. Soil was sifted in the field through a <6.3 mm sieve and samples were collected for multi-element analysis. Slurry tests using the sampled medium and de-ionized water in a 1:1 volumetric ratio were conducted to measure oxidation-reduction potential, EC, pH, acidified pH (to test the soil's buffering capacity) and free-chlorine content.

GORE-SORBER® hydrocarbon collectors were inserted at the bottom of each sampled hole, including duplicate holes, for approximately 40 days. The collectors are composed of activated carbon within a GORE-TEX® sheath, which allows the carbon to passively sequester volatile organic and inorganic compounds within the soil through a

water-impermeable yet gas-permeable membrane (Anderson, 2006). A total of 187 sample modules have been analyzed by Amplified Geochemical Imaging (Newark, Delaware) for volatile organic and inorganic compounds; sensitive gas chromatography and mass spectrometry were used to detect these compounds in a parts per trillion range (Anderson, 2006). Results are to be interpreted alongside the rest of the geochemical data and in the context of the regolith maps to determine their efficacy in geochemical surveys over deeply buried sulphide mineralization.

Fieldwork completed in the 2016 season included soil-profile microsampling at 5 cm intervals down a soil profile to assess the influence of anthropogenic inputs, if any, to the soil surface as well as demonstrate the most ideal soil horizon to sample from for the purpose of exploratory soil sur-

veys. Tree coring was conducted to temporally understand the influence of anthropogenic inputs and decouple them from mineralization-derived and background signals.

Laboratory Analysis Techniques

Soil samples were submitted to Bureau Veritas Commodities Canada Limited (Vancouver) for drying at <60 °C and screening to <180 µm, with separate de-ionized water extraction and aqua-regia digestion, both followed by multi-element inductively coupled plasma–mass spectrometry. Total organic carbon was also measured by combustion furnace and infrared spectrometry. The multi-element analytical data from these tests will be subjected to various statistical techniques to identify the surficial response to the presence of buried mineralization.

In addition, pulps from the 2015 soil samples were analyzed for total element concentrations using an Innov-X field-portable X-ray fluorescence (XRF) analyzer manufactured by Olympus. This exercise assessed the use of a hand-held XRF unit as a quicker and cost-effective method to carry out total chemical analysis of soil samples on site instead of sending them out to commercial facilities.

Discussion and Ongoing Work

The pulps from selected 2015 soil samples will additionally be analyzed using X-ray diffraction to identify clay minerals. This will give insight into the relative cation-exchange capacities of the different materials and their ability to adsorb trace elements, both naturally sourced and from anthropogenic inputs.

Split portions of selected 2015 soil samples will be screened to two fractions: <2 mm and 2–6.3 mm. These fractions will be visually investigated under a binocular microscope to determine the presence and abundance of any relict sulphide grains that occur in each sample. This step will help identify glacially transported clastic sulphide material in the samples.

Eighteen soil samples, nine from each target, were selected and submitted for Cu-isotope studies in-house at UBC's Pacific Centre for Isotopic and Geochemical Research to help determine the source of Cu-ion migration (e.g., clastic contribution from till versus migration from buried sulphide mineralization). Sequential leaching on these samples will be completed to further constrain the source and residency of Cu as well as to determine the most effective leaching method to use in routine exploration geochemical soil surveys.

All chemical and physicochemical data from the research and fieldwork will be integrated and evaluated in the context of the regolith maps to identify the controls on the presence and abundance of elemental signatures. This work will generate more applicable exploration models, which

will expand beyond traditional frameworks and make use of new technologies.

Acknowledgments

This research is being undertaken as a M.Sc. research project of the primary author as part of the National Sciences and Engineering Research Council (NSERC) and Canadian Mining Innovation Council (CMIC)'s mineral exploration Footprints Project as well as the Mineral Deposit Research Unit's Exploration Geochemistry Initiative. The authors sincerely appreciate all financial and technical support that has helped to make this research possible. Funding was provided by NSERC and CMIC through the NSERC Collaborative Research and Development Program. The authors would like to thank J. Stemler and G. Grubisa from Teck Resources Limited for providing field support and allowing access to historical data. Special thanks are extended to S. Cook (Teck Resources Limited) and R. Beckie (University of British Columbia) for being a part of the advisory committee. Geoscience BC and Endeavour Silver Corporation are thanked for their support in the form of scholarships. The authors appreciate the assistance of L. Yeung and D. Kamal in the field, the hospitality of the community of Logan Lake, and the guidance and expertise of K. Byrne and G. Lesage. The authors also thank P. Bradshaw for providing a critical review of this manuscript. MDRU publication 373 and NSERC-CMIC Exploration Footprints Network Contribution 116 (<http://cmic-footprints.ca>).

References

- Anderson, H. (2006): Amplified geochemical imaging: an enhanced view to optimize outcomes; *First Break*, v. 24, no. 8, p. 77–81.
- Bobrowsky, P., Cathro, M. and Paulen, R. (2002): Quaternary geology reconnaissance studies (921/2 and 7); *in* Geological Fieldwork 2001, British Columbia Geological Survey, Paper 2002 1, p. 397–204.
- Byrne, K., Stock, E., Ryan, J., Johnson, C., Nisenson, J., Alva Jimenez, T., Lapointe, M., Stewart, H., Grubisa, G. and Sykora, S. (2013): Porphyry Cu-(Mo) deposits in the Highland Valley district, south central British Columbia; *in* Porphyry Systems of Central and Southern BC: Tour of Central BC Porphyry Deposits from Prince George to Princeton, J. Logan. and T. Schroeter (ed.), Society of Economic Geologists, Guidebook Series, v.44, p. 99–116.
- Deblonde, C., Plouffe, A., Boisvert, É., Buller, G., Davenport, P., Everett, D., Huntley, D., Inglis, E., Kerr, D., Moore, A., Paradis, S.J., Parent, M., Smith, I.R., St. Onge, D., Weatherston, A. (2012): Science language for an integrated Geological Survey of Canada data model for surficial geology maps, version 1.2, Geological Survey of Canada, Open File 7003, 238 p., doi: 10.4095/290144
- Logan, J.M. and Schroeter, T.G., ed. (2013): Porphyry systems of central and southern BC: tour of central BC Porphyry deposits from Prince George to Princeton; Society of Economic Geologists, Guidebook Series, v. 44, 143 p.

- Logan, J.M. and Schroeter, T.G., ed. (2016): Porphyry systems of central and southern British Columbia; Society of Economic Geologists, Guidebook Series, v. 52, 110 p.
- McMillan, W.J. (1976): J.A.; *in* Porphyry Deposits of the Canadian Cordillera, A. Sutherland Brown (ed.), Canadian Institute of Mining, Metallurgy and Petroleum, Special Volume 15, p. 144–162.
- McMillan, W.J. and Panteleyev, A. (1995): Porphyry copper deposits of the Canadian Cordillera; Arizona Geological Society Digest, v. 20, p. 203–218.
- McMillan, W.J., Anderson, R.G, Chan R. and Chow, W. (2009): Geology and mineral occurrences (MINFILE), the Guichon Creek Batholith and Highland Valley porphyry copper district, British Columbia; Geological Survey of Canada, Open File 6079, 2 sheets, doi: 10.4095/248060
- Northcote, K. (1969): Geology and geochronology of the Guichon Creek Batholith, BC; British Columbia Department of Mines and Petroleum Services, Bulletin 56, 73 p.
- Plouffe, A. and Ferbey, T. (2015): Surficial geology, Gnawed Mountain area, British Columbia (Parts of NTS 92-I/6, 92-I/7, 92-I/10, and 92-I/11); Geological Survey of Canada, Canadian Geoscience Map 214 (preliminary) and British Columbia Geological Survey, Geoscience Map 2015-3, scale 1:50 000.
- Reed, A. and Jambor, J. (1976): Highmont: linearly zoned copper-molybdenum porphyry deposits and their significance in the genesis of the Highland Valley ores; *in* Porphyry Deposits of the Canadian Cordillera, A. Sutherland Brown (ed.), Canadian Institute of Mining, Metallurgy and Petroleum, CIM Special Volume 15, p. 163–181.
- Soil Classification Working Group (1998): The Canadian system of soil classification; Agriculture and Agri-Food Canada, Publication 1646 (revised) 187 p.

Rapid, Field-Based Hydrogeochemical-Survey Analysis and Assessment of Seasonal Variation Using a Field-Portable Photometer and Voltammeter, Marmot Lake NTS Area, South-Central British Columbia (NTS 093B/13)

R. Yehia, MYAR Consulting, Vancouver, BC, myar@telus.net

D.R. Heberlein, Heberlein Geoconsulting, North Vancouver, BC

R.E. Lett, Consultant, Victoria, BC

Yehia, R., Heberlein, D.R., and Lett, R.E. (2017): Rapid, field-based hydrogeochemical-survey analysis and assessment of seasonal variation using a field-portable photometer and voltammeter, Marmot Lake NTS area, south-central British Columbia (NTS 093B/13); in Geoscience BC Summary of Activities 2016, Geoscience BC, Report 2017-1, p. 133–140.

Introduction

Water geochemistry can provide useful information in support of many resource sectors, such as mineral (Taufen 1997; Leybourne and Cameron, 2010), geothermal (Yehia et al., 2013), petroleum and environmental (Saha and Sahu, 2015). Building on the successful outcome of the 2014 project (Yehia and Heberlein, 2015) and on the wealth of data available in the TREK project area (Angen et al., 2015; Jackaman et al., 2015; Lett and Jackaman, 2015; Bordet and Hart, 2016), this project aims to extend the real-time hydrogeochemical-survey methodology to a regional setting and, at the same time, investigate the effects of seasonal variations and the potential for rapid, field-based detection of anomalous hydrogeochemistry indicative of mineral occurrences. As well, this project assesses the application of another technology for the rapid, field-based analysis of water-sample chemistry, the Modern Water PDV6000*ultra* voltammeter (PDV; Braungardt et al., 2010; Lewtas et al., 2010), an electrochemical method based on anodic stripping voltammetry (ASV).

Photometer technology and field-data-collection methodology are discussed in detail in Yehia and Heberlein (2015). This project aims to expand upon the results of that study by achieving the following objectives:

- Provide a regional-scale hydrogeochemistry dataset to supplement the QUEST and TREK SE stream-sediment, lake-sediment and till geochemical surveys in the Marmot Lake NTS area (NTS 093B/13), using field-based portable photometer and voltammeter instrumentation

- Investigate seasonal variability of water chemistry by repeating the sampling campaign in spring, summer and fall
- Investigate known mineral occurrences to determine their associated hydrogeochemical responses
- Produce accurate, precise and cost-effective analytical results for selected cations and anions that are relevant to the mineral-exploration community
- Investigate the capabilities of the PDV for rapid hydrogeochemical surveys

Orientation Survey

One of the recommendations in Yehia and Heberlein (2015) was to carry out a small orientation survey prior to the field surveys. This orientation survey was designed to optimize sampling, sample preservation (Hall, 1998; Khanna et al., 2009) and analytical methods for the Palintest[®] Photometer 8000 and the PDV. It was carried out at three locations: 1) Furry Creek and Britannia Creek, which drain the Britannia mine area; 2) Lynn Creek in the Lynn Headwaters Regional Park; and 3) a creek flowing southwest of Fraser-view Golf Course in Vancouver. The sites were chosen for 1) ease of access during the spring runoff, 2) detecting potential mineralization in the water with the chosen methods, and 3) potential for mineralization comparison between laboratory and field-based water analyses. The survey included the collection of four samples at each of these localities: two filtered samples, one with acidification and a second without acidification; and two unfiltered samples, also acidified and non-acidified. Following the procedures outlined in Yehia and Heberlein (2015), duplicate unfiltered and acidified samples were sent to the ALS Environmental laboratory (Burnaby, BC) for comparative analysis.

Results from photometer tests were inconclusive in defining a single preferred sampling type for routine collection. This was due mainly to a small sample set and lower-than-expected mineral concentrations for most sites. Unfortunately, the PDV was unavailable for the orientation survey.

Keywords: British Columbia, hydrogeochemistry, photometer, voltammeter, rapid, field analysis, regional geochemistry, seasonal variation

This publication is also available, free of charge, as colour digital files in Adobe Acrobat[®] PDF format from the Geoscience BC website: <http://www.geosciencebc.com/s/DataReleases.asp>.

The survey was successful, however, in identifying photometer reagents (Table 1) that seemed to have reacted adequately with the nitric-acid preservation. Further testing could be continued for Al and Fe. Previous photometer and laboratory analysis of samples by Yehia and Heberlein (2015) revealed that the photometer Al and Fe values were much lower than the laboratory analyses due to lack of water-sample preservation.

Project Area

Location and Access

The project area is located south of Nazko (Figure 1), approximately 75 km west of Quesnel in the Marmot Lake NTS area (NTS 093B/13). As well, two mineral prospects occur in the study area, and recently collected water, soil and gas investigation data are available (Lett and Jackman, 2015) for comparison. The aim of sampling in the area was to determine if rapid hydrogeochemistry surveys will work in an environment that is hydrologically complex and challenging. In addition, the Nazko Economic Development Corporation was interested in assessing potential for resource-based economic development.

Table 1. Tests performed by the portable devices chosen for this project. Abbreviation: PDV, Modern Water PDV6000ultra voltammeter.

Type	Photometer detection limit (mg/l)	Typical PDV detection limit in clean water (mg/l) ¹
Aluminum (Al) ²	0.005	
Arsenic (As)		0.0005
Cadmium (Cd)		0.0005
Calcium hardness	0.5	
Chloride (Cl)	0.05	
Copper (Cu, ionic and total)	0.005	0.0005
Fluoride (F)	0.005	
Hardness	0.5	
Iron (Fe) ²	0.005	
Lead (Pb)		0.0005
Magnesium (Mg) ²	0.5	
Manganese (Mn)	0.0005	
Molybdate (MoO ₄)	0.005	
Nickel (Ni)	0.005	
Potassium (K)	0.05	
Silica (High Range, SiO ₂)	0.05	
Sulphate (SO ₄)	0.5	
Zinc (Zn)	0.005	

¹published by Modern Water Inc. (http://www.modernwater-monitoring.com/product_limits-of-detection.html)

²photometer reagent capable of nitric-acid preservation

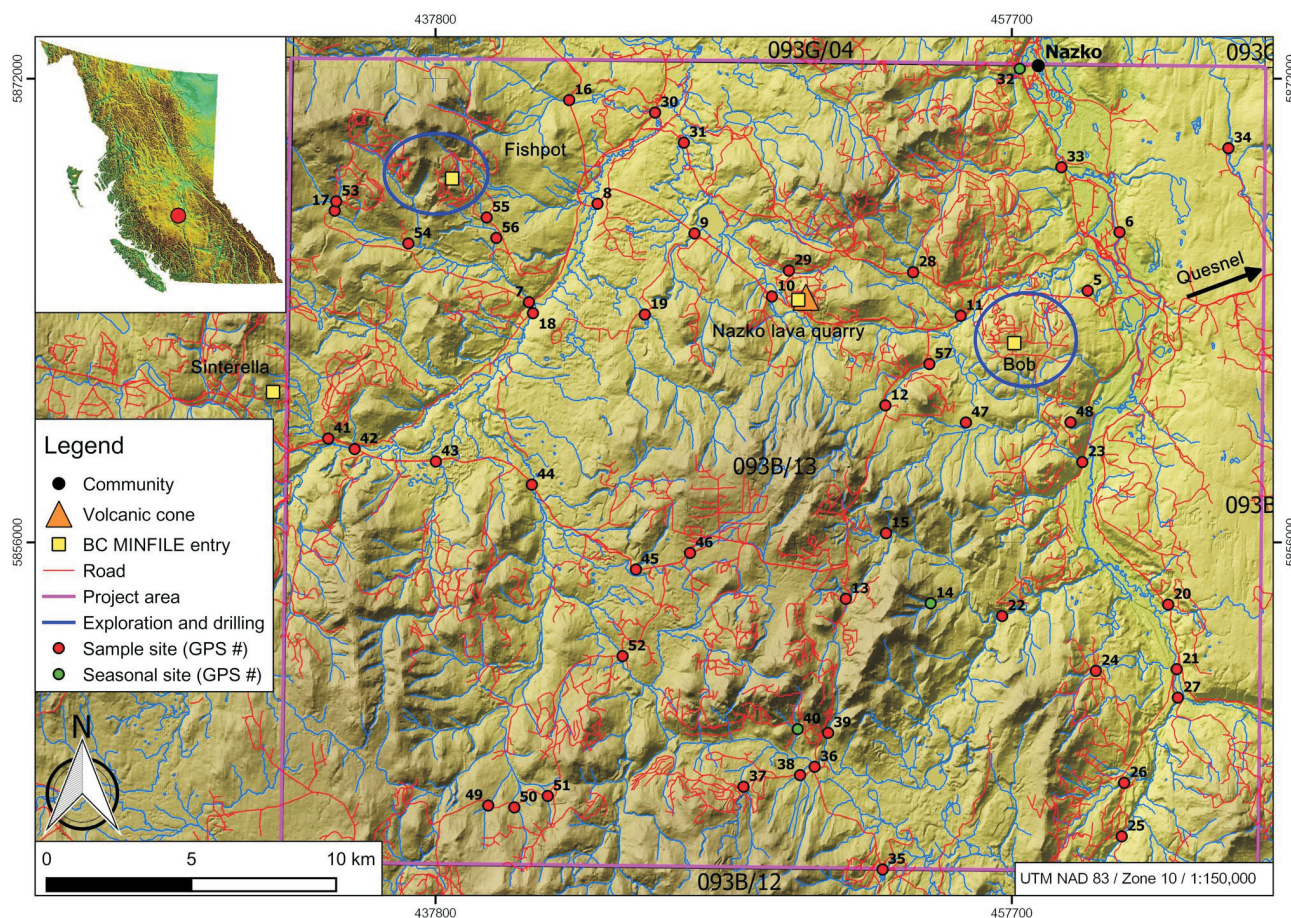


Figure 1. Locations of samples in the Marmot Lake NTS area (NTS 093B/13). Base map from GeoBase® (2016).

Access to the study area is via the paved Nazko Road (HW 59) and an extensive system of forestry roads throughout the project area. Elevations in the study area range from 850 to 1250 m above mean sea level. The north-flowing Nazko River traverses the eastern part of the study area. Another large river, the Baezaeko, flows from southwest to northeast in the northwestern part of the study area. The area has an abundance of water and the various types (creeks, lakes, wetlands) of water bodies, including bogs at higher elevations. Drainage patterns are predominantly dendritic. Some creeks flow in and out of wetland. A few of the wetlands are the result of beaver activity. The forest is dominated by lodgepole pine, which has been severely affected by the mountain pine beetle infestation; the resulting increase in logging activity has opened up road access to much of the area. Accommodation and logistical staging were provided partly as in-kind support from the Nazko Economic Development Corporation, and residence and laboratory space for the project crew were provided at the Blackwater logging camp.

Geology and Surface Environment

The youngest rocks exposed in the survey area are volcanic rocks of the Miocene to Holocene Anahim volcanic belt, the easternmost limit of which is represented by the Nazko volcanic cone that erupted approximately 7200 years ago (Cassidy et al., 2011). Older volcanic and sedimentary rocks are the Miocene to Pliocene Chilcotin Group basalts along the east side of the Nazko River. Underlying the Chilcotin sedimentary rocks are volcanic rocks of the Eocene Ootsa Lake Group, which are the most extensive in the

study area, while sandstone and conglomerate of the Cretaceous Skeena Group are widespread in the northeastern part of the area, around the Bob Au-Ag prospect (MINFILE 093B 054; BC Geological Survey, 2016). Volcanic rocks of the Lower to Middle Jurassic Hazelton Group occur in the northeast corner of the study area (Massey et al., 2005). Recent mapping and an interpretation of airborne geophysical-survey data by Angen et al. (2015) revised the geology of the project area and identified several new faults, including an inferred dextral fault along the Nazko River valley.

The area has an abundance of glacial deposits of various thicknesses, till being the dominant surficial material that overlies much of the bedrock. The most recent ice-flow direction in the area is generally from south-southwest to north-northeast (Jackaman et al., 2015).

In the northwestern part of the study area, Cu-As-Au mineralization at the Fishpot showing (MINFILE 093B 066) is hosted in an Eocene pyritic quartz rhyolite porphyry plug that intrudes Late Jurassic Hazelton Group pebble conglomerate, shale and tuffaceous sandstone. The Hazelton volcanic sequence consists mainly of andesitic and basaltic flows, and lesser amounts of pyroclastic rocks. Two major alteration zones identified on the prospect consist of carbonate-limonite staining and local quartz veining (Kennedy, 2012).

The Bob prospect, which has been more thoroughly explored, lies just south of Nazko and east of the Nazko volcanic cone. It is underlain by Lower Cretaceous to Lower

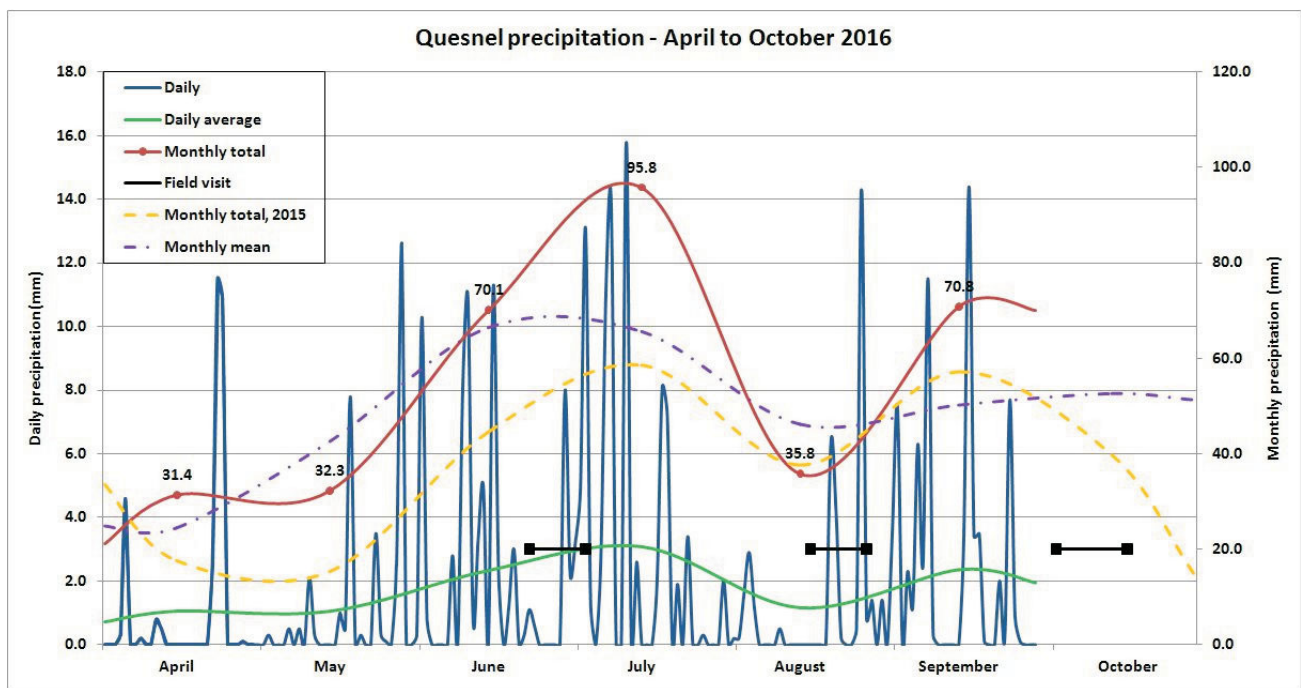


Figure 2. Precipitation for Quesnel at the time of the sampling campaign (Environment Canada, 2016).

Paleogene Skeena Group conglomerate, sandstone and argillite that are unconformably overlain by Paleocene to Eocene andesite, basalt, basalt breccia and rhyolite breccia. Tertiary quartz-feldspar porphyry dikes intrude the Skeena Group sedimentary rocks. Anomalous Au, As, Ag, Sb and Hg levels have been reported from Skeena Group sedimentary rocks that have undergone silicification and argillic alteration, and contain carbonate minerals and pyrite (MIN-FILE 093B 054).

Field Conditions

Although precipitation in the month of June for the last couple of years had been below the mean of 66 mm, the June sampling campaign was carried out under wet conditions. Precipitation recorded for Quesnel in April and May had been 25 mm, but totals for June and July were 56 and 82 mm, respectively (Figure 2), with potentially more precipitation noted in the Nazko area (Nazko is 600 m higher than Quesnel). June's precipitation turned creek water turbid with high or overflowing banks, a noticeable change from the previous two months.

Vehicle access to some parts of the area was complicated by widespread mud on the secondary logging roads, and foot access was complicated by high water levels in creeks and wetlands. This made sampling at some sites and subsequent follow-up challenging. Conditions were drier in August compared to July, but water levels were still above average because of July precipitation. Regardless, road and foot access was markedly improved from the June campaign.

Sample Collection and Analysis

Water samples were collected directly from mid-stream sites; where streams were too wide or the banks unsafe, samples were collected using a water-sampling pole. Samples were stored in two sizes of #2 high-density polyethylene (HDPE) bottles: non-acidified samples in 1 L bottles and acidified samples (with 3 mL ultrapure nitric acid) in 250 mL bottles. Both samples were unfiltered. Sample bottles were reused and rinsed thoroughly three times with the water to be sampled, with the cap on before sample collection. Collected water was transported in a cooler after collection and stored in a refrigerator at the camp until analysis (except for some samples that were analyzed the same afternoon). Analysis was carried out within 24 hours of collection for both photometer and PDV (within 48 hours in the orientation survey). Sample locations were tested for temperature, pH, conductivity, total dissolved solids (TDS) and salinity using an Oakton PCStestr 35 meter. The samples were retested as a quality-control procedure with a second PCStestr for the same parameters prior to analysis to prevent sample mix-up and record any changes after collection. Both meters were calibrated weekly. No unusual differences were observed between the two sets of results, except for the expected slight pH variations and normal

analytical variations caused by using a different instrument.

Identical procedures were used for samples sent to the ALS Environmental laboratory, except for filtering on site for dissolved-metals analysis. Dissolved tests involved filtering the sample through a 0.45 µm filter and preserving the metals in the solution with 3 mL nitric acid. Water in the 250 mL bottles was used for cation analysis, whereas the 1 L sample was required by the laboratory for TDS determination, conductivity, turbidity, anion analysis, quality-control monitoring and reanalysis (if required). Water samples for laboratory analysis were transported in coolers to the ALS Environmental laboratory in Burnaby by the lead author the day after returning from the field trips. Laboratory determinations were for dissolved constituents, since both photometer and PDV measure the dissolved component of the sample (except for the photometer Cu test, which analyzes for ionic Cu as well as total dissolved Cu—after reaction with a decomplexing agent).

The number of sites sampled around mineral occurrences turned out to be lower than initially estimated. This was due to the lack of suitable sample sites draining directly from the Bob prospect and inactive (dry glacial outwash) channels around the Fishpot showing. A second stage of sampling involved follow-up around both mineral occurrences, as well as more regional sampling over the broader NTS area. Sample sites for the latter were chosen for their safe access from the primary logging roads in spring, due to the high water levels.

Quality Control

Quality-control measures used for the project included

- use of the manufacturer's standard solutions and government-certified reference solutions for calibration and drift monitoring;
- triplicate readings for each photometer test, which helps to monitor analytical precision as well as identify any reagent problem; and
- for every batch of 20 samples, the following:
 - 15 field samples
 - 1 field duplicate
 - 1 analytical duplicate (second test from same sample bottle)
 - 1 government-certified standard
 - 1 blank using ultrapure deionized water (18 MΩ)
 - 1 laboratory duplicate for every tenth sample.

Analysis

Table 2 shows the samples that had been collected and analyzed by the time this paper was written. In the June survey, the photometer analyzed many samples with high turbidity (tested by the photometer), whereas previous surveys

Table 2. Sampling completed to August 31, 2016.

Type	Sampled and tested	Laboratory samples
Orientation survey	4 sample sites (16 tests) 1 deionized 1 SLRS-6 Standard	4
June field survey	49 sample sites 3 deionized 3 SLRS-6 Standard 3 analytical duplicates 3 field duplicates	8
August field survey	50 sample sites 3 deionized 3 SLRS-6 Standard 3 analytical duplicates 3 field duplicates	5
Total	141	17

(Yehia et al., 2013; Yehia and Heberlein, 2015) included only a very few turbid samples. Reagents that did not involve a high-wavelength colour test (Figure 3), such as Cu and MoO₄, appeared to be affected by the higher turbidity levels. As the photometer uses light to analyze the samples, higher turbidity levels appear to produce a high bias in the measured concentrations.

Figure 4 shows examples of the influence of turbidity on the June Cu and MoO₄ results. Both analytes display strong positive correlations with turbidity in the photometer results (left), but this effect is not reproduced in the corresponding laboratory turbidity analyses (right). Variations in turbidity are likely to cause a similar trend in the laboratory results.

The photometer uses a separate tube as a ‘blank’, against which all reagent tests are compared. In the past, the pho-



Figure 3. Collection of reagents ready for photometer testing. Note the clear Cu test (third from the left) that could be susceptible to turbidity interference, which occurs when the photometer records a false concentration because the solution is darker due to turbidity.

tometer tests used deionized water for the blank, as it was a method of measuring maximum turbidity differences between the clear water and the sample. Palintest states that, when turbidity is below 10 Formazin Turbidity Units (FTU), the turbidity test is not as precise as can be achieved with a dedicated turbidity meter (Palintest, pers. comm., 2016). At these low turbidity levels, reagent tests, including the clear-water ones, should not be affected by the turbidity. Palintest further states that, when turbidity is between 10 and 80 FTU, test accuracy is adequate and should not affect the results. Following consultation with Palintest and further field tests in August, it was decided to follow Palintest’s recommendations for using filtered sample water for each suite and continuing with the deionized water blank for turbidity monitoring. Using filtered sample water as a blank counteracts the turbidity effect to try and keep FTU below 10 for accurate reagent results. Initial testing and photometer analysis for elements in August is promising, and more comprehensive analysis of water samples is ongoing.

The PDV was included in the June and August surveys. The team had to overcome some initial challenges with the instrument in June. Some of the issues were related to outdated Modern Water documentation (initially supplied with the device) and a high learning curve for the device operators during the actual survey, since the PDV was not available before the survey to allow adequate training time. Consequently, testing was limited to just As, Cd, Cu and Pb. Lengthy preparation time required for analysis of each element suite also prevented the team from performing additional tests, such as Zn or Mn.

Conclusions and Recommendations

Preliminary observations from the program so far are as follows:

- The rapid nature and low cost of this field methodology can allow for higher density surveys, thus
 - enabling increased sampling of first- and second-order streams, closer to the stream source or groundwater influx; and
 - offsetting lower concentrations in samples during times of higher precipitation (e.g., some follow-up was already possible during the short field-survey time for this project due to the rapid nature of the methodology).
- Differences were recorded between June and August in field observations with higher TDS, conductivity, etc., and higher concentrations in analytical results in August. These observations will be incorporated into the seasonal variation analysis.
- For a large survey, the PDV requires a controlled, logistically convenient operating environment because

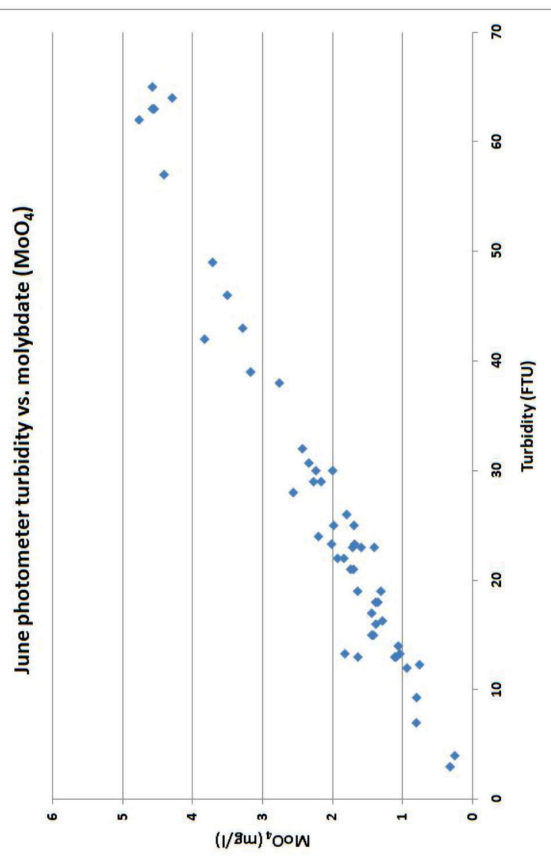
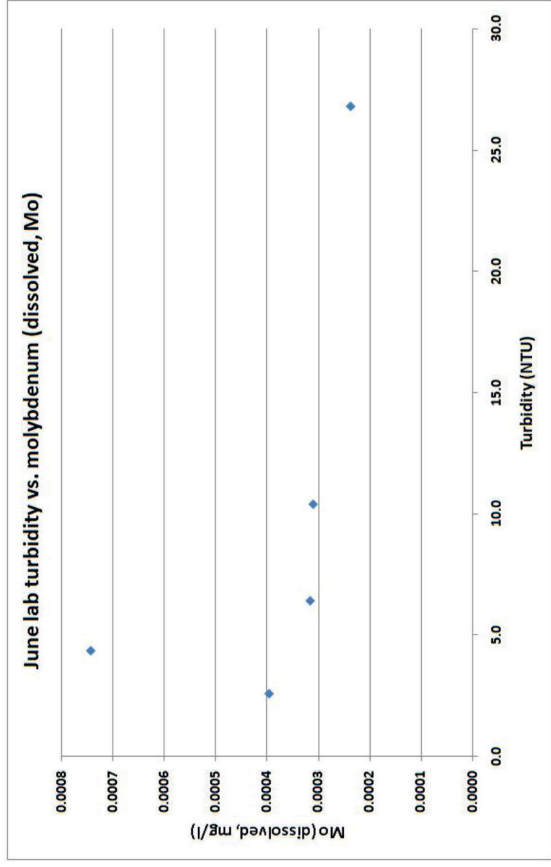
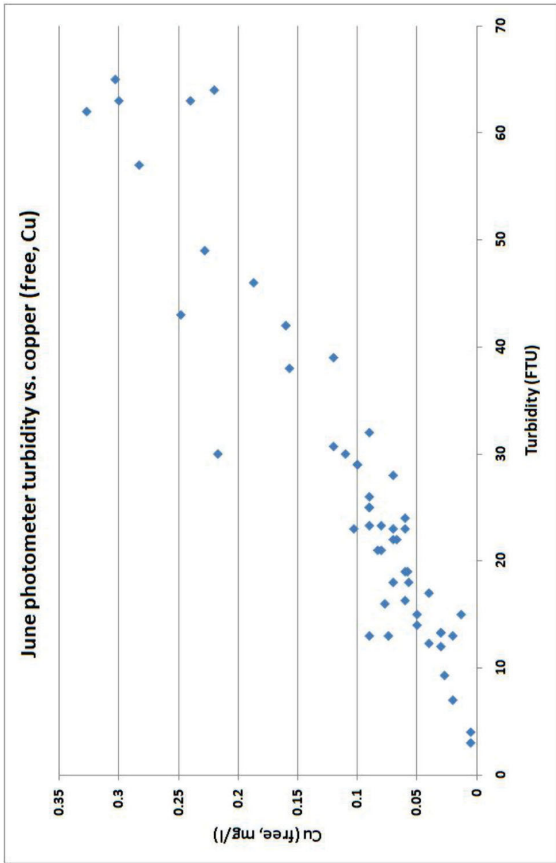
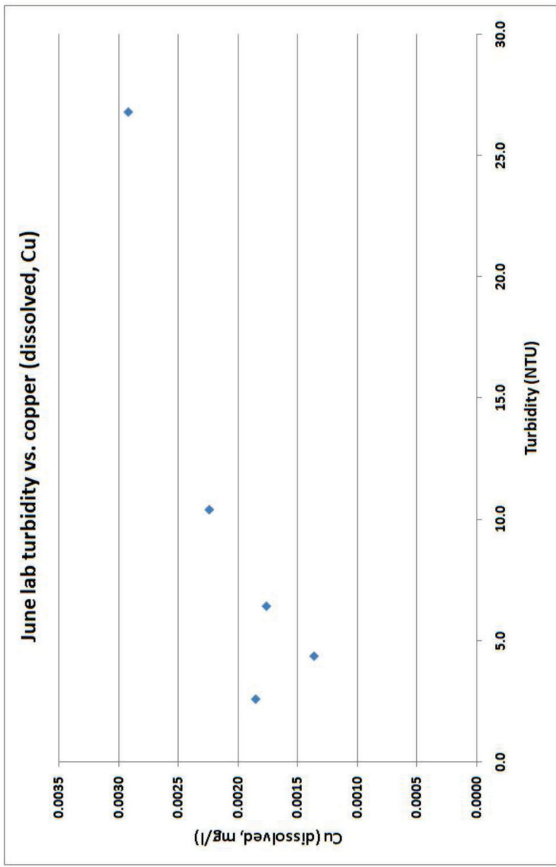


Figure 4. Scatterplots showing the potential for turbidity effect on element concentrations determined by photometer analysis (left) and laboratory analysis (right). Note the negative turbidity versus concentration correlation in the plot of Mo laboratory concentrations (bottom right).

- each analyte suite requires a certain amount of preparation time. For large sample sets, any technical difficulties encountered during that time cause significant delays and analytical backlog.
- lack of a Canadian distributor and technical support caused delays and supply difficulties, and is an issue to consider for surveys under a strict timetable.
- unlike the photometer, a higher technical skill level and additional training time are required.
- The PDV has the ability to detect concentrations at much lower levels than the photometer, and offers additional cation tests that the Palintest photometer does not include (Table 1).

Continuing Fieldwork

The lead author returned to the project site in October for repeat sampling at the time this paper was written. Once all of the data has been analyzed, the following reporting is planned:

- final report documenting methodologies used
- discussion of data quality and description of results
- set of digital maps showing concentrations of the measured analytes
- digital database of the analytical and quality-control results

The project is expected to be complete in early 2017, at which time a final report will be submitted to Geoscience BC.

Acknowledgments

The authors thank Geoscience BC for project funding and the Nazko Economic Development Corporation for their in-kind and logistical support; L. Schlechtleitner and C. Craig for their dedicated and valuable work on the devices and in the field; J. Chapman and N. Vigouroux for reviewing a draft of this paper; and the University of Victoria School of Earth and Ocean Sciences for their support in loaning a micropipette.

References

Angen, J.J., Wesberg, E., Hart, C.J.R., Kim, R. and Rahami M. (2015): Preliminary geological map of the TREK project area, central British Columbia (parts of NTS 093B, C, F and G); Geoscience BC, Report 2015-10, URL <<http://www.geosciencebc.com/s/Report2015-10.asp>> [November 2016].

BC Geological Survey (2016): MINFILE BC mineral deposits database; BC Ministry of Energy and Mines, URL <<http://minfile.ca>> [November 2016].

Braungardt, C., Butterfield, M. and Wajrak M. (2010): On-site mine water analysis: application note for the PDV6000plus; International Mine Water Association Conference, Sydney Nova Scotia, Proceedings, p. 331–334.

Bordet, E. and Hart, J.R. (2016): Distribution and nature of the Eocene Ootsa Lake Group in the Chilcotin Plateau, parts of Quesnel and Anahim Lake map areas (NTS 093B and 093C), central British Columbia; Geoscience BC, Report 2016-12, URL <<http://www.geosciencebc.com/s/Report2016-12.asp>> [November 2016].

Cassidy, J.F., Balfour, N., Hickson, C., Kao, H., White, R., Caplan-Auerbach, J., Mazzotti, S., Rogers, G.C., Al-Khoubbi, I., Bird, A.L., Esteban, L., Kelman, M., Hutchinson, J. and McCormack, D. (2011): The 2007 Nazko, British Columbia, earthquake sequence: injection of magma deep in the crust beneath the Anahim volcanic belt; Bulletin of the Seismological Society of America, v. 101, no. 4, p. 732–1741.

Environment Canada 2016: Historical data; Environment Canada, URL <http://climate.weather.gc.ca/historical_data/search_historic_data_e.html> [November 2016].

GeoBase[®] (2016): Canadian digital elevation model; Natural Resources Canada, Geospatial Data Extraction, URL <<http://www.geogratis.gc.ca/site/eng/extraction>> [November 2016].

Hall, G.E.M. (1998): Relative contamination levels observed in different types of bottles used to collect water samples; Explore, no. 101, p. 1–7.

Jackaman, W., Sacco, D.A. and Lett, R.E. (2015): Regional geochemical and mineralogical data – TREK project year 2, Interior Plateau, British Columbia (NTS 093B, C, F, G); Geoscience BC, Report 2015-12, 13 p. and appendices, URL <<http://www.geosciencebc.com/s/Report2015-12.asp>> [November 2016].

Kennedy, S. (2012): Rock geochemistry report, Hottie mineral claims, NTS 93B 091; BC Ministry of Energy and Mines, Assessment Report 33 447, URL <http://aris.empr.gov.bc.ca/search.asp?mode=repsum&rep_no=33447> [November 2016].

Khanna, P.P., Ahmad, T. and Islam R. (2009): Effect of acidification in water samples before and after filtration: a caution for hydro-geochemical studies; Current Science, v. 96, no. 7, p. 896–897.

Lett, R.E and Jackaman, W. (2015): Tracing the source of anomalous geochemical patterns in soil, water and seepage gas near the Nazko volcanic cone, BC (NTS 93B/13); Geoscience BC, Report 2015-16, 75 p., URL <<http://www.geosciencebc.com/s/Report2015-16.asp>> [November 2016].

Lewtas, P., Fujikawa Y., Hamasaki, T., Sugahara, M. and Yoneda, D. (2010): Field analysis of arsenic by voltammetry – practical techniques for reduction of interferences; Arsenic in Geosphere and Human Diseases, Taylor & Francis Group, London, United Kingdom.

Leybourne, M.I. and Cameron, E.M. (2010): Groundwater in geochemical exploration; Geochemistry: Exploration, Environment, Analysis, v. 10, p. 99–118.

Massey, N.W.D., MacIntyre, D.G., Desjardins, P.J. and Cooney, R.T. (2005): Digital geology map of British Columbia: whole province; BC Ministry of Energy and Mines, GeoFile 2005-1, scale 1:250 000, URL <<http://www.empr.gov.bc.ca/Mining/Geoscience/PublicationsCatalogue/GeoFiles/Pages/2005-1.aspx>> November 2016].

Saha, D and Sahu, S. (2015): A decade of investigations on groundwater arsenic contamination in Middle Ganga Plain, India; Environmental Geochemistry and Health, v. 38, no. 2, p. 315–337. doi:10.1007/s10653-015-9730-z

Taufen, P.M. (1997): Ground waters and surface waters in exploration geochemical surveys; *in* Proceedings of Exploration 97: Fourth Decennial International Conference on Mineral Exploration, p. 271–284.

Yehia, R., Vigouroux, N. and Hickson, C. (2013): Use of a portable photometer for accelerated exploration: testing for geothermal indicators in surface waters; GRC Transactions, v. 37, p. 375–381.

Yehia, R. and Heberlein, D.R. (2015): Use of a field portable photometer for rapid geochemical analysis of stream and spring waters: a case history from Poison Mountain, British Columbia (NTS 092O/02); Geoscience BC, Report 2015-17, URL <<http://www.geosciencebc.com/s/2014-009.asp>> [November 2016].

Preliminary Results of a Geochemical Investigation of Halogen and Other Volatile Compounds Related to Mineralization, Part 1: Lara Volcanogenic Massive-Sulphide Deposit, Vancouver Island (NTS 092B/13)

D.R. Heberlein, Heberlein Geoconsulting, North Vancouver, BC, dave@hebgeoconsulting.com

C.E. Dunn, Colin Dunn Consulting Inc., North Saanich, BC

Heberlein, D.R. and Dunn, C.E. (2017): Preliminary results of a geochemical investigation of halogen and other volatile compounds related to mineralization, part 1: Lara volcanogenic massive-sulphide deposit, Vancouver Island (NTS 092B/13); *in* Geoscience BC Summary of Activities 2016, Geoscience BC, Report 2017-1 p. 141–150.

Introduction

The halogens (F, Cl, Br and I) are common constituents of igneous, metamorphic and sedimentary rocks (Billings and Williams, 1967). They are particularly enriched in differentiated magmas; the hydrothermal fluids and volatile compounds derived from them play an important role in the mobilization and transport of metals in ore-forming systems. In the primary environment, they reside in a variety of hydrous minerals, including micas, amphiboles, scapolite, topaz and apatite. High halogen concentrations are also documented in high-salinity liquid phases or in tiny secondary-mineral phases in fluid inclusions in igneous and hydrothermal minerals (Kendrick et al., 2012; Kendrick and Burnard, 2013). In the hydrothermal environment, halogens can be concentrated in alteration minerals such as micas, clays and topaz, and the gangue mineral fluorite. On exposure to surface conditions, these minerals weather and release their halogens as volatile gases (Br and I) and/or their more stable compounds, or water soluble ions (F and Cl) that disperse to form detectable anomalies in the surficial environment (Trofimov and Rychkov, 2004).

In mineral exploration there are case histories that demonstrate positive responses for all these elements and compounds over zones of concealed mineralization (Al Ajely et al., 1985; Ridgway, 1989, 1991; Ridgway et al., 1990; Trofimov and Rychkov, 2004). However, these methods have seen little or no application to the exploration for minerals in the extensively overburden-covered terrains of British Columbia (BC).

In 2005, Geoscience BC sponsored a project entitled 'Halogens in surface exploration geochemistry: evaluation and development of methods for detecting buried mineral de-

posits' (Dunn et al., 2007). This initial study investigated the optimal analytical procedures available at the time for determining halogen concentrations in soil and vegetation, and provided new halogen data from the Mount Polley, QR and 3Ts deposits. A recommendation from this study was that, since a clear response of labile halogens in soils and vegetation over known mineralization had been established, targets concealed by overburden (both Quaternary and volcanic) needed to be tested and analytical methodology needed to be refined. Bissig et al. (2013), as part of a wider study looking at geochemical responses of blind Cu-Au porphyry-style mineralization beneath Chilcotin basalt cover at the Woodjam property (near the community of Horsefly, central BC), demonstrated that the partial-extraction techniques Bioleach and Enzyme LeachSM produced robust Br and I anomalies over blind mineralization at the Three Firs prospect.

The current project expands on the 2005 study. It aims to further investigate responses of halogen and other volatile compounds (not included in the 2005 study) in organic media over blind and thinly covered mineralization. Two study sites, both on Vancouver Island, have been selected for this investigation: Lara is a volcanogenic massive-sulphide (VMS) target that is buried by 5–10 m of glacial till; Mount Washington is an epithermal system with a thin veneer of overburden. This paper summarizes the field program and objectives of the first of these—Lara. A second paper in this volume outlines the approach at Mt. Washington (Heberlein and Dunn, 2017). Objectives of this study are to broaden the range of sample media tested and to look at the effectiveness of commercially available analytical methods and new instrumentation (some not available in 2005) for detecting mineralization-related halogen and volatile-compound responses.

This project aims to test the geochemical responses of halogens and other mineralization-related compounds (e.g., NH₄, PO₄ and SO₄) in a variety of organic media, including 1) soil Ah horizon, 2) foliage from the most prevalent tree species, and 3) foliage from selected understorey species. Volatile-element distributions are to be compared with

Keywords: *British Columbia, deep-penetrating geochemistry, Lara, base metals, biogeochemistry, halogens, western hemlock, salal, Oregon grape, sword fern, Ah horizon, oxyanions, ammonium, nitrate, nitrite, sulphate, phosphate, Bioleach*

This publication is also available, free of charge, as colour digital files in Adobe Acrobat® PDF format from the Geoscience BC website: <http://www.geosciencebc.com/s/DataReleases.asp>.

commodity- and pathfinder-element signatures for the same media.

An ongoing geochemistry-research project of the Mineral Deposit Research Unit (MDRU) at The University of British Columbia is investigating the processes and controls of labile-element mobility. That project aims to develop a process-based model of trace-element dispersion in the surface environment above concealed massive-sulphide mineralization, and provides a useful context and backdrop to this study.

Relevance to the Exploration Community

This study is designed to provide the mineral-exploration community with an understanding of the potential advantages of determining volatile components, derived from zones of VMS and epithermal Au mineralization, that accu-

mulate in surface soils and common coniferous trees and shrubs in regions with glacial-sediment cover. It assesses the relative capabilities of each medium for preserving the secondary geochemical-dispersion patterns related to a blind mineral deposit. The study assesses the value to the exploration community of an alternative analytical approach for geochemical-sampling programs in areas where conventional soil-sampling methods are found to be ineffective and/or where contamination from mining activities might present a problem for the use of other geochemical-exploration sampling media.

Study Area

The test site at the Lara VMS deposit (Coronation zone), located near Chemainus, is readily accessible by a good road network, thus minimizing the logistical costs required for the field component of the study (Figure 1).

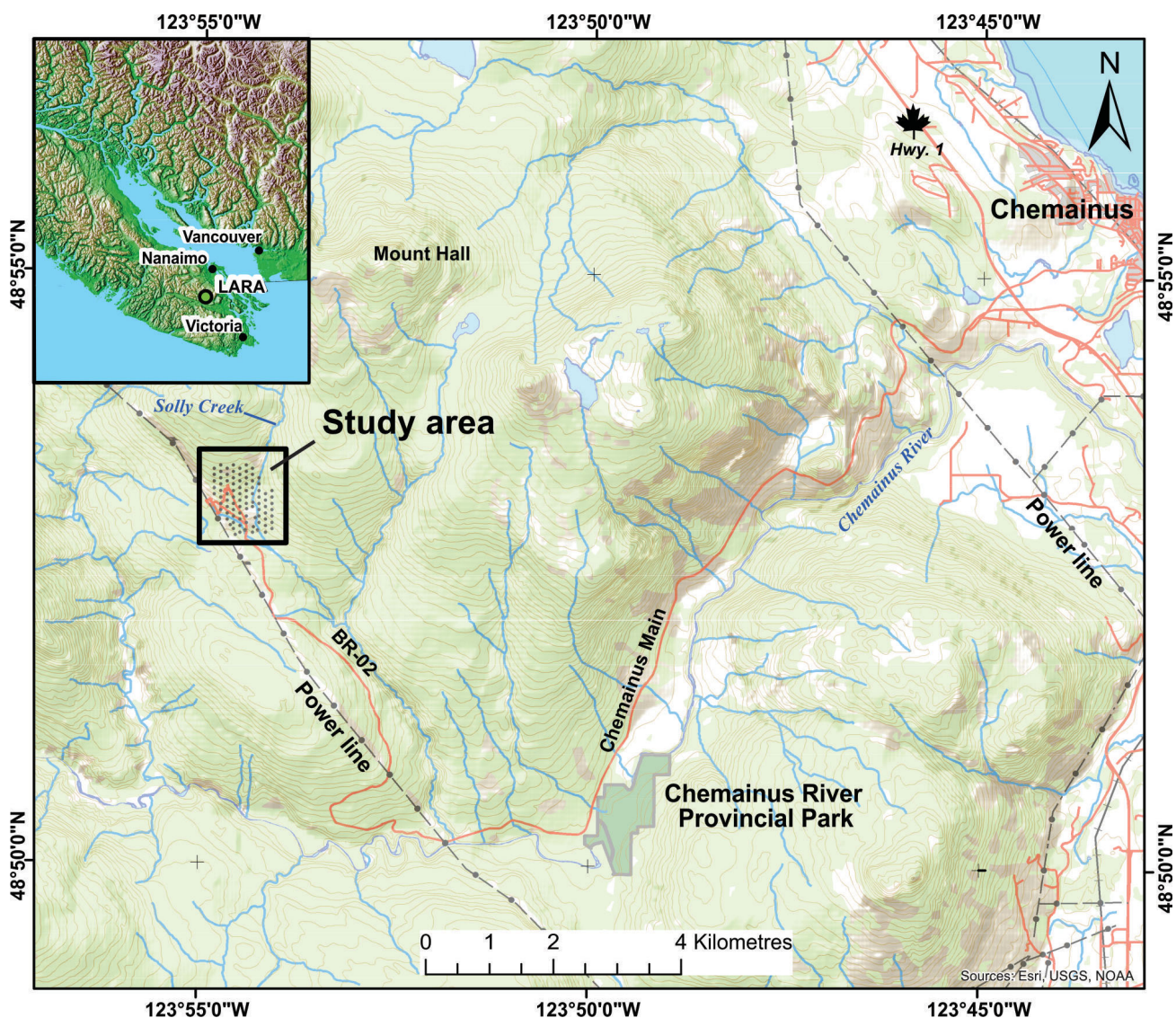


Figure 1. Location of the Lara study area (grey box), east-central Vancouver Island, showing sample stations. Contains information licensed under the Open Government Licence – Canada.

Location and Access

The Lara deposit ('Lara') lies in the Victoria Mining Division of southern Vancouver Island, some 75 km north of Victoria, 15 km northwest of Duncan and 25 km west-southwest of Chemainus, which was the logistical base for the field portion of the study. Access to the project area is via the active Chemainus Main logging road to Kilometre 19 and then the BR-02 Mount Brenton Forest Service Road to Kilometre 7.5. From there, a network of secondary logging roads, drilling roads and a BC Hydro right-of-way provide access to parts of the sampling area.

Surficial Environment

Lara is located at the boundary between the Vancouver Island Ranges to the north and west, and the Nanaimo Lowlands to the south and east (Holland, 1976), in an area of rolling topography. The study site lies on the lower southern slopes of Coronation Mountain and Mount Hall, between elevations of 610 and 770 m (Figure 2). Solly Creek is the main drainage separating the two peaks. It crosses the study area from north to south before turning southeastward to drain into the Chemainus River.

The entire project area was logged in the 1950s. Consequently, the present-day vegetation consists of mixed second-growth forest comprising mostly western redcedar (*Thuja plicata*), western hemlock (*Tsuga heterophylla*) and Douglas-fir (*Pseudotsuga menziesii*). Other species present include western white pine (*Pinus monticola*), paper birch (*Betula papyrifera*) and red alder (*Alnus rubra*). Understorey species vary considerably from place to place. Western sword fern (*Polystichum munitum*) is common in moist coniferous forests at low elevations. It grows best in a well-drained acidic soil of rich humus. Salal (*Gaultheria shallon*), a leathery-leaved shrub in the heather family, is tolerant of both sunny and shady conditions at low to moderate elevations. It is a common coniferous-forest understorey species and may dominate large areas and form dense, nearly impenetrable thickets. Oregon-grape (*Mahonia sp.*) has holly-like leaves and prefers the more canopied areas.

There are no published surficial-geology maps for the immediate Lara area, only the area to the east where the general ice-flow direction is indicated (Blyth and Rutter, 1993). The distribution of surficial materials shown in Figure 2 has been interpreted primarily from field observations and aerial photographs. Regolith mapping, undertaken by M. Bodnar for his M.Sc. thesis at MDRU, is incorporated into this interpretation.

Figure 2 shows that the northern two-thirds of the project area are underlain by a veneer or blanket of glacial till (dark green; Figure 2). This is interpreted to be a basal or lodgment till; it is exposed in roadcuts, stream banks, trenches

and the large open-cut adjacent to the Coronation zone underground portal. Although its thickness is difficult to estimate from present-day exposures, drilling and trenching records show that it varies between <1 m and >50 m (Kapusta, 1990; Archibald, 1999). The presence of outcrops and bedrock-derived colluvium within the till-covered area (Figure 2, reddish brown and brown units) suggest that there is a well-developed buried bedrock topography. In general, there is a gradual thinning of the till deposits upslope.

Recent mapping by M. Bodnar (pers. comm., 2016) has augmented the interpretation of the surficial geology in the central part of the study area. Alluvial deposits, consisting of coarse sand, gravel and channel conglomerate (Figure 2, pale green unit), define a paleochannel system that is now occupied by Solly Creek. First-order tributaries show evidence of erosional recession to the northwest, with backscarps incised into and causing reworking of the till blanket. A recent landslide in the northernmost tributary on Figure 2 has delivered large amounts of unsorted sediment into Solly Creek. The apparently rapid incision of the drainage system has caused it to dissect its own alluvial deposits. Remnants of older alluvial terraces occur along the hillside to the west of Solly Creek between elevations of 660 and 675 m (Figure 2, pale yellow unit). These deposits define the upper edge of a 200 m wide alluvial sand and gravel plain bordering the present-day creek and extending down to the base of slope, where it spreads out into what appears to be an alluvial fan (Figure 2, pale green stipple unit). A remnant of an even older alluvial ridge or terrace (Figure 2, orange unit) is preserved as an interfluvium on the west side of Solly Creek.

Alluvium related to the active drainages is shown by yellow stippled patterns in Figure 2. Solly Creek is the main drainage in the study area. Its upper reaches (above 650 m) are constrained by a steep-sided canyon that has incised through the till and into the underlying bedrock. Upper slopes on the east side of the canyon are covered with colluviated till deposits (Figure 2, pale brown unit). The steeper lower slopes adjacent to the creek are made up of bedrock-derived colluvial veneer overlying bedrock (Figure 2, dark brown unit). Bedrock exposures (too small to be visible at the scale of Figure 2) can be found along the eastern canyon wall, as well as in the streambed itself. Similar colluvial deposits and outcrops are present on the west side of the canyon, but these are capped by unmodified till and the older alluvial gravel ridge mentioned above.

A shallow colluvial veneer over bedrock is also present in the northwestern corner of the study area (medium brown; Figure 2). Two separate areas are mapped, but they could be part of a larger area of bedrock-derived colluvium extending upslope to the northwest. Downslope, the colluvium forms a thin veneer over glacial till.

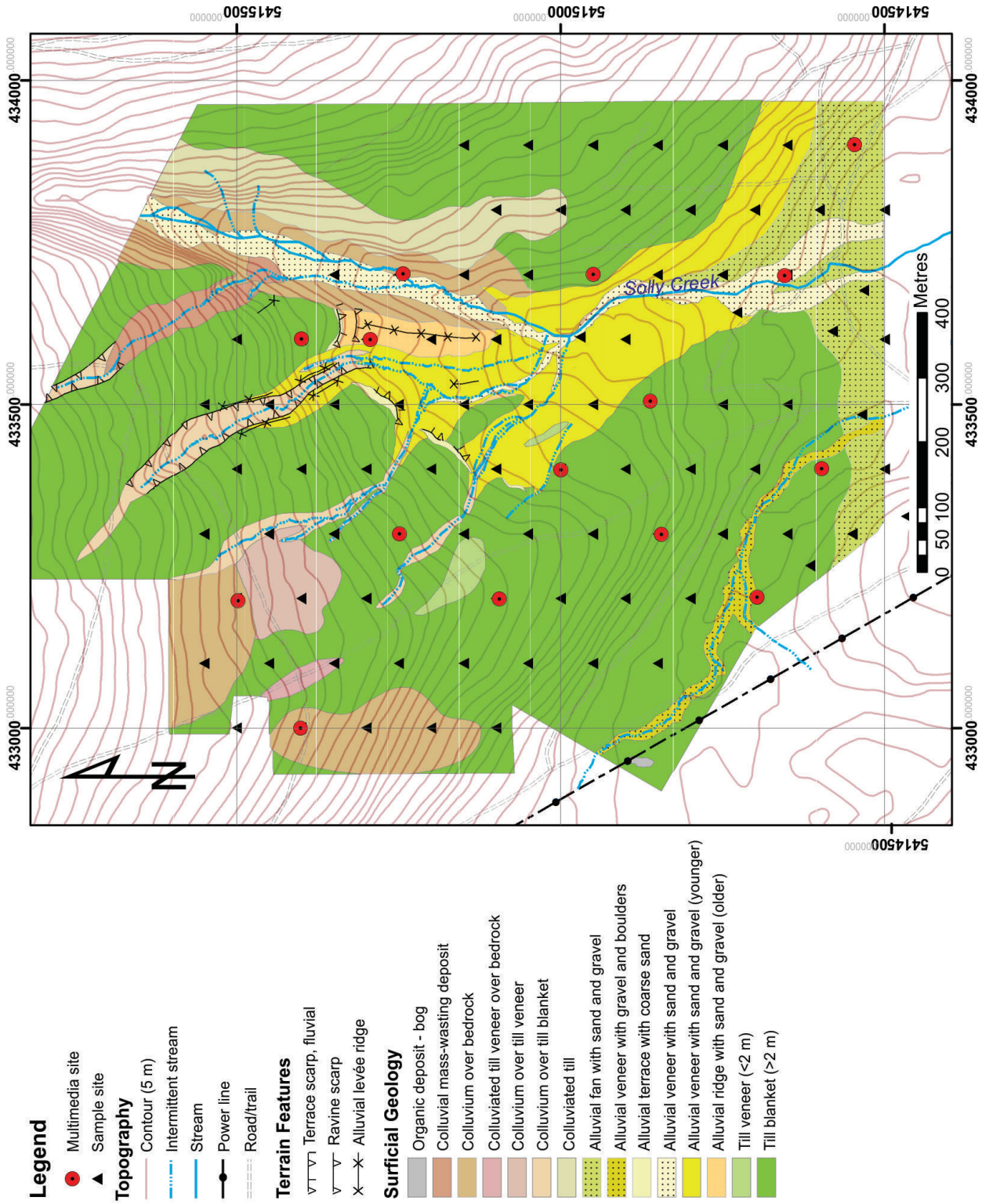


Figure 2. Surficial geology of the Lara study area, east-central Vancouver Island, showing sample stations. Contains information licensed under the Open Government Licence – Canada.

Soil profiles developed on the tills are typical dystric Brunisols. They include a surface LFH layer and an underlying thin Ah horizon lying on top of a generally undifferentiated brown Bm horizon. Iron enrichment at the top of the Bm horizon (Bf horizon) is present at some localities, particularly over alluvial and colluvial deposits. The presence of a discontinuous eluviated horizon (Aej) at some of these localities indicates incipient podzolization over better drained areas.

Geology

The Lara study area is underlain by volcanic and volcanoclastic sedimentary units belonging to the McLaughlin Ridge Formation of the Sicker Group (Massey, 1992; Krockner, 2014). The Sicker Group is known as an important host for Kuroko-type VMS mineralization, the principal economic deposits being the H-W, Lynx, Myra and Price deposits from the Buttle Lake camp (Juras, 1987), located in the Buttle Lake uplift west of Courtenay. Lara lies in a separate uplift, the Cowichan–Horne Lake uplift, in the southern part of the island. Volcanogenic massive-sulphide–style mineralization is hosted by a west-northwest-striking, northeast-dipping package of volcanoclastic sedimentary rocks consisting mostly of sandstone, siltstone, argillite and tuffite (Krockner, 2014). Volcanic rocks are volumetrically subordinate to the volcanoclastic sedimentary rocks. They include aphyric and porphyritic (feldspar, pyroxene and hornblende) rocks, lapilli tuff and breccia of intermediate to mafic composition that lie in the immediate hangingwall to the Coronation trend (Figure 3). Felsic units are relatively common in the Lara area. A narrow quartz-phyric rhyolite-crystal and ash tuff package, known as the Southern Rhyolite sequence, hosts mineralization at the Coronation zone. The unit is intruded by a number of sill-like gabbro bodies. A footwall rhyolite, possibly a dome complex consisting of quartz- and feldspar-phyric rhyolite, has also been identified by a few drillholes in the footwall of the Coronation zone.

South of the Coronation zone, the Sicker Group is abruptly truncated by the Fulford fault, a bedding-subparallel reverse fault that thrusts Sicker Group over younger Nanaimo Group sedimentary units.

Lara mineralization occurs in seven discrete zones (Krockner, 2014). Three of these, the Coronation zone, the Coronation extension and the Hanging wall zone, which together make up the Coronation trend, occur in the area covered by this study. The most important of these is the Coronation zone, which hosts massive, banded/laminated and stringer-style polymetallic sulphide mineralization. The position of these zones, as compiled from historical drilling results, is shown in Figure 3 (Bodnar, pers. comm., 2016). Treasury Metals Inc., holder of the mineral claims to these zones, had reported an indicated-resource estimate (for a 1% Zn block

cutoff) of approximately 1 146 700 tonnes averaging 3.01% Zn, 32.97 g/t Ag, 1.05% Cu, 0.58% Pb and 1.97 g/t Au for the Coronation trend, with an additional 669 600 tonnes averaging 2.26% Zn, 32.99 g/t Ag, 0.90% Cu, 0.44% Pb and 1.90 g/t Au of inferred resource (Treasury Metals Inc., 2013). The Coronation trend crosses the southern third of the study area.

Hydrothermal alteration, present mostly in the structural hangingwall east of the Coronation zone, consists of strong pervasive sericitization, defined chemically by Na depletion and K enrichment. It is associated with elevated Zn values and local silicification and disseminated pyrite.

Sampling and Analysis

The aim of the 2016 sampling program was to collect a selection of organic media to test for halogens and other mineralization-related compounds (including NH₄, SO₄ and PO₄). Considerably more samples were collected than could be analyzed under the scope of the project. However, sampling is quick and easy, and it was unknown which medium might provide the most informative response to the concealed mineralization. Therefore, emphasis was placed on collecting the most common species at all sample stations so that samples not initially analyzed would be available for focusing on detailed analysis once initial baseline data were established.

Samples of the dominant tree species (Douglas-fir, western hemlock and western redcedar) were collected from 89 stations arranged in a 100 m spaced offset grid (Figure 4). Ah horizon soils and samples for soil pH and electrical conductivity readings were also collected at these locations. Soil pH and conductivity measurements were done on samples from the top 5 mm of the B horizon. Approximately every fifth sample was designated as a multimedia site, where additional understory species, including Western sword fern, Oregon-grape and salal, were collected to provide background information on different species. Numbers and types of samples collected are summarized in Table 1 and Figure 4. Limitations on the availability of sample media at some sample stations meant that not all media could be collected at all of the desired sites. This was especially true in areas of ground disturbance caused by road building, mining and drilling activities, as well as in swamps and major drainages.

Twigs and foliage comprising the most recent 5–7 years of growth were collected from each of the dominant tree species. Each sample comprised 5–7 lengths, each of about 25 cm, snipped from around the circumference of a single tree. Samples of outer bark from Douglas-fir and western hemlock were obtained by scraping the scales from around the circumference of neighbouring trees, using a hardened-steel paint scraper, and pouring the scales into a standard ‘Kraft’ paper soil bag (about 50 g, a fairly full bag).

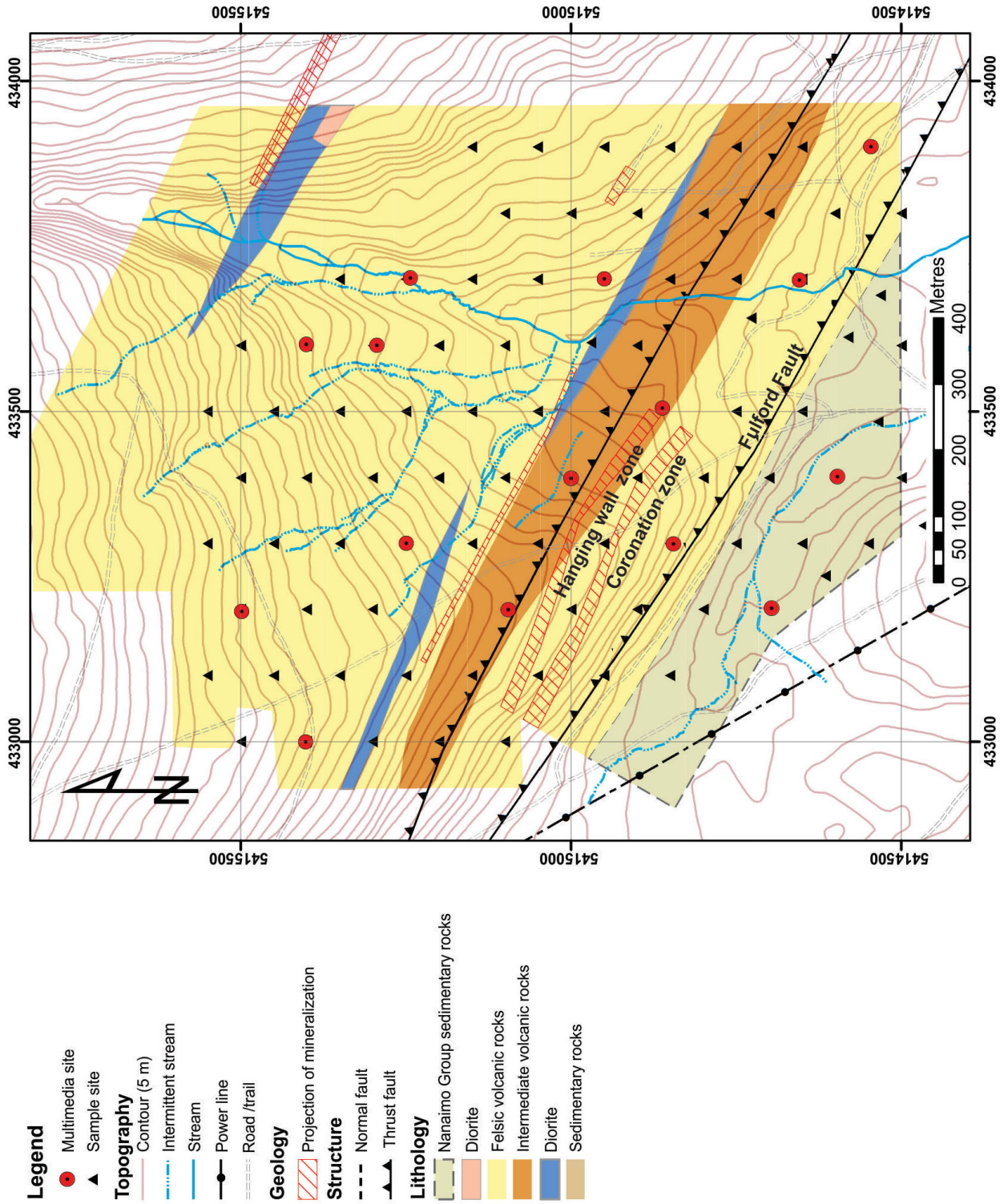


Figure 3. Geology of the Lara study area, east-central Vancouver Island, showing surface projections of the mineralized horizons (red hatching). Contains information licensed under the Open Government Licence – Canada.

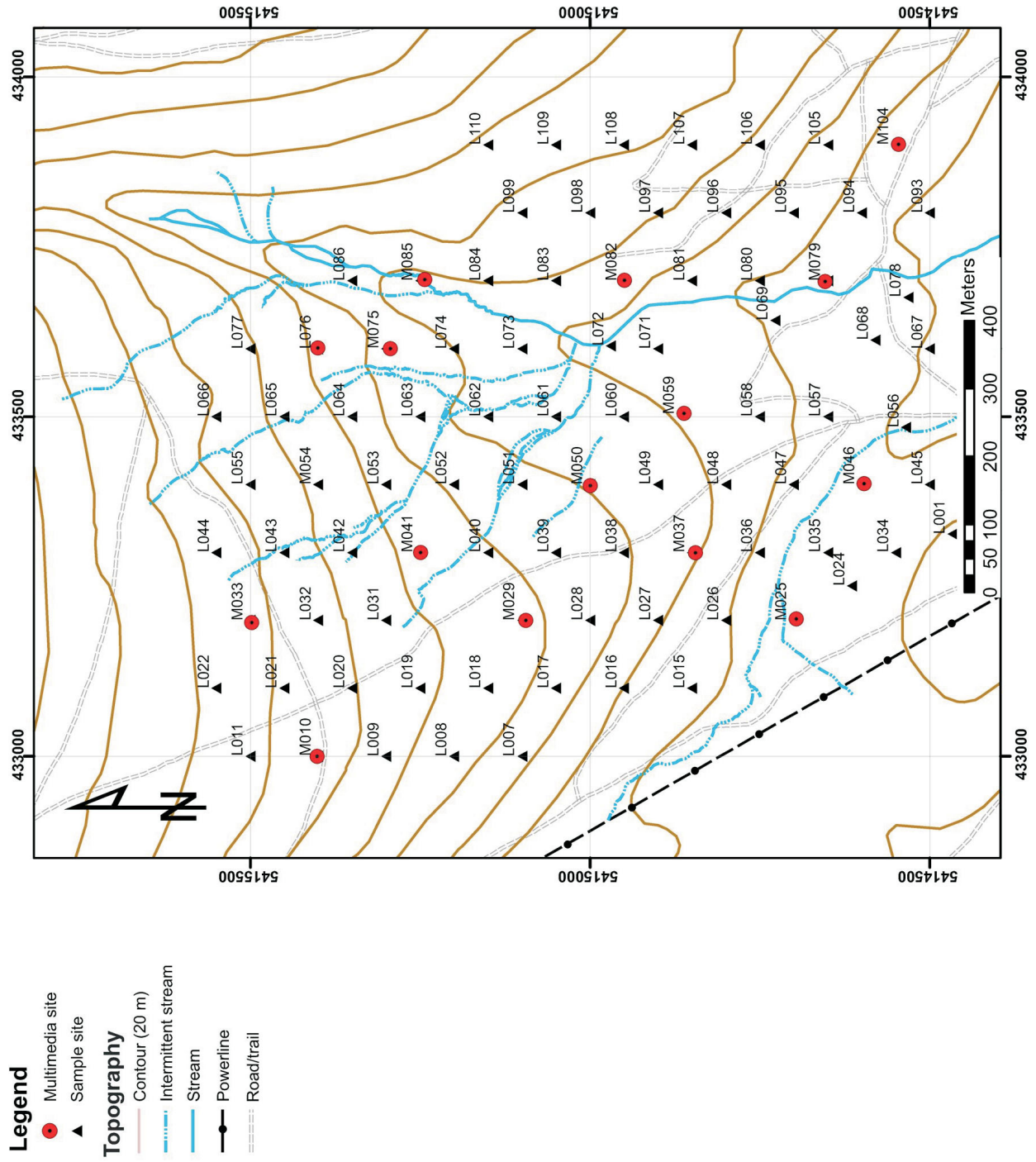


Figure 4. Locations of samples in the Lara study area, east-central Vancouver Island. Contains information licensed under the Open Government Licence – Canada.

Table 1. Numbers and types of samples collected in the Lara study area, east-central Vancouver Island.

Sample medium	No. of samples
Western hemlock foliage (WHF)	89
Douglas-fir bark (DFB)	79
Western redcedar foliage (RCF)	89
Western hemlock bark (WHB)	68
Salal foliage (SALF)	17
Western Sword fern foliage (SF)	8
Oregon-grape foliage (OGF)	8
Ah horizon soil	88
Soil pH & electrical conductivity	81

Foliage from the understorey species collected at the multimedia sites was sampled by gripping a stem near the base and pulling upward to strip off the leaves. Leaves were collected from two or three plants and placed in a 13 by 9 inch Hubco New Sentry[®] fabric sample bag.

Vegetation and soil samples were oven dried at 80° C for 24 hours to remove all moisture. Ah horizon soil samples were sieved to –80 mesh (177 µm) in preparation for analysis of the finer fraction. Foliage was separated from twigs. All foliage and bark samples were then milled to a fine powder. Each sample medium was split into either two or three subsets for submission to several laboratories for different treatments (Table 2). This table is a work in progress that will be refined once experimental work has been completed

Initially, a split of each sample of western hemlock needles was subjected to a warm-water leach in accord with the method developed by G. Hall (Dunn et al., 2007):

“Soil and vegetation samples were leached by placing a 1 g sample in 10 mL deionized water which was then vortexed and allowed to sit for 1 hour at 30°C in an incubator. Samples were then centrifuged and filtered through a 0.45 micron filter.”

Leachates from approximately 200 vegetation samples were analyzed by high-performance liquid chromatography–ion chromatography (HPLC-IC) for Cl, Br, I, PO₄ and

SO₄. The same solutions were analyzed on an AutoAnalyzer (an automated analyzer using continuous-flow analysis [CFA]), for nitrate (NO₃) and ammonium (NH₄), and for fluoride (F⁻) using an ion-selective electrode (ISE) and ion chromatography. Separate splits of the milled western hemlock needles and sieved Ah soils were sent to Activation Laboratories Ltd. (‘Actlabs’; Ancaster, ON) for analysis by their proprietary Bioleach method. Actlabs states that:

“It has been proven that microbiological processes [in the subsurface] are exceptionally important. Electrochemical Redox cells mobilize metals from the mineral deposit to the surface which become adsorbed on soil particles and create unique surficial conditions that bacteria then feed upon. Bioleach digests bacteria and their proteins from the collected surficial samples to analyze for the elements related to the blind mineralization. A 0.75 g sample is leached in a proprietary matrix at 30°C for 1 hour, and the solutions are analyzed on a Perkin Elmer ELAN 6000, 6100 or 9000 ICP/MS.”

Quality Control

Quality-control measures employed in the Lara study include collection of field-duplicate samples for each sample type, as well as insertion of ‘blind’ control samples (milled vegetation of similar matrix and known composition) for the vegetation and Ah horizon samples. Table 3 summarizes the control samples employed.

Results

The only data received by the time of writing were:

- 1) Ah soils and Western hemlock foliage by Bioleach; completed and excellent precision for almost all elements, including Br and I
- 2) Ah soils by aqua regia
- 3) preliminary numbers for NO₃ and NH₄ from the AutoAnalyzer and F⁻ by ISE, with an updated analytical report expected in the near future; moderate variability in the and is reported, and there are unusually high concentrations of F⁻ in all eight of the sword fern samples collected

Table 2. Summary of analytical methods used for samples from the Lara study area, east-central Vancouver Island.

Sample media ¹	Laboratory	Digestion	Analytical methods
Ah horizon – all sites	ALS Minerals, North Vancouver, BC	Aqua regia	ME-ICP41L
Ah horizon – all sites	ALS Minerals, North Vancouver, BC	Warm water leach	ME-MS14L including all halogens
Ah horizon – all sites	Actlabs, Ancaster, ON	Bioleach	ICP-MS
WHF – all sites	Actlabs, Ancaster, ON	Bioleach	ICP-MS
WHF - all sites	BC MOE Laboratory, Victoria, BC	Warm H ₂ O	HPLC-IC for Cl, Br, I, PO ₄ and SO ₄ ; F by ISE
WHB, RCF, SAL, SF, OGF	BC MOE Laboratory, Victoria, BC	Warm H ₂ O	ICP-MS
WHF, WHB, RCF, SAL, SF, OGF	BC MOE Laboratory, Victoria, BC	Microwave HNO ₃	ICP-MS
WHB, RCF, SAL, SF, OGF	ALS Minerals, North Vancouver, BC	Warm H ₂ O	ME-MS14L including all halogens

¹See Table 1 for abbreviation definitions

Abbreviations: BC MOE, BC Ministry of Environment (Environmental Sustainability and Strategic Policy Division, Knowledge Management Branch); HPLC-IC, high-performance liquid chromatography–ion chromatography; ISE, ion-selective electrode

Table 3. Summary of quality-control samples used in the Lara study, east-central Vancouver Island.

Sample medium	No. of samples	Standards		Field duplicates
		V14	LIM-2011	
Western redcedar foliage (RCF)	90	2		8
Western hemlock foliage (WHF)	89	9		8
Douglas-fir bark (DFB)	79	2		7
Western hemlock bark (WHB)	68	9		2
Salal foliage (SALF)	17	2		0
Western sword fern foliage (SF)	8	1		0
Oregon-grape foliage (OGF)	8	1		0
Ah horizon	88	8	9	8

Analytical development work will be ongoing through the fourth quarter of 2016. Interpretation of the analytical results and preparation of the final report will be completed following the snow-sampling program in January 2017.

Acknowledgments

The authors thank the following, and their analytical staff, for their ongoing contributions in developing the analytical technology relevant to this study: B. MacFarlane (Vice-President, Analytical Technology, ALS Minerals–Geochemistry, Vancouver, BC) and C. Dawson (Head, Analytical Chemistry, BC Ministry of Environment, Environmental Sustainability and Strategic Policy Division, Knowledge Management Branch, Technical Services (Laboratory), Victoria, BC). A. Hoffman (Actlabs, Ancaster, ON) is thanked for the discounted rate for the Bioleach analysis of a suite of samples. The authors also thank S. Willder for his efficient assistance that greatly expedited the field component of this study. They are most grateful to R. Lett for his constructive comments on the draft of this paper.

Treasury Metals Inc. is thanked for access to their mineral claims at Lara, and Island Timberlands is thanked for providing access to their forestry lands within which the Lara claims are located.

References

- Al Ajely, K.O., Andrews, M.J. and Fuge, R. (1985): Biogeochemical dispersion patterns associated with porphyry-style mineralization in the Coed Y Brenin forest, North Wales; *in* *Prospecting in Areas of Glaciated Terrain*, Institute of Mining and Metallurgy, London, United Kingdom, v. 6, p. 1–10.
- Archibald, J.C. (1999): Summary report on the Laramide property diamond drilling program, Lara VMS Project, Victoria Mining Division, NTS 092B/13E, Vancouver Island, BC; BC Ministry of Energy and Mines, Assessment Report 26021, 150 p., URL <http://aris.empr.gov.bc.ca/search.asp?mode=repsum&rep_no=26021> [September 2016].
- Billings, G.K. and Williams, H.H. (1967): Distribution of chlorine in terrestrial rocks: a discussion; *Geochimica et Cosmochimica Acta*, v. 31, p. 22–47.
- Bissig, T., Heberlein D.R. and Dunn, C.E. (2013): Geochemical techniques for detection of blind porphyry copper-gold mineralization under basalt cover, Woodjam property, south-central British Columbia (NTS 093A/03, 06); Geoscience BC, Report 2013-17, p. 1–54, URL <<http://www.geosciencebc.com/s/Report2013-17.asp>> [October 2016].
- Blyth, H.E. and Rutter, N.W. (1993): Surficial geology of the Duncan area (NTS 92B/13); BC Ministry of Energy and Mines, Open File 1993-27, 1:50 000 scale map, URL <<http://www.empr.gov.bc.ca/Mining/Geoscience/Publications/Catalogue/OpenFiles/1993/Pages/1993-27.aspx>> [October 2016].
- Dunn, C.E., Cook, S.J. and Hall, G.E.M. (2007): Halogens in surface exploration geochemistry: evaluation and development of methods for detecting buried mineral deposits; Geoscience BC, Report 2007-10, p. 1–74, URL <<http://www.geosciencebc.com/s/2007-10.asp>> [October 2016].
- Heberlein, D.R. and Dunn, C.E. (2017): Preliminary results of a geochemical investigation of halogen and other volatile compounds related to mineralization, part 2: Mount Washington epithermal gold prospect, Vancouver Island (NTS 092F/14); *in* *Geoscience BC Summary of Activities 2016*, Geoscience BC, Report 2017-1, p. 151–158.
- Holland, S.S. (1976): Landforms of British Columbia: a physiographic outline (second edition); BC Ministry of Energy and Mines, Bulletin 48, 136 p., URL <<http://www.empr.gov.bc.ca/Mining/Geoscience/PublicationsCatalogue/BulletinInformation/BulletinsAfter1940/Pages/Bulletin48.aspx>> [October 2016].
- Juras, S. (1987): Geology of the polymetallic volcanogenic Buttle Lake camp, with emphasis on the Price hillside, central Vancouver Island, British Columbia, Canada; Ph.D. thesis, The University of British Columbia, 299 p., URL <<https://open.library.ubc.ca/cIRcle/collections/ubctheses/831/items/1.0052424>> [October 2016].
- Kapusta, J.D. (1990): 1990 drilling report on the Lara Group 1, Victoria Mining Division, NTS 092B/13W, BC; BC Ministry of Energy and Mines, Assessment Report 20981, 71 p., URL <http://aris.empr.gov.bc.ca/search.asp?mode=repsum&rep_no=20981> [September 2016].
- Kendrick, M.A., Woodhead, J.D. and Kamenetsky, V.S. (2012): Tracking halogens through the subduction cycle; *Geology*, v. 40, no. 12, p. 1075–1078.
- Kendrick, M.A. and Burnard, P. (2013): Noble gases and halogens in fluid inclusions: a journey through the Earth's crust; *in* *The Noble Gases as Chemical Tracers, Advances in Isotope Geochemistry*, Springer-Verlag, Berlin-Heidelberg, Germany, p. 319–369. doi:10.1007/987-3-642-28836-4_11
- Krocker, R. (2014): Mapping, whole rock geochemical sampling and preliminary environmental baseline study, Lara polymetallic property, Victoria Mining Division, NTS

- 092B/13, BC; BC Ministry of Energy and Mines, Assessment Report 35428, 198 p., URL <<http://aris.empr.gov.bc.ca/ArisReports/35428.PDF>> [October 2016].
- Massey, N.W.D. (1992): Geology and mineral resources of the Duncan sheet, Vancouver Island (92B/13); British Columbia Ministry of Energy and Mines, Paper 1992-4, 124 p., URL <<http://www.empr.gov.bc.ca/Mining/Geoscience/PublicationsCatalogue/Papers/Pages/1992-4.aspx>> [October 2016].
- Ridgway, J. (1989): Ammonium geochemistry in the search for hydrothermal gold mineralization: final report to the Overseas Development Administration; British Geological Survey, Technical Report WC/89/13 (open file).
- Ridgway, J. (1991): Ammonium geochemistry in the search for hydrothermal gold deposits (II): final report to the Overseas Development Administration, November, 1991; British Geological Survey, Technical Report WC/91/41, 8 p., URL <www.bgs.ac.uk/research/international/dfid-kar/WC91041_col.pdf> [October 2016].
- Ridgway, J., Appleton, J.D. and Levinson, A.A. (1990): Ammonium geochemistry in mineral exploration – a comparison of results from the American cordilleras and the southwest Pacific; *Applied Geochemistry*, v. 5, p. 475–489, URL <<http://www.sciencedirect.com/science/article/pii/088329279090022W>> [October 2016].
- Treasury Metals Inc. (2013): Lara property; Treasury Metals Inc., URL <www.treasuremetals.com/s/lara_property.asp> [November 2016].
- Trofimov, N.N. and Rychkov A.I. (2004): Iodine and Bromine: Geochemical Indicators of Deep Ore Deposits (translated by E. Erlich and M.-M. Coates); Colorado Mountain Publishing House, Denver, Colorado, 205 p.

Preliminary Results of a Geochemical Investigation of Halogen and Other Volatile Compounds Related to Mineralization, Part 2: Mount Washington Epithermal Gold Prospect, Vancouver Island (NTS 092F/14)

D.R. Heberlein, Heberlein Geoconsulting, North Vancouver, BC, dave@hebgeoconsulting.com

C.E. Dunn, Colin Dunn Consulting Inc., North Saanich, BC

Heberlein, D.R. and Dunn, C.E. (2017): Preliminary results of a geochemical investigation of halogen and other volatile compounds related to mineralization, part 2: Mount Washington epithermal gold prospect, Vancouver Island (NTS 092F/14); in Geoscience BC Summary of Activities 2016, Geoscience BC, Report 2017-1, p. 151–158.

Introduction

The halogens (F, Cl, Br and I) are common constituents of igneous, metamorphic and sedimentary rocks (Billings and Williams, 1967). Heberlein and Dunn (2017) provide a discussion of the rationale behind determining the concentrations of the halogens and other volatile compounds in the exploration for concealed mineral deposits. At the Mount Washington (epithermal) Au prospect on Vancouver Island, sample media and methods are used that are similar to those employed in the Lara VMS study (Heberlein and Dunn, 2017). However, to assist in understanding natural processes, a key component of this study is the use of ion-collection devices (traps). Activated charcoal and alkaline ion-exchange resin packages were buried in the soil profile for three months to capture volatile anions and cations emanating from the ground. In addition, the flux of these components through vegetation will be measured through the analysis of transpired fluids exuded from mountain hemlock (*Tsuga mertensiana*) twigs, and in snow.

Study Area

The Mount Washington epithermal Au prospect is located near the city of Courtenay on Vancouver Island. A biogeochemical study of the area, conducted by the Geological Survey of Canada in 1990, revealed strong geochemical signals of the commodity and pathfinder elements related to the underlying mineralization (Dunn, 1995, 2007). This indicated that Mount Washington would be a suitable area for testing the volatile components sought in this study. Furthermore, archived samples from the 1990 survey were available for additional analysis.

Keywords: *British Columbia, deep-penetrating geochemistry, Mount Washington, biogeochemistry, halogens, ion traps, mountain hemlock, transpired fluids, Ah horizon, snow, ammonium, halogens, multi-element analysis*

This publication is also available, free of charge, as colour digital files in Adobe Acrobat® PDF format from the Geoscience BC website: <http://www.geosciencebc.com/s/DataReleases.asp>.

At Mount Washington, the sampling approach was somewhat different from that at Lara. In addition to collecting plants and soils to assess their volatile-compound concentrations and spatial patterns around the mineralized zone, artificial media were placed in the ground to collect ions that may be migrating to the surface from the underlying rocks. By using this novel approach, the aim is to establish if there is, indeed, a vertical flux of volatile compounds emanating from the bedrock. Activated carbon and alkaline ion-exchange resin are used as collectors for these mobile cations and anions. Results from the artificial media will be compared to patterns in natural media, including Ah horizon soil, vegetation (mountain hemlock and yellow-cedar) and transpired fluids collected from the dominant species (mountain hemlock).

Location and Access

The study area lies immediately north of the Mount Washington Alpine Resort (Figure 1). Access from the nearest logistical centre at Courtenay is via Highway 19 north to the Strathcona Parkway and then west for 10 km to the alpine resort, all on well-maintained paved roads. From the alpine lodge, the sampling area is accessible on foot via mountain biking trails and ski runs to the Boomerang chairlift and then by a network of old drilling and mining roads to the northwest. Alternative access can be gained by four-wheel-drive vehicle from the Raven Lodge parking area via a network of variably maintained logging roads (Figure 1).

Surficial Environment

The sampling area is at midslope (approximately 1360 m elevation) on the western flank of Mount Washington, just above the transition between steeper colluvial slopes above and more gentle, poorly drained slopes below. Drainage development at the elevation of the sampling area is poor.

Much of the area has been previously logged. Present-day vegetation consists of fairly open subalpine woodland containing a variety of tree species, including yellow-cedar (*Chamaecyparis nootkatensis*), mountain hemlock (*Tsuga*

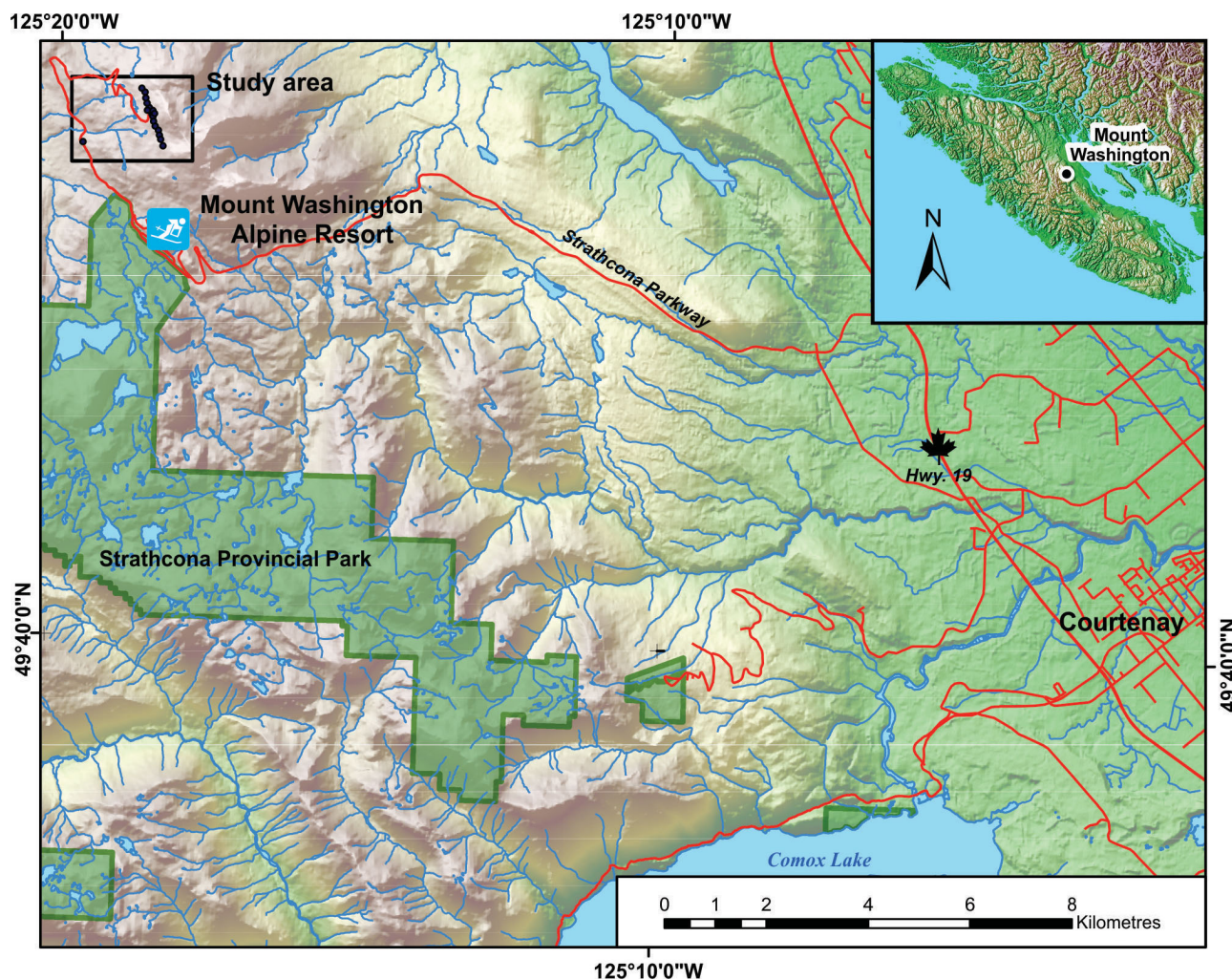


Figure 1. Location of the Mount Washington study area (black box), east-central Vancouver Island. Sample locations indicated by black dots. Contains information licensed under the Open Government Licence – Canada.

mertensiana), Pacific silver fir (or *Amabilis* fir; *Abies amabilis*) and subalpine fir (*Abies lasiocarpa*). The dominant understorey species is white-flowered rhododendron (*Rhododendron albiflorum*).

Surficial geology is relatively simple. Above about 1320 m, the hillsides are covered with a veneer of colluvium. Exposures in roadcuts show that this material rarely exceeds 2 m in thickness and, over much of the sampled area, it is less than 0.5 m thick. A thin soil profile is developed on this sandy matrix material. Observations from sample holes and roadcuts show that the most common profile consists of poorly developed dystric Brunisol, typified by a surface LFH layer and a thin Ah horizon (<2 cm) overlying a uniform, brown, undifferentiated Bm horizon. Incipient podzolization, marked by the presence of an intermittent eluvial Ae_j horizon and Fe-enriched Bf horizon, is present at about 10% of the sample locations.

Below the 1320 m contour, particularly in the northwest corner of the survey area, there is an abrupt transition from

well-drained colluvium to water-saturated ground. This elevation is marked by an almost continuous line of meltwater-fed springs and seeps that form a series of small raised bogs, which feed downslope into a number of ponds and lakes. These water bodies define the headwaters of several streams that drain the slope westward into the northwest-flowing Goss Creek.

Geology

This study was carried out over the western part of the Lakeview-Domineer resource area (Houle, 2013), which is defined by a number of shallow-dipping, Au-Ag-Cu-bearing quartz-sulphide veins (Figure 2).

The Lakeview-Domineer zones have been exploited in two small open pits and explored by extensive diamond-drilling, trenching, bulk sampling and underground drifts. Production by Mount Washington Copper Co. Ltd. between 1964 and 1967 was 381 733 tonnes grading 0.34 g/t Au, 19 g/t Ag and 0.93% Cu (Houle, 2013).

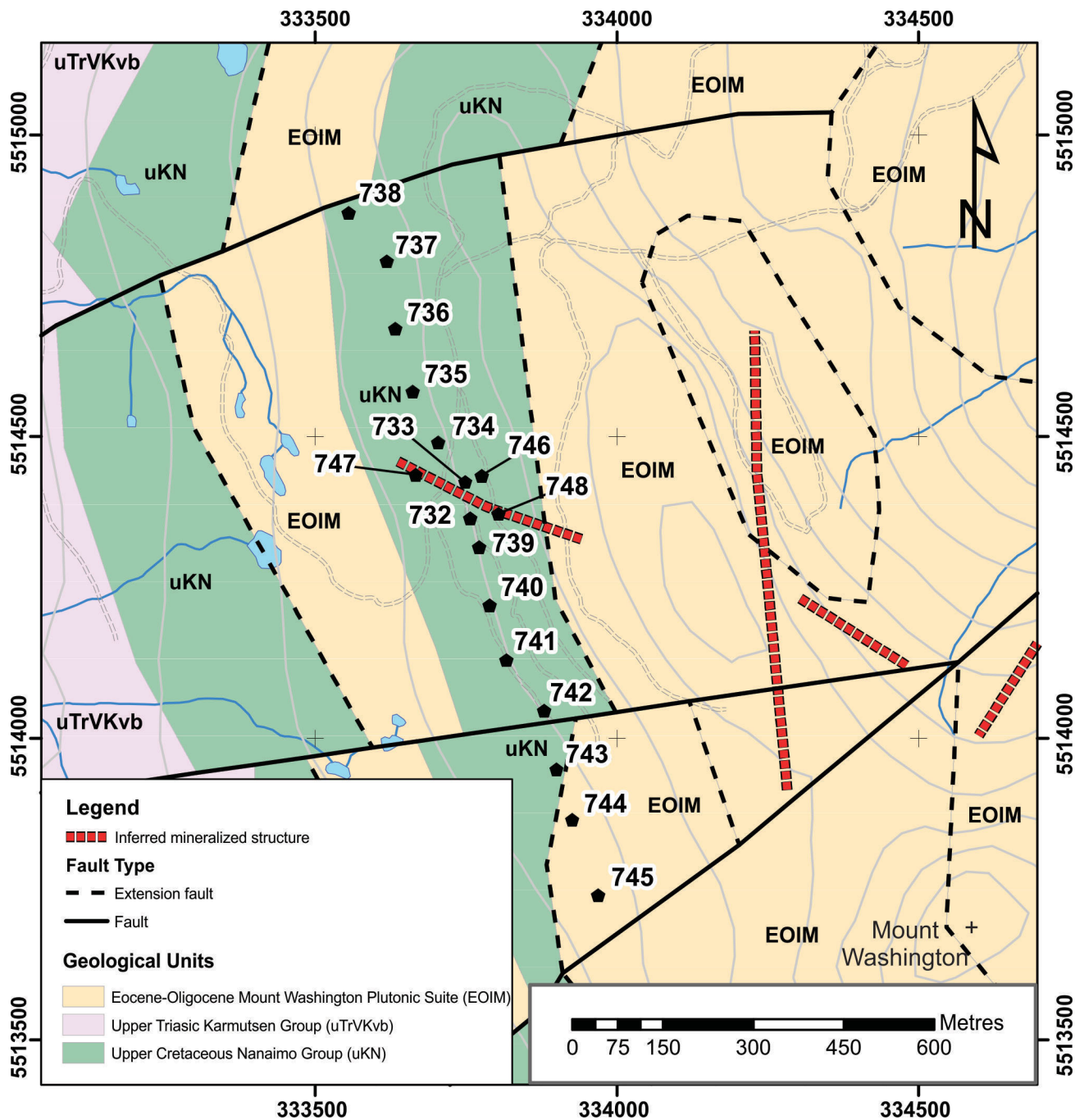


Figure 2. Geology of the Mount Washington study area (after Massey et al., 2005), east-central Vancouver Island, showing sample locations (black pentagons).

From the most up-to-date geological mapping of the Mount Washington area, it is apparent that most of the area to the west of Mount Washington is underlain by pillow basalts of the Triassic Karmutsen Formation. Close to Mount Washington itself, the basalts are unconformably overlain by a gently east-dipping sequence of sandstone, siltstone and conglomerate of the Upper Cretaceous Nanaimo Group. This is the main unit underlying the sampled area. The ridges and upper elevations of the mountain are defined by intrusive rocks, consisting of quartz diorite and feldspar-

hornblende dacite porphyry that together make up the Eocene–Oligocene (41–35.5 Ma; Madsen et al., 2006) Mount Washington Plutonic Suite. The intrusions occur as stocks, sills and dike-like bodies that intrude the Nanaimo Group.

At least seven different breccia bodies, some pipe like and others more flat lying, have been recognized in the Domineer-Lakeview resource area (Houle, 2013). Zones of brecciation are localized along the intrusive contacts and

on north- and northwest-trending structures. They vary widely in texture and composition, and appear to be the principal controls for polymetallic sulphide mineralization. Mineralization also occurs in veins and stringers. The style of mineralization is considered to be high-sulphidation epithermal Au-Ag-Cu (BC Mineral Deposit Profile L04; Panteleyev, 1995) or ‘subvolcanic’ Cu-Au-Ag (Houle, 2013).

Sampling

The Mount Washington sampling campaign is divided into three parts. **Part 1**, carried out between June 27 and 30, involved the installation of 18 passive ion collectors along a south-southeast-trending traverse over the Domineer Au zone (Figure 3) and the collection of foliage and transpired fluids from mountain hemlock at the same sample stations.

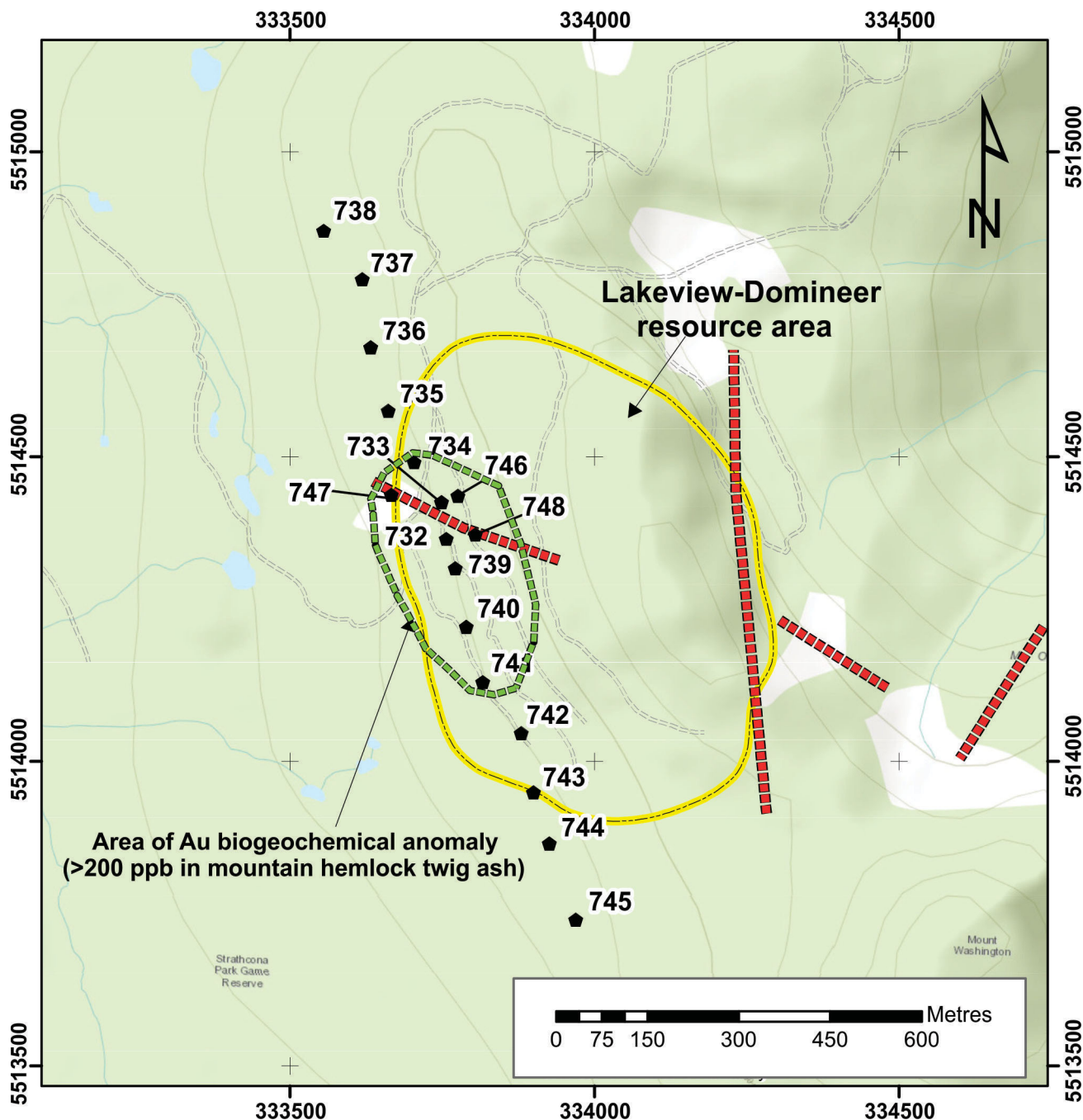


Figure 3. Location of passive ion-collector sites, showing also the locations of the Lakeview-Domineer resource area (yellow outline), the 1990 biogeochemical anomaly (green outline) and the approximate positions of mineralized structures (red). White areas are devoid of trees. Contains information licensed under the Open Government Licence – Canada.

Collectors were installed at nominal 100 m intervals. A single collector was also installed in a presumed unmineralized area located 1500 m to the west, to act as a background/control site. A summary of samples collected to date is presented in Table 1.

The ion collectors contain two different collection media: activated charcoal for cations and alkali ion-exchange resin for anions (Sigma Aldrich Amberlite IRA743®). The media were accurately weighed into 10 by 7 cm porous nylon sachets (15 and 20 g, respectively) and the bags were heat sealed. In the field, they were placed on a 2 cm thick bed of pure silica sand housed in an 18 cm diameter by 15 cm deep cardboard tube that was buried to 20 cm in the ground. The silica sand serves to isolate the collectors from the soil, so as to avoid capture of endogenic ions: a filter paper was used to isolate the collectors from the silica sand. A ceramic tile was placed between the collectors in order to avoid the possibility of cross-contamination between the charcoal and resin sachets. The apparatus was capped with an overlapping plastic plate to prevent entry of rain water and surface debris, and shallowly buried. Each site was sprayed with animal repellent to discourage disturbance by curious bears. One of the collectors is illustrated in Figure 4.

Duplicate collectors were planted at two of the sites: one over mineralization and the other in a background location.

In addition to installing the passive collectors, mountain hemlock (*Tsuga mertensiana*) foliage (MHF; 16) and transpired-fluid samples (16) were collected at each location. Transpired fluids (from mountain hemlock) were obtained



Figure 4. Partly installed ion collector showing sachets of activated carbon (right) and ion-exchange resin (left) separated by a ceramic partition. Cardboard tube is 18 cm in diameter.

Table 1. Numbers and types of samples collected for the Mount Washington study.

Sample medium	No. of samples	No. of duplicates	Comment
Mountain hemlock foliage (MHF)	22	2	Collected June 2016
Ion collectors (IC)	18	2	Put in place June 2016
Transpired fluids (TFMH)	18	2	Collected August 2016
Ah soils			To be collected October 2016
Additional MHF			To be collected October 2016
Snow	18	2	To be collected January 2017
Archived MHF	~50		Collected August 1990
Archived yellow-cedar bark ash (YCB)	17		Collected August 1990

by enclosing several 25 cm lengths of twig with needles in plastic bags and leaving them for a minimum of 24 hours during a period of sunny weather (Figure 5). After that time, the transpired fluid was recovered by removing the bag and taking up the fluid in a 100 ml syringe. A 0.45 µm filter was then attached to the end of the syringe and the liquid filtered into 25 ml glass vials. The glass vials were placed in a cooler with ice packs for transportation to Vancouver.

The ion collectors were left in the ground for three months. **Part 2** of the program, carried out in early October, involved recovery of the ion collectors and collection of Ah horizon soil samples. Ion collectors were carefully exposed and each medium placed in individual Ziploc® bags. Both bags were then placed in a third bag to isolate the samples from the atmosphere. All of the used materials were removed from the sample sites and disposed of.

Collection of additional vegetation samples included repeats of the Part 1 sites to permit an evaluation of temporal changes in foliage chemistry, and collection of samples from parallel sample lines 100 m to the east and west of the ion-collector line.



Figure 5. Collection of transpired fluid (left) and filtration of fluid into glass vial (right).

The final part of the Mount Washington sampling program (**Part 3**) is planned for January, 2017, when base-of-snow samples will be collected from selected collector sites. This part of the program is contingent on snow conditions at that time.

Sample Preparation and Analysis

Mountain hemlock samples will be oven dried at 80°C and the foliage will be separated from the twigs and milled to a fine powder. Aliquots of the powdered samples (0.5 g) will be leached in warm water and analyzed, initially, for ammonium (NH₄); additional anions will be determined if a suitable methodology can be successfully developed. In addition, all samples will be microwave-digested in HNO₃ and analyzed at the ALS Geochemistry Laboratories (North Vancouver, BC) by ICP-ES/MS for all of the same elements and compounds listed in the accompanying paper (Heberlein and Dunn, 2017), as well as F⁻ by ion chromatography (IC) using a newly developed method. Tests comparing element concentrations in dry and ashed vegetation will be made to determine if ashing provides a similar halogen signature to analysis of the dry tissue, even though a portion of the halogens will volatilize during ashing. If signatures are similar, ashing might be the preferred method because it eliminates many of the analytical interferences encountered during analysis of organic-rich media by IC. Transpired fluids are to be analyzed by ICP-MS and IC at ALS Geochemistry Laboratories.

Ah horizon samples will be oven dried at 80°C and sieved to -80 mesh (177 µm). A 0.5 g aliquot of the fine fraction will be digested by a 1:1 nitric:hydrochloric acid mixture and analyzed for multiple elements by ICP-ES/MS. Halogens will be determined by IC (F and Cl) and ICP-MS (Cl, Br and I) on a warm-water leach. Other tests to be conducted will depend on results obtained from the ongoing analytical research component of this study.

All vegetation and Ah horizon samples will be analyzed by Bioleach at Activation Laboratories Ltd. ('Actlabs'; Ancaster, ON). Analytical methods for the ion collectors had yet to be determined at the time of writing. Snow samples will be analyzed as water samples following the protocols used for the transpired fluids.

All field components of the study will have been completed by early October 2016, except for the snow collection, which will be undertaken in mid- to late winter when snow-pack conditions are suitable and it is considered that there has been sufficient time for a signature to have developed for elements fluxing from mineralization into the snow profile. In the meantime, all other analytical components will be completed and results will be prepared for preliminary presentation at the Mineral Exploration Roundup in January 2017. A final report is expected to be completed by the end of April 2017.

Quality Control

Quality-control measures employed at Mount Washington include the collection of field duplicates (2) and the use of reference materials for biogeochemistry (control V14) and Ah horizon soils (LIM-2011).

Acknowledgments

The authors thank the following and their analytical staff for their ongoing contributions in developing the analytical technology relevant to this study: W. MacFarlane (Vice President, Analytical Technology, ALS Minerals–Geochemistry, North Vancouver, BC) and C. Dawson (Head, Analytical Chemistry, BC Ministry of Environment, Environmental Sustainability and Strategic Policy Division, Knowledge Management Branch, Technical Services Laboratory, Victoria, BC). Natural Resources Canada (Geological Survey of Canada, Ottawa, ON) is thanked for supplying archived material to assist in this survey. K. Willder is thanked for her efficient assistance that greatly expedited the first field component of this study. The authors are most grateful to R. Lett for his constructive comments on the draft of this paper.

They are also grateful to P. Leopold (President, North Bay Resources Inc.) and D. Zamida for their permission to access the mineral claims.

References

- Billings, G.K. and Williams, H.H. (1967): Distribution of chlorine in terrestrial rocks: a discussion; *Geochimica et Cosmochimica Acta*, v. 31, p. 22–47.
- Dunn, C.E. (1995): Mineral exploration beneath temperate forests: the information supplied by trees; *Exploration and Mining Geology*, v. 4, no. 3, p. 197–204.
- Dunn, C.E. (2007): Biogeochemistry in Mineral Exploration; *Handbook of Exploration and Environmental Geochemistry* (M. Hale, ser. ed.), v. 9, Elsevier, Amsterdam, 462 p.
- Heberlein, D.R. and Dunn, C.E. (2017): Preliminary results of a geochemical investigation of halogen and other volatile compounds related to mineralization, part 1: Lara volcanogenic massive-sulphide deposit, Vancouver Island (NTS 092B/13); *in* Geoscience BC Summary of Activities 2016, Geoscience BC, Report 2017-1 p. 141–150.
- Houle, J. (2013): NI 43-101 technical report on the Mount Washington property, Vancouver Island, British Columbia, NTS 092F/11 and 092F/14, North Bay Resources Inc.; BC Ministry of Energy and Mines, Assessment Report 34200, 206 p. URL <<http://aris.empr.gov.bc.ca/AriseReports/34200.PDF>> [October 2016].
- Madsen, J.K., Thorkelson, D.J., Friedman, R.M. and Marshall, D.D. (2006): Cenozoic to Recent plate configurations in the Pacific Basin: ridge subduction and slab window magmatism in western North America; *Geosphere*, v. 2, no. 1, p. 11–34.
- Massey, N.W.D., MacIntyre, D.G., Desjardins, P.J. and Cooney, R.T. (2005): Digital geology map of British Columbia – whole province; BC Ministry of Energy and Mines, BC

Geological Survey, GeoFile 2005-1, scale 1:1 000 000, URL <<http://www.empr.gov.bc.ca/Mining/Geoscience/PublicationsCatalogue/Geofiles/Pages/2005-1.aspx>> [November 2016].

Panteleyev, A. (1995): Porphyry Cu±Mo±Au; *in* Selected British Columbia Mineral Deposit Profiles, Volume 1 – Metallics

and Coal, D.V. Lefebure and G.E. Ray (ed.), BC Ministry of Energy and Mines, BC Geological Survey, Open File 1995-20, p. 87–92.

Surficial Geochemical Map Packages for British Columbia Porphyry Systems

C.J.R. Hart, Mineral Deposit Research Unit (MDRU), The University of British Columbia, Vancouver, BC, chart@eos.ubc.ca

S. Jenkins, Mineral Deposit Research Unit (MDRU), The University of British Columbia, Vancouver, BC

Hart, C.J.R. and Jenkins, S. (2017) Surficial geochemical map packages for British Columbia porphyry systems; *in* Geoscience BC Summary of Activities 2016, Geoscience BC, Report 2017-1, p. 159–164.

Introduction

The application of geochemical methods to surficial materials for the exploration and discovery of British Columbia (BC) porphyry deposits has resulted in many successes, but is fraught with challenges that contribute toward decreasing success in areas of cover. Porphyry systems themselves are invariably diverse, large and zoned; their geochemical signatures can vary considerably over large areas, depending on sample and survey location within the system. Post-mineralization dispersion of surficial materials by glacial, alluvial and mass-wasting processes further diffuses the signal. Additionally, the pedogenic processes involved in soil formation, such as oxidation, bio- and cryoturbation, leaching and hydromorphic dispersion, further contribute to modifying the geochemical signal and patterns.

Savvy explorers are well aware of these challenges, and tools have been developed to assist in their recognition. Geochemical-exploration models, for example, were first developed and presented by Bradshaw (1975) for deposits in the Canadian Cordillera and Canadian Shield. General, conceptual geochemical-exploration models (GEMs) were created for ore deposits in BC based on fundamental scientific principles and a limited number of case histories. These preliminary models summarized the potential controls on geochemical dispersal, and the expected results of the modified geochemical distributions. Subsequent efforts emphasized GEMs in volcanogenic massive-sulphide and shale-hosted Pb-Zn-Ag deposits in the Canadian Cordillera (Lett and Jackman, 2000; Lett, 2001; Lett and Bradshaw, 2003). Although it was recognized by Lett and Bradshaw (2003) that greater development and refinement of GEMs related to Cordilleran porphyry deposits was required, little progress was made and advances in the scientific literature were few.

This Geoscience BC-sponsored MDRU research project aims to create a framework to considerably expand on the conceptual models presented by Bradshaw (1975), by providing an abundance of spatially enabled data that can contribute toward the development of real and constrained, empirically defined geochemical-exploration models for BC porphyry deposits in various surficial environments. The largest step toward improving GEMs comprises the compilation and updating of information relevant to evaluating such models, which can be sourced from the accumulated historical exploration data from both industry and government sources.

The purpose of this project and these results is to provide the mineral-exploration community with easy access to surficial geochemistry data and related information that facilitates exploration and discovery of BC porphyry deposits. For a selected group of porphyry deposits, geochemical information available in print form has been compiled, digitized and updated to meet modern geospatial standards, and paired with spatial datasets related to the physiographic setting, glacial history, surficial materials and other geological factors that may influence geochemical distributions. Examples of how such data can be utilized to understand the importance of surficial process, terrain and climate in modifying the geochemical signals are provided in Blaine and Hart (2012).

Location Selection

Initially, 44 BC porphyry deposits were evaluated for this project according to a range of features related to their geographic and physiographic settings. These included pedogenic and geomorphic factors potentially affecting geochemical dispersions, such as the glacial history, the thickness and type of glacially derived cover, topography and climate. From these, 15 porphyry deposits and/or groups of deposits were selected as localities deserving of greater attention due to availability of Assessment Report Indexing System (ARIS) data (Table 1). These deposits are Brenda, Getty, Iron Mask region (contains Afton, Ajax and Galaxy deposits), Mount Polley, Primer, Mouse Mountain, Davidson, Louise Lake, Pitman, Hearne Hill and Morrison, Takla-Rainbow, Mount Milligan, Shaft Creek North, Alwin and Red Chris (Figure 1).

Keywords: *British Columbia, geochemical exploration model, surficial geochemistry, ARIS, geochemical survey, porphyry deposit, soil*

This publication is also available, free of charge, as colour digital files in Adobe Acrobat® PDF format from the Geoscience BC website: <http://www.geosciencebc.com/s/DataReleases.asp>.

Table 1: Classification of three major types of British Columbia porphyry deposits based on factors affecting surficial geochemical expression. Climatic factors include temperature (classified by the length of the frost-free period [ffp]), and precipitation (classified by the annual amount of non-snow precipitation [nsp]). Topographic factors include a general expression of relief (steep, moderate or slight). Deposits selected for delivery as geochemical-data compilations for this project are shown in bold text.

		Calc-Alkalic			Alkalic			Molybdenum		
Topography:		Steep	Moderate	Slight	Steep	Moderate	Slight	Steep	Moderate	Slight
Climate	Wet (nsp >500 mm)	Ok North, Hushamu	Louise Lake	Gambier Island	Kena Gold, Kena (Gold Mountain)	-	-	Pitman	-	-
	Dry (nsp <500 mm)	Hearne Hill, Indata, May, Morrison, Schaft Creek	Brenda, HED, Poplar, Highmont, Alwin	Getty South, Jean	Mt. Polley, Mt. Milligan, Col	Getty, Mouse Mtn., Primer	Ajax, Galaxy, Woodjam	Carmi Mo, Davidson, Stewart	Mineral Hill	-
	Wet (nsp >500 mm)	Taseko, Huckleberry, New Nanik, Whiting Creek	-	-	-	-	-	-	-	-
	Dry (nsp <500 mm)	Takla-Rainbow, Kemess, Red Chris	Gnat Pass, Eaglehead	-	Chuchi Lake	-	-	Storie	-	-

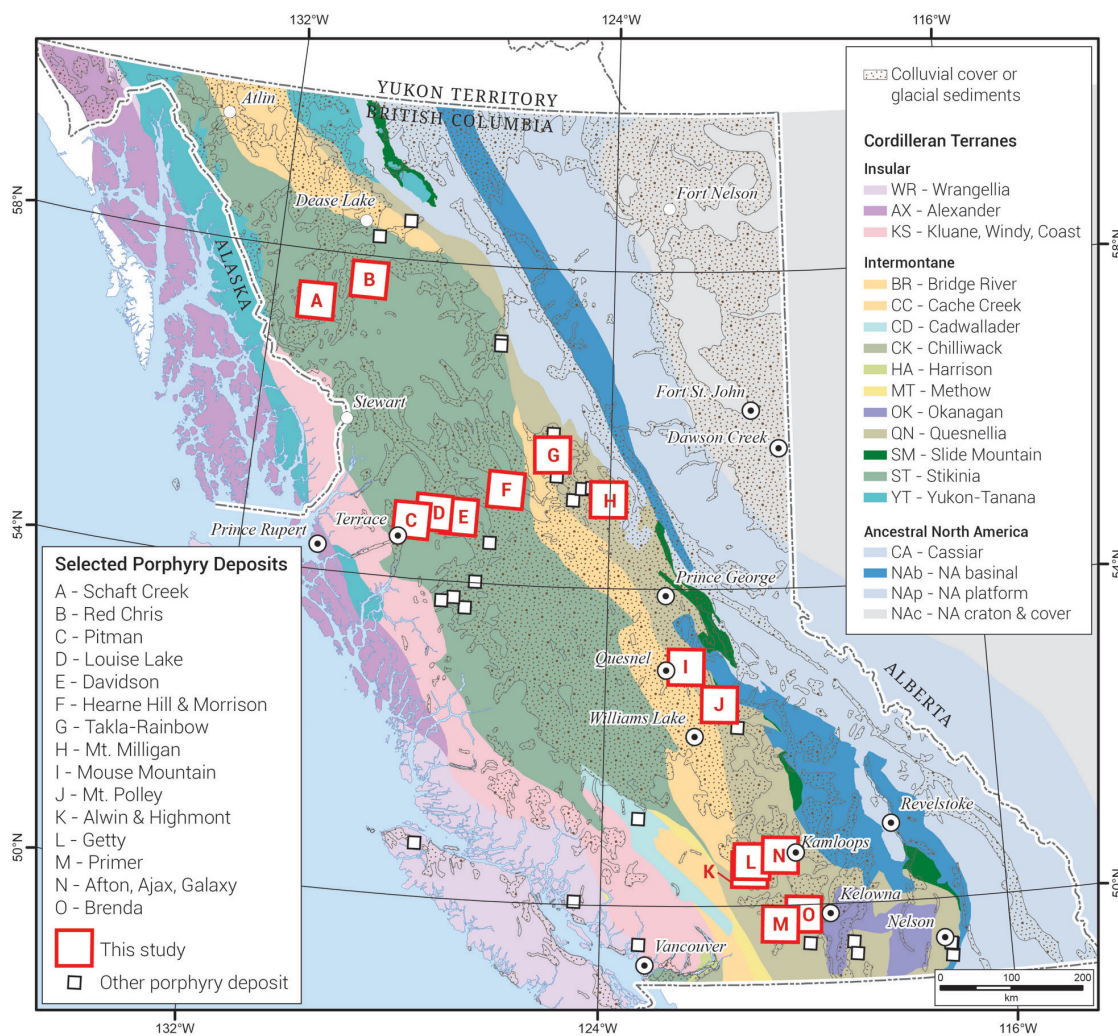


Figure 1: British Columbia porphyry deposits evaluated for this project (white squares with black or red borders) and those selected for geochemical-data compilations (white squares with red border), shown in reference to the distribution of Quaternary glacial deposits and older cover, as well as major terrane boundaries (Colpron and Nelson, 2011). Label refers to the legend key and to the name of the geochemical-data compilation associated with this project (e.g., Schaft Creek is package 2016-15-A).

Capturing Archival Data

Geochemical-sample data have been captured from many industry and government sources, including regional geochemical surveys carried out by the Geological Survey of Canada (Lett, 2011) and the BC Geological Survey (BCGS); the results of updated sampling and archival-sample analysis available from Geoscience BC; deposit- and area-specific studies carried out by the BCGS and Geoscience BC; and historical geochemical data generated through exploration by industry.

The primary source for the geochemical data compiled in this study is the ARIS archives, maintained by the BC Ministry of Energy and Mines. The ARIS documents are generally stored as scanned-to-PDF documents and vary widely in scan quality. Data of good quality for the selected deposits were retrieved through optical character recognition

(OCR) of the scanned PDF documents and manually reviewed for errors, or entered into tables manually. Where text quality of the scanned document was too poor to determine the values, they were entered as null values.

This process resulted in the creation of approximately 50 000 spatial data points pertaining to individual geochemical samples for the 15 selected porphyry deposits shown in Figure 1. Compiled geochemical data were then re-projected into either geographic (latitude and longitude) or UTM co-ordinate systems for ease of use and to provide internal spatial confidence. The breakdown of these data by sample type is given in Table 2.

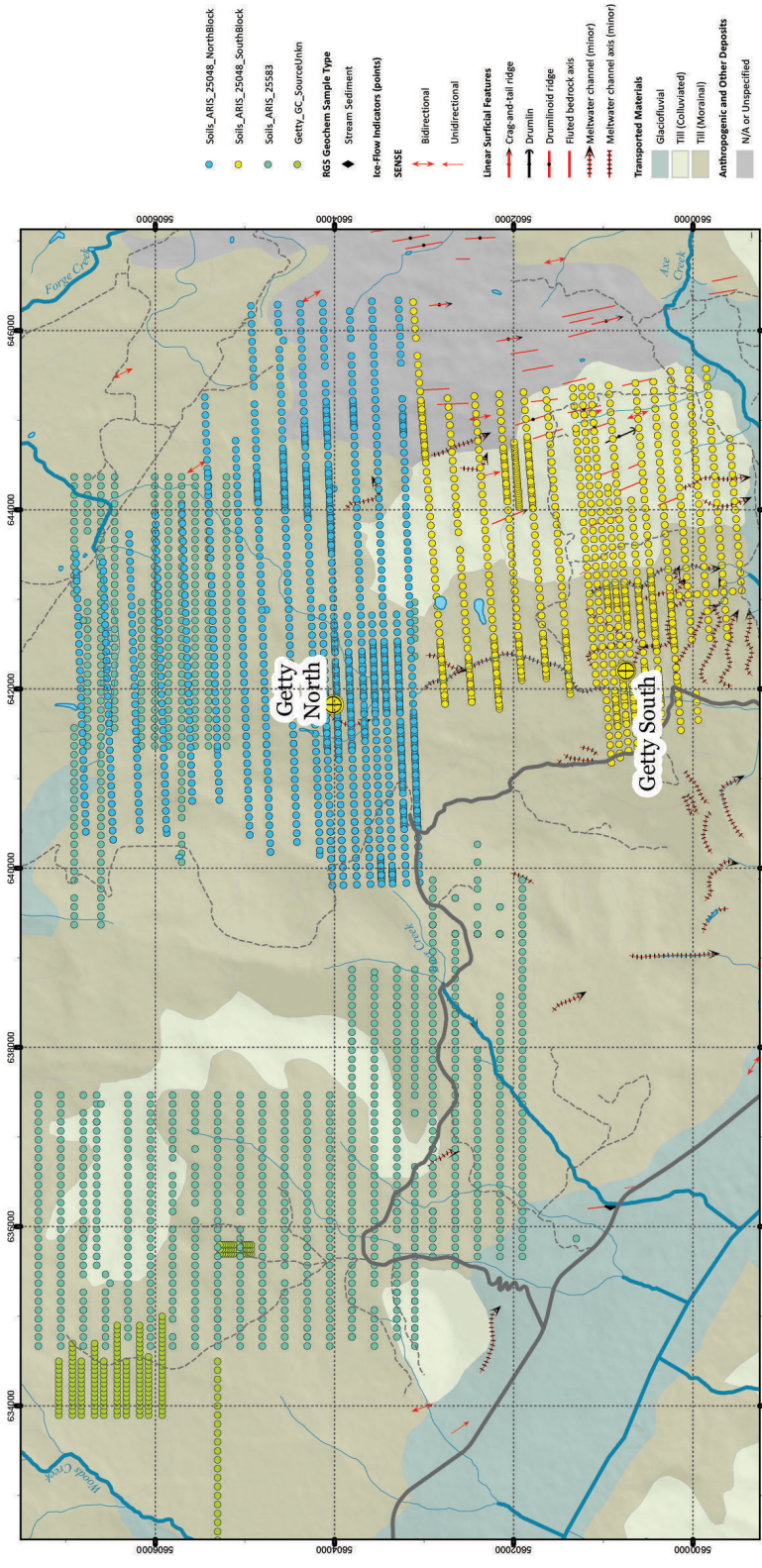
Products

Following geochemical-data compilation, additional relevant datasets were integrated with the geochemical data and packaged as self-extracting ArcGIS® map packages

Table 2: Distribution of sample type within the Assessment File Indexing System (ARIS) datasets digitized for each porphyry deposit in the GIS map packages. Abbreviation: BLEG, bulk leach extractable gold.

Compilation	Porphyry	Data source	Sample type											
			Soil	Silt	Stream sediment	Moss mat	Lake sediment	Till or outwash	Rock	Grab	Vegetation	BLEG	Unclear	
A	Schaft Creek	ARIS RGS (Lett, 2011)	183									17		
B	Red Chris	ARIS RGS (Lett, 2011)	2463											
C	Pitman	ARIS RGS (Lett, 2011)	872											
D	Louise Lake	ARIS RGS (Lett, 2011)	1101	534				22						
E	Davidson	ARIS RGS (Lett, 2011)	446					50						
F	Hearne Hill & Morrison	ARIS RGS (Lett, 2011)	807						1228					
G	Takla-Rainbow	ARIS RGS (Lett, 2011)	19701		1978	165			1275	1751				8
H	Mt. Milligan	ARIS RGS (Lett, 2011) Other sources	2519	32	59			606			121		133	33
I	Mouse Mtn	ARIS RGS (Lett, 2011)	3403							1	15	2		2
J	Mt Polley	ARIS RGS (Lett, 2011) Other sources	5625						85					
K	Alwin & Highmont	ARIS RGS (Lett, 2011)	712										100	
L	Getty	ARIS RGS (Lett, 2011) Other sources	4298											318
M	Primer	ARIS RGS (Lett, 2011)	1151											
N	Afton, Ajax & Galaxy	ARIS RGS (Lett, 2011)	2403		27			3	341					
O	Brenda	ARIS RGS (Lett, 2011)	3788											

SURFICIAL GEOCHEMISTRY OF THE GETTY PORPHYRY DEPOSIT, BRITISH COLUMBIA, CANADA



- Solt_ARIS_25048_NorthBlock
 - Solt_ARIS_25048_SouthBlock
 - Solt_ARIS_25583
 - Getty_GC_Sources/Units
- RGS Geochem Sample Type**
- ◆ Stream Sediment
- Ice-Flow Indicators (points)**
- SENSE**
- ↔ Bidirectional
 - Unidirectional
- Linear Surficial Features**
- Crag-and-tail ridge
 - Drumlin
 - Drumlinoid ridge
 - Fluted bedrock axis
 - Melwater channel (minor)
 - Melwater channel axis (mmor)
- Transported Materials**
- Glaciifluvial
 - Till (Colluviated)
 - Till (Morainal)
- Anthropogenic and Other Deposits**
- N/A or Unspecified

Surficial Geochemistry of the Getty Porphyry Deposit, British Columbia, Canada

Version: 07/05/2016, 07/10/11

Fred Blaine, Sara Jenkins and Craig E. Hart
MDRU - Mineral Deposit Research Unit
The University of British Columbia

1:50,000

MAP SPECIFICATIONS

Coordinate System: NAD 1983 UTM Zone 10N
 Projection: Transverse Mercator
 Datum: North American 1983
 Units: Meter
 Printing Date: 08/11/2016

SUGGESTED CITATION

Blaine, F., Jenkins, S., and Hart, C.E., 2016. Surficial geochemistry of the Getty Porphyry Deposit, British Columbia, Canada. Geoscience BC Report 2016-15-L. MDRU - Mineral Deposit Research Unit, The University of British Columbia. Available at: <http://www.geosciencebc.com/s2009-048.asp>

CONTACT

MDRU - Mineral Deposit Research Unit
 The University of British Columbia
 2020 - 2207 Main Mall
 Vancouver BC V6T 1Z4 Canada
 Ph: +1-604-822-6138
 Email: mdru@geos.ubc.ca
<http://www.mdr.u.ubc.ca/>

MAP DOCUMENTATION

The surficial geochemistry data were obtained, digitized and compiled here from various sources. Most of the soil geochemical data were captured from historical assessment reports filed with the Ministry of Energy, Mines and Petroleum Resources of British Columbia's ARIS system, and other public data sources.

This map and related data and map products are results from the "Geochemical Models for BC Porphyry Deposits: An Integrating, Blind and Banded Example" project conducted by MDRU and funded by Geoscience BC (Project 2009-048) and Gabriel Barbosa da Silva. Source information for the various data provided in this map package can be found in the accompanying Project Documentation file.

Although all attempts have been made to ensure that the information provided herein is valid, due to the historical nature of most of the geochemical data, neither Geoscience BC nor MDRU can be held responsible for the accuracy of the data or their use in this or any derivative products.

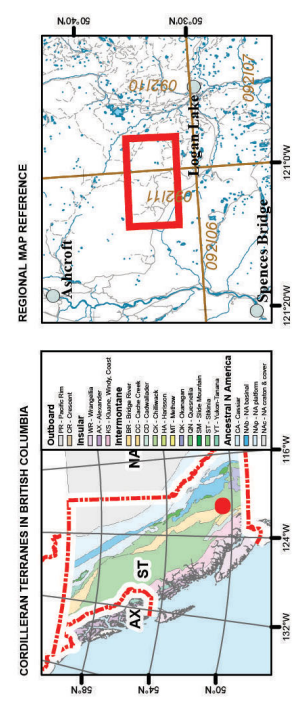


Figure 2: Surficial geochemistry of the Getty porphyry deposit, as an example of a self-extracting map package that is designed to be displayed or printed in 11 x 17 inch format. Features and text displayed here are representative and not intended to be utilized.

(.mpk) to allow users to undertake their own interpretations of geochemical signatures based on interrelated influences of physiography, geology, mineralization, surficial materials and glacial history at each porphyry deposit (Figure 2). For these packages, all GIS layers have been clipped to an area of 50 by 50 km around the deposit or group of deposits, but the maps are best displayed at the scale that incorporates the range of compiled soil-geochemical data. Users ultimately have the flexibility to view at whatever scale they wish.

Additional layers for each map package vary depending on availability of data at the highest level of detail, and may include

- digital elevation data and rendered hillshade images built from 30 m images resampled to 12 m resolution (Alaska Satellite Facility, 2015);
- National Topographic System (NTS) 1:50 000 scale gridlines and UTM zones;
- bedrock geology and faults (Colpron and Nelson, 2011; Cui et al., 2015);
- surficial geology (Fulton, 1995; Hashmi et al., 2015; Plouffe and Ferbey, 2015);
- glacial indicators (Ferbey et al., 2013);
- soils (BC Ministry of Environment, 2015);
- hydrological features (BC Ministry of Forests, Lands and Natural Resource Operations, 2016);
- geophysical imagery from various sources;
- scanned geological maps from assessment reports; and
- cultural and transportation information sourced from OpenStreetMap contributors (2016).

The packages open as a fully symbolized ArcGIS map project at a fixed scale (between 1:24 000 and 1:75 000), and display in a format suitable for printing on ledger/tabloid (11 by 17 inch) paper. Metadata for each layer are populated according to the ISO 19139 Metadata Implementation Specification.

Packages are accompanied by tabulated files (.xlsx) of geochemical data with map co-ordinates for manipulation outside ArcGIS; Geological Survey of Canada (GSC) fonts and layer files for third-party reproduction of symbologies in map packages; and a report summarizing the work conducted on the project, with a full list of ARIS reports and references for each map package. The project will also deliver georeferenced TIFF and PDF exports of the maps to ensure broad usability within the exploration sector. These files are available for download from the [Project 2009-048: Geochemical Models for BC Porphyry Deposits: Outcropping, Blind and Buried Examples](#) page of the Geoscience BC website.

Please note that, although reasonable efforts have been made to ensure that the data presented are of the highest quality, there may be errors due to the historical nature of

the data, transcription and OCR errors, and spatial re-projections necessary to provide the data in modern GIS formats. Neither Geoscience BC, MDRU nor the authors assume any liability for the correctness of the data or decisions based upon its use.

Conclusion

The success or failure of a geochemical exploration program designed to discover a porphyry Cu system can depend on the practitioner's ability to interpret the data and effectively drill targets. Understanding how geochemical signatures respond and are modified according to various physiographic, glacial, pedogenic, climatic and related features is essential to effective exploration decision-making. Datasets provided as part of this project offer the ultimate, made-in-BC opportunity for geologists to discover and understand the various controlling features related to surficial geochemical responses and patterns.

References

- Alaska Satellite Facility (2015): ALOS PALSAR_Radiometric_Terrain_Corrected_hi_res; Alaska Satellite Facility (ASF) Distributed Active Archive Center (DAAC), ALOS PALSAR Global Radar Imagery, 2006–2011 (includes material © JAXA/METI 2007), doi:10.5067/jbyk3j6hfsvf [August 2016].
- BC Ministry of Environment (2015): British Columbia soil mapping spatial data (a compilation of digital soil mapping datasets); BC Ministry of Environment, Environmental Stewardship Division, URL <http://www.env.gov.bc.ca/esd/distdata/ecosystems/Soil_Data/SOIL_DATA_FGDB/> [August 2016].
- BC Ministry of Forests, Lands and Natural Resource Operations (2016): Freshwater atlas – lakes; GeoBC, <<https://catalogue.data.gov.bc.ca/dataset/freshwater-atlas-lakes>> [December 2016].
- Blaine, F.A. and Hart, C.J.R. (2012) Geochemical-exploration models for porphyry deposits in British Columbia; *in* Geoscience BC Summary of Activities 2011, Report 2012-1, p. 29–40, URL <http://www.geosciencebc.com/i/pdf/summaryofactivities2011/soa2011_blaine.pdf> [November 2016].
- Bradshaw, P.M.D. (1975) Conceptual models in exploration geochemistry – the Canadian Cordillera and Canadian Shield; *Journal of Geochemical Exploration*, v. 4. p. 1–213.
- Cui, Y., Miller, D., Nixon, G. and Nelson, J. (2015): British Columbia digital geology; BC Ministry of Energy and Mines, BC Geological Survey, Open File 2015-2, URL <<http://www.empr.gov.bc.ca/Mining/Geoscience/Publications/Catalogue/OpenFiles/2015/Pages/2015-2.aspx>> [November 2016].
- Colpron, M. and Nelson, J.L. (2011): A digital atlas of terranes for the northern Cordillera; BC Ministry of Energy and Mines, BC Geological Survey, GeoFile 2011-11, URL <<http://www.empr.gov.bc.ca/mining/geoscience/publications/catalogue/geofiles/pages/2011-11.aspx>> [November 2016].
- Ferbey, T., Arnold, H. and Hickin, A.S. (2013): Ice-flow indicator compilation, British Columbia; BC Ministry of Energy and Mines, BC Geological Survey, Open File 2013-06, URL

- <http://www.empr.gov.bc.ca/mining/geoscience/publicationscatalogue/openfiles/2013/pages/2013-06.aspx> [November 2016].
- Fulton, R.J. (1995): Surficial materials of Canada; Geological Survey of Canada, Map 1880A, scale 1:5 000 000. doi:10.4095/205040
- Hashmi, S., Plouffe, A. and Ward, B.C. (2015): Surficial geology, Bootjack Mountain area, British Columbia, parts of NTS 93-A/5, NTS 93-A/6, NTS 93-A/11, and NTS 93-A/12; Geological Survey of Canada, Canadian Geoscience Map 209 (preliminary) or BC Geological Survey, Geoscience Map 2015-02, scale 1:50 000. doi:10.4095/296029
- Lett, R.E. (2001): Geochemical exploration models, volume 2: shale-hosted Pb-Zn-Ag deposits in NE BC; BC Ministry of Energy and Mines, BC Geological Survey, Open File 2001-7, 70 p. plus maps and appendices, URL <<http://www.empr.gov.bc.ca/mining/geoscience/publicationscatalogue/openfiles/2001/pages/2001-7.aspx>> [November 2016].
- Lett, R.E. (2011): Regional geochemical survey database; BC Ministry of Energy and Mines, BC Geological Survey, GeoFile 2011-07, URL <<http://www.empr.gov.bc.ca/mining/geoscience/publicationscatalogue/geofiles/pages/gf2011-7.aspx>> [November 2016].
- Lett, R.E. and Bradshaw, P. (2003): Atlas of landscape geochemical models for porphyry copper, VMS and gold deposits in the Cordillera from Alaska to Nevada; Association of Applied Geochemists, Explore newsletter, no. 118, p. 20–23.
- Lett, R.E. and Jackaman, W. (2000) Geochemical exploration models, volume 1: VMS deposits in south central BC; BC Ministry of Energy and Mines, BC Geological Survey, Open File 2000-31, URL <<http://www.empr.gov.bc.ca/Mining/Geoscience/PublicationsCatalogue/OpenFiles/2000/Pages/2000-31.aspx>> [November 2016].
- OpenStreetMap contributors (2016): British Columbia populated places and roads; Geofabrik GmbH, Karlsruhe, Germany, URL <<http://download.geofabrik.de/north-america/canada/british-columbia.html>> [November 2016].
- Plouffe, A. and Ferbey, T. (2015): Surficial geology, Gnawed Mountain area, British Columbia, parts of NTS 92-I/6, NTS 92-I/7, NTS 92-I/10, and NTS 92-I/11; Geological Survey of Canada, Canadian Geoscience Map 214 (preliminary) or BC Geological Survey, Geoscience Map 2015-3, scale 1:50 000. doi:10.4095/296285

Synthesis of U-Pb and Fossil Age, Lithochemical and Pb-Isotopic Studies of the Paleozoic Basement of the Quesnel Terrane in South-Central British Columbia and Northern Washington State

J.K. Mortensen, The University of British Columbia, Vancouver, BC, jmortensen@eos.ubc.ca

K. Lucas, The University of British Columbia, Vancouver, BC

J.W.H. Monger, Natural Resources Canada, Geological Survey of Canada–Pacific, retired

F. Cordey, Laboratoire de Géologie de Lyon, Lyon, France

Mortensen, J.K., Lucas, K., Monger, J.W.H. and Cordey, F. (2017): Synthesis of U-Pb and fossil age, lithochemical and Pb-isotopic studies of the Paleozoic basement of the Quesnel terrane in south-central British Columbia and northern Washington state; *in* Geoscience BC, Report 2017-1, p. 165–188.

Introduction

The Quesnel terrane underlies a large region in south-central and east-central British Columbia (BC), and extends both northward as a narrow fault-bounded sliver into south-central Yukon and southward into northern Washington state (Figure 1; Nelson and Colpron, 2007). The main defining feature of the Quesnel terrane in south-central BC is the Late Triassic Nicola arc assemblage and associated plutons (Figure 1), which have been well studied (e.g., Mortimer, 1987; Mihalynuk et al., 2014), not least because they host several large copper-porphyry deposits.

The basement rocks that unconformably underlie strata of the Nicola arc in this area are much less well understood (Monger, 1977). This basement includes a number of variably deformed and metamorphosed volcanic and sedimentary rock assemblages that include the Harper Ranch, Chapperon, Apex Mountain, Kobau, Knob Hill, Attwood and Anarchist groups. Paleozoic basement rocks of the Quesnel terrane are age equivalent with the Paleozoic Stikine assemblage in Stikinia (Nelson and Colpron, 2007). There has been considerable debate about whether the Quesnel terrane represents an allochthonous terrane that became attached to the edge of North America during Early Jurassic accretion, or comprises continental-margin-arc rocks and underlying Paleozoic basement that formed close to their present position with respect to the North American craton (e.g., Monger et al., 1991; Thompson et al., 2006).

A Geoscience BC-funded project was begun in 2010 aimed at better understanding the nature and origin of the Paleo-

zoic volcanic and sedimentary rocks that make up the basement of the Quesnel terrane in the southern Okanagan area of south-central BC, and contributing new information regarding the mineral potential of the region (Mortensen et al., 2011; Mortensen, 2014). The Paleozoic rocks in this part of the Cordillera were involved in Mesozoic compressional deformation, and early Cenozoic crustal extension has divided them into a series of blocks bounded by large normal faults (Parrish et al., 1988). In addition to the complex deformation, the basement assemblages have been intruded by extensive Late Triassic to Early Jurassic and younger plutonic suites, and are widely overlain by mainly Paleogene volcanic and sedimentary sequences. As a result, the basement rocks are now exposed in a number of scattered outcrop areas (Figure 1), making regional correlations difficult.

In addition, the basement rocks in this region have been the subject of little modern study, especially in the western part (Hedley–Keremeos–Osoyoos area), prior to this work and, although the general distribution of rock units is reasonably well defined by existing mapping, only limited fossil or U-Pb isotopic age information was available and the petro-tectonic affiliations of the Paleozoic igneous rocks were not well understood. The general geology of these areas has been documented or compiled at either 1:250 000 (Tempelman-Kluit, 1989) or 1:63 360 scales, although some mapping is quite dated (e.g., Bostock, 1939, 1940, 1941), and parts of the Greenwood and Rock Creek areas have been recently remapped at a 1:50 000 or 1:25 000 scale (e.g., Little, 1983; Church, 1985; Fyles, 1990; Massey, 2006, 2007; Massey and Duffy, 2008). Several small areas have also been the focus of these or other topical studies over the years (e.g., Okulich, 1969, 1973; Peatfield, 1978; Milford, 1984; Lewis et al., 1989; Ray and Dawson, 1994). Reconnaissance-scale lithochemical studies have been carried out on the basement rock units in the Greenwood–Rock Creek area (Dostal et al., 2001; Massey and Dostal, 2013a) and in adjoining portions of northern Washington state (Gaspar,

Keywords: *British Columbia, Quesnel terrane, Paleozoic, basement, volcanic, sedimentary, fossils, U-Pb, geochronology, lithochemistry, detrital zircons, VMS deposits, paleotectonic setting*

This publication is also available, free of charge, as colour digital files in Adobe Acrobat® PDF format from the Geoscience BC website: <http://www.geosciencebc.com/s/DataReleases.asp>.

2005). However, there has been no comprehensive study of the basement rocks and major questions still remain regarding the nature of rock units in the various areas of exposure, their ages and the tectonic setting(s) in which they formed.

Overview of Paleozoic Basement Rocks in the Southernmost Part of the Quesnel Terrane

Basement rocks in the Hedley–Keremeos–Osoyoos area (Figure 2) have been subdivided into several ‘assemblages’, based mainly on the relative proportions of volca-

nic (mainly variably altered basalt or ‘greenstone’ and associated intrusions) and sedimentary rocks (mainly chert, fine-grained clastic rocks and minor carbonate rocks). Note that the past and current usage of stratigraphic and litho-demic terms such as ‘assemblage’, ‘formation’, ‘complex’, in this region do not follow strict nomenclature guidelines as defined by the Lexicon of Canadian Geologic Units; however, the terms as currently in use have been retained to minimize confusion. In the Keremeos, Oliver and Okanagan Falls areas Bostock (1939, 1940, 1941) identified several lithological assemblages that he called formations,

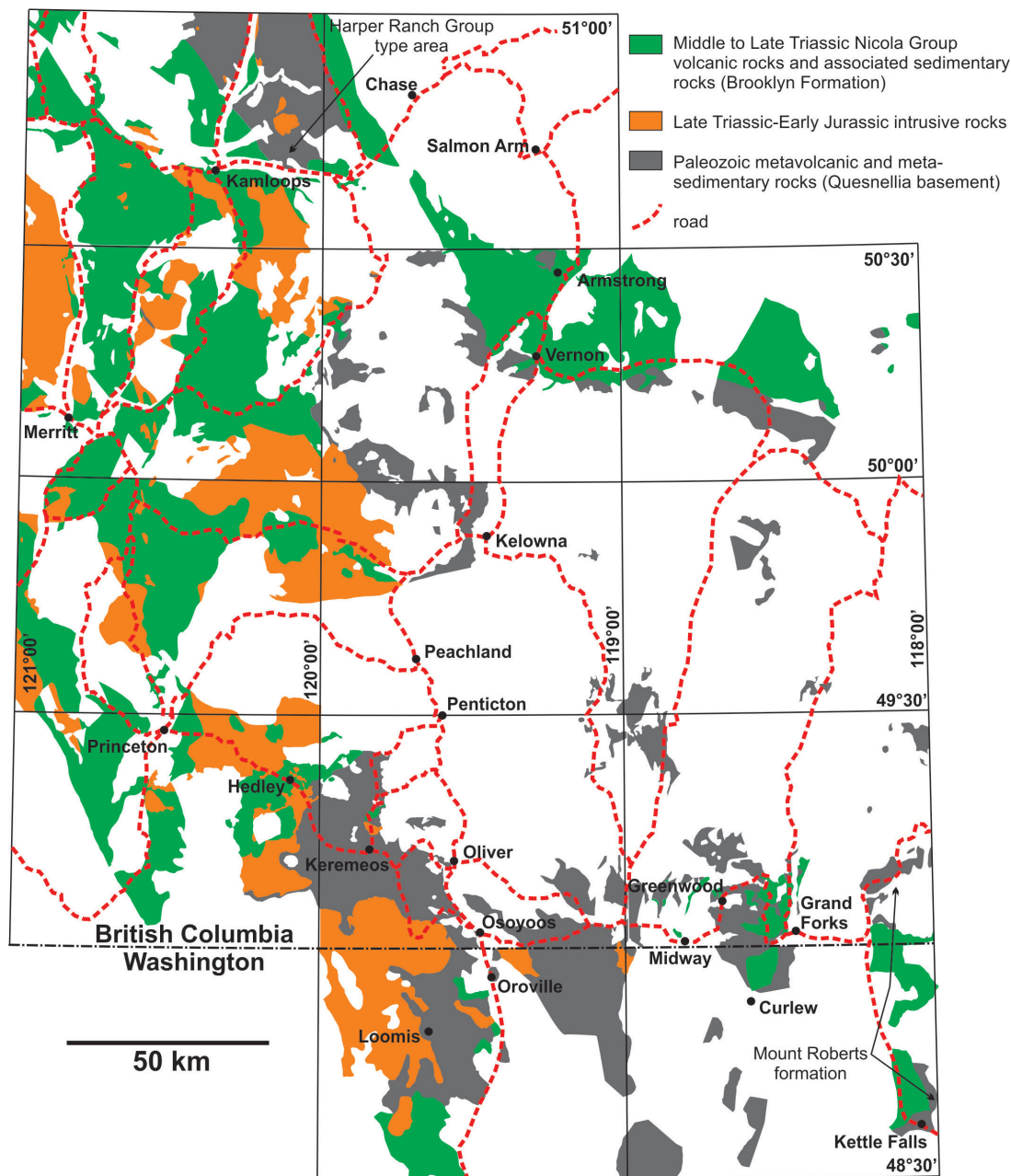


Figure 1. Distribution of Middle and Late Triassic volcanic and sedimentary rocks, Late Triassic and Early Jurassic intrusive rocks, and Paleozoic basement rocks of the Quesnel terrane in south-central British Columbia and northern Washington state.

including the Independence, Bradshaw, Old Tom, Shoemaker and Barslow, based mainly on the relative proportions of mafic volcanic and intrusive rocks, chert and clastic rocks. Rock assemblages that Bostock mapped as Independence and Bradshaw formations (Figure 2) were mainly derived from fine-grained clastic protoliths, locally interlayered with mafic volcanic-flow rocks. In the field, there was little basis on which to distinguish these assemblages one from the other, and they are therefore herein considered together. The Old Tom assemblage (mainly

greenstone plus minor mafic intrusive rocks and chert) and Shoemaker assemblage (mainly chert with minor greenstone) underlie much of the Keremeos area. The distinction between Independence–Bradshaw, Old Tom and Shoemaker is not clear in the area southwest of the Similkameen River between Hedley and Keremeos (Figure 2; Bostock, 1939; Monger, 1989; Tempelman-Kluit, 1989). The Barslow assemblage in the Cawston area (Figure 2) comprises fine- to locally coarse-grained clastic strata (including pebble and minor cobble conglomerate) with locally

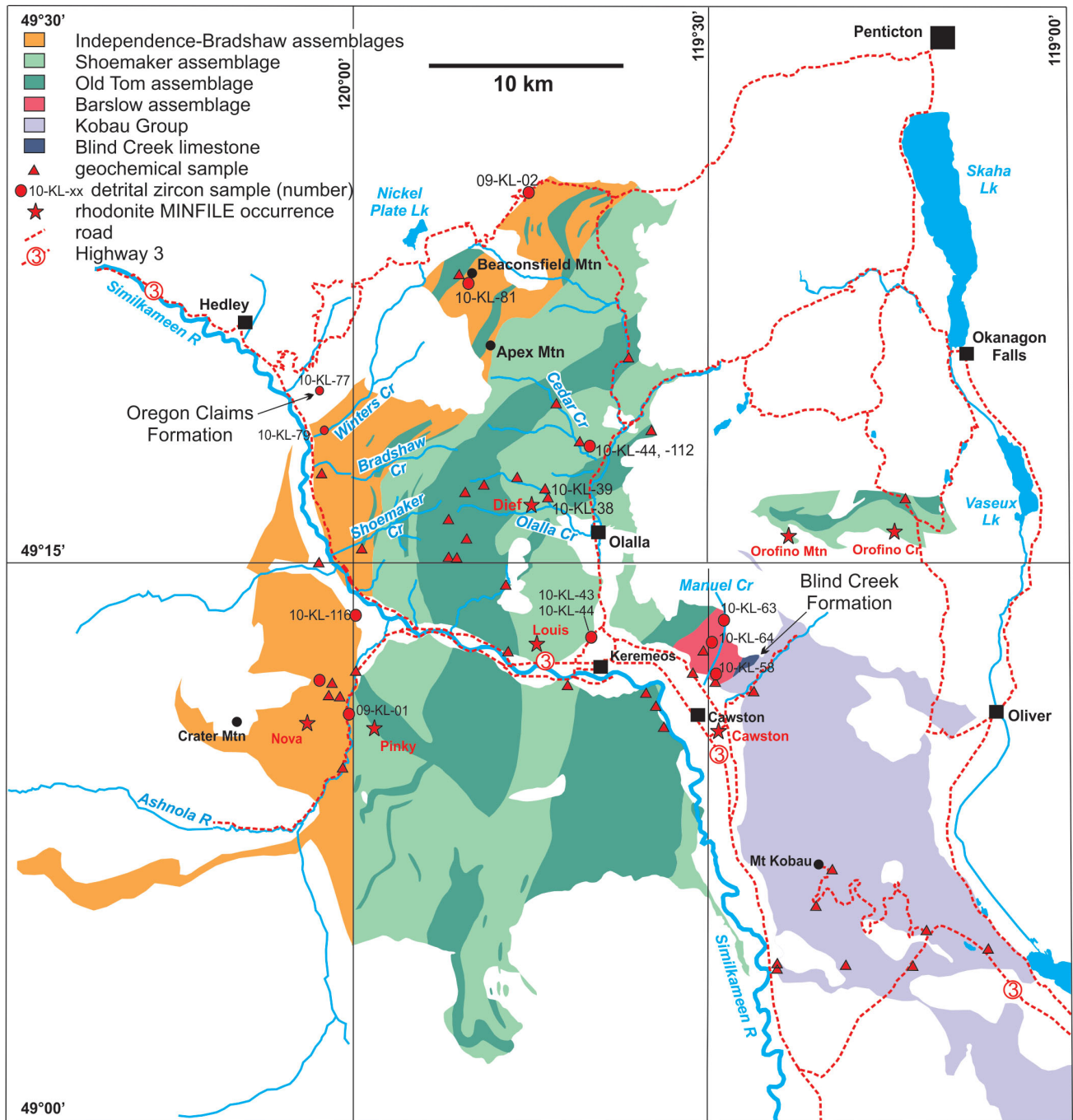


Figure 2. Simplified geology of the Hedley–Keremeos–Osoyoos area in south-central British Columbia. Abbreviations: Cr, Creek; Lk, Lake; Mt, Mount; Mtn, Mountain; R, River.

interlayered greenstone. Milford (1984), in his study of the Apex Mountain area, lumped all but the Barslow assemblage into a single unit that he termed the Apex Mountain Group (later renamed the Apex Mountain Complex by Monger, 1989), a term that was also subsequently used by Ray and Dawson (1994). Farther to the east, the Kobau Group (Figure 2) of Bostock (1939), Okulich (1969, 1973), Lewis et al. (1989) and Tempelman-Kluit (1989) consists of more strongly metamorphosed and deformed mafic volcanic rocks (now amphibolite) and fine-grained quartzite that probably was derived mainly from a chert protolith. A sequence of mafic tuffs and flows, together with sandstone, siltstone, argillite and minor polymictic conglomerate and carbonate rock, that immediately underlies the Late Triassic volcanic and sedimentary rocks of the Nicola Group in the Hedley area (Figure 2) has been called the 'Oregon Claims formation' (Figure 2) by Ray et al. (1994, 1996). Although the age of this assemblage is unknown at this time, Ray et al. (1996) considered it to be part of the Paleozoic Apex Mountain Complex.

The nature of the contacts between the various lithological assemblages is uncertain. In some cases it appears to be gradational (e.g., the Old Tom assemblage could simply represent a facies of the Shoemaker assemblage). However, there is some evidence for fault imbrication within the Old Tom and Shoemaker assemblages; for example, on Shoemaker Creek just west of Keremeos (Figure 2; see later discussion).

A large composite body of massive to bedded limestone termed the 'Blind Creek limestone' (Figure 2; Bostock,

1939; Barnes and Ross, 1975) that is in fault contact with the Old Tom, Barslow and Kobau assemblages near Cawston (Figure 2) has yielded numerous robust Carboniferous fossil ages and overlaps in age with at least some of the other basement rock units in the area, although the original stratigraphic relationships between this limestone body and adjacent rock packages are uncertain.

Farther to the east, Paleozoic basement rocks between the Okanagan Valley and Grand Forks (Figure 3) occur within a series of north-dipping thrust panels, with the intervening thrust surfaces commonly marked by the presence of thin tectonic slices of serpentinite, all cut and offset by numerous Eocene normal faults (Figure 3; Fyles, 1990; Massey, 2007; Massey and Duffy, 2008; Massey and Dostal, 2013a). Three main lithological assemblages have been distinguished in this area. The Knob Hill Complex in the Greenwood area comprises mafic volcanic flows and locally abundant diabase and gabbro intrusions, together with subordinate amounts of interlayered chert, chert breccia and argillite. The two other assemblages, the sedimentary Attwood Group near Greenwood and the more metamorphosed Anarchist Schist, exposed mainly between Rock Creek and the Okanagan Valley, consist mostly of metasedimentary rocks. The interpreted areal distribution of these two groups has changed considerably over the last two decades. Church (1985) and Fyles (1990) included all of the sediment-dominated basement rocks in the Greenwood area in the Attwood Group, whereas Anarchist Schist was reserved for the more metamorphosed metasedimentary packages. Massey and Duffy (2008) redefined the An-

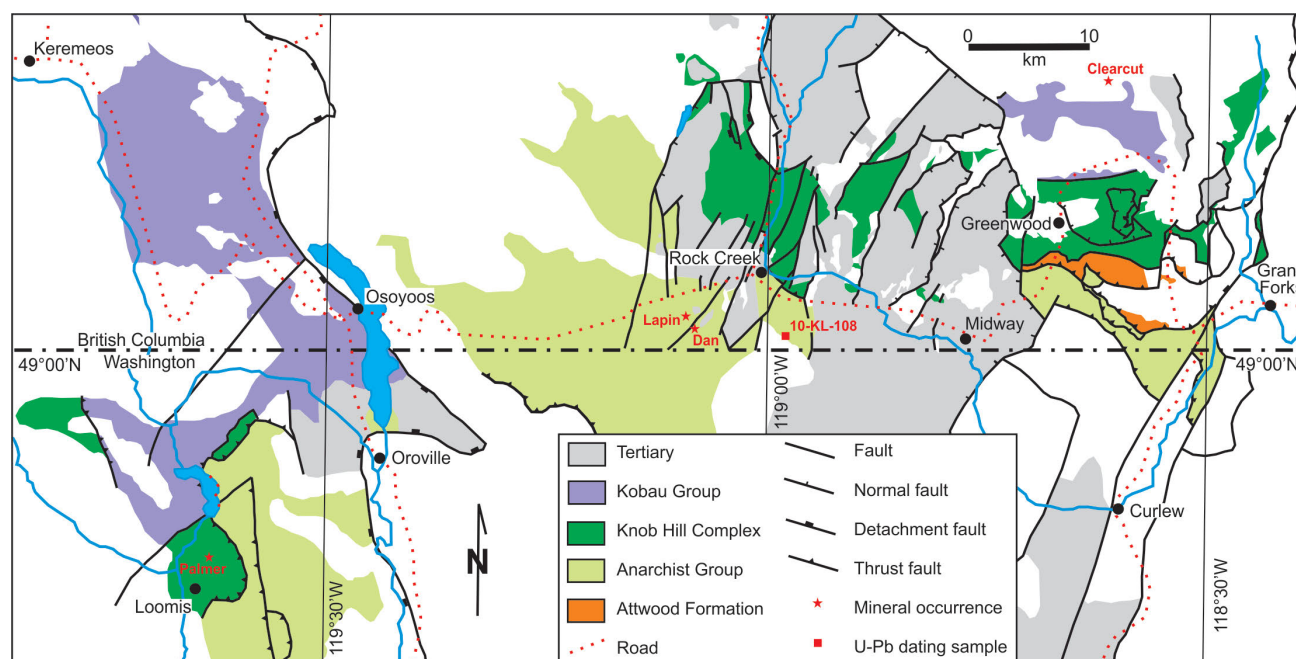


Figure 3. Distribution of, and structural relationships between, Paleozoic assemblages in the southern part of the Quesnel terrane between Keremeos and Grand Forks (modified from Massey and Dostal, 2013a).

archist Schist as the ‘Anarchist Group’, and included most of the metasedimentary rock units previously mapped as Attwood in this more regionally extensive package (Figure 3). The term ‘Attwood Formation’ is now restricted by Massey and Dostal (2013a) to a package of argillite, siltstone, greywacke and sandstone, with locally abundant limestone, chert-pebble conglomerate and minor mafic volcanic rocks, in a small area southeast of Greenwood (Figure 3). The Anarchist Group, as now defined, comprises chert, argillaceous chert and argillite, with minor interlayered mafic flows and tuffs, limestone, and rare felsic tuff. The Mount Roberts Formation east of Grand Forks (Figure 1; Roback and Walker, 1995) comprises metaclastic rocks that may be correlative with the Anarchist Group.

A large area in northern Washington state near Loomis and Oroville (Figure 3) is underlain by mafic volcanic and metaclastic rocks that have been variably correlated with the Knob Hill, Anarchist and Kobau groups (e.g., Cheney et al., 1994; Massey and Dostal, 2013a). The ‘Palmer Mountain greenstone’ north of Loomis (Figure 3) consists of mafic volcanic and volcanoclastic rocks together with gabbro and serpentinite (Rinehart and Fox, 1972) that lithologically closely resemble the Knob Hill Complex (e.g., Massey and Dostal, 2013a) or possibly the Old Tom assemblage.

Biochronology

A limited number of macro- and microfossil ages were available for the Paleozoic basement rocks in the southernmost part of the Quesnel terrane prior to this study. During this study, extensive sampling of chert for radiolarian and/or conodonts was carried out to better constrain the age of the various assemblages present. Although chert in many localities in the study area contains visible radiolarians, in most cases these fossils are too recrystallized to give confident age determinations. A total of eight limestone samples were processed for possible conodonts; however, all proved to be barren. A small number of new localities did produce reliable radiolarian or conodont ages, and resampling of some localities that had previously given preliminary age determinations yielded more confident age assignments. One locality also produced a reliable macrofossil age assignment. All of the new fossil ages produced during this study are listed in Table 1 and these results are summarized below, along with previous fossil information from the region.

The only fossil age constraints available thus far for rock units that are unequivocally part of the Independence–Bradshaw assemblage are from three collections of brachiopods and tentaculitids from a single locality northeast of Highway 3 between Shoemaker and Bradshaw creeks, 10 km southeast of Hedley (Figure 2), that gave Cambrian to Devonian, Devonian, and mid-Early to early Late Devo-

nian (Pragian–Frasnian) ages (Dawson, 1994; Ray and Dawson, 1994). A crinoidal limestone located 3.5 km east of Crater Mountain, north of the Ashnola River (Figure 2), that is interlayered with argillite, sandstone, and minor chert pebble conglomerate and greenstone, is herein tentatively correlated with the Independence–Bradshaw assemblage and gave a Middle Devonian (late Eifelian to early Givetian) conodont age (identified by M.J. Orchard in Nebocat, 1996).

The Old Tom and Shoemaker assemblages have produced a number of fossil ages. A Middle Devonian age (M.J. Orchard, unpublished data, 2006) was obtained for ichthyoliths and conodonts from a limestone interlayered with greenstone and chert of the Old Tom and Shoemaker assemblages 4 km northeast of Olalla (Figure 2; W.R. Danner, unpublished data, 1987). A thinly laminated red radiolarian chert that occurs as a large local talus block on the northern side of Highway 3 about 2 km west of Keremeos (Figure 2) gave a Late Devonian (middle–late Famennian) conodont age (this study; Cordey, 1998; see Table 1). Late Devonian to Mississippian and Pennsylvanian to Permian radiolarian ages were also obtained from grey chert at several localities above the Keremeos garbage dump site, 1 km north of Keremeos, and on the mountain top approximately 3 km northwest of Keremeos (this study; Table 1).

Three localities within the Old Tom and Shoemaker assemblages yielded somewhat puzzling fossil age results. On Shoemaker Creek north of the Similkameen River, 13.5 km northwest of Keremeos (Figure 2), two lenses of limestone that either overlie, or are stratigraphically or structurally interlayered with mainly chert at, or near, the mapped contact between the Independence–Bradshaw and Shoemaker assemblages (Bostock 1939), yielded Middle to Late Triassic (late Ladinian to early Carnian) conodont ages (Read and Okulitch, 1977; Milford, 1984). However, this same limestone also locally contains Silurian corals and Carboniferous foraminifera, both of which are considered to represent reworked fossils incorporated from older, as yet unidentified rock units in the immediate area. Read and Okulitch (1977) interpreted the Triassic rocks on Shoemaker Creek to be small erosional remnants of Triassic clastic rocks that were deposited unconformably on top of the Old Tom or Shoemaker units. An alternative interpretation is that the Triassic rocks are fault-bounded bodies that were imbricated with the Paleozoic rocks during Jurassic folding and thrust faulting. At another locality on the western side of the Similkameen River, approximately 6 km south of Cawston (Figure 2), Tempelman-Kluit (1989) reports a Middle Triassic (Ladinian) conodont age from an argillaceous limestone at a locality that is mapped as being within the Shoemaker assemblage. The presence of these Triassic rock units apparently within the Old Tom and/or

Table 1. New fossil age determinations from the Old Tom, Shoemaker and Barslow assemblages in the Hedley–Keremeos–Cawston area.

Field number	Collector	Zone	UTM		Location	Rock unit	Description	Fossil type	Age
			Northing	Easting					
K10-01 ¹	Cordey, F	11	287494	5460776	Olalla Creek, float	Old Tom-Shoemaker	Red chert	Conodonts	Latest Devonian to Mississippian
K10-02 ¹	Cordey, F	11	286955	5459885	Olalla Creek, float	Old Tom-Shoemaker	Red chert	Radiolarians	Late Paleozoic
K10-03 ¹	Cordey, F	11	286557	5459966	Olalla Creek, float	Old Tom-Shoemaker	Red chert	Radiolarians	Late Paleozoic
K10-05 ¹	Cordey, F	11	289210	5460384	Olalla Creek, in situ	Old Tom-Shoemaker	Grey ribbon chert	Radiolarians	Probably Mississippian
K10-09 ¹	Cordey, F	11	291316	5454405	Float block in talus sheet ~2 km west of Keremeos	Old Tom-Shoemaker	Red chert	Conodonts	Late Devonian to middle-late Famennian
K07-05 ¹	Cordey, F	11	293338	5455818	Above Keremeos dump site, in situ	Old Tom-Shoemaker	Grey chert	Radiolarians	Pennsylvanian to Permian
K07-07 ¹	Cordey, F	11	293517	5455870	Above Keremeos dump site, in situ	Old Tom-Shoemaker	Grey chert	Radiolarians	Late Devonian to Mississippian
K07-23 ¹	Cordey, F	11	291200	5456040	Top of mountain 3 km northwest of Keremeos, in situ	Old Tom-Shoemaker	Grey chert	Radiolarians	Possibly Mississippian
K10-12 ¹	Cordey, F	11	293244	5455470	Above Keremeos dump site, in situ	Old Tom-Shoemaker	Grey chert	Conodonts, radiolarians	P'robably Late Devonian or Mississippian (conodonts); Mississippian (radiolarians)
K10-15-8 ¹	Cordey, F	11	298683	5454383	Float block in talus sheet north of Cawston	Barslow	Green chert	Conodonts	Likely Late Mississippian or Pennsylvanian
10-KL-60 ²	Monger, JWH	11	298738	5454102	3.5 km due north of Cawston; float at bottom of talus cone	Barslow	Fossiliferous argillite, crinoid-bearing limestone	Brachiopods	Early Carboniferous, probably Tournaisian

¹Sample processing and fossil identification by F. Cordey, Laboratoire de Géologie de Lyon, Université Claude Bernard, Lyon, France

²Fossil identification by W. Bamber, Geological Survey of Canada-Calgary, Calgary, Alberta

Shoemaker assemblages led Tempelman-Kluit (1989) to assign a probable Triassic age to all of these units. More detailed examination of both localities is needed to resolve these problems.

On Cedar Creek approximately 3 km north of Olalla (Figure 2), a large block of limestone within an area mapped as Shoemaker assemblage yielded Middle to Late Ordovician conodont ages (Pohler et al., 1989). Red radiolarian chert on Olalla Creek approximately 3 km southwest of the Cedar Creek locality gave latest Devonian to Mississippian conodonts and probably Mississippian radiolarians (this study; Table 1). Tempelman-Kluit (1989) and Orchard (1993) also reported a Mississippian conodont age from a nearby locality on Olalla Creek. It thus appears that the Shoemaker assemblage in this area is mostly of Late Devonian to Mississippian age, and the Ordovician limestone body is interpreted to be either a large olistolith contained within argillite and sandstone of the Shoemaker assemblage, or alternatively it could be a thrust-fault-bounded body that was structurally imbricated with the Shoemaker rock units. Either of these interpretations is complicated by the fact that there are no known limestone of Ordovician age anywhere west of the Rocky Mountains in BC, from which the limestone block could have been sourced.

The Blind Creek limestone unit (Figure 2) has given consistent Middle Mississippian to Early Pennsylvanian conodont ages from numerous samples (Barnes and Ross, 1975; Tempelman-Kluit, 1989; Orchard, 1993). The Barslow assemblage in the Cawston area (Figure 2) contains a heterogeneous clastic package, including pebbles and cobbles of crinoidal limestone, brachiopod-bearing argillite and chert, as well as greywacke with well-preserved plant fossils. A chert clast gave a probably Late Mississippian or Pennsylvanian conodont age (this study; Table 1) and brachiopods from an argillite layer that included abundant brachiopod fragments and wood debris gave an Early Carboniferous, probably Tournaisian, age (this study; Table 1).

The high degree of strain and strong metamorphic recrystallization that has affected the Kobau Group precludes any possibility of preservation of fossils. Middle to Late Devonian conodont ages have been obtained from the lower part of the Knob Hill Complex (Orchard, 1993; note that this same limestone bed had previously been interpreted as “Carboniferous or Permian” by Little, 1983, based on corals and bryozoans), and chert in the upper part of the Group has given a Late Pennsylvanian or earliest Permian radiolarian age (identified by F. Cordey in Massey, 2007). The Anarchist Group has not yet yielded any fossil ages; however, a number of collections of brachiopods, crinoids, corals and bryozoans from the Attwood Group have given “Carboniferous or Permian” ages (Little, 1983). Limited fossil age constraints for the Paleozoic volcanic and sedimentary packages in adjacent parts of northern Washington

state include fusulinids of possible Early Permian age in the southeastern part of the Curlew quadrangle, approximately 30 km south of Grand Forks (Figure 3; Parker and Calkins, 1964), and fusulinids, corals, bryozoans, gastropods and crinoid of Early Permian age in the Marcus and Kettle Falls quadrangles, approximately 55 km south-southeast of Grand Forks (Figure 1; Mills and Davis, 1962; Mills, 1985). The latter locality has been included in the Mount Roberts Formation by Roback and Walker (1995).

U-Pb Geochronology

Rock Ages

Nearly all of the igneous rocks present within the Paleozoic basement of the Quesnel terrane in south-central BC are mafic in composition and only rarely contain igneous zircon; hence, there are very few rock units that can be dated using the U-Pb method. Massey et al. (2013) reported U-Pb zircon ages, ranging from 389 to 380 Ma (late Middle Devonian), for four separate samples of gabbro of the Knob Hill Complex in the Greenwood area. A quartz-muscovite schist unit sampled from the Anarchist Group south of Rock Creek (sample 10-KL-108; Figure 3) is interpreted to be a felsic metavolcanic rock, likely a metatuff. The sample yielded abundant clear, colourless, euhedral zircons. The analytical results are given in Table 2 and shown graphically in Figure 4. Nineteen zircon grains were analyzed using the laser ablation inductively coupled plasma-mass spectrometry method, as described in Massey et al. (2013). One grain gave a Paleoproterozoic age (2.33 Ga) and is clearly a detrital zircon that was incorporated into the sample. The remaining grains form one loose cluster between ~390 and 375 Ma, and a second, tight cluster at ~365 Ma. This younger cluster of seven analyses gives a weighted average $^{206}\text{Pb}/^{238}\text{U}$ age of 365.2 ± 1.0 Ma (MSWD = 0.02; probability of fit = 1.0), which is interpreted to be the crystallization age of the volcanic protolith for the sample. The older cluster represents somewhat older detrital (late Middle to early Late Devonian) zircons. One zircon grain gave a younger $^{206}\text{Pb}/^{238}\text{U}$ age (359 Ma), which is interpreted to be the result of post-crystallization Pb loss. The latest Devonian U-Pb zircon age reported here is the first depositional age that has ever been produced for rocks of the Anarchist Group.

Detrital Zircon Ages

A major goal of the present study was to use the ages of detrital zircons from clastic rock units within the various Paleozoic assemblages to constrain their depositional age, which cannot be older than the youngest significant detrital zircon age population present. In addition, the detrital zircon ages were used to evaluate linkages between the assemblages, and between them and the North American craton. This approach is particularly useful when there is no possibility of using fossil information to test such linkages. De-

Table 2. Results of U-Pb zircon analysis for a felsic metavolcanic rock of the Anarchist Group (sample 10-KL-108) in the Rock Creek area.

Fraction	Isotopic ratios					Isotopic ages (Ma)					Background corrected mean counts per second at specified mass									
	$^{207}\text{Pb}/^{235}\text{U}$	$1\sigma(\%)$	$^{206}\text{Pb}/^{238}\text{U}$	$1\sigma(\%)$	$^{207}\text{Pb}/^{206}\text{Pb}$	$1\sigma(\%)$	$^{207}\text{Pb}/^{235}\text{U}$	1σ	$^{206}\text{Pb}/^{238}\text{U}$	1σ	202	204	206	207	208	232	235	238		
Sample 10-KL-108 (UTM 355293E, 5430667N, Zone 11, NAD 83):																				
1	0.0066	0.44787	0.00694	0.06028	0.0003	0.32	27.86	375.8	4.87	377.3	1.81	15	50404	2732	11986	119868	3182	396780		
2	0.05367	0.00069	0.45656	0.00728	0.0609	0.32	28.66	381.9	5.07	381.1	1.85	0	26954	1473	5446	54746	1683	209992		
3	0.05501	0.00078	0.46334	0.00829	0.06222	0.32	31.3	386.6	5.75	389.1	2.16	22	28080	1572	7018	64770	1771	214051		
4	0.05348	0.0004	0.44854	0.00412	0.06092	0.32	16.87	376.3	2.89	381.2	1.12	8	86035	4682	27048	264512	5450	669784		
5	0.05378	0.00053	0.45243	0.00558	0.06048	0.32	22.3	379	3.9	378.5	1.46	19	60803	3326	16158	168476	3840	476715		
6	0.0533	0.00057	0.43242	0.00567	0.05832	0.33	23.89	364.9	4.02	365.4	1.5	32	0	45104	2443	10389	110069	366561		
7	0.05227	0.00075	0.44467	0.00791	0.06096	0.31	32.2	373.5	5.56	381.5	2.07	29	38454	2042	7674	76886	2401	298934		
8	0.0529	0.00063	0.43017	0.00623	0.06078	0.32	32.4	363.3	4.43	380.4	1.68	41	22465	1206	4553	50812	1467	175096		
9	0.05287	0.00087	0.41306	0.00837	0.05733	0.32	37.05	351.1	6.01	359.4	2.25	0	24857	1333	4418	47917	1690	205362		
10	0.05354	0.00059	0.44696	0.00612	0.06094	0.32	24.73	375.1	4.29	381.3	1.62	19	9	40512	2197	7693	79359	2577		
11	0.14829	0.00086	8.5601	0.12674	0.42837	0.24	9.93	2292.3	13.46	2298.3	6.89	12	0	124908	18758	18267	31733	1149		
12	0.05466	0.00066	0.44687	0.00663	0.06157	0.32	26.59	375.1	4.65	385.2	1.79	5	14	41550	2299	10026	104103	2699		
13	0.05262	0.00061	0.43249	0.00623	0.05827	0.32	312.2	364.9	4.42	365.1	1.63	40	0	59484	3166	12051	121533	3843		
14	0.04897	0.00052	0.17361	0.00201	0.02466	0.35	146.5	162.5	1.74	157	0.61	0	20	28796	1426	4123	109104	4313		
15	0.05345	0.00057	0.4268	0.00556	0.05827	0.32	347.7	360.9	3.95	365.1	1.48	27	7	29268	1580	5306	57924	1946		
16	0.0536	0.00053	0.43205	0.00519	0.05833	0.33	354.1	364.6	3.68	365.5	1.38	0	0	58811	3183	9115	95193	3873		
17	0.05363	0.00051	0.43552	0.00504	0.05831	0.33	355.5	367.1	3.57	365.3	1.32	0	22	40670	2202	8473	91072	2659		
18	0.05401	0.00052	0.43892	0.00518	0.05825	0.32	371.4	369.5	3.66	365	1.35	55	0	56010	3052	14132	161129	3659		
19	0.0535	0.00051	0.43355	0.00498	0.0583	0.33	350	365.7	3.53	365.3	1.31	103	13	37468	2022	8641	87292	2454		

U-Pb analyses done at the Pacific Centre for Isotopic and geochemical Research, University of British Columbia, Vancouver

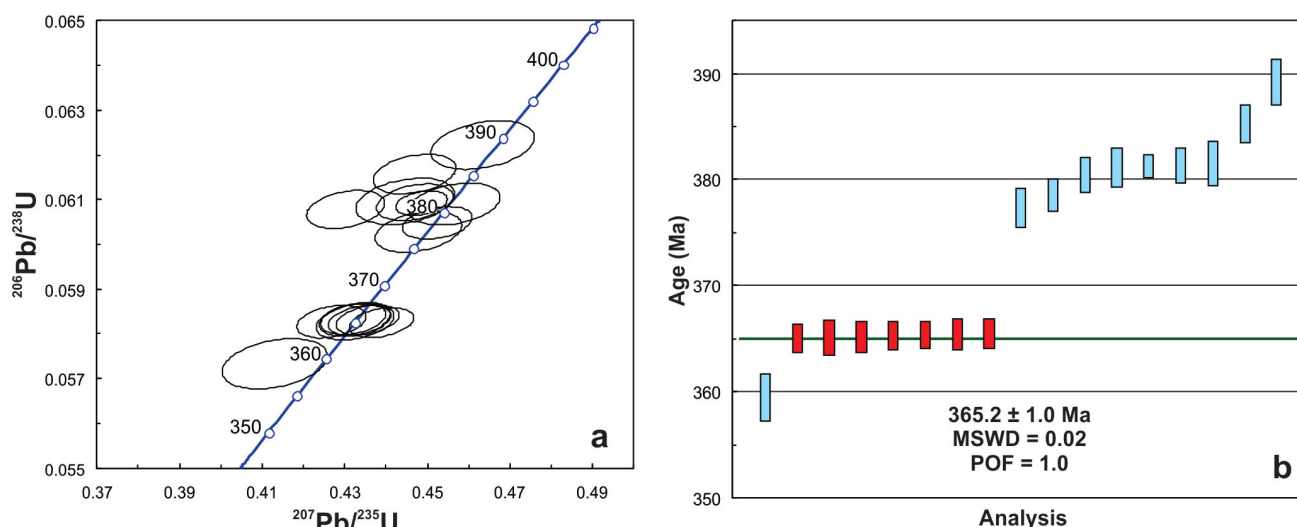


Figure 4. Conventional concordia diagrams and plots of **a)** U-Pb analyses by laser ablation inductively coupled plasma–mass spectrometry of zircon from a felsic metatuff of the Anarchist Group (sample 10-KL-108; Figure 3). Analytical errors are shown at the 2 σ uncertainty level; **b)** analyses shown as blue error boxes were excluded from the calculated weighted-average age for the sample. Abbreviations: MSWD, mean square of weighted deviates; POF, probability of fit.

trital zircons had previously been dated from a sample (n=44) of Barslow assemblage (J.E. Wright, unpublished data, 2007). Although it was not expected there would be any difficulty finding suitable clastic rock units from which to recover detrital zircons from the more sediment-dominated lithological assemblages in the southern part of the Quesnel terrane (e.g., Independence–Bradshaw, Barslow, Anarchist and Attwood), there was some concern at the beginning of the study about whether any clastic rocks were actually present within some of the greenstone/chert-dominated assemblages such as Old Tom and Shoemaker, which appeared to represent deposition in deep oceanic settings. However, a large number of localities, where the presence of greywacke, lithic sandstone and, in some cases, quartz sandstone was noted as thin clastic units interlayered with the greenstone and chert within most of the various assemblages, were located and sampled during the course of the study.

A total of 1410 individual zircon grains were dated in the study, from a total of 21 samples from the Independence–Bradshaw, Old Tom, Shoemaker, Barslow, Anarchist and Attwood assemblages. No samples for detrital zircon dating were collected in this study from either the Blind Creek or Knob Hill assemblages. Several samples of highly metamorphosed quartzite from the Kobau Group were processed but did not yield zircons; these units are now thought to have likely been derived from chert protoliths. Detrital zircons were also separated and dated from the Oregon Claims formation in the Hedley area to test possible correlations with the other Paleozoic assemblages in the area (see earlier discussion). The complete results of the work will be presented in detail in a separate paper. In this contribution, summary probability plots for zircon ages from each sample are shown; these are stacked for each assem-

blage or group of assemblages so that the detrital zircon signature can be compared between samples.

Independence–Bradshaw Assemblage and Oregon Claims Formation

Zircons recovered from the Independence–Bradshaw assemblage metasandstone on Winters Creek (sample 10-KL-79; Figure 2) are all euhedral to subhedral. The youngest grain recovered gave an age of 301 Ma, and a total of 15 grains gave ages in the 315–300 Ma range (early Middle to latest Pennsylvanian; Figure 5a). The remaining 50 grains gave ages ranging from 372 to 316 Ma (mid-Late Devonian to Middle Pennsylvanian). Zircons recovered from the Oregon Claims formation (sample 10-KL-77; Figure 2) are all euhedral to subhedral, and are mainly very young (Figure 5b). A single grain gave an age of 296 Ma (Early Permian), 33 grains gave ages of 315–300 Ma (Middle and Late Pennsylvanian), most of the rest of the grains ranged from 332 to 315 Ma (Middle Mississippian to Middle Pennsylvanian); and a single grain gave an age of 363 Ma (latest Devonian). Taken together the detrital zircon age signature is very similar between the two samples. This could either indicate that the Oregon Claims formation is equivalent to the Independence–Bradshaw assemblage (as previously suggested by Ray and Dawson, 1994), or alternatively, that the Oregon Claims formation is younger but all the zircons within it were reworked from the underlying Independence–Bradshaw units. In any case, neither of the two samples can be older than Early Permian.

Two samples (10-KL-30, -34) were collected from quartz-rich sandstone from within a sequence of grey argillite, sandstone, grit and minor chert pebble conglomerate and dark grey chert 5 km east of Crater Mountain (Figure 2), which is tentatively correlated on lithological grounds with

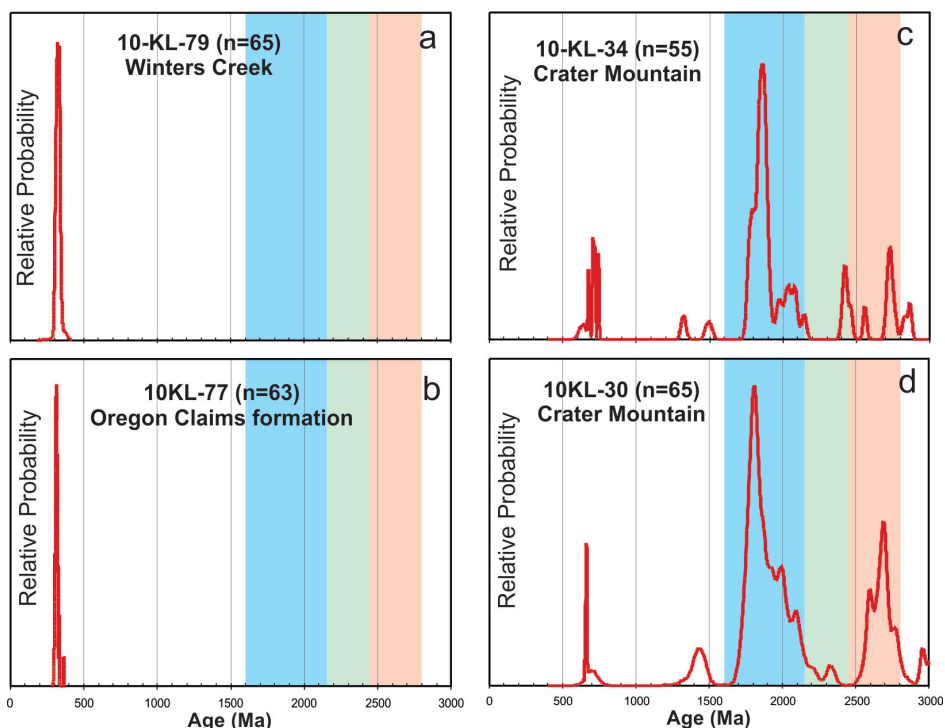


Figure 5. Probability density plots for detrital zircon ages from samples of **a)** the Independence–Bradshaw assemblage; **b)** the Oregon Claims formation; **c)** and **d)** the Crater Mountain area. Colour bands are: pink, 2450–2800 Ma; green, 2150–2450 Ma; blue, 1600–2150 Ma. These age ranges are typical for detrital zircons shed from the northwestern part of the North American craton (Gehrels et al., 1995; Gehrels and Ross, 1998; Leslie, 2009; Lemieux et al., 2011; Kraft, 2013).

the Independence–Bradshaw assemblage. Each yielded abundant detrital zircon, most of which was subrounded. Zircons from both samples gave predominantly Mesoproterozoic and older ages (Figures 5c–d). The youngest grains from the two samples were late Proterozoic (743–662 Ma; Figure 5c, d).

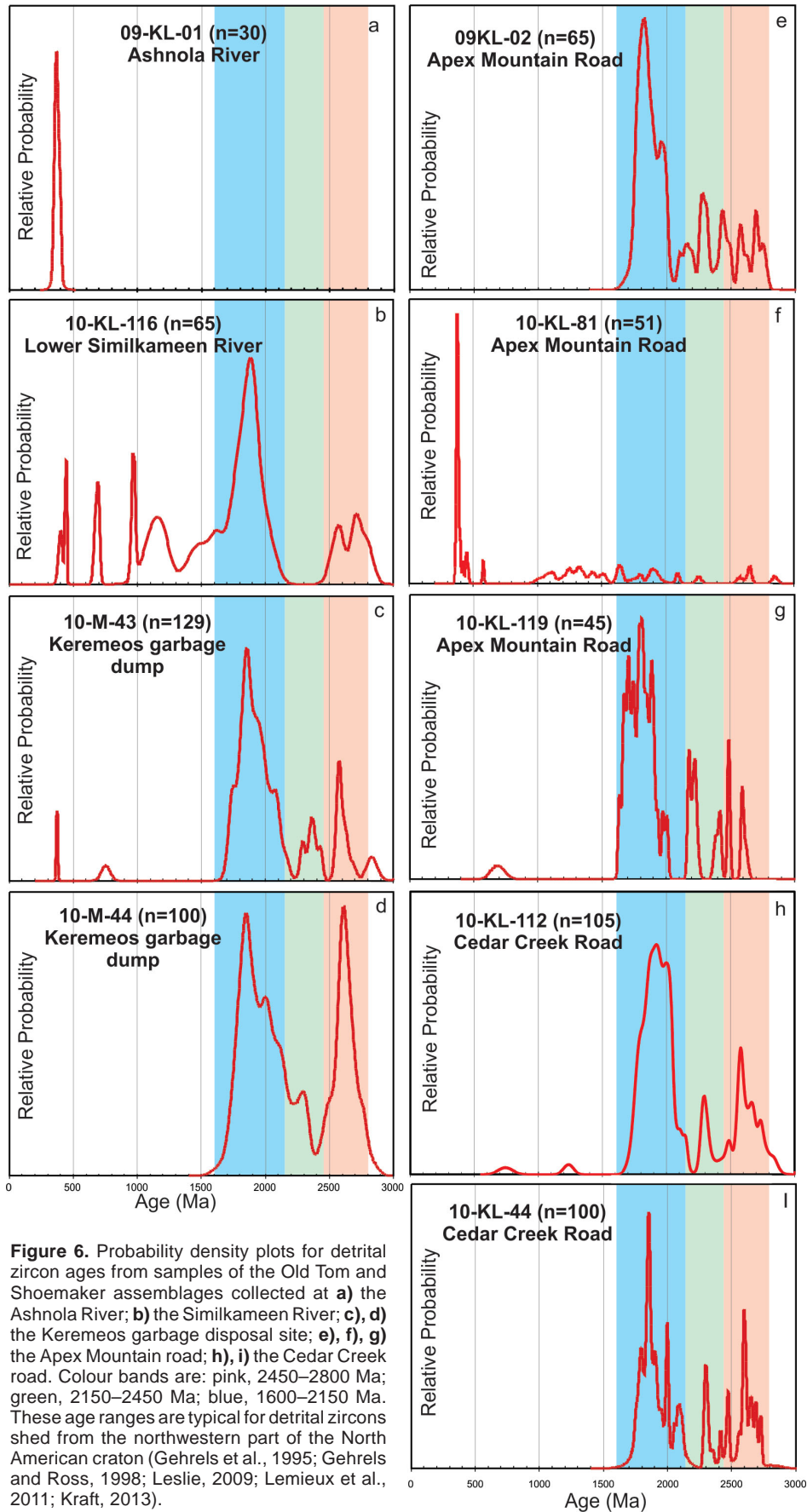
The mid-Early to early Late Devonian brachiopod/tentaculitid age reported by Ray and Dawson (1994) from metasandstone in the Independence–Bradshaw metasedimentary units was from a locality approximately 4 km to the southeast of the Winters Creek sample locality that gave an Early Permian maximum depositional age. The combined data suggest that as much as 80 million years of sedimentation may be represented by the Independence–Bradshaw assemblage. In view of the fine-grained nature of most of the sedimentary rocks of this package, and the lack of any obvious marker horizons within it, such a long period of sedimentation is entirely possible.

Detrital zircon age spectra from the two Crater Mountain area samples show prominent peaks in the 2800–2450 Ma and 2150–1600 Ma ranges (pink and blue bands, respectively, in Figure 5c, d). These age ranges are typical of zircon in early and middle Paleozoic sedimentary units that were shed off the western part of the North American craton and deposited in the continental margin (e.g., Gehrels et al., 1995; Gehrels and Ross, 1998; Leslie, 2009; Lemieux et al.,

2011; Kraft, 2013). The data therefore suggest that the Independence–Bradshaw assemblage was likely deposited along the western edge of the North American craton. Zircons in the range of 2450–2150 Ma (green band in Figures 5c, d), which are present in minor amounts in both Crater Mountain samples, are generally thought to indicate a provenance from a specific part of the northwestern portion of the craton, namely from the Buffalo Head and Hottah terranes of northern Alberta and southwestern Northwest Territories (e.g., Gehrels and Ross, 1998; Kraft, 2013).

Old Tom and Shoemaker Assemblages

Detrital zircons were separated and dated from a total of nine samples of clastic rock from the Old Tom and Shoemaker assemblages, from localities throughout much of the outcrop area of these units. The data from each of the samples are shown in Figure 6 a–i. Many (but not all) of the samples have prominent age peaks from zircon grains that show rounded and frosted morphologies (and therefore are probably multiply reworked) in the ranges of 2150–1600 Ma and 2800–2450 Ma, and most samples also contained a substantial number of grains in the 2450–2150 Ma range, which is interpreted to indicate derivation from the northwestern part of the North American craton. This suggests that, although the abundance of chert, scarcity of clastic sedimentary rocks and absence of carbonate rocks



indicate deposition in deep water at some distance from a continental margin, the Old Tom and Shoemaker assemblages were likely deposited offshore of the northwestern part of the North American craton. Several of the samples contain small populations of zircons that yielded late Mesozoic and early Neoproterozoic (~1500–1000 Ma) ages, and a few samples also contain a small number of early Paleozoic zircons. Again, this is consistent with detrital-zircon age spectra that have been reported for sedimentary units in the miogeocline of the northwestern North American craton (e.g., Gehrels et al., 1995; Leslie, 2009; Lemieux et al., 2011; Hadlari et al., 2012).

In addition, a small number of samples also contain prominent Devonian to Early Mississippian age populations. A greywacke unit (sample 09-KL-01; see Figure 2) interlayered with greenstone on the Ashnola River contained only euhedral zircon grains, which yielded consistently mid- to late Paleozoic ages. Thirty grains were dated (Figure 6a); of these, ten gave ages of 360–350 Ma, and the remainder ranged from 404 to 360 Ma. Three samples were processed from localities along the Apex Mountain resort road (Figure 2). A modest proportion of the zircons recovered from one sample (10-KL-81; Figure 6f) were euhedral in outline. One grain gave an age of 360 Ma, and fifteen additional grains gave ages ranging from 393 to 367 Ma (Middle to Late Devonian). All the rest of the zircons in this sample, and all zircons from both of the other Apex Mountain road samples (09-KL-02 and 10-KL-119; Figures 6g, i), are subrounded to rounded, and yielded older ages (mostly in the 1600–2150 Ma and 2450–2800 Ma brackets; Figure 5).

The range of rock units present, especially the local abundance of radiolarian chert, together with detrital zircon information for the Old Tom and Shoemaker assemblages, suggests that these rocks were deposited in a relatively deep ocean setting somewhat distant from the continental margin of the northwestern North American craton, but also received sporadic input of first-cycle igneous zircon grains ranging from 404 to as young as 350 Ma (Early Devonian to Early Mississippian). The fact that one sample (Ashnola River; Figure 2, 6a) contains only Late Devonian–Early Mississippian zircons and that, of three samples from relatively closely spaced samples in the Apex Mountain road area, only one contains any young zircons, suggests that the source(s) of these younger grains could probably have been volcanoes that were located within the depositional basin (i.e., relatively proximal to the sample site), rather than on the continental margin.

The constraints on possible depositional ages for the Old Tom and Shoemaker assemblages provided by the youngest detrital zircons present in each sample are generally consistent with the fossil-age constraints for the units (Middle Devonian to Pennsylvanian or possibly Permian; see discussion above). Unfortunately the fossil and detrital zir-

con age constraints are too sparse to provide the basis for firm conclusions regarding the relative stratigraphic position of the various exposure areas of Old Tom and Shoemaker units. It was hoped that detrital zircon age data from rocks associated with the blocks of Ordovician limestone on Cedar Creek would shed some light on the nature and origin of these units. The youngest detrital zircons dated from two samples of sandstone, one of which forms the immediate host for the Ordovician limestone block, and one of which occurs along stratigraphic strike from it (samples 10-KL-44 and 10-KL-112), are 1727 and 743 Ma (Figure 6 h, i), respectively; therefore, the detrital zircon ages unfortunately do not provide any useful constraints on the actual depositional age of the sedimentary rocks that host the Ordovician limestone body.

Barslow Assemblage

Three samples of clastic rocks from the Barslow assemblage were collected in the Manuel Creek area, north of Cawston (Figure 2); these were a coarse-grained sandstone (10-KL-61), a fine-grained sandstone (10-KM-63) and a pebble conglomerate (10-KL-64). The conglomerate consisted mainly of chert pebbles; however, rare pebbles of quartz-feldspar porphyry clasts, along with some aphanitic felsic volcanic material, were also present. The two sandstone samples yielded abundant zircon, most of which comprised euhedral, first-cycle grains. One grain from sample 10-KL-61 gave an age of 312 Ma (Middle Pennsylvanian); 53 grains gave ages ranging from 360 to 333 Ma (Early to Middle Mississippian), and nine additional grains gave ages of 383–360 Ma (Late Devonian; Figure 7a). A single grain gave a Neoproterozoic age of 2684 Ma. In sample 10-KL-63, forty-three grains gave ages of 360–342 Ma (Early Mississippian), fifteen grains gave ages ranging from 392 to 360 Ma (Middle to Late Devonian), and the seven remaining grains gave Neoproterozoic to Neoproterozoic ages (Figure 7b). Zircons recovered from the conglomerate sample (10-KL-64) were mainly subrounded to rounded, and the youngest ages that were obtained were 631 and 506 Ma (Figure 7c). Six grains gave ‘Grenvillian’ ages (1160–936 Ma) and the remaining grains gave Mesoproterozoic to Mesoarchean zircons, whose ages suggest derivation from the northwestern North American craton. The age ranges for detrital zircons from this latter sample are very similar to those obtained from a nearby sample (n=44; J.E. Wright, unpublished data, 2007).

The detrital zircon age data for the Barslow assemblage samples are consistent with the Early Mississippian to Pennsylvanian depositional age that was inferred from fossil-age information (see discussion above).

Attwood and Anarchist Groups and Mount Roberts Formation

One sample of pebble conglomerate from the Attwood Group in the Greenwood area (Figure 3), together with four

samples of sandstone and conglomerate from the Greenwood and Rock Creek areas, all yielded very similar detrital zircon age signatures, with abundant Devonian to Pennsylvanian ages (Figure 8a–e). The Attwood conglomerate sample (09-KL-11) yielded one grain at 327 Ma and five more in the range of 355–344 Ma (Early to Middle Mississippian). Two samples of coarse- and fine-grained sandstone from a single locality in the Anarchist assemblage (10-KL-91,-92) each contain one or more zircons at 300–299 Ma (earliest Permian), significant populations of zircons at 310–300 Ma (Late Pennsylvanian) and abundant

grains that are only slightly older. A calcarenite sample from the Anarchist group (10-KL-94) yields a similar age signature, with the three youngest grains giving ages of 310–308 Ma (Middle Pennsylvanian). The final Anarchist sandstone sample (10-KL-107) yielded a significant number of 800 Ma and older grains (Figure 8e); however, it also contains a large proportion of euhedral zircon grains with one grain at 340 Ma and five in the range of 365–350 Ma (Late Devonian to Early Mississippian). This sample was collected less than 1 km from the felsic tuff sample that yielded a latest Devonian U-Pb zircon depositional age of 365.2 ± 1.0 Ma (see discussion above). Collectively the detrital zircon age information from the Greenwood–Rock Creek area shows that much of the Attwood and Anarchist groups are Middle or Late Pennsylvanian in age, and part(?) may be younger than earliest Permian but that the Anarchist, at least locally, also includes felsic metatuff that is latest Devonian in age.

Detrital zircons from a sample of Mount Roberts Formation in the Kettle Falls area in northern Washington state were analyzed by Roback and Walker (1995) using the isotope dilution–thermal ionization mass spectrometry method. The Mount Roberts assemblage is generally thought to be correlative with the Anarchist Group. Only 23 single zircon grains were analyzed; however, the age signature (Figure 8f) shows a substantial population of grains with ages ranging from 2719 to 1001 Ma, but four grains with ages of 378–375 Ma (early Late Devonian), which is generally consistent with the ages obtained from some of the Anarchist samples in this study.

Most of the samples contained minor Mesoproterozoic and Archean populations, whose ages suggest derivation from the northwestern part of the North American craton.

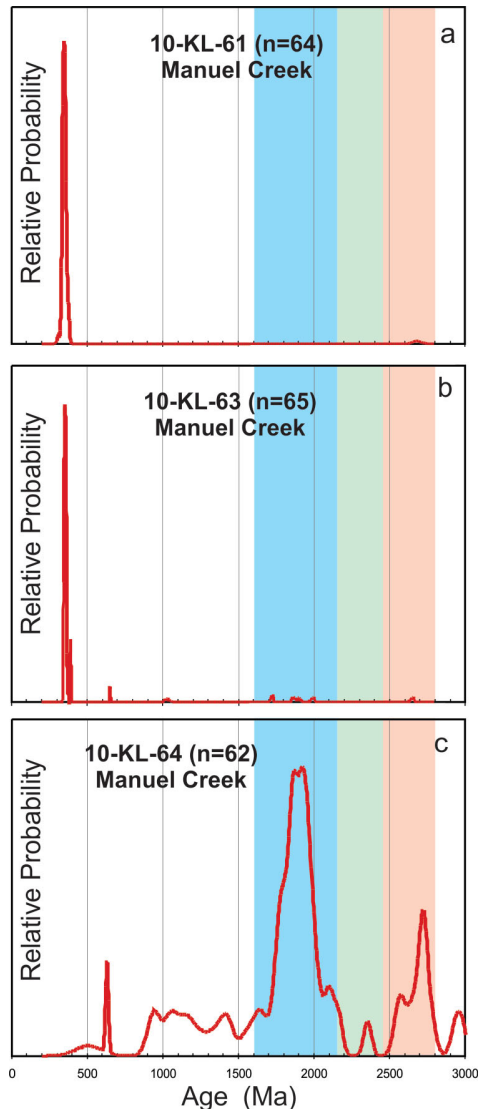


Figure 7. Probability density plots for detrital zircon ages from samples of the Barslow assemblage collected from **a)** a coarse-grained sandstone; **b)** a fine-grained sandstone; **c)** a pebble conglomerate at Manuel Creek. Colour bands are: pink, 2450–2800 Ma; green, 2150–2450 Ma; blue, 1600–2150 Ma. These age ranges are typical for detrital zircons shed from the northwestern part of the North American craton (Gehrels et al., 1995; Gehrels and Ross, 1998; Leslie, 2009; Lemieux et al., 2011; Kraft, 2013).

Lithogeochemical Studies

A total of 61 samples of greenstone (and some mafic intrusive rocks) was collected during this study, with the goal of geochemically characterizing the igneous components of each of the Paleozoic assemblages, and to use these results in an attempt to establish the tectonic setting in which the rocks were erupted. The new data has been compiled along with extensive datasets from the Greenwood and Rock Creek areas (Dostal et al., 2001; Massey and Dostal, 2013a), and from potentially correlative successions in northern Washington state (Gaspar, 2005). The data generated by this study will be presented in detail in a separate publication, but the main characteristics of the various assemblages are described briefly herein, along with the overall tectonic significance of these results.

Hedley–Keremeos–Osoyoos Area

Geochemical data from greenstone contained within the Independence–Bradshaw, Old Tom, Shoemaker, Barslow

and Kobau assemblages are plotted on a variety of geochemical and tectonic discrimination diagrams in Figure 9. Analyses for two samples from a thick gabbro sill within the Old Tom greenstone on the southwestern side of the Silmilkameen River near Cawston are also included, along with two analyses of mafic tuff in the Oregon Claims formation near Hedley (from Ray et al., 1996). There is a large degree of scatter on the total alkalis versus silica diagram (Figure 9a) of Le Bas et al. (1986), and at least some of this is likely due to mobility of alkalis and other elements during alteration that these rock units experienced after they were erupted on the seafloor, or during greenschist- to locally lower-amphibolite-facies regional metamorphism and later surface weathering. However, on a plot of immobile-element ratios (Figure 9b), the data also shows a significant

amount of scatter, suggesting that a substantial range of protolith compositions is represented within this suite of samples. Most of the samples yielded basalt to alkaline-basalt compositions. One sample of greenstone from the Independence–Bradshaw assemblage yielded an anomalously high Zr/TiO₂ ratio (Figure 9b). This may reflect contamination by mixing of a trace amount of detrital zircon into a mafic volcanoclastic rock unit. On a Shervais-type discrimination diagram of V versus Ti (Shervais, 1982; Figure 9c) samples fall in both arc and non-arc fields; however, some consistent trends are observed. All of the Barslow samples plot as arc rocks, whereas all but one of the Kobau samples yield non-arc (mid-ocean ridge basalt [MORB] and within-plate) compositions. Old Tom and Shoemaker greenstone samples are equally split between arc and non-arc signa-

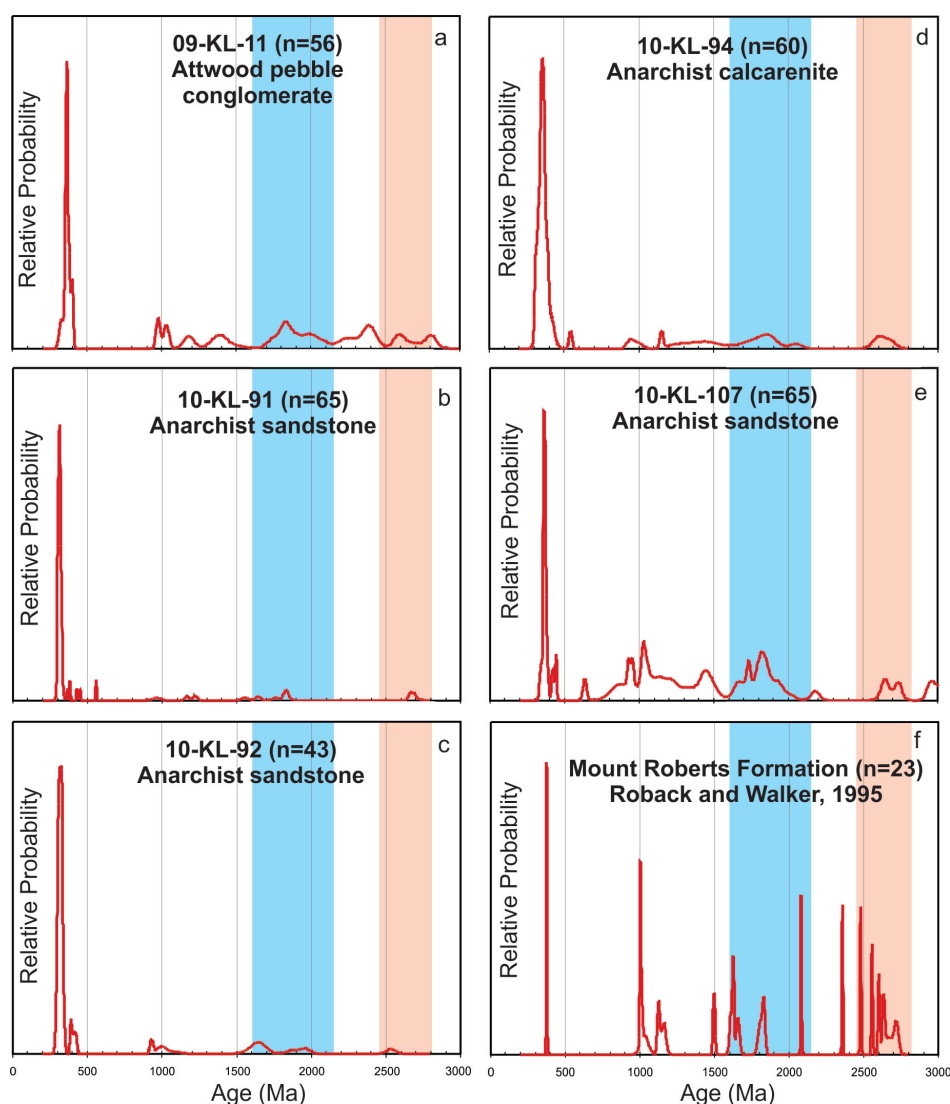


Figure 8. Probability density plots for detrital zircon ages from samples of **a)** Attwood pebble conglomerate; **b), c)** Anarchist sandstone; **d)** Anarchist calcarenite; **e)** another Anarchist sandstone; **f)** the Mount Roberts assemblage. Colour bands are: pink, 2450–2800 Ma; green, 2150–2450 Ma; blue, 1600–2150 Ma. These age ranges are typical for detrital zircons shed from the northwestern part of the North American craton (Gehrels et al., 1995; Gehrels and Ross, 1998; Leslie, 2009; Lemieux et al., 2011; Kraft, 2013).

tures in Figure 9c. Two samples from a thick gabbro sill that intrudes Old Tom greenstone on the southwestern side of the Similkameen River across from Cawston (Figure 2) plot as alkaline basalt on the Nb/Y versus Zr/TiO₂ plot (Winchester and Floyd, 1977; Figure 9b) and in the alkaline field on the Shervais plot (Figure 9c); these samples also

fall in the enriched mid-ocean ridge basalt (E-MORB) and ocean-island basalt fields on a Wood (1980) ternary plot (Figure 9d). The Barslow greenstone, as well as a few greenstone samples from the Old Tom and Shoemaker assemblages, one sample from the Independence–Bradshaw assemblage and interestingly, both samples from the Ore-

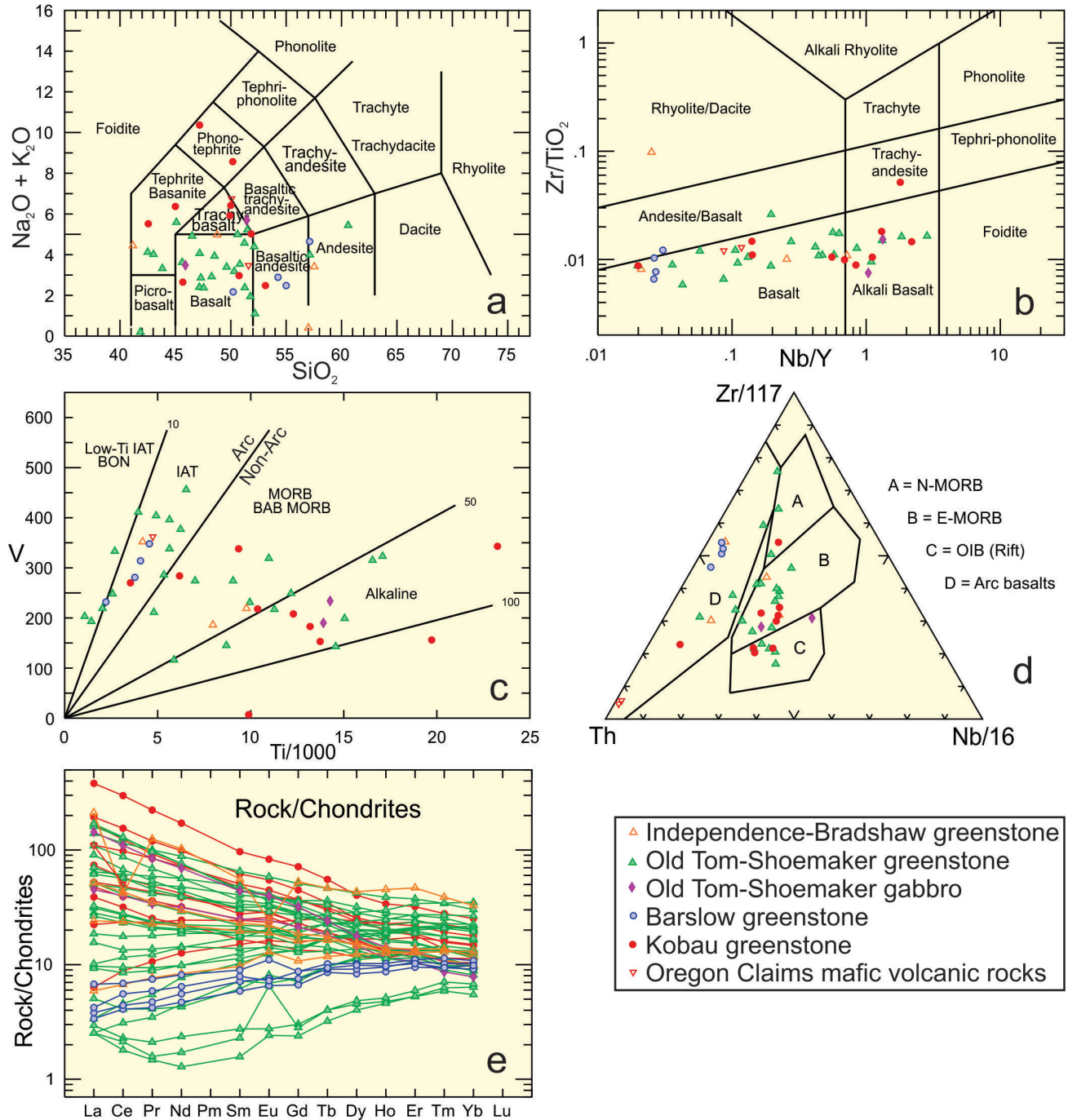


Figure 9. Lithogeochemical discrimination diagrams for samples from the Independence–Bradshaw, Old Tom, Shoemaker, Barslow and Kobau assemblages. Data are from this study, except two analyses of samples from the Oregon Claims formation that are from Ray et al. (1996). References for the various discrimination diagrams are **a)** Le Bas et al. (1986); **b)** Winchester and Floyd (1977) as revised by Pearce (1996); **c)** Shervais (1982); **d)** Wood (1980); **e)** Sun and McDonough (1989). Abbreviations: BAB MORB, back-arc basin mid-ocean ridge basalt; BON, boninite; E-MORB, enriched mid-ocean ridge basalt; IAT, island-arc tholeiite; MORB, mid-ocean ridge basalt; N-MORB, normal mid-ocean ridge basalt; OIB, ocean-island basalt.

gon Claims formation (data from Ray et al., 1996), also plot as arc rocks on the Wood (1980) discrimination diagram (Figure 9d). On a plot of rare earth elements (REE), normalized to chondritic values (Sun and McDonough, 1989; Figure 9e), the Barslow samples show consistent minor light-REE depletion, as do several samples from the Old Tom and Shoemaker and one from the Independence–Bradshaw assemblage. Most other samples show slight to strong light-REE enrichment.

The paucity of depositional ages for igneous rock units analyzed in this study from each of the assemblages makes it difficult to establish whether rock units of similar age throughout the whole area show comparable compositions, possibly reflecting a similar evolution of tectonic setting over time (see later discussion).

Greenwood–Rock Creek and Loomis (Washington State) Areas

Dostal et al. (2001) and Massey and Dostal (2013a, b) have produced an extensive set of lithogeochemical data for mafic volcanic rocks and gabbro from the Greenwood and Rock Creek areas. A limited number of additional samples from the area were analyzed for this study, and the entire dataset is presented in a series of geochemical and tectonic discrimination diagrams in Figure 10a–e. A substantial number of lithogeochemical analyses were also reported for samples from the ‘Palmer Mountain greenstone’ unit in the Loomis area of northern Washington state by Gaspar (2005; see earlier discussion). Massey and Dostal (2013a) demonstrate that the Knob Hill greenstone and gabbro show a mainly island-arc tholeiite (IAT) affinity, with minor MORB and E-MORB units present as well. They suggest that greenstone from the Anarchist Group mainly shows within-plate E-MORB compositions, along with some units that give IAT and MORB signatures. Most Knob Hill greenstone and all Knob Hill gabbro, as well as the Palmer Mountain greenstone analyses, show a very limited range of lithogeochemical compositions, with almost all plotting as arc rocks on the Shervais (1982)- and Wood (1980)-type plots (Figure 10c, d).

As with the sample suite discussed previously from the Hedley–Keremeos–Osoyoos area, the data from the Greenwood–Rock Creek–Loomis areas show a considerable range of compositions and inferred paleotectonic settings. The limited age constraints from this area indicate that depositional ages of the various rock units range from Middle Devonian to Middle or Late Pennsylvanian, but there is insufficient age information to identify any significant geochemical trends over time.

Pb-Isotopic Studies of VMS and Related Mineralization the Southern part of the Quesnel Terrane

Numerous stratabound, apparently stratiform rhodonite occurrences, commonly associated with abundant hematitic jasperoid, have been recognized within the volcanic rock- and chert-dominated Paleozoic assemblages in the Quesnel terrane in south-central BC (Figures 2, 3). The presence of these occurrences, together with a single occurrence of massive iron formation interpreted to be >100 m thick and associated with widespread Cu and minor Zn anomalies in soil samples (Nova occurrence; MINFILE 092HSE249, BC Geological Survey, 2016; Nebocat, 1993, 1996; Figure 2), suggest that there could be potential for volcanogenic massive sulphide (VMS) mineralization in the region. Although no stratiform sulphide occurrences have been identified thus far in south-central BC, a significant stratiform Cu-Zn massive sulphide deposit (the Copper World Extension mine) is present in the Palmer Mountain area near Loomis, approximately 20 km south of the BC–Washington state border (Figure 3). This deposit was mined on a small scale in the early 1900s, and produced approximately 3500 tonnes of ore grading 3.1% Cu (Caron, 2008). Recent diamond drilling is reported to have intersected massive sulphide lenses up to 8 m thick, and up to 40 m of stratigraphically underlying footwall stringer-type mineralization (Caron, 2008). The deposit is hosted in the Palmer Mountain greenstone, which has been variably correlated with the Old Tom, Kobau, Knob Hill and/or Anarchist assemblages in the past by various workers. Although no reliable depositional ages are available for the Palmer Mountain greenstone, the lithogeochemical signature of the greenstone indicates that it formed in a magmatic arc environment, and this signature, together with the overall lithological character of the rocks, suggests that the Palmer Mountain greenstone most likely correlates with the Knob Hill Complex in the Greenwood area (as suggested by Massey and Dostal, 2013a; see discussion above).

A Pb-isotopic study of several samples of massive sulphides from drillcore from the Palmer Mountain deposit was undertaken to determine whether the massive sulphide mineralization is indeed syngenetic. Analytical data is given in Table 3, together with a Pb-isotopic analysis of mineralization from the deposit that was reported by Church (2010). The analytical results are shown on a $^{207}\text{Pb}/^{204}\text{Pb}$ versus $^{206}\text{Pb}/^{204}\text{Pb}$ diagram in Figure 11. Fields of Pb-isotopic compositions for Paleozoic VMS deposits and occurrences in other terranes in the northern Cordillera that occupy a similar ‘pericratonic’ position as the Quesnel terrane area are also shown for comparison.

The Pb-isotopic analyses from the Palmer Mountain deposit are well clustered and relatively nonradiogenic (Figure 11). The data are entirely consistent with a VMS origin

for the deposit, and suggest an association with very juvenile igneous source rocks. As shown in Figure 11, the deposit has some of the least radiogenic (most ‘primitive’) isotopic signatures of any Paleozoic VMS mineralization in the northern Cordillera. This would be consistent with the hostrocks (Palmer Mountain greenstone) representing a ju-

venile arc and/or ophiolitic complex. It is not possible at this time to correlate the Palmer Mountain greenstone with the assemblages north of the border. However, it was suggested above that these rocks are lithologically and geochemically very similar to the mainly Middle Devonian Knob Hill Complex. Greenstone and chert of Middle Devo-

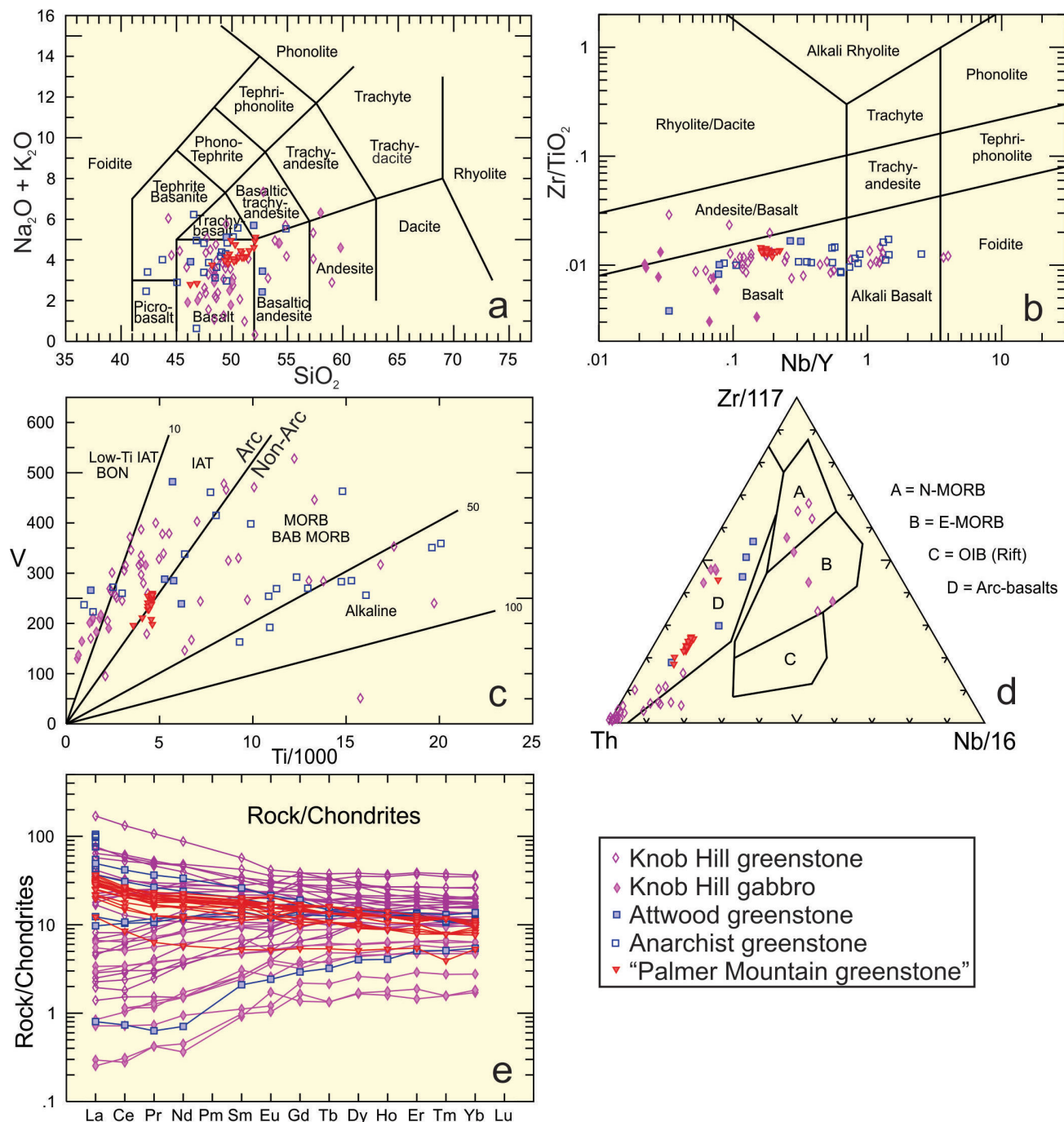


Figure 10. Litho-geochemical discrimination diagrams for samples from Knob Hill greenstone and gabbro, and Attwood and Anarchist greenstone (data from Dostal et al., 2001; Massey and Dostal, 2013a; this study), and the ‘Palmer Mountain greenstone’ in the Loomis area of northern Washington state (from Gaspar, 2005). References for the various discrimination diagrams are **a**) Le Bas et al. (1986); **b**) Winchester and Floyd (1977) as revised by Pearce (1996); **c**) Shervais (1982); **d**) Wood (1980); **e**) Sun and McDonough (1989). Abbreviations: BAB MORB, back-arc basin mid-ocean ridge basalt; BON, boninite; E-MORB, enriched mid-ocean ridge basalt; IAT, island-arc tholeiite; MORB, mid-ocean ridge basalt; N-MORB, normal mid-ocean ridge basalt; OIB, ocean-island basalt.

Table 3. Lead-isotopic compositions of volcanogenic massive sulphide mineralization on the Palmer Mountain property near Loomis, Washington state.

Sample no.	Mineralogy	$^{206}\text{Pb}/^{204}\text{Pb}$	1 σ error	$^{207}\text{Pb}/^{204}\text{Pb}$	1 σ error	$^{208}\text{Pb}/^{204}\text{Pb}$	1 σ error	$^{207}\text{Pb}/^{206}\text{Pb}$	1 σ error	$^{208}\text{Pb}/^{206}\text{Pb}$	1 σ error
PM-7-150.5-a ¹	py + sl	18.124	0.11	15.503	0.05	37.798	0.15	0.8554	0.09	2.0855	0.11
PM-7-150.5-b ¹	py + sl	18.198	0.03	15.502	0.02	37.633	0.03	0.8518	0.02	2.068	0.01
PM-5-186-a ¹	py+cp+sl	18.16	0.03	15.517	0.03	37.725	0.03	0.8545	0	2.0774	0.01
PM-5-186-b ¹	py+cp+sl	18.15	0.01	15.507	0.01	37.692	0.01	0.8544	0	2.0767	0.01
PM-5-186-b ¹	py+cp+sl	18.139	0.03	15.47	0.02	37.572	0.03	0.8529	0.02	2.0713	0.02
PM-5-186-b ¹	py+cp+sl	18.194	0.02	15.523	0.02	37.746	0.03	0.8532	0.01	2.0746	0.01
PM-5-145-a ¹	py	18.141	0.02	15.469	0.02	37.57	0.02	0.8527	0.01	2.071	0.01
PM-5-145-b ¹	py	18.111	1	15.404	1	37.51	1.02	0.8505	0.12	2.0711	0.18
86WACWE 3 ²	py+cp+po	18.16		15.54		37.793					

¹Source of data: this study

²Source of data: Church (2010)

All analyses done at the Pacific Centre for Isotopic and Geochemical Research, University of British Columbia, Vancouver

nian age are also recognized in the Old Tom, Shoemaker and Independence–Bradshaw assemblages in the Hedley–Keremeos–Osoyoos area, and it is interesting to note that many of the known rhodonite occurrences in the Paleozoic rocks in southern BC occur within the Old Tom and Shoemaker assemblages (Figure 2). None of these rhodonite occurrences, or the Nova iron formation in the Crater Mountain area (Nebocat, 1996; Figure 2), contain significant amounts of sulphides, with the exception of trace amounts of pyrite, pyrrhotite and chalcopyrite in the Clearcut rhodonite occurrence (MINFILE 082ESE241), 13 km northeast of Greenwood (Caron, 1996; Simandl and Church, 1996; Figure 3). It is therefore not possible to compare the Pb-isotopic signature of these occurrences with that of the Copper World Extension mineralization. Caron (1996) briefly describes small zones of massive pyrite, pyrrhotite and chalcopyrite in the vicinity of the Clearcut occurrence that contain up to 0.4% Cu and anomalous levels of Pb and Zn. However, the relationship, if any, between these sulphide occurrences and the rhodonite exhalite is uncertain. The area has experienced strong contact metamorphism and it is possible that the massive sulphides result from later skarn development (Caron, 1996).

Stratabound, apparently syngenetic, lenses of recrystallized barite are interlayered with clastic rocks of the Anarchist Group at the Lapin and Dan occurrences (BC MINFILE 082ESW256 and 082ESW168, respectively), approximately 8 km southwest of Rock Creek (Figure 3). These occurrences are not obviously associated with geochemical anomalies that would suggest a relationship with base-metal-rich sedimentary exhalative- or volcanogenic massive sulphide-type deposits. However, the presence of stratiform barite within the Anarchist Group, does suggest that there may be potential for other syngenetic deposits in this assemblage, especially in light of the 365 Ma felsic tuff unit that was dated approximately 9 km east of the barite mineralization (this study; see earlier discussion).

Tectonic Synthesis and VMS Potential of the Paleozoic Basement of the South-Central Part of the Quesnel Terrane

Limited fossil-age constraints indicate that the Paleozoic volcanic and sedimentary assemblages of the southern part of the Quesnel terrane get as old as late Middle and Late Devonian, but most are Mississippian to Pennsylvanian, and some are as young as Early Permian in age (this study). Several gabbro bodies that are part of the Knob Hill Complex in the Greenwood area have yielded consistent Middle Devonian U-Pb zircon ages (Massey et al., 2013). A thin felsic metavolcanic (probably metatuff) unit within the Anarchist Group yields a 365 Ma (latest Devonian) U-Pb zircon age (this study). However, detrital zircon ages of euhedral grains from several clastic rock units, especially in the Greenwood area but also in the Independence–Bradshaw assemblage near Hedley, are as young as 315–300 Ma (Middle Pennsylvanian to earliest Permian), indicating that depositional ages for some of the assemblages get at least as young as Early Permian (this study). Collectively therefore, the ages of the Quesnel terrane basement rocks in south-central BC are now known to span at least 90 million years.

Detrital zircon age signatures for the various Paleozoic assemblages that were investigated during this study are all very similar in terms of specific age populations that are present in each assemblage (although there are wide variations in the relative size of each age population between assemblages, and between individual samples within each assemblage). This is taken as strong evidence for a close primary stratigraphic linkage between all of the various assemblages that make up the Paleozoic basement of the southern part of the Quesnel terrane. Furthermore, the specific Mesoproterozoic to Neoproterozoic detrital zircon age populations indicate that all of the assemblages likely formed in a near-offshore position adjacent to the northwestern margin of the North American craton.

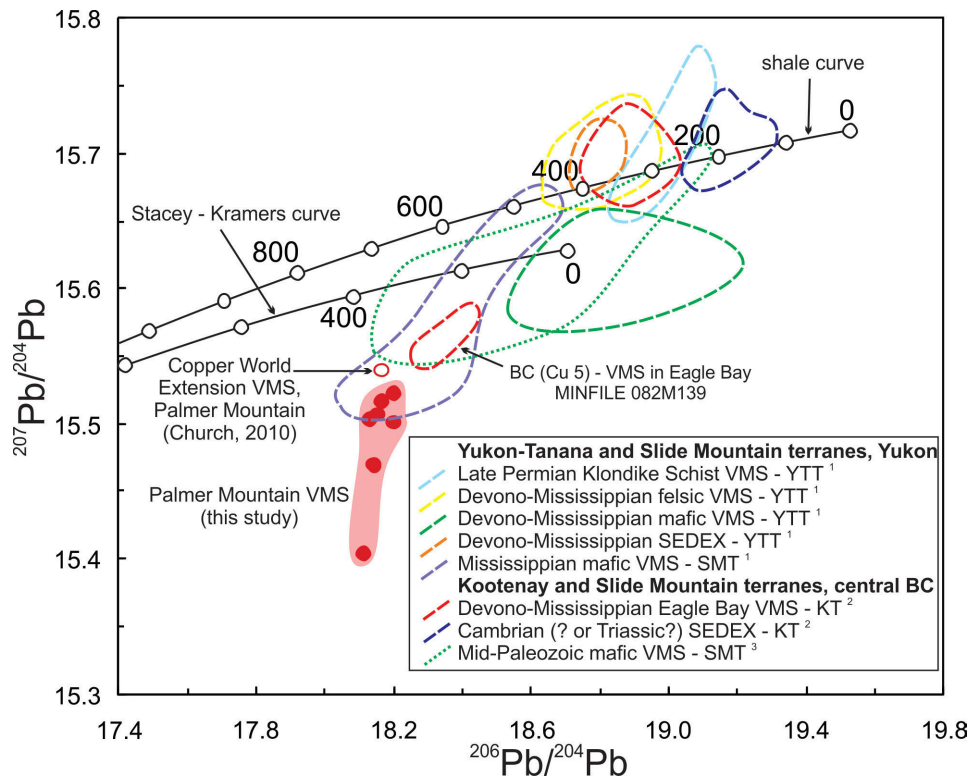


Figure 11. Plot of $^{207}\text{Pb}/^{204}\text{Pb}$ versus $^{206}\text{Pb}/^{204}\text{Pb}$ for sulphides from volcanogenic massive sulphide (VMS) mineralization in the Palmer Mountain greenstone near Loomis, Washington state (solid and open red circles, and dark pink field), together with data from VMS deposits and occurrences in a variety of other VMS deposits elsewhere in the northern Cordillera. The 'shale curve' of Godwin and Sinclair (1982), which is an approximation of the evolution of upper crustal Pb isotopes in the miogeocline of western North America and adjacent pericratonic terranes (Mortensen et al., 2006), and the global average upper crustal Pb-isotopic growth curve of Stacey and Kramers (1975) are shown for reference, as is a MINFILE occurrence in Eagle Bay (BC Geological Survey, 2016). Sources of data for outlined fields are: (1) Mortensen et al. (2006); (2) Goutier (1987); (3) Aggarwal and Nesbitt (1984). Abbreviations: KT, Kootenay terrane; SEDEX, sedimentary exhalative sulphides; SMT, Slide Mountain terrane; VMS, volcanogenic massive sulphides; YTT, Yukon-Tanana terrane.

A considerable range of tectonic affinities is indicated by the lithogeochemical studies of the metavolcanic rocks in the southern part of the Quesnel terrane (Gaspar, 2005; Massey and Dostal, 2013a; this study). Some packages (especially the Barslow, parts of Knob Hill and parts of Old Tom assemblages) show definitive magmatic arc chemistry; however, most assemblages yield mainly non-arc chemistry (normal mid-ocean ridge basalt, enriched mid-ocean ridge basalt and ocean-island basalt). Existing age constraints are not sufficient to establish whether consistent correlations exist between age and indicated paleotectonic affinity. Detailed lithogeochemical and U-Pb studies of the Knob Hill Complex by Massey and Dostal (2013a) and Massey et al. (2013), respectively, suggest that magmas typical of both arc and possibly fore-arc settings were erupting more or less simultaneously in that part of the Quesnel terrane in Middle and Late Devonian time. The presence of nearly coeval igneous suites with markedly different petrotectonic affinities is well recognized in many of the pericratonic terranes that make up the easternmost part of the North American Cordillera (e.g., Piercey et al.,

2006). Recent detailed lithogeochemical and isotopic studies of the middle Paleozoic Sicker Group on Vancouver Island by Ruks (2015) has shown that such a 'mixed' petrotectonic signature also appears to be relatively common in some more juvenile arc settings. The Harper Ranch assemblage, which is mainly exposed farther to the north within the Quesnel terrane, was not investigated in the present study; however, limited lithogeochemical work on that package suggests a more clearly magmatic arc/back-arc affinity than is observed in most of the Paleozoic assemblages of south-central BC (e.g., Monger et al., 1991; Beatty, 2003).

Extensive U-Pb-dating studies of detrital zircons extracted from thin clastic units (greywacke to fine-grained quartz sandstone) that are interlayered with the mafic volcanic and chert-dominated assemblages (Old Tom and Shoemaker, Independence, Bradshaw) indicate variable mixtures of well-rounded, probably extensively recycled Neoproterozoic to Mesoproterozoic zircons, whose age ranges are consistent with having been derived mainly from the northwest-

ern part of the North American craton, and subhedral to euhedral grains that are much less travelled and yield Late Devonian and younger ages. Assemblages that are dominantly clastic in nature (Attwood and parts of the Barslow and Anarchist assemblages) show a similar mix of detrital zircon ages; however, these samples typically contain a much higher proportion of the middle and late Paleozoic grains, and locally also contain felsic porphyry and rhyolite clasts. Preliminary detrital zircon dating of euhedral grains (n=25) from a single sample from the oldest known, Late Devonian, part of the Harper Ranch assemblage near Kamloops (J.E. Wright, unpublished data, 2007) shows a nearly unimodal age range of Late Devonian to Early Mississippian. The detrital zircon dating results of this study are therefore interpreted as indicating that the Attwood Formation and probably much of the Anarchist Group are likely correlative with the Harper Ranch Group to the north, as has been suggested by some previous workers (e.g., Nelson et al., 1995). The complete overlap between the detrital zircon age signatures of the various Paleozoic assemblages that make up the Quesnel terrane in south-central BC strongly suggests that these assemblages probably formed in close proximity to one another, in an original position off the northwestern margin of the North American craton.

The different assemblages that make up the Paleozoic basement of the southern part of the Quesnel terrane comprise varying proportions of 1) rocks that were deposited in a mainly oceanic setting (mafic volcanic rocks and chert) and 2) clastic rocks that include a large proportion of material that was likely shed off of a magmatic arc (as first recognized by Peatfield, 1978). The latter component is correlated with the Harper Ranch Group as defined in the Kamloops area (Beatty et al., 2006), on the basis of both rock units and detrital zircon age signature. Although the mafic volcanic rock and chert component reflects deposition in a submarine basin, a minor component of clastic rocks with close similarities to the Harper Ranch equivalents is present throughout the package, indicating that this basin was not far removed from the site of eruption and deposition of the Harper Ranch Group and its equivalents.

Lithochemical studies indicate a diversity of paleotectonic settings for Paleozoic magmatism in the Quesnel terrane in south-central BC. There is insufficient information as yet to determine whether there was any consistent change in paleotectonic setting with time; however, in at least some of the assemblages (e.g., Knob Hill) both arc and non-arc magmatism was occurring simultaneously.

Lead-isotopic studies of stratabound Zn-Cu massive sulphide mineralization in the Palmer Mountain area immediately south of the BC–Washington state border, which is hosted in mafic volcanic rocks that are coextensive with the Paleozoic mafic rocks of the southern part of the Quesnel

terrane, confirm that this mineralization is indeed volcanogenic in nature. This emphasizes the potential for similar VMS mineralization within the volcanic-rock-dominated Paleozoic assemblages north of the border, especially because of the known occurrence of stratiform rhodonite in several localities. In addition, two occurrences of apparently stratiform barite are known within clastic rocks of the Anarchist Group southwest of Rock Creek, which suggests that there may be potential for SEDEX- or (distal) Kuroko-type VMS mineralization in that assemblage as well.

Acknowledgments

The authors thank N. Massey for providing guidance in the field in the Greenwood area in 2010, and A. Okulitch for useful discussions about the nature and origin of the Kobau Group. L. Caron is also thanked for providing samples of the sulphide mineralization from the Palmer Mountain VMS deposit and for a copy of an unpublished company report on the property. The final version of the paper benefited from an insightful critical review of the manuscript by J. Nelson. The project was funded by a grant from Geoscience BC, as well as a Natural Science and Engineering Research Council (NSERC) Discovery Grant to J.K. Mortensen.

References

- Aggarwal, P.K. and Nesbitt, B.E. (1984): Geology and geochemistry of the Chu Chua massive sulfide deposit, British Columbia; *Economic Geology*, v. 79, p. 815–825.
- Barnes, W.C. and Ross, J.V. (1975): The Blind Creek limestone, Keremeos, British Columbia: Structure and regional tectonic significance; *Canadian Journal of Earth Sciences*, v. 12, p. 1929–1933.
- BC Geological Survey (2016): MINFILE BC mineral deposits database; BC Ministry of Energy and Mines, BC Geological Survey, URL <<http://minfile.ca/>> [January 2016].
- Beatty, T.W. (2003): Stratigraphy of the Harper Ranch Group and tectonic history of the Quesnel terrane in the area of Kamloops, British Columbia; M.Sc. thesis, Simon Fraser University, Vancouver, British Columbia, 168 p.
- Beatty, T.W., Orchard, M.J. and Mustard, P.S. (2006): Geology and tectonic history of the Quesnel terrane in the area of Kamloops, British Columbia; *in* Paleozoic Evolution and Metallogeny of Pericratonic Terranes at the Ancient Pacific Margin of North America, Canadian and Alaskan Cordillera, M. Colpron and J.L. Nelson (ed.), Geological Association of Canada, Special Paper 45, p. 483–504.
- Bostock, H.S. (1939): Geology, Keremeos; Geological Survey of Canada, Map 341A, scale 1:63 360.
- Bostock, H.S. (1940): Geology, Olalla; Geological Survey of Canada, Map 628A, scale 1:63 360.
- Bostock, H.S. (1941): Geology, Okanagan Falls; Geological Survey of Canada, Map 627A, scale 1:63 360.
- Caron, L. (1996): Assessment report on the Clearcut property; assessment report 24,414, prepared for Kettle River Resources Ltd., 5 p.

- Caron, L. (2008): Summary report on the Palmer Mountain property; technical report prepared for W. Hallauer, November 28, 2008, 36 p.
- Cheney, E.S., Rasmussen, M.G. and Miller, M.G. (1994): Major faults, stratigraphy, and identity of Quesnellia in Washington and adjacent British Columbia; Washington Division of Geology and Earth Resources, Bulletin 80, p. 49–71.
- Church, B.N. (1985): Geology and mineralization in the Mount Attwood-Phoenix area, Greenwood, B.C.; BC Ministry of Energy, Mines and Petroleum Resources, Preliminary Map 59.
- Church, S.E. (2010): Lead isotope database of unpublished results from sulfide mineral occurrences – California, Idaho, Oregon, and Washington; U.S. Geological Survey Open-File Report 2010-1157, 9 p.
- Cordey, F. (1998): Radiolaires des complexes d'accrétion cordilléraires; Geological Survey of Canada, Bulletin 509, 210 p., 28 p.
- Dawson, G.L. (1994): Geological setting of the Hedley gold skarn camp with specific reference to the French Mine, south-central British Columbia; M.Sc. thesis, University of British Columbia, Vancouver, British Columbia, 208 p.
- Dostal, J., Church, B.N. and Hoy, T. (2001): Geological and geochemical evidence for variable magmatism and tectonics in the southern Canadian Cordillera: Paleozoic to Jurassic suites, Greenwood, southern British Columbia; Canadian Journal of Earth Sciences, v. 38, p. 75–90.
- Fyles, J.T. (1990): Geology of the Greenwood-Grand Forks area, British Columbia; BC Ministry of Energy, Mines and Petroleum Resources, Open File 1990-25, 19 p.
- Gaspar, L.M.G. (2005): The Crown Jewel gold skarn deposit; Ph.D. thesis, Washington State University, Pullman, Washington, 325 p.
- Gehrels, G.E., Dickinson, W.R., Ross, G.M., Stewart, J.H. and Howell, D.G. (1995): Detrital zircon reference for Cambrian to Triassic miogeoclinal strata of western North America; Geology, v. 23, p. 831–834.
- Gehrels, G. and Ross, G.M. (1998): Detrital zircon geochronology of Neoproterozoic to Permian miogeoclinal strata in British Columbia and Alberta; Canadian Journal of Earth Sciences, v. 35, p. 1380–1401.
- Godwin, C.I. and Sinclair, A.J. (1982): Average lead isotope growth curves for shale-hosted zinc-lead deposits, Canadian Cordillera; Economic Geology, v. 77, p. 675–690.
- Goutier, F.N. (1987): Galena lead isotope study of mineral deposits in the Eagle Bay Formation, southeastern British Columbia; M.Sc. thesis, University of British Columbia, Vancouver 152 p., URL <<https://open.library.ubc.ca/cIRcle/collections/ubctheses/831/items/1.0052653>> [January 2014].
- Kraft, J.L. (2013): Stratigraphy, paleogeography and tectonic evolution of early Paleozoic to Triassic pericratonic strata in the northern Kootenay Arc, southeastern Canadian Cordillera, British Columbia; Ph.D. thesis, University of Alberta, Edmonton, 361 p.
- Le Bas, M.J., Le Maitre, R.W., Streckeisen, A. and Zanettin, B. (1986): A chemical classification of volcanic rocks based on the total alkali-silica diagram; Journal of Petrology, v. 27, p. 745–750.
- Lemieux, Y., Hadlari, T. and Simonetti, A. (2011): Detrital zircon geochronology and provenance of Devonian-Mississippian strata in the northern Canadian Cordillera miogeoclinal; Canadian Journal of Earth Sciences, v. 48, p. 515–541.
- Leslie, C.D. (2009): Detrital zircon geochronology and rift-related magmatism: central Mackenzie Mountains, Northwest Territories; M.Sc. thesis, The University of British Columbia, 236 p., URL <<https://open.library.ubc.ca/cIRcle/collections/ubctheses/24/items/1.0052744>> [January 2015].
- Lewis, P.D., Mäder, U. and Russell, J.K. (1989): Geology and structure of the Kobau Group between Oliver and Cawston, British Columbia (NTS 82E/4E); BC Ministry of Energy, Mines and Petroleum Resources, Open File 1989-2.
- Little, H.W. (1983): Geology of the Greenwood map-area, British Columbia; Geological Survey of Canada, Paper 79-29, 37 p.
- Massey, N.W.D. (2006): Boundary project: Reassessment of Paleozoic rock units of the Greenwood area (NTS 82E/02), southern British Columbia; BC Ministry of Energy, Mines and Petroleum Resources, Geological Fieldwork 2005, Paper 2006-1, p. 99–107.
- Massey, N.W.D. (2007): Geology and mineral deposits of the Rock Creek area, British Columbia, scale 1:25 000; BC Ministry of Energy, Mines and Petroleum Resources, Open File 2007-17.
- Massey, N.W.D. and Duffy, A. (2008): Boundary project: McKinney Creek (NTS 82E/03) and Beaverdell (NTS 82E/06E, 07W, 10W, 11W) areas, south-central British Columbia; BC Ministry of Energy, Mines and Petroleum Resources, Geological Fieldwork 2007, Paper 2008-1, p. 87–102.
- Massey, N.W.D. and Dostal, J. (2013a): Geochemistry of metabasalts from the Knob Hill complex and Anarchist Group in the Paleozoic basement to southern Quesnellia; BC Ministry of Energy, Mines and Natural Gas, Geological Fieldwork 2012, Paper 2013-1, p. 45–52.
- Massey, N.W.D. and Dostal, J. (2013b): Boundary Project: Geochemistry of metabasalts from the Knob Hill Complex and Anarchist Group: Report, data tables and ancillary diagrams; BC Ministry of Energy, Mines and Natural Gas, GeoFile 2013-01.
- Massey, N.W.D., Gabites, J.E. and Mortensen, J.K. (2013): LA-ICP-MS geochronology of the Greenwood gabbro, Knob Hill complex, southern Okanagan, British Columbia; BC Ministry of Energy, Mines and Natural Gas, Geological Fieldwork 2012, Paper 2013-1, p. 35–44.
- Mihalynuk, M.G., Logan, J.M., Diakow, L.J., Friedman, R.M. and Gabites, J. (2014): Southern Nicola Arc Project (SNAP): Preliminary results; BC Ministry of Energy and Mines, Geological Fieldwork 2013, Paper 2014-1, p. 29–57.
- Milford, J.C. (1984): Geology of the Apex Mountain Group, north and east of the Similkameen River, south-central British Columbia; M.Sc. thesis, University of British Columbia, Vancouver, 108 p.
- Mills, J. W. (1985): Geologic maps of the Marcus and Kettle Falls quadrangles, Stevens and Ferry Counties, Washington; Washington Department of Natural Resources and Division of Geology and Earth Resources Geologic Map GM-32, scale 1:24 000.
- Mills, J. W. and Davis, J. R. (1962): Permian fossils of the Kettle Falls area, Stevens County, Washington; Contributions from the Cushman Foundation for Foraminiferal Research, v. 13, part 2, p. 41–51.
- Monger, J.W.H. (1977): Upper Paleozoic rocks of the western Canadian Cordillera and their bearing on Cordilleran evolu-

- tion; *Canadian Journal of Earth Sciences*, v. 14, p. 1832–1859.
- Monger, J.W.H. (1989): *Geology of Hope and Ashcroft map areas, British Columbia*; Geological Survey of Canada, Map 42-1989, scale 1:250 000.
- Monger, J.W.H., Wheeler, J.O., Tipper, H.W., Gabrielse, H., Harms, T., Struik, L.C., Campbell, R.B., Dodds, C.J., Gehrels, G.E. and O'Brien, J. (1991): Part B. Cordilleran terranes, Upper Devonian to Middle Jurassic assemblages (Chapter 8), in H. Gabrielse C.J. Yorath (ed.), *Geology of the Cordilleran orogen in Canada*: Geological Survey of Canada, *Geology of Canada*, no. 4, also *Geological Society of America, The Geology of North America*, v. G-2, p. 281–327.
- Mortensen, J.K. (2014): U-Pb ages, geochemistry and Pb-isotopic compositions of Jurassic intrusions, and associated Au(-Cu) skarn mineralization, in the southern Quesnel terrane, southern British Columbia (NTS 082E, F, L, 092H, I); in *Geoscience BC Summary of Activities 2013, Report 2014-1*, p. 83–98.
- Mortensen J.K., Dusel-Bacon C., Hunt J. and Gabites J.E. (2006): Lead isotopic constraints on the metallogeny of middle and late Paleozoic syngenetic base metal occurrences in the Yukon–Tanana and Slide Mountain/Seventymile terranes and adjacent portions of the North American miogeocline; in *Paleozoic Evolution and Metallogeny of Pericratonic Terranes at the Ancient Pacific Margin of North America*, Canadian and Alaskan Cordillera, Geological Association of Canada Special Paper, M. Colpron and J.L. Nelson (ed.), p. 261–280.
- Mortensen, J.K., Lucas, K., Monger, J.W.H. and Cordey, F. (2011): Geological investigations of the basement of the Quesnel Terrane in southern British Columbia (NTS 082E, F, L, 092H, I): progress report; in *Geoscience BC Summary of Activities 2010, Geoscience BC, Report 2011-1*, p. 133–142.
- Mortimer, N. (1987): The Nicola Group: Late Triassic and Early Jurassic subduction-related volcanism in British Columbia; *Canadian Journal of Earth Sciences*, v. 24, p. 2521–2536.
- Nebocat, J. (1993): Geological, geochemical and hand trenching report – NOVA 1-13 mineral claims; Assessment Report 23,178, 20 p.
- Nebocat, J. (1996): Soil geochemical survey report for NOVA 1-13 mineral claims; Assessment Report 24,237, 22 p.
- Nelson, J. and Colpron, M. (2007): Tectonics and metallogeny of the British Columbia, Yukon and Alaskan Cordillera, 1.8 Ga to the present; in *Mineral Deposits of Canada: A Synthesis of Major Deposit-Types, District Metallogeny, the Evolution of Geological Provinces, and Exploration Methods*, edited by W.D. Goodfellow, Geological Association of Canada, Mineral Deposits Division, Special Publication No. 5, p. 755–791.
- Nelson, J., Ferri, F. and Roback, R. (1995): Introduction: raising the questions; Geological Association of Canada–Mineralogical Association of Canada, Joint Annual Meeting, May 17–19, 1995, Victoria, Field Trip Guidebook B2, p. 40–49.
- Okulitch, A.V. (1969): *Geology of Mount Kobau*; Ph.D. thesis, University of British Columbia, Vancouver, 140 p.
- Okulitch, A.V. (1973): Age and correlation of the Kobau Group, Mount Kobau, British Columbia; *Canadian Journal of Earth Sciences*, v. 10, p. 1508–1518.
- Orchard, M.J. (1993): Report on conodonts and other microfossils, Penticton (82E); Geological Survey of Canada Report Number Open File 1993-19.
- Parker, R.L. and Calkins, J.A. (1964): *Geology of the Curlew quadrangle, Ferry County, Washington*; U.S. Geological Survey, Bulletin 1129, 95 p.
- Parrish, R.R., Carr, S.D. and Parkinson, D.L. (1988): Eocene extensional tectonics and geochronology of the southern Omineca Belt, British Columbia and Washington; *Tectonics*, v. 7, p. 181–122.
- Pearce, J.A. (1996): A user's guide to basalt discrimination diagrams; in *Trace Element Geochemistry of Volcanic Rocks: Applications for Massive Sulphide Exploration*, A.H. Bailes, E.H. Christiansen, A.G. Galley, G.A. Jenner, J.D. Keith, R. Kerrich, D.R. Lentz, C.M. Leshner, S.B. Lucas, J.N. Ludden, J.A. Pearce, S.A. Peloquin, R.A. Stern, W.E. Stone, E.C. Syme, H.S. Swinden and D.A. Wyman (ed.), Geological Association of Canada, Short Course Notes-12, p. 79–113.
- Peatfield, G.R. (1978): *Geologic history and metallogeny of the 'Boundary District', southern British Columbia and northern Washington*; Ph.D. thesis, Queen's University, Kingston, 462 p.
- Piercey, S.J., Nelson, J.L., Colpron, M., Dusel-Bacon, C., Simard, R.-L. and Roots, C.F. (2006): Paleozoic magmatism and crustal recycling along the ancient Pacific margin of North America, northern Cordillera; in *Paleozoic Evolution and Metallogeny of Pericratonic Terranes at the Ancient Pacific Margin of North America*, Canadian and Alaskan Cordillera, M. Colpron and J.L. Nelson (ed.), Geological Association of Canada, Special Paper 45, p. 281–322.
- Pohler, S.M.L., Orchard, M.J. and Tempelman-Kluit, D.J. (1989): Ordovician conodonts identify the oldest sediments in the Intermontane Belt, Olalla, south-central British Columbia; in *Current Research, Part E, Geological Survey of Canada, Paper 89-1E*, p. 61–67.
- Ray, G.E. and Dawson, G.L. (1994): The geology and mineral deposits of the Hedley gold skarn district, southern British Columbia; BC Ministry of Energy, Mines and Petroleum Resources, Bulletin 87, 156 p.
- Ray, G.E., Dawson, G.L. and Webster, I.C.L. (1996): The stratigraphy of the Nicola Group in the Hedley district, British Columbia, and the chemistry of its intrusions and Au skarns; *Canadian Journal of Earth Sciences*, v. 33, p. 1105–1126.
- Read, P.B. and Okulitch, A.V. (1977): The Triassic unconformity of south-central British Columbia; *Canadian Journal of Earth Sciences*, v. 14, p. 606–638.
- Rinehart, C.D. and Fox, K.F., Jr. (1972): *Geology and mineral deposits of the Loomis Quadrangle, Okanogan County, Washington*; Washington Division of Mines and Geology Bulletin 64, 124 p.
- Roback, R.C. and Walker, N.W. (1995): Provenance, detrital zircon U-Pb geochronometry, and tectonic significance of Permian to Lower Triassic sandstone in southeastern Quesnellia, British Columbia and Washington; *Geological Society of America Bulletin*, v. 107, p. 665–675.
- Ruks, T.W. (2015): Stratigraphic and paleotectonic studies of Paleozoic Wrangellia and its contained volcanogenic massive sulfide (VMS) occurrences, Vancouver Island, British Columbia, Canada; Ph.D. thesis, University of British Columbia, Vancouver, 375 p., URL <<https://open.library.ubc.ca/cIRcle/collections/ubctheses/24/items/1.0166640>> [January 2016].

- Shervais, J.W. (1982): Ti-V plots and the petrogenesis of modern and ophiolitic lavas; *Earth and Planetary Science Letters*, v. 59, p. 101–118.
- Simandl, G.J. and Church, B.N. (1996): Clearcut pyroxmangite/rhodonite occurrence, Greenwood area, southern British Columbia (82/E2); BC Ministry of Energy, Mines and Petroleum Resources, Geological Fieldwork 1995, Paper 1996-1, p. 219–222.
- Stacey, J.S. and Kramers, J.D. (1975): Approximation of terrestrial lead isotope evolution by a two-stage model; *Earth and Planetary Science Letters*, v. 26, p. 207–221.
- Sun, S.S. and McDonough, W.F. (1989): Chemical and isotopic systematics of oceanic basalts: Implications for mantle composition and processes; *in* *Magmatism in the Ocean Basins*, A.D. Saunders and M.J. Norry (ed.), Geological Society Special Publication 42, p. 313–345.
- Tempelman-Kluit, D.J. (1989): *Geology*, Penticon, British Columbia; Geological Survey of Canada, Map 1736A, scale 1:250 000.
- Thompson, R.I., Glombick, P., Erdmer, P., Heaman, L.M., Lemieux, Y. and Daughtry, K.L. (2006): Evolution of the ancestral Pacific margin, southern Canadian Cordillera: Insights from new geologic maps; *in* *Paleozoic Evolution and Metallogeny of Pericratonic Terranes at the Ancient Pacific Margin of North America*, Canadian and Alaskan Cordillera, M. Colpron and J.L. Nelson (ed.), Geological Association of Canada, Special Paper 45, p. 505–515.
- Winchester, J.A. and Floyd, P.A. (1977): Geochemical discrimination of different magma series and their differentiation products using immobile elements; *Chemical Geology*, v. 20, p. 325–343.
- Wood, D. A. (1980): The application of a Th-Hf-Ta diagram to problems of tectonomagmatic classification and to establishing the nature of crustal contamination of basaltic lavas of the British Tertiary volcanic province; *Earth and Planetary Science Letters*, v. 50, p. 11–30.

Mineralogical and Geochemical Characteristics of Porphyry-Fertile Plutons: Guichon Creek, Takomkane and Granite Mountain Batholiths, South-Central British Columbia (NTS 092I, P, 093A, B)

F. Bouzari, Mineral Deposit Research Unit, The University of British Columbia, Vancouver, BC,
fbouzari@eos.ubc.ca

C.J.R. Hart, Mineral Deposit Research Unit, The University of British Columbia, Vancouver, BC

T. Bissig, Mineral Deposit Research Unit, The University of British Columbia, Vancouver, BC

G. Lesage, Mineral Deposit Research Unit, The University of British Columbia, Vancouver, BC

Bouzari, F., Hart, C.J.R., Bissig, T. and Lesage, G. (2017): Mineralogical and geochemical characteristics of porphyry-fertile plutons: Guichon Creek, Takomkane and Granite Mountain batholiths, south-central British Columbia (NTS 092I, P, 093A, B); *in* Geoscience BC Summary of Activities 2016, Geoscience BC, Report 2017-1, p. 189–200.

Introduction

Distinguishing metal-fertile from barren plutons provides a significant advantage for exploration for porphyry Cu deposits, particularly in British Columbia (BC), where many porphyry systems occur within or around the edges of large batholiths. The fundamental relationship of porphyry Cu (Au, Mo) deposits with bodies of intrusive rocks is well established (e.g., Sillitoe, 1973, 2010), but distinguishing metal-fertile from barren plutons remains a significant challenge for exploration. This is largely because porphyry-related intrusive rocks are common in convergent-margin settings, yet very few host ore deposits. Information that contributes such *a priori* knowledge provides guidance early in the exploration process to make decisions more effectively and efficiently, in order to focus exploration resources on the most prospective targets. This research project, therefore, provides tools and strategies that emphasize porphyry fertility in the BC context.

The formation of porphyry Cu deposits is fundamentally controlled by magmatic processes that generate hydrothermal fluids enriched in metals, Cl and S (e.g., Dilles and Einaudi, 1992). These buoyant fluids are focused in cupolas above the batholiths at shallow depths of 2–4 km, which leads to the formation of porphyry Cu deposits. In many districts, large deposits are hosted within or adjacent to the large plutons that form part of the mineralizing system. These plutons host mineralogical evidence that records fertility characteristics, such as presence of Cl and S, favourable oxidation state and suitable depths of emplacement. The relationship between magmatic processes and ore deposits has long been the focus of ore-deposit research (e.g., Dilles et

al., 2015), but past studies have generally concentrated on the deposit scale. This project investigates district- to batholith-scale porphyry fertility in the Guichon Creek, Takomkane and Granite Mountain batholiths (Figure 1), which will provide a level of assessment not previously documented in BC.

Field and Laboratory Work

Field and laboratory work focused on the characterization of accessory minerals in various intrusive bodies of three well-documented and mapped batholiths, the Guichon Creek, Takomkane and Granite Mountain batholiths, located in south-central BC (Figure 1). In total, 113 rock samples were collected: 52 from Guichon Creek, 35 from Takomkane and 26 from Granite Mountain. Samples were collected from various intrusive phases that constitute each batholith. Samples were disaggregated using an electric-pulse disaggregator (EPD) at Overburden Drilling Management Limited (Nepean, Ontario) to break the rock along mineral-grain boundaries, providing a larger number of unbroken mineral grains. Subsequently, mineral separation was performed at the Mineral Deposit Research Unit (MDRU), The University of British Columbia using Frantz[®] magnetic separation and heavy liquids.

Mineral grains were handpicked, mounted and polished in preparation for electron-probe microanalysis (EPMA) and trace-element laser-ablation inductively coupled plasma-mass spectrometry (LA-ICP-MS) at The University of British Columbia. More than 3000 grains of apatite, titanite, zircon and amphibole were separated. These grains were studied and characterized by binocular, petrographic and cathodoluminescence (CL) microscopy, as well as by scanning electron microscope (SEM). Properties such as colour, shape, inclusion populations, zoning and replacements were documented for each grain. Mineral grains were then analyzed by EPMA for major elements and some trace ele-

Keywords: British Columbia, fertility, plutons, porphyry copper

This publication is also available, free of charge, as colour digital files in Adobe Acrobat[®] PDF format from the Geoscience BC website: <http://www.geosciencebc.com/s/DataReleases.asp>.

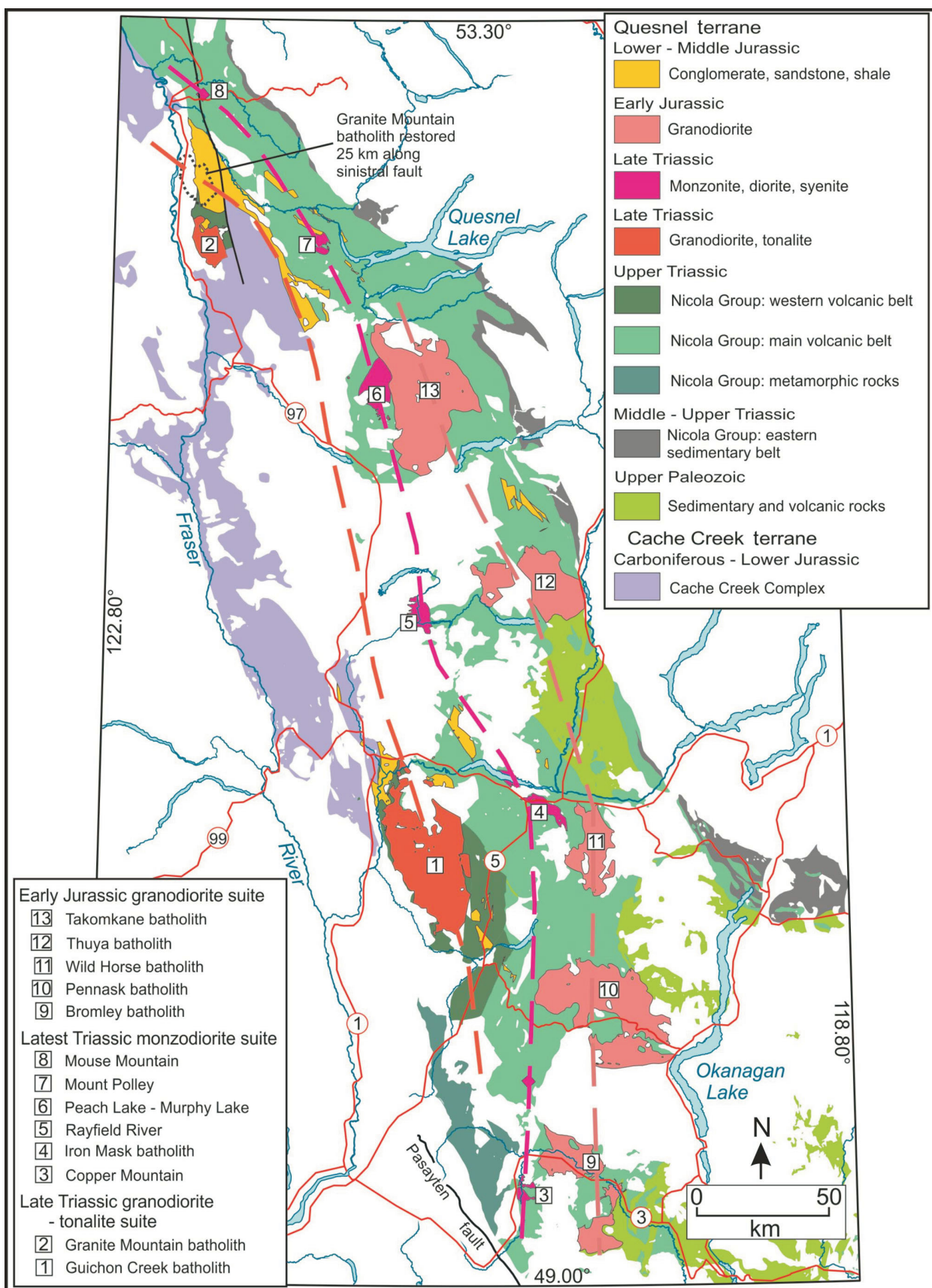


Figure 1. Simplified geology of south-central British Columbia, showing the location of major plutonic bodies. Dashed lines illustrate parallel belts of calcalkaline or alkaline plutons that show progressive younging from west to east (from Schiarizza, 2015).

ments. Subsequently, the same grains were analyzed by LA-ICP-MS for a full trace-element characterization.

Whole-rock samples were analyzed for major and trace elements at Bureau Veritas Minerals (Vancouver, BC; formerly Acme Analytical Laboratories Ltd.), to characterize the geochemical signature of each intrusive unit and to compare the mineral chemistry with whole-rock chemistry. Polished thin sections were prepared from representative samples for petrography.

This paper summarizes initial mineral-grain chemistry results from selected samples based on EPMA and LA-ICP-MS.

Guichon Creek Batholith

The Late Triassic Guichon Creek batholith (Figure 2) is a north-trending, approximately 65 by 30 km body that intruded and thermally metamorphosed the Upper Triassic Nicola Group basaltic to andesitic volcanic and volcanoclastic rocks (Casselman et al., 1995) that form part of the Quesnel terrane. The batholith is composite, with diorite

and quartz diorite border phases flanking a younger granodiorite phase in the centre (Casselman et al., 1995; Byrne et al., 2013). These phases, from the margins inward, are: the Border phase, the Highland Valley phases (consisting of Guichon and Chataway subphases), the Bethlehem phases (consisting of Bethlehem and Skeena subphases) and the Bethsaida phase. The Bethlehem and Skeena subphases and the Bethsaida phase host most of the Highland Valley porphyry Cu-Mo deposits (Valley, Lornex, Highmont, Alwin, Bethlehem and JA). Two mineralization events are recognized: an older event that formed the deposits in the Bethlehem area and was associated with the emplacement of the Bethlehem phase, followed by the formation of the Valley, Lornex and Highmont deposits in conjunction with the emplacement of the Skeena and Bethsaida phases (Byrne et al., 2013).

Takomkane Batholith

The Takomkane batholith (Figure 3) is a large (40 by 50 km) Late Triassic–Early Jurassic composite intrusive body that hosts several mineralized centres. It intrudes the Spout Lake pluton and is cut by Early Jurassic ultramafic–mafic

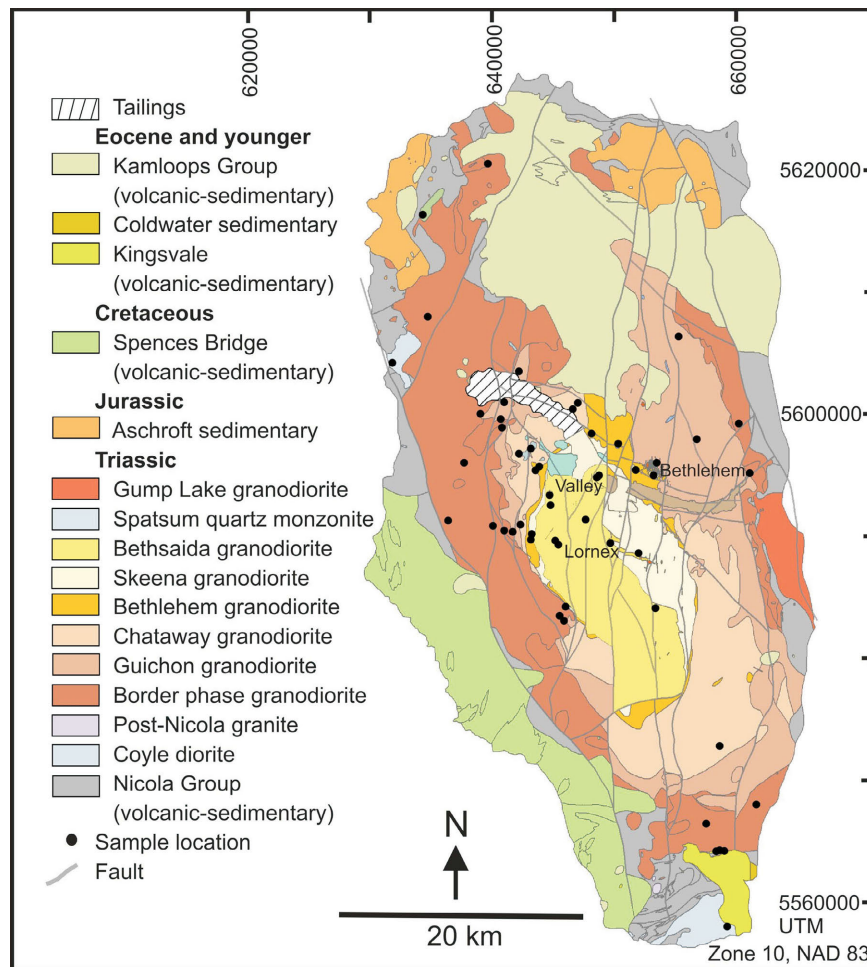


Figure 2. Simplified geology of the Guichon Creek batholith, showing the main intrusive units and sample locations (summarized and redrafted after McMillan et al., 2009).

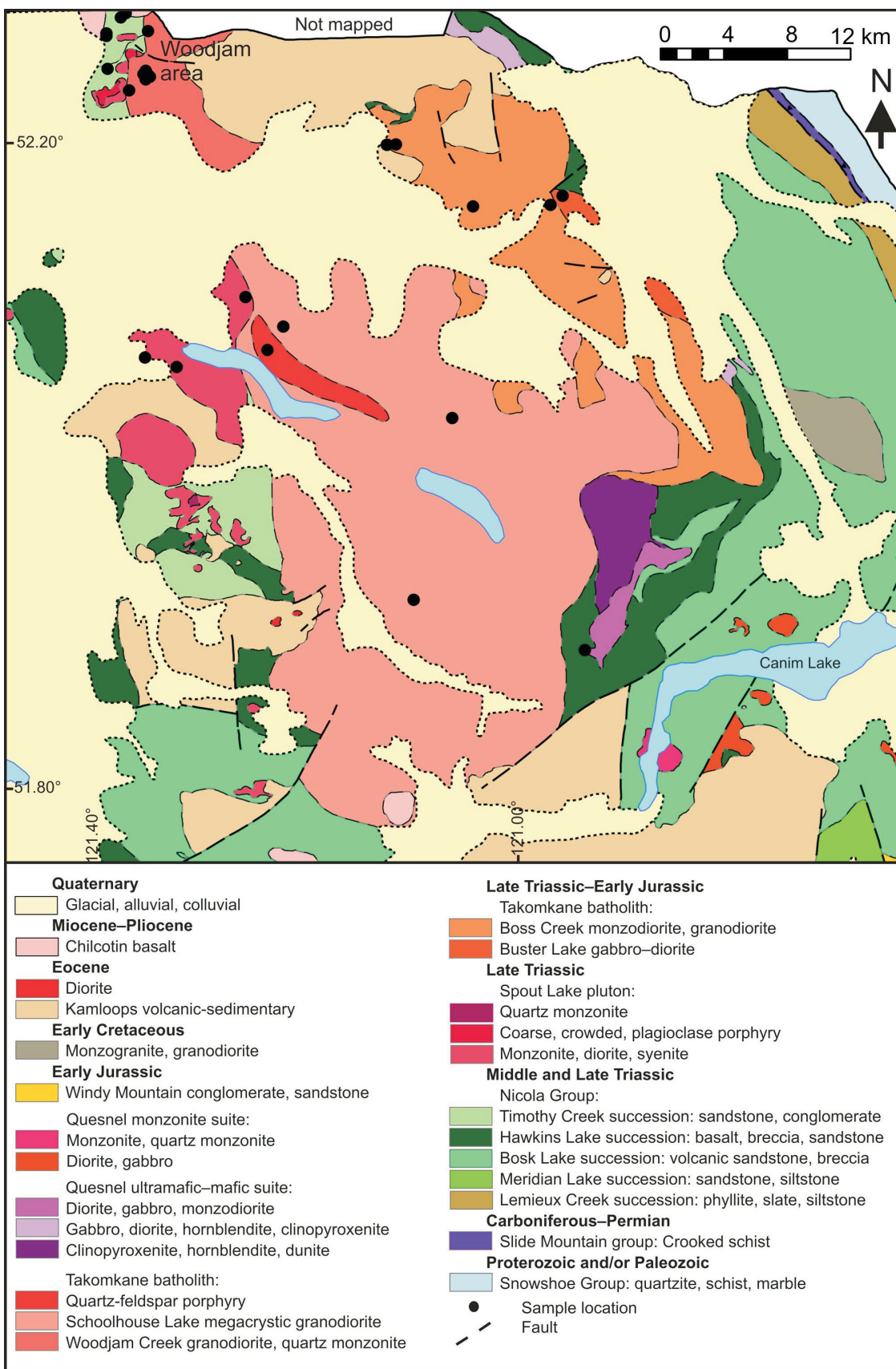


Figure 3. Simplified geology of the Takomkane batholith, showing the main intrusive units and sample locations (summarized and redrafted after Schiarizza et al., 2013).

plutons and the Early Cretaceous Boss Mountain Mine stock. The Takomkane batholith consists of two major units: the Late Triassic–Early Jurassic Boss Creek unit and the Early Jurassic megacrystic Schoolhouse Lake unit. A smaller-volume unit of quartz-feldspar porphyry occurs within the Schoolhouse Lake unit. The Woodjam Creek unit is texturally distinct but compositionally similar to the Schoolhouse Lake unit and forms the northwestern part of the batholith (Schiarizza et al., 2009).

Several small Cu showings occur within the Spout Lake pluton and, to a lesser extent, within the Boss Creek and Schoolhouse units (Schiarizza et al., 2009). However, economically more significant Cu-Mo-Au porphyry mineralization occurs along the northwestern boundary of the batholith in the Woodjam area (Megabuck, Takom, Southeast and Deerhorn deposits). These deposits are hosted within the Woodjam Creek unit or in small porphyry dikes and adjacent volcanic rocks. The Takomkane batholith records a magmatic evolution lasting 11 m.y., with three separate mineralizing events identified at Woodjam (del Real, 2015). The presence of Cu-Au and Cu-Mo deposits, together with the regional northwest tilting of geological units, provides an insight into different levels of exposure and potentially subtle geochemical variations within the intrusive bodies.

Granite Mountain Batholith

The Late Triassic Granite Mountain batholith (18 by 10 km) occurs near McLeese Lake in south-central BC and hosts the Gibraltar porphyry Cu-Mo mine (Figure 4). The batholith is subdivided into three main units, from south-

west to northeast: Border phase diorite to quartz diorite, Mine phase tonalite and Granite Mountain phase leucocratic tonalite. The Burgess Creek stock (Panteleyev, 1978), to the northeast, comprises a heterogeneous assemblage of tonalite, quartz diorite and diorite that intrudes the Nicola Group. Panteleyev (1978) considered the stock to be younger than the Granite Mountain batholith, but more recent dating by Schiarizza (2015) has shown that it is 4–5 m.y. older than the adjacent Granite Mountain phase of the batholith. As suggested by Ash et al. (1999), the Burgess Creek stock may represent the border phase part of the batholith.

It was originally thought that the Granite Mountain batholith intruded the Cache Creek terrane (Bysouth et al., 1995). However, mapping by Schiarizza (2015) recognized Nicola Group strata on the northeastern margin of the batholith and suggested that it is more likely a part of the Quesnel terrane. This is also supported by recent interpretation of aeromagnetic data that has assigned the Granite Mountain area to the Quesnel terrane (Sánchez et al., 2015). Thus, the Granite Mountain batholith is correlative with the Late Triassic, calcalkaline Guichon Creek batholith, host to the Highland Valley porphyry Cu-Mo deposits, 250 km to the south-southeast. Mineralization at the Gibraltar mine is hosted in the Mine phase tonalite of the Granite Mountain batholith, but small porphyry-style mineral occurrences are also known in the Border phase and the Granite Mountain phase (Schiarizza, 2015).

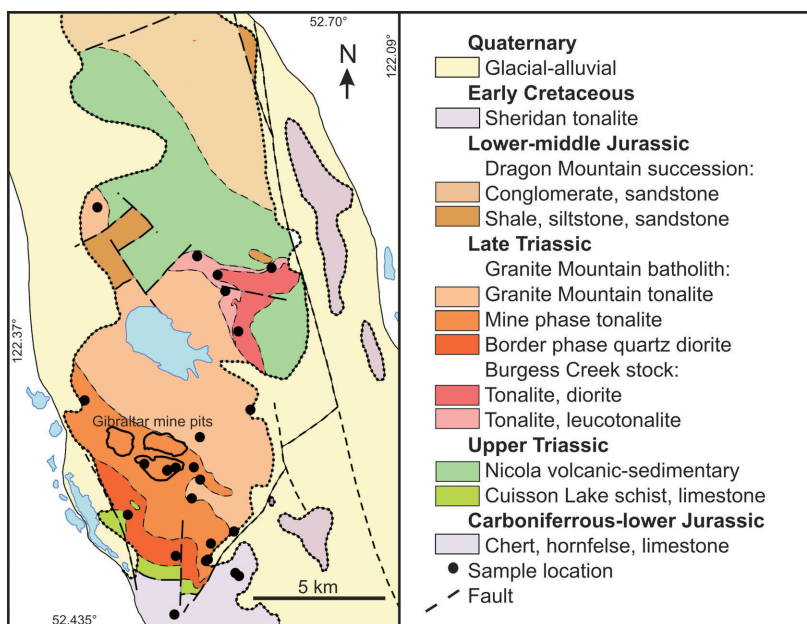


Figure 4. Geology of the Granite Mountain batholith, showing the main intrusive units and sample locations (redrafted after Schiarizza, 2015).

Apatite Chemistry

Trace-element compositions of apatite ($\text{Ca}_5(\text{PO}_4)_3(\text{F},\text{Cl},\text{OH})$) have been used to recognize the characteristics of mantle fluids, assimilation, degree of fractionation and the oxidation state of magma (summarized in Bouzari et al., 2016). Zoned magmatic apatite commonly has S-rich cores that abruptly change to S-poor rims, indicating that early SO_4 -rich magma evolved to SO_4 -poor magma via crystallization of anhydrite (e.g., Streck and Dilles, 1998). Moreover, apatite associated with porphyry Cu deposits is Cl rich (e.g., Roegge et al., 1974). Thus, apatite records the chloride content of the crystallizing melt, which may have played a key role in transporting Cu (Holland, 1972). Mao et al. (2016) used apatite compositions to discriminate their various hostrock and deposit types. Bouzari et al. (2016) showed that apatite luminescence and chemistry can record differing types of hydrothermal alteration in BC porphyry deposits.

Apatite luminescence in the studied samples varied from brown to green and yellow. Apatite grains in largely nonmineralized phases display mostly uniform to zoned brown luminescence (Figure 5a). Some apatite grains have narrow rims of green luminescence or the green luminescence occurs along fractures across the apatite (Figure 5b), suggesting weakly developed zoning or replacement processes. Apatite grains from mineralized rocks have well-developed green luminescence. The green-luminescent apatite typically has darker cores, in most cases a dark brown domain that is zoned outward to green-brown- and green-luminescent apatite (Figure 5c). Apatite grains in mineralized units, particularly the Bethsaida phase of the Guichon Creek batholith, the Woodjam Creek unit of the Takomkane batholith and the Mine phase of the Granite Mountain batholith, display well-developed green luminescence. Locally, the entire apatite grain has green luminescence (Figure 5d). The main exception is the poorly mineralized Schoolhouse Lake unit of the Takomkane batholith, which shows apatite with brown luminescent cores but well-developed green luminescent zones (Figure 5e). Apatite grains from altered-mineralized hostrocks typically display both green and patchy grey luminescence (Figure 5f), reflecting proximal hydrothermal-alteration effects (Bouzari et al., 2016).

Detailed electron-probe microanalyses of several zoned apatite grains show a correlation between luminescence and chemistry. The brown-luminescent cores are S and Cl rich but with low Fe/Mn ratios. Green-luminescent apatite rims have relatively low concentrations of S and Cl but higher Fe/Mn ratios (Figure 6). In zoned apatite, there is generally a decrease in S and Cl concentrations and an increase in Fe/Mn ratio from the core to rim (see Figure 5c).

Chemical analyses of apatite grains show distinct variations between mineralized and barren phases of the batholiths. In the Bethsaida phase of the Guichon Creek batholith, which is the main host to the Highland Valley porphyry deposits, apatite grains have less Cl and S relative to the Chataway phase. The Cl concentration of apatite in both phases is less than that of apatite in the Guichon phase (Figure 7a). Similarly, apatite from the Mine phase of the Granite Mountain batholith, which is the main host to the Gibraltar deposit, has lower Cl and S concentrations than apatite from the unmineralized Burgess Creek stock (Figure 7b). The Granite Mountain phase shows Cl and S concentrations similar to the Mine phase. The apatite composition of the Takomkane batholith shows some variability. Apatite from the Late Triassic Spout Lake monzodiorite and the Jurassic Woodjam Creek monzogranite has variable Cl and S concentrations from high to low, roughly displaying a trend from high S and Cl values to low values (Figure 7c). Both of these units are the main host to the Cu mineralization, although the known extent of mineralization in the Woodjam Creek is larger than that in the Spout Lake (Schiarizza et al., 2009). The Late Triassic–Early Jurassic Boss Creek monzodiorite and Jurassic Schoolhouse Lake megacrystic granodiorite have apatite with largely moderate to low S and low Cl concentrations. The Boss Creek apatite has uniform brown luminescence, whereas Schoolhouse Lake apatite has locally brown luminescent cores surrounded by green luminescent rims. Both of these units host only a few subeconomic Cu occurrences (Rodeo and Lucy Jack occurrences).

These observations suggest that, in each batholith, the mineralized intrusive bodies evolved from early Cl- and S-rich phases toward phases with less Cl and S. This can be seen in zoned apatite grains, which became progressively depleted in Cl and S from core to rim. Therefore, the apatite from mineralized intrusive bodies displays a depletion trend for Cl and S and commonly has lower concentrations of these elements relative to the barren or less mineralized bodies. Apatite with scattered but low Cl and S concentrations and commonly uniform CL texture, such as those from Boss Creek, suggests a probable low budget of Cl and S in the crystallizing melt. This apatite differs clearly from that in mineralized rock units.

Titanite Chemistry

Titanite (CaTiSiO_5) is a common accessory mineral occurring in amounts of about 2–4% in various phases of the studied batholiths. Titanite grains are 1–2 mm, range from colourless to dark brown and locally contain inclusions of an opaque phase, most commonly ilmenite. Less commonly, inclusions of apatite and quartz are also noted (Figure 8a). Titanite textures under SEM vary from uniform to zoned, and more rarely display irregular mottled rims. Titanite is a robust and stable phase in a magmatic system and

can incorporate geochemically important trace elements into its structure, thus providing a powerful tool for petrogenetic studies (e.g., Kowallis, 1997; Piccoli et al., 2000) and studies of ore deposit-related alteration processes (e.g., Che et al., 2013; Celis, 2015). Electron-microprobe

data were used to calculate mineral formulas based on five oxygens in the ideal titanite formula, $ABOT_4$, where the A site is filled by Ca^{2+} , Mn^{2+} , Na^+ , K^+ and REE^{3+} , the B site is filled by Ti^{4+} , Fe^{3+} and Al^{6+} , and the T site is filled by Si^{4+} and Al^{4+} .

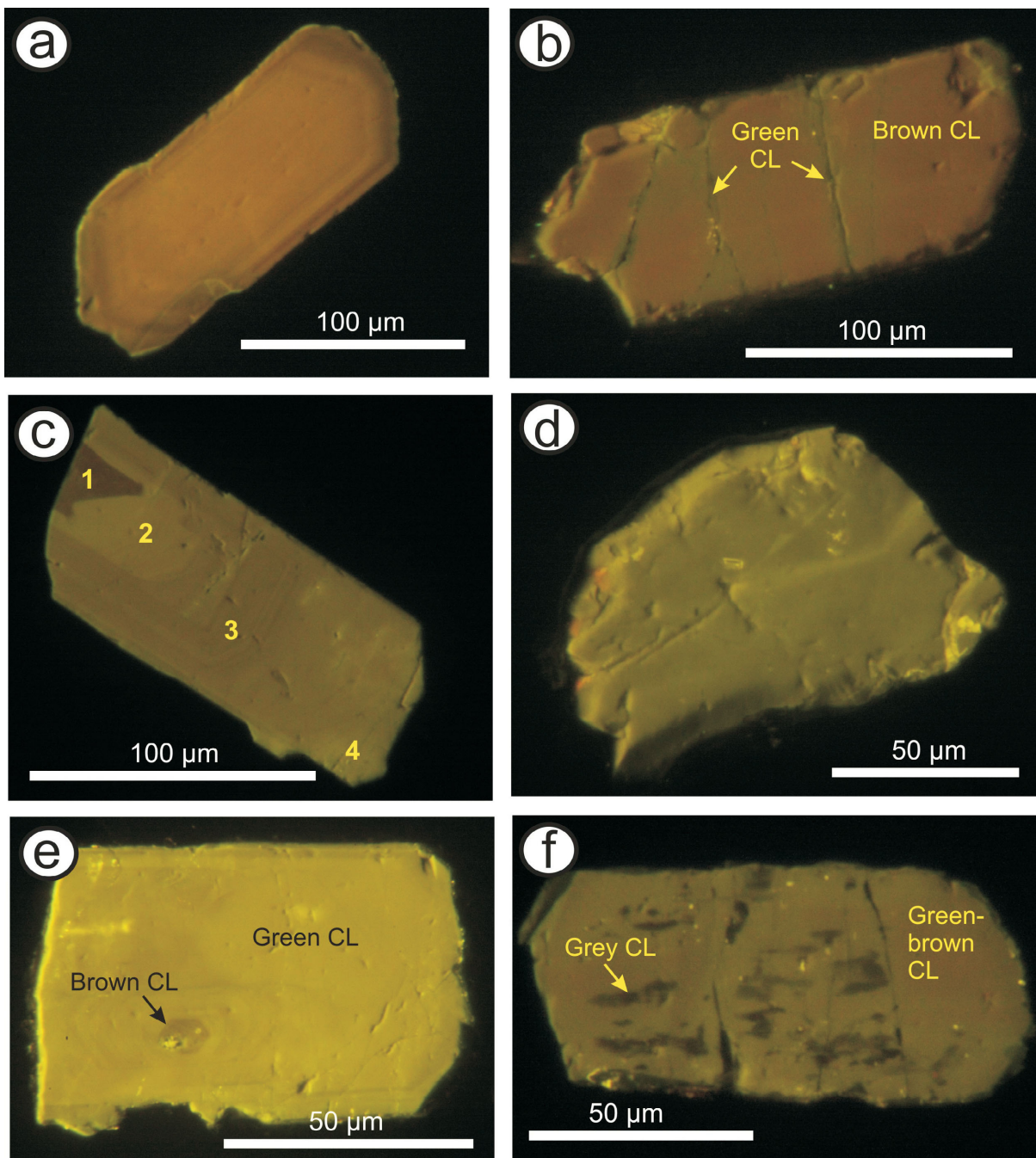


Figure 5. Cathodoluminescence images of apatite grains from the Guichon Creek, Takomkane and Granite Mountain batholiths: **a)** zoned apatite with brown luminescence from the Spout Lake pluton, Takomkane batholith; **b)** apatite from the Granite Mountain phase of the Granite Mountain batholith with brown luminescence and weak green luminescence developed along fractures; **c)** zoned apatite from the Woodjam Creek unit of the Takomkane batholith, showing a core with brown luminescence and a rim with green luminescence; numbers represent location of spots analyzed by EPMA (see Figure 6); **d)** apatite from the Bethesda phase of the Guichon Creek batholith, showing green luminescence; **e)** apatite from the Schoolhouse Lake unit of the Takomkane batholith with a brown luminescent core surrounded by yellow-green luminescent apatite; **f)** apatite from the altered and mineralized Mine phase of the Granite Mountain batholith with green luminescence, as well as remnants of brown luminescence overprinted by grey luminescence. Abbreviations: CL, cathodoluminescence; EPMA, electron-probe microanalysis.

The chemical composition of titanite from the Guichon Creek batholith shows a correlation between rock type and Fe, Al and Mn concentrations, specifically a positive correlation between Fe/Al and Mn/Ca ratios. More importantly, titanite in the Bethsaida and Skeena granodiorite (host to the mineralization) has the highest Fe/Al and Mn/Ca ratios, whereas titanite in the other phases of batholith has lower Fe/Al and Mn/Ca (Figure 9a). In fact, the Fe/Al and Mn/Ca ratio increases from the older border phase to the (younger) central mineralized phase (Bethsaida) of the batholith.

Titanite from the Takomkane batholith has similar variations. The mineralized Woodjam Creek granodiorite has high Fe/Al and moderate Mn/Ca ratios. Titanite in the older Boss Creek unit and the younger Schoolhouse Lake unit has lower Fe/Al relative to that in the Woodjam Creek unit but similar moderate Mn/Ca (Figure 9b). The quartz-feldspar porphyry, which occurs as a small body inside the Schoolhouse Lake unit, has titanite with similar Fe/Al and Mn/Ca ratios, but some grains have ratios that are distinctly higher than those in the Woodjam Creek unit. The Late Triassic Spout Lake monzodiorite has Fe/Al and Mn/Ca ratios similar to those in the Schoolhouse Lake unit. The Quesnel diorite, which cuts the Takomkane batholith units, has ti-

tanite with low Mn/Ca and moderate Fe/Al ratios. Overall, Takomkane titanite, similar to Guichon Creek titanite, shows a positive correlation between Fe/Al and Mn/Ca ratios, with the mineralized unit showing high Fe/Al compositional ratios. However, unlike the Guichon Creek batholith, that shows a single trend of Fe/Al and Mn/Ca ratios for titanite, the Takomkane batholith shows at least two distinct trends, possibly reflecting more complex intrusive relationships.

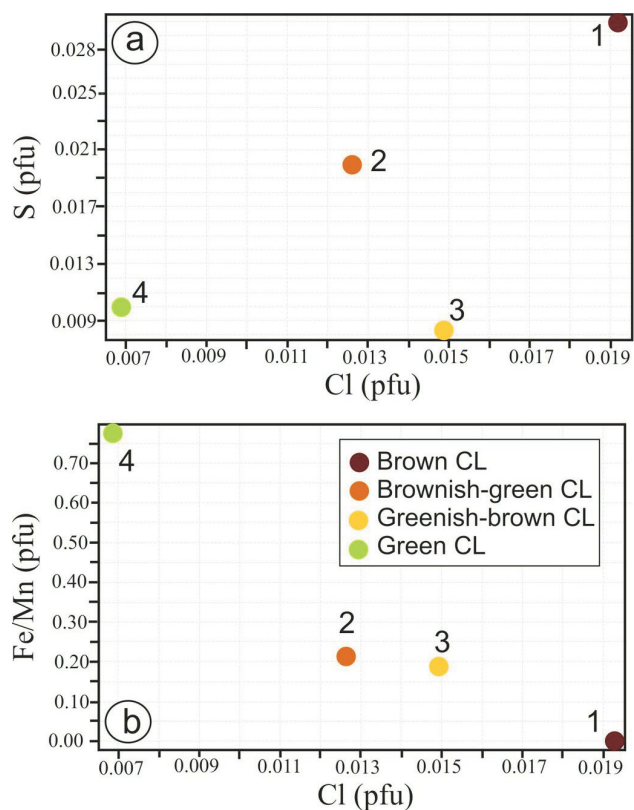


Figure 6. Binary diagram showing correlation of apatite luminescence in a single zoned apatite grain from the Woodjam Creek unit of the Takomkane batholith with Cl and S concentrations (see Figure 5c for location of analyzed spots). Abbreviations: CL, cathodoluminescence; pfu, per formula unit.

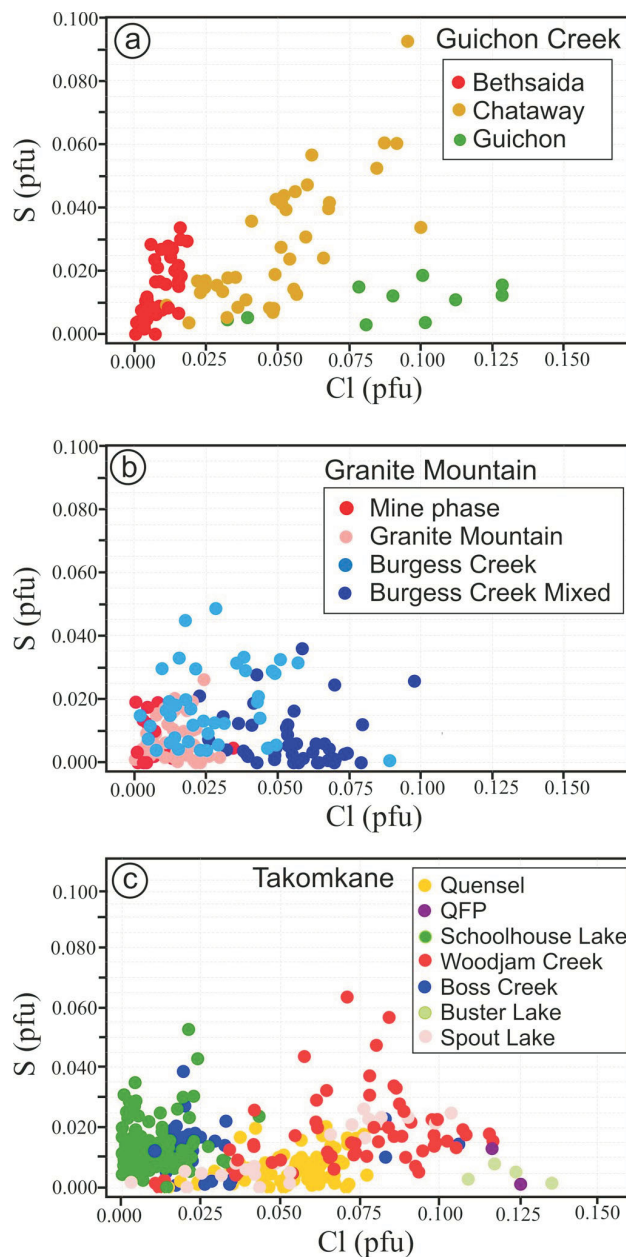


Figure 7. Binary diagrams of apatite compositions in various mineralized and barren pluton phases of the Guichon Creek, Takomkane and Granite Mountain batholiths; Cl and S values are calculated per formula unit (pfu). Abbreviation: QFP, quartz-feldspar porphyry.

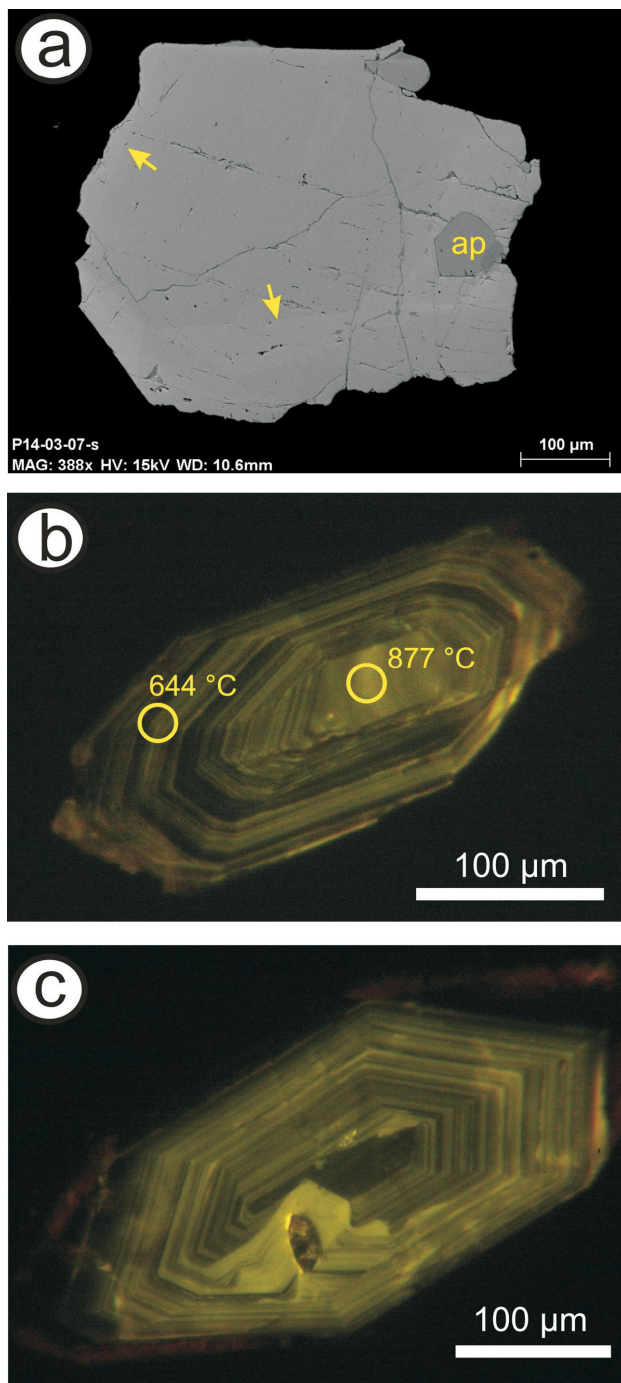


Figure 8. a) Scanning electron microscope image of a zoned titanite grain from the Bethlehem phase of the Takomkane batholith; the rim shown by arrows has higher Fe/Al and Mn/Ca ratios relative to the core. b) Cathodoluminescence image of a zircon grain from the quartz-feldspar porphyry unit of the Takomkane batholith, showing oscillatory zoning and, on the basis of Ti-in-zircon thermometry, a lower crystallization temperature at the rim; yellow circles represent areas analyzed by LA-ICP-MS. c) Cathodoluminescence image of zircon from the Schoolhouse Lake unit of the Takomkane batholith, showing oscillatory zoning with some irregularity causing termination of some zones, especially near a mineral inclusion.

Zircon Chemistry

Zircon (ZrSiO_4) is a geochemically robust mineral that records orthomagmatic chemical compositions that influence formation of porphyry Cu deposits. Zircon trace-element behaviour, as recorded during its growth, can be used to examine crystal fractionation, crustal assimilation and magma mixing. Zircon incorporates a suite of lithophile elements, including rare-earth elements (REE), U, Th and Hf, in concentrations that are dependent upon the pressure, temperature and composition of the magma (Hanchar and Watson, 2003). In addition, the Ti-in-zircon geothermometer can determine zircon-crystallization temperatures (Ferry and Watson 2007). Zircon is also a sensitive indicator of the magmatic oxidation state because of its multivalent Ce and Eu contents. Investigation by Ballard et al. (2002) and more recently by Shen et al. (2015) correlated the relative $\text{Ce}^{4+}/\text{Ce}^{3+}$ in zircon with the oxidation state of barren and Cu-mineralized intrusive rocks in northern Chile and central Asia. Dilles et al. (2015) showed similar relationships for porphyry deposits in Chile using the Eu concentration in zircon and suggested that small negative Eu anomalies ($\text{Eu}_N/\text{Eu}_N^* = 0.4$) indicate oxidizing magmatic conditions that reflect oxidation due to SO_2 degassing from magmas.

Zircon typically forms 100–500 μm long grains with complex internal oscillatory and sector zoning; in some cases, the grains have inherited cores. Cathodoluminescence imaging was used to characterize zircon grains. Oscillatory zoning typically forms fine concentric zones of dark- and light-coloured domains (Figure 8b). The zoning, in some cases, becomes irregular and new growth zones may cross-cut older zones (Figure 8c), probably due to chemical disequilibrium or a pronounced change in temperature. Results from LA-ICP-MS analysis of selected Takomkane batholith rock samples demonstrate the application of zircon chemistry to BC porphyry-fertility studies.

Results of the calculated Ti-in-zircon temperature, corrected to an activity for TiO_2 of ~ 0.7 , are plotted against Hf concentration in Figure 10a. Despite some scatter in the data, probably due to analytical uncertainties and small variations in the activity of TiO_2 in melt, Figure 10a illustrates that the Hf content in zircon increases with a decrease in Ti-in-zircon temperature, as has been previously documented in other felsic melts (e.g., Claiborne et al., 2010). Zircons from the Boss Creek unit show variable temperatures ranging from 950°C to below 650°C, whereas the Schoolhouse Lake unit has temperatures above 850°C (Figure 10a). Zircons from the mineralized Woodjam Creek granodiorite and the late quartz-feldspar porphyry unit have modelled Ti-in-zircon temperatures of 750–650°C, consistent with zircon crystallization in near-eutectic conditions close to the solidus of hydrous granite. Zircons from the youngest smaller unit of quartz-feldspar

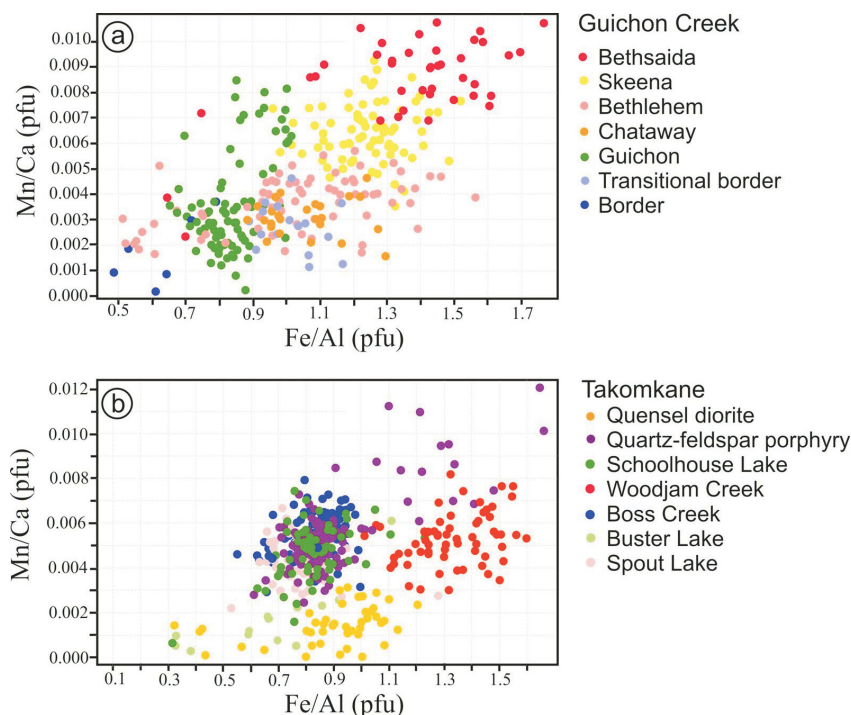


Figure 9. Binary diagrams of titanite compositions in various mineralized and barren pluton phases of **a)** the Guichon Creek batholith, showing that the Bethsaida and Skeena phases have high Fe/Al and Mn/Ca; and **b)** the Takomkane batholith, showing that the Woodjam Creek unit has high Fe/Al but moderate Mn/Ca.

porphyry have a temperature range similar to or less than that of the Woodjam Creek unit.

The chondrite-normalized negative Eu anomaly (Eu_N/Eu_N^* , where $Eu_N^* = (Sm_N \times Gd_N)^{1/2}$) of zircon has been used to characterize the fertility of igneous rocks (Ballard et al., 2002; Dilles et al., 2015). Chemical compositions of zircon grains from the Takomkane batholith indicate that the unmineralized Boss Creek unit has a more pronounced Eu anomaly ($Eu_N/Eu_N^* < 0.35$) compared to the other rock suites. Zircons from the mineralized Woodjam Creek unit have relatively small negative Eu anomalies (mostly $Eu_N/Eu_N^* > 0.35$). The younger phases of batholith, Schoolhouse Lake and the quartz-feldspar porphyry unit, are both similar to the Woodjam Creek unit in displaying $Eu_N/Eu_N^* < 0.35$, but these phases have a larger range of Eu_N/Eu_N^* values (Figure 10b).

Discussion

The results of this study suggest that the chemical compositions of apatite, titanite and zircon can be used to characterize porphyry-fertile intrusive rocks. Porphyry-fertile plutons contain apatite that becomes progressively depleted in Cl and S, but enriched in Fe relative to Mn, during crystallization. The depletion in S is attributed to the evolution of an early magma that is oxidizing and SO_4 rich to a melt that is SO_4 poor as a result of crystallization of anhydrite (Streck and Dilles, 1998). The increase in the Fe/Mn ratio in apa-

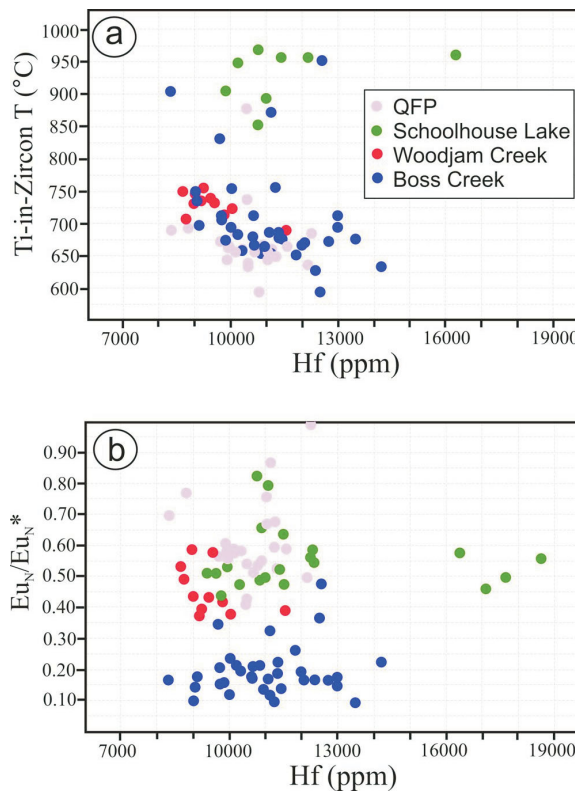


Figure 10. Rare-earth element concentrations in zircon from the Takomkane batholith: **a)** Ti-in-zircon temperature versus Hf concentration, assuming a melt activity for TiO_2 of ~ 0.7 , calculated after Ferry and Watson (2007); **b)** zircon Eu anomaly (Eu_N/Eu_N^*) versus Hf concentration. Abbreviation: QFP, quartz-feldspar porphyry.

tite, which is largely responsible for green luminescence, is also interpreted to be controlled by magmatic evolution toward a higher oxidation state. Further cooling of the melt caused saturation in a water-rich fluid phase, and probably the breakdown of crystalline anhydrite and the release of SO₂ to a vapour phase (Dilles et al., 2015). The depletion in both Cl and S of apatite from the mineralized pluton provides evidence for degassing of SO₂-rich magmatic volatiles from SO₄-rich melts. These Cl- and S-rich volatiles generated from such fertile plutons are capable of carrying Cu and producing porphyry Cu ores.

The change of oxidation state is also recognized from the titanite chemistry. Titanite from the mineralized pluton has high Fe/Al, attributed to an increase in oxygen fugacity that controls the abundance of Fe³⁺ substituting for Ti in the B site (Kowallis, 1997). The same conditions were probably responsible for an increase of Mn substituting for Ca in the A site. Evidence from ilmenite in the cores of titanite and higher Fe/Al and Mn/Ca in the rims, also suggest that the mineralized plutons became progressively oxidized over time.

Titanium-in-zircon temperatures calculated for the mineralized units indicate that these magmas were largely crystallized at 750–650°C in near-eutectic conditions close to the solidus of hydrous granite. These data provide additional information about the conditions for metal and S behaviour as they are partitioned into the hydrothermal phase, rather than incorporated into earlier-formed minerals or forming magmatic sulphide (Burnham and Ohmoto, 1980; Candela, 1986). Barren or weakly mineralized plutonic phases show evidence of the initiation of crystallization at higher temperature compared to fertile phases.

Zircon REE compositions indicate that fertile granitic bodies have small negative Eu anomalies (EuN/EuN* = 0.35). This reflects 1) high water content and consequent suppression of early plagioclase crystallization (e.g., Ballard et al., 2002) and 2) late magmatic oxidation resulting in the loss of SO₂-rich magmatic-hydrothermal ore fluids during late-stage crystallization of granite (Dilles et al., 2015). The smaller Eu anomalies observed in zircons from mineralized intrusions compared to nonmineralized intrusions may result from suppression of plagioclase crystallization at high pressure and water content (Richards et al., 2012), or they could be due to the higher oxidation state of melts (e.g., Dilles et al., 2015). However, evidence from the Fe/Al ratios in titanite independently suggests higher oxidation state, which is consistent with only moderate Eu anomalies in the zircons of fertile intrusions. Moreover, S and Cl depletion in apatite indicates degassing of SO₂-rich magmatic volatiles, thus supporting the required oxidation state.

This study shows that apatite, titanite and zircon can provide tools to characterize fertility factors in plutonic rocks,

in particular Cl and S contents, temperature and oxidation state. The use of these three indicator minerals together provides a means of assessing the Cu fertility of plutons.

Acknowledgments

Geoscience BC is thanked for its financial contribution in support of this project. Additional samples from the Granite Mountain batholith were provided by P. Schiarizza of the BC Geological Survey and N. Mostaghimi of The University of British Columbia. B. Najafian helped with mineral separation, E. Chan helped with mineral-grain photographing and H. McIntyre helped with drafting maps and LA-ICP-MS. The authors also thank A. Wainwright of the Mineral Deposit Research Unit, The University of British Columbia for his review and comments on this paper.

References

- Ash, C.H., Rydman, M.O., Payne, C.W. and Panteleyev, A. (1999): Geological setting of the Gibraltar mine, south-central British Columbia (93B/8, 9); *in* Exploration and Mining in British Columbia 1998, BC Ministry of Energy and Mines, BC Geological Survey, p. A1–A15.
- Ballard, J.R., Palin, J.M. and Campbell, I.H. (2002): Relative oxidation states of magmas inferred from Ce(IV)/Ce(III) in zircon: application to porphyry copper deposits of northern Chile; *Contributions to Mineralogy and Petrology*, v. 144, p. 347–364.
- Bouzari, F., Hart, C.J.R., Bissig, T. and Barker, S. (2016): Hydrothermal alteration revealed by apatite luminescence and chemistry: a potential indicator mineral for exploring covered porphyry copper deposits; *Economic Geology*, v. 111, p. 1397–1410, URL <<http://econgeol.geoscienceworld.org/content/111/6/1397>> [November 2016].
- Burnham, C.W. and Ohmoto, H. (1980): Late-stage processes of felsic magmatism; *in* Granitic Magmatism and Related Mineralization, S. Ishihara and S. Takenouchi, S. (ed.), *Mining Geology*, Special Issue 8, p. 1–11.
- Byrne, K., Stock, E., Ryan, J., Johnson, C., Nisenson, J., Alva Jimenez, T., Lapointe, M., Stewart, H., Grubisa, G. and Sykora, S. (2013): Porphyry Cu-(Mo) deposits in the Highland Valley district, south-central British Columbia; *in* Porphyry Systems of Central and Southern BC, Tour of Central BC Porphyry Deposits from Prince George to Princeton, J. Logan, and T. Schroeter (ed.), *Society of Economic Geologists, Field Guidebook Series*, v. 44, p. 99–116.
- Bysouth, G.D., Campbell, K.V., Barker, G.E. and Gagnier, G.K. (1995): Tonalite trondhjemite fractionation of peraluminous magma and the formation of syntectonic porphyry copper mineralization, Gibraltar mine, central British Columbia; *in* Porphyry Deposits of the Northwestern Cordillera of North America, T.G. Schroeter (ed.), *Canadian Institute of Mining, Metallurgy and Petroleum, Special Volume 46*, p. 201–213.
- Candela, P.A. (1986): The evolution of aqueous vapor from silicate melts: effect on oxygen fugacity; *Geochimica et Cosmochimica Acta*, v. 50, p. 1205–1211.
- Casselmann, M.J., McMillan, W.J. and Newman, K.M. (1995): Highland Valley porphyry copper deposits near Kamloops, British Columbia: a review and update with emphasis on the Valley deposit; *in* Porphyry Deposits of the Northwestern Cordillera of North America, T.G. Schroeter (ed.), *Canadian*

- Institute of Mining and Metallurgy, Special Volume 46, p. 161–191.
- Celis, M.A. (2015): Titanite as an indicator mineral for alkalic Cu-Au porphyry deposits in south-central British Columbia; M.Sc. thesis, The University of British Columbia, 247 p.
- Che, X.D., Linnen, R.L., Wang, R.C., Groat, L.A. and Allison, A.B. (2013): Distribution of trace and rare earth elements in titanite from tungsten and molybdenum deposit in Yukon and British Columbia, Canada; *The Canadian Mineralogist*, v. 51, p. 415–438.
- Claiborne, L.L., Miller, C.F. and Wooden, J.L. (2010): Trace element composition of igneous zircon: a thermal and compositional record of the accumulation and evolution of a large silicic batholith, Spirit Mountain, Nevada; *Contributions to Mineralogy and Petrology*, v. 160, p. 511–531.
- del Real, I. (2015): Geology, alteration, mineralization and magmatic evolution of the Southeast Zone (Cu-Mo) and Deerhorn (Cu-Au) porphyry deposits, Woodjam, central British Columbia, Canada; M.Sc. thesis, The University of British Columbia, 315 p.
- Dilles, J.H. and Einaudi, M.T. (1992): Wall-rock alteration and hydrothermal flow paths about the Ann-Mason porphyry copper deposit, Nevada: a 6-km vertical reconstruction; *Economic Geology*, v. 87, p. 1963–2001.
- Dilles, J.H., Kent, A.J.R., Wooden, J.L., Tosdal, R.M., Koleszar, A., Lee, R.G. and Farmer, L.P. (2015): Zircon compositional evidence for sulfur-degassing from ore-forming arc magmas; *Economic Geology*, v. 110, p. 241–251.
- Ferry, J.M., and Watson, E.B. (2007): New thermodynamic models and revised calibrations for the Ti-in-zircon and Zr-in-rutile thermometers; *Contributions to Mineralogy and Petrology*, v. 154, p. 429–437.
- Hanchar, J.M. and Watson, E.B. (2003): Structure and chemistry of zircon and zircon group minerals; *in* Zircon, J.M. Hanchar and P.W.O. Hoskin (ed.), *Reviews in Mineralogy and Geochemistry*, v. 53, p. 89–112.
- Holland, H.D. (1972): Granites, solutions, and base metal deposits; *Economic Geology*, v. 67, p. 281–301.
- Kowallis, B.J. (1997): Compositional variations in titanite; *Geological Society of America, Abstracts with Programs*, v. 29, p. 402.
- Mao, M., Rukhlov A.S., Rowins, S.M., Spence, J. and Coogan, L.A. (2016): Apatite trace element compositions: a robust new tool for mineral exploration; *Economic Geology*, v. 111, p. 1187–1222, URL <<http://econgeol.geoscienceworld.org/content/111/5/1187>> [November 2016].
- McMillan, W.J., Anderson, R.G., Chan, R. and Chow, W. (2009): Geology and mineral occurrences (MINFILE), the Guichon Creek Batholith and Highland Valley porphyry copper district, British Columbia; Geological Survey of Canada, Open File 6079, 2 maps, URL <<http://geogratis.gc.ca/api/en/nrcan-rncan/ess-sst/78e93fdd-50d0-5877-a024-310362144149.html>> [November 2016].
- Panteleyev, A. (1978): Granite Mountain project (93B/8); *in* Geological Fieldwork 1977, BC Ministry of Energy and Mines, BC Geological Survey, Paper 1977-1, p. 39–42.
- Piccoli, P., Candela, P. and Rivers, M. (2000): Interpreting magmatic processes from accessory phases: titanite – a small-scale recorder of large-scale processes; *Transactions of the Royal Society of Edinburgh, Earth Sciences*, v. 91, p. 257–267.
- Richards, J.P., Spell, T., Rameh, E., Raziq, A. and Fletcher, T. (2012): High Sr/Y magmas reflect arc maturity, high magmatic water content, and porphyry Cu±Mo±Au potential: examples from the Tethyan arcs of central and eastern Iran and western Pakistan; *Economic Geology*, v. 107, p. 295–332.
- Roegge, J.S., Logsdon, M.J., Young, H.S., Barr, H.B., Borcsik, M. and Holland, H.D. (1974): Halogens in apatite from the Providencia area, Mexico; *Economic Geology*, v. 69, p. 229–240.
- Sánchez, M.G., Bissig, T. and Kowalczyk, P. (2015): Toward an improved basis for beneath-cover mineral exploration in the QUEST area, central British Columbia: new structural interpretation of geophysical and geological datasets (NTS 093A, B, G, H, J, K, N); *in* Geoscience BC Summary of Activities 2014, Geoscience BC, Report 2015-1, p. 53–62, <http://www.geosciencebc.com/i/pdf/SummaryofActivities2014/SoA2014_Sanchez.pdf> [November 2016].
- Schiarizza, P. (2015): Geological setting of the Granite Mountain batholith, south-central British Columbia; *in* Geological Fieldwork 2014, BC Ministry of Energy and Mines, BC Geological Survey, Paper 2015-1, p. 19–39, <http://www.empr.gov.bc.ca/Mining/Geoscience/PublicationsCatalogue/Fieldwork/Documents/2014/02_Schiarizza.pdf> [November 2016].
- Schiarizza, P., Bell, K. and Bayliss, S. (2009): Geology and mineral occurrences of the Murphy Lake area, south-central British Columbia (NTS 093A/03); *in* Geological Fieldwork 2008, BC Ministry of Energy and Mines, BC Geological Survey, Paper 2009-1, p. 169–188, <http://www.empr.gov.bc.ca/Mining/Geoscience/PublicationsCatalogue/Fieldwork/Documents/2008/15_Schiarizza.pdf> [November 2016].
- Schiarizza, P., Israel, S., Heffernan, S., Boulton, A., Blich, J., Bell, K., Bayliss, S., Macauley, J., Bluemel, B., Zuber, J., Friedman, R.M., Orchard, M.J. and Poulton, T.P. (2013): Bedrock geology between Thuya and Woodjam creeks, south-central British Columbia, NTS 92P/7, 8, 9, 10, 14, 15, 16; 93A/2, 3, 6; BC Ministry of Energy and Mines, BC Geological Survey, Open File 2013-05, 4 sheets, 1:100 000 scale, <<http://www.empr.gov.bc.ca/mining/geoscience/publications/catalogue/openfiles/2013/pages/2013-5.aspx>> [November 2016].
- Shen, P., Hattori, K., Pan, H., Jackson, S. and Seitmuratova, E. (2015): Oxidation condition and metal fertility of granitic magmas: zircon trace-element data from porphyry Cu deposits in the Central Asian orogenic belt; *Economic Geology*, v. 110, p. 1861–1878.
- Sillitoe, R.H. (1973): The tops and bottoms of porphyry copper deposits; *Economic Geology*, v. 68, p. 799–815.
- Sillitoe, R.H. (2010): Porphyry copper systems; *Economic Geology*, v. 105, p. 3–41.
- Streck, M.J. and Dilles, J.H. (1998): Sulfur evolution of oxidized arc magmas as recorded in apatite from a porphyry copper batholith; *Geology*, v. 26, p. 523–526.

Detrital Gold as a Deposit-Specific Indicator Mineral, British Columbia: Analysis by Laser-Ablation Inductively Coupled Plasma–Mass Spectrometry

R.J. Chapman, School of Earth and Environment, Leeds University, Leeds, United Kingdom,
r.j.chapman@leeds.ac.uk

D.A. Banks, School of Earth and Environment, Leeds University, Leeds, United Kingdom

C. Spence-Jones, School of Earth and Environment, Leeds University, Leeds, United Kingdom

Chapman, R.J., Banks, D.A. and Spence-Jones, C. (2017): Detrital gold as a deposit-specific indicator mineral, British Columbia: analysis by laser-ablation inductively coupled plasma–mass spectrometry; in Geoscience BC Summary of Activities 2016, Geoscience BC, Report 2017-1, p. 201–212.

Introduction

The northern cordillera has been the focus of traditional prospecting for nearly 200 years. Placer-gold occurrences are widespread and have supported an industry that has underpinned many local economies. In some cases, further prospecting has identified significant in situ mineralization that has also been profitably exploited, but the relationship between placer gold and its source lode is less clear at other localities, either as a consequence of extensive surficial sediments or because complex solid geology provides several potential geological settings for source mineralization. Both these factors have constrained exploration in British Columbia (BC). The use of gold compositional studies has elevated the potential value of detrital gold from a simple physical marker to an indicator of the source style of mineralization. For example, regional studies in the Yukon and the Fortymile district of the Yukon and Alaska have identified the importance of gold derived from orogenic systems in local placer inventories, even when an intrusion-related source type has been proposed (Wrighton, 2013). This approach has also been used in BC to elucidate detailed variation in the mineralogy of detrital gold in the Cariboo gold district and to infer the relative importance of lode sources (Chapman and Mortensen, 2016). The alkalic copper-gold porphyries of BC are both potential sources of detrital gold and located within wider auriferous areas. Consequently, the region provides an excellent study area in which to explore the potential of gold compositional studies in the context of exploration in a challenging environment.

Exploration for porphyry mineralization is increasingly focused on techniques that can identify mineralization concealed by Quaternary cover. Studies of the trace-element mineralogy of minerals formed in porphyry systems (e.g.,

Bouzari et al., 2010, 2016; Celis et al., 2014; Pisiak et al., 2015) have identified mineralogical markers indicative of the environment of formation within an evolving magmatic-hydrothermal system. The overall aim of these studies has been to permit informed interrogation of heavy-mineral concentrates (HMC) collected during exploration campaigns.

Native gold grains derived from such mineralization may also be present in panned concentrates. However, the simple presence of gold grains is not necessarily indicative of derivation from the exploration target. For example, Kelley et al. (2011) reported that the nature of gold-dispersion trains in glacial sediments in the environs of the Pebble porphyry in Alaska may have been influenced by the influx of gold from different sources. The dispersion of particulate gold from the Mt. Polley porphyry deposit through glacial transport was investigated by Plouffe et al. (2013), who noted that the presence of a large, auriferous paleoplacer deposit lying stratigraphically below till near the deposit could have resulted in gold grains being recycled into the more recent sediments. The information flowing from the identification and character of particulate gold in HMC would be far greater if it were possible to establish its genetic origin.

Studies of gold-grain chemistry have been undertaken by several workers since the advent of the electron microprobe, which facilitates rapid determination of the major alloying elements (Ag, Cu, Hg, Pd) within native gold particles. Antweiler and Campbell (1977) identified systematic spatial variation in both Ag and Cu contents of native gold in the environs of Circle City, Alaska and speculated that gold composition was a consequence of the temperature at which the source mineralization was emplaced. Subsequent studies in important placer districts, such as the Cariboo (Mctaggart and Knight, 1993) and the Klondike (Knight et al., 1999), also identified variation in the alloy compositions of populations of gold grains collected from different localities. Knight et al. (1999) applied these data

Keywords: British Columbia, detrital gold, indicator mineral, LA-ICP-MS

This publication is also available, free of charge, as colour digital files in Adobe Acrobat® PDF format from the Geoscience BC website: <http://www.geosciencebc.com/s/DataReleases.asp>.

to speculate that some in situ sources of Klondike placer gold remained to be discovered.

In the late 1980s, the British Geological Survey developed a refined approach to gold-grain characterization that involved systematic screening of grain sections to identify inclusions of other minerals preserved within the gold grains. They successfully correlated inclusion suites with variation in alloy composition to refine the characteristics of populations of detrital gold grains. This approach of ‘microchemical characterization’ has been applied to gold from many localities worldwide, (e.g., Chapman et al., 2000, 2010; Chapman and Mileham, 2016), with a view to developing a global template by which detrital gold can act as an indicator for the source style of mineralization. The use of inclusions in the characterization process has permitted clarification of placer-lode relationships in the Lone Star area of the Klondike, where consideration of inclusion signatures distinguished between populations of gold from different sampling sites that were previously indistinguishable in terms of their alloy composition.

Although distinction between populations of grains derived from different mineralizing events and different source styles of mineralization are commonly identified using this approach, the methodology depends upon analyses of much larger gold grain populations than are routinely collected in HMC. Such gold-grain studies normally require a separate dedicated sampling exercise by personnel experienced in collecting gold particles in areas of low abundance. Any analytical method that could reduce the number of gold grains required to establish provenance would effectively remove this major barrier to using detrital gold as an indicator mineral.

The determination of trace metals by laser-ablation inductively coupled plasma–mass spectrometry (LA-ICP-MS) has only rarely been applied to particulate gold, principally because gold commonly contains mercury, which takes considerable time to be flushed through the instrument and is a major interference when the instrument is used for U-Pb isotopic dating of other minerals. Unlike many other LA-ICP-MS installations available in Canada and elsewhere, the equipment at Leeds is not used for dating by Pb determination, and thus may be routinely employed for gold analysis. The data flowing from LA-ICP-MS analysis would allow characterization of gold based on a far larger array of trace elements and at lower detection limits than is currently possible using electron microprobe (EMP) methods, but has the disadvantage that the method is destructive.

This project involves analysis of populations of gold grains from throughout BC whose microchemical signature has already been determined (Figure 1, Table 1). The aims of the project are to provide the first large-scale dataset that would allow:

- 1) evaluation of the suitability of LA-ICP-MS for gold analyses,
- 2) comparison of microchemical signatures with trace-element signatures, and
- 3) identification of any trace-element signatures diagnostic for gold formed in specific environments.

This paper contains the preliminary findings of this study, which commenced in August 2016. Analysis of some target sample suites is complete, while others remain to be analyzed. Consequently, it is not yet possible to interrogate the full database to answer points 1–3 (above).

Methodology

Sample Suites

Various sample suites studied in previous projects were available to the present study. They include those that underpinned studies of the Cariboo gold district (Chapman and Mortensen, 2016) and studies of gold derived from alkalic porphyry systems (Chapman and Mileham, 2016). Populations of gold grains previously collected had been mounted in resin blocks and polished to reveal grain core to facilitate earlier microchemical studies. It has not been possible to analyze every grain in all these collections because of the large numbers involved. Nevertheless, complete datasets will be generated for some sample populations that are considered important to the study. The samples analyzed are indicated in Table 1.

Analytical Method

Images of the polished block surface were used to identify each grain within each sample population, while enabled correlation of previous microchemical data with that obtained by laser-ablation inductively coupled plasma–mass spectrometry (LA-ICP-MS). The LA-ICP-MS system uses an Agilent 7500c quadrupole mass spectrometer, combined with a Geolas ablation system to determine the composition of individual grains. The Geolas ablation system uses a Compex 103 ArF excimer laser operating at a wavelength of 193 nm and delivering an energy density of up to 20 J/cm on the sample surface at a pulse frequency of up to 20 Hz, with spot sizes ranging from 5 to 160 μm. The ablated material is transported from the ablation cell to the ICP-MS us-

Figure 1. Locations of gold-grain sampling in central British Columbia: **a)** location of the Cariboo gold district (box; see part b) and sample locations near Kamloops (Afton mine, MINFILE 092INE023; Tranquille River placer, MINFILE 092INE106; and Cherry Creek) and in the Princeton area (Copper Mountain mine, MINFILE 092HSE001; Similkameen River placer, MINFILE 092HSE233; Whipsaw Creek placer, MINFILE 092HSE236; and Friday Creek); **b)** detail of sample locations in the Cariboo gold district (Spanish Mountain, MINFILE 093A 043; Mount Polley, MINFILE 093A 008); geology adapted from Mortensen and Chapman (2010); grid references for other placer localities provided in Table 1; place names with the generic in lower case are unofficial; refer to BC Geological Survey (2016) for MINFILE records.

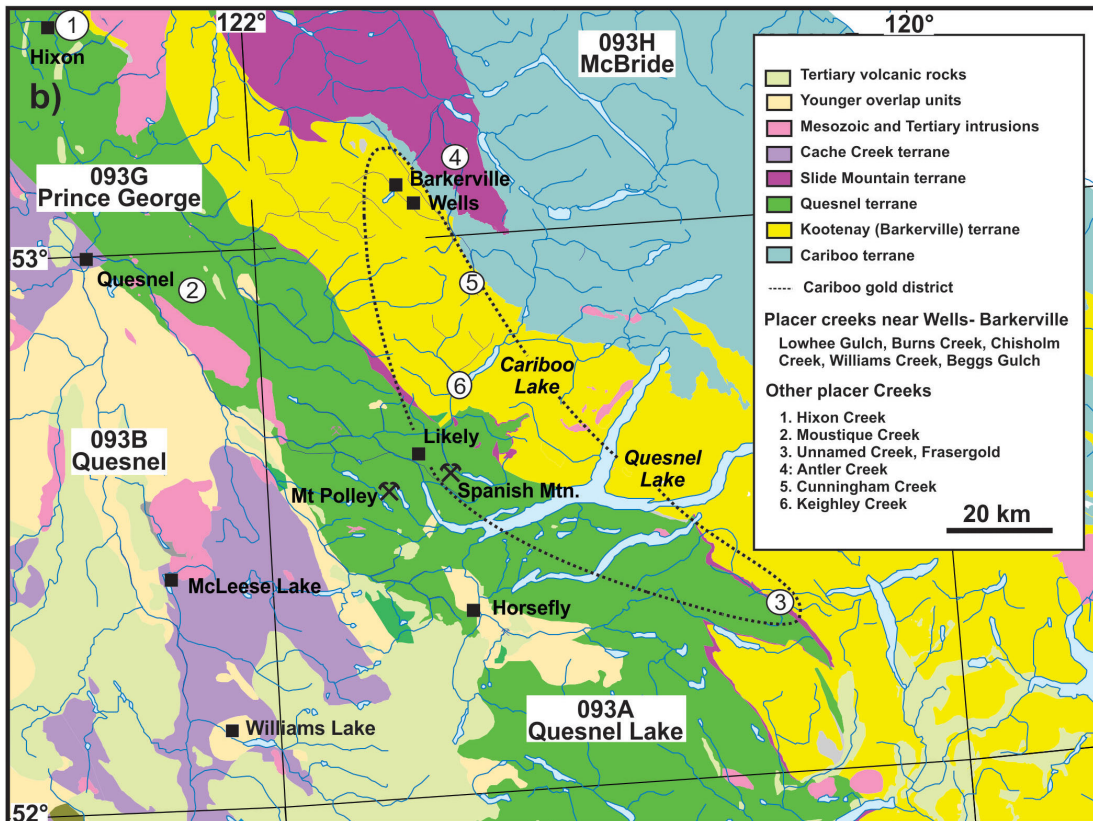
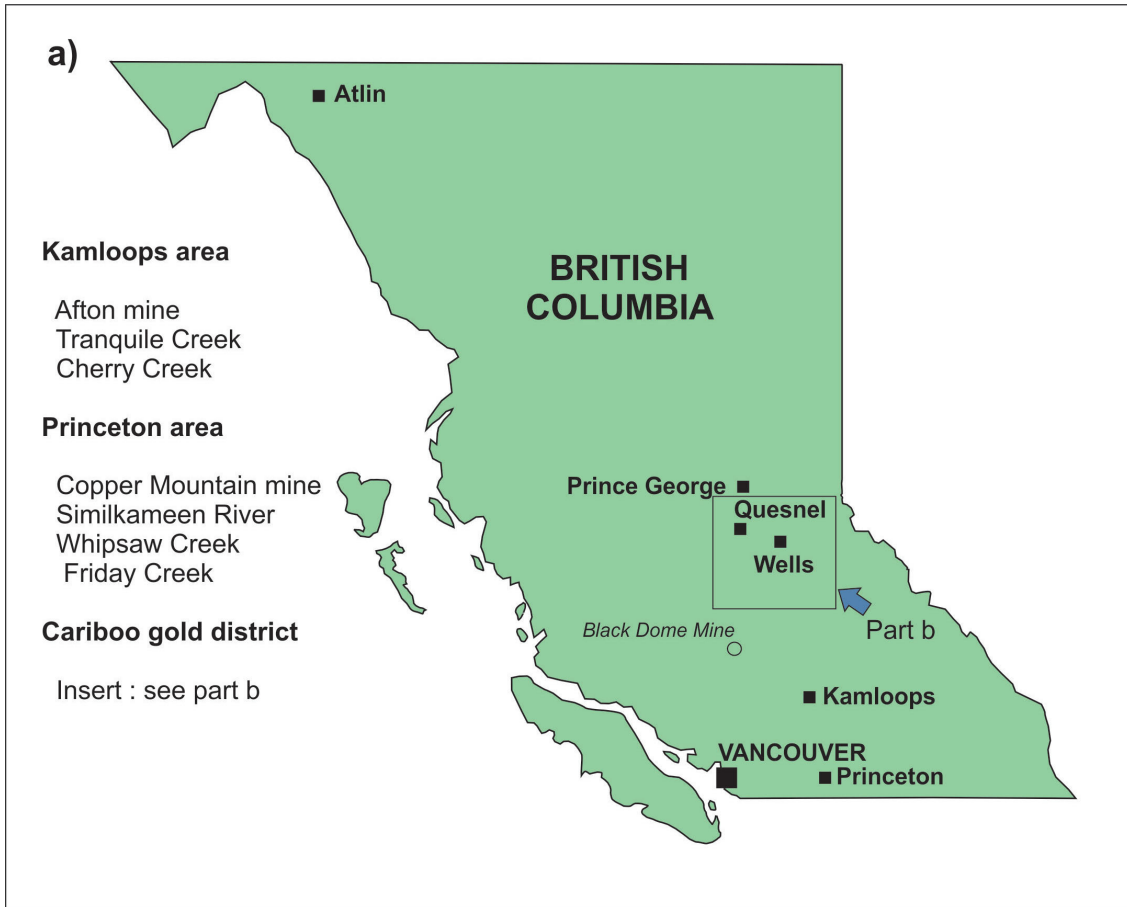


Table 1. Sample localities, indicating progress of the experimental program in the context of the original proposal.

Sample location	UTM Zone 10N, NAD 83		No. of grains	
	Easting	Northing	Identified ⁷	Analyzed ⁸
CGD: lode samples²				
Cow Mountain vein	596050	5883280	2*	0
Wells adit	595950	5883250	30	0
Warspite	601518	5876958	30	0
BC vein	596343	5883218	30	0
Myrtle	597414	5881788	24	0
Hibernia	586345	6011100	76	16
Midas adit	606400	5856400	22	0
Frasergold ⁵	665083	5797785	30	0
CGD: placer samples²				
Williams Creek	599830	5881613	54	41
Beggs Gulch	606300	5875500	30	30
Keighley Creek	604183	5849514	30	16
Amador Creek	588853	5876180	30	0
Burns Creek	590031	5881840	30	26
Lowhee Creek	596500	5883750	30	56
Antler Creek	606750	5871205	60	15
Cunningham Creek	610520	5865900	30	22
Dragon Creek	583016	5885903	12	26
Spanish Mountain ⁵	604674	5827518	30	30
Chisholm Creek	586791	5878197	0	20
Frasergold Creek	666389	5797008	28	8
Moustique Creek	569250	5873350	40	26
Hixon Creek	529328	5922040	30	54
Alkalic porphyry: lode samples³				
Mount Milligan (P)	434363	6109388	18	5
Mount Milligan (Pr)	434698	6109464	5	0
Mount Polley (P)	Wight Pit stockpile		16	6
Afton (P)	¹		4	0
Copper Mountain (P)	679873	5466653	5	2
Alkalic porphyry: placer samples³				
King Richard Creek	434721	6108928	30	36
Similkameen River	678215	5468502	60	117
Friday Creek ⁶	677785	5463800	30	54
Whipsaw Creek ⁶	677057	5471100	30	46
Cherry Creek	672106	5615716	30	42
Tranquille Creek	675305	5624270	40	62
Low sulphidation epithermal				
Black Dome ^{4,5}	535537	5685967	0	20

¹samples from Leeds University archive collection, labelled as 'Afton Pit'

²gold grains studied by Chapman and Mortensen (2016)

³grains studied by Chapman and Mileham (2016)

⁴sample obtained from The University of British Columbia collections

⁵co-ordinates taken from MINFILE reports

⁶approximate co-ordinates, as samples were donated from placer miners

⁷for study in proposal

⁸to date

Abbreviations: P, zone of potassic alteration; Pr, zone of propylitic alteration; CGD, Cariboo gold district (see Figure 1)

ing 99.9999% He flowing at 2 ml/min into a cyclone mixer, where it is combined with the Ar carrier gas flowing at 1.02 ml/min. The instrument can be operated in reaction-cell mode using 2.5 ml/min 99.9999% H₂ to remove interferences from ⁴⁰Ar on ⁴⁰Ca and from ⁵⁶ArO on ⁵⁶Fe; however, this also reduces the signal intensity of both the background and the analyte. In general, the target elements analyzed had low background signals and the only benefit would have been the ability to use the major ⁵⁶Fe isotope for analysis, but it was found that operating without the reaction cell enhanced sensitivity for the isotopes analyzed.

Figure 2 shows the effects of ablating gold grains for 150 laser pulses. The predominant feature is the rim of metal that has condensed on the surface around the ablation pit. This is much less than the volume of material that has been transported into the ICP-MS, but analysis of these rims does not indicate there has been any elemental fractionation between what has been transported and what has been condensed. As gold is easily ablated at the 193 nm wavelength, the laser energy was reduced to 6 J/cm and the pulse rate tuned to 5 Hz. The best analytical data are gained from conditions where a stable ablation profile is achieved for periods of around 10 seconds (Figure 3), as this allows the mass spectrometer to cycle through the elements a number of times to produce the most reproducible ratios relative to the internal standard element. At higher energies or higher pulse rates, the gold was ablated all the way through too quickly and analyses were less reproducible and accurate. As an estimate, it was found that 150 pulses was ablating the gold to a depth of around 100–120 µm. The lower en-

ergy did result in a lower ablation rate and, accordingly, a lower ICP-MS response, but this was not overly significant. The size of the laser pulse determined the depth to which ablation was possible and hence the duration of the ICP-MS elemental signal. For spot sizes of 5, 10 and 15 µm, there was an initial signal whose duration increased with the size of spot but rapidly diminished prior to the selected target of 150 laser pulses. The laser energy could penetrate to the bottom of the smaller diameter laser pits as effectively and hence ablation of the gold ceased. Therefore, all the gold grains were analyzed with spot diameters of 25–100 µm, with 50 µm being the most frequent size used, to ensure ablation continued for the full 150 pulses.

Calibration and Quantification

The gold grains were analyzed for a large number of elements to see which were detectable and to provide an appraisal of which would be useful in distinguishing different deposits and metallogenic types, and potentially be indicative of processes operating during precipitation. The suite of elements was ²⁷Al, ²⁹Si, ³²S, ⁴⁷Ti, ⁵¹V, ⁵³Cr, ⁵⁵Mn, ⁵⁷Fe, ⁵⁹Co, ⁶⁰Ni, ⁶³Cu, ⁶⁶Zn, ⁶⁹Ga, ⁷²Ge, ⁷⁵As, ⁸²Se, ⁸⁹Y, ⁹³Nb, ⁹⁵Mo, ¹⁰³Rh, ¹⁰⁵Pd, ¹⁰⁷Ag, ¹¹¹Cd, ¹¹⁵In, ¹¹⁸Sn, ¹²¹Sb, ¹²⁵Te, ¹³⁹La, ¹⁸²W, ¹⁹⁵Pt, ¹⁹⁷Au, ²⁰²Hg, ²⁰⁸Pb, ²⁰⁹Bi, ²³²Th, ²³⁸U, all at 10 ms dwell times and with a total cycle time of 0.442 seconds.

The LA-ICP-MS quantification requires that elements are measured as ratios relative to an internal standard of known concentration. Therefore, all elements were measured using Au as the internal standard. Integration of the standard and sample signals was achieved with the SILLS software

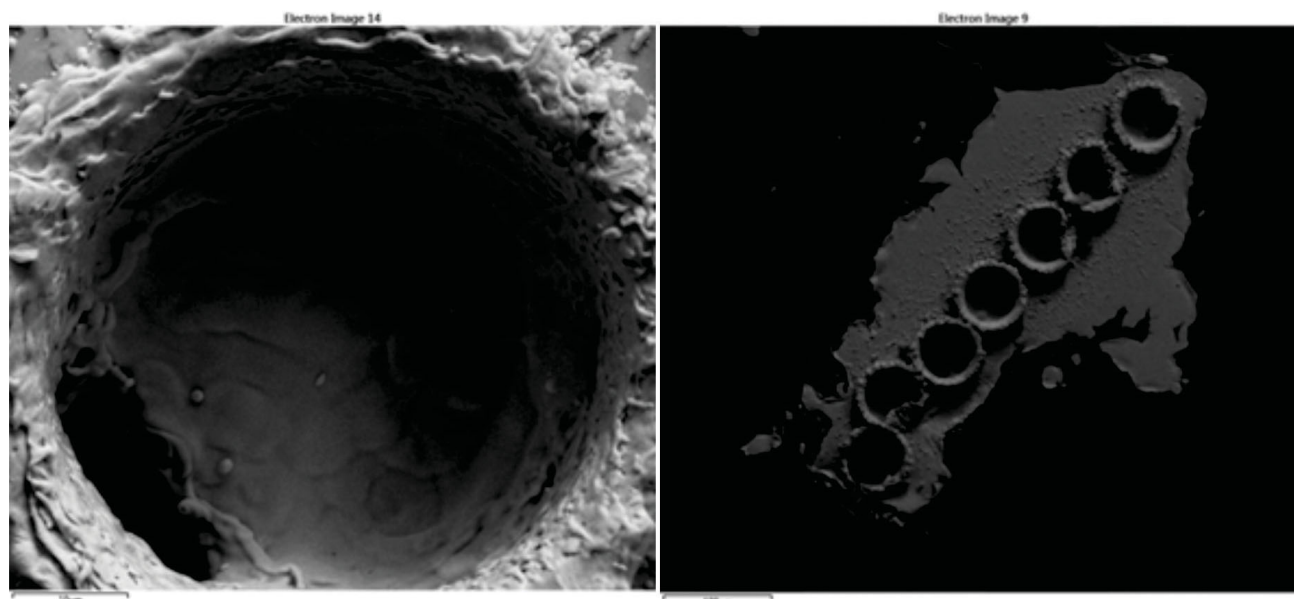


Figure 2. Scanning electron microscope images of laser-ablation pits in gold after ablation for 150 laser pulses. Penetration depth into the gold is approximately 100 µm. Re-precipitated metal forms a rim around the ablation pit, but the majority of material is transported as an aerosol to the ICP-MS. The image on the left shows where the laser has penetrated through the gold grain (hole at bottom left). On the right, a series of closely spaced 50 µm pits shows how spatial compositional variations in a single gold grain could be determined.

package (Allan, 2005; Guillong et al., 2008). The London Bullion Market Association Reference Standard AuRM2 was used as the primary standard for Ag, Al, As, Bi, Cr, Cu, Fe, Mn, Ni, Pb, Pd, Pt, Rh, Sb, Se, Sn, Te and Zn, with the

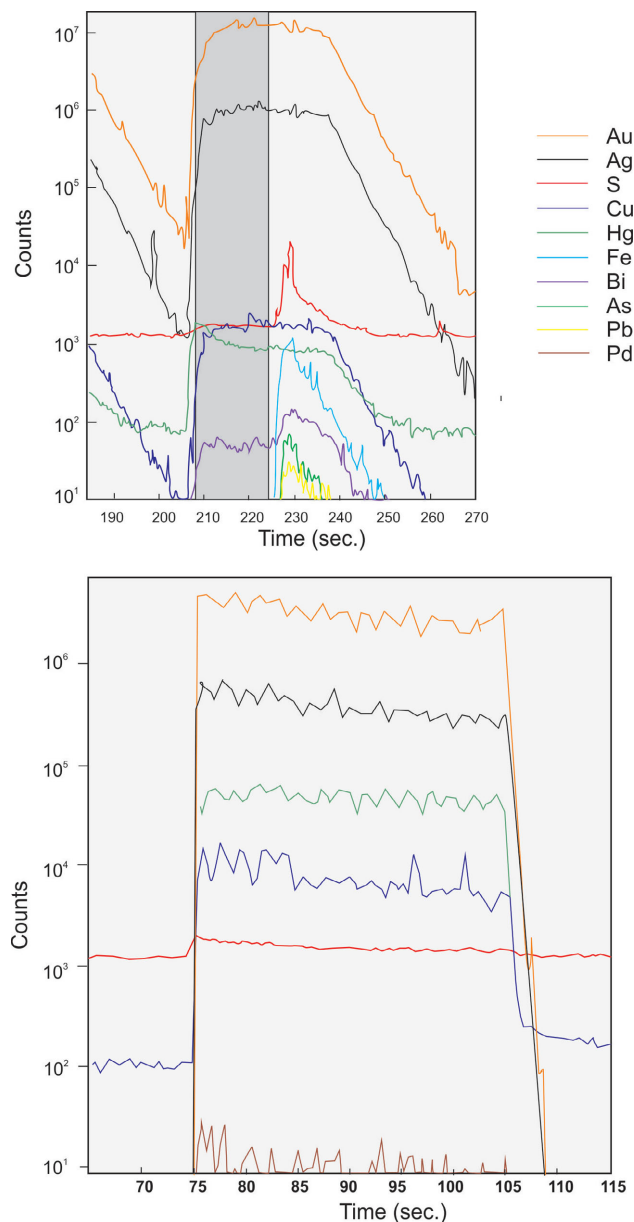


Figure 3. Visualization of ablation of a gold grain with 150 laser pulses over 30 seconds using the SILLS software package (Allan, 2005; Guillong et al., 2008). The elemental traces are a depth profile through the gold going down to approximately 100 μm : **a)** ablation-depth profile initially shows elements in gold but then ablates a sulphide inclusion; with SILLS, it is possible to integrate the gold separately from the inclusion, as the shaded area indicates; in the gold area, the elements are (from bottom to top) Bi, Hg, Cu, S, Ag and Au and, in the inclusion, they are (from bottom to top) Pb, As, Bi, Fe, Hg, Cu, S, Ag and Au; the elements Hg, Cu, Ag and Au do not vary as the inclusion is ablated, so the inclusion is composed of Bi, As, Pb, Fe and S; **b)** ablation-depth profile of a gold grain without inclusions; the elements shown (from bottom to top) are Pd, S, Cu, Hg, Ag and Au; for each element, the signals are quite constant and parallel; in this case, the period of ablation would be integrated and processed with SILLS.

remaining elements calibrated against NIST 610 glass, again using Au as the internal standard element. However, AuRM2 was not suitable for accurate determination of the Ag/Au ratio, as the Ag/Au ratio of the standard is 9.96^{-5} , whereas most of the gold grains have Ag/Au ratios of 0.25 to 0.66 (corresponding to ratios of 80:20 to 60:40 percent Au:Ag, respectively). Hence, this would require extrapolating the calibration many orders of magnitude above the value of the standard. The NIST 610 standard has a Ag/Au ratio of 0.106, which is closer to the sample values and did produce more accurate results. The Ag/Au ratio used in the final quantification was calibrated against NIST standard 481, which is a set of Au-Ag wires ranging in composition from pure Au and Ag to intermediate compositions of 80:20, 60:40 and 40:60 percent Au:Ag respectively. The 80:20 standard was used for quantification and, despite the difference in matrix and in the concentration of both elements, gave a calibration that was almost identical to that obtained using NIST 610. Determining the calibration for Hg used the USGS synthetic sulphide standard MASS-1, as Hg is not present in the NIST standards or the AuRM2 standard. In this instance, the calibration was based on using Ag as the internal standard element, as there is no Au in MASS-1, and manually extracting the counts per second ratio for Hg/Ag from the SILLS output to use with the Hg/Ag wt./wt. ratio of the standard. A combination of calibrations based on the S/Au from NIST 610 and S/Ag from MASS-1 (calibration procedure was the same as for Hg/Ag) was used to determine the S wt./wt. ratio in the gold grains.

Standards SRM-610 and AuRM2 were used to monitor instrumental drift, which was found to be insignificant over each day's analyses. The slope of the calibration graphs converting the counts per second ratios to weight ratios was consistent during the 2–3 week analysis period, indicating the stability of the instrumentation. Using SILLS, it was possible to determine the wt./wt. ratios of elements in the samples using either NIST 610 or AuRM2 as the calibration standard. Element concentrations of the samples, with the exception of Pd and Pt, were within 10% of each other, which indicates that matrix effects are negligible using this analytical system.

Processing of the ICP-MS output using SILLS produces a series of background-corrected wt./wt. ratios for each of the elements analyzed relative to the internal standard element, Au, which is given a value of 1. If the value of the internal element is known for each area ablated, then that can be input instead and the concentration of the other elements will be output as concentrations; however, the concentration of Au in the grains is unknown. The approach used here was to sum the wt./wt. ratios of all the elements/Au that were above the detection limit and divide 1 000 000 ppm (100%) by that number, which when multiplied by the individual element/Au ratio gives the ppm value for that element. In effect, element concentrations were determined by

normalizing the total to 100%, thereby eliminating the need for a true internal standard, because everything with a significant concentration has been analyzed and the total will be 100%.

Figure 4 compares the alloy compositions of gold grains from a low-sulphidation epithermal deposit (Black Dome) with those from the Similkameen River placer adjacent to Copper Mountain. Results are included for Au, Ag, Hg and Cu obtained using both electron microprobe and LA-ICP-MS. In both examples, the median and distribution of analytical results are quite comparable except for Cu from the epithermal deposit, where the LA-ICP-MS data are at significantly lower concentrations. However, this is likely to be a due to the microprobe analysis having a detection limit

that is much higher (~300 ppm), so it cannot accurately determine lower concentrations. When the Cu concentration is greater, as in the porphyry deposit, both methods give very similar results. Thus, the good comparisons mean that the analytical approach is valid and the LA-ICP-MS data are comparable with EMP analyses.

Initial Results

This paper has detailed the application of LA-ICP-MS to the analysis of gold grains and shown that the amount of additional data that can be obtained is greater than was possible using only the electron microprobe as the analytical method of choice. The analysis (to date) of 776 grains for 36 elements from different localities and different deposit

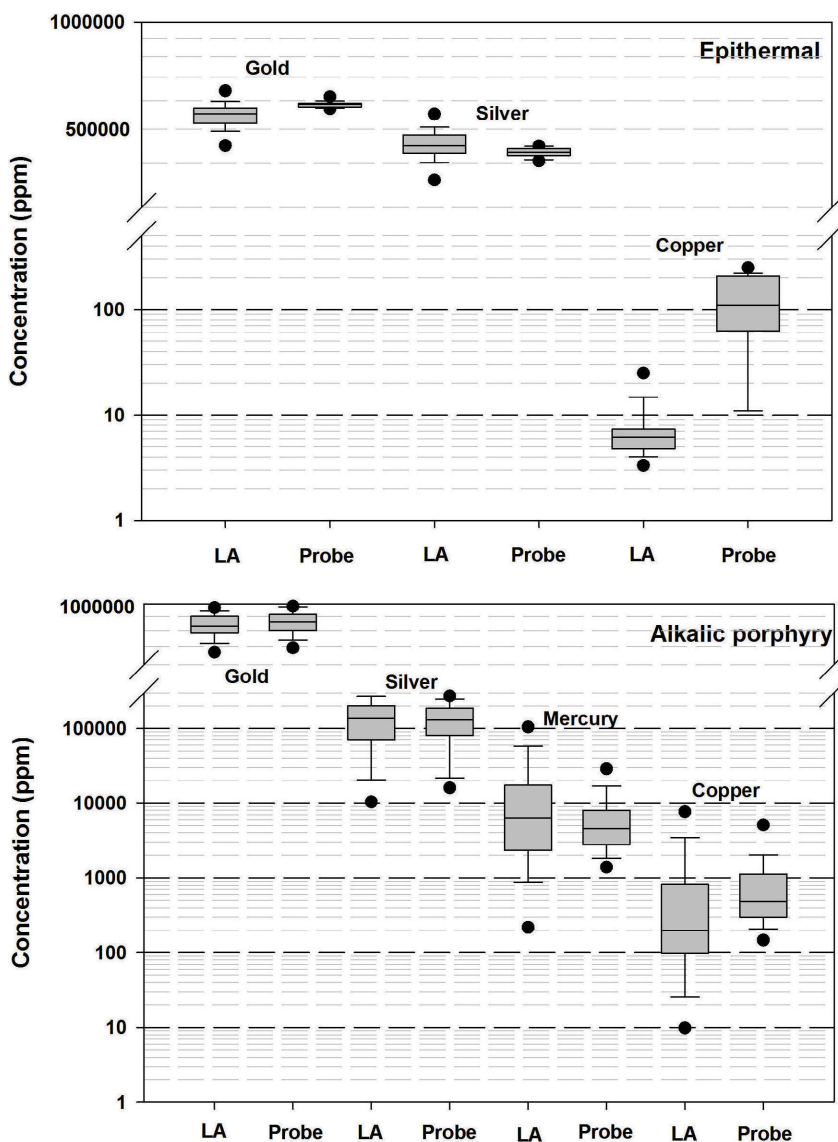


Figure 4. Comparison of the Au, Ag, Hg and Cu concentrations in placer-gold populations from two deposit types by electron microprobe and LA-ICP-MS. The statistical distribution of concentrations (median, box is 25th to 75th percentile, upper and lower lines are 5th and 95th percentiles) compare well except for Cu in the epithermal deposit. However, the microprobe analysis for Cu is at the detection limit for the technique.

types in BC has made it possible to define the elements that are most commonly present at sufficient concentrations to be used as potential discriminators of the origins of the gold. Figures 5–7 show that it is possible to interrogate the dataset at low concentrations of various elements to obtain useful information. However, a full interpretation of the data is not possible at present owing to the incomplete dataset (Table 1).

In Figure 5, bivariate plots of the major elements in the gold are shown for all the grains analyzed so far, differentiated on the basis of the deposit type from which the gold originated. The alkali porphyry deposits have, in general, the highest concentrations of elements other than the Au and Ag that dominate the gold-grain composition as a binary mixture. The alkali porphyry deposits plot below a binary mixing line due to the high concentrations of Hg, up to

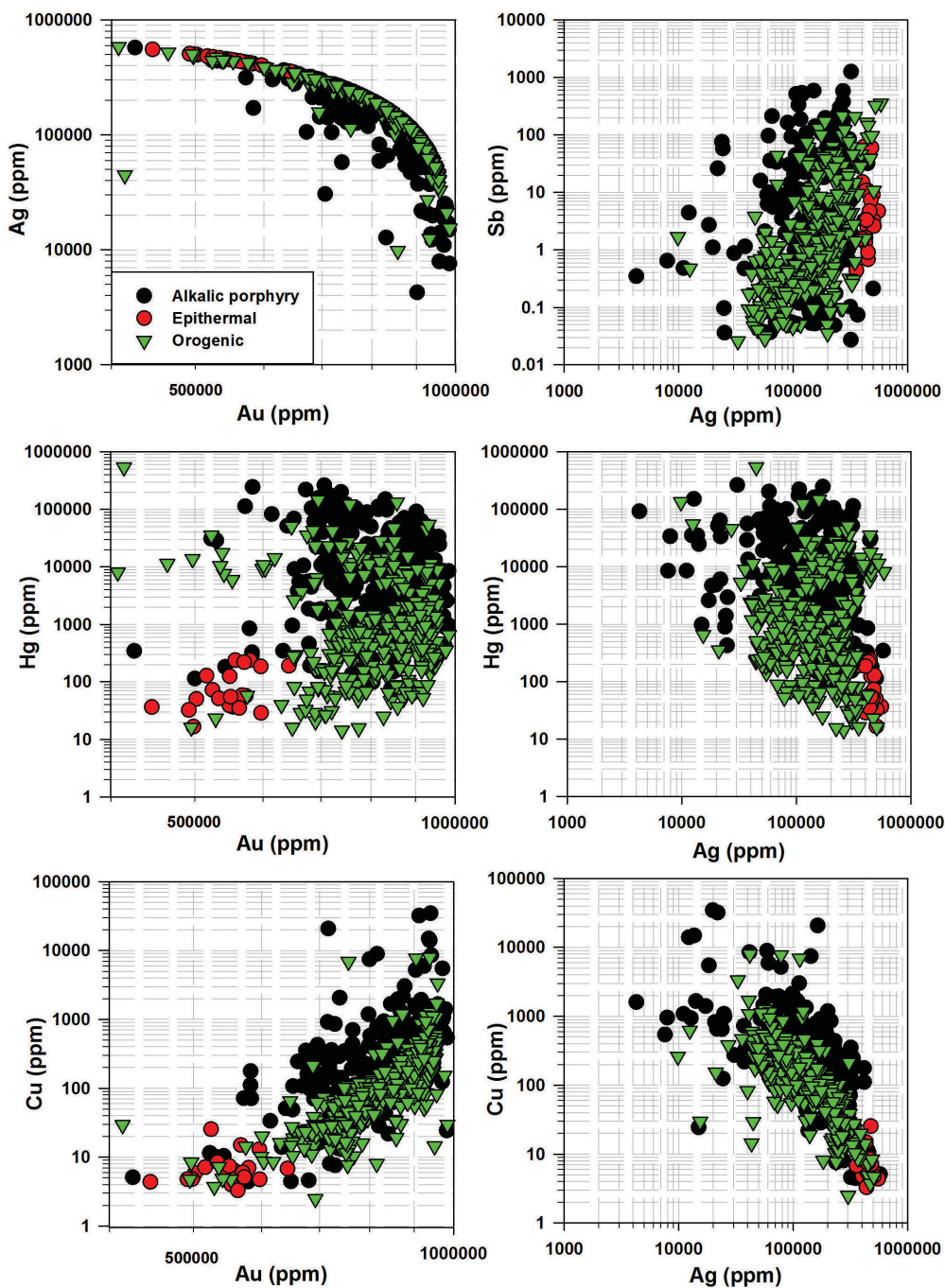


Figure 5. Major elements in all gold grains analyzed, differentiated on the basis of the type of deposit from which the placer grains originated.

10%, in these grains. There are reasonably good negative correlations of Hg with Au and Ag, over a large range in Hg concentrations, which is indicative of Hg replacing both Au and Ag in the porphyry gold grains. The dataset available that relates to epithermal deposits is relatively restricted when compared to the other two types. Nevertheless, the initial indication is that, for these types of deposit, there may be distinction based on the higher Ag and the low Cu and Hg concentrations. The number of gold grains from orogenic deposits analyzed is relatively large and some clearly defined trends have emerged. The majority of gold grains are binary Au and Ag mixtures, with these elements making up well over 99% of the composition, a result that is well known from previous alloy studies using EMP. In general, other elements are present at lesser concentrations than the alkalic porphyry deposits but greater than the single epithermal deposit studied here. There is a good positive correlation of Ag and Sb, and good negative correlations of Ag with Cu and Hg. These trends have not been previously observed in EMP datasets because of the higher detection limits. It is encouraging, at this level of data interpretation, that different sources of gold grains do seem to have observable differences when looking at the dataset as a whole. The observed correlations from measurement of trace elements at low concentrations show that these are not just random analyses, but may be related to processes during gold deposition.

In Figure 6, three individual deposits (Spanish Creek, Black Dome and Similkameen) have been chosen as examples of gold derived from orogenic, low-sulphidation epithermal and alkalic porphyry systems, respectively. Although some differences in alloy compositions can be identified in the EMP data (and corresponding inclusion assemblages), a number of further differences can be observed in the suite of minor elements whose concentrations have been measured using LA-ICP-MS. Gold from the Similkameen placer (alkalic porphyry related) shows the most complex elemental signatures and with trace elements at the highest concentrations. Gold from the Black Dome deposit contains fewer elements and at lower levels, whereas the signature of gold from Spanish Mountain (orogenic) falls midway between the other two. Three elements are worthy of particular attention: Hg, Cu and Pd. Concentrations of Hg in gold alloy from the alkalic porphyry system are around ten times higher than in the gold from Spanish Mountain, which in turn exhibits Hg concentrations ten times those of the gold from Black Dome. The detection limit for Hg by EMP is around 0.3%, so the use of LA-ICP-MS allows measurement and interpretation of Hg in the alloy at far lower levels. Copper concentrations were generally highest in gold from the alkalic porphyry system, although most grains from this sample suite and the Spanish Mountain suite returned similar values for Pd; however, some individual grains from the Similkameen River exhibited far

higher Pd values. Palladium was absent in the gold from Black Dome, where Cu concentrations were also very low.

Figure 7 compares LA-ICP-MS analyses of three placer samples taken in the vicinity of the Copper Mountain alkalic porphyry. The Similkameen River sampling locality was immediately downstream of the main ore zone, whereas those at Friday and Whipsaw creeks were more distal. The three sets of analyses look similar, which is consistent with derivation from similar distal sources surrounding the porphyry. Minor deviations in signature (e.g., elevated Hg and Cd in the Similkameen River sample) are likely to be a consequence of element zonation superimposed on the different catchments. The As content of some gold grains from Whipsaw Creek was higher than those encountered elsewhere. The reasons for this difference remain unclear, although they are clearly related to a subpopulation of grains specific to that drainage. However, the overall similarity between the three signatures supports the assertion that the technique yields reproducible results from individual primary sources of mineralization.

Preliminary Observations and Concluding Remarks

Successive ablation of natural gold yields datasets that reveal whether specific elements are present as alloy components or as inclusions. The ability of the SILLS software to visualize and filter out these modes of occurrence has enabled the authors to establish which elements have the potential to act as discriminators when comparing alloy compositions. Consideration of the relatively small number of data points described in this paper has highlighted advantages of gold alloy analysis by LA-ICP-MS. The differences between alloy signatures in gold from different deposit types previously identified by EMP analysis are evident in the LA-ICP-MS data, but the quantitative analysis of Cu, Hg and Pd at trace levels permits additional interrogation of these datasets. Most importantly, the use of LA-ICP-MS has identified the potential for other elements (e.g., Sb) to be used as discriminators and the ability to spot trends in element ratios where analyses were close to the detection limit by EMP. Regardless of the preliminary nature of the data, it appears that there are reproducible compositional similarities between populations of gold derived from the same source, and that differences exist between signatures of gold from different source types. The authors stress that, as yet, there are insufficient data to establish whether such differences are generic or a consequence of specific environments of mineralization. Ongoing studies will seek to clarify this question while also focusing on the detailed examination of the new datasets in the context of existing characterization of the microchemical signatures.

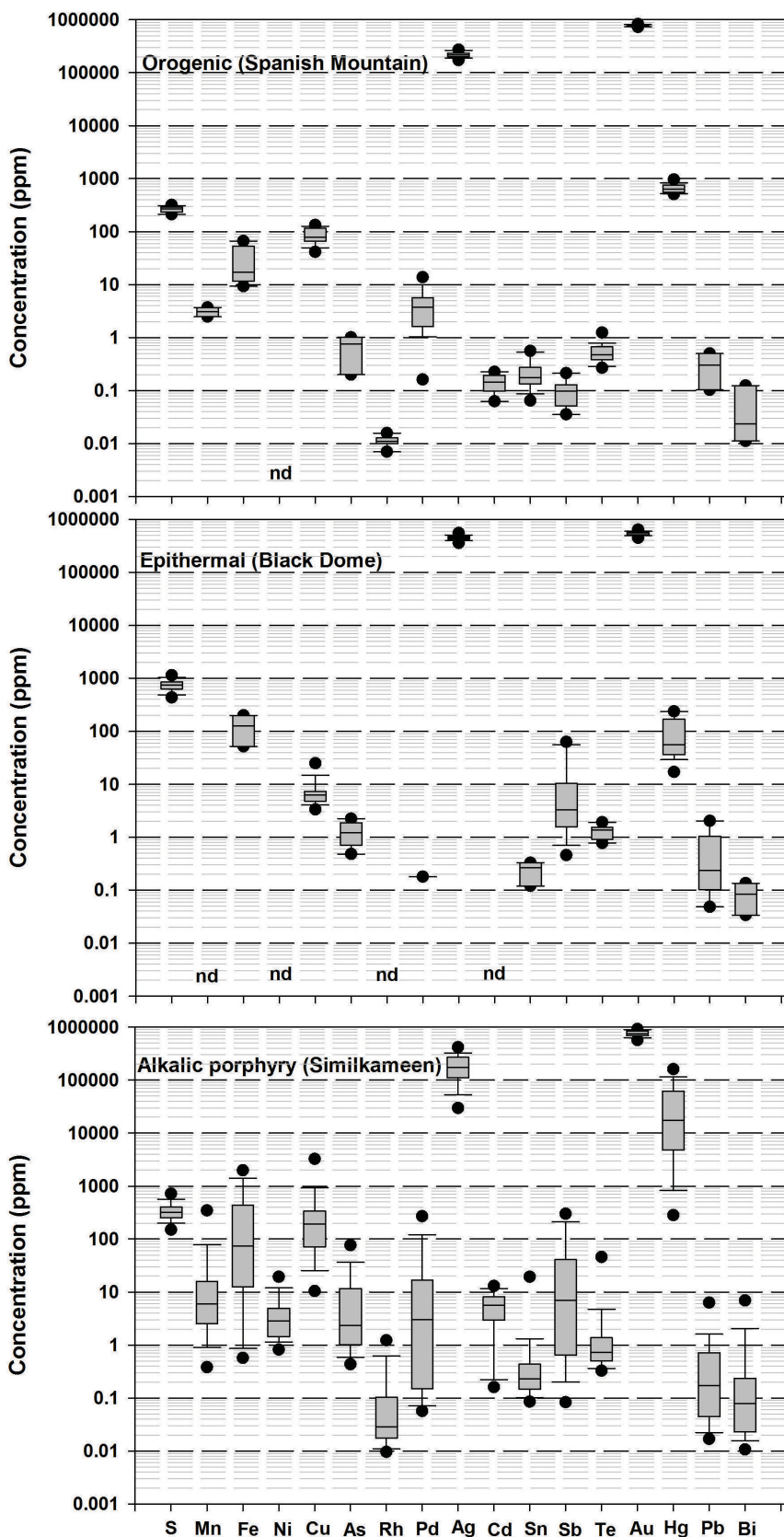


Figure 6. Analyses of the most common elements from three deposits that are representative of the different styles of mineralization. In this initial presentation, it is clear that there are significant differences in the concentrations of elements, other than Au and Ag, from the three deposit types.

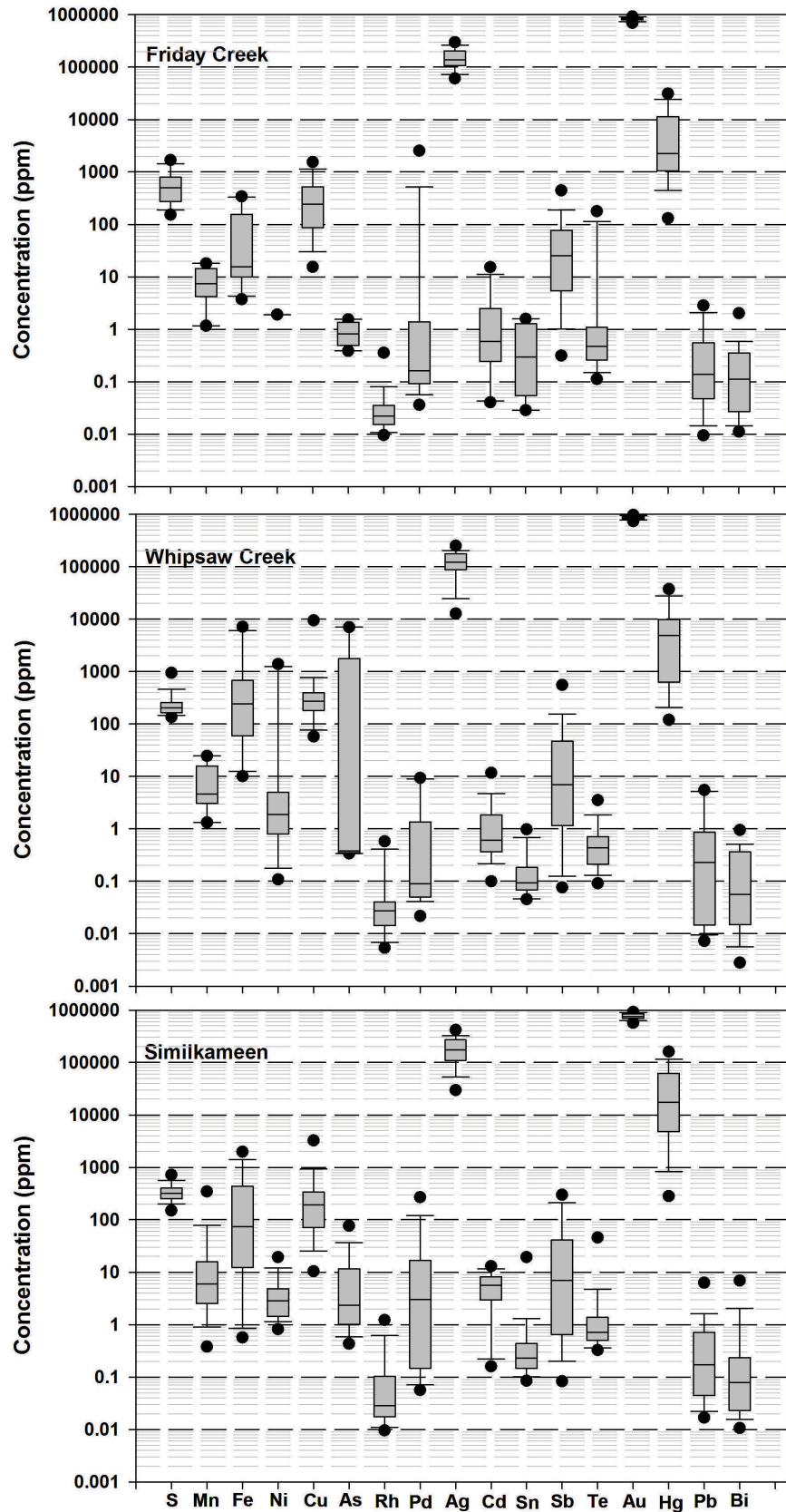


Figure 7. Analyses of placer grains from different streams in the vicinity of the Copper Mountain porphyry. Elements shown are those that are most prevalent in the grains. In general, the analyses show a good degree of similarity, but Hg, for example, is much higher at Similkameen than the other two placers.

The initial results of the study reported here have built upon the foundations of gold compositional work established using microchemical characterization. British Columbia provides an excellent testing ground to develop this methodology, by virtue of the diverse nature of gold mineralization and the overall gold endowment. Ongoing studies will constitute a novel approach to illuminating regional gold metallogeny through the studies of detrital gold, which is relevant not only to a better understanding of Cordilleran geology but to application in comparable areas of exploration interest globally. Consequently, the authors will continue to evaluate the possibility of establishing a low-cost, early-stage exploration methodology that would form a valuable addition to the suite of techniques available to explorationists in BC.

Acknowledgments

The authors are extremely grateful to M. Allan for an efficient and helpful review of this manuscript.

References

- Allan, M.M. (2006): Hydrothermal processes in the Mouth Leyshon Intrusive Complex, Australia: microanalytical insights; Ph.D. thesis, University of Leeds, Leeds, United Kingdom, 321 p.
- Antweiler, J.C. and Campbell, W.L. (1977): Application of gold compositional analyses to mineral exploration in the United States; *Journal of Exploration Geochemistry*, v. 8, p. 17–29.
- BC Geological Survey (2016): MINFILE BC mineral deposits database; BC Ministry of Energy and Mines, URL <<http://minfile.ca>> [November 2016].
- Bouzari, F., Hart, C.J.R., and Barker, S. (2016): Hydrothermal alteration revealed by apatite luminescence and chemistry: a potential indicator mineral for exploring covered porphyry copper deposits. *Economic Geology*, v. 111, pp. 1397–1410.
- Bouzari, F., Hart, C.J.R., Barker, S. and Bissig, T. (2010): Porphyry indicator minerals (PIMs): exploration for concealed deposits in south-central British Columbia (NTS 092I/06, 093A/12, 093N/01, /14); *in* Geoscience BC Summary of Activities 2009, Geoscience BC, Report 2010-1, p. 25–32, URL <http://www.geosciencebc.com/i/pdf/SummaryofActivities2009/SoA2009_Bouzari.pdf> [October 2016].
- Celis, M.A., Bouzari, F., Bissig, T., Hart, C.J.R. and Ferbey, T. (2014): Petrographic characteristics of porphyry indicator minerals from alkalic porphyry copper-gold deposits in south-central British Columbia (NTS 092, 093); *in* Geoscience BC Summary of Activities 2013, Geoscience BC, Report 2014-1, p. 53–62, URL <http://www.geosciencebc.com/i/pdf/SummaryofActivities2013/SoA2013_Celis.pdf> [October 2016].
- Chapman, R.J. and Mileham, T.J. (2016): Detrital Au grains as indicators of alkalic Cu-Au porphyry mineralization; Geoscience BC, Report 2016-06 (unpublished internal report), 48 p.
- Chapman, R.J., and Mortensen, J.K. (2016): Characterization of gold mineralization in the northern Cariboo Gold District, British Columbia through integration of compositional studies of lode and detrital gold with historical placer production: a template for evaluation of orogenic gold districts; *Economic Geology*, v. 111, p. 1321–1345.
- Chapman, R.J., Leake, R.C., Moles, N.R., Earls, G., Cooper, C., Harrington, K. and Berzins, R. (2000): The application of microchemical analysis of gold grains to the understanding of complex local and regional gold mineralization: a case study in Ireland and Scotland; *Economic Geology*, v. 95, no. 8, p. 1753–1773.
- Chapman, R.J., Mortensen, J.K., Crawford, E. and LeBarge, W. (2010): Microchemical studies of placer and lode gold in the Klondike District, Yukon, Canada: 1. evidence for a small, gold-rich, orogenic hydrothermal system in the Bonanza and Eldorado Creek area; *Economic Geology*, v. 105, p. 1369–1392.
- Guillong, M., Meier, D.L., Allan, M.M., Heinrich, C. and Yardley, B.W.D. (2008): SILLS – a MATLAB-based program for the reduction of laser ablation ICP-MS data of homogeneous materials and inclusions; *in* Laser Ablation ICP-MS in the Earth Sciences: Current Practices and Outstanding Issues, P. Sylvester (ed.), Mineralogical Association of Canada, Short Course 40, p. 328–333.
- Kelley, K.D., Eppinger, R.G., Lang, J., Smith, S.M and Fey, D.L. (2011): Porphyry Cu indicator minerals in till as an exploration tool: example from the giant Pebble porphyry Cu-Au-Mo deposit, Alaska, USA; *Geochemistry: Exploration, Environment, Analysis*, v. 11, p. 321–334.
- Knight, J.B., Mortensen, J.K. and Morison, S.R. (1999): Lode and placer gold composition in the Klondike District, Yukon Territory, Canada: implications for the nature and genesis of Klondike placer and lode gold deposits; *Economic Geology*, v. 94, p. 649–664.
- McTaggart K.C. and Knight, J. (1993): Geochemistry of lode and placer gold of the Cariboo District, BC; BC Ministry of Energy and Mines, Open File 1993-30, 25 p.
- Mortensen, J.K. and Chapman, R. (2010): Characterization of placer- and lode-gold as an exploration tool in east-central British Columbia (parts of NTS 093A, B, G, H); *in* Geoscience BC Summary of Activities 2010, Geoscience BC, Report 2011-1, p. 109–122.
- Pisiak, L.K., Canil, D., Grondahl, C., Plouffe, A., Ferbey, T. and Anderson, R.G. (2015): Magnetite as a porphyry copper indicator mineral in till: a test using the Mount Polley porphyry copper-gold deposit, south-central British Columbia (NTS 093A); *in* Geoscience BC Summary of Activities 2014, Geoscience BC, Report 2015-1, p. 141–150.
- Plouffe, A., Ferbey, T., Anderson, R.G., Hashmi, S. and Ward, B.C. (2013): New TGI-4 till geochemistry and mineralogy results near the Highland Valley, Gibraltar, and Mount Polley mines, and Woodjam District: an aid to search for buried porphyry deposits; Geological Survey of Canada, Open File 7473, 58 p.
- Wrighton, T.M., (2013) Placer gold microchemical characterization and shape analysis applied as an exploration tool in western Yukon; M.Sc. thesis, The University of British Columbia, 140 p.

Large-Scale Sodic-Calcic Alteration Around Porphyry Copper Systems: Examples from the Highland Valley Copper District, Guichon Batholith, South-Central British Columbia

K. Byrne, University of Alberta, Edmonton, AB, kbyrne@ualberta.ca

G. Lesage, Mineral Deposit Research Unit, The University of British Columbia, Vancouver, BC

S.A. Gleeson, Helmholtz Centre Potsdam GFZ German Research Centre for Geosciences, Potsdam, Germany

R.G. Lee, Mineral Deposit Research Unit, The University of British Columbia, Vancouver, BC

Byrne, K., Lesage, G, Gleeson, S.A. and Lee, R.G. (2017): Large-scale sodic-calcic alteration around porphyry copper systems: examples from the Highland Valley Copper district, Guichon batholith, south-central British Columbia; *in* Geoscience BC Summary of Activities 2016, Geoscience BC, Report 2017-1, p. 213–222.

Introduction

Porphyry Cu deposits are the primary source of Cu globally and, although demand ebbs and flows and recycling is increasing, a pipeline of quality projects and resources is needed to replace decreasing inventories (Seedorff et al., 2005; Sillitoe, 2010; Thompson, 2016). Exploration costs and expenditures have increased approximately threefold during the last 12 years (Wilburn et al., 2015; Wood, 2016), yet discovery rates are down and very few new deposits have been found (Sillitoe, 2013). As a result, exploration is moving into underexplored, high-risk political jurisdictions and beneath cover (systems with no surface expression) in known productive belts, necessitating more effective and efficient exploration methodologies and techniques (Sillitoe, 2013; Schodde, 2014; Wood, 2016).

The volume of hydrothermally altered rocks outboard of economically significant concentrations of Cu-Fe-sulphide minerals is termed the porphyry footprint. An understanding of the fluid types that can be present during porphyry Cu formation, how they manifest in the footprint and their spatial distribution with respect to Cu-mineralized portions of the system is critical to developing better exploration tools. This work is part of the Porphyry Copper Footprints Subproject of the Canada Mining Innovation Council (CMIC) and Natural Sciences and Engineering Research Council of Canada (NSERC). Its purpose is to investigate the petrophysical, structural, mineralogical, geochemical and isotopic footprints of the porphyry Cu (\pm Mo) deposits in the Highland Valley Copper (HVC) district of south-central British Columbia (BC; Figure 1). The Teck Highland

Valley Copper Partnership ('Highland Valley Copper') is wholly owned and operated by Teck Resources Limited. The district contains proven and probable reserves of

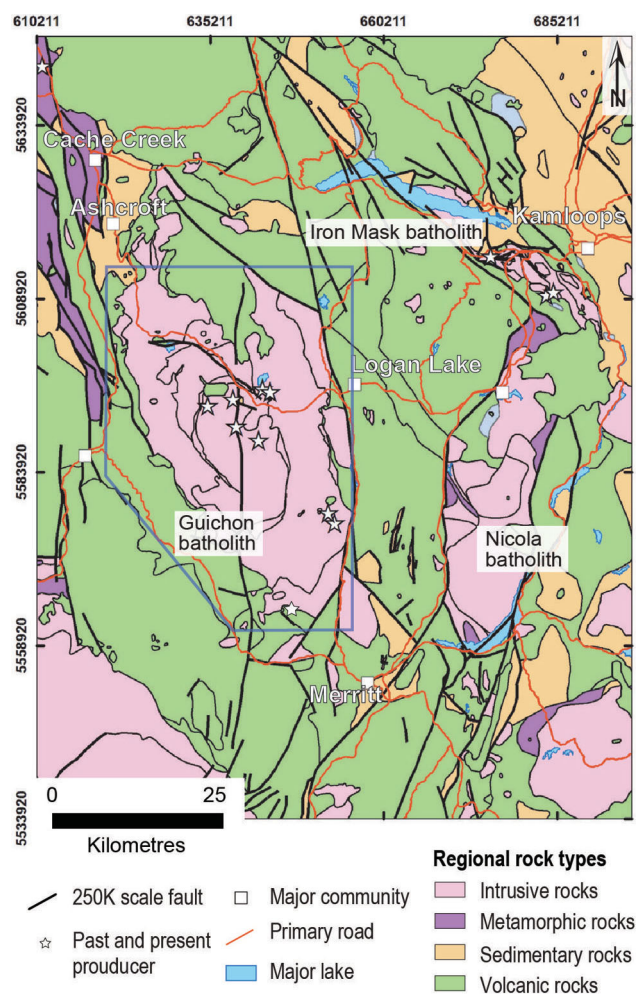


Figure 1. Simplified geology of the Quesnel terrane in southern British Columbia. Geological data from Massey et al. (2005). Blue outline indicates the area shown in Figure 2a.

Keywords: British Columbia, Guichon batholith, Highland Valley Copper, actinolite, albite, alteration, epidote, Na-Ca, nonmagmatic, porphyry Cu, seawater, sodic-calcic

This publication is also available, free of charge, as colour digital files in Adobe Acrobat® PDF format from the Geoscience BC website: <http://www.geosciencebc.com/s/DataReleases.asp>.

577 200 tonnes at 0.29% Cu and 0.007% Mo (Teck Resources Limited, 2016).

Four major porphyry Cu (\pm Mo) systems, hosted in various intrusive facies of the Late Triassic Guichon batholith, occur in the HVC district (Figure 2a). Exposure and airborne magnetic data indicate that the batholith has an oval shape, elongate to the northwest, with a long axis of approximately 60 km and a short axis of 25 km. Due to its size and low degree of exposure (\sim 3%), the HVC district is a realistic natural laboratory in which to investigate the large-scale footprint of porphyry Cu deposits, integrate disparate geological and geochemical datasets, and develop new methodologies and genetic understanding to aid modern exploration geoscientists.

Two field seasons of mapping and sample collection have been completed. Whole-rock litho-geochemistry, representative rock slabs and thin sections have been processed and analyzed for mineralogy and paragenesis. McMillan (1976, 1985) described argillic and propylitic alteration at HVC; however, the district-scale footprint of sodic-calcic (Na-Ca) alteration had not been recognized in the Guichon batholith before the current study (Figure 2b). This paper presents a description of the Na-Ca alteration in the Guichon batholith and outlines the research question concerning its genesis.

Geological Setting

Regional Geology

The Quesnel terrane in the Canadian Cordillera is characterized by Mesozoic island-arc assemblages comprising volcanic and sedimentary rocks and associated intrusions. The most important rocks for this study are the Late Triassic Nicola Group and the Guichon batholith (Coney et al., 1980; Logan and Mihalynuk, 2014). The Nicola Group consists primarily of andesitic submarine volcanic and associated volcano-sedimentary rocks of island-arc affinity (Preto, 1979; Mortimer, 1987; Ray et al., 1996) that were deposited in a rifted marine basin above an east-dipping subduction zone (Colpron et al., 2007). The I-type, low-K tholeiitic to medium-K calcalkalic Guichon batholith (Figures 1, 2a; Northcote, 1969; McMillan, 1976; D'Angelo, 2016) intruded the ca. 238–202 Ma Nicola Group between ca. 211 and 204 Ma, prior to docking with ancestral North America (Logan and Mihalynuk, 2014; Mihalynuk et al., 2016). The region subsequently underwent Cretaceous shortening and localized Paleogene–Neogene extensional deformation (Colpron et al., 2007).

District Geology

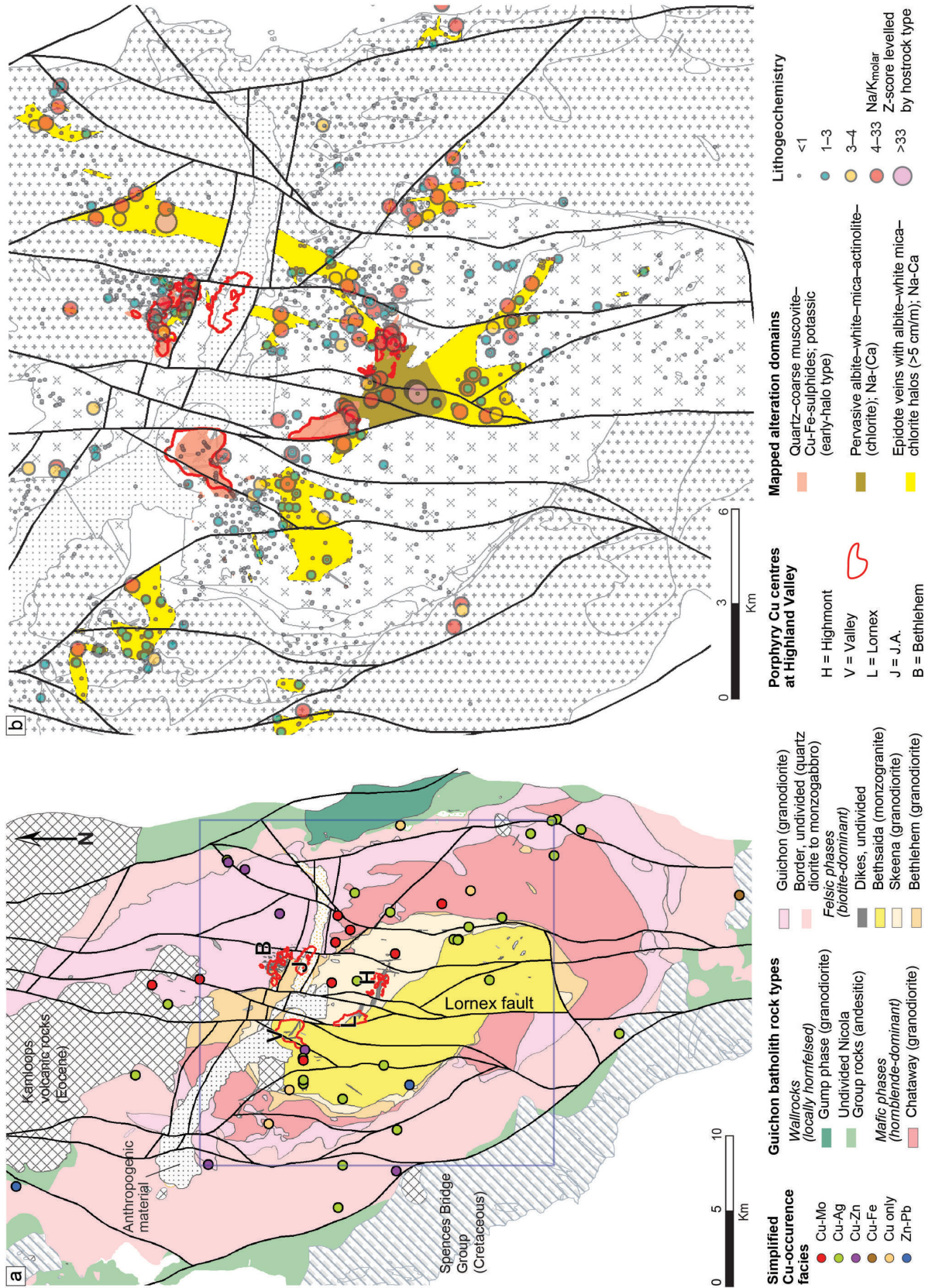
Several texturally and compositionally distinct intrusive facies are recognized in the Guichon batholith (Northcote, 1969; McMillan, 1976; D'Angelo, 2016). Older marginal

and equigranular mafic rocks transition to younger, centrally located, inequigranular to porphyritic felsic facies (Figure 2a). A cluster of at least four porphyry Cu deposits, hosted by the inner intrusive facies, and \sim 160 additional Cu showings occur in the HVC district (Figure 2a; McMillan et al., 2009; Byrne et al., 2013). Two main stages of mineralization are recognized at HVC (McMillan, 1985; Byrne et al., 2013), and these are separated by \sim 1 m.y. and intrusion and crystallization of the most evolved intrusive rocks (D'Angelo, 2016). A postmineral, north-trending, dextral strike-slip fault cuts the Valley and Lornex deposits (Figure 2a). Restoring approximately 3.5 km of dextral movement suggests that the Valley and Lornex deposits were once a single porphyry centre (Hollister et al., 1976; McMillan, 1976).

Several features indicate that some of the porphyry centres at HVC were deeply emplaced. Plutonic hostrocks, hornblende bathymetry (D'Angelo, 2016), presence of unidirectional solidification textures and coarse muscovite-dominated (Byrne et al., 2013) early halo-type (or greisen-like) veins imply that the Valley-Lornex cupola and porphyry Cu system was likely emplaced between 4 and 5 km deep (Seedorff et al., 2008; Proffett, 2009; Riedell and Proffett, 2014). A 4–5 km emplacement depth for the Valley-Lornex porphyry system (Figure 3) is also consistent with stratigraphic-thickness estimates for southern Quesnel Nicola Group rocks of between 3 and 6 km (Preto, 1979). At depths greater than approximately 4 km, a single-phase supercritical fluid (of moderate salinity, \sim 10%) would likely have been stable, possibly leading to mineralization styles and an alteration footprint that are atypical of porphyry environments (Rusk et al., 2008; Richards, 2011b; D'Angelo, 2016). The exposure and prevalence of Na-Ca alteration indicates a deep level of erosion (Figure 3; Seedorff et al., 2008; Halley et al., 2015).

Sodic-Calcic Footprint and Characteristics

Field mapping of domains of high vein density ($>$ 0.5 cm/m) highlights fluid pathways within the district (Figure 2b). The Na-Ca facies in the Guichon batholith consists primarily of light green epidote veins with haloes of albite \pm fine-grained white mica \pm epidote \pm chlorite \pm actinolite (Figures 4, 5). A key characteristic of the Na-Ca facies is the selective replacement of primary K-feldspar by secondary albite \pm fine-grained white mica. Within Na-Ca haloes, primary mafic minerals are replaced by chlorite and localized actinolite, with accessory titanite (Figure 5g). Sodic-calcic veins and haloes occur in \sim 0.5–2 km wide, north-northeast- and northwest-trending domains that extend along trend from Cu centres for up to 7 km in a nonconcentric pattern (Figure 2b). At the Bethlehem porphyry centre, Na-Ca alteration is most common at depth beneath biotite-altered and Cu-mineralized breccias but is exposed at higher elevations in structurally controlled domains in the



west and south pit walls. Some isolated domains of Na-Ca facies occur in mafic Border facies rocks. Individual vein orientations are similar to the trend of the larger alteration domains. Outcropping Na-Ca-altered rocks are typically white and fractured, and contrast with surrounding wallrock (Figures 4a, b). Isolated veinlets with narrow haloes, however, are less conspicuous (Figure 4c). Epidote veins typically have an irregular morphology and diffuse walls, and can vary in thickness along strike and down dip (Figures 4c, d). In all examples, K-feldspar is altered to albite within the alteration halo (e.g., Figures 5a–d), whereas plagioclase appears to be less susceptible and only albitized within intense alteration haloes (Figure 5e). Alteration haloes typically range in width between 0.5 and 2 cm but can be up to 1 m wide on large veins. More pervasive albite alteration, locally accompanied by actinolite and relict garnet (mostly retrograded to pumpellyite and chlorite) formed close (150–1000 m) to the porphyry-Cu centres and stocks (Figures 2b, 4b). In hand sample, albite haloes are opaque and the primary twinning and lamellae in igneous feldspars are absent. In thin section, albite-altered feldspar is turbid and associated with coeval, disseminated, fine-grained (~5–10 μm) white mica and microporosity (Figures 5f, g).

Prehnite veinlets (±epidote) with plagioclase-destructive white mica–prehnite haloes (±chlorite-vermiculite in hornblende and biotite) constitute the most abundant and widespread alteration facies in the Guichon batholith. The K-feldspar is generally stable within prehnite-vein alteration haloes (Figures 5c, d). Initial shortwave-infrared spectral analysis (TerraSpec 4) of this facies identified a mixed spectrum of white mica (illite), prehnite and subordinate chlorite. Hyperspectral analysis of rock slabs, completed by P. Lypaczewski (CMIC Ph.D. student, University of Alberta), more clearly showed prehnite morphology (vein-fill and disseminated grains in the halo) in rock slabs, and its distribution in the HVC district. Prehnite in rock slabs varies from opaque to light mint-green or dark green and the mineral is susceptible to amaranth stain after etching with HF (Figure 5d). In hand sample, plagioclase altered to white mica is typically pale mint-green in colour. In thin section, small grains (20–100 μm) of prehnite and more abundant fine-grained clusters (5–20 μm) of white mica occur together in altered plagioclase crystals. Prehnite veins exhibit a wide range of orientations throughout the

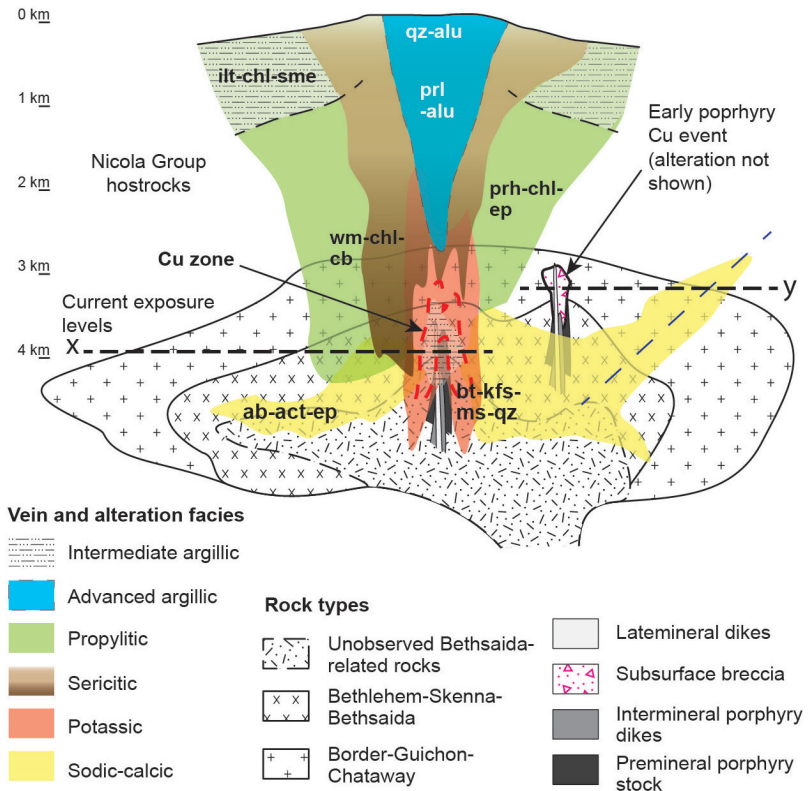


Figure 3. Schematic alteration zonation through the Valley-Lornex porphyry Cu centre hosted in the Guichon batholith (modified after Halley et al., 2015). Note 1) the structural control on Na-Ca-alteration facies; 2) the interpreted emplacement depths and exposure levels of the Valley-Lornex centre (labelled 'x') and the shallower Bethlehem breccia-hosted porphyry centre (labelled 'y'); and 3) the exclusion of the alteration at Bethlehem for clarity. Mineral abbreviations: ab, albite; act, actinolite; alu, alunite; bt, biotite; cb, carbonate mineral; chl, chlorite; ep, epidote; ift, ilmenite; kfs, K-feldspar; ms, muscovite (coarse grained); prh, prehnite; prl, pyrophyllite; qz, quartz; sme, smectite; wm, white mica-sericite (fine grained).

batholith. Prehnite veinlets and their associated white mica–chlorite alteration commonly refracture and overprint earlier-formed veins and haloes, resulting in complex alteration patterns in hand sample.

Paragenetic Sequence

Most of the Na-Ca alteration appears to have occurred between the main stages of Cu introduction in the HVC district (Figure 6). Sodic-calcic alteration overprinted biotite–K-feldspar–bornite–chalcocite veins and alteration, and magmatic-hydrothermal breccia, in the Bethlehem system (Figure 4e; Byrne et al., 2013). Narrow (0.2–1 cm) K-feldspar fracture haloes, with and without trace chalcocite patina, are found up to 4 km away from the Valley-Lornex and Highmont Cu centres (Lesage et al., 2016). These early-mineral K-feldspar fracture haloes were overprinted by Na-Ca veins at most locations. Locally within the Highmont porphyry Cu centre, however, quartz–chalcocite–K-feldspar veinlets appear to crosscut epidote veins with albite haloes (Figures 5a, b). Main-stage veins containing quartz, coarse muscovite and Cu-Fe–sulphide crosscut epi-

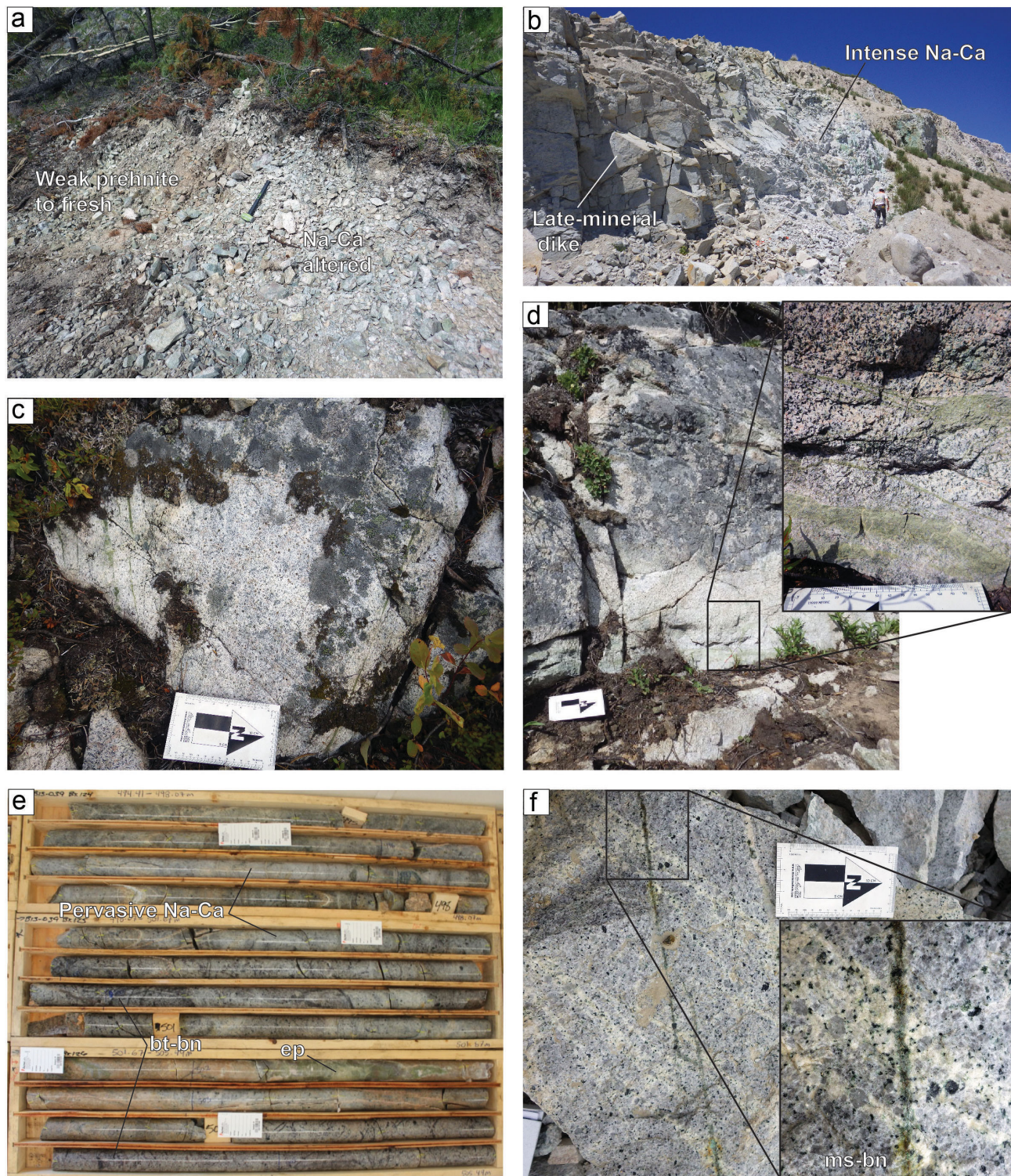
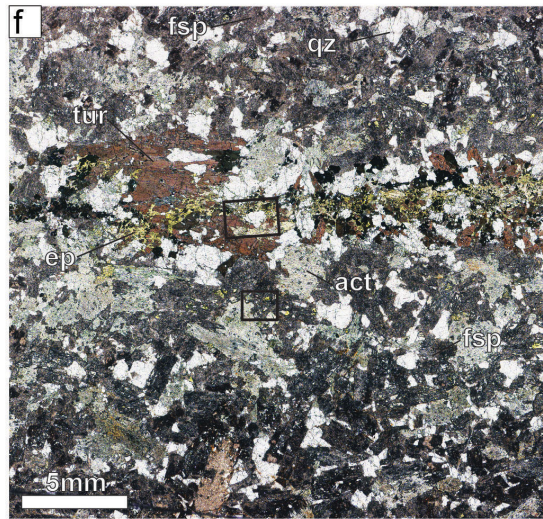
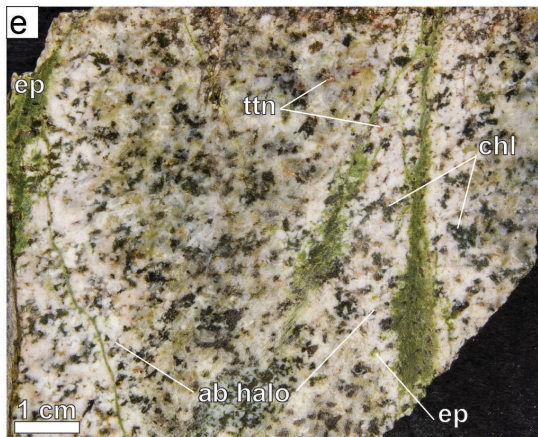
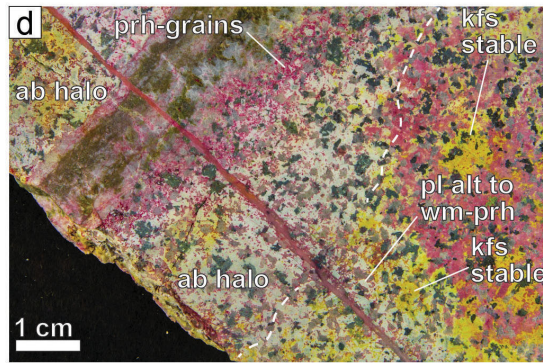
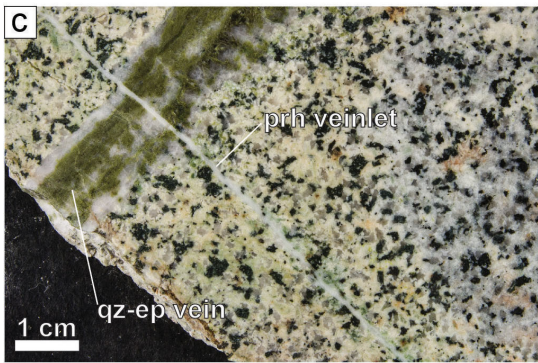
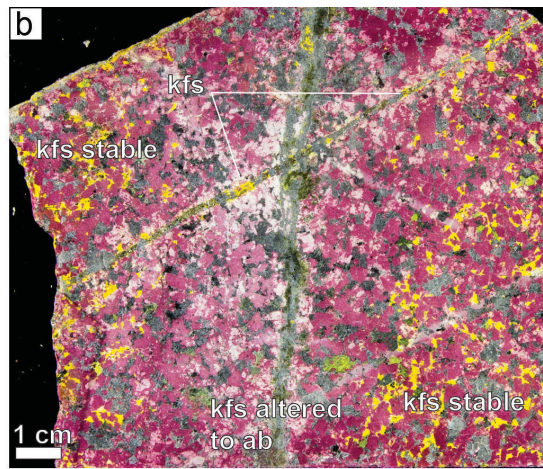
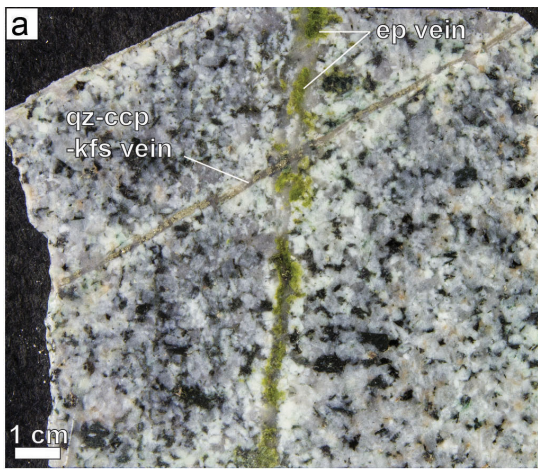
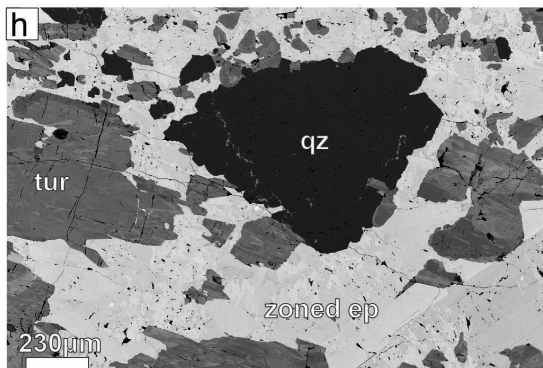
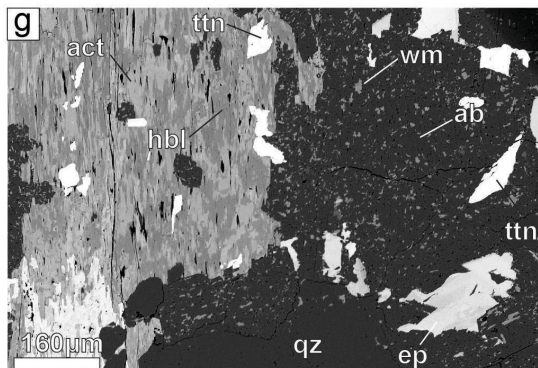


Figure 4. **a)** Fresh roadcut exposure of Na-Ca alteration in the northeastern part of the batholith. **b)** Intense albite–white-mica alteration above the Bethlehem pit; note the highly fractured Na-altered domain compared to the blocky fracture pattern of a late-mineral dike on the left side of the image. **c)** and **d)** Examples of epidote veins with albite haloes hosted in Guichon granodiorite. **e)** Drillcore from the centre of the Jersey (Bethlehem) porphyry system, showing biotite veins and alteration, and Cu mineralization overprinted by intense albite and epidote-albite (hematite stained); the Na-Ca facies is Cu-grade destructive and leaches Fe. **f)** Premineral quartz and feldspar porphyry stock at Highmont crosscut by albite-fracture haloes (white coloured), which are in turn cut by coarse muscovite-bornite veins. Mineral abbreviations: bn, bornite; bt, biotite; ep, epidote.



	Al/Ti	Ca/K	Na/K	Na/Ba	Sr/Ba	K/Th	Rb/Ti
Stg. Na-Ca	26.7	10.0	9.3	3.9	4.4	0.1	28.0
Least alt.	24.8	2.8	1.9	0.6	1.0	0.4	82.6



dote veinlets with albite haloes and pervasive albite-altered rocks (Figure 4f) at Valley-Lornex and Highmont. North and east of Bethlehem, rare tourmaline veinlets, with and without haloes of K-feldspar or intense white mica, are overprinted by epidote veins with albite–white mica haloes (Figure 5h). Sodic–calcic–altered rocks are crosscut by prehnite veinlets with plagioclase–destructive white mica haloes (Figures 5c, d) but still have distinctive major- and minor-element enrichments and depletions: elevated Na₂O, CaO and Cl; a decrease in K₂O and FeO; and high Na/Ba and Sr/Ba (e.g., Figure 5e).

Discussion

The recognition and study of the Na–Ca alteration assemblage is important because

- mapping has shown that large domains of strongly Na–Ca–metasomatized rocks are along strike of the porphyry Cu centres (Figure 2b);
- it locally removed magnetite and hornblende, thus changing the rock petrophysical properties; and
- where it overprinted Cu mineralization, it is destructive of the Cu grade.

Isotope and fluid-inclusion studies have shown that meteoric (Sheets et al., 1996; Taylor, 1979; Selby et al., 2000), formational brine (Dilles et al., 1992) and magmatic-derived (Dilles et al., 1992; Harris et al., 2005; Rusk et al., 2008) fluids of varying salinities can all be present in various proportions at different locations and times in an evolving porphyry system. Additionally, sericite at Koloula and Waisoi in Papua New Guinea is interpreted to have formed from seawater in young (1.5–5 Ma) and shallowly emplaced porphyry systems (Chivas et al., 1984). Similarly, calculated initial O and D isotopic compositions of coarse muscovite from the Valley system at HVC suggest mixing

of seawater with high-temperature (370–500°C), Cu-bearing magmatic fluids (Osatenko and Jones, 1976).

Widespread Na–Ca alteration may be caused by the flow of external hypersaline formation waters, heated during inflow to the magmatic cupola regions along the margins of potassic alteration (Dilles et al., 1992; Dilles et al., 2000). Highly oxidized felsic magmas can produce fluids capable of Na-, Fe-, Ca- or K-rich alteration (Arancibia and Clark, 1996). Similarly, fluids evolved from special alkalic melts can cause Na metasomatism (Lang et al., 1995). The magmatic-derived Na–Ca–alteration examples, however, are inconsistent with the scale and distribution features of Na–Ca alteration in the Guichon batholith. Sodium-rich alteration is widely developed in Permian to Jurassic arc igneous rocks of the western United States, where it is attributed to moderate- to high-salinity fluids of marine, formation and/or meteoric origin, with or without a magmatic component (Battles and Barton, 1995). The hypothesis that will be tested in this study is that seawater drawn down and inward along regional structures toward cupola regions caused Na–Ca alteration during the upwelling of the magmatic-hydrothermal fluids that formed the porphyry Cu mineralization. If this is the case, this process may be more prevalent in island-arc porphyry systems than previously recognized.

This hypothesis will be tested using a combination of field and laboratory techniques. First, field maps, feldspar-stained rock slabs, hyperspectral images and petrography will be used to establish the Na–Ca facies distribution, mineralogy and its paragenesis at HVC. This will be followed by geochemical characterization by electron microprobe analysis (EMPA) and laser-ablation inductively coupled plasma–mass spectrometry (LA-ICP-MS) of the associated minerals (epidote, albite, actinolite, titanite). Results will be compared to Na, Ca and Na–Ca assemblages in other systems: Yerington, Anne-Mason and Royston in Nevada (Carten, 1986; Dilles and Einaudi, 1992); Sierrita-Esperanza and Kelvin-Riverside in Arizona (Seedorff et al., 2008); and Island Copper, Mt. Milligan, Gibraltar and Woodjam in BC (Arancibia and Clark, 1996; Jago et al., 2014; Chapman et al., 2015; Kobylinski et al., 2016). Whole-rock ⁸⁷Sr/⁸⁶Sr values of unaltered samples will be compared to the Sr-isotope composition of strongly Na–Ca–altered samples to test for shifts from initial HVC magmatic compositions of 0.7034 (D’Angelo, 2016) to Triassic seawater values of ~0.7076 (Tremba et al., 1975). Additionally, the Sr, O and D isotope compositions of epidote, albite and actinolite will be measured and evaluated with respect to magmatic and other fluid-reservoir (e.g., meteoric and seawater) compositions. Minerals formed from magmatic fluids are expected to have initial δ¹⁸O and δD values close to 6‰ and –60‰, respectively (Taylor, 1979), whereas minerals formed from a fluid with seawater input may move toward the composition of standard mean ocean water (SMOW; ~0‰ for both δ¹⁸O and δD).

Figure 5. a) Epidote vein with albite halo in Skeena granodiorite crosscut by a quartz–K-feldspar–chalcopyrite veinlet. **b)** Feldspar-stained image of photo (a); dark yellow indicates K-feldspar and pink indicates calcic plagioclase; weak pink-stained to white plagioclase is associated with fine-grained, pale green, white mica and small grains of prehnite. **c)** and **d)** Epidote-quartz vein with K-feldspar–destructive albite halo crosscut, offset and overprinted by a prehnite veinlet with strong white mica–prehnite–chlorite halo; host rock is Chataway-facies granodiorite. **e)** Irregular epidote veins with albite–chlorite haloes in Guichon granodiorite, also showing lithochemical response of the corresponding sample. **f)** Photomicrograph of albite- and white mica–altered feldspar and actinolite–epidote–altered hornblende in Guichon granodiorite; tourmaline vein fill is crosscut by epidote. **g)** Back-scattered electron image of partially actinolite-altered primary hornblende; note accessory titanite; primary feldspar is altered to albite and contains numerous disseminated inclusions of white mica and very fine grained pore space (black). **h)** Fragments of tourmaline in compositionally zoned (Fe–Al substitution) epidote. Mineral abbreviations: ab, albite; act, actinolite; ccp, chalcopyrite; chl, chlorite; ep, epidote; fsp, feldspar; hbl, hornblende; kfs, K-feldspar; pl, plagioclase; prh, prehnite; qz, quartz; ttn, titanite (sphene); tur, tourmaline; wm, white mica.

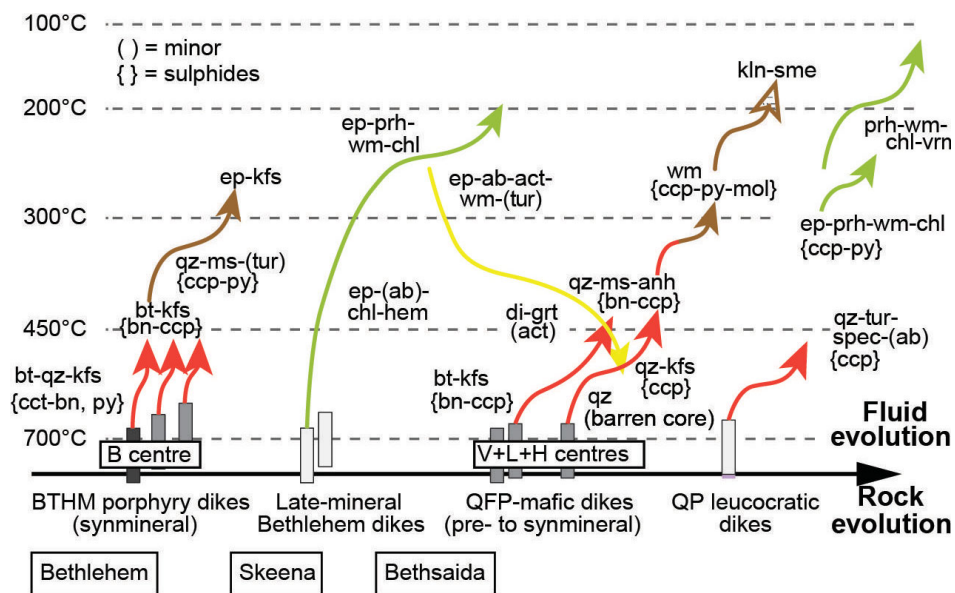


Figure 6. Paragenetic sequence of intrusion facies (rectangles) and vein and alteration facies (coloured arrows) at Highland Valley Copper (HVC). The colour scheme of the vein and alteration arrows is explained in Figure 3. The arrows are schematic representations of fluid evolution through time (x axis) and temperature changes (y axis). Abbreviations: B, Bethlehem; V, L and H, Valley, Lornex and Highmont, respectively. Mineral abbreviations: ab, albite; act, actinolite; anh, anhydrite; bn, bornite; bt, biotite; ccp, chalcopyrite; chl, chlorite; di, diopside; ep, epidote; grt, garnet; hem/spec, hematite; kln, kaolinite; kfs, K-feldspar; mol, molybdenite; ms, muscovite (coarse grained); prh, prehnite; py, pyrite; qz, quartz; sme, smectite; tur, tourmaline; vm, vermiculite; wm, white mica-sericite (fine grained).

Impact of Proposed Work

Porphyry Cu deposits provide the world with most of its Cu and have likely been the focus of more academic research than any other class of base-metal deposit. Significant advances in genetic understanding of porphyry systems, at various scales, have been made. Exploration tools and models (e.g., Holliday and Cooke, 2007) applicable to the exploration geoscientist, however, have not advanced to the same degree, with a few notable exceptions: fertility (Richards, 2011a; Loucks, 2014); epidote-vector geochemistry (Jago, 2008; Cooke et al., 2014); lateral and vertical metal zonation (Jones, 1992; Halley et al., 2015); shortwave-infrared spectroscopy (Thompson et al., 1999; Halley et al., 2015); and porphyry-indicator minerals (Averill, 2011).

The research outlined in this paper is designed to test for evidence of nonmagmatic fluid flow around porphyry Cu deposits, and how these fluids interacted with and affected wallrock with increasing distance from the Cu centres. The nonconcentric distribution of Na-Ca alteration is an important modifier to typical alteration-zonation models. Results from this research have the potential to refine exploration models and leverage existing datasets, thus leading to more cost-efficient and successful exploration programs.

Acknowledgments

Funding was provided by the Natural Sciences and Engineering Council of Canada (NSERC) and the Canada Mining Innovation Council (CMIC) through the NSERC Collaborative Research and Development Program, for which the authors are grateful (NSERC-CMIC Exploration Footprints Network Contribution 115). Additionally, the authors thank the Strategic Planning Group at HVC and Teck Resources Limited for support during the summer fieldwork periods. This contribution benefited from review by L. Marshall, Regional Chief Geoscientist at Teck, and L. Pyrer.

References

- Arancibia, O.N. and Clark, A. (1996): Early magnetite-amphibole-plagioclase alteration-mineralization in the Island Copper porphyry copper-gold-molybdenum deposit, British Columbia; *Economic Geology*, v. 91, p. 402–438.
- Averill, S.A. (2011): Viable indicator minerals in surficial sediments for two major base metal deposit types: Ni-Cu-PGE and porphyry Cu; *Geochemistry: Exploration, Environment, Analysis*, v. 11, no. 4, p. 279–291. doi:10.1144/1467-7873/10-IM-022

- Battles, D.A. and Barton, M.D. (1995): Arc-related sodic hydrothermal alteration in the western US; *Geology*, v. 23, no. 10, p. 913–916.
- Byrne, K., Stock, E., Ryan, J., Johnson, C., Nisenson, J., Alva-Jimenez, T., Lapointe, M., Stewart, H., Grubisa, G. and Sykora, S. (2013): Porphyry Cu-(Mo) deposits in the Highland Valley District, South Central British Columbia; *in* Porphyry Systems of Central and Southern BC: Tour of Central BC Porphyry Deposits from Prince George to Princeton, J. Logan and T. Schroeter (ed.), Society of Economic Geologists, Guidebook Series, v. 44, p. 99–116, URL <<http://www.segweb.org/store/detail.aspx?id=GB44-DISC>> [November 2016].
- Carten, R.B. (1986): Sodium-calcium metasomatism: chemical, temporal, and spatial relationships at the Yerington, Nevada porphyry copper deposit; *Economic Geology*, v. 81, no. 6, p. 1495–1519. doi:10.2113/gsecongeo.81.6.1495
- Chapman, J., Plouffe, A. and Ferbey, T. (2015): Tourmaline chemistry as a tool for porphyry exploration: the Woodjam Cu-Au deposits, central British Columbia; Association for Mineral Exploration (AME) Roundup 2015, poster presentation.
- Chivas, A.R., O’Neil, J.R. and Katchan, G. (1984): Uplift and submarine formation of some Melanesian porphyry copper deposits: stable isotope evidence; *Earth and Planetary Science Letters*, v. 68, p. 326–334.
- Colpron, M., Nelson, J.A.L. and Murphy, D.C. (2007): Northern Cordilleran terranes and their interactions through time; *GSA Today*, v. 17, no. 4, p. 4–10. doi:10.1130/GSAT01704-5A.1
- Coney, P.J., Jones, D.L. and Monger, J.W.H. (1980): Cordilleran suspect terranes; *Nature*, v. 288, p. 329–333.
- Cooke, D.R., Baker, M., Hollings, P., Sweet, G., Zhaoshan, C., Danyushevsky, L., Gilbert, S., Zhou, T., White, N.C., Gemmell, J.B. and Inglis, S. (2014): New advances in detecting the distal geochemical footprints of porphyry systems: epidote mineral chemistry as a tool for vectoring and fertility assessments; *in* Building Exploration Capability for the 21st Century, K.D. Kelley and H.C. Golden (ed.), Society of Economic Geologists, Special Publication 18, p. 127–152.
- D’Angelo, M. (2016): Geochemistry, petrography and mineral chemistry of the Guichon Creek and Nicola batholiths, south-central British Columbia; M.Sc. thesis, Lakehead University, Thunder Bay, Ontario, 435 p., URL <http://cmic-footprints.ca/home/publications/files/Theses/088_D%27Angelo_2016%20Lakehead%20MSc_Guichon%20Creek%20Batholith.pdf> [November 2016].
- Dilles, J.H. and Einaudi, M.T. (1992): Wall-rock alteration and hydrothermal flow paths about the Ann-Mason porphyry copper deposit, Nevada: a 6-km vertical reconstruction; *Economic Geology*, v. 87, p. 1963–2001.
- Dilles, J.H., Einaudi, M.T., Proffett, J.M. and Barton, M.D. (2000): Overview of the Yerington porphyry copper district: magmatic to nonmagmatic sources of hydrothermal fluids, their flow paths, alteration affects on rocks, and Cu-Mo-Fe-Au ores; Society of Economic Geologists, Post-Meeting Field Conference, v. 32, p. 55–66.
- Dilles, J.H., Solomon, G.C., Taylor, H.P. and Einaudi, M.T. (1992): Oxygen and hydrogen isotope characteristics of hydrothermal alteration at the Ann-Mason porphyry copper deposit, Yerington, Nevada; *Economic Geology*, v. 87, no. 1, p. 44–63. doi:10.2113/gsecongeo.87.1.44
- Halley, S.W., Dilles, J.H. and Tosdal, R.M. (2015): Footprints: hydrothermal alteration and geochemical dispersion around porphyry copper deposits; SEG Newsletter, no. 100.
- Harris, A.C., Golding, S.D. and White, N.C. (2005): Bajo de la Alumbrera copper-gold deposit: stable isotope evidence for a porphyry-related hydrothermal system dominated by magmatic aqueous fluids; *Economic Geology*, v. 100, no. 5, p. 863–886. doi:10.2113/gsecongeo.100.5.863
- Holliday, J.R. and Cooke, D.R. (2007): Advances in geological models and exploration methods for copper±gold porphyry deposits; *in* Proceedings of Exploration 07: Fifth Decennial International Conference on Mineral Exploration, p. 791–809.
- Hollister, V.F., Allen, J.M., Anzalone, S.A. and Seraphim, R.H. (1976): Structural evolution of porphyry mineralization at Highland Valley, British Columbia: reply; *Canadian Journal of Earth Sciences*, v. 13, p. 612–613. doi:10.1139/e76-065
- Jago, C.P. (2008): Metal- and alteration-zoning, and hydrothermal flow paths at the moderately-tilted, silica-saturated Mt. Milligan Cu-Au alkalic porphyry deposit; M.Sc. thesis, The University of British Columbia, Vancouver, BC, 227 p.
- Jago, C., Tosdal, R., Cooke, D. and Harris, A. (2014): Vertical and lateral variation of mineralogy and chemistry in the Early Jurassic Mt. Milligan alkalic porphyry Au-Cu deposit, British Columbia, Canada; *Economic Geology*, v. 109, p. 1005–1033. doi:10.2113/econgeo.109.4.1005
- Jones, B.K. (1992): Application of zoning to Au exploration in porphyry copper systems; *Journal of Geochemical Exploration*, v. 43, p. 127–155.
- Kobylnski, C., Hattori, K., Smith, S. and Plouffe, A. (2016): Mineral chemistry of greenrock alteration associated with the porphyry Cu-Mo mineralization at the Gibraltar deposit, south central British Columbia, Canada; paper presented at Geological Association of Canada–Mineralogical Association of Canada, Joint Annual Meeting, Whitehorse, Yukon.
- Lang, J., Stanley, C., Thompson, J.F.H. and Dunne, K. (1995): Na-K-Ca magmatic-hydrothermal alteration in alkalic porphyry Cu-Au deposits, British Columbia; *in* Magmas, Fluids and Ore Deposits, J.F.H. Thompson (ed.), Mineralogical Association of Canada, p. 339–366.
- Lesage, G., Byrne, K., Lypaczewski, P., Lee, R.G. and Hart, C.J.R. (2016): Characterizing the district-scale alteration surrounding a large porphyry Cu system: the footprint of Highland Valley Copper, British Columbia; paper presented at Geological Association of Canada–Mineralogical Association of Canada, Joint Annual Meeting, Whitehorse, Yukon, <http://cmic-footprints.ca/home/publications/files/Posters/Lesage_2016_GAC_MAC_HVC_alteration_Poster.pdf> [November 2016].
- Logan, J.M., and Mihalynuk, M.G. (2014): Tectonic controls on early Mesozoic paired alkaline porphyry deposit belts (Cu-Au±Ag-Pt-Pd-Mo) within the Canadian Cordillera; *Economic Geology*, v. 109, no. 4, p. 827–858. doi:10.2113/econgeo.109.4.827
- Loucks, R.R. (2014): Distinctive composition of copper-ore-forming arc magmas; *Australian Journal of Earth Sciences*, v. 61, no. 1, p. 5–16. doi: 10.1080/08120099.2013.865676
- Massey, N.W.D., MacIntyre, D.G., Desjardins, P. and Cooney, R.T. (2005): Digital geology map of British Columbia – whole province; BC Ministry of Energy and Mines, BC Geological Survey, GeoFile 2005-1, <<http://www.empr.gov.bc.ca/Mining/Geoscience/Publications/Catalogue/GeoFiles/Pages/2005-1.aspx>> [December 2016].

- McMillan, W.J. (1976): Geology and genesis of the Highland Valley ore deposits and the Guichon Creek Batholith; *in* Porphyry Deposits of the Canadian Cordillera, A. Sutherland Brown (ed.), Canadian Institute of Mining and Metallurgy, Special Volume 15, p. 85–104.
- McMillan, W.J. (1985): Geology and ore deposits of the Highland Valley camp; Geological Association of Canada, Mineral Deposits Division, Field Guide and Reference Manual Series (A.J. Sinclair, ser. ed.), no. 1, 121 p.
- McMillan, W.J., Anderson, R.G., Chen, R. and Chen, W. (2009): Geology and mineral occurrences (MINFILE), the Guichon Creek Batholith and Highland Valley porphyry copper district, British Columbia; Geological Survey of Canada, Open File 6079, 3 maps. doi:10.4095/248060
- Mihalynuk, M.G., Diakow, L.J., Friedman, R.M. and Logan, J.M. (2016): Chronology of southern Nicola arc stratigraphy and deformation; *in* Geological Fieldwork 2015, BC Ministry of Energy and Mines, BC Geological Survey, Paper 2016-1, p. 31–63.
- Mortimer, N. (1987): The Nicola Group: Late Triassic and Early Jurassic subduction related volcanism in British Columbia; Canadian Journal of Earth Sciences, v. 24, p. 2521–2536.
- Northcote, K.E. (1969): Geology and geochronology of the Guichon Creek Batholith; BC Ministry of Energy and Mines, Bulletin 56, 77 p.
- Osatenko, M.J. and Jones, M.B. (1976): Valley Copper; *in* Porphyry Deposits of the Canadian Cordillera, A. Sutherland Brown (ed.), Canada Institute of Mining and Metallurgy, Special Volume 15, p. 130–143.
- Preto, V.A. (1979): Geology of the Nicola Group between Merritt and Princeton; BC Ministry of Energy and Mines, Bulletin 69, 100 p.
- Proffett, J.M. (2009): High Cu grades in porphyry Cu deposits and their relationship to emplacement depth of magmatic sources; *Geology*, v. 37, no. 8, p. 675–678. doi:10.1130/G30072A.1
- Ray, G.E., Dawson, G.L. and Webster, I.C. (1996): The stratigraphy of the Nicola Group in the Hedley district, British Columbia, and the chemistry of its intrusions and Au skarns; Canadian Journal of Earth Sciences, v. 33, p. 1105–1126.
- Richards, J.P. (2011a): High Sr/Y arc magmas and porphyry Cu±Mo±Au deposits: just add water; *Economic Geology*, v. 106, no. 7, p. 1075–1081.
- Richards, J.P. (2011b): Magmatic to hydrothermal metal fluxes in convergent and collided margins; *Ore Geology Reviews*, v. 40, no. 1, p. 1–26.
- Riedell, K.B. and Proffett, J.M. (2014): Batholithic and early halo type Cu-Mo deposits; Geological Society of America, 2014 Annual Meeting, paper 247-4, <[https://gsa.confex.com/gsa/2014AM/webprogram/Handout/Paper245644/Bath and EHT deposits_Riedell-Proffett_300dpi_rev-d-141027.pdf](https://gsa.confex.com/gsa/2014AM/webprogram/Handout/Paper245644/Bath_and_EHT_deposits_Riedell-Proffett_300dpi_rev-d-141027.pdf)> [November 2016].
- Rusk, B.G., Reed, M.H. and Dilles, J.H. (2008): Fluid inclusion evidence for magmatic-hydrothermal fluid evolution in the porphyry copper-molybdenum deposit at Butte, Montana; *Economic Geology*, v. 103, no. 2, p. 307–334. doi:10.2113/gsecongeo.103.2.307
- Schodde, R. (2014): The global shift to undercover exploration: how fast? how effective?; presentation at Society of Economic Geologists, 2014 Annual Meeting, Keystone, Colorado, September 30, 2014.
- Seedorff, E., Barton, M.D., Stavast, W.J. and Maher, David, J. (2008): Root zones of porphyry systems: extending the porphyry model to depth; *Economic Geology*, v. 103, p. 939–956.
- Seedorff, E., Dilles, J.H., Proffett, J.M., Einaudi, M.T., Zurcher, L., Stavast, W.J.A., Johnson, D.A. and Barton, M.D. (2005): Porphyry deposits: characteristics and origin of hypogene features; *in* Economic Geology 100th Anniversary Volume, J. Hedenquist, J.F. Thompson, R. Goldfarb and J. Richards (ed.), Society of Economic Geologists, p. 251–298.
- Selby, D., Nesbitt, B.E., Muehlenbachs, K. and Prochaska, W. (2000): Hydrothermal alteration and fluid chemistry of the Endako porphyry molybdenum deposit, British Columbia; *Economic Geology*, v. 95, no. 1, p. 183–202.
- Sheets, R.W., Nesbitt, B.E. and Muehlenbachs, K. (1996): Meteoric water component in magmatic fluids from porphyry copper mineralization, Babine Lake area, British Columbia; *Geology*, v. 24, no. 12, p. 1091–1094.
- Sillitoe, R.H. (2010): Porphyry copper systems; *Economic Geology*, v. 105, no. 1, p. 3–41. doi:10.2113/gsecongeo.105.1.3
- Sillitoe, R.H. (2013): Metallogenic and regulatory inequalities around the northern Pacific Rim: implications for discovery; *in* Tectonics, Metallogeny, and Discovery: The North American Cordillera and Similar Accretionary Settings, M. Colpron, T. Bissig, B.G. Rusk and J.F.H. Thompson (ed.), Special Publication 17, p. 1–16.
- Taylor, H.P. (1979): Oxygen and hydrogen isotope relationships in hydrothermal mineral deposits; *in* Geochemistry of Hydrothermal Ore Deposits, H.L. Barnes (ed.), John Wiley & Sons, New York, New York, p. 236–277.
- Teck Resources Limited (2016): Annual information form, 117 p., <http://www.teck.com/media/Investors-aif_march_2016_T5.1.2.pdf> [November 2016].
- Thompson, A.J.B., Hauf, P.L. and Robitaille, A.J. (1999): Alteration mapping in exploration: applications of short-wave infrared (SWIR) spectroscopy; *SEG Newsletter*, no. 39, p. 13.
- Thompson, J.F.H. (2016): The future of mineral exploration; presentation at Association for Mineral Exploration (AME) Roundup 2016, Vancouver, BC.
- Tremba, E.L., Faure, G., Katsikatos, G.C. and Summerson, C.H. (1975): Strontium isotope composition in the Tethys Sea, Euboea, Greece; *Chemical Geology*, v. 16, p. 109–120.
- Wilburn, D.R., Stanley, K.A. and Karl, N.A. (2015): Exploration review; *Mining Engineering, Annual Review 2014*, v. 67, no. 5, p. 16–38. <<http://me.smenet.org/abstract.cfm?preview=1&articleID=5905&page=16>> [December 2016].
- Wood, D. (2016): We must change exploration thinking in order to discover future orebodies; *SEG Newsletter*, no. 105, p. 16–19.

Nature and Origin of the Brucejack High-Grade Epithermal Gold Deposit, Northwestern British Columbia (NTS 104B)

D.F. McLeish, Department of Earth and Planetary Sciences, McGill University, Montréal, QC, duncan.mcleish@mail.mcgill.ca

A.E. Williams-Jones, Department of Earth and Planetary Sciences, McGill University, Montréal, QC

W.S. Board, Pretium Resources Inc., Vancouver, BC

McLeish, D.F., Williams-Jones, A.E. and Board, W.S. (2017): Nature and origin of the Brucejack high-grade epithermal gold deposit, northwestern British Columbia (NTS 104B); in *Geoscience BC Summary of Activities 2016*, Geoscience BC, Report 2017-1, p. 223–232.

Introduction

A major challenge in understanding the genesis of epithermal gold deposits is that existing genetic models do not satisfactorily explain the mechanisms responsible for high-grade gold deposition and transport at temperatures characteristic of the epithermal realm (150–300°C). Although transport by dissolution in an aqueous hydrothermal liquid is the widely proposed mechanism for mobilizing gold within Earth's upper crust (e.g., Helgeson and Garrels, 1968; Krupp and Seward, 1987; Sillitoe and Hedenquist, 2003; Simmons and Brown, 2006; Williams-Jones et al., 2009; Zhu et al., 2011), experiments have shown that the solubility of gold is too low in hydrothermal liquids at temperatures less than approximately 400°C to account for the extraordinarily high grades observed in some epithermal deposits (e.g., Seward 1973; Gammons and Williams-Jones, 1995; Heinrich et al., 2004; Stefánsson and Seward, 2004; Zevin et al., 2011; Hurtig and Williams-Jones, 2014). It is therefore necessary to consider alternative explanations for the high grades, including 1) that the temperatures commonly assumed for gold transport greatly underestimate the true temperature because they are based on estimates of the conditions of deposition; 2) that high fluid fluxes and steep physicochemical gradients can be maintained in single fractures for exceptional periods of time (unlikely); and 3) that the capacity of a fluid to transport gold is not controlled by simple solubility, either in a vapour or a liquid, but is also determined by other processes. For example, the development of boiling-mediated nanoparticle suspensions (colloids) could greatly increase the capacity of the fluid to carry gold. Resolving the issue of how exceptionally high grade epithermal gold deposits form will be an important step in elucidating the broader

question of how these deposits truly relate to the higher temperature copper–molybdenum±gold porphyry systems with which they are commonly associated.

The Brucejack deposit of Pretium Resources Inc. (MIN-FILE 104B 193 and 104B 199; BC Geological Survey, 2016), currently undergoing preproduction mine development in the Stewart–Eskay Creek district of northwestern British Columbia (Figure 1), is host to one of the highest grade (up to 41 000 g/tonne Au) and best exposed intermediate-sulphidation or possibly low-sulphidation epithermal gold deposits in the world. The well-explored nature of epithermal gold mineralization on the Brucejack property, combined with its proximity to well-explored, world-class copper-gold-molybdenum porphyry deposits (Snowfield and Kerr-Sulphurets-Mitchell; Figure 2) of the Stikine Arc, offer an unparalleled opportunity to study the genesis of epithermal gold deposits, investigate their hydrothermal evolution and, importantly, test their relationship to spatially associated porphyry systems.

This paper presents preliminary results from a recently initiated study of the Brucejack deposit, the purpose of which is to petrographically and chemically (including isotopically) characterize its ores and associated hydrothermal alteration, and determine the composition of its mineralizing fluids through fluid-inclusion analysis. These data will be used to reconstruct, through thermodynamic analysis, the physicochemical conditions that controlled gold mineralization, and to quantitatively test plausible models of ore formation. If successful, the study will improve on existing models for the genesis of epithermal Au deposits and the strategies that guide their exploration.

Regional Geology

The Brucejack deposit is situated in the Stewart–Eskay Creek district of the northwestern Stikine terrane (Figures 1, 2), a paleo-island arc system akin to that of the modern-day Philippine archipelago (Marsden and Thorkelson, 1992). The Stikine terrane formed as an intraoceanic island arc in the mid-Paleozoic and was accreted to the western

Keywords: *British Columbia, Stikine terrane, Hazelton Group, Brucejack, geochemistry, gold, solubility, hydrothermal fluids, epithermal, veins, electrum*

This publication is also available, free of charge, as colour digital files in Adobe Acrobat® PDF format from the Geoscience BC website: <http://www.geosciencebc.com/s/DataReleases.asp>.

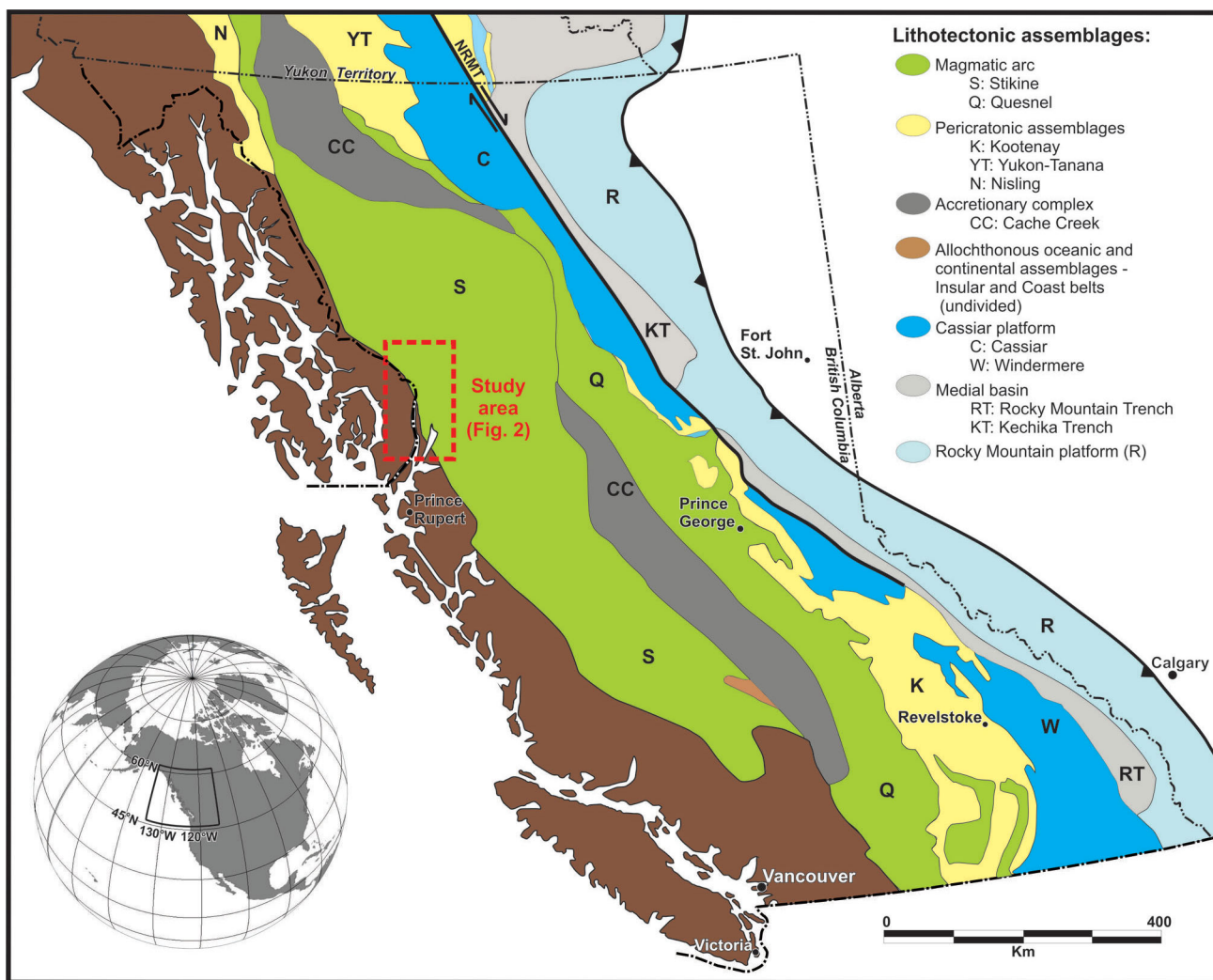


Figure 1: Location of the study area in reference to the major lithotectonic subdivisions of the Canadian Cordillera (modified after McLeish, 2013 with lithotectonic boundaries from Johnston, 2008). Abbreviation: NRMT, Northern Rocky Mountain Trench (fault).

continental margin of Laurentia in the Middle to Late Jurassic (Monger et al., 1991; Anderson, 1993). Volcano-sedimentary rocks of the Late Triassic Stuhini Group and Early Jurassic Hazelton Group dominate the stratigraphy of the Stikine terrane. Two distinct episodes of magmatism in the Late Triassic and in the Jurassic (229–221 Ma and 195–175 Ma, respectively; Macdonald et al., 1996) affected the Stuhini-Hazelton succession, which was deformed in the Middle to Late Jurassic during accretion and during later Cretaceous compressional tectonism (Greig and Brown, 1990; Alldrick, 1993). Porphyry magmatism is known to span ca. 220–186 Ma on a terrane scale (Logan and Mihalyuk, 2014); however, within the Stewart–Eskay Creek district, uranium-lead ages for porphyry intrusions are generally limited to the ca. 197–193 Ma range (Kirkham and Margolis, 1995).

Brucejack Property Geology

Five zones of mineralization have been explored in detail at Brucejack (West, Valley of the Kings, Bridge, Gossan Hill and Shore zones; Figure 3), all of which are hosted within hornblende- and/or feldspar-phyric volcanic flows, lapilli tuff, locally derived pyroclastic and volcanic conglomerate, volcanic sandstone, siltstone and mudstone of the lowermost Hazelton Group, proximal to the regional-scale unconformity between the Stuhini and Hazelton groups (Board and McNaughton, 2013). To the immediate west and northwest of these zones, monzonitic, syenitic and granitic rocks of the Mitchell suite intrude volcanoclastic rocks of the Stuhini and Hazelton groups; these intrusions are closely associated with porphyry-style copper-gold-molybdenum mineralization on the adjacent Kerr-Sulphurets-

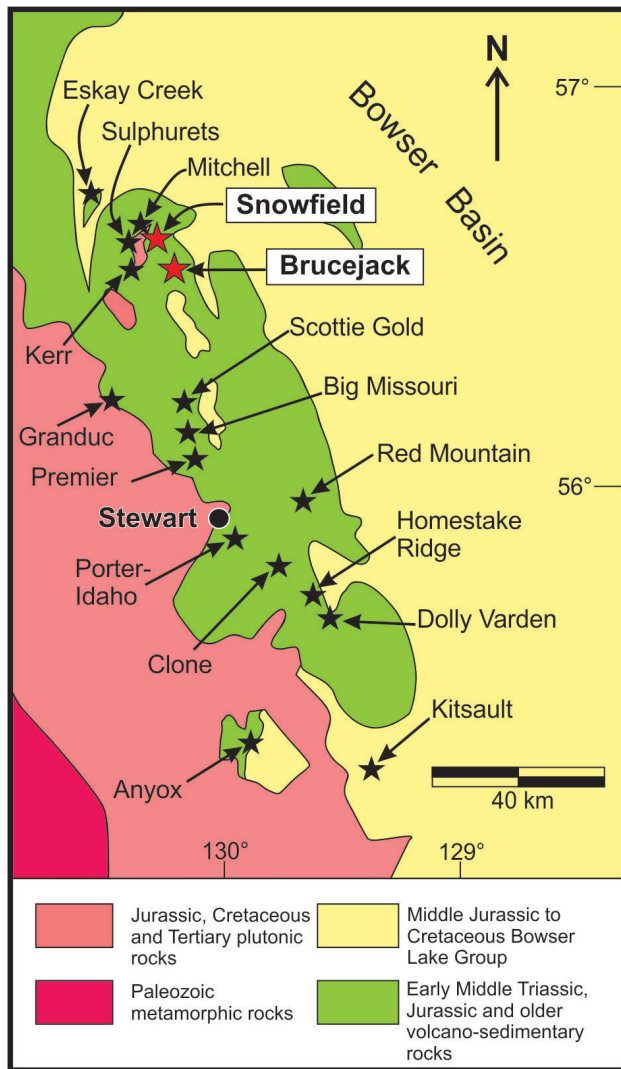


Figure 2: Major porphyry, epithermal and volcanogenic massive-sulphide deposits of the Stewart–Eskay Creek district (modified after Ghaffari et al., 2012), with the locations of the Brucejack and Snowfield properties highlighted.

Mitchell and Snowfield properties (Kirkham and Margolis, 1995). Uranium-lead zircon ages from various phases of these intrusions suggest that the porphyry-style mineralization was emplaced at 195–192 Ma (Margolis, 1993; Macdonald et al., 1996). Large areas of hydrothermal alteration affected and surround the intrusive complexes of the Mitchell suite. These consist of 1) early potassic alteration closely associated with porphyry copper and gold mineralization; 2) locally overprinting propylitic and chlorite-sericite alteration; and 3) widespread and well-developed, late quartz-sericite-pyrite alteration that pervasively overprints earlier alteration and extends distally into the surrounding hostrocks of the Stuhini and Hazelton groups (Ghaffari et al., 2012).

The intrusions of the Mitchell suite and the surrounding rocks of the Stuhini and Hazelton groups were strongly de-

formed during Cretaceous tectonism. This deformation is manifested by the development of 1) schistose and mylonitic fabrics within the weakest, most intensely altered intrusions and wallrocks; 2) prominent east-verging thrust faulting, including the Mitchell and Sulphurets thrusts, which penetrate and offset the Kerr-Sulphurets-Mitchell deposit; and 3) steeply dipping to vertical, north-trending, late-stage brittle faults, including the Brucejack fault (Board, 2014; Febbo et al., 2015). The third group of structures has been interpreted to have reactivated a system of pre-existing syndepositional basin-margin growth faults that were initially active during deposition of the Hazelton Group rocks (Nelson and Kyba, 2014).

Deposit Mineralization

Within the Valley of the Kings zone (VOK; Figure 3), gold mineralization is hosted by extensive, predominantly subvertical, quartz-carbonate-sulphide vein stockworks and subordinate vein breccias. Five stages of veins have been recognized in the VOK: 1) discontinuous pyrite-stringer veins containing carbonate and quartz (V_{N0}); 2) electrum-bearing quartz-carbonate±sericite sheeted, stockwork and brecciated veins (V_{N1a} , V_{N1b} and V_{N1c} , respectively); 3) zinc-lead±copper sulphide veins containing common silver sulphosalts and electrum (V_{N2}); 4) carbonate±quartz veins containing abundant orange-coloured, manganese-bearing calcite, and electrum (V_{N3}); 5) post-mineral, Cretaceous, orogenic quartz±carbonate shear veins with rare, remobilized pyrite, electrum and base-metal sulphides in thrust-related shear bands (V_{N4a} , V_{N4b}) and subhorizontal, barren, white bull-quartz tension-gash veins with adjacent chlorite alteration (V_{N4c} ; classification modified after Tombe et al., 2014). The V_{N0} , V_{N1a-c} , V_{N2} and V_{N3} veins are largely undeformed to weakly deformed, except within localized strain zones where they are moderately to rarely strongly deformed. Evidence from crosscutting relationships paired with hostrock uranium-lead zircon and vein-hosted molybdenite rhenium-osmium age determinations have constrained the age of V_{N1a-c} , V_{N2} and V_{N3} vein formation to ca. 188–183 Ma (Board, 2014; Tombe, 2015). Variably developed but generally intense quartz-sericite-pyrite alteration occurs throughout the deposit but is strongest proximal to the Brucejack fault and the unconformity between the Stuhini and Hazelton groups, which suggests that these structures may have acted as important fluid conduits during hydrothermal alteration and mineralization. Preliminary paleotemperature vectors derived from alteration, mineralization and vein textures suggest a down-temperature thermal gradient toward the east (up stratigraphy) and away from the Snowfield and Kerr-Sulphurets-Mitchell higher temperature porphyry centres, located northwest of the deposit (Board and McNaughton, 2013).

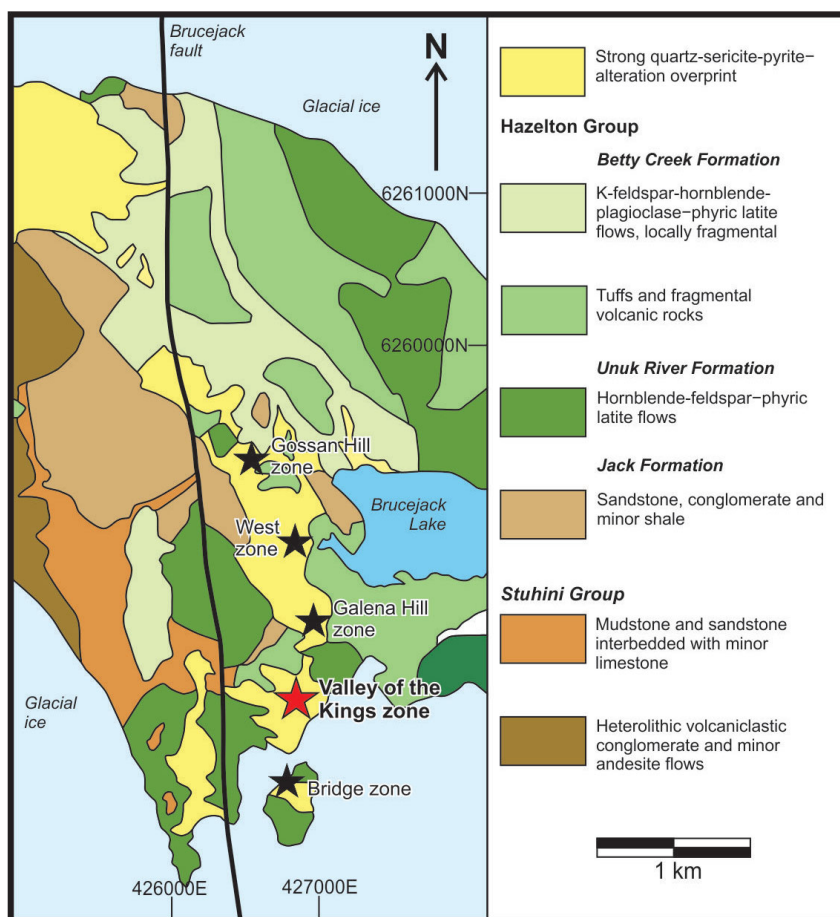


Figure 3: Geology of the Brucejack deposit area (modified after Tombe, 2015), showing five main zones of mineralization that are hosted within a moderately to strongly quartz-pyrite-altered sequence of hornblende- and/or feldspar-phyric volcanic flows, lapilli tuffs, locally derived pyroclastic and volcanic conglomerate, volcanic sandstone, siltstone and mudstone of the lowermost Hazelton Group. All zones are proximal to a regional-scale unconformity between the Stuhini and Hazelton groups.

Methods and Preliminary Findings

Fieldwork

Fieldwork completed to date has involved logging selected north-south and east-west drillcore transects of the VOK, and targeted mapping of mineralized showings on surface and in the VOK underground-development workings. This work has allowed for initial, field-level characterization of the alteration, ore and temporal relationships of the five vein stages, as well as familiarization with the broader lithological nature, including pervasive alteration, of the major mineralized zones on the property. Sampling of drillcore, underground workings and a limited number of outcrops has been carried out on the different vein and alteration types for the purpose of detailed petrographic and geochemical investigations (discussed below). This has been complemented by logging of core from selected drillholes and mapping. Reconnaissance visits have also been made to the adjacent Snowfield porphyry deposit to collect samples for comparison.

Petrography and Mineral Chemistry

Textural relationships among the various ore, gangue and alteration minerals are currently being established using a combination of optical and scanning electron microscopy. Results of this work will be used to develop a detailed mineral paragenesis for each vein stage. This information will provide important insights into the physicochemical evolution of the fluids responsible for each vein stage.

From the work completed to date, there are several important petrographic observations that point to a complex, multistage evolution of the Brucejack hydrothermal system during the ca. 188–183 Ma mineralizing event. In brief, these are 1) at least three texturally distinct generations of quartz, in veins representing the Vn₁ electrum-mineralization stage, that are locally well-organized into discrete millimetre-scale domains, which may cut one another (Figure 4c, d); 2) evidence for silica dissolution as part of the electrum-precipitation event(s), in the form of textures reflecting extensive corrosion of quartz-grain boundaries

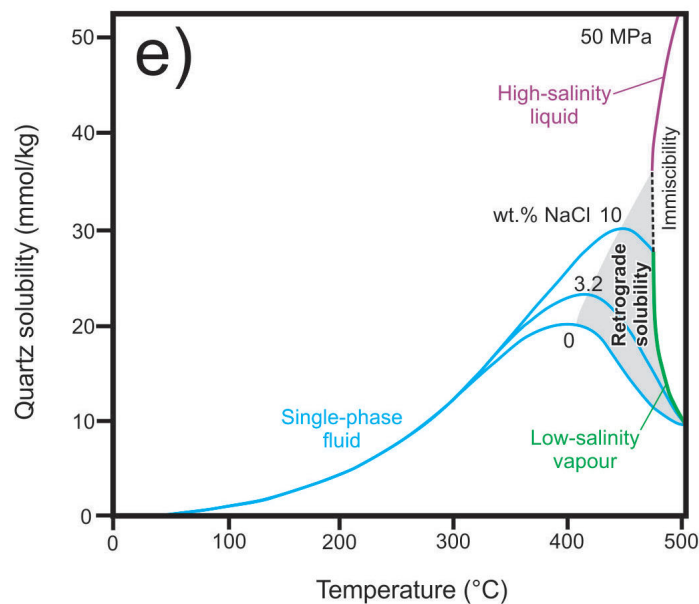
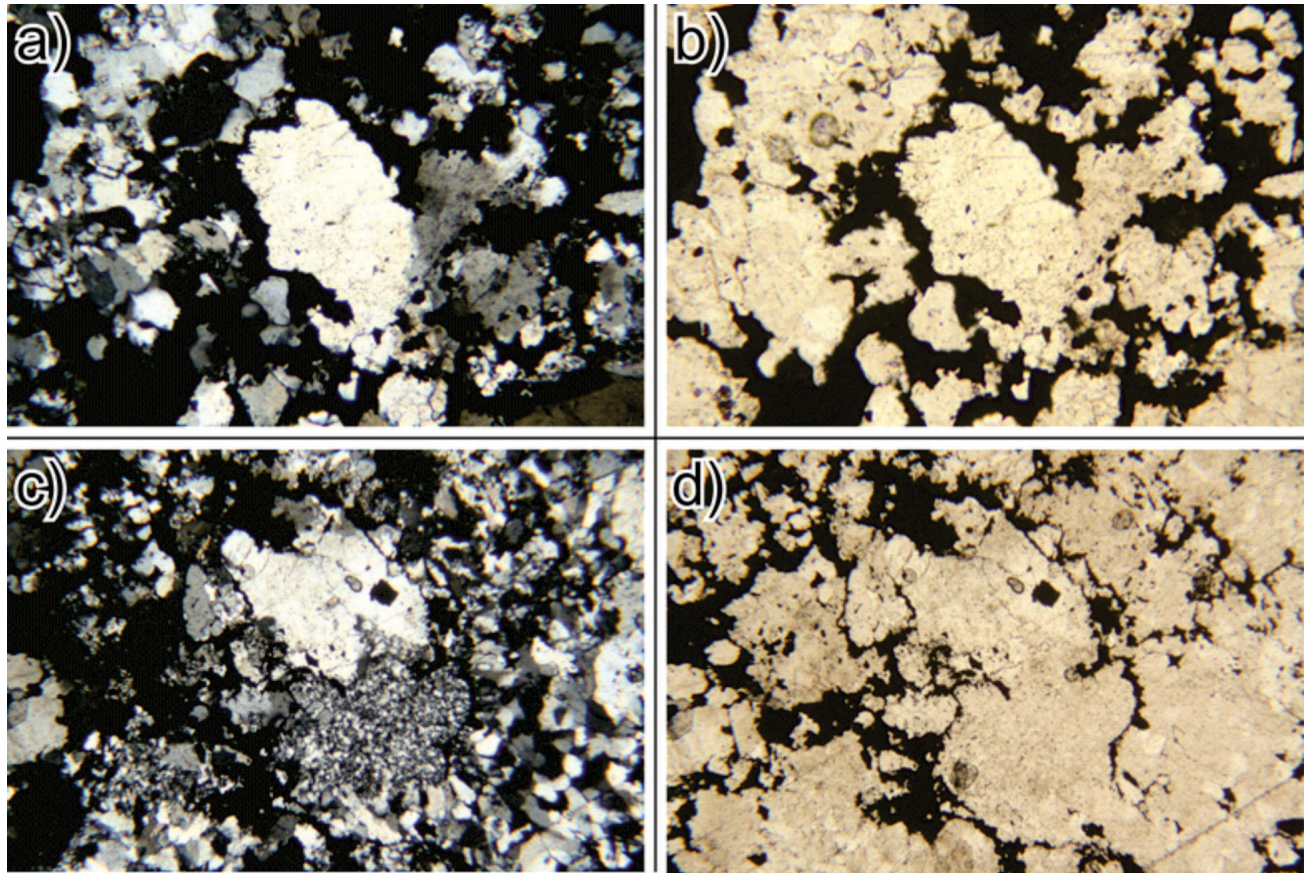


Figure 4: Photomicrographs of quartz and electrum (dendritic opaque mineral) in Brucejack (Valley of the Kings zone) Vn_{1c} veins and plot of quartz solubility versus temperature at 50 MPa: **a)** and **b)** large quartz grain in centre of images has highly irregular, corroded grain boundaries where in contact with electrum; **c)** and **d)** at least three texturally distinct types of quartz are clearly evident, the finest grained type appearing to be cut by the medium-grained type at the bottom of the images. **e)** isobaric quartz solubility plotted as a function of temperature in pure H_2O , $H_2O + 3.2$ wt. % NaCl, and $H_2O + 10$ wt. % NaCl fluids (modified after Steele-MacInnis et al., 2012). Images on the left and right are in cross-polarized and plane-polarized light, respectively, and all have a 1 mm wide field of view. See text for further explanation.

where they are in contact with electrum (Figure 4a, b); 3) well-developed arsenic zonation in abundant early pyrite, which is cut by electrum and locally destroyed by possible chemical resorption (Figure 5); 4) an apparently regular, systematic variation in the gold:silver ratio of electrum among different vein stages and substages (Figure 6); and 5) variations in the style of electrum mineralization, both within and among vein stages, including volumetrically dominant, dendritic electrum, lesser proportions of coarse subhedral clots and aggregates, and rare subhedral to euhedral sheet- to plate-like crystals.

Although preliminary, these observations point to the possibility that electrum mineralization was strongly influenced by fluid overpressure, as does the corroded nature of the quartz (see below). The randomly oriented nature of dendritic to arborescent electrum radiating into, and dying out in, masses of quartz is suggestive of potential hydraulic fracturing associated with the influx of the mineralizing fluids.¹ The multiple, distinct domains of fine-, medium- and coarse-grained quartz indicate that multiple pulses of fluid were likely involved in the formation of each of the individual vein types. In samples from the Vn₁ vein generation, the very fine grained to cryptocrystalline quartz appears to have been locally cut by coarser grained quartz. Collectively, these textures are consistent with a model in which conditions varied between those of prograde and retrograde solubility of quartz (Figure 4e; Steele-MacInnis et al., 2012; Seward et al., 2014) during the evolution of the Vn₁ vein generation. The very fine grained quartz is interpreted to indicate extremely rapid cooling under conditions of prograde solubility (high levels of quartz-grain nucleation and no significant quartz-grain growth), which was probably caused by adiabatic expansion that led to fluid pressure-induced fracturing of the rocks. In principle, quartz dissolution should imply heating. However, at temperatures above 350°C and relatively low pressure (such as might be associated with fracturing of the rocks) and low salinity, quartz undergoes retrograde solubility (~370–500°C; Figure 4e). It is therefore tentatively proposed that the observed dissolution textures reflect this retrograde effect of cooling. Thus, a regime is envisaged in which pressure oscillated from values that exceeded the strength of the rock to hydrostatic values and, in the process, controlled temperature and ultimately the nature of quartz growth and dissolution.

Summary and Future Work

Results from the preliminary petrographic and mineral-chemistry studies of mineralized quartz–electrum±carbonate veins from the Brucejack deposit indicate that the de-

posit formed from a hydrothermal system that had a complex history comprising multiple and possibly long-lived mineralizing events. The formation of the five synmineral vein stages and substages defined from drillcore logging and underground mapping (Vn_{1a}, Vn_{1b}, Vn_{1c}, Vn₂, Vn₃) appear to have resulted from multiple pulses of fluid that circulated through the deposit under dynamic physicochemical conditions, including possible fluid-overpressure and silica-dissolution events. Although the chemical evolution of individual vein stages is not well constrained at present, evidence from preliminary pyrite and electrum mineral chemistry from vein samples across the Valley of the Kings zone suggests that vein composition varied temporally and possibly spatially during formation of the Brucejack deposit. Finally, the observation that electrum appears to post-date most of the pyrite in veins and along vein margins supports the suggestion by Board (2014) that widespread premineral phyllic alteration of the Brucejack country rock, likely related to earlier emplacement of the neighbouring Snowfield and Kerr-Sulphurets-Mitchell porphyry deposits, pre-sulphidized the Brucejack hostrocks and increased the ability of mineralizing fluids at Brucejack to transport elevated concentrations of gold as a bisulphide complex (Au(HS)₂⁻), following the model of Heinrich et al. (2004).

Future petrographic, mineral-chemistry, fluid-inclusion and thermodynamic-modelling studies will further test these interpretations and explore for other insights into the physicochemical evolution of the fluids responsible for each vein stage. In particular, the composition of key ore and alteration minerals, and their evolution through the different stages in the paragenesis, will be determined using a combination of electron microprobe wavelength-dispersive spectrometry and laser-ablation inductively coupled plasma–mass spectrometry (LA-ICP-MS) analysis. Petrographic, chemical and microthermometric analysis of fluid inclusions will be carried out in an attempt to determine the composition and temperatures of the fluids forming different veins. Sulphur and oxygen isotopic compositions will be analyzed using ICP-MS and thermal-ionization mass spectrometry in order to obtain temperature data from the different vein stages using appropriate mineral pairs (e.g., sphalerite-galena and quartz-adularia). High-resolution transmission electron microscopy imaging of electrum and cryptocrystalline silica will be carried out to explore for evidence of colloid formation (presence of nanocrystals). Ultimately, the aim is to complement all of this work with thermodynamic analyses of mineral equilibria to evaluate the evolving physicochemical conditions in the Brucejack hydrothermal system, particularly those accompanying gold mineralization. This information will provide the basis for thermodynamic-path modelling that will incorporate mineral and aqueous species, and will be used to evaluate potential mechanisms for ore deposition, including boiling, fluid mixing and fluid-rock interaction (e.g., Heinrich,

¹*Dendritic electrum textures have also been cited as evidence for gold transport by colloidal processes at Brucejack (Harrichhausen et al., 2016).*

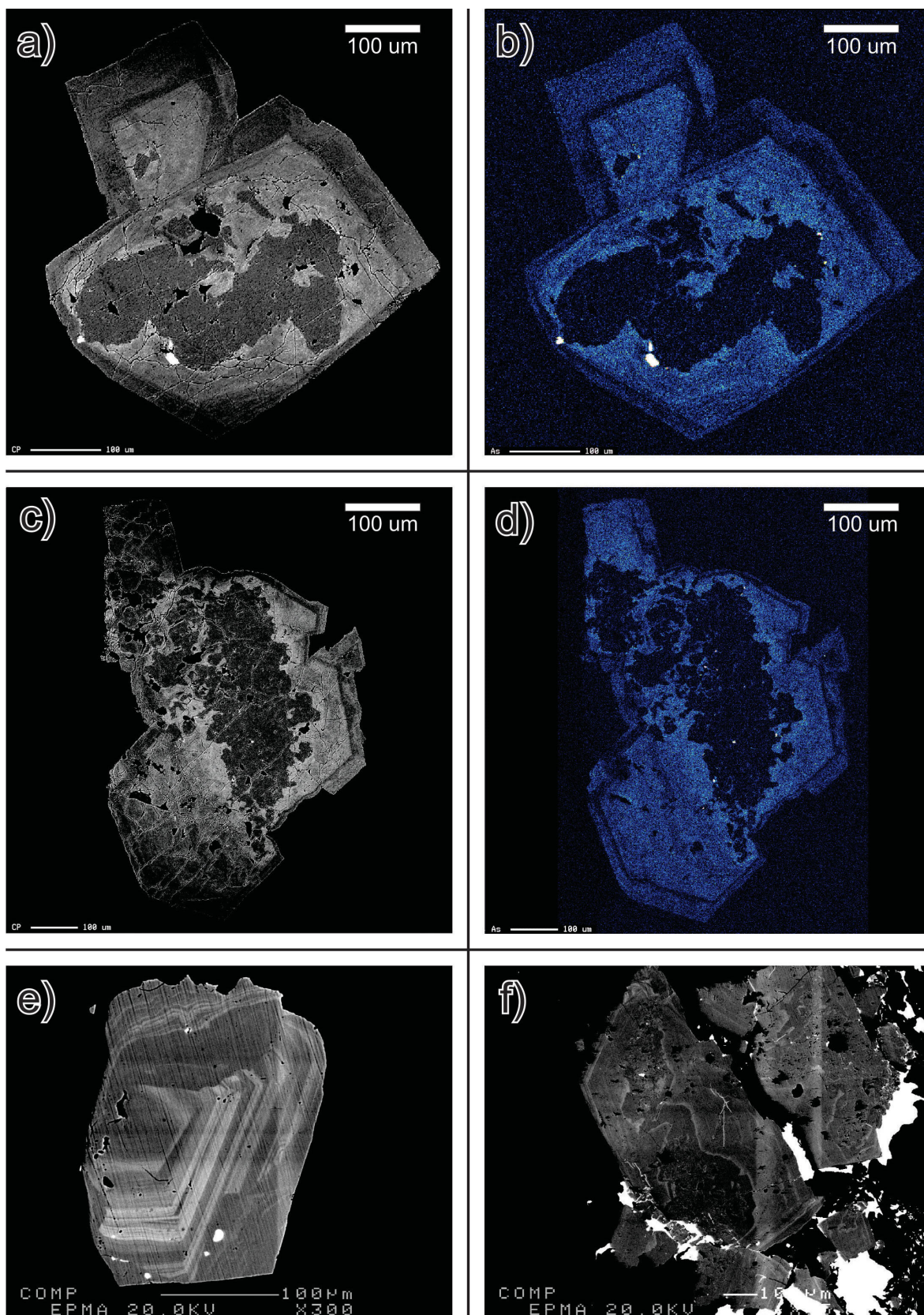


Figure 5: Images of the Vn₁ vein generation at Brucejack (Valley of the Kings zone): **a), c)** and **e)** electron microscope back-scattered electron (BSE) images of pyrite showing complex internal zoning patterns; **f)** BSE image of electron cutting arsenic zonation and filling fractures in pyrite; **b)** and **d)** electron-microprobe maps showing relative levels of arsenic in grains (a) and (c), respectively.

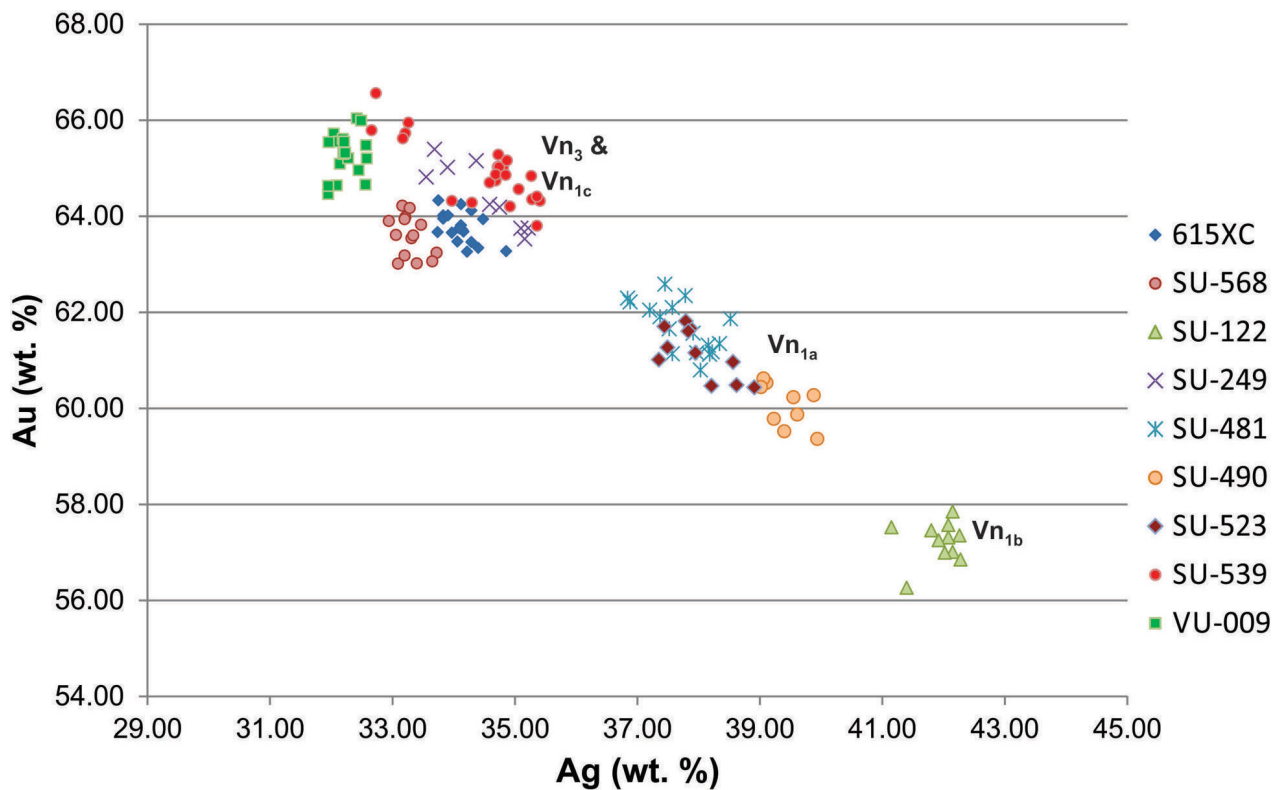


Figure 6: Preliminary results from electron-microprobe wavelength-dispersive spectrometry (WDS) analysis of Brucejack (Valley of the Kings zone) electrum: gold:silver ratio of electrum appears to vary considerably with vein type; further investigation will determine whether or not this variation is also reflective of a spatial zonation in gold:silver across the deposit; no significant variation in the gold:silver ratio of electrum is observed within individual samples; analyses were taken across electrum grains (rim-core-rim) for both quartz matrix-hosted and pyrite inclusion-hosted electrum with no obvious gold:silver differences observed.

2005). In particular, the modelling will address the fundamental question of whether the large, high-grade Brucejack resource can be explained using simple solubility considerations.

Acknowledgments

Funding for this project is provided by the Natural Sciences and Engineering Research Council of Canada (NSERC) and Pretium Resources Inc. The authors thank O. Vasyukova for providing a careful and constructive review of this paper. The lead author also thanks Geoscience BC for their financial support through the Geoscience BC Scholarship program. Lastly, the authors gratefully acknowledge logistical support and accommodation generously provided by Pretium during the summer field season.

References

Alldrick, D.J. (1993): Geology and metallogeny of the Stewart mining camp, northwestern British Columbia; BC Ministry of Energy and Mines, BC Geological Survey, Bulletin 85, 105 p.

Anderson, R.G. (1993): A Mesozoic stratigraphic and plutonic framework for northwestern Stikinia (Iskut River area), northwestern British Columbia, Canada; *in* Mesozoic Paleogeography of the Western United States, II, G.C.

Dunne and K.A. McDougall (ed.), Society of Economic Paleontologists and Mineralogists, Pacific Section, Los Angeles, California, p. 477–494.

BC Geological Survey (2016): MINFILE BC mineral deposits database; BC Ministry of Energy and Mines, BC Geological Survey, URL <<http://minfile.ca/>> [November 2016].

Board, W.S. (2014): Brucejack geology summary; Pretium Resources Inc., URL <http://s1.q4cdn.com/222336918/files/doc_downloads/geology/2013429_Geology_for_website_APRIL2013_WSB.pdf> [November 2016].

Board, W.S. and McNaughton, K.C. (2013): The Brucejack high-grade gold project, northwest British Columbia, Canada; *in* Proceedings of NewGenGold Conference, Perth, Australia, November 26–27, 2013, p. 177–191.

Febbo, G.E., Kennedy, L.A., Savell, M., Creaser, R.A. and Friedman, R.M. (2015): Geology of the Mitchell Au-Cu-Ag-Mo porphyry deposit, northwestern British Columbia, Canada; *in* Geological Fieldwork 2014, BC Ministry of Energy and Mines, BC Geological Survey, Paper 2015-1, p. 59–86.

Gammons, C.H. and Williams-Jones, A.E. (1995): The solubility of Au-Ag alloy + AgCl in HCl/NaCl solutions at 300°C: new data on the stability of Au (1) chloride complexes in hydrothermal fluids; *Geochimica et Cosmochimica Acta*, v. 59, p. 3453–3468.

Ghaffari, H., Huang, J., Hafez, S.A., Pelletier, P., Armstrong, T., Brown, F.H., Vallat, C.J., Newcomen, H.W., Weatherly, H., Wilchek, L. and Mokos, P. (2012): Technical report and updated preliminary economic assessment of the Brucejack

- project; NI-43-101 report by Tetra Tech, Wardrop, Rescan, PE Mining, Geospark and AMC Mining, 327 p.
- Greig, C.J. and Brown, D.A. (1990): Geology of the Stikine River–Yehiniko Lake area, northwestern British Columbia; Geological Association of Canada–Mineralogical Association of Canada, Joint Annual Meeting, Program with Abstracts, v. 15, p. A51.
- Harrichhausen, N.J., Rowe, C.D., Board, W.S. and Greig, C.J. (2016): Relationship between amorphous silica and precious metals in quartz veins: examples from Brucejack, British Columbia and Dixie Valley, Nevada; Association for Mineral Exploration (AME) Roundup, conference poster, URL <http://www.geosciencebc.com/i/pdf/Roundup2016/2016%20poster_Harrichhausen.pdf> [November 2016].
- Heinrich, C.A. (2005): The physical and chemical evolution of low- to medium-salinity magmatic fluids at the porphyry to epithermal transition: a thermodynamic study; *Mineralium Deposita*, v. 39, p. 864–889.
- Heinrich, C.A., Driesner, T., Stefánsson, A. and Seward, T.M. (2004): Magmatic vapour contraction and transport of gold from the porphyry environment to epithermal ore deposits; *Geology*, v. 32, no. 9, p. 761–764.
- Helgeson, H.C. and Garrels, R.M. (1968): Hydrothermal transport and deposition of gold; *Economic Geology*, v. 63, p. 622–635.
- Hurtig, N.C. and Williams-Jones, A.E. (2014): An experimental study of the transport of gold through hydration of AuCl in aqueous vapour and vapour-like fluids; *Geochimica et Cosmochimica Acta*, v. 127, p. 305–325.
- Johnston, S.T. (2008): The Cordilleran ribbon continent of North America; *Annual Review of Earth and Planetary Sciences*, v. 36, p. 495–530.
- Kirkham, R.V. and Margolis, J. (1995): Overview of the Sulphurets area, northwestern British Columbia, in *Porphyry Deposits of the Northwestern Cordillera of North America*, T.G. Schroeter (ed.), Canadian Institute of Mining, Metallurgy and Petroleum, Special Volume 46, p. 473–508.
- Krupp, R.E., and Seward, T.M. (1987): The Rotokawa geothermal system, New Zealand: an active epithermal ore-depositing environment; *Economic Geology*, v. 82, p. 1109–1129.
- Logan, J.M. and Mihalynuk, M.G. (2014): Tectonic controls on Early Mesozoic paired alkaline porphyry deposit belts (Cu-Au±Ag-Pt-Pd-Mo) within the Canadian Cordillera; *Economic Geology*, v. 109, p. 827–858.
- Macdonald, A.J., Lewis, P.D., Thompson, J.F.H., Nadaraju, G., Bartsch, R., Bridge, D.J., Rhys, D.A., Roth, T., Kaip, A., Godwin, C.I. and Sinclair, A.J. (1996): Metallogeny of an Early to Middle Jurassic arc, Iskut River area, northwestern British Columbia; *Economic Geology*, v. 91, p. 1098–1114.
- Margolis, J. (1993): Geology and intrusion related copper-gold mineralization, Sulphurets, British Columbia: Ph.D. thesis, University of Oregon, Eugene, Oregon, 289 p.
- Marsden, H. and Thorkelson, D.J. (1992): Geology of the Hazelton Volcanic Belt in British Columbia: implications for the Early to Middle Jurassic evolution of Stikinia; *Tectonics*, v. 11, p. 1266–1287.
- McLeish, D.F. (2013): Structure, stratigraphy, and U-Pb zircon-titanite geochronology of the Aley carbonatite complex, northeast British Columbia: evidence for Antler-aged orogenesis in the Foreland Belt of the Canadian Cordillera; M.Sc. thesis, University of Victoria, Victoria, British Columbia.
- Monger, J.W.H., Wheeler, J.O., Tipper, H.W., Gabrielse, H., Harms, T., Struik, L.C., Campbell, R.B., Dodds, C.J., Gehrels, G.E. and O'Brien, J. (1991): Upper Devonian to Middle Jurassic assemblages; Chapter 8 in *Geology of the Cordilleran Orogen in Canada*, H. Gabrielse and C.J. Yorath (ed.), Geological Survey of Canada, *Geology of Canada*, No. 4, p. 281–328.
- Nelson, J. and Kyba, J. (2014): Structural and stratigraphic control of porphyry and related mineralization in the Treaty Glacier–KSM–Brucejack–Stewart trend of western Stikinia; in *Geological Fieldwork 2013*, BC Ministry of Energy and Mines, BC Geological Survey, Paper 2014-1, p. 111–140.
- Seward, T.M. (1973): Thio complexes of gold and the transport of gold in hydrothermal ore solutions; *Geochimica et Cosmochimica Acta*, v. 37, p. 379–399.
- Seward, T.M., Williams-Jones, A.E. and Migdisov, A.A. (2014): The chemistry of metal transport and deposition by ore-forming hydrothermal fluids; in *Geochemistry of Mineral Deposits*, Volume 13 of *Treatise on Geochemistry* (Second Edition), H. Holland and K. Turekian (ed.), Elsevier Science, p. 29–57.
- Sillitoe, R.H. and Hedenquist, J. W. (2003): Linkages between volcanotectonic settings, ore-fluid compositions, and epithermal precious metal deposits; in *Volcanic, Geothermal, and Ore-Forming Fluids: Rulers and Witnesses of Processes within the Earth*, S.F. Simmons and I. Graham (ed.), Society of Economic Geologists, Special Publication 10, p. 315–345.
- Simmons, S.F. and Brown, K.L. (2006): Gold in magmatic hydrothermal solutions and the rapid formation of a giant ore deposit; *Science*, v. 314, p. 288–190.
- Steele-MacInnis, M., Han, L., Lowell, R.P., Rimstidt, J.D. and Bodnar, R.J. (2012): The role of fluid phase immiscibility in quartz dissolution and precipitation in sub-seafloor hydrothermal systems; *Earth and Planetary Science Letters*, v. 321–322, p. 139–151.
- Stefánsson, A. and Seward, T.M. (2004): Gold(I) complexing in aqueous sulphide solutions to 500°C at 500 bar; *Geochimica et Cosmochimica Acta*, v. 68, p. 4121–4143.
- Tombe, S.P. (2015): Tectonomagmatic setting of the Sulphurets Cu-Au porphyry-epithermal district, northwestern British Columbia. M.Sc. thesis, University of Alberta, Edmonton, Alberta.
- Tombe, S.P., Greig, C.J., Board, W.S., Richards, J.P., Friedman, R.M. and Creaser, R.A. (2014): The Brucejack porphyry-related epithermal Au deposit, northwestern British Columbia; PDAC-CMIC-SEG Canada Student Minerals Colloquium, conference abstracts; URL <http://cmic-footprints.ca/smc/files/2014/Tombe_2014SMC_British%20Columbia_Porphyry_Gold%20Silver%20Brucejack.pdf> [November 2016].
- Williams-Jones, A.E., Bowell, R.J. and Migdisov, A.A. (2009): Gold in solution; *Elements*, v. 5, p. 281–287. doi:10.2113/gselements.5.5.281
- Zein, D.Y., Migdisov, A.A. and Williams-Jones, A.E. (2011): The solubility of gold in H₂O–H₂S vapour at elevated temperature and pressure; *Geochimica et Cosmochimica Acta*, v. 76, p. 5140–5153.
- Zhu, Y., Fang, A. and Tan, J. (2011): Geochemistry of hydrothermal gold deposits: a review; *Geoscience Frontiers*, v. 2, p. 367–374.

Magmatic History of the Kerr-Sulphurets-Mitchell Copper-Gold Porphyry District, Northwestern British Columbia (NTS 104B)

M.E. Campbell, College of Earth, Ocean, and Atmospheric Sciences, Oregon State University, Corvallis, Oregon, campbemi@oregonstate.edu

J.H. Dilles, College of Earth, Ocean, and Atmospheric Sciences, Oregon State University, Corvallis, Oregon

Campbell, M.E. and Dilles, J.H. (2017): Magmatic history of the Kerr-Sulphurets-Mitchell copper-gold porphyry district, northwestern British Columbia (NTS 104B); in *Geoscience BC Summary of Activities 2016*, Geoscience BC, Report 2017-1, p. 233–244.

Introduction

Porphyry deposits contain the world’s most important reserves of Cu and are important sources of Au, Mo, Ag and Re (e.g., Sillitoe, 2010). Globally, these deposits are concentrated along convergent plate margins, including western Canada. The economic importance of porphyry Cu-Au and related magmatic-hydrothermal deposits to Canada is profound, and the total of past production, reserves and resources of Cu-Au deposits in the Canadian Cordillera has likely surpassed \$200 billion in net contained metal value (Lydon, 2007). Furthermore, a recent study, based on statistical modelling, estimated that only 60% of the total Cu contained within porphyry deposits in western Canada has been discovered to date (Mihalasky et al., 2011).

Porphyry deposits in British Columbia (BC) are located mainly within two volcanic-arc terranes, the Quesnel and Stikine terranes, where most porphyry mineralization occurred within a relatively short (~15 m.y.) time span during the Late Triassic and Early Jurassic (Figure 1; Logan and Mihalynuk, 2014). The Kerr-Sulphurets-Mitchell (KSM) project, owned by Seabridge Gold Inc., is located approximately 65 km northwest of the town of Stewart in the Iskut-Stikine River region of northwestern BC (Figure 2). The KSM project is situated within the Stikine terrane and features four distinct centres of early Jurassic Cu-Au-Ag-Mo porphyry mineralization, located along a northerly trend and contained within an area measuring roughly 2 km by 10 km. From south to north, these deposits are Kerr, Sulphurets, Mitchell and Iron Cap. The KSM project has proven and probable reserves totalling 1.08 million kilograms (38 million ounces) of Au, 4.5 billion kilograms (9.9 billion pounds) of Cu, 5.41 million kilograms (191 million ounces) of Ag and 96.6 million kilograms (213 million pounds) of Mo, for a total of 2.2 billion tonnes averaging 0.55 g/t Au, 0.21% Cu, 2.6 g/t Ag and 42.6 ppm

Mo (Seabridge Gold Inc., 2016). The KSM district represents one of the largest undeveloped Cu-Au deposits in the world, with significant potential economic importance for the surrounding region of northwestern BC.

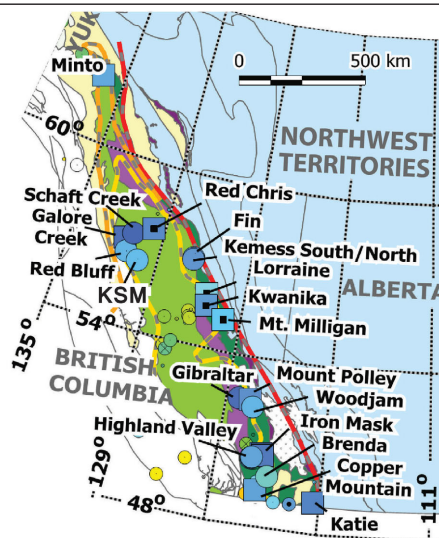
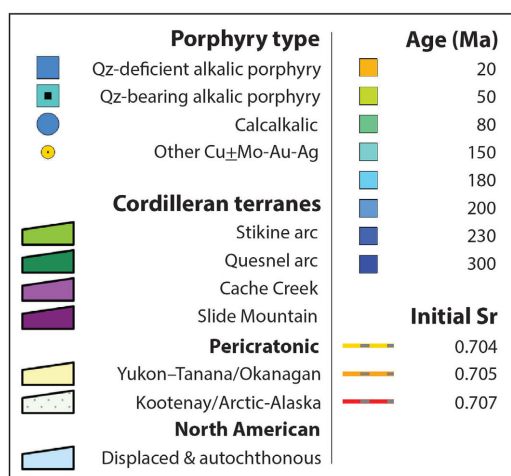


Figure 1. Locations of the principal porphyry deposits in the cordillera of western Canada, including the KSM district in northwestern BC (modified from Logan and Mihalynuk, 2014); shapes of porphyry-deposit symbols reflect the classification of the deposit, with alkalic deposits represented by squares and calcalkalic deposits by circles; symbols are also colour coded according to age.

Keywords: British Columbia, Stikine terrane, Early Jurassic, porphyry deposit, igneous petrology, calcalkaline, magmatism

This publication is also available, free of charge, as colour digital files in Adobe Acrobat® PDF format from the Geoscience BC website: <http://www.geosciencebc.com/s/DataReleases.asp>.

Fundamentally, porphyry Cu-Au deposits result from the emplacement of porphyry intrusions and accompanying metalliferous hydrothermal fluids (e.g., Titley and Beane, 1981). A single porphyry deposit may contain a range of plutonic bodies, including precursor plutons, multiple syn-mineral intrusive phases and post-mineral dikes or stocks. Unravelling the magmatic phases of a porphyry deposit is critical for an understanding of the evolution of the ore system, including the distribution of contained metals. To date, studies of the intrusive rocks at KSM have been marred by problems common to Mesozoic magmatic-hydrothermal deposits in active tectonostratigraphic terranes: hydrothermal alteration, deformation, faulting and low-grade metamorphism. Issues such as texturally destructive phyllic alteration, penetrative foliation and extensive remobilization of major and trace elements by hydrothermal fluids can result in the partial to total destruction of the primary mineralogy and textures in large swaths of the deposits, and masking of litho-geochemical signatures. The primary aim of this ongoing study is to establish the magmatic history of the district, by cataloguing, describing and determining the chronology and spatial extent of the intrusive phases at each of the four porphyry centres in the KSM district. This will be accomplished through 1) relogging and sampling of drillcore at each of the four deposits; 2) petrographic analysis of the intrusive phases at each deposit, to determine primary mineralogy; 3) whole-rock geochemistry; 4) geochronology; and 5) refractory-mineral geochemistry. In addition, the authors aim to unravel the spatial and temporal relationships between the intrusive phases and hydrothermal alteration and mineralization, with the objective of gaining new insight into the primary controls on mineralization within the KSM district.

Regional Geology

The KSM district, located in the western Stikine terrane (Figure 1), is situated on an approximately 60 km long, discontinuous, northerly trend of mineralization centres (Figure 2; Nelson and Kyba, 2014). Major mineralized deposits along this trend consist of porphyry, epithermal and volcanogenic massive-sulphide (VMS) deposits, including Red Mountain, Silbak-Premier, Granduc, Scottie Gold, Big Missouri, Brucejack, KSM, Treaty and Eskay Creek (Figure 2). These deposits are hosted mainly within the volcaniclastic and sedimentary strata of the Lower Jurassic Haz-

elton Group and are often related to early Jurassic intrusions, including the 197–187 Ma Texas Creek plutonic suite (Alldrick, 1993; Logan and Mihalyuk, 2014). The Texas Creek plutonic suite includes the Premier porphyry intrusions, named for the syn-mineral intrusions at the Premier mine (Figure 2; Alldrick, 1993). Premier porphyry intrusions are characterized by K-feldspar megacrysts and plagioclase phenocrysts in a fine-grained groundmass (Alldrick, 1993); as will be discussed in the ‘Kerr Deposit’ and ‘Mitchell Deposit’ sections, roughly contemporaneous intrusions of similar mineralogy and texture have been noted within the KSM district. The Hazelton Group, which records several successive pulses of arc volcanism, unconformably overlies the Triassic Stuhini Group, which is composed of arc and marine sedimentary strata (Nelson and Kyba, 2014). Several younger plutons unrelated to mineralization, Eocene to Middle Jurassic in age, are also found within the region.

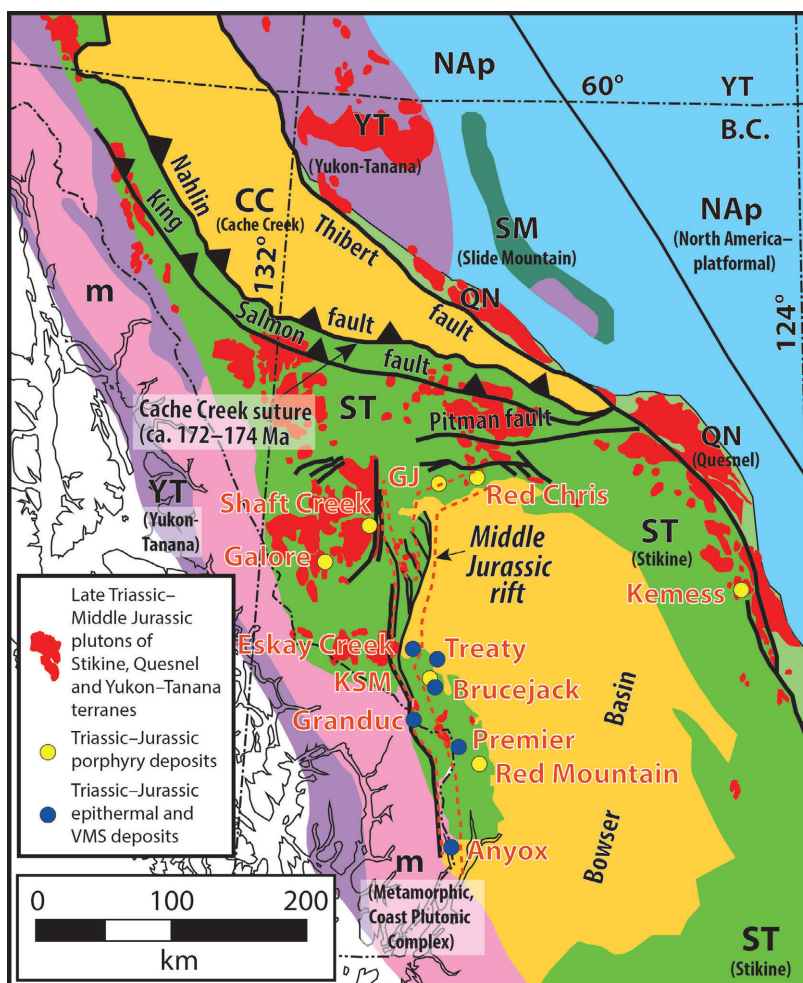


Figure 2. Tectonostratigraphy of the northern Stikine terrane, northwestern BC, showing the locations of major faults and Triassic–Jurassic magmatic-hydrothermal deposits (modified from Nelson et al., 2013); note that the KSM district is situated along a rough alignment of several of these deposits, extending from Red Mountain to Eskay Creek. Abbreviations: CC, Cache Creek terrane; m, Metamorphic, Coast Plutonic Complex; NAP, North America – platformal; QN, Quesnel terrane; ST, Stikine terrane; VMS, volcanogenic massive-sulphide; YT, Yukon-Tanana terrane.

The western part of the Stikine terrane is a structurally complex region, with important northerly- to northeasterly-trending structures resulting from mid-Cretaceous sinistral transpression associated with the Skeena fold-and-thrust belt (Figure 2; Nelson and Kyba, 2014). Structural controls on mineralization have also been proposed at several magmatic-hydrothermal deposits within the region, including Silbak-Premier, Big Missouri and Scottie Gold (Alldrick, 1993).

District Geology

The KSM district is composed mainly of Late Triassic Stuhini Group and Early Jurassic Hazelton Group volcanic and sedimentary basement strata, with numerous Early Jurassic intrusions ranging in composition from diorite to syenite. The structural geology of the region is complex, largely due to Cretaceous deformation caused by the development of the Skeena fold-and-thrust belt. Imbricate thrust faults, including the Sulphurets thrust fault (STF) and the Mitchell thrust fault (MTF), have dismembered the district into multiple panels. Differential strain accommodation within the district has also resulted in localized zones of intense deformation and foliation, most notably within zones of strong phyllic alteration (and, thus, relatively low competency) within the Kerr and Mitchell deposits (Febbo et al., 2015).

As previously mentioned, the KSM district includes four Cu-Au-Ag-Mo porphyry deposits with defined resources on property owned by Seabridge Gold Inc. (Figure 3). Adjoining the KSM project, Pretium Resources Inc. owns the Brucejack epithermal Au system and Snowfield Cu-Au porphyry deposit (Figure 3). The Snowfield deposit, which contains measured and indicated resources of 1.37 billion tonnes averaging 0.59 g/t Au and 0.10% Cu, for a total of 25.9 million ounces Au and 2.98 billion pounds Cu (Pretium Resources, 2016), is actually the displaced cap of the Mitchell deposit, which was transported approximately 2 km ESE by the Mitchell thrust fault (Febbo et al., 2015). The occurrence of multiple Cu-Au porphyry deposits within the KSM district, as well as their approximate northerly alignment, is not unusual; global porphyry districts commonly feature clusters or alignments of ore deposits, each separated by hundreds to thousands of metres, distributed over a total distance of up to 30 km (Sillitoe, 2010). Alignments may occur either parallel or orthogonal to the magmatic arc, and porphyry deposits throughout a single district may display significant ranges of formational age (e.g., up to ~18 m.y. in the Cadia district; Wilson et al., 2007; Sillitoe, 2010).

Global Cu-Au porphyry deposits can be broadly classified into two principal groups: 1) calcalkalic porphyry deposits, and 2) comparatively rare alkalic porphyry deposits (e.g., Titley and Beane, 1981). British Columbia and the south-

west Pacific are the two regions where alkalic Cu-Au porphyry deposits are relatively common (Bissig and Cooke, 2014). As of 2011, a total of 431 alkalic prospects and 904 calcalkalic prospects had been documented in BC (BC Geological Survey, 2011). The characteristic styles of hydrothermal alteration and mineralization of archetypal calcalkalic porphyry deposits differ markedly from alkalic equivalents, so the implementation of strategic and successful mineral-exploration campaigns for porphyry Cu-Au deposits in BC hinges upon the correct identification of the porphyry class within the district.

Although the porphyry deposits of the KSM district have, in the past, been referred to as alkalic (e.g., Bissig and Cooke, 2014), the four deposits with defined reserves at KSM display distinctly calcalkaline features. Notably, as will be discussed in the deposit descriptions, the four deposits contain abundant disseminated pyrite (pyrite > chalcopyrite) and considerable molybdenite. Kerr, Sulphurets and Mitchell feature extensive peripheral propylitic alteration zones. Furthermore, the Kerr, Mitchell and Iron Cap deposits also feature zones of strong phyllic alteration, as well as quartz-stockwork zones with >50% quartz veins ('A-veins' and 'B-veins', based upon standard porphyry vein nomenclature; e.g. Gustafson and Hunt, 1975; Sillitoe, 2010). The KSM district, therefore, is dominated by calcalkaline porphyry Cu-Au mineralization. However, certain zones of relatively weak mineralization within the KSM district, peripheral to the calcalkaline porphyry deposits, display features that are more consistent with typical alkalic deposits. These zones are associated with monzonite to syenite porphyry intrusions (Figure 4), little quartz veining, potassic alteration and a reddening of feldspars via hematite dusting, all of which are characteristics typical of alkalic porphyry deposits (e.g., Logan and Mihalynuk, 2014). The total metal contained within these apparently alkalic zones, however, is subordinate to the mineralization found within the footwall of the STF, which hosts the bulk of the ore at KSM.

KSM Cu-Au Porphyry Deposits

This section contains brief overviews of the Kerr, Sulphurets, Mitchell and Iron Cap Cu-Au porphyry deposits, covering the morphology, the principal hydrothermal alteration assemblages, the degree of deformation, and the range of important intrusions encountered at each deposit. All of the deposits are roughly contemporaneous in age and hosted by wallrocks of the Early Jurassic Hazelton Group and/or Late Triassic Stuhini Group (Figure 3). Figure 5 shows, in plan view, the lateral distribution of Au and Cu at each of the four deposits. The lateral extent and orientation of mineralization is different at each deposit, with Kerr and Sulphurets rather elongate, and Mitchell displaying concentric zoning of metals (Figure 5). Thus, while the four deposits display certain distinct similarities, they also feature

notable differences, resulting in a unique character for each deposit.

Kerr Deposit

Located in the southern part of the KSM district, the Kerr deposit contains probable reserves of 242 million tonnes averaging 0.45% Cu and 0.24 g/t Au, for a total of 1.09 billion kilograms (2.4 billion pounds) of Cu and 54.9 million grams (1.9 million ounces) of Au (Seabridge Gold Inc., 2016). The Deep Kerr zone, which is the deeper extension of the Kerr deposit, contains an inferred resource of 782 million tonnes averaging 0.54% Cu and 0.33 g/t Au, for a total of 4.2 billion kilograms (9.3 billion pounds) of Cu and 232 million grams (8.2 million ounces) of Au (Seabridge Gold Inc., 2016). The Kerr deposit has a roughly planar, north-striking and steeply west-dipping form (Figure 5), reflecting the morphologies of the Kerr intrusions themselves: a suite of steeply west-dipping dikes. The morphologies of certain porphyry Cu-Au orebodies replicate the forms of their porphyry intrusions (Sillitoe, 2010), especially those emplaced at shallow crustal levels (Proffett, 2009). Porphyry deposits with narrow elongate shapes similar to that of Kerr have also been noted elsewhere in the world (e.g., Hugo Dummett, Mongolia; Khashgerel et al., 2008).

The wallrocks to the dikes comprise a range of sedimentary and volcanoclastic strata, including finely bedded argillite, mudstone, massive sandstone, conglomerate, turbidite sequences and various volcanoclastic units, which likely encompass both the Stuhini and Hazelton groups (Bridge, 1993; Rosset and Hart, 2015). The zones of strongest mineralization in the Kerr deposit occur within the porphyry dikes. However, the wallrocks can also carry significant mineralization, with the grade typically decreasing with increasing distance from the dikes. There are two principal zones of increased intrusion density, or dike swarms, within the Kerr deposit, that correlate to two zones of higher grade: an 'eastern limb' and a 'western limb' of mineralization, which are separated by a central septum of wallrock.

The range of different intrusive phases found at Kerr is, in approximate chronological order from oldest to youngest:

- high-quartz-vein zones, with >80% quartz veins, where the nature of the intrusive protolith is largely obscured by the veins, primarily A-veins (Figure 6)
- plagioclase-hornblende-phyric, fine- to medium-grained subporphyritic intrusions, with >10% quartz veins (A-veins and B-veins) that typically envelop pods of the high-quartz-vein zones and are well mineralized (Figure 6)
- plagioclase-K-feldspar-hornblende-phyric, medium-grained subporphyritic intrusions, typically with potassic alteration and well mineralized

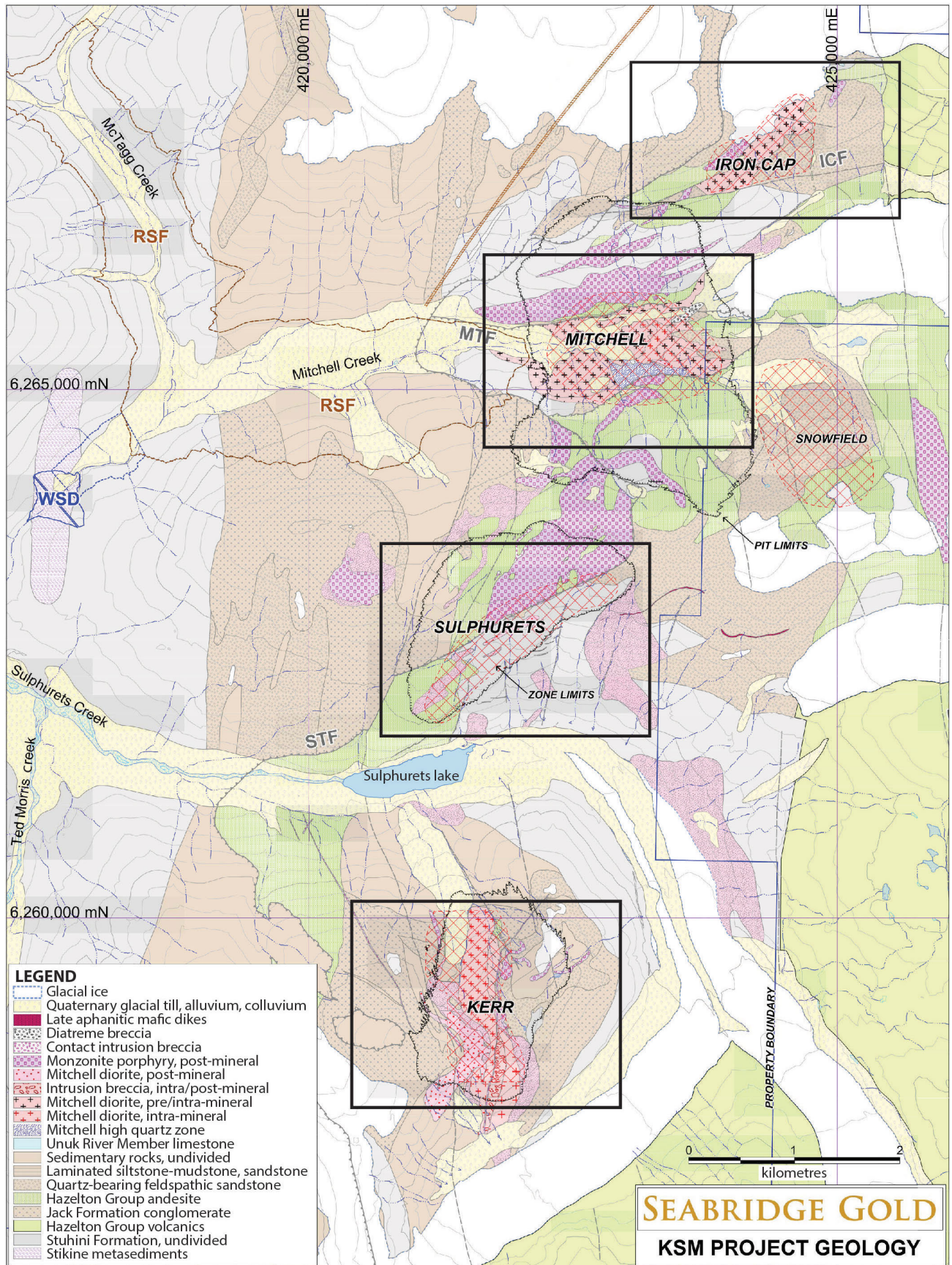
- plagioclase-hornblende-phyric, fine- to medium-grained subporphyritic intrusions, with <10% quartz veins and variable mineralization (Figure 6)
- augite-plagioclase-phyric dikes, sometimes megacrystic, that are typically unmineralized or very weakly mineralized
- K-feldspar-megacrystic (up to ~2 cm), plagioclase-hornblende-phyric dikes, that resemble the Premier porphyry intrusions described by Alldrick (1993), that are typically unmineralized (Figure 6)
- aphanitic to very fine grained mafic dikes, with pervasive chlorite alteration, that are post-mineral
- lamprophyre dike that is post-mineral

As discussed by Rosset and Hart (2014) and Bridge (1993), the Kerr deposit features early potassic alteration, characterized by an assemblage of chloritized hydrothermal biotite±K-feldspar±magnetite, centred upon the dike swarms but also affecting proximal wallrocks. Propylitic alteration (chlorite±epidote) is distal to potassic alteration. Chlorite-sericite-pyrite alteration commonly overprints these earlier assemblages, varying in intensity from weak to intense and affecting both intrusions and wallrock. The bornite and some of the sulphosalts at Kerr, accompanied by dickite±pyrophyllite, were formed within intermediate- to high-sulphidation alteration zones, which typically overlap with the high-quartz-vein zones. Regions with networks of anhydrite veins and veinlets are common at Kerr. In near-surface parts of the deposit, the hydration of anhydrite to gypsum, and eventual dissolution of the latter, have led to the formation of apparent rubble zones.

Mineralization at Kerr is primarily hypogene, although small amounts of supergene mineralization, including chalcocite, occur in the near-surface environment (Bridge, 1993). Hypogene mineralization includes chalcopyrite, pyrite, bornite, molybdenite, enargite, tennantite, tetrahedrite and base-metal sulphides, all closely associated with quartz veins, as well as pervasive disseminated pyrite. Quartz-stockwork zones are commonly, but not exclusively, associated with the highest grade zones at Kerr. See Rosset and Hart (2015) for a further overview of vein types and mineralization at Kerr.

Finally, the Kerr deposit features considerable deformation related to the development of the Cretaceous Skeena fold-and-thrust belt. Zones with strong sericitic alteration in particular, within both intrusive and wallrock protoliths, have

 Figure 3. Geology of the Kerr-Sulphurets-Mitchell district, showing the locations of Seabridge Gold's Kerr, Sulphurets, Mitchell and Iron Cap deposits, as well as Pretium Resources' Snowfield deposit (courtesy of Seabridge Gold Inc.). The black rectangles indicate the locations of the deposit maps in Figure 5. Abbreviations: MTF, Mitchell thrust fault; STF, Sulphurets thrust fault. Place names with the generic in lower case are unofficial.



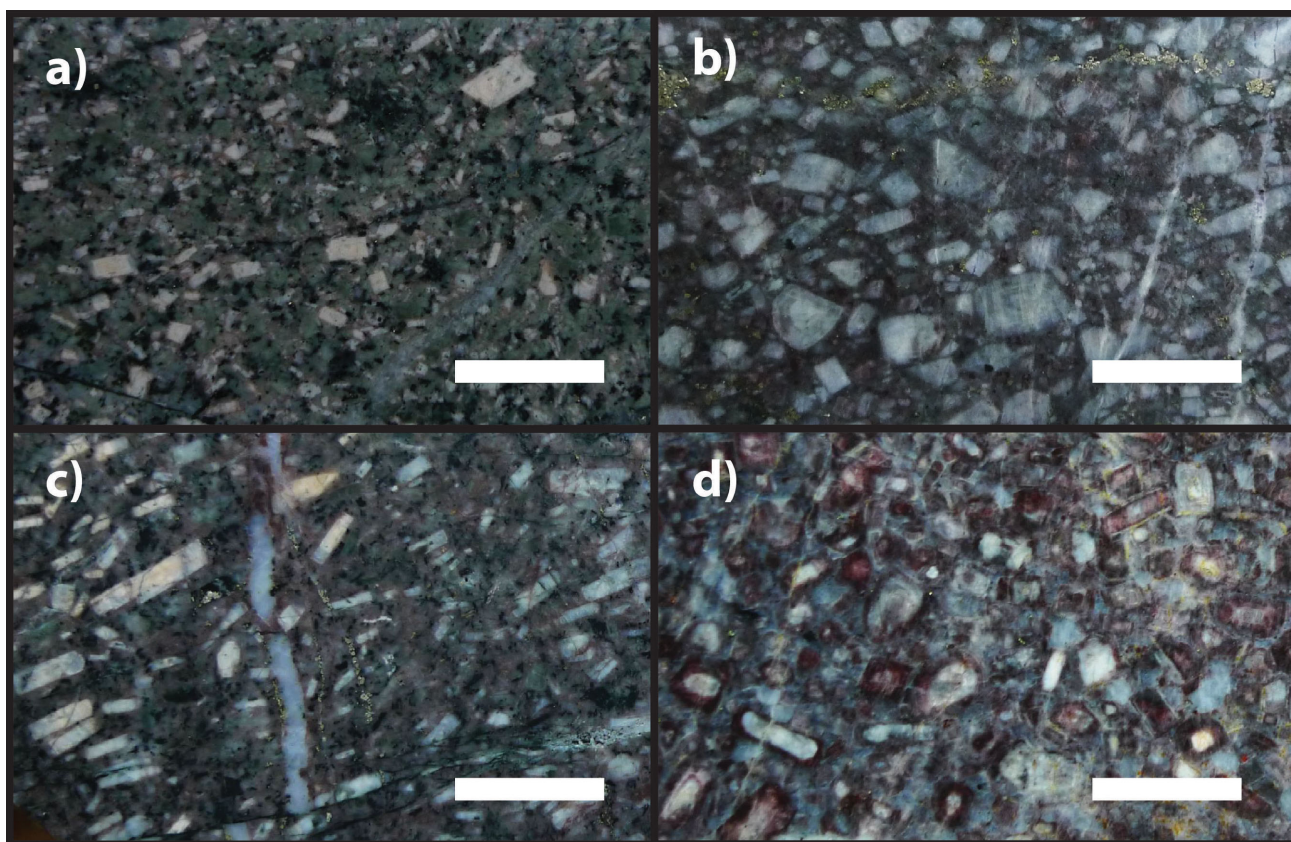


Figure 4. Hand-specimen photographs of weakly mineralized syenite and monzonite porphyry intrusions in the Kerr-Sulphurets-Mitchell district: **a)** intrusion northeast of the Kerr deposit (diamond-drill hole MQ-14-07, 621.1 m depth); **b)** intrusion peripheral to the Iron Cap deposit (IC-10-034, 353.4 m); **c)** and **d)** intrusions in the hangingwall of the Mitchell thrust fault, above the Mitchell deposit (c – M-15-130, 474.5 m; d – M-11-128, 535.2 m). Scale bars are 2 cm in length.

been extensively folded and foliated. Areas with strong anhydrite veining sometimes appear brecciated.

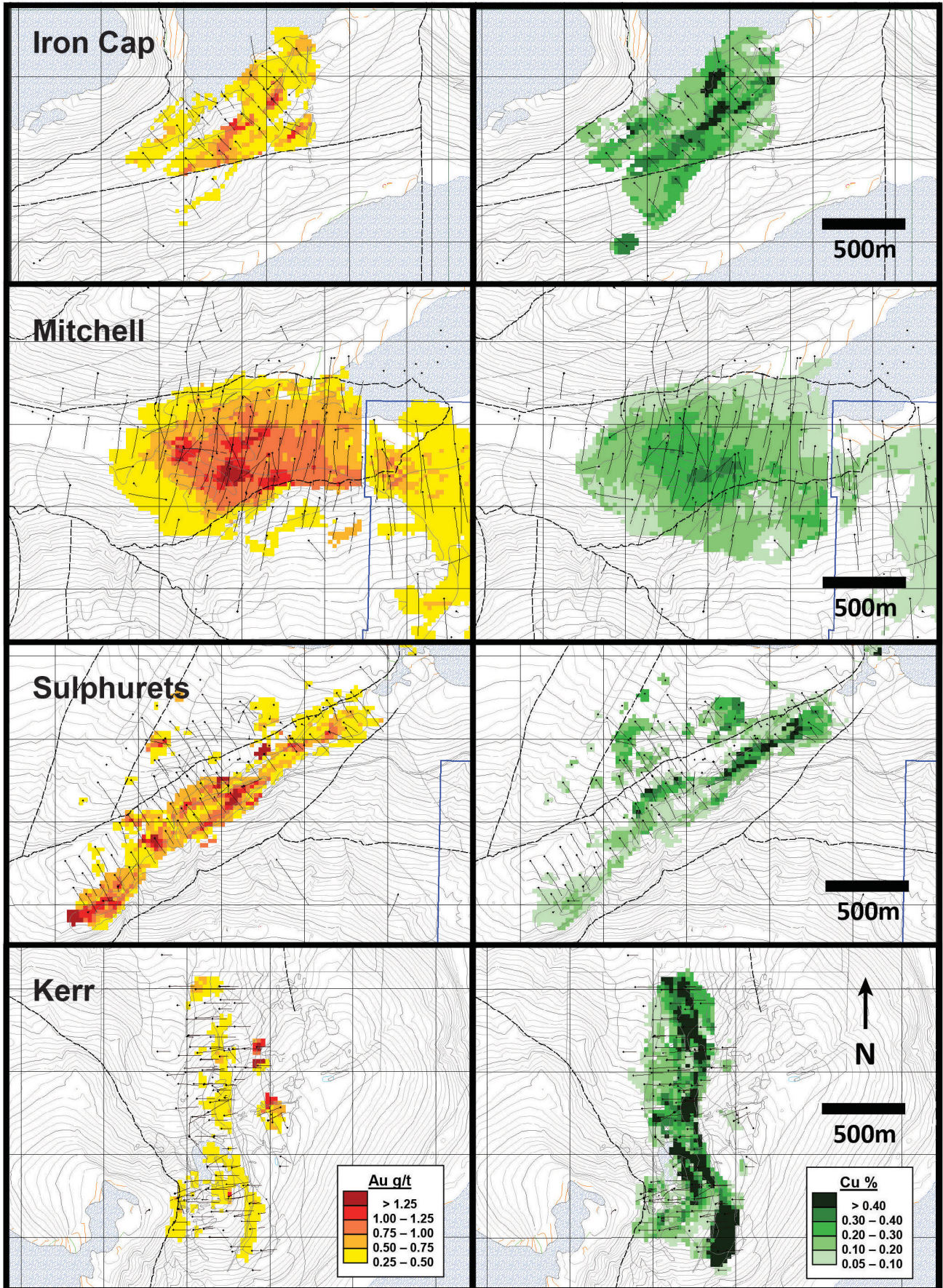
Sulphurets Deposit

The Sulphurets deposit, located approximately 2 km north of the Kerr deposit (Figure 3), contains probable reserves of 304 million tonnes averaging 0.59 g/t Au, 0.22% Cu, 0.8 g/t Ag and 51.6 ppm Mo (Seabridge Gold Inc., 2016). In plan view, Sulphurets is elongated in a northeasterly direction and is truncated to the south by the Sulphurets cliff (Figures 3, 5). The Sulphurets orebody is cut by the Sulphurets thrust fault (STF) and related splays, and features mineralization in both the hangingwall and footwall of the STF. The geology of the two panels is, however, quite different. In the hangingwall of the STF, mineralization is closely associated with monzonite to syenite porphyry intrusions (Figure 6) that commonly display potassic alteration and reddish hematite dusting—features typically associated with alkalic Cu-Au porphyries. These intrusions are not observed in the footwall of the STF, where intrusions are volumetrically subordinate and mineralization is hosted primarily within sedimentary wallrock. The wallrock is composed of a range of sedimentary rock types, including massive mudstone, massive to bedded siltstone and sandstone, and

polymictic pebbly conglomerate beds. Mineralized wallrocks commonly show strong hornfels development, with patches of fine, dark brown hydrothermal biotite, or dark chlorite alteration. Peripheral to the well-mineralized zone, propylitic chlorite±epidote alteration dominates, and the degree of hornfels development diminishes.

The intrusions observed below the STF at Sulphurets are typically shallowly-dipping dikes, primarily fine- to medium-grained, subporphyritic, plagioclase-hornblende-phyric dioritic intrusions with chlorite-dominant alteration, and plagioclase-K-feldspar-hornblende-phyric monzodiorite porphyry intrusions with <5% K-feldspar phenocrysts (Figure 6). No monzonite or syenite intrusions resembling the mineralized intrusions in the hangingwall are observed in the panels immediately below the STF. Due to uncertainty in the total displacement along the STF, the original spatial relationship, or genetic link (if any), between the mineralization in the hangingwall and footwall of

Figure 5. Plan views of, from top to bottom, the Iron Cap, Mitchell, Sulphurets and Kerr deposits, showing the distribution and intensity of the Au grade (left) and Cu grade (right) for each deposit (courtesy of Seabridge Gold Inc.) See Figure 3 for location of each deposit within the district.



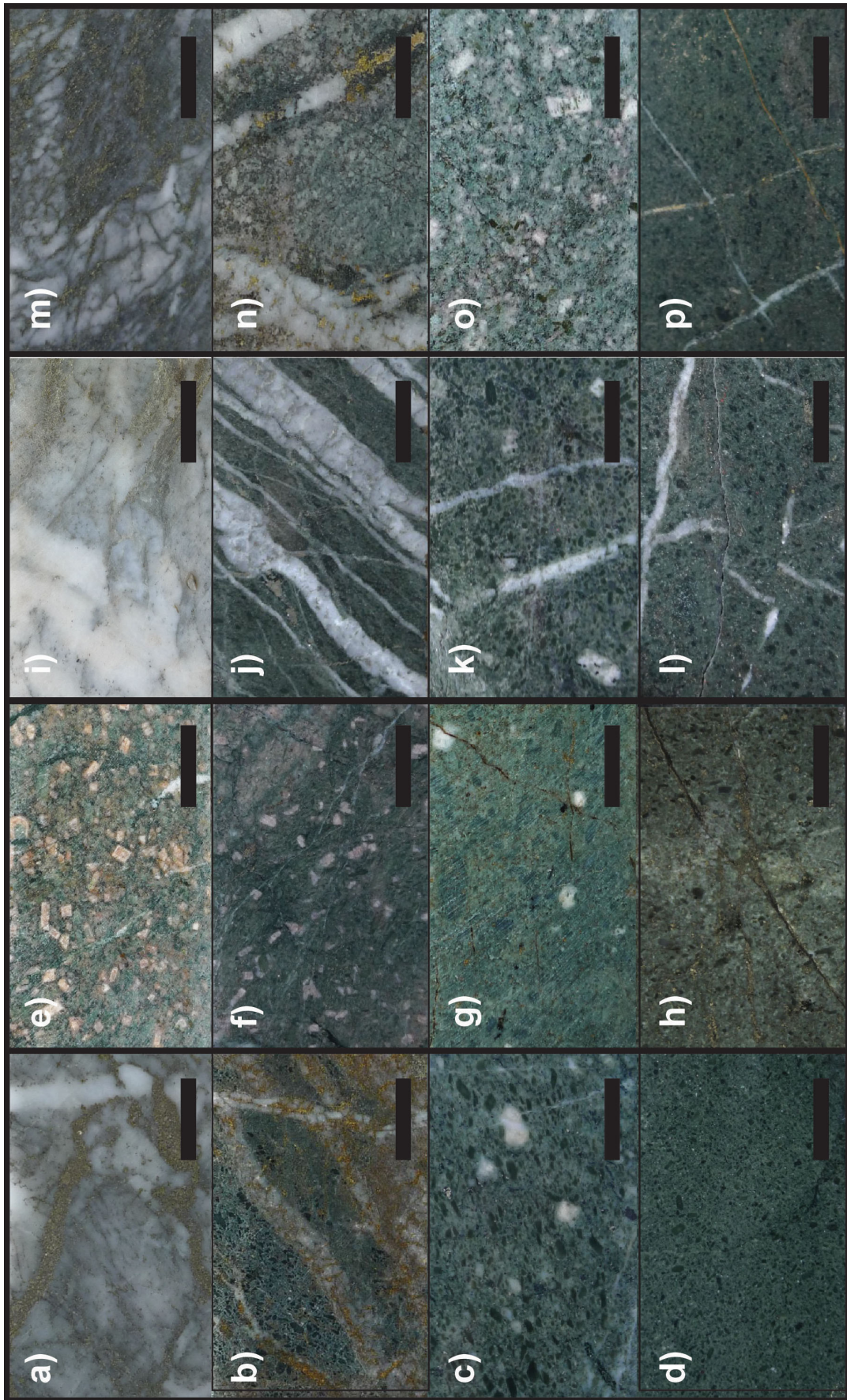


Figure 6. Typical intrusive phases of the Kerr (a, b, c, d), Sulphurets (e, f, g, h), Mitchell (i, j, k, l) and Iron Cap (m, n, o, p) deposits: **a)** K-13-29, 749.5 m (diamond-drill hole and depth); **b)** K-13-29, 461.8 m; **c)** K-13-23, 1416 m; **d)** K-13-31A, 608.4 m; **e)** S-12-75, 159.6 m; **f)** S-14-79, 42.2 m; **g)** S-11-52, 286.2 m; **h)** S-11-62, 109 m; **i)** M-08-090, 325.5 m; **j)** M-08-094, 293.6 m; **k)** M-08-073, 546.0 m; **l)** M-08-073, 199.9 m; **m)** IC-16-062, 236.4 m; **n)** IC-13-051, 919.0 m; **o)** IC-13-051A, 1165 m; **p)** IC-12-047, 306.0 m. All photographs are shown at the same scale and the scale bars are 2 cm in length.

the STF at Sulphurets is currently unclear. However, the total displacement on the STF is likely significant, and probably exceeds 1 km.

The Sulphurets deposit is dissimilar to the other three deposits with defined reserves at KSM in several important ways. Firstly, the Sulphurets orebody straddles the STF, whereas the other KSM deposits are uniquely in the footwall of this thrust fault. Furthermore, there are no quartz-stockwork zones at Sulphurets, and typically only minor quartz veining (<2%). Finally, Sulphurets lacks the zones of extensive phyllic alteration found at Kerr, Mitchell and Iron Cap, although it still features abundant disseminated pyrite. Altogether, the characteristics of Sulphurets above the STF are more consistent with an alkalic classification, whereas an appropriate classification for the largely wallrock-hosted mineralization below the STF is still pending. However, the principal dikes below the STF at Sulphurets texturally and mineralogically resemble syn-mineral porphyry intrusions found at the distinctly calcalkaline Kerr and Mitchell deposits. An ongoing aim of this study is to test the potential affinity between the porphyry intrusions at these neighbouring deposits via petrography and geochemistry.

Mitchell Deposit

The Mitchell deposit, located between the Sulphurets and Iron Cap deposits, currently holds the largest Au reserves of the four KSM porphyry deposits, with measured and indicated resources of 1.794 billion tonnes averaging 0.60 g/t Au, 0.16% Cu, 3.1 g/t Ag and 58 ppm Mo, for a total of 964 million grams (34 million ounces) of Au and 3.0 billion kilograms (6.6 billion pounds) of Cu (Seabridge Gold, 2016). The Mitchell deposit forms a roughly cylindrical orebody plunging steeply to the northwest (Figure 5). As previously mentioned, the neighbouring Snowfield deposit is the displaced cap of the Mitchell deposit, dismembered by the Mitchell thrust fault (~1600 m total offset) during the Cretaceous (Febbo et al., 2015).

Unlike the Kerr deposit, in which mineralization is partially hosted within wallrock adjacent to the syn-mineral intrusions, mineralization at Mitchell is almost entirely intrusion hosted. The major intrusive phases at Mitchell are, in approximate chronological order from oldest to youngest:

- high-quartz zones, with >80% quartz veins, where the nature of the intrusive protolith is largely obscured by the veins (primarily A-veins Figure 6)
- plagioclase-hornblende-phyric, fine- to medium-grained subporphyritic intrusions, with >30% quartz veins (A-veins and B-veins) that typically envelop pods of the high-quartz-vein zones and are well mineralized (Figure 6)

- plagioclase-hornblende-phyric, fine- to medium-grained subporphyritic intrusions with <10% quartz veins and variable mineralization (Figure 6)
- plagioclase-K-feldspar-hornblende-quartz-phyric, medium-grained intrusions, with occasional K-feldspar phenocrysts up to approximately 1 cm in size, that are similar to the Premier porphyry intrusions described by Alldrick (1993) and typically weakly mineralized (Figure 6)
- aphanitic to very fine grained mafic dikes, with pervasive chlorite alteration, that are post-mineral

The principal styles of hydrothermal alteration at Mitchell are early K-feldspar+magnetite+biotite potassic alteration and peripheral chlorite±epidote alteration. Extensive zones of chlorite+sericite alteration overprint sections of the Mitchell deposit, including areas of strong sericite+pyrite phyllic alteration, especially in the southern and eastern parts of the deposit (Febbo et al., 2015). The Mitchell deposit contains a central high-quartz zone, with >50% quartz A-veins and B-veins (Febbo et al., 2015). This zone, as well as the plagioclase-hornblende-phyric porphyry stocks and dikes containing >10% quartz A-veins and B-veins, host the bulk of the mineralization. Molybdenite-bearing quartz veins are concentrated in a halo around the centre of the deposit. Finally, a pipe-like brecciated zone of high-sulphidation bornite+pyrite+tennantite+tetrahedrite+dickite/pyrophyllite, with abundant fragmented anhydrite veins, occurs near the centre of the deposit. Veining and mineralization in the Mitchell deposit are described in further detail by Febbo et al. (2015).

Although the Kerr and Mitchell deposits are on completely opposite sides of the morphological spectrum, they share many important similarities: early high-quartz-vein zones (>50% quartz veins), partially overprinted by late high-sulphidation assemblages of bornite+pyrite+tennantite+tetrahedrite±dickite/pyrophyllite; very similar plagioclase-hornblende-phyric syn-mineral intrusions; late syn-mineral to post-mineral K-feldspar-phyric dikes; and zones of strong anhydrite veining. These similarities indicate that the Kerr and Mitchell deposits formed by similar genetic processes.

Weak mineralization is also found immediately north of the Mitchell deposit, above the MTF, associated with monzonite to syenite porphyry intrusions, low quartz-vein densities and reddish hematite dusting (Figure 4). As the displacement along the MTF is constrained by the modern positions of the Snowfield and Mitchell orebodies, which the MTF dismembered, it is possible to estimate that these weakly mineralized alkalic intrusions north of the deposit were originally situated ~1600 m west-northwest of the deposit. Thus, the mineralization within these alkalic intrusions

probably was not generated by the Mitchell hydrothermal system.

Iron Cap Deposit

The northernmost Cu-Au porphyry deposit in the KSM district, Iron Cap, is a roughly cylindrical orebody plunging steeply to the northwest. Iron Cap is composed of numerous stocks and dikes hosted within sedimentary and volcanoclastic wallrock. The wallrock comprises mainly massive mudstone, sandstone, polymict pebbly conglomerate and volcanic breccia. As is the case with the Kerr deposit, the zones of strongest mineralization at Iron Cap are contained within syn-mineral porphyry intrusions, although significant mineralization is also hosted by the surrounding wallrock. Iron Cap features central potassic alteration, with hydrothermal K-feldspar and magnetite in the monzonite intrusions, whereas the plagioclase-hornblende-phyric intrusions commonly display chlorite±sericite-dominant alteration. The wallrocks are commonly altered to hornfels and often display strong silicification in addition to sericite+pyrite alteration.

The Iron Cap intrusions include the following:

- plagioclase-hornblende-phyric, fine- to medium-grained subporphyritic intrusions, with little to no quartz veining, that are pre-mineral or early syn-mineral (Figure 6)
- high-quartz-vein zones, with >80% quartz veins, where the nature of the intrusive protolith is largely obscured by the veins primarily A-veins that are well mineralized and syn-mineral (Figure 6)
- plagioclase-K-feldspar-hornblende-phyric, medium-grained monzonite intrusions, with seriate texture, 10–30% K-feldspar phenocrysts, 2–50% quartz veins and variable mineralization, that are syn-mineral (Figure 6)
- aphanitic to very fine grained mafic dikes, with pervasive chlorite alteration, that are post-mineral

Within the Kerr and Mitchell deposits, the dioritic plagioclase-hornblende-phyric intrusions are commonly well mineralized and often contain significant volumes of quartz veins. The analogous intrusions at Iron Cap, however, are only weakly mineralized to unmineralized and are apparently precursors to the monzonite stocks and dikes, which are commonly very well mineralized. The Iron Cap deposit also presents interesting similarities to the Red Chris deposit, another Late Triassic–Early Jurassic porphyry deposit within the Stikine terrane (Figure 2), which features pre-mineral plagioclase-hornblende-phyric diorite and syn-mineral monzonite intrusions (Rees et al., 2015).

Future Work

This ongoing study will utilize a range of techniques to further unravel the magmatic history of the KSM district, in-

cluding whole-rock geochemistry, petrography, refractory-mineral geochemistry, and geochronology, to accurately classify, order and compare the intrusions found at each of the KSM deposits. Furthermore, as the KSM district contains many texturally destructive features, including extensive deformation and hydrothermal alteration, the authors will seek to gain insights into the intrusive history at KSM through the study of primary refractory trace-mineral phases, such as zircon and apatite. The geochemistry of these resistive minerals contains valuable records of conditions within the parental magma, and allows researchers to gain insights into the intrusive histories of areas where poor textural preservation precludes the possibility of traditional petrographic and lithochemical studies.

Finally, although the KSM district is dominated by calc-alkaline porphyry mineralization, zones containing features typical of alkalic porphyry mineralization are also represented. The authors will aim to understand the genetic and temporal relationships between these two styles of mineralization within the KSM deposits and peripheral areas, and investigate whether these relationships may be linked to the fertility, or unusually Au-rich nature, of the district. Finally, they will investigate how the Early Jurassic magmatism within the district resulted in the formation of such a large, and unusually Au-rich, suite of porphyry deposits.

Acknowledgments

This study is being undertaken at Oregon State University, in collaboration with Seabridge Gold Inc. The authors acknowledge the Seabridge Gold team of geologists for their support and insights, especially M. Savell, T. Dodd, P. Erwich and W. Threlkeld. G. Febbo is thanked for years of thoughtful discussions regarding the mysteries of the KSM project. The authors acknowledge the helpful reviews of this paper by J. Osorio. M.E.C. gratefully acknowledges financial support from Seabridge Gold Inc., Geoscience BC and the Natural Sciences and Engineering Research Council of Canada (NSERC).

References

- Alldrick, D.J. (1993): Geology and metallogeny of the Stewart mining camp, northwestern BC; BC Ministry of Energy and Mines, BC Geological Survey, Bulletin 85, 105 p.
- BC Geological Survey (2011): MINFILE BC mineral deposits database: BC Ministry of Energy and Mines, URL <<http://minfile.ca/>> [October 2016].
- Bissig, T. and Cooke, D.R. (2014): Introduction to the special issue devoted to alkalic porphyry Cu-Au and epithermal deposits; *Economic Geology*, v. 109, p. 819–825.
- Bridge, D.J. (1993): The deformed Early Jurassic Kerr copper-gold porphyry deposit, Sulphurets gold camp, northwestern British Columbia; M.Sc. thesis, The University of British Columbia, 319 p.

- Febbo, G.E., Kennedy, L.A., Savell, M., Creaser, R.A. and Friedman, R.M. (2015): Geology of the Mitchell Au-Cu-Ag-Mo porphyry deposit, northwestern British Columbia, Canada; *in* Geological Fieldwork 2014, BC Ministry of Energy and Mines, BC Geological Survey, Paper 2015-1, p. 59–86, URL <http://www.em.gov.bc.ca/Mining/Geoscience/PublicationsCatalogue/Fieldwork/Documents/2014/04_Febbo_etal.pdf> [October 2016].
- Gustafson, L.B. and Hunt, J.P. (1975): The porphyry copper deposit at El Salvador, Chile; *Economic Geology*, v. 70, p. 857–912.
- Khashgerel, B.-E., Kavalieris, I. and Hayashi, K. (2008): Mineralogy, textures, and whole-rock geochemistry of advanced argillic alteration: Hugo Dummett porphyry Cu-Au deposit, Oyu Tolgoi mineral district, Mongolia; *Mineralium Deposita*, v. 43, p. 913–932.
- Logan, J.M., and Mihalynuk, M.G. (2014): Tectonic controls on early Mesozoic paired alkaline porphyry deposit belts (Cu-Au ± Ag-Pt-Pd-Mo) within the Canadian Cordillera; *Economic Geology*, v. 109, p. 827–858.
- Lydon, J.W. (2007): An overview of the economic and geological contexts of Canada’s major mineral deposit types; *in* Mineral Deposits of Canada: a Synthesis of Major Deposit-Types, District Metallogeny, the Evolution of Geological Provinces, and Exploration Methods, W.D. Goodfellow (ed.), Geological Association of Canada, Mineral Deposits Division, Special Publication 5, p. 3–48.
- Mihalasky, M.J., Bookstrom, A.A., Frost, T.P. and Ludington, S. (2011): Porphyry copper assessment of British Columbia and Yukon Territory, Canada; United States Geological Survey, Scientific Investigations Report 2010-5090-C, v. 1.1, 128 p.
- Nelson, J. and Kyba, J. (2014): Structural and stratigraphic control of porphyry and related mineralization in the Treaty Glacier–KSM–Brucejack–Stewart trend of western Stikinia; *in* Geological Fieldwork 2013, BC Ministry of Energy and Mines, BC Geological Survey, Paper 2014-1, p. 111–140, URL <http://www.empr.gov.bc.ca/Mining/Geoscience/PublicationsCatalogue/Fieldwork/Documents/2013/07_Nelson_Kyba.pdf> [October 2016].
- Nelson, J.L., Colpron, M. and Israel, S. (2013): The cordillera of British Columbia, Yukon and Alaska: tectonics and metallogeny; Chapter 3 *in* Tectonics, Metallogeny and Discovery: the North American Cordillera and Similar Accretionary Settings, M. Colpron, T. Bissig, B.G. Rusk and J.F.H. Thompson (ed.), Society of Economic Geologists, Special Publication 17, p. 53–109.
- Pretium Resources (2016): Snowfield property, February 2011 resource estimate; Pretium Resources Inc., URL <<http://www.pretium.com/projects/snowfield/overview/>> [October 2016].
- Proffett, J.M. (2009): High Cu grades in porphyry Cu deposits and their relationship to emplacement depth of magmatic sources; *Geology*, v. 37, no. 8, p. 675–678.
- Rees, C., Riedell, K.B., Proffett, J.M., MacPherson, J. and Robertson, S. (2015): The Red Chris porphyry copper-gold deposit, northern British Columbia, Canada: igneous phases, alteration, and controls of mineralization; *Economic Geology*, v. 110, p. 857–888.
- Rosset, S. and Hart, C.J.R. (2016): Hydrothermal alteration and mineralization at the Kerr and Deep Kerr copper-gold porphyry deposits, northwestern British Columbia (parts of NTS 104B/08); *in* Geoscience BC Summary of Activities 2015, Geoscience BC, Report 2016-1, p. 175–184, URL <http://www.geosciencebc.com/i/pdf/SummaryofActivities2015/SoA2015_Rosset.pdf> [October 2016].
- Seabridge Gold Inc. (2016): Mineral reserves and resources; Seabridge Gold Inc., URL <<http://www.seabridgegold.net/resources.php>> [September 2016].
- Sillitoe, R.H. (2010): Porphyry copper systems; *Economic Geology*, v. 105, no. 1, p. 3–41.
- Titley, S.R. and Beane, R.E. (1981): Porphyry Copper Deposits, Part 1: Geologic Settings, Petrology, and Tectogenesis; *Economic Geology*, 75th Anniversary Volume, p. 214–269.
- Wilson, A.J., Cooke, D.R., Stein, H.J., Fanning, C.M., Holliday, J.R. and Tedder, I.J. (2007): U-Pb and Re-Os geochronologic evidence for two alkalic porphyry ore-forming events in the Cadia district, New South Wales, Australia; *Economic Geology*, v. 102, p. 3–26.

Geology of the Northern Extension of the Rock Creek Graben, Christian Valley Map Area, South-Central British Columbia (NTS 082E/10)

T. Höy, Consultant, Sooke, BC, thoy@shaw.ca

G.M. DeFields, Assistant, Sooke, BC

Höy, T. and DeFields, G.M. (2017): Geology of the northern extension of the Rock Creek graben, Christian Valley map area, south-central British Columbia (NTS 082E/10); in Geoscience BC Summary of Activities 2016, Geoscience BC, Report 2017-1, p. 245–256.

Introduction

The Christian Valley project, funded by Geoscience BC, is a continuation to the north of geological mapping of the Rock Creek graben located in south-central British Columbia (BC) that was begun in 2015 in the Almond Mountain map area (Figure 1; Höy, 2016; Höy and Jackaman, 2016). The project is part of a regional mapping, compilation and mineral-potential evaluation of the east half of the 1:250 000 scale Pentiction map area (NTS 082E) that has focused mainly on the structural, stratigraphic and magmatic controls of base- and precious-metal mineralization in an area dominated by Eocene extensional tectonics.

Geological and Exploration History

The Christian Valley area appears on the Pentiction map area (NTS 082E), mapped and compiled at a scale of 1:250 000 by Tempelman-Kluit (1989). The area was first mapped by Little (1957) as part of a regional mapping project that covered the east half of the Pentiction map area. Considerable mapping at more detailed scales has been done in the western and southwestern portions of the area by Christopher (1978) and Massey and Duffy (2008), and by junior exploration companies that were mainly concentrating on the uranium potential of the area. Geological mapping in the Christian Valley map area in 2016 focused on the western part of the area dominated by the north-trending Rock Creek graben. Additional work will include compilation in digital format of all regional geological, geophysical and geochemical data collected under the National Geochemical Reconnaissance and BC Regional Geochemical Survey programs, Ar-Ar and U-Pb dating of both volcanic and intrusive rocks within the area, an update of the BC MINFILE database, and final publication of the 1:50 000 scale Christian Valley map area.

Exploration in the western part of the Christian Valley map area has been directed mainly toward the discovery of uranium deposits and, to a lesser extent, base- and precious-metal mineralization due largely to the successful exploitation of the veins in the Highland Bell mine to the southwest and of base- and precious-metal deposits in the Greenwood camp farther south (Figure 2).

A number of exploration programs for uranium in the area north of Beaverdell Creek and in the Trapping Creek area were conducted during the 1970s, prior to the moratorium on uranium exploration that was enacted in BC in 1980. This work included geological mapping (e.g., McCandless and Hughes, 1977) and a number of core and percussion drilling programs with ancillary radiometric and geochemical sampling surveys (e.g., Okuno, 1972; Inazumi, 1973; Turner et al., 1980). The work focused mainly on uranium deposits hosted in basal sedimentary rocks that underlie Pliocene plateau basalt. In 1978, the BC Geological Survey initiated a study of the potential for uranium mineralization in the district with resultant publication of several reports (Christopher, 1977, 1978). In 1999, exploration work, mainly sampling programs, was renewed on these uranium deposits and continued intermittently through to 2008 (e.g., Brickner, 2003; McLelland, 2008).

Regional Geology

The Christian Valley map area occupies the central part of the Pentiction map area in south-central BC. The area is mainly underlain by a variety of igneous intrusive rocks that range in age from Jurassic to Eocene (Tempelman-Kluit, 1989). Basement rocks comprise late Paleozoic metasedimentary and metavolcanic rocks of the Quesnel terrane, which includes the oceanic rocks of the Knob Hill Group and Anarchist Schist, and the arc-related Harper Ranch subterrane (Wheeler and McFeely, 1991). Overlying arc-volcanic rocks include the Triassic Nicola Group, exposed in the Greenwood area to the south and throughout the Thompson Plateau area to the west (Preto, 1979), and the Early Jurassic Rossland Group along the southeastern margin of Quesnellia (Höy and Dunne, 2001).

Regional extension during the Eocene had a profound effect on the physiography and metallogeny of south-central

Keywords: British Columbia, geology, regional compilation, Eocene stratigraphy and magmatism, Eocene extensional tectonics, uranium, base- and precious-metal mineralization

This publication is also available, free of charge, as colour digital files in Adobe Acrobat® PDF format from the Geoscience BC website: <http://www.geosciencebc.com/s/DataReleases.asp>.

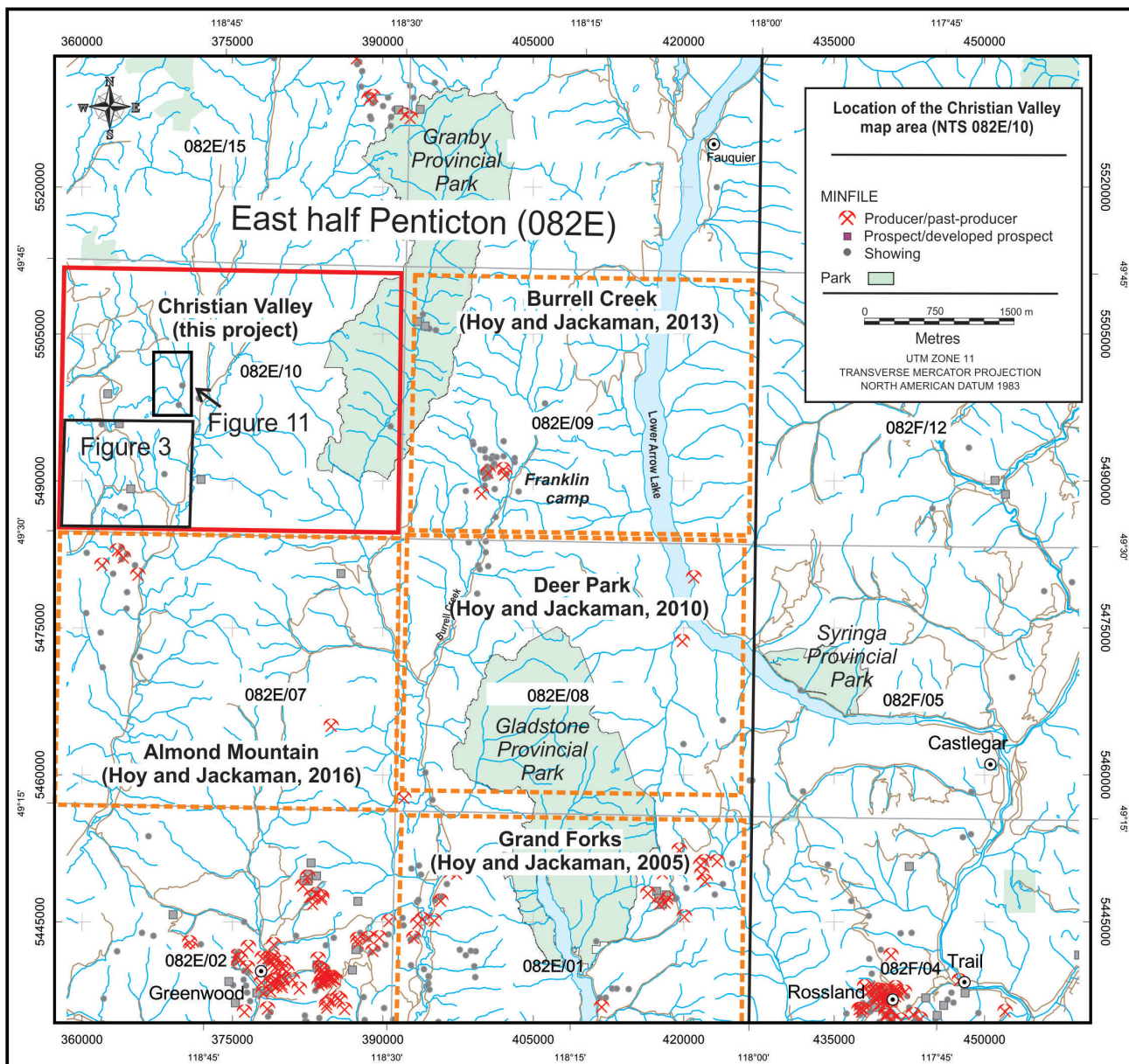


Figure 1. Location of the 1:50 000 scale Christian Valley map sheet (NTS 082E/10) in south-central British Columbia; modified from BC MapPlace (BC Geological Survey, 2016a).

BC, with low-angle detachment faults exhuming Proterozoic and Paleozoic gneissic and platform rocks that formed the metamorphic-core complexes of the southern Monashee Mountains, including the Grand Forks complex in the southeastern part of the Penticton map area (Preto, 1970). Extension in the hangingwall terrane, between the Granby fault at the western margin of the Grand Forks complex and the Okanagan detachment fault to the west (Figure 2) produced north-trending grabens that preserved Eocene volcanic rocks, resulted in the intrusion of Eocene granitic and alkalic intrusive rocks and localized both base -and precious-metal mineralization throughout the eastern portion of the Penticton map area.

Geology of the Christian Valley Area

The Rock Creek graben extends northward through the central part of the Christian Valley map area (Figure 3). The graben in this area is filled with Eocene alkaline volcanic rocks, referred to as the Kamloops Group (Christopher, 1978) and, to the south and west, the Penticton Group (Figure 4; Church, 1973; Fyles, 1990). Older granitic rocks of the Okanagan batholith, and metasedimentary and meta-volcanic rocks of the Paleozoic Wallace group (Massey and Duffy, 2008) are exposed west of the graben and the Okanagan batholith, and Eocene Coryell syenite is exposed to the east (Figure 3). The 'Kallis formation' (Massey and

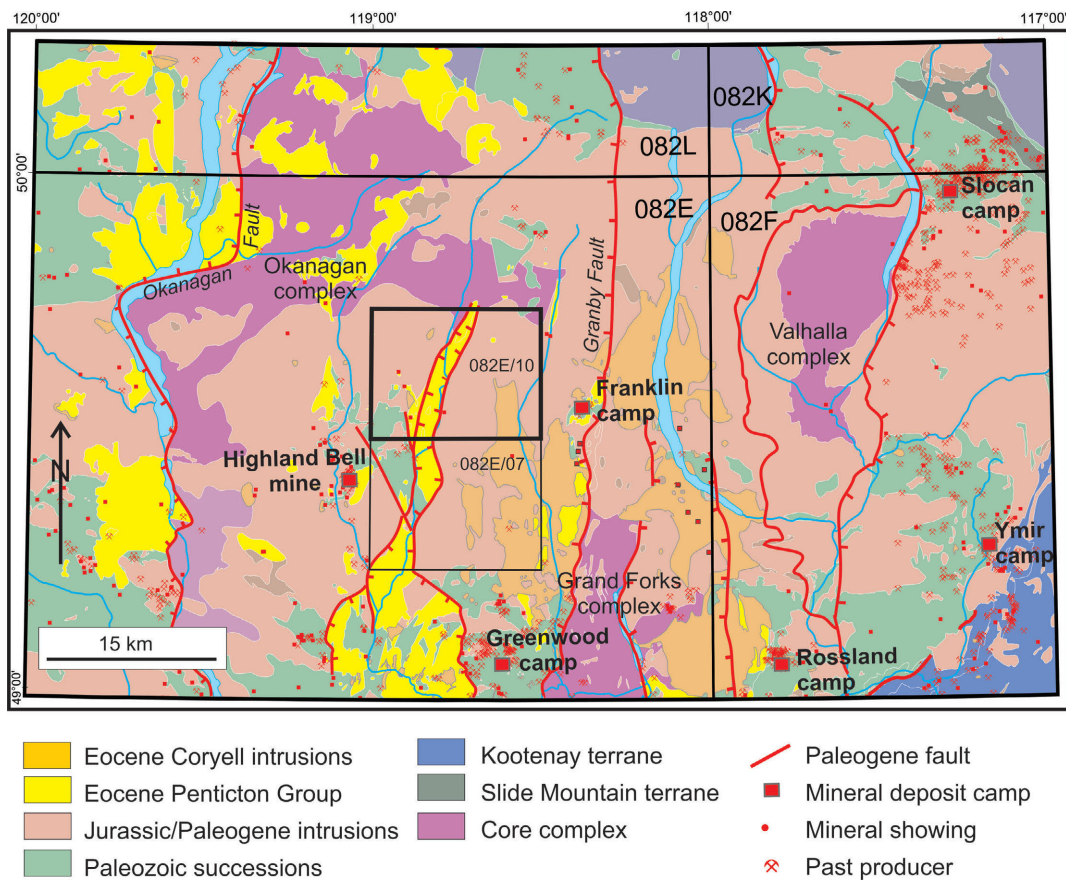


Figure 2. Geology of part of the Pentiction map area, showing the location of the Christian Valley (NTS 082E/10) and Almond Mountain (NTS 082E/07) map areas (modified from Tempelman-Kluit, 1989).

Duffy, 2008), remnants of widespread Pliocene plateau basalt, is preserved in isolated topographic highs throughout the area.

Wallace Group

The Wallace group was initially defined by Reinecke (1915) to include Paleozoic metasedimentary and metavolcanic rocks in the Beaverdell area to the southwest. These rocks have been studied in detail by Massey and Duffy (2008) in the Almond Mountain map area; they are poorly exposed in the southwestern part of the Christian Valley map area, where they comprise mainly rusty-weathering argillite and siltstone, and minor greenstone that may represent mafic tuff.

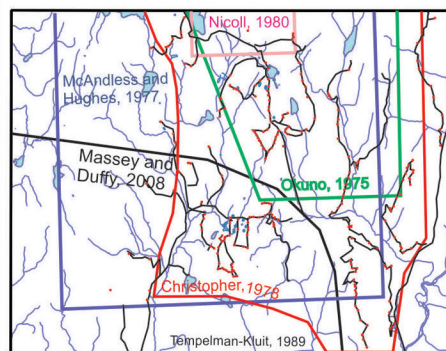
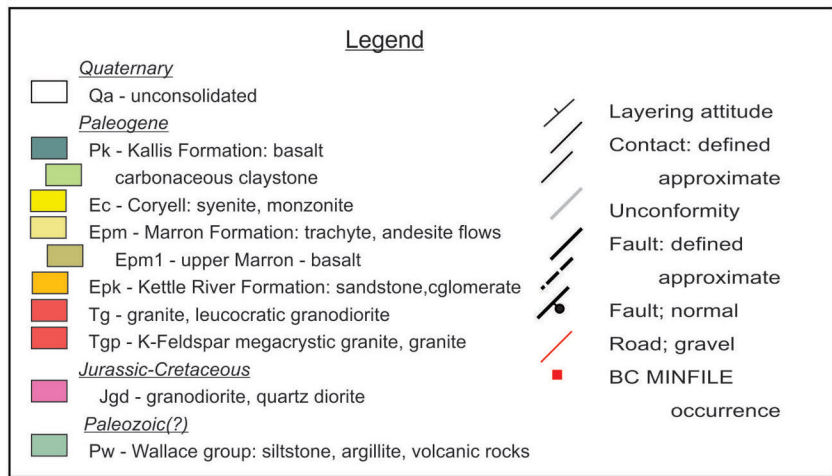
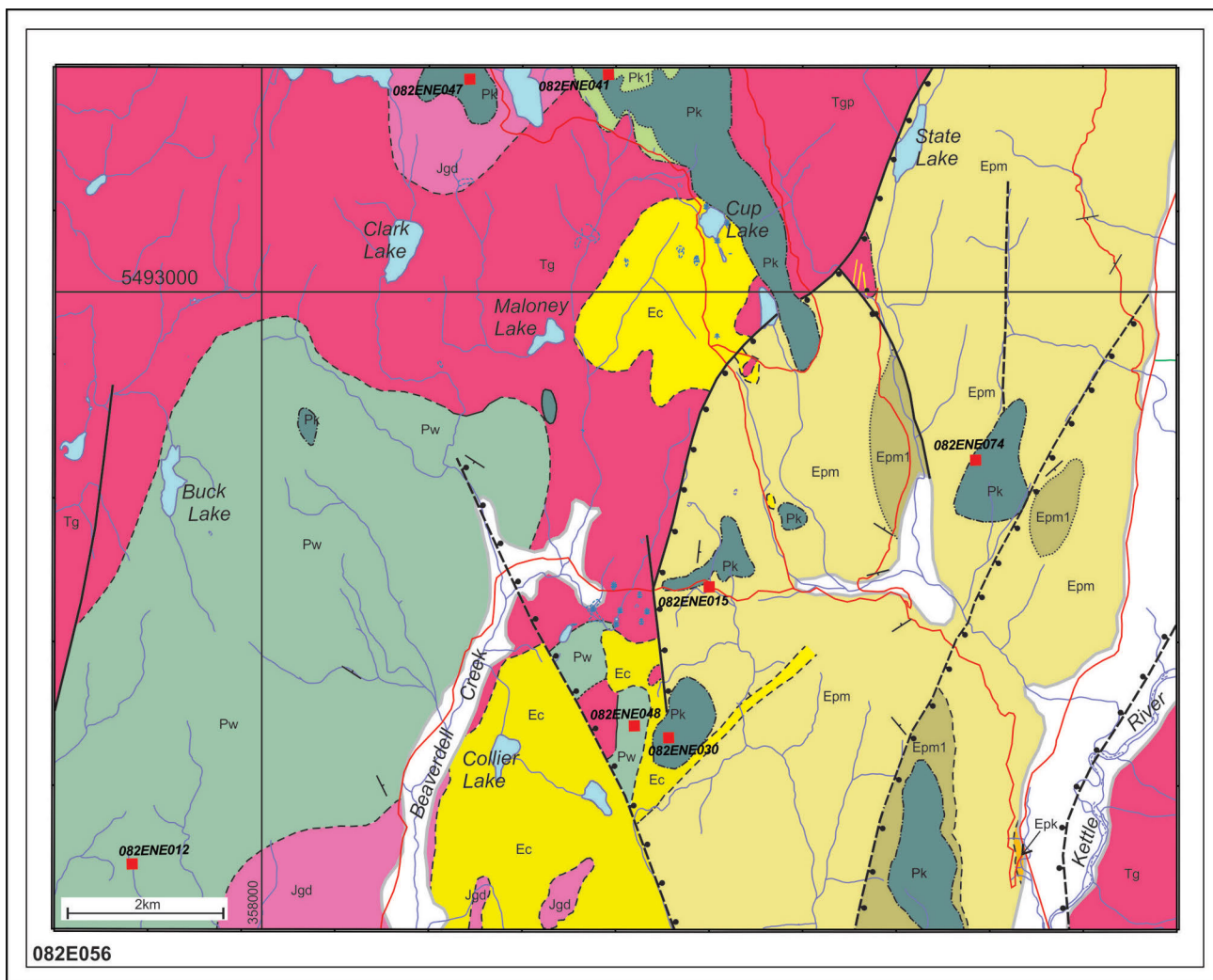
Triassic–Jurassic Intrusive Rocks

‘Middle Jurassic’ granodiorite (mJg) was originally mapped by Little (1957) in several small stocks in the western part of the Christian Valley map area. These are shown on subsequent geological maps by Christopher (1978), Tempelman-Kluit (1989) and Massey and Duffy (2008). Exposures are foliated to massive biotite-hornblende granodiorite, typical of rocks of the Middle Jurassic Nelson plutonic suite. The Westkettle batholith, which hosts many of the veins in

the Highland Bell mine (Reinecke, 1915), is lithologically similar to the granodiorite intrusions in the Christian Valley map area, but has been dated at 213.5 Ma by U-Pb zircon geochronology (Massey et al., 2010). Additional samples of these intrusive rocks have been submitted to the geochronology laboratory of the University of British Columbia for testing by both the $^{40}\text{Ar}/^{39}\text{Ar}$ and U-Pb methods of age determination.

Granite (Unit Tg)

Granite and granodiorite of the ‘Cretaceous and/or Jurassic’ Okanagan batholith (Tempelman-Kluit, 1989) underlie a large part of the Christian Valley map area west and east of the Rock Creek graben. These comprise mainly medium-grained, fresh white to pink-tinged quartz-plagioclase-orthoclase granite, with variable but generally minor biotite and hornblende. Porphyritic phases, with large white to pink feldspar crystals, are common in exposures east of the Rock Creek graben (Figure 3). Based on lithological similarities to Eocene ‘Ladybird’ granite in the Deer Park and Burrell Creek areas to the east, granitic rocks in the Christian Valley map area are assumed to be Paleogene in age. This is supported by a K-Ar date on biotite of 56.3 Ma from a sample of the ‘Ladybird’ granite located along Trapping



Data sources

Figure 3. Geology of 1:20 000 TRIM map area 082E/056. Inset shows the data sources in coloured outline and the 2016 traverse locations are indicated by the black line.

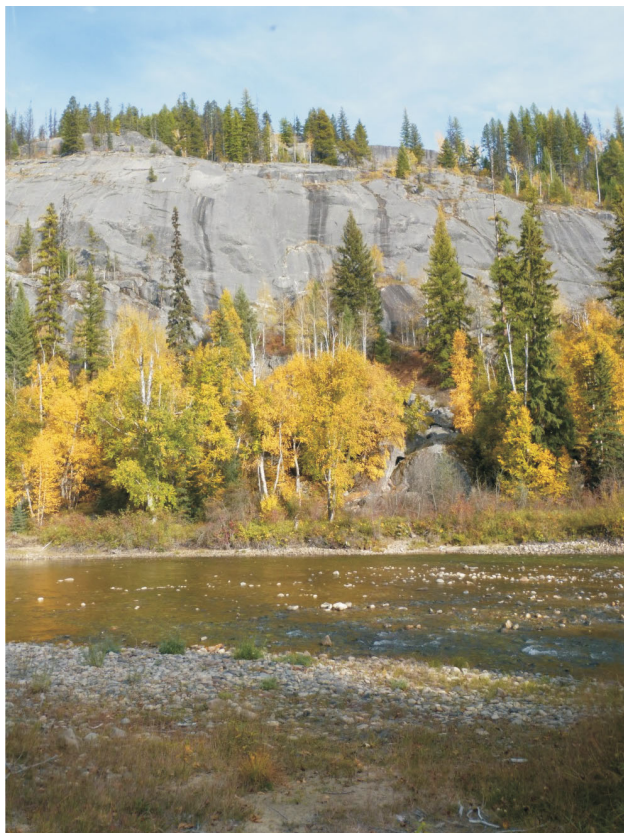


Figure 4. Large exposure of the Marron Formation of the Pentiction Group in the core of the Rock Creek graben on the eastern shore of the Kettle River in 1:20 000 TRIM map area 082E/057 (UTM 370500E, 5492000N, NAD83).

Creek in the central part of the Christian Valley (Hunt and Roddick, 1992).

Eocene Coryell Intrusive Suite (Unit Ec)

The alkalic to subalkalic Coryell intrusions occur as a number of small stocks that intrude Okanagan batholith rocks west of the Rock Creek graben and as part of a larger batholith that extends north from the Almond Mountain map area into the southern part of the Christian Valley area, east of the graben. Coryell rocks range from massive to porphyritic, typically varying in composition from syenite to monzonite. A suite of north-trending Coryell dikes are common in the area between Lassie Lake and Trapping Creek.

The Coryell intrudes granitic rocks of unit Tg throughout the Christian Valley map area, and dikes and small syenite intrusions locally cut Marron Formation in the Rock Creek graben. Several of these are shown west of Cup Lake and Collier Lake in Figure 3.

Pentiction Group

The Eocene Pentiction Group is described and defined by Church (1973) as comprising six formation members: basal

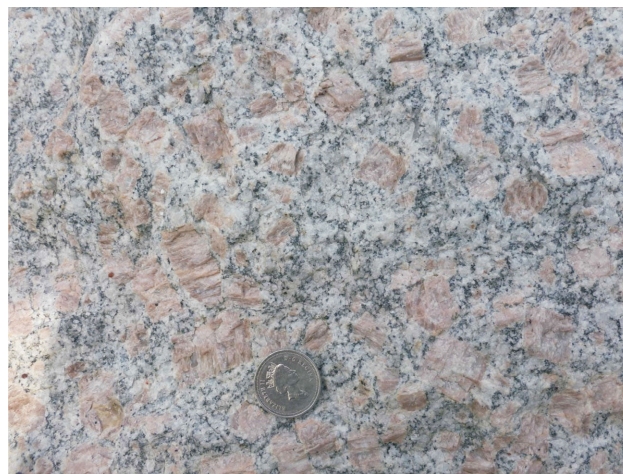


Figure 5. Unit Tg K-feldspar megacrystic granite from the eastern side of the Rock Creek graben in 1:20 000 TRIM map area 082E/057 (UTM 375153E, 5494488N, NAD83).

Springbrook and coeval Kettle River formations, volcanic rocks of the Marron and Marama formations, and dominantly sedimentary rocks of the White Lake and Skaha formations (Figure 6). In the Christian Valley area, the lower two formations of the Pentiction Group are exposed in the Rock Creek graben: a basal succession of conglomerate and siltstone of the Kettle River Formation and dominantly volcanic rocks of the Marron Formation. The overlying 'Kallis formation', separated from the Marron by a regional unconformity, is not included in the Pentiction Group.

Kettle River Formation (Unit Epk)

The Kettle River Formation is only exposed in the southern part of the map area, along a roadcut in the Kettle River valley. It comprises coarse conglomerate, with numerous large subrounded clasts of dominantly feldspar porphyry in a granular, green to tan silty or sandy matrix (Figure 7). It is in sharp contact with overlying green andesite and lapilli tuff of the Marron Formation. As the base of this conglomerate is not exposed, it is possible that it represents a coarse clastic unit within the Marron Formation; however, as similar units farther south are located mainly at the base of the Pentiction Group (Höy, 2016), this exposure is assumed to be Kettle River Formation.

Marron Formation (Unit Epm)

The Marron Formation comprises a thick package of dominantly alkalic volcanic rocks that are exposed in the Rock Creek graben. The formation overlies the Kettle River Formation and older rocks of the Nelson and Valhalla plutonic suites, or late Paleozoic metasedimentary or metavolcanic rocks of the Wallace group. It is unconformably overlain by basalt of the Pliocene 'Kallis formation'. Subdivision of the Marron Formation within the map area (Figure 3) is difficult due largely to the lack of distinctive marker units and structural complexity caused by the numerous high-angle block faults that occur throughout the graben.

		Christian Valley (1) Almond Mountain	East Okanagan (2)	Greenwood (3)	White Lake basin (4)	Republic, Wash. (5)
Neogene	Pliocene	Kallis	plateau basalt			
				Klondike Mountain	Skaha	Klondike Mountain
Paleogene	Eocene				White Lake	
					Marama	Sandpoil
		← Coryell	← Coryell			←
		Marron	Kamloops	Marron	Marron	
		Kettle River	Kettle River	Kettle River	Springbrook	O'Brien
Mesozoic	Pal.	← Tg	← Valhalla			
	Jurassic	← mJg	← Nelson			
		Triassic			Brooklyn	
Paleozoic		Wallace	Anarchist	Attwood Knob Hill		

Figure 6. Correlation chart of units in the Christian Valley map area with other successions; note relative ages of intrusive rocks (Coryell, unit Tg, Valhalla, Nelson and unit mJg) and regional unconformities (grey lines). Data sources are shown in 'References' section: (1) this study, Massey (2010); (2) Christopher (1978); (3) Church (1986), Fyles (1990); (4) Church (1973); (5) Cheney and Orr (1987). Abbreviation: Pal, Paleocene.

In general, the Marron Formation (unit Epm) can be subdivided into two units: a basal subunit dominated by green to mauve-tinged tuff and andesitic flows, and an overlying subunit of more massive basalt (subunit Epm1). These units are relatively well displayed along several of the roads that climb westward from the Kettle River valley road in the southeastern part of the map area (Figure 3).

The Marron Formation comprises dominantly pale to medium green, massive to amygdaloidal lava flows; pale to medium green to grey crystal and lithic tuff, occasional well-bedded sandstone and siltstone (Figure 8); and rare conglomerate beds in the central part of the succession. The lower part of the Marron, exposed mainly at lower elevations in the Kettle River valley (Figure 3), is highly vari-



Figure 7. Conglomerate of the Kettle River Formation, exposed in a roadcut in Christian Valley; note chloritic alteration of arkosic matrix (1:20 000 TRIM map area 082E/056; UTM 367706E, 5485601N, NAD83).

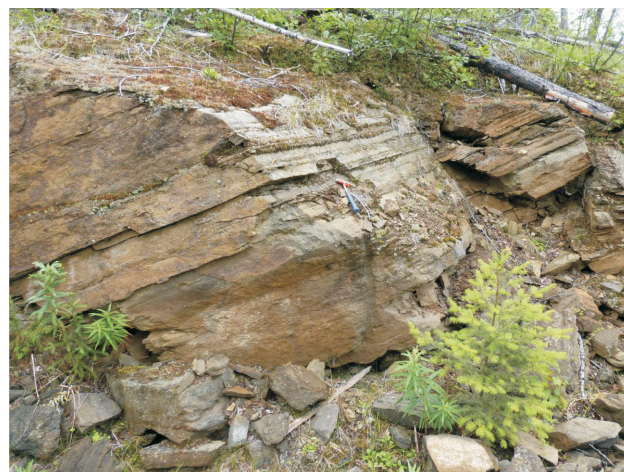


Figure 8. Well-layered sandstone beds within the central part of the Marron Formation on 1:20 000 TRIM map area 082E/056 (UTM 366387E, 5487419N, NAD83).

able, with pale green to light grey feldspar-phyric flows (Figure 9) and pale green to mauve-tinged lithic and crystal tuff. It is overlain by a thick section of dominantly pale green crystal and lithic tuff and, less commonly, grey to mauve-tinged tuff and massive plagioclase-pyroxene-phyric flows. Sections of pale salmon pink trachyte flows, commonly with pink K-feldspar and biotite phenocrysts, occur throughout the middle part of the Marron, and thin successions of well-layered green tuffaceous beds, agglomerate, shale and siltstone occasionally occur in the upper part of the formation.

Subunit Epm1, the uppermost unit in the Marron Formation, comprises hard, compact, massive basalt with occasional biotite and pyroxene phenocrysts. Locally, it is unconformably overlain by massive basalt of the 'Kallis formation'.

Discussion

Church (1973) described the type section of the Marron Formation in the White Lake basin area, where five distinctive members are recognized (Figure 6). It is difficult to correlate these members with specific units in the Rock Creek graben, although many of the rock units identified by Church (op. cit.) are recognized here as well. As noted above, this may be due to the difficulty in subdividing the Marron Formation in the Rock Creek graben into distinct, mappable units or, alternatively, the detailed breakdown of the Marron Formation into these constituent members does not apply here. However, it would appear that the uppermost subunit (Emp1) may correlate with the lithologically similar Park Rill member, the uppermost member of the Marron Formation in the White Lake basin (Church, 1973).

The age of the Marron Formation is constrained by the age of the unconformably underlying megacrystic Kettle River

granite, which has been mapped in the Almond Mountain map area to the south (Massey and Duffey, 2008; Höy, 2016), and the age of the Coryell suite, which intrudes the Marron in several locations, notably in the western part of the Rock Creek graben as shown in Figure 3. In the Almond Mountain map area to the south, megacrystic K-feldspar granite is bleached and eroded, and overlying Kettle River Formation contains conglomerate and grit that is clearly derived from the granite. A K-Ar date of 49.4 ± 1.9 Ma was obtained from a lithologically similar megacrystic granite south of Beaverdell (Church, 1996), and a U-Pb zircon date of 56.0 ± 1.0 Ma (Parrish, 1992) as well as a $^{39}\text{Ar}/^{40}\text{Ar}$ date on hornblende of 52.8 ± 1.6 Ma (Höy, 2013) for a similar granite in the Burrell Creek area. Coryell intrusive rocks throughout the Penticton map area have been dated at approximately 51–52 Ma (Parrish et al., 1988). Hence, the Marron Formation is assumed to have been extruded in middle Eocene time, between ~57 and 51 Ma.

'Kallis Formation' (Unit Pk)

The 'Kallis formation' is preserved in isolated topographic highs throughout the area (Figure 10). It unconformably overlies the Marron Formation and older units, and represents the remnants of widespread Pliocene plateau basalt. It consists typically of a black, fine-grained, aphyric or olivine basalt.

Structure

The structure of the Kettle River area in the Christian Valley map area is dominated by the north-trending Rock Creek graben. A west-dipping normal fault along the eastern margin of the graben, juxtaposes Eocene(?) granitic rocks of unit Tg with Marron Formation in the core of the graben. The fault is not exposed as it is covered by alluvium in the floor of the Kettle River valley (Figure 3). The western



Figure 9. Unusual feldspar-phyric flow in the central part of the Marron Formation on 1:20 000 TRIM map area 082E/067 (UTM 370986E, 5499578N, NAD83); plagioclase crystals are up to 1 cm long.



Figure 10. Columnar basalt of the Pliocene 'Kallis formation'; paleochannels at the base of this formation have been explored extensively for uranium (1:20 000 TRIM map area 082E/056; UTM 364970E, 5497380N, NAD83).

margin of the graben in the southern part of the map area (Figure 3) is defined by an east-dipping normal fault that is closely constrained by exposures of Marron Formation within the graben and the Coryell syenite to the west. Farther north, a north-northeast-trending normal fault marks the western margin of the graben, constrained by mainly Paleogene granite (unit Tgp) to the west and the Marron Formation (unit Epm) to the east. These faulted contacts appear to be relatively sharp, with little observed alteration in rocks that are within a few tens of metres of either hanging-wall or footwall rocks. However, immediately north, in 1:20 000 scale map area 082E/066, the western margin fault is more complicated, showing several splays that expose altered and sheared Middle Jurassic granodiorite and Wallace group rocks (Figure 11). These altered rocks have been explored for base- and precious-metal skarn and vein mineralization (Whiting, 1985). The internal structure of the graben is more complex than shown in Figure 3. Several, generally north-northwest-trending high-angle faults are recognized within the graben, mainly by offsets and truncation of units.

Movement along the bounding graben faults clearly post-dates Marron Formation deposition, supporting a model in which late fault movement down-dropped and hence preserved remnants of more widespread Marron Formation within the north-trending grabens. However, it is possible that movement on the faults began earlier and controlled in part the distribution of Marron Formation rocks throughout the area. Although the Marron is broadly similar in all down-dropped blocks throughout the Okanagan and Boundary areas, correlation of the well-recognized succession of the White Lake basin (Church, 1973) is not possible in other basins, specifically in the Rock Creek graben. As noted above, the fault at the western margin of the graben is locally characterized by several fault splays, shearing, brecciation and alteration. In one of these exposures (Figure 11), highly broken Eocene(?) granite contains large blocks of crushed Wallace group, but is cut by a fresh, unaltered north-trending hornblende-porphyry dike that is lithologically similar to some phases of the Marron Formation and unlike the syenite dikes of the younger Coryell suite (Figures 12, 13). An isotopic date on this dike would constrain the timing of movement on this splay of the fault and conceivably provide evidence for movement during deposition of the Marron Formation.

Mineralization

Most exploration in the Christian Valley map area has been focused on uranium mineralization that occurs near the base of the Pliocene ‘Kallis formation’. Exploration peaked in the 1970s and continued until the BC Provincial Government enacted a moratorium on uranium exploration in the province that was in effect from 1980 to 1987, and again after 2008, when the moratorium was reinstated. Limited ex-

ploration for base and precious metals, based in part on the successful exploration in the area of the Carmi, Beaverdell and Greenwood mining camps has continued intermittently throughout the Christian Valley map area. Descriptions of these mineral occurrences are taken mainly from Provincial Government assessment reports and BC MINFILE.

Uranium mineral occurrences and deposits in the Kettle River valley area (Figure 3) are generally found in poorly consolidated sandstone and conglomerate that have been preserved below a cap of Pliocene basalt of the ‘Kallis formation’. The deposits occur in fluvial sediments that unconformably overlie the Marron Formation, Wallace group or Anarchist Schist, and Jurassic and Eocene intrusive rocks (Christopher, 1977). The Fuki deposits occur within a northeast-trending paleochannel that overlies the Eocene

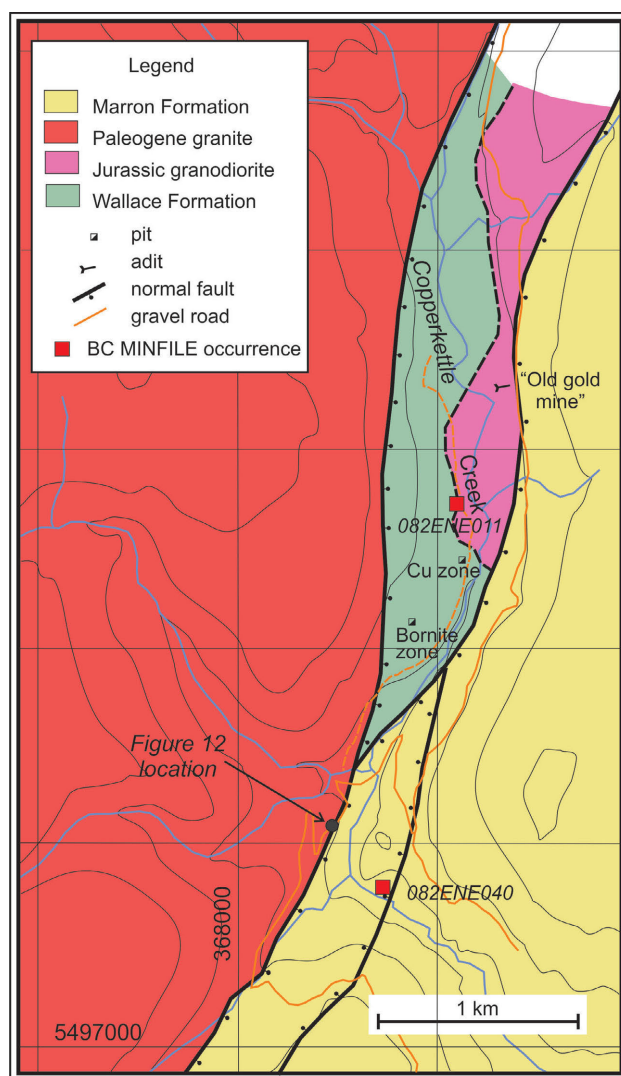


Figure 11. Geology of the western margin of the Rock Creek graben in the Christian Valley, showing several fault splays and exposures of Middle Jurassic granodiorite and Wallace group rocks (1:20 000 TRIM map area 082E/066; UTM 368478E, 5498097N, NAD83), and location of mineralization on the Copket property (modified from Whiting, 1991).

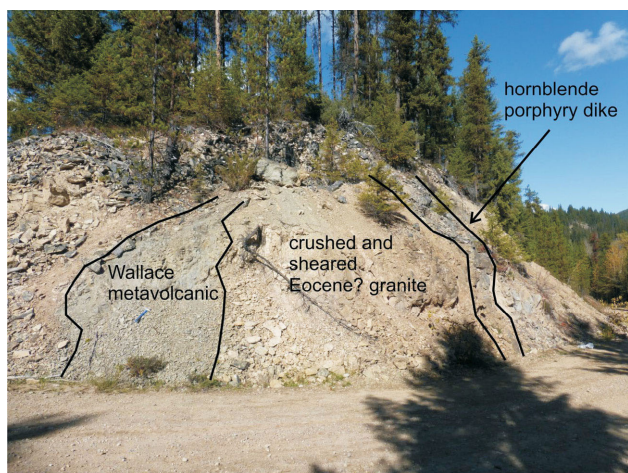


Figure 12. Crushed and sheared Eocene(?) granite in the fault along the western margin of the Rock Creek graben contains blocks of altered and sheared Paleozoic Wallace group metavolcanic rocks, and is cut by a fresh, unaltered hornblende-phyric dike (Figure 13). The age of the dike constrains timing of movement on this splay of the fault; the location of the fault is shown in Figure 11 on 1:20 000 TRIM map area 082E/066 (UTM 368478E, 5498097N, NAD83).

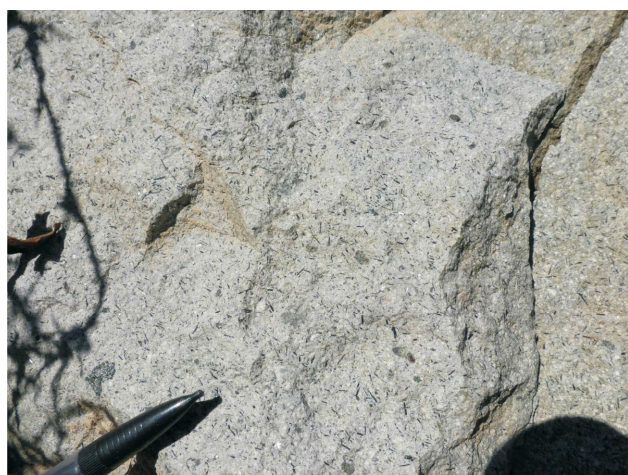


Figure 13. Detail of the hornblende-phyric dike shown in Figure 12, which is lithologically similar to some phases of the Eocene Marron Formation; the dike is located on the western margin of the Rock Creek graben in the Christian Valley.

Marron Formation. Hostrocks are poorly consolidated interbedded arkosic sandstone, siltstone, carbonaceous mudstone and conglomerate that form the lowermost member of the 'Kallis formation' (e.g., Nicoll, 1980; Turner et al., 1980; Brickner, 2003). Secondary uranium mineralization is largely concentrated in the basal conglomerate, occurring as films on pebbles and in the matrix of the conglomerate. Autunite is the only uranium mineral identified.

The Copket (MINFILE 082ENE11, BC Geological Survey, 2016b) and Sand (MINFILE 082ENE040) mineral occurrences are located in the Copperkettle Creek valley, along the western edge of the Rock Creek graben, in an area of extensional north-south faulting and locally intense alter-

ation (Figure 11). The Sand occurrence is a narrow zone of disseminated chalcopyrite, galena and pyrite that was intersected in the Marron Formation in a 1970 diamond drilling program that was focused on locating uranium mineralization (Kikuchi, 1970). There is no reported surface mineralization. The Copket showings comprise a number of shafts, adits, pits and mineralized outcrops that record exploration that dates back to the early 1900s. Two styles of mineralization are documented: copper-gold-silver skarn in Wallace or Anarchist metasediments and limestone along the contact with Jurassic granodiorite, and later copper-zinc mineralization developed along a north-trending Eocene normal fault (Whiting, 1991). These mineralized areas are shown in Figure 11 as the Bornite and Cu zones, respectively. Whiting (1991) notes that considerable alteration, brecciation and disseminated sulphide mineralization occurs in the Jurassic granodiorite and that an "old gold mine" occurs farther along strike, to the north of the Copket mineralization. Altered granodiorite and Wallace metasedimentary rocks, both containing disseminated pyrite, are conspicuous within the fault zone several kilometres farther north of these showings.

Summary and Conclusions

The geology of the Christian Valley area is dominated by the north-trending Rock Creek graben, which is filled with Eocene volcanic rocks of the Marron Formation and bounded by mainly granitic rocks, also of predominantly Eocene age. Remnants of a Paleozoic basement, metavolcanic and metasedimentary rocks of the Wallace group are exposed in a tectonic high in the southwestern part of the area (Figure 3), and in splays of normal faults that bound the western margin of the graben (Figure 11). Several magmatic pulses are recorded throughout the area. Middle Jurassic granodiorite intrudes the Wallace group and two magmatic pulses are recorded in the Paleogene. Massive to megacrystic K-feldspar granite intrudes both Wallace and Jurassic granodiorite and locally forms the basement to unconformably overlying Kettle River and Marron formations. In contrast, Coryell syenite intrudes the granite and locally the Marron Formation within the graben. Hence, the Marron Formation was deposited between these two magmatic pulses, sometime between 57 and 51 Ma ago, which are the respective ages of the two magmatic suites.

The Rock Creek graben may have formed after deposition of the volcanic rocks of the Marron Formation that are preserved in its core, or by growth faulting during their deposition. At least some movement along the bounding graben faults clearly postdates the Marron, supporting a model in which these Eocene volcanic rocks are represented as remnants of widespread volcanism, preserved from erosion in down-dropped blocks (e.g., Cheney, 1994). However, it is equally possible that initiation of graben development occurred earlier and controlled, at least in part, the distribu-

tion of Eocene volcanism. Fault zones along the western margin of the graben are locally cut by fresh, undeformed dikes that include both younger Coryell and hornblende-phryic dikes that are lithologically similar to some phases of the Marron Formation. Dating of these dikes, and more robust dating of the Marron Formation and granitic rocks that form the margins of the Rock Creek graben, will help constrain the timing of movement of the bounding faults and the age span of the Marron.

Mineral exploration in the Christian Valley map area has been mainly directed toward finding unconformity-related uranium that occurs in paleochannels beneath Pliocene plateau basalt. Minor exploration for base- and precious-metal mineralization has taken place along the faulted western margin of the Rock Creek graben, with discovery of mineralized skarn in Wallace group rocks adjacent to Middle Jurassic granodiorite, and both vein and disseminated mineralization in both Eocene Marron Formation and older granitic rocks. This suggests that several stages of mineralization occurred during Jurassic and Eocene time, as has been demonstrated in the Highland Bell and Carmi mines to the south (e.g., Watson et al., 1982).

Acknowledgments

Geoscience BC is gratefully acknowledged for its financial support of this study. W. Jackaman is thanked for help in preparing base maps, and G.E. Ray and reviewers from Geoscience BC and RnD Technical for editing the manuscript.

References

- BC Geological Survey (2016a): MapPlace GIS internet mapping system; BC Ministry of Energy and Mines, BC Geological Survey, MapPlace website, URL <<http://www.MapPlace.ca>> [November 2016]
- BC Geological Survey (2016b): MINFILE BC mineral deposits database; BC Ministry of Energy and Mines, BC Geological Survey, URL <<http://minfile.ca>> [November 2016].
- Brickner, R. (2003): Blizzard claims; BC Ministry of Energy and Mines, Assessment Report 27,257, 24 p.
- Cheney, E.S. (1994): Cenozoic unconformity-bounded sequences of central and eastern Washington; Washington Division of Geology and Earth Resources, Bulletin 80, p. 115–139.
- Cheney, E.S. and Orr, K.E. (1987): Kettle and Okanagan domes, northeastern Washington and southern British Columbia; Washington Division of Geology and Earth Resources, Bulletin, p. 55–71.
- Christopher, P.A. (1977): Uranium reconnaissance program (82E, 82L, and 82M); BC Ministry of Energy and Mines, BC Geological Survey, Paper 1977-1, p. 11–14.
- Christopher, P.A. (1978): Geology of the East Okanagan uranium area (NTS 082E/10, 11, 14, 15), south-central British Columbia; BC Ministry of Energy and Mines, Preliminary map 29, 1:50 000 scale.
- Church, B.N. (1973): Geology of the White Lake basin; BC Ministry of Energy and Mines, Bulletin 61, 120 p.
- Church, B.N. (1986): Geological setting and mineralization in the Mount Attwood–Phoenix area of the Greenwood camp; BC Ministry of Energy and Mines, Paper 1986-2, 65 p.
- Church, B.N. (1996): Several new industrial mineral and ornamental stone occurrences in the Okanagan–Boundary district (82E, 82L); *in* Exploration in British Columbia 1995, BC Ministry of Energy and Mines, p. 123–130.
- Fyles, J.T. (1990): Geology of the Greenwood–Grand Forks area, British Columbia; BC Ministry of Energy and Mines, Open File 1990-25.
- Höy, T. (2013): Burrell Creek map area: setting of the Franklin mining camp, southeastern British Columbia; *in* Geoscience BC Summary of Activities 2012, Geoscience BC, Report 2013-1, p. 91–101.
- Höy, T. (2016): Geology of the Kettle River area, Almond Mountain project, southern British Columbia (NTS 082E/07); *in* Geoscience BC, Summary of Activities 2015; Report 2016-1, p. 23–34.
- Höy, T. and Dunne, K.P.E (2001): Metallogeny and mineral deposits of the Nelson–Rossland area, Part II: The early Jurassic Rossland Group, southeastern British Columbia; BC Ministry of Energy and Mines, Bulletin 109, 195 p.
- Hoy, T. and Jackaman, W. (2005): Geology of the Grand Forks map sheet, British Columbia (NTS 082E/01); BC Ministry of Energy and Mines, Geoscience Map 2005-2, scale 1:50 000.
- Höy, T. and Jackaman, W. (2010): Geology of the Deer Park map sheet (NTS 82E/08); Geoscience BC, Map 2010-7-1, scale 1:50 000.
- Höy, T. and Jackaman, W. (2013): Geology of the Burrell Creek map sheet (NTS 82E/09); Geoscience BC, Map 2013-07-1, scale 1:50 000.
- Höy, T. and Jackaman, W. (2016): Geology of the Almond Mountain map sheet (NTS 82E/07); Geoscience BC, Map 2016-07-1, scale 1:50 000.
- Hunt, P.A. and Roddick, J.C. (1992): A compilation of K–Ar ages report 21; *in* Radiogenic and Isotopic Studies, Report 5; Geological Survey of Canada, Paper 91-2, p. 207–252.
- Inazumi, S. (1973): Diamond drilling report on Donen (281 to 320 inclusive) mineral claims; BC Ministry of Energy and Mines, Assessment Report 4630, 45 p., URL <https://aris.empr.gov.bc.ca/search.asp?mode=repsum&rep_no=04630> [November 2016].
- Kikuchi, T. (1970): Geological, radiometric and diamond drilling report on Sand, Cup and Lassie mineral claims, Greenwood Mining Division; BC Ministry of Energy and Mines, Assessment Report 2482, 36 p., URL <https://aris.empr.gov.bc.ca/search.asp?mode=repsum&rep_no=02482> [November 2016].
- Little, H.W. (1957): Kettle River (East half); Geological Survey of Canada, Map 6-1957, scale 1:253 440.
- Massey, N.W.D. and Duffy, A. (2008): Boundary project: McKinney Creek and Beaverdell areas, south-central BC; *in* Geological Fieldwork 2007, BC Ministry of Energy and Mines, BC Geological Survey, Paper 2008-1, p. 87–102.
- Massey, N.W.D., Gabites, J.E., Mortensen, J.K. and Ullrich, T.D. (2010): Boundary project: geochronology and geochemistry of Jurassic and Eocene intrusions, southern British Columbia (NTS 082E); *in* Geological Fieldwork 2009, BC Ministry of Energy and Mines, BC Geological Survey, Paper 2010-1, p. 127–142.

- McCandless, P. and Hughes, B. (1977): Assessment report: combined geological and geochemical survey on the CL#1, Dell and State mineral claims; BC Ministry of Energy and Mines, Assessment report 6319, 81 p., URL <https://aris.empr.gov.bc.ca/search.asp?mode=repsum&rep_no=02482> [November 2016].
- McLelland, D. (2008): Gamma-ray spectrometer ground verification exploration and prospecting program of the Trapping Creek–Sandrift Lake claims; BC Ministry of Energy and Mines, Assessment Report 27,791, 496 p., URL <https://aris.empr.gov.bc.ca/search.asp?mode=repsum&rep_no=27791> [November 2016].
- Nicoll, L. (1980): Diamond drilling report on Done, Fuki mineral claims, Greenwood Mining Division, and aerial photography on PB and Donen 361 mineral claims, Osoyoos, Vernon and Greenwood Mining divisions; BC Ministry of Energy and Mines, Assessment Report 8105, 360 p., URL <https://aris.empr.gov.bc.ca/search.asp?mode=repsum&rep_no=08105> [November 2016].
- Okuno, T. (1972): Diamond drilling report on Donen (281 to 320 inclusive) mineral claims; BC Ministry of Energy and Mines, Assessment Report 3775, 49 p., URL <https://aris.empr.gov.bc.ca/search.asp?mode=repsum&rep_no=03775> [November 2016].
- Parrish, R.R. (1992): Miscellaneous U-Pb zircon dates from south-east British Columbia; *in* Radiogenic Age and Isotopic Studies, Geological Survey of Canada, Report 5, Paper 91-2, p. 143–153.
- Parrish, R.R., Carr, S.D. and Parkinson, D.L. (1988): Eocene extensional tectonics and geochronology of the southern Omineca belt, British Columbia and Washington; *Tectonics*, v. 72, p. 181–212.
- Preto, V.A. (1970): Structure and petrology of the Grand Forks Group, BC; Geological Survey of Canada, Paper 69-22.
- Preto, V.A. (1979): Geology of the Nicola Group between Merritt and Princeton; BC Ministry of Energy and Mines, Bulletin 69, 90 p.
- Reinecke, L. (1915): Ore deposits of the Beavertell map area; Geological Survey of Canada, Memoir 79, 172 p.
- Tempelman-Kluit, D. J. (1989): Geology, Penticton, British Columbia; Geological Survey of Canada, Map 1736A, scale 1:250 000.
- Turner, A.T., Sawyer, D.A. and Cann, R. (1980): Geochemical survey and percussion drilling project, Beverly-Blizzard Group, Greenwood Mining Division, British Columbia; BC Ministry of Energy and Mines, Assessment Report 7822, 267 p., URL <https://aris.empr.gov.bc.ca/search.asp?mode=repsum&rep_no=07822> [November 2016].
- Watson, P.H., Godwin, C.I. and Christopher, P.A. (1982): General geology and genesis of silver and gold veins in the Beavertell area, south-central British Columbia; *Canadian Journal of Earth Sciences*, v. 19, p. 1264–1274.
- Wheeler, J.O. and McFeely, P. (1991): Tectonic assemblage map of the Canadian Cordillera and adjacent parts of the United States of America; Geological Survey of Canada, Map 1712A, scale 1:2 000 000.
- Whiting, F.B. (1985): Copket Group, Greenwood Mining Division; BC Ministry of Energy and Mines, Assessment Report 13,795, 22 p., URL <https://aris.empr.gov.bc.ca/search.asp?mode=repsum&rep_no=13795> [November 2016].
- Whiting, F.B. (1991): Geological sampling report, Copket Group, Copperkettle Creek; BC Ministry of Energy and Mines, Assessment Report 21,534, 23 p., URL <https://aris.empr.gov.bc.ca/search.asp?mode=repsum&rep_no=21534> [November 2016].

Merging Geological, Seismic-Reflection and Magnetotelluric Data in the Purcell Anticlinorium, Southeastern British Columbia

F.A. Cook, Salt Spring Imaging, Ltd., Salt Spring Island, BC, fcook@ucalgary.ca

Cook, F.A. (2017): Merging geological, seismic-reflection and magnetotelluric data in the Purcell Anticlinorium, southeastern British Columbia; in Geoscience BC Summary of Activities 2016, Geoscience BC, Report 2017-1, p. 257–258.

Introduction

The purpose of this project is to combine geological, seismic-reflection and magnetotelluric (MT) data in southeastern British Columbia (BC) to target concentrations of sulphide mineralization in the subsurface. Existing MT data will be reprocessed with two-dimensional (2-D) inversions, where possible, and the results will be combined with reprocessed seismic-reflection profiles and drillhole information. The seismic data and drillholes allow detailed mapping of structural and stratigraphic variations, while the MT data will help to characterize the electrical properties, and thus perhaps the presence or not of metals, at different stratigraphic levels.

The Belt-Purcell Basin of southeastern BC and northern Montana (Figure 1) contains a number of stratigraphically controlled massive-sulphide deposits, most notably the now-closed Sullivan mine near Kimberley, BC. Ever since Cominco began to phase out their mining operations at the Sullivan, there have been a number of efforts to find ‘another Sullivan’. Most of the efforts have focused on the stratigraphic interval between the top of the Mesoproterozoic Lower Aldridge Formation and the middle part of the Middle Aldridge Formation (colloquially known as the ‘Sullivan zone’ or ‘Sullivan horizon’). However, there are also stratigraphic intervals, either above or below the Sullivan zone, that may contain economic quantities of metals. For example, the Creston Formation (Revett Formation in the United States) is a major producing interval for copper minerals in the Troy, Montanore, Rock Creek and other deposits in Montana, and the upper Aldridge is host to the St. Eugene vein system near Moyie, BC. Thus, the approach described here may also be helpful for finding metals in various stratigraphic levels (Cook and Jones, 1995).

Previous Work

Seismic reflection profiling was undertaken in the mid-1980s for petroleum exploration and for regional studies

throughout the Purcell Anticlinorium (Figure 1). Regional data were recorded by LITHOPROBE but are not of sufficiently high resolution for this study. Data acquired for hydrocarbon exploration were recorded by Duncan Energy Inc. and then provided to the University of Calgary for analysis (Cook and van der Velden, 1995). The data were initially reprocessed for large-scale regional studies (Cook and van der Velden, 1995). Even though the data were recorded nearly 30 years ago, they provide a unique view of the Belt-Purcell Basin that is not available with any other geological or geophysical dataset. A deep (3.477 km) exploration drillhole (‘DEI’ location shown in Figure 1) was drilled by Duncan Energy in 1985 and provides definitive correlations of seismic reflections to stratigraphic (in this case, sill) horizons along a number of seismic profiles.

More than 200 MT stations were recorded during the 1980s in a series of lines that cross the eastern part of the Purcell Anticlinorium in Montana and BC (Cook and Jones, 1995; Gupta and Jones, 1995). Seventy-eight MT stations were acquired in BC along eight lines or partial lines, three of which were analyzed by Gupta and Jones (1995). Initial (1-D) inversions of the MT data by Gupta and Jones (1995) indicated that there is a strong, regional, electrically conductive zone at a depth of a few kilometres beneath the anticlinorium. However, when the work was done, 2-D inversions were not commonly applied. Thus, more advanced techniques may provide enhanced detail so that the electrical structure can be correlated to stratigraphic and structural features that are observed in the seismic data. This approach was undertaken by Cook and Jones (1995) for data in the vicinity of the DEI drillhole.

Project Plan

Available data have been obtained from the Geological Survey of Canada. The MT inversions will be completed by a contractor such that the results can be combined with the seismic geometry, surface geology and drillhole data to map the subsurface variations in electrical conductivity. The inversions should be completed by the end of 2016, so merging of the results with the seismic data should be completed in early 2017. The results should help to delineate stratigraphically controlled zones with high electrical conductivity in the subsurface that may contain concentrations of sulphides but which, at the present time, are not visible.

Keywords: *British Columbia, geophysics, seismic reflection, magnetotelluric, Purcell Anticlinorium, Sullivan deposit*

This publication is also available, free of charge, as colour digital files in Adobe Acrobat® PDF format from the Geoscience BC website: <http://www.geosciencebc.com/s/DataReleases.asp>.

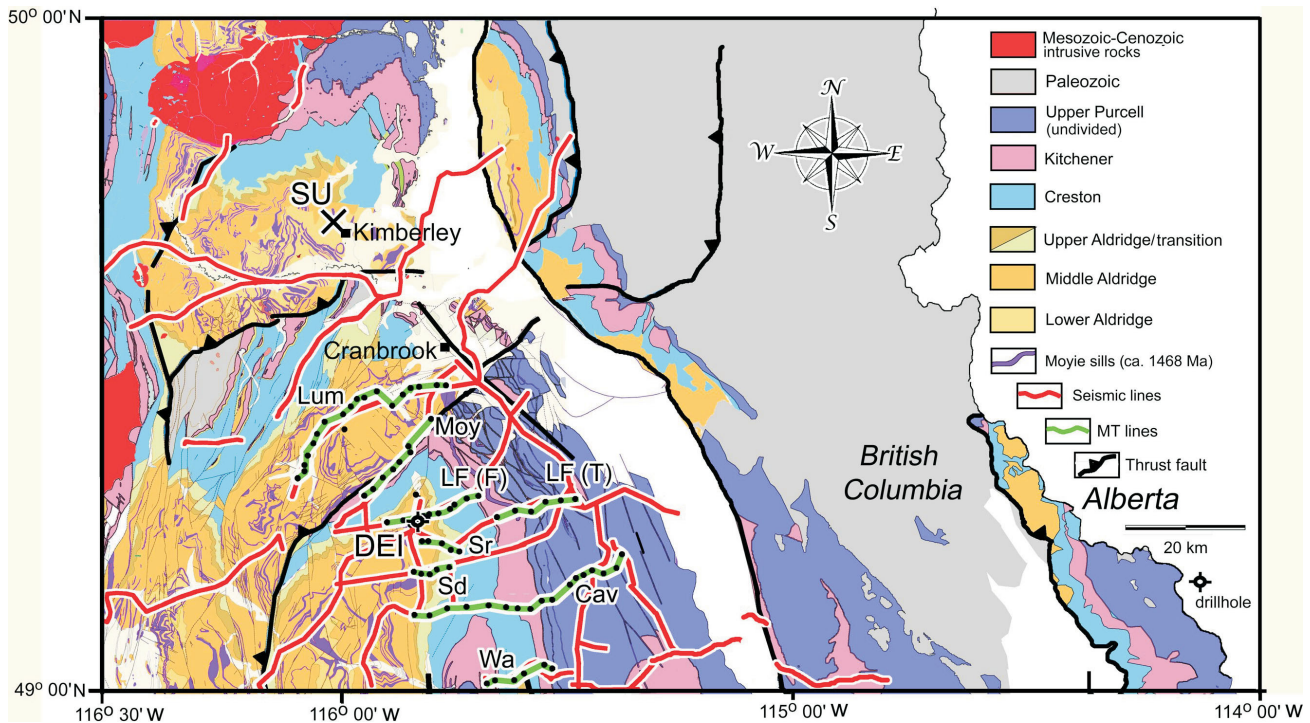


Figure 1. Geology of southeastern British Columbia (modified from Cook and van der Velden, 1995). Red lines are locations of seismic-reflection profiles and green lines with dots are MT station locations. Both datasets were acquired in the mid-1980s. Abbreviations: DEI, Duncan Energy Inc. drillhole; LF, Longfarrell MT profile in two segments; Cav, Caven Creek profile; Lum, Lumberton profile; Moy, Moyie fault profile; Sd, Sundown Creek; Sr, Sunrise Creek; SU, Sullivan mine; Wa, Ward Creek.

References

- Cook, F. and Jones, A. (1995): Seismic reflections and electrical conductivity: a case of Holmes' curious dog?; *Geology*, v. 23, p. 141–144.
- Cook, F.A. and Van der Velden, A.J. (1995): Three dimensional crustal structure of the Purcell anticlinorium in the Cordil-

lera of southwestern Canada; *Geological Society of America Bulletin*, v. 107, p. 642–664.

- Gupta, J. and Jones, A. (1995): Electrical conductivity structure of the Purcell anticlinorium in southeast British Columbia and northwest Montana; *Canadian Journal Earth Sciences*, v. 32, p. 1564–1583.

Unlocking the Value of Open Data in British Columbia: A Mining Industry Knowledge Hub

M.J. Flynn, Canada Mining Innovation Council, Vancouver, BC, mflynn@cmic-ccim.org

B.E. Madu, Geoscience BC, Vancouver, BC

Flynn, M.J. and Madu, B.E. (2017): Unlocking the value of open data in British Columbia: a Mining Industry Knowledge Hub; in Geoscience BC Summary of Activities 2016, Geoscience BC, Report 2017-1, p. 259–264.

Introduction

In January 2016, the Canada Mining Innovation Council (CMIC) and Geoscience BC signed a one-year working agreement for the development of an initiative entitled Mining Industry Knowledge Hub ('Knowledge Hub'). The central aims of the initiative are to compile, centralize and disseminate key water quality data that are related to the mining sector.

The working agreement covers the pilot/proof-of-concept phase of the initiative. This allows the project participants to evaluate the technical feasibility of the project while gauging stakeholder buy-in. As CMIC is a national organization, the initiative may be used as a model for the development of additional Knowledge Hubs in other major mining jurisdictions across Canada.

The strategic partnership between CMIC and Geoscience BC capitalizes on the unique skills and expertise of the organizations. The project lead is CMIC, with its role as a key mining industry association for developing innovation projects. It provides overall project management and is the interface between the project participants and project stakeholders (i.e., mining companies, regulatory agencies, communities, etc.). Given Geoscience BC's strong track record of collecting, curating and distributing earth-science data, it serves as the technical lead for the initiative.

Project Background

Geoscience BC Project Background

In 2014, Geoscience BC began identifying challenges associated with accessibility to environmental data for the mining sector and the public. Water quality data was highlighted as a key priority, given the importance of sound

water management to both the resource sector and to all British Columbians.

To do so, the organization engaged in outreach to determine initiatives that would address some of the challenges surrounding access to water quality data, while also exploring many of the opportunities that exist in the realm of environmental data.

At the same time, Geoscience BC sought strategic partnerships with organizations within the mining ecosystem. This would leverage the skills and expertise of the partnering organizations and create new avenues for collaboration.

CMIC Project Background

The Canada Mining Innovation Council is a national, member-based and industry-led organization. Its mandate is to lead innovation in the Canadian mining sector. Members of CMIC—through its technical working groups—define the challenges facing the sector and then develop innovative solutions in the form of collaborative projects and programs.

The Environmental Stewardship Initiative is one of four technical working groups within CMIC. Its role is to collaborate on innovation projects and programs that address sustainability issues facing the mining sector. In 2014, CMIC completed an environmental management scoping study (Hatch Ltd., 2014), which identified water management as a key area of the mining sector requiring innovation.

In turn, the Environmental Stewardship Initiative established the water working group to develop water management initiatives. The water working group defined many challenges surrounding water management; water quality monitoring and the associated data management were identified as key challenges.

Problem Definition

Importance of Water Quality Data

Monitoring is an integral component of water management activities for mine development and operations. The data and interpretations are critical for:

Keywords: *British Columbia, environmental data, water quality data, baseline data, data preservation, open data, transparency, innovation, social acceptance*

This publication is also available, free of charge, as colour digital files in Adobe Acrobat® PDF format from the Geoscience BC website: <http://www.geosciencebc.com/s/DataReleases.asp>.

- establishing baseline water quality conditions;
- determining any deleterious effects of mining operations on water resources;
- devising water management strategies, including impact mitigation strategies;
- implementing corrective actions;
- informing water treatment strategies and their efficacy; and
- characterizing the potential cumulative impact of mining activities on the surrounding environment.

Mine operators expend significant resources collecting, storing and analyzing water quality data that are used by regulators to meet their legislated mandates. This includes predicting impacts to water resources at the outset of project development, devising operating permits and ensuring compliance with the permits.

Disparate Nature of Regulatory Water Quality Data

Individual mine developers and operators collect and store their own water quality data. The methods and tools for doing so vary by company. Additionally, companies submit their data to the following regulatory bodies throughout various stages of the mine life cycle (i.e., assessment and permitting through to operations and closure/post-closure):

- BC Environmental Assessment Office (BC EAO)
- BC Ministry of Energy and Mines (BC MEM)
- BC Ministry of the Environment (BC MoE)
- Canadian Environmental Assessment Agency (federal)
- Environment and Climate Change Canada (ECCC; federal)

Each of the above agencies have different requirements for data submission, ranging from data submission in simple PDF to electronic submission into storage platforms. For example, the BC EAO requires that baseline water quality data be appended in PDF to environmental impact statements (EIS) as part of an overall environmental assessment. Conversely, the ECCC requires Metal Mining Effluent Regulations compliance data to be submitted via an electronic platform, namely the Regulatory Information Submission System. The data are then stored in an electronic database.

Data Loss

Environmental data loss is problematic across the mining sector. A predominant point at which this occurs is when mine projects are transferred between companies. This may occur at the project development stage (e.g., exploration, assessment) and/or during the operational stage.

Data loss can occur where mining companies submit data to regulatory agencies for assessment and/or permitting purposes and subsequently withdraw their application. In other cases, following the submission of the data, a project may be cancelled and/or the company dissolves. For both

instances, there is risk that the data-management systems and retention policies may result in data loss.

Sector Transparency

Despite high levels of regulatory compliance with respect to water quality, there is often a broad perception that the mining sector must improve its environmental stewardship. There may be distrust of mining companies as well as apprehension of the real and perceived impacts to the environment. In turn, this affects social acceptance of the sector's activities. Movement in the sector with respect to sharing information, reporting on sustainability and deeper engagement are some examples of transparency that might lead to greater social acceptance.

Government regulators are increasing transparency as well through the release of water quality data and summary reports that traditionally were used internally to determine compliance.

Developing a Solution: a Mining Industry Knowledge Hub

The Knowledge Hub initiative is exploring platforms that can ingest and store water quality data related to developing and operating mines across Canada.

Data Preservation

A key deliverable of the Knowledge Hub initiative is to compile and centralize disparate water quality data so it will be accessible for future use. Some of it is publicly available already, but not in a form that is broadly usable.

The three sources of data have been identified for inclusion in the pilot phase of the Knowledge Hub are

- baseline data submitted as part of environmental assessments to the BC EAO,
- compliance data submitted to regulatory bodies (i.e., BC MoE and BC MEM), and
- select datasets that are held by mining companies.

The above data are being stored in a temporary platform (Figures 1, 2) that uses the existing hardware and software of Geoscience BC (i.e., the Geoscience BC Earth Science Viewer). Parallel scoping work is being completed to identify a permanent platform for the data.

Extracting Value from Data

A goal of the Knowledge Hub is to enhance data-driven decision making. This requires that data is curated and presented in a way that facilitates use by a broad group of stakeholders.

Significant efforts are being made to ensure that the data platform is sufficiently user-friendly. These efforts are guided by the principle that the user experience of the

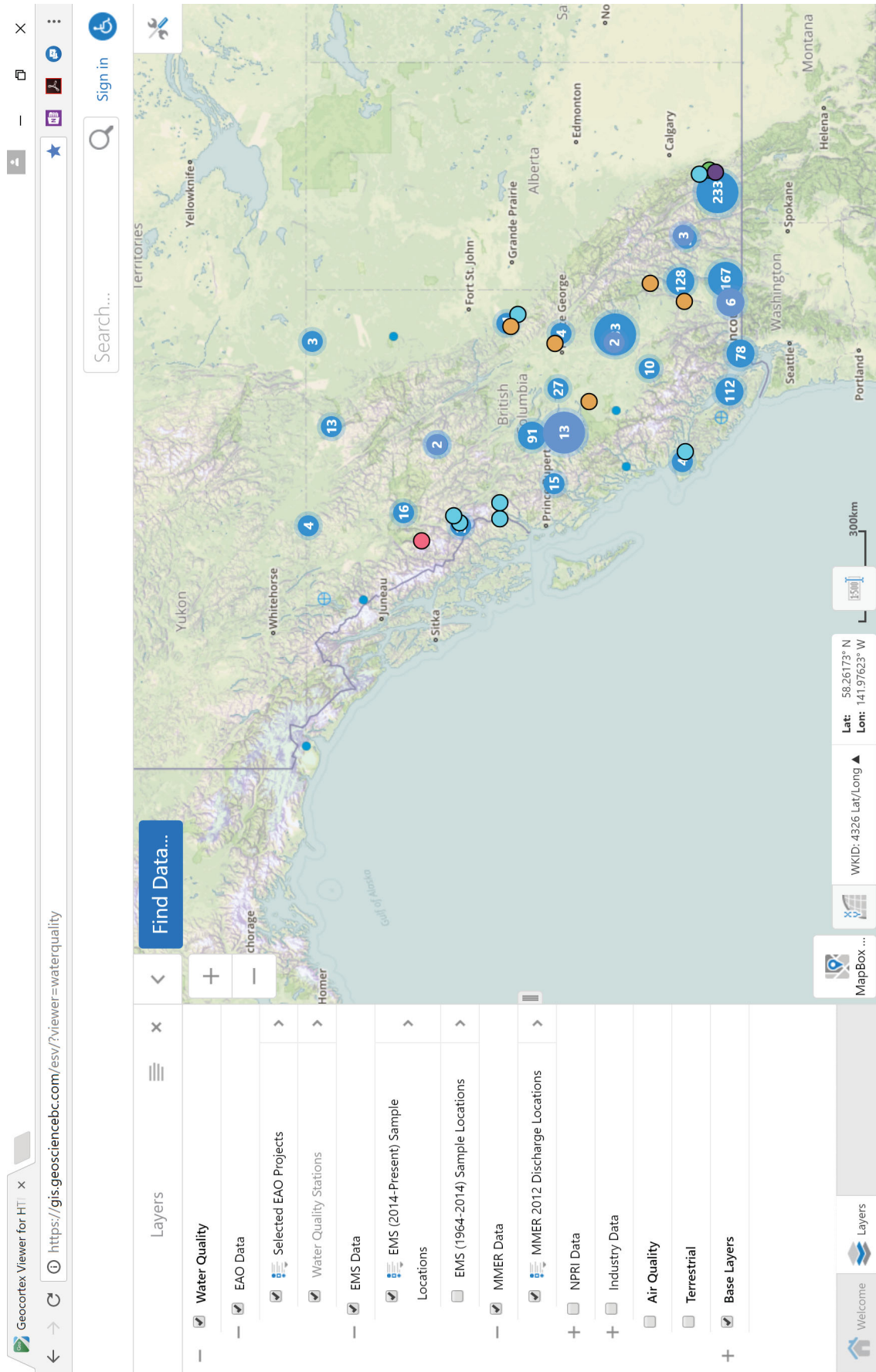


Figure 1. Screen capture showing a report (in PDF) selected that contains baseline water quality for a project in environmental assessment. A user can view the report data by clicking 'View Additional Details' or following a link back to the British Columbia Environmental Assessment Office website.

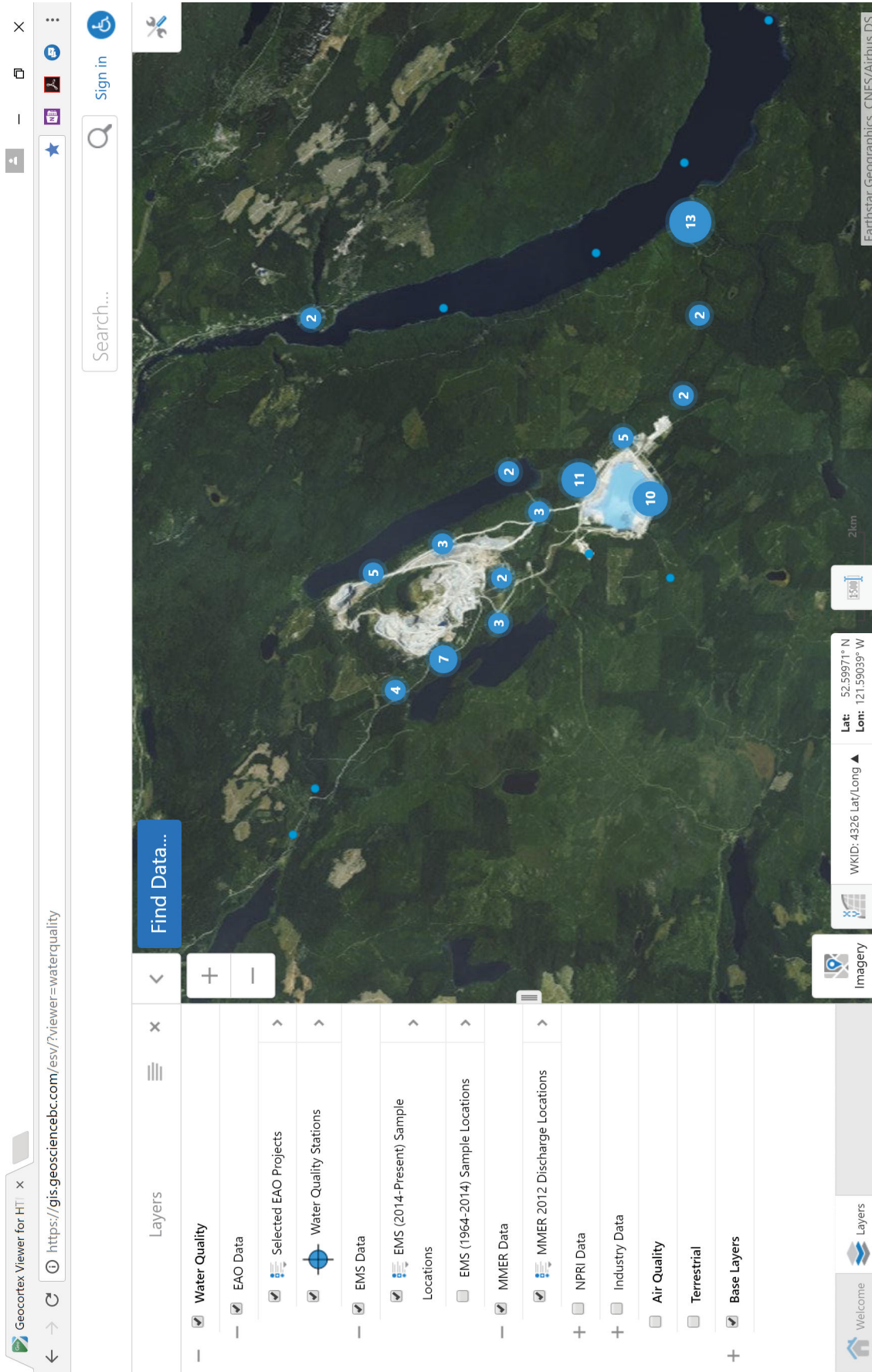


Figure 2. Screen capture from the temporary platform showing a satellite image of a mine operation with water quality monitoring points from the British Columbia Ministry of Environment Environmental Management System. A user can select a point to see what the water quality parameters are at that point. Additional functionality allows the changes in water quality parameters over time to be charted.

Knowledge Hub should be similar to that of consumer-based platforms.

Quality assurance (QA) and quality control (QC) protocols are critical for data usability and defensibility. To address this, the project team has developed a QA-QC strategy to guide data collection and ingestion. A key component of the strategy is presenting existing, publicly available data in an ‘as is, where is’ format. Although less than ideal, this approach mitigates validation and verification risks that may arise during data conversion. Where possible, the project team is working with mining companies and analytical labs to access datasets directly. This approach further helps to mitigate QA-QC risks.

Transparency Through ‘Open Data’

The concept of ‘open data’—defined generally as data that can be accessed and used by anyone—is rapidly capturing the attention of stakeholders, from governments and regulatory agencies to local communities and the public. The value and possibilities of ‘open data’ are myriad, including within the mining sector.

The Knowledge Hub is a first step toward capturing and unlocking these opportunities. The initiative will increase transparency within the mining sector by making water quality data publicly available. By doing so, the sector demonstrates the efficacy of their water management strategies and highlights the sustainability trends of the industry.

Acknowledgments

Special thanks are extended to the Knowledge Hub steering committee members: D. Sanguinetti (Committee Chair), Sanguinetti Engineering; M. Sarfi, JDS Silver; C. Hughes, Imperial Metals; and M. Thorpe, Torex Gold. Special thanks are also extended to the peer reviewer, J. Milette, Corporate Responsibility Initiative at Harvard Kennedy School.

References

Hatch Ltd. (2014): Environmental management in the mining industry: scoping report; Canada Mining Innovation Council, Report 2014, 114 p.



VISION

Earth science for everyone

MISSION

We are a trusted partner providing earth science to encourage investment that benefits all British Columbians

1101 – 750 West Pender Street
Vancouver BC, V6C 2T7

info@geosciencebc.com
www.geosciencebc.com